Universidade do Porto
Faculdade de Engenharia
FEUP

Celina Maria Godinho da Silva Pinto Leão

Modelling and Simulation of Separation/Reaction Process

DEQ/LSRE
Porto, 2003

FEUP

Modelling and Simulation of Separation/Reaction Process

Thesis Dissertation for the Degree of Doctor
in Engineering Sciences
from School of Engineering of University of Porto

by

Celina Maria Godinho da Silva Pinto Leão

Supervision
Professor Alírio E. Rodrigues
Full Professor

Department of Chemical Engineering
School of Engineering
University of Porto
Porto, Portugal

February 2003

Acknowledgements

First of all, I have to acknowledge Prodep and University of Minho for supporting my work. Also, wish to thanks the given opportunity to work at the LSRE, Chemical Engineering Department, Faculty of Engineering of Porto University, in particular Prof. Alírio E. Rodrigues for accepting to be my supervisor and for his constant encouragement and advisable guidelines to explore and keeping me in the right direction.

To Prof. Pedro Oliveira, my scientific supervisor, and all my colleagues from the Production and System Department at the School of Engineering of University of Minho, where I academically belong, specially the colleagues of the Numerical and Statistic Methods Group, for having encouraged and helping me towards this enterprise.

During the development of my work, I came across with different peoples, that directly or indirectly, helping me to carry on this project. I especially thanks to Luís Pais for his valuable aid at the beginning of my work. To Manuela Vilarinho and Ana Mafalda Ribeiro to their refreshing friendship, the 'coffee' times, and for helping me in difficult moments. Also, my sincere thanks to Susana Cruz for her friendship, advises and truthfulness. I enjoyed to working in the LSRE group, not only due to the best work environment but also the opportunity to know new friends.

Last, but not least, Francisco, to his tolerance and entirely support in the most difficult moments, keeping me on the right way. My mother and my sister, the two flowers in my life, tons of thanks.

To My Mother, Guidinha

and Francisco

«O homem é mais genial quando descobre o génio que há em cada um de nós,

e não quando convida a ser seguido.»

Agustina Bessa Luís (1983)

Meninos de Ouro

Resumo

Nos últimos anos, o processo de Leito Móvel Simulado, SMB, tem vindo a ser cada vez mais utilizado como uma poderosa alternativa à cromatografia convencional, nomeadamente na indústria farmacêutica e na purificação de extractos naturais. Os processos de SMB, complexos e altamente interactivos, são de difícil projecto e operação. Duas diferentes abordagens de modelização podem ser aplicadas ao sistema de SMB para a separação de uma mistura binária: o modelo de Leito Móvel Verdadeiro (True Moving Bed, TMB) e o modelo de Leito Móvel Simulado (Simulated Moving Bed, SMB). O modelo de TMB permite uma redução significativa na complexidade computacional mesmo usando uma descrição mais rigorosa de diversos fenómenos (transferência de massa do seio do líquido para o filme que rodeia a partícula do adsorvente, sua penetração através dos poros procurando locais para adsorção/reacção, reacção, adsorção, difusão no estado não estacionário em partículas porosas, convecção). Dois tipos de aproximação LDF foram incluídas e comparadas: aproximação LDF para partículas porosas e aproximação LDF para partículas homogéneas. Com as equivalências apropriadas entre as duas abordagens, TMB e SMB, resultados idênticos foram obtidos.

Os modelos de simulação são intensivamente utilizados no desenvolvimento de processos de separação, reduzindo quer o esforço experimental quer os custos associados. A separação fructose-glicose, é usada como o sistema de teste. Dependendo do interesse do utilizador, os modelos matemáticos resultantes podem ser escritos como um sistema de equações diferenciais às derivadas parciais (PDEs) ou como um sistema de equações algébrico-diferencial às derivadas parciais (PDAEs) para modelos de estado de transiente e, como um sistema de equações diferenciais ordinárias (ODEs) ou como um sistema de equações algébrico-diferenciais (DAEs) para modelos de estado estacionário. Todos os diferentes modelos apresentados foram numericamente resolvidos com pacotes disponíveis: PDECOL e COLNEW para PDEs e ODEs, respectivamente, e DASSL e COLDAE para PDAEs e DAEs, respectivamente.

A tecnologia de SMB também é desenvolvida e aplicada nos processos híbridos, isto é, quando a separação e a reacção dos produtos ocorre simultaneamente e na mesma unidade (Simulated Moving Bed Reactor, SMBR). Como sistema de teste, a inversão da sacarose e separação dos produtos fructose e glicose, foi utilizado. Numa primeira fase, a reacção química foi considerada ocorrer na fase líquida e a sacarose não adsorvida. A influência das condições de operação no desempenho do SMBR, baseado na analogia de TMBR, foi estudada. O desenvolvimento do modelo foi feito a fim de considerar não só a reacção na fase líquida como também no interior da partícula do adsorvente. O modelo detalhado desenvolvido, que inclui reacção química, define um sistema de equações diferenciais parciais com duas variáveis espaciais, axial e radial. Simulações, quer em estado estacionário quer em estado transiente, foram realizadas e apresentadas. Uma metodologia diferente para resolver o modelo detalhado desenvolvido pode ser feita calculando a média da difusão, da adsorção e da reacção nos poros da partícula do adsorvente sobre o volume da partícula. Uma aproximação polinomial foi feita definindo um novo modelo de aproximação LDF com reacção química. Diversas comparações foram feitas entre os perfis de concentração no estado estacionário obtidos com os diferentes modelos.

A separação baseada no SMB é também aplicada à separação de proteínas, separação BSA-Myoglobin. Neste caso, partículas perfusivas são utilizadas onde a transferência de massa ocorre por difusão e convecção dentro dos macroporos. O modelo detalhado, fiável e exacto foi desenvolvido e apresentado.

Abstract

In the last years the SMB process was increasingly used as a powerful alternative to conventional batch chromatography, namely in the fine chemical and pharmaceutical industry and in the purification of natural extracts. SMB processes, which are often complex and highly interactive, are difficult to design and operate. Two different modelling approaches can be applied to a SMB system for the separation of a binary mixture: the true moving bed (TMB) model and the real simulated moving bed (SMB) model. The TMB model allows a significant reduction of the computational complexity even using a more rigorous description of several phenomena (mass transfer from the bulk fluid to the liquid film surrounding the adsorbent particle, and then the penetration through the pores of the adsorbent particle seeking sites for adsorption/reaction, reaction, adsorption, unsteady-state diffusion on porous particles, convection). In the SMB approach a LDF approximation for porous particle was included and compared with the results obtained by using a LDF approximation for homogeneous particle. Keeping in mind the proper relations of equivalence between the two approaches, TMB and SMB, identical results are obtained.

Simulation models are intensively used in the development of separation processes, reducing the experimental effort and the costs associated. The fructose-glucose separation is used as a test system. The resulting mathematical models can be written in terms of systems of Partial Differential Equations (PDEs) or Partial Differential-Algebraic Equations (PDAEs) for transient situations, and Ordinary Differential Equations (ODEs) or Differential Algebraic Equations (DAEs) for steady-state situations, depending on the user interest. All four different models were numerically solved with available software packages: PDECOL and COLNEW for PDEs and ODEs, respectively, and DASSL and COLDAE for PDAEs and DAEs, respectively.

The SMB technology is also developed and applied in hybrid processes, where chromatography separation and chemical reaction take place in the same unit. The sucrose inversion and fructose/glucose separation was the system used. As a first approach, the chemical reaction was only considered to take place in the liquid phase and the sucrose is not adsorbed. The influence of the operating conditions on the SMBR performance based on the TMBR analogy was addressed. Developments in the model were done in order to consider the reaction in the fluid phase and inside the adsorbent particle. The detailed model presented, which takes into account chemical reaction, defines a system of partial differential equations in two spatial variables, axial and radial coordinates. Transient and steady-state simulations were carried out. A different methodology for solving the new detailed model can be done by averaging the pore diffusion, adsorption and reaction over the particle volume equation. A polynomial approximation was done defining a new LDF approximation model with chemical reaction. Several comparisons were made with the final steady-state profile concentrations obtained with the different models.

The design of a SMB separation is also applied to the proteins separation, namely BSA - Myoglobin separation. In this case perfusive particles are used where mass transfer occurs by diffusion and convection inside large-pores. An optimal design depends on various factors such as columns numbers and length, flowrates, switching time. A detailed, reliable and accurate model has been developed and presented.

Résumé

Le procédé de SMB est devenu une alternative puissante à la chromatographie conventionnelle, en particulier dans l'industrie pharmaceutique et dans la purification des extraits normaux. Les procédés de SMB, souvent complexes et fortement interactifs, sont de difficile conception et opération. Deux approches pour la modélisation peuvent être appliquées à un système de SMB pour la séparation d'un mélange binaire: les modèles du lit mobile vrai (TMB) et du lit mobile simulé (SMB). Le modèle de TMB permet une réduction significative du temps de calcul avec une description de plusieurs phénomènes (transfert de masse a travers du film entourant la particule d'adsorbant, et puis la diffusion dans les pores de l'adsorbant, réaction, adsorption, convection). Dans l'approche SMB une approximation LDF pour la particule poreuse était utilisée et comparée aux résultats obtenus avec une approximation LDF pour la particule homogène. Avec les relations appropriées d'équivalence, des résultats identiques sont obtenues.

Des modèles de simulation sont employés dans le développement des procédés de séparation, réduisant l'effort expérimental et les coûts associés. La séparation fructose-glucose, est employée comme système d'essai. Les modèles mathématiques résultants peuvent être écrits en termes de systèmes d'équations partielles (PDEs) ou d'équations Différentielles-Algébriques partielles (PDAEs) pour des situations transitoires et, de systèmes d'équations ordinaires (ODEs) ou d'équations algébriques différentielles (DAEs) pour l'état stationnaire, selon l'intérêt d'utilisateur. Chacun des modèles différents a été numériquement résolu avec les softwares disponibles: PDECOL et COLNEW pour PDEs et ODEs, respectivement, et DASSL et COLDAE pour PDAEs et DAEs, respectivement.

La technologie de SMB est également développée et appliquée dans des processus hybrides, où la séparation chromatographie et la réaction chimique de produit aient lieu dans la même unité. L'inversion du sucrose et la séparation fructose/glucose étaient le système utilisé. Comme première approche, la réaction chimique a été seulement considérée dans la phase liquide et la sucrose n'est pas adsorbé. L'influence des conditions de fonctionnement sur l'opération du SMBR basée sur l'analogie de TMBR a été adressée. Des développements dans le modèle ont été faits afin de considérer la réaction dans la phase liquide et à l'intérieur de la particule d'adsorbant. Le modèle détaillé présenté, qui tient compte de la réaction chimique, définit un système des équations partielles dans deux variables spatiales, axial et radial. Une méthodologie différente pour résoudre le modèle détaillé peut être faite en faisant la moyenne de la diffusion, de l'adsorption et de la réaction dans les pores sur le volume de la particule. Une approximation polynomial a été faite définissant un nouveau modèle d'approximation LDF avec la réaction chimique.

La conception d'une séparation de SMB est aussi appliquée à la séparation de protéines, BSA - Myoglobine. Dans ce cas des particules perfusives sont employées où le transfert de masse se produit par diffusion et convection à l'intérieur des macropores. Un modèle détaillé, fiable et précis a été développé et présenté.

Table of Contents

List of Figures iv

List of Tables xvi

List of Symbols xx

1. Introduction 01

1.1 Simulated Moving Bed (SMB) / Simulated Moving Bed Reactor (SMBR) 01
1.2 Motivation 02
1.3 Thesis objectives and organization 03
1.4 References 05

2. Simulated Moving Bed: Fundamentals and Numerical Strategies to Solve Transient and Steady-State Models 09

2.1 Simulated Moving Bed Technology 10
2.1.1 Theoretical Aspects: Separation Region and Process Parameters 14
2.1.2 Model Description 21
2.2 Numerical Methods and Differential Equations Solvers 26
2.2.1 Orthogonal collocation on finite elements 27
2.2.2 Method of Lines 28
2.2.3 Boundary-Value Problems for Differential-Algebraic Equations 30
2.2.3.1 Orthogonal collocation on finite elements 31
2.2.4 Parabolic Partial-Algebraic Differential Equations 32
2.2.4.1 Method of Lines 32
2.2.5 Mathematial software applied to the case study 32
2.2.5.1 Boundary-Value Problems for Differential-Algebraic Equations 33
2.2.5.2 Parabolic Partial Differential-Algebraic Equations 35
2.2.5.3 Boundary-Value Problems for Ordinary Differential Equations 47
2.2.5.4 Parabolic Partial Differential Equations 49
2.3 Simulation Results and Discussion 51
2.4 Conclusions 58

2.5 References 58

3. Modeling and Simulation of SMB Chromatography 63

3.1 The Case of Gl/Fr Separation 64
3.1.1 Steady-State Simulation Results from T-TMB and S-TMB Models using LDF approximation for homogeneous particles 64
3.1.2 Evolution of the Internal Profiles for Transient Operation of the TMB 70
3.1.3 Effect of Operating Variables 70
3.1.3.1 Effect of the Rotation Period 72
3.1.3.2 Effect of the Extract Flow Rate 74
3.1.3.3 Effect of the Feed Flow Rate 76
3.1.3.4 Effect of Feed Concentration 77
3.1.3.5 Effect of the Section Length and Configuration 79
3.1.3.6 Effect of the Number of Intraparticle Mass Transfer Unit 80
3.1.3.7 γ_{II} - γ_{III} Plane Analysis 83
3.1.4 Influence of the Type of Isotherms on the Behaviour of the SMB 87
3.1.5 Effect of the Operating Conditions on the TMB Performance 98
3.2 TMB and SMB Models usig LDF Approximation Model for Porous Particles 102
3.2.1 Effect of Operating Variables 111
3.2.1.1 Effect of the Rotation Period 111
3.2.1.2 Effect of the Extract Flow Rate 113
3.2.1.3 Effect of the Feed Flow Rate 113
3.2.1.4 Effect of the Section Length 116
3.2.1.5 Effect of the Number of intraparticle Mass Transfer Unit 116
3.2.2 Evolution of the Internal Profiles for the Transient Operation of the TMB 118
3.2.3 Influence of the LDF Type Model Approximation 118
3.3 Conclusions 126
3.4 References 128

4. Simulated Moving Bed Adsorptive Reactor: Modelling and Simulation 131

4.1 Basic Idea of the SMBR. 131
4.1.1 Model Description. 133
4.1.2 Performance Criteria. 137
4.2 Numerical Methods. 137
4.3 Simulation Results and Discussion 138
4.3.1 Evolution of the internal profiles for the transient of the TMBR. 140
4.3.2 Comparison between the transient TMBR model and the steady-state TMBR 142
4.4 Effect of operating variables 146
4.4.1 Effect of the rotation period. 146
4.4.2 Effect of the extract flowrate. 148
4.4.3 Effect of the feed flowrate. 150
4.4.4 Effect of feed concentration. 150
4.4.5 Effect of the section length and configuration. 152
4.4.6 Effect of the number of intraparticle mass transfer units. 154
4.5 Comparison between the transient TMBR and TMB models 155
4.6 Conclusions 158
4.7 References 158

5. Modelling of TMBR Adsorber: New Developments 161

5.1 Model Formulation and Development 162
5.2 Operating Conditions and Model Parameters Estimation 174
5.2.1 OperatingConditions. 174
5.2.2 Model Parameters. 176
5.3 Performance Criteria 177
5.4 Simulation Results and Discussion 178
5.4.1 Effect of Particle Radius. 179
5.4.2 Complete Separation Region. 181
5.5 New Developments on the TMBR System 183
5.6 Simulation Results 191
5.6.1 Transient Solutions. 192
5.6.2 Steady-state Solutions. 198
5.6.3 Model Without Reaction. 202
5.6.4 Model With Non Linear Reaction. 203
5.7 Conclusions 206
5.8 References 207

6. Model With Intraparticle Diffusion and Convection Development in Proteins Separation 209

6.1 Introduction 209
6.2 TMB steady-state intraparticle diffusion/convection model equations 214
6.2.1 γ_{II} - γ_{III} plane analysis. 218
6.2.2 The optimisation problem and procedure. 221
6.2.3 Design results and discussion. 222
6.2.3.1 Effect of the Purity Requirements 224
6.2.3.2 Effect of the Particle Size 226
6.3 Equilibrium Stage Model 228
6.4 Conclusions 232
6.5 References 233

7. Conclusions and Suggestions for Future Work 235

Appendices

A. Source code for the Steady-State TMB model using COLDAE 237

B. Source code for the Transient TMB model using DASSL 241

C. Source code for the Steady-State TMB model using COLNEW 253

D. Source code for the Transient TMB model using PDECOL 257

E. Modelling intraparticle diffusion, adsorption and reaction (with spatial discretization) 261

List of Figures

Chapter 2

Figure 2.1 Moving Bed Chromatographic Separation 11

Figure 2.2 Scheme of a four-section True Moving Bed separation unit. It also shows the flow rates direction of the two components in each section; fructose, represented by letter B, and glucose, represented by letter A, in each section ... 12

Figure 2.3 Scheme of an equivalent SMB unit with 3-3-3-3 configuration..... 13

Figure 2.4 Region of complete separation on the planes $\gamma_{II} - \gamma_{III}$ and $\gamma_{IV} - \gamma_{I}$ in terms of purity of the outlet streams, in the case of a system described by a linear isotherm with K_A=0.50 and K_B=0.88. The region of complete separation is defined by the triangle AWB on the $\gamma_{II} - \gamma_{III}$ plane, and by the square CWDE on the $\gamma_{IV} - \gamma_{I}$ plane. See next section for the definition of γ_{II} and γ_{III}..... 17

Figure 2.5 Regions of the (γ_{II}, γ_{III}) plane with different separation regimes in terms of purity of the outlet streams. The constraints on γ_{I} and γ_{IV} must be fulfilled in order to obtain complete separation. System with linear isotherms with K_A = 0.50 and K_B = 0.88. Point W and point C correspond, respectively, to the lower and upper limits on the safety coefficient β, $1 < \beta < \sqrt{\alpha}$ 20

Figure 2.6 Flow diagram of computer program to numerically solve the models presented in Table 2.4. The subroutine PACKAGE refers to the package used depending on the type of problem to be solved. 33

Figure 2.7 Flow diagram of subroutine HERMCOL (one of the PACKAGE subroutine) that develops the discretization elements for the first and second derivatives carried out sequentially for each finite element, initial conditions are set and the problem takes the ODE form, defined in RES, to be integrated using the DASSL. 36

Figure 2.8 (a) Subdivision of the solution domain into 14 finite elements. Two collocation points, NC=2, were chosen in each finite element considered. | , end points, ı , continuity between interior finite elements, •, interior collocation points within each finite element. Global numbering i. **(b)**

Representation of the finite element 2 (k = 1, ..., NE) normalised between 0 and 1, with the two collocation points, u_1 and u_2, considered. Local numbering system I. 38

Figure 2.9 **HaMAT** matrix representation considering three finite elements, $NE = 3$, with two collocation points in each finite element. 46

Figure 2.10 Transient T-TMB internal concentration profiles for the TMB, under conditions described in Table 2.7, obtained by using the PDECOL, (a), and by using the DASSL, (b), for cycles 1, 2 and 10. 53

Figure 2.11 Steady-state T-TMB internal concentration profiles solutions, under conditions described in Table 2.7, obtained by using the PDECOL, (a), DASSL, (b), COLNEW, (c), and COLDAE, (d). 54

Figure 2.12 Steady-state T-TMB internal concentration profiles solutions, under the new conditions described in Table 2.8, obtained by using the PDECOL, (a), DASSL, (b), COLNEW, (c), and COLDAE, (d). 56

Figure 2.13 Steady-state internal concentration profiles for the TMB, (a) under conditions described in Table 2.7, (b) under the new conditions described in Table 2.8, obtained by using the PDECOL (straight and dash lines) and DASSL (• and ♦ points). 56

Chapter 3

Figure 3.1 Steady-state internal profiles for the case study under conditions described in Table 3.1 and 3.2, obtained by (a) using PDECOL package and the COLNEW package, for the PDE/ODE system; and obtained by (b) using the DASSL package and the COLDAE package, for the PDAE/DAE system. Full squares and circles for fructose (Fr) and glucose (Gl), respectively, obtained with PDECOL/DASSL, and white squares and circles for fructose (Fr) and glucose (Gl), respectively, obtained with COLNEW/COLDAE. 67

Figure 3.2 Relative error, (a) and (c), and absolute error, (b) and (d), for the case study, comparing the obtained results using COLNEW/ PDECOL and COLDAE/DASSL, respectively. 69

Figure 3.3 Transient TMB internal profiles for the case study under conditions described in Table 3.1 and 3.2, obtained by using PDECOL (a) and DASLL (b), for cycles 1, 2, 3 and 10. 71

Figure 3.4 Evolution of the transient internal profiles for the case study under conditions described in Table 3.1 and 3.2. Squares represent the internal profile in cycle 1 and the circles the internal profiles in cycle 10, the diamonds and triangles represent the internal profiles for cycle 2 and 3, respectively (full glucose and white, fructose). The two arrows show the way of the evolution, one for each outlet stream. 72

Figure 3.5 Effect of the rotation period on the SMB performance parameters for the case study. The rotation period varied between 106 and 136 sec. The other operating conditions and model parameters were kept constant and the same as described in Table 3.1. (a) Rotation period versus Purity, (b) Rotation period versus Recovery, (c) Rotation period versus Solvent Consumption, (d) Rotation period versus Productivity. 73

Figure 3.6 Recovery versus purity for extract (a) and raffinate (b), obtained for different values of rotation period (106-136 sec), for the base case study. The other operating conditions and model parameters were kept constant and the same as described in Table 3.4. The two limits considered for the rotation period, 106 sec and 136 sec, are referred with the equivalent values for the purity and recovery. The arrows show the evolution of the performance with the increase of the rotation period. 74

Figure 3.7 Effect of the extract flowrate on the SMB performance parameters for the case study. The extract flowrate changed between 3.62 and 11.62 ml/min. The other operating conditions and model parameters were kept constant and the same as described in Table 3.4, except the raffinate flowrate that changed with the extract flowrate in order to keep constant the total balance. (a) Extract flowrate versus Purity, (b) Extract flowrate versus Recovery, (c) Extract flowrate versus Solvent Consumption, (d) Extract flowrate versus Productivity. 75

Figure 3.8 Recovery versus purity for extract (a) and raffinate (b), obtained for different values of the extract flowrate (4.12-12.12 ml/min), for the base case study. The other operating conditions and model parameters were kept constant and the same as described in Table 3.4, except the raffinate flowrate that changed with the extract flowrate in order to keep constant the total balance ($Q_R+Q_E=Q_D+Q_F$). The two limits considered for the rotation period, 4.12 ml/min and 12.12 ml/min are referred with the equivalent values for the purity and recovery. The arrows show the evolution of the performance with the increase of the extract flowrate. 76

Figure 3.9 Effect of the feed flowrate on the SMB performance parameters for the case study. The feed flowrate changed between 0.23 and 8.23 ml/min. The other operating conditions and model parameters were kept constant and the same as described in Table 3.4, except the eluent flowrate that changed with the feed flowrate in order to keep constant the total balance ($Q_R+Q_E=Q_D+Q_F$). (a) Feed flowrate vs. Purity, (b) Feed flowrate vs. Recovery, (c) Feed flowrate vs. Solvent Consumption, (d) Feed flowrate vs. Productivity. 77

Figure 3.10 Recovery versus purity for extract (a) and raffinate (b), obtained for different values of the feed flowrate (0.23-8.23 ml/min), for the base case study. The other operating conditions and model parameters were kept constant and the same as described in Table 3.4, except the eluent flowrate that changed with the feed flowrate in order to keep constant the total balance ($Q_R+Q_E=Q_D+Q_F$). The two limits considered for the rotation period, 0.23 ml/min and 8.23 ml/min are referred with the equivalent values for the purity and recovery. The arrows show the evolution of the performance with the increase of the feed flowrate 78

Figure 3.11 Effect of the feed concentration on the Solvent Consumption and on the Productivity on the SMB for the case study. The feed concentration varied between 5 and 100 g/l. The other operating conditions and model parameters were kept constant and the same as described in Table 3.4. (a) Productivity versus Feed concentration, (b) Solvent Consumption versus Feed concentraion. 78

Figure 3.12 Effect of the zone length in the performance parameters: (a) purity, (b) recovery. The other operating conditions and model parameters were kept constant and the same as described in Table 3.1. 79

Figure 3.13 Effect of the intraparticle mass transfer rate on the SMB steady-state internal profile. (a) α=3.60 or k=0.01 s^{-1}; (b) α=7.20 or k=0.02 s^{-1}; (c) α=10.8 or k=0.03 s^{-1}; (d) α=18.0 or k=0.05 s^{-1}. The other operating conditions and model parameters were kept constant and the same as described in Table 3.1. . 80

Figure 3.14 Recovery vs. purity of extract (a) and Recovery vs. purity of raffinate (b) for different values of the intraparticle mass transfer rate (--□-- k=0.1 s^{-1}, --○-- k=0.05 s^{-1}, -- Δ-- k=0.03 s^{-1}, --×-- k=0.02 s^{-1}, --◊-- k=0.01 s^{-1}) each for different values of rotation period, $t^* \in [106, 136]$ sec. The other operating conditions and model parameters were kept constant and the same as described in Table 3.1. The arrow shows the evolution of the performance parameters with the increase of the rotation period. 81

Figure 3.15 Recovery vs. purity of extract (a) and Recovery vs. purity of raffinate (b) for different values of the intraparticle mass transfer rate (--□-- k=0.1 s^{-1}, --○-- k=0.05 s^{-1}, -- Δ-- k=0.03 s^{-1}, --×-- k=0.02 s^{-1}, --◊-- k=0.01 s^{-1}) each for different values of extract flow, $Q_E \in [4.12, 12.12]$ ml/min. The other operating conditions and model parameters were kept constant and the same as described in Table 3.1. The arrow shows the evolution of the performance parameters with the increase of the extract flowrate. 82

Figure 3.16 Recovery vs. purity of extract (a) and Recovery vs. purity of raffinate (b) for different values of the intraparticle mass transfer rate (--□-- k=0.1 s^{-1}, --○-- k=0.05 s^{-1}, -- Δ-- k=0.03 s^{-1}, --×-- k=0.02 s^{-1}, --◊-- k=0.01 s^{-1}) each for different values of feed flow, $Q_F \in [0.23, 8.23]$ ml/min. The other operating conditions and model parameters were kept constant and the same as described in Table 3.4. The arrow shows the evolution of the performance parameters with the increase of the feed flowrate. 83

Figure 3.17 Regions of operation of the TMB in a plot of the ratio of fluid solid velocities in zone III versus Ratio of fluid solid velocities in zone II considering linear isotherms for both components under conditions described in Table 3.4 and 3.1; the full squares (■) represent numerical simulation results corresponding to purity values ≥99.5% for one or both outlet streams; the —— line represents the theoretical limits; × and + represents the effect of extract and feed flowrates changes on the separation region of operating of the TMB, respectively. The performance parameters obtained for A, B, C and D points are described in Table 3.6. 85

Figure 3.18 Regions of operation of the TMB in a plot of the ratio of fluid solid velocities in zone III versus Ratio of fluid solid velocities in zone II considering linear isotherms for both components under conditions described in Table 3.4 and 3.1; the full diamonds (♦), the full squares (■), and the full triangles (▲) represent the numerical simulation results corresponding to purity values ≥99.5% for one or both outlet streams, for k=0.1 s^{-1}, k=0.5 s^{-1}, and k=2.0 s^{-1}, respectively; the —— line represents the theoretical limits (Vertex: ♦ γ_I = 1.47, ■ γ_I = 1.34, ▲ γ_I = 1.32). 87

Figure 3.19 Regions of operation of the TMB in a plot of the ratio of fluid solid velocities in zone III versus Ratio of fluid solid velocities in zone II considering linear

isotherms for both components under conditions described in Table 3.1, with k=2.0 s^{-1}, for different values of total balances; the full squares (■),the full diamonds (♦), and the full triangles (▲) represent the numerical simulation results corresponding to purity values ≥99.5% for one or both outlet streams, for 12.92, 17.62, and 22.62 ml/min, respectively; the —— line represents the theoretical limits (Vertex: ■ $\gamma_I = 1.32$, ♦ $\gamma_I = 1.64$, ▲ $\gamma_I = 2.08$). 88

Figure 3.20 (a) Steady-state internal profiles for the study case obtained using linear isotherms (3.2) for both components, with K_{Gl}=0.3401 and K_{Fr}=0.5634, and the operating conditions and model parameters as described in Table 3.7 and 3.2, and (b) corresponding relative error. 90

Figure 3.21 Isotherms of glucose in the presence of fructose using (3.3a). Results taken from Strube and Schmidt-Traub (1996). The dots represent the experimental results and the lines the values obtained using the model similar to the multicomponent Langmuir. 91

Figure 3.22 Isotherms of glucose in the presence of fructose using (3.4), Langmuir equation modelled by using the experimental values obtained Strube and Schmidt-Traub (1996). The dots represent the experimental results and the lines the values obtained by using the new model (3.4) 92

Figure 3.23 (a) 3-dimensional representation of the Langmuir equation model (3.3a) obtained by Strube and Schmidt-Traub (1996); and (b) 3-dimensional representation of the Langmuir equation model used in the present work using the experimental values of Strube and Schmidt-Traub (1996) (3.4). (1) variation of q_{Gl} for different values of c_{Gl} and c_{Fr}; (2) 2-D plane showing the variation of q_{Gl} dor different values of c_{Gl}; (3) 2-D plane showing the variation of q_{Gl} for different values of c_{Fr}. 93

Figure 3.24 Relative error, eqaution (3.5), versus glucose concentration for the obtained values by using the Langmuir equation (3.4) and by using the multicomponent Langmuir equation (3.3a). 94

Figure 3.25 Steady-state internal profiles for each TMB component obtained using the new Langmuir isotherm (3.4) for glucose and the linear isotherm for fructose equation (3.2a). The model parameters and operating conditions are as described in Table 3.7. 95

Figure 3.26 Steady-state internal profiles for the TMB obtained using linear isotherms for glucose and fructose, equation (3.3), for a feed concentration, C=225 g/l. The model parameters and operating conditions are as described in Table 3.7. 96

Figure 3.27 Steady-state internal profiles for the TMB obtained using non linear Langmuir isotherm, equation (3.4), for glucose and linear isotherm, equation (3.2a), for fructose, for a concentration feed, C=225 g/l. The model parameters and operating conditions are as described in Table 3.7. 97

Figure 3.28 Regions of operation of the TMB in a γ_{III} - γ_{II} plot considering linear isotherms for both components under conditions described in Table 3.12; the full diamonds (♦) represent the numerical simulation results obtained for mass transfer resistance k=0.1 s^{-1}, the full squares (■) represent the numerical simulation results obtained for k=0.5 s^{-1}, the full triangles (▲) represent the numerical simulation results obtained for negligible mass transfer resistance

k=2.0 s^{-1}, the —— line represents the theoretical limits (Vertex: ♦ γ_I = 1.56, ■ γ_I = 1.46, ▲ γ_I = 1.45)..... 99

Figure 3.29 Regions of operation of the TMB in a γ_{III} - γ_{II} plot considering linear isotherms for fructose and Langmuir for glucose under conditions described in Table 3.12; the full diamonds (♦) represent the numerical simulation results obtained for mass transfer resistance k=0.1 s^{-1}, the full squares (■) represent the numerical simulation results obtained for k=0.5 s^{-1}, the full triangles (▲) represent the numerical simulation results obtained for negligible mass transfer resistance k=2.0 s^{-1}, the —— line represents the theoretical limits; the open diamonds (◊) and triangles (Δ) represents the numerical simulation results obtained for k=0.1and 2.0 s^{-1}, respectively for Q_{BAL} =12.89 ml/min (Vertex: ♦ γ_I = 0.97, ◊ γ_I = 1.17, ▲ γ_I = 0.85, Δ γ_I = 0.95)..... 102

Figure 3.30 Schematic stagnant particle representation..... 103

Figure 3.31 Adsorption isotherms for the bi-naphthol enantiomers: (a) for the more retained component; (b) for the less retained component. Thin line for the LDF model for homogeneous particles, equation (3.9), and thick line for LDF model considering porous particle, equation (3.14). 109

Figure 3.32 Internal profiles for the reference case. Solid line for the less retained component, dashed line for the more retained component, under operating conditions as in Table 3.17..... 111

Figure 3.33 Effect of the rotation period on the SMB performance parameters $t^* \in$[105, 210] sec. The others operating conditions and model parameters were kept constant as described in Table 3.17. (a) Rotation Period vs. Purity (b) Rotation Period vs. Recovery (c) Rotation Period vs. Solvent Consumption (d) Rotation Period vs. Productivity (e) Recovery vs. purity for extract (f) Rotation Period vs. purity for raffinate (the arrows show the way of the rotation period increase)..... 112

Figure 3.34 Effect of the extract flowrate on the SMB performance parameters $Q_E \in$[11.98, 23.98] ml/min. The others operating conditions and model parameters were kept constant as described in Table 3.17. (a) Extract flowrate vs. Purity (b) Extract flowrate vs. Recovery (c) Extract flowrate vs. Solvent Consumption (d) Extract flowrate vs. Productivity (e) Recovery vs. purity for extract (f) Rotation Period vs. purity for raffinate (the arrows show the way of the extract flowrate increase). 114

Figure 3.35 Effect of the feed flowrate on the SMB performance parameters $Q_F \in$[0.94, 9.14] ml/min. The others operating conditions and model parameters were kept constant as described in Table 3.17, except the eluent flowrate that changed with the feed flowrate in order to keep constant the total balance ($Q_R+Q_E=Q_D+Q_F$). (a) Feed flowrate vs. Purity (b) Feed flowrate vs. Recovery (c) Feed flowrate vs. Solvent Consumption (d) Feed flowrate vs. Productivity (e) Recovery vs. purity for extract (f) Rotation Period vs. purity for raffinate (the arrows show the increase of the feed flowrate). 115

Figure 3.36 Effect of the section length on the performance parameters: (a) purity, (b) recovery, (c) solvent consumption, (d) productivity. The others operating conditions and model parameters were kept constant and the same as described in Table 3.17. 116

Figure 3.37 Effect of the mass transport coefficient in the pores on the cyclic SMB steady-state internal profiles. (a) k_{pA}=0.1395 s^{-1} and k_{pB}=0.2015 s^{-1} (or α_{pA}=50.22 and α_{pB}=72.54), (b) k_{pA}=1.395 s^{-1} and k_{pB}=2.015 s^{-1} (or α_{pA}=502.2 and α_{pB}=725.4). The others operating conditions and model parameters were kept constant and the same as described in Table 3.17. 117

Figure 3.38 Transient TMB internal profiles for the reference case obtained fot cycles 1, 2, 3, and 10. 118

Figure 3.39 Internal profiles for the case of LDF model for homogeneous particles (full circles for raffinate (A) and full triangles for extract (B)), and LDF model for porous particles (white circles for raffinate (A) and white triangles for extract (B)). 119

Figure 3.40 Concentration profiles in (a) the extract and (b) raffinate for the SMB at cyclic-state and during a full cycle obtained by using the LDF model for porous particle. Dotted lines are for the more retained component, full line is for the less retained component. 122

Figure 3.41 Cyclic steady-state internal concentration profiles during a switch time internal (fraction) for the SMB obtained by using the LDF model for porous particle. Profiles for the less retained component (a) and for the mores retained component (b) at the beginning, 25%, 50%, 75%, and at the end of a switch time interval (eluent at the beginning of column 1; extract between columns 2 and 3; feed between columns 4 and 5; raffinate between columns 6 and 7). 123

Figure 3.42 Transient evolution (first five cycles) of the concentration (a) of the more retained component in the extract (b) of the less retained component in the raffinate, obtained by using the LDF model for porous particle. The full line represents the values obtained in the TMB approach, the dotted line in the SMB approach, the step dotted line is the SMB approach with the average concentration over a switch time interval, the ooo line is the SMB instantaneous concentration evaluated between switching. 124

Figure 3.43 Steady-state internal concentration in the TMB approach and SMB case at half-time between switching obtained by using the LDF model for porous particle: less retained component A, more retained component B. The full circles and triangles are for the SMB approach; the white circles and triangles are for the TMB (extract outlet column 2, feed inlet column 4, raffinate outlet column 6). 126

Chapter 4

Figure 4.1 SMBR system configuration, with four sections, different number of columns per section, 2 2 6 2, respectively. 133

Figure 4.2 Results obtained for the inversion of sucrose and glucose/fructose separation under conditions in Table 4.2 and numerical parameters described in Table 4.3, by using PDECOL solver. 140

Figure 4.3 Results obtained for the inversion of sucrose and glucose/fructose separation under conditions in Table 4.2 and numerical parameters described in Table 4.3, by using PDECOL solver, the 3-3-3-3 configuration. 140

Figure 4.4 Transient TMBR internal profiles for the case study under conditions described in Table 4.2 obtained by PDECOL solver for cycles 1, 2, 3 and 10, respectively, with numerical parameters described in Table 4.3. 141

Figure 4.5 Evolution of the transient internal profiles for the reference case under conditions described in Table 4.2 and 4.3. Squares represent the internal profiles in cycle 1 and circles represent the internal profiles in cycle 10 (full, glucose, and white, fructose), the continuous lines correspond to sucrose. The two arrows show the way of the evolution, one for each outlet stream. 142

Figure 4.6 Results obtained for the inversion of sucrose and glucose/fructose separation under conditions in Table 4.2 and 4.3 by using COLNEW solver. 144

Figure 4.7 Relative error (a) and absolute error (b), obtained for case study, comparing the obtained results by using PDECOL (transient model) and COLNEW (steady-state model) solvers. 144

Figure 4.8 Effect of the rotation period on the TMBR performance parameters for the case study. The rotation period varied between 110 and 130 sec. The others operating conditions and model parameters were kept constant and the same as described in Table 4.2 and numerical parameters in Table 4.3. (a) Rotation Period versus Purity, (b) Rotation Period versus Recovery, (c) Rotation Period versus Solvent Consumption, (d) Rotation Period versus Productivity, (e) Rotation Period versus Conversion..... 147

Figure 4.9 Recovery vs purity for extract (a) and raffinate (b), obtained for different values of rotation period (110-130 sec) for the base case study. The others operating conditions and model parameters were kept constant and the same as described in Table 4.2. The two limits considered for the rotation period, 106 sec and 136 sec are referred with the equivalent values for the purity and recovery. The arrows show the evolution of the performance with the increase of the rotation period. 148

Figure 4.10 Effect of the extract flowrate on the SMB performance parameters for the case study. The extract flowrate changed between 4.0 and 11.0 ml/min. The others operating conditions and model parameters were kept constant as described in Table 4.2, except the raffinate flowrate that changed with the extract flowrate in order to keep constant the total balance ($Q_R+Q_E=Q_D+Q_F$) and numerical parameters in Table 4.3. (a) Extract Flowrate versus Purity, (b) Extract Flowrate versus Recovery, (c) Extract Flowrate versus Solvent Consumption, (d) Extract Flowrate versus Productivity, (e) Extract Flowrate versus Conversion. 149

Figure 4.11 Recovery versus purity for extract (a) and raffinate (b) obtained for different values of the extract flow rate (4.0-11.0 ml/min), for the case study. The others operating conditions and model parameters were kept constant and the same as described in Table 4.2, except the raffinate flowrate that changed with the extract flowrate in order to keep constant the total balance ($Q_R+Q_E=Q_D+Q_F$). The two limits considered for the extract flowrate, 4.0 ml/min and 11.0 ml/min are referred with the equivalent values for the purity and recovery. The arrows show the evolution of the performance with the increase of the extract flowrate. 150

Figure 4.12 Effect of the feed flow rate on the SMB performance parameters for the case study. The feed flowrate varied between 0.15 and 11.15 ml/min. The others

operating conditions and model parameters were kept constant and the same as described in Table 4.2, except the eluent flowrate that changed with the feed flowrate in order to keep constant the total balance ($Q_R+Q_E=Q_D+Q_F$). (a) Feed Flowrate versus Purity, (b) Feed Flowrate versus Recovery, (c) Feed Flowrate versus Solvent Consumption, (d) Feed Flowrate versus Productivity, (e) Feed Flowrate versus Conversion. 151

Figure 4.13 Recovery versus purity for extract (a) and raffinate (b) obtained for different values of the feed flow rate (0.15-11.15 ml/min), for the case study. The others operating conditions and model parameters were kept constant and the same as described in Table 4.2, except the eluent flowrate that changed with the feed flowrate in order to keep constant the total balance ($Q_R+Q_E=Q_D+Q_F$). The two limits considered for the feed flowrate, 0.15 ml/min and 11.15 ml/min are referred with the equivalent values for the purity and recovery. The arrows show the evolution of the performance with the increase of the feed flowrate 152

Figure 4.14 Effect of the feed concentration on the Solvent Consumption and on the Productivity on the SMBR for the study case. The feed concentration varied between 2.5 and 250 gr/l. The others operating conditions and model parameters were kept constant and the same as described in Table 4.2 and 4.3. (a) Feed concentration versus Solvent Consumption, (b) Feed concentration versus Productivity 153

Figure 4.15 Effect of the section configuration on the TMBR steady-state internal profile. 2 2 6 2 black circles (full glucose, white fructose) and black line sucrose; and 3 3 3 3 grey squares (full glucose, white fructose) and grey line sucrose. The operating conditions and model parameters were as described in Table 4.2. Extract: 2, feed: 4 and raffinate: 10, for 2-2-6-2 configuration; extract: 3, feed: 6 and raffinate: 9, for 3-3-3-3 configuration 154

Figure 4.16 Effect of the length of section I and II on the TMBR steady-state internal profile. 2 2 6 2 black circles (full glucose, white fructose) and black line sucrose; and 3 3 3 3 grey squares (full glucose, white fructose) and grey line sucrose. The operating conditions and model parameters used are described in Table 4.2. Extract: 2, feed: 4 and raffinate: 10, for 2-2-6-2 configuration; extract: 3, feed: 4 and raffinate: 10, for 3-1-6-2 configuration 155

Figure 4.17 Effect of the intraparticle mass transfer rate on the SMB steady-state internal profile. (a) $k=0.02\ s^{-1}$; (b) $k=0.1\ s^{-1}$; (c) $k=0.5\ s^{-1}$, (d) $k=1.0\ s^{-1}$. The others operating conditions and model parameters were kept constant and the same as described in Table 4.2 156

Figure 4.18 Results obtained for the inversion of sucrose and glucose/fructose separation, black circles (full glucose, white fructose) and black line for sucrose concentration profiles; and for the glucose/fructose separation, grey squares (full glucose, white fructose), under conditions described in Table 4.2 and in Table 4.7, respectively, by using the COLNEW solver. 157

Chapter 5

Figure 5.1 Column and film and intraparticle diffusion of component i.. 162

Figure 5.2 Volume element of the column (a) and spherical particle shell element (b).. ... 163

Figure 5.3 ϕ versus s_1/s_2 168

Figure 5.4 Fit of a second order polynomial $\overline{s_1/s_2} = 15 + 1.4932\phi + 2.0039\phi^2$. The dots correspond to the values of s_1/s_2 for various ϕ values. 169

Figure 5.5 Steady-state internal concentration profiles for the reference case, under operating conditions and model parameters in Table 5.4..... 179

Figure 5.6 SMBR/TMBR steady-state internal profiles obtained for three different value of R_p, 0.016, 0.064, and 0.256 cm, for (a) sucrose, (b) glucose, and (c) fructose, Table 5.6, the others model parameters and operating conditions in Table 5.4..... 180

Figure 5.7 SMBR/TMBR performance for the sucrose inversion and glucose/fructose separation in the (γ_{II},γ_{III}) plane. Different regions are defined in terms of purity of the two outlet products, as legend in the figure. (a) The presented points define parallel lines to the diagonal at different feed flowrate, Q_F, (b) effects of the reaction rate coefficient k_r, on the reaction/separation region; the dot point (•) corresponds to the reference case under conditions described in Table 5.4..... 182

Figure 5.8 Effect of the purity specification on the separation/reaction region for the SMBR/TMBR for the sucrose inversion and glucose/fructose separation in the (γ_{II},γ_{III}) plane. 183

Figure 5.9 **HMAT** and **HVEC** matrix representation, considering four finite elements, NE(=Ner)=4, with two collocation points in each.. 189

Figure 5.10 Solution strategy, considering NE finite elements for the radial coordinate..... 190

Figure 5.11 Internal pore concentration of the three components, Suc, Gl and Fr, in a specific position of the TMBR, after the feed point (beginning of section III), for 6 different time, θ.. 194

Figure 5.12 Internal pore concentration of the three components, in the four most important positions on the TMBR: beginning of section II, III, IV, and I, for different time: θ = 1(a-d), and θ = 40 (e-h). 195

Figure 5.13 Transient TMBR internal profiles (a-c-e) for liquid concentration, and (b-d-f) mean pore concentration of component i in section j averaged over the particle, obtained by using (5.41), for different time θ. 196

Figure 5.14 Transient internal concentration profiles evolution, for the two reaction products, glucose and fructose. 197

Figure 5.15 Transient steady-state internal concentration profiles for the sucrose reaction and glucose-fructose separation under operating conditions described in Table 5.7. 197

Figure 5.16 (a) isovolumetric, (b) equidistant, and (c) user defined, discretization of the spatial particles domain, ρ, for Ner=3 with two collocation point in each subinterval. 199

Figure 5.17 Steady-state internal concentration profiles for the sucrose reaction and glucose-fructose separation obtained by using the steady-state model, under operating conditions described in Table 5.7..... 200

Figure 5.18 Transient Steady-state internal concentration profiles for the sucrose reaction and glucose-fructose separation obtained with Ne=3, Nint=20 and tol=10^{-5}. ..201

Figure 5.19 Internal pore concentration of the three components, Suc, Gl and Fr, in a specific position of the TMBR, after the feed point (beginning of section III), for 4 different time, θ=2, 4, 12 and 40, with Ne=3 Nint=20 and tol=10^{-5}. 201

Figure 5.20 Steady-state internal concentration profiles for the glucose-fructose separation obtained with Ner=3 and Nint=20.....203

Figure 5.21 Radial position for the steady-state internal concentration profiles for the glucose-fructose separation obtained with Ner=3 and Nint=20, in a specific position of the TMB, after the feed point (beginning of section III). 203

Figure 5.22 Relative error between the transient steady-state internal concentration profiles with linear and non-linear reaction; Ner=3 and Nint=20.....205

Chapter 6

Figure 6.1 The enhancement factor, $1/f(\lambda_b)$, of diffusivity by convection (Rodrigues, 1997).....210

Figure 6.2 Conventional and perfusion chromatography stationary phase particle (from Garcia et al., (2000)).. 213

Figure 6.3 Steady-state concentration profiles for a simulated moving bed separation under conditions summarised in Table 6.2, full dots for the case without intraparticle convection white dots for the case with intraparticle convection. 218

Figure 6.4 TMB/SMB performance for the proteins separation in the γ_{II} - γ_{III} plane. Four regions are defined in terms of purity of the two components, no separation, pure extract, pure raffinate and complete separation triangle region. The circle, (●), represents the location of the system under conditions summarised in Tables 6.1 and 6.2, the diamond, (♦), represents the location of the system with higher productivity, and the square, (▪), represents the location of the optimal operating condition for η=0.8. 220

Figure 6.5 (a) Diagram of the optimisation algorithm; (b) procedure to obtain the value of $\tilde{D}_{pe}$, when intraparticle convection is considered on the model.....223

Figure 6.6 Productivity and optimal column length as a function of η with purity equal to 99% for the system described in Tables 6.1 and 6.2. Straight and dash lines correspond to obtained simulation values with and without intraparticle convection, respectively. The maximum corresponds to the optimal point (▲ for raffinate and ▪ for extract).....224

Figure 6.7 Optimal productivity (▲ for raffinate and ▪ for extract) and column length (♦) for various purities specifications for the system described in Table 6.1 and 6.2. 225

Figure 6.8 Values of η leading to productivity for various purities specifications for the system described in Table 6.1 and 6.2 226

Figure 6.9 Column length as a function of particle radius for a purity specification of 99%, for the system described in Table 6.1 and 6.2.....227

Figure 6.10 Productivity as a function of particle radius for a purity specification of 99%, (▲ for raffinate and ▪ for extract), for the system described in Table 6.1 and 6.2 227

Figure 6.11 Triangle- shaped complete separation region obtained for R_p=10 and 20μm, thin lines, for the system described in Table 6.1 and 6.2. The several points correspond to the simulation point for several values of η (♦ R_p=10μm, ● R_p=20μm, ■ R_p=40μm). The arrow shows the way of η increasing..... 228

Figure 6.12 Steady-state concentration profiles for the two models defined: intraparticle diffusion/convection model (6.11-6.14), white dots, and the equilibrium stage model (6.21), full dots, under conditions described in Table 6.1 and 6.2..... 230

Figure 6.13 Steady-state concentration profiles for the two models considered: intraparticle diffusion/convection model defined by (6.11-6.14), white dots, and the equilibrium stage model defined by (6.21), full dots for the optimal conditions described in Table 6.5..... 231

Figure 6.14 Steady-state concentration profiles for the equilibrium stage model (6.20-6.21), with (white dots) and without (full dots) the intraparticle convection term, for the optimal operating conditions described in Table 6.5. 232

List of Tables

Chapter 2

Table 2.1 The equivalence between the SMB and TMB systems. 13

Table 2.2 Constraints for good separation. 15

Table 2.3 Model equations for the Transient and Steady-State TMB. 24

Table 2.4 Dimensionless model equations for the transient TMB and for the Steady-State TMB described in the Table 2.3. 25

Table 2.5 Dimensionless parameters for the TMB system. 26

Table 2.6 Relevant parameters for the four packages used. 49

Table 2.7 Operating conditions and models parameters used in the simulations of the TMB/SMB system, for the two models. 52

Table 2.8 New operating conditions and models parameters used in the simulations of the TMB/SMB system, for the two models, to obtain higher purity and recovery performances. 55

Table 2.9 Final results for the performance parameters obtained by using the four different packages in the resolution of the mathematical model, as the run time needed. T. 2.7 and T. 2.8 conditions described in Table2.7 and Table 2.8, respectively. The values in parenthesis correspond to the values obtained by considering lower number of finite elements, for the case of using the DASSL. 57

Table 2.10 Comparison between the relative concentrations values obtained for the two components, fructose and glucose, in the four nodes extract, feed, raffinate and eluent, obtained for the TMB, under conditions described in Table2.7 and in Table 2.8, by using the PDECOL and DASSL. With these values the concentration balance can be verified. 57

Chapter 3

Table 3.1a Operating conditions and model parameters for the base case study. The flow rates were estimated using the equilibrium model for the SMB, as in Zhong and Guiochon (1996).... 65

Table 3.1b Equivalence between TMB and SMB flowrates.... 65

Table 3.2 Numeric parameters used in the four packages.... 66

Table 3.3 Relative concentration values obtained for the two components, Gl and Fr, in the four nodes: extract, feed, raffinate and eluent, and the T-TMB system performance parameters and run time obtained by using the four packages, for the case study.... 68

Table 3.4 Range of the operating variables for the study of the effect on the TMB performance. The other parameters are described in Table 3.1.... 72

Table 3.5 Effect of the section length in the performance parameters. The other operating conditions and model parameters were kept constant and the same as described in Table 3.1.... 79

Table 3.6 TMB performance parameters obtained for A, B, C, and D points illustrated in Figure 3.17.. 86

Table 3.7a Operating conditions and model parameters for the study case. The flowrates were estimated using the equilibrium model for the SMB/TMB as in Zhong and Guiochon (1996) 89

Table 3.7b Equivalence between TMB and SMB flowrates.... 89

Table 3.8 T-TMB system performance parameters and run time, for the case study, under conditions as described in Table 3.7 and 3.2, obtained by using the four solvers.... 90

Table 3.9 T-TMB system performance parameters and run time, for the case study, under conditions as described in Table 3.7, obtained by using the four packages, considering, for glucose, the new Langmuir isotherm (3.4) and a linear isotherm (3.2a) for fructose.... 95

Table 3.10 T-TMB system performance parameters and run time, for the case study, under conditions as described in Table 3.7, for a feed concentration C=225 g/l, obtained by using the four packages, considering, for glucose, the new Langmuir isotherm (3.4) and a linear isotherm (3.2a) for fructose.... 96

Table 3.11 Performance parameters obtained, by using COLNEW, for a feed concentration30 and 225 g/l, under conditions as described in Table 3.7. 97

Table 3.12 Operating conditions and model parameters that were kept constant to study the influence in the process performance 98

Table 3.13 Operating conditions and γ_j parameters obtained for two values of total balance. Q_{BAL} = 9.51 and 12.89 ml/min, with Q_{Rec} = 19.89 ml/min, t^* = 1.75 min and k = 2.0s^{-1}. 101

Table 3.14 Transient TMB model equations. 104

Table 3.15 Transient TMB dimensionless model equations. 105

Table 3.16 Steady-state TMB dimensionless model equations. 107

Table 3.17 SMB and equivalent TMB operating conditions and model parameters used in the steady-state TMB model, with a feed concentration of $C_A = C_B = 2.9$ g/l.. 110

Table 3.18 Effect of the mass transport coefficient in the pores on the performance parameter. 117

Table 3.19 Transient SMB dimensionless model equations. 120

Table 3.20 Equivalence between TMB and SMB flow-rates. 125

Table 3.21 Comparison between extract and raffinate purities and recoveries in the TMB and SMB approach obtained by using the LDF model for porous particle. 126

Chapter 4

Table 4.1 Dimensionless parameters for the TMBR system. 136

Table 4.2a Operating parameters conditions and models parameters used in the simulations of the transient and steady-state TMBR models. 139

Table 4.2b Equivalence between TMBR and SMBR flowrates. 139

Table 4.3 Numerical parameters used in the two software packages. 139

Table 4.4 TMBR system performance parameters, Gl and Fr components concentrations values obtained in and outlet points, and the run time needed by using the PDECOL for the transient model, and COLNEW for the steady-state model, solvers, under conditions described in Table 4.2, and the numerical parameters in Table 4.3. 145

Table 4.5 Range of the operating variables for the study of the effect on the TMBR performance. The other parameters are described in Table 4.2. 146

Table 4.6 Effect of the section length in the performance parameters. The other operating conditions and model parameters were kept constant and the same as described in Table 4.2. The numerical parameters are in Table 4.3. 153

Table 4.7 Operating parameters conditions and models parameters used in the simulation of the steady-state TMB model The equivalence between the TMB and SMB flowrates are the same as described in Table 4.2b. 156

Table 4.8 Performance parameters obtained for the TMBR and TMB models under conditions as described in Table 4.2 and Table 4.7, respectively 157

Chapter 5

Table 5.1 Coefficient in LDF formulas. Source: Kim (1989). 168

Table 5.2 Coefficient in LDF formulas, s_1/s_2, obtained by Kim (1989), by the second order polynomial, $\overline{s_1/s_2}$ and the squares deviations, for different values of ϕ. 169

Table 5.3 Dimensionless parameters for the SMBR/TMBR system defined. 173

Table 5.4 Model parameters and operating conditions for the SMBR/TMBR system defined. 174

Table 5.5 Performance parameters obtained for the reference case, under operating conditions and model parameters in Table 5.4. 178

Table 5.6 Model parameters used for the study of the radius particle effects in the SMBR/TMBR performance parameters.... 181

Table 5.7 Model parameters and operating conditions for the SMBR/TMBR system defined (similar to the operating conditions used for the previous model, Table 5.4). 192

Table 5.8 Equivalence between TMBR and SMBR flow-rates 192

Table 5.9 Numeric parameters used in the solvers 193

Table 5.10 Parameters used in the radial position discretization for the steady-state model. The run time was obtained for 3, 4 and 5 collocation points per finite element in the radial position ρ, respectively; (-) indicates that the stop criteria error was not verified after the maximum number of iterations, k_{max}, was reached 199

Table 5.11 Concentration values for the two components, Gl and Fr, in the extract and raffinate nodes obtained by using PDECOL (transient model) and COLNEW (steady-state model) for the case study. 200

Chapter 6

Table 6.1 Parameters values for Rodrigues equation (6.6) from Leitão et al., (2002).. 211

Table 6.2 Model parameters and operating conditions for the SMB/TMB system defined **(a)** with intraparticle convection, $\lambda_p \neq 0$; **(b)** equivalence between TMB and SMB flow-rates; **(c)** model parameters for $\lambda_p = 0$. 217

Table 6.3 TMB concentrations values obtained for the two components in the four nodes without or with intraparticle convection, under the conditions described in Table 6.1 and Table 6.2. 218

Table 6.4 Some operating conditions for the SMB and the concentrations values obtained for the two components in the four nodes for $\lambda_p \neq 0$, (♦) point on Figure 6.4. 220

Table 6.5 TMB concentrations values obtained for the two components in the four nodes and the flowrates with or without intraparticle convection through the optimisation procedure for $\eta = 0.8$ 225

Table 6.6 Enhancement factor, $1/f(\lambda)$, of diffusivity by convection, under the conditions described in Table 6.1 and Table 6.2. 227

Table 6.7 Number of theoretical plates HETP, and the number of stages n, in each section, for the model (6.21).. 230

Table 6.8 TMB concentrations values obtained for the two components in the four nodes by using the two models, intraparticle diffusion convection model defined by (6.11-6.14) and the equilibrium stage model defined by (6.21), under the conditions described in Table 6.1 and Table 6.2. 231

List of Symbols

Symbol	Description	Units (SI)
A	cross section area of a SMB column	m^2
Bi_m	mass Biot number	
$\tilde{Bi}_m$	mass Biot number in the intraparticle diffusion/convection model	
c	bulk fluid phase concentration	kg/m^3
c_p	concentration in the fluid phase in the pores of an adsorbent particle	kg/m^3
$\langle c_p \rangle$	pore fluid phase concentration averaged over the particle volume	kg/m^3
c_s	fluid phase concentration at the surface of an adsorbent particle	kg/m^3
D_L	axial dispersion coefficient	m^2/s
D_m	Molecular diffusivity	m^2/s
D_{pe}	Effective pore diffusion coefficient	m^2/s
$\tilde{D}_{pe}$	augmented effective diffusivity by intraparticle convection	m^2/s
d_c	column diameter	m
d_p	diameter of adsorbent particle	m
er	Global error	%
er_E, er_R	relative error of the average concentrations of the two components in the extract and raffinate, respectively, for two successive iterations	%
er_A, er_B	relative error between the amount of the less and more, respectively, retained component that enters and leaves the system	%
$f(\phi)$	Polynomial in ϕ for the new LDF approximation	
$1/f(\lambda)$	Enhancement factor of diffusivity by convection	
h_k	size of finite interval k	
k	intraparticle mass transfer/reaction rate constant	s^{-1}

K	adsorption constant as defined in the LDF approximation	
k'	Reaction rate constant	s^{-1}
k_f	film mass transfer coefficient	m^2/s
k_h	Mass transport coefficient for homogeneous particle	s^{-1}
$\tilde{k}_p$	Mass transport coefficient in the pores in the intraparticle diffusion/convection model	s^{-1}
k_r	rate constant of the inversion reaction kinetics	s^{-1}
K_m	Michaelis-Menten constant	kg/m^3
L_c	column length in the SMB	m
N_s	number of columns per section in the SMB	
L_j	length of section j in the TMB	m
ℓ	porous slab half-thickness	m
n_j	number of columns in the section j in the SMB	m
Nd	Number of pore diffusion units	
Pe	Peclet number	
Q_j^*	liquid flow rate in the SMB	m^3/s
Q_j	liquid flow rate in the equivalent TMB	m^3/s
Q_S	solid flow rate in the equivalent TMB	m^3/s
$\langle q_{ij} \rangle$	average adsorbed phase concentration of component i in section j of the TMB, g adsorbed/ l of particle.	
q	adsorbed phase concentration	kg/ m^3
q^*	adsorbed phase concentration in equilibrium with fluid phase	kg/ m^3
q_h	adsorbed phase concentration in a homogeneous solid	kg/ m^3
$\mathcal{R}$	Michaelis-Menten reaction rate	$kg/ m^3/s^{-1}$
$\langle \mathcal{R}(c_{p_{ij}}) \rangle$	Average reaction rate	$kg/ m^3/s^{-1}$
R_p	particle radius	m
s_1/s_2	coefficient defined in Kim, 1989	
t	time	s
t^*	switching time or rotation period	s
T	absolute temperature	K
u_s	interstitial solid velocity in a TMB	m/s
u_t	Collocation points	

V_c	column volume in the SMB	m^3
v_j^*	interstitial fluid velocity in a SMB	m/s
v_j	interstitial fluid velocity in a TMB	m/s
v_0	Intraparticle convective velocity inside large pores	m/s
X	reaction conversion (%)	
x	Dimensionless space co-ordinate in TMB-based model	
z	axial coordinate	m

Greek letters

α	number of mass transfer or reaction rate units	
α_p	number of intraparticle mass transfer units for porous particle	
β	safety margin applied on TMB/SMB flowrate ratios	
γ	ratio between fluid and solid interstitial velocities in a TMB	
γ_j^*	dimensionless key parameter, defined as in (2.1)	
ΔP	pressure drop across a SMB column	Pa
ε	bed porosity	
ε_p	particle porosity	
ϕ	Thiele modulus	
η	dimensionless feed flowrate	
θ	dimensionless time co-ordinate in TMB-based model	
τ_j	liquid space time	
τ_s	solid space time	
λ	intraparticle Peclet number	
ρ	relative error of the solutions obtained by the ordinary/algebraic equation solvers and the partial algebraic/ordinary algebraic equation solvers	%
υ	stoichiometric reaction parameter	
Ω	scale factor	

Indexes

1, ..., 4	index to indicate TMB/SMB sections
D	eluent
des	desired
enz	enzyme

F	feed
Fr (B)	fructose
Gl (A)	glucose
h	referring to a homogeneous solid
i	chemical species
in	at the inlet of a column (superscript)
j	TMB section
k	SMB column
o	referring to initial condition
p	particle
r	reaction
R	raffinate
Rec	recycle
Suc	sucrose
sp	specified
E	extract

Abbreviations

DAE	Differential-Algebraic Equations
HETP	Height Equivalent to a Theoretical Plate
LDF	Linear Driving Force
ODE	Ordinary Differential Equations
P	purity
PDAE	Partial Differential Algebraic Equations
PDE	Partial Differential Equations
Pr	productivity
$QBAL$	sum of inlet (eluent+feed) or outlet (extract+raffinate) SMB streams
R	recovery
S	solvent consumption
SMB	Simulated Moving Bed
SMBR	Simulated Moving bed Reactor
TMB	True moving Bed
TMBR	True Moving Bed Reactor

UOP Universal Oil Products

1. Introduction

In this chapter both context and objective of this work are presented.

A brief reference to the Simulated Moving Bed (SMB) and to the Simulated Moving Bed Reactor (SMBR) concepts is made in relation with the developments made in the modelling, simulation and optimization of the process of separation/reaction processes.

Finally, the thesis objective and organization are presented.

1.1 Simulated Moving Bed (SMB) / Simulated Moving Bed Reactor (SMBR)

The developments of models that describe separation and reaction process are far from complete. Due to the advances in computer hardware, the models can now be solved by using a common PC.

The new concept of the Simulated Moving Bed (SMB) technology has been known since 1961 when the first patent by UOP (Universal Oil Products, Des Plaines, Illinois, USA) appeared (Broughton and Gerhold, 1961). This technology, a well-known process in the areas of petroleum refining and petrochemicals where it was originally developed, becomes known commonly as the Sorbex process (Broughton, 1968, 1984; Gembicki *et al.*, 1977). A large amount of Sorbex units have been licensed until now, leading to a production of more than 10 millions tons per year of desired products (Gattuso *et al.*, 1994). An alternative process for the

production of p-xylene using the SMB technology was also developed in 1973 by the Toray Industries (Tokyo, Japan) (Otani, 1973; Otani *et al.*, 1973). Other successful SMB process in the carbohydrate industry is the production of "high" fructose corn syrup (HFCS) and the recovery of sucrose from molasses. This technology was also originally developed by UOP in the late 1970s, known as the Sarex process (de Rosset *et al.*, 1981; Gembicki *et al.*, 1977). With the expiration of the UOP patents, other companies developed alternative process for the sugars separation, such as Illinois Water Treatment (USA), Mitsubishi (Japan), Finnish Sugar (Finland), and Amalgamated Sugar Co. (USA) (Heikkilä, 1983; Nicoud, 1992; Rearick *et al.*, 1997).

SMB is one of the most powerful and promising techniques for preparative scale chromatography and has found new applications in the areas of biotechnology, fine chemistry and pharmaceuticals. In particular, this technology is attractive to separate racemic mixture into the corresponding enantiomers, since the process essentially splits a feed into two fractions (Kaspereit *et al.*, 2002; Haag *et al.*, 2001; Azevedo *et al.*, 1999). Briefly, the SMB technology allows the continuous injection and separation of binary mixtures. The simulated countercurrent contact between the solid and liquid phases maximizes the mass-transfer driving force, leading to a significant reduction in mobile was developed in order to overcome the stationary phases consumption when compared with elution chromatography.

The Simulated Moving Bed concept was developed in order to overcome the limitations of conventional batch chromatography, mainly the discontinuous character of the process and its high cost due to the large eluent and adsorbent requirements.

The Simulated Moving Bed Reactor (SMBR) process applies the knowledge of the SMB involving reaction, i.e., SMBR combines two processes, separation and reaction, in the same unit. The system that will be studied is the production of glucose and fructose by the inversion of sucrose, in presence of an invertase enzyme. The application of the SMB technology is also applied to the proteins separation (BSA and Myoglobin).

1.2 Motivation

In the last years the SMB process was increasingly used as a powerful alternative to conventional batch chromatography. New applications are developed namely in the pharmaceutical area such as the purification of an ascomycin derivative (Küsters, *et al.*, 2000) and the purification of the anti-cancer agent paclitaxel (Wu, *et al.*, 1999).

Modelling and simulation of a chemical engineering process always attracted a special attention since it could lead to significant savings in time and materials.

In the present work, due to the characteristics of the system of equations that describes the process in study, they can be defined as partial differential equation (PDE), ordinary differential equations (ODE), partial differential algebraic equations (PDAE), and differential algebraic equations (DAE). Due to the differences between the four types of models, it is necessary to implement suitable algorithms to solve them. In a first approach, public domain solvers were used to integrate numerically the model equations. The different strategies to solve the mathematical models were compared in order to predict the transient and steady-state behaviour of SMB and SMBR units. New extensions to the existing models were also proposed.

The optimization of the moving bed is a subject that is still under development. The optimization algorithm used, allow the choice of the unit operating conditions in order to obtain the specified performance. Usually the objective in the optimization process is of economic order. However, it can be other depending on the material and conditions available, *i.e.*, maximum specific productivity without exceeding given pressure drop limits imposed by the material used. Depending on the objective function, the parameters to be estimated and/or initially considered as fixed are different.

Nowadays the development and optimization of SMB processes usually starts after the choice concerning suitable mobile and stationary phases has been made (Pais *et al.*, 1997). Then the established theories are adapted to identify attractive operating conditions (Azevedo and Rodrigues, 1999; Mazzotti *et al.*, 1997).

1.3 Thesis objectives and organization

The main objective of this thesis is to pursue and give continuity to the developments that have been made at the LSRE, concerning the study of the Simulated Moving Bed (SMB) and the Simulated Moving Bed Reactor (SMBR) processes, (Pais, 1999; Azevedo, 2001). The main stages that were followed in this work are: a) modelling and simulation of the separation and separation/reaction processes considering a detailed description of the adsorbent particle; the two test examples used are the Glucose/Fructose separation for the SMB/TMB and the Sucrose inversion and Glucose/Fructose separation for the SMBR/TMBR; b) application of an optimization procedure for SMB, where the mass transfer inside particles includes not only

diffusion but also convection; the separation of Bovine Serum Albumin (BSA) and Myoglobin (MYO) was used to validate this procedure.

In chapter 2 the fundamental concepts of the Simulated Moving Bed (SMB) technology and the mathematical models developed are presented. Models can be formulated in terms of systems of Partial Differential Equations (PDEs) and Ordinary Differential Equations (ODEs) or Partial Differential-Algebraic Equations (PDAEs) and Differential Algebraic Equations (DAEs) for transient and steady-state situations, respectively. Transient and steady-state models are used depending on the user interest. The algebraic equation for the adsorption equilibrium isotherm can be substituted in the model equations or kept as an independent equation defining a PDAE or DAE system. This partition, when relevant, is used in the following chapters.

In chapter 3 the study of the effects of operating parameters on the SMB/TMB separation region is discussed. The influence of the type of the equilibrium isotherms on the complete separation region is also studied. A new model for the mass transfer on porous particle, LDF for porous, is included and compared with the LDF model for homogenous particles. The two models are presented under the TMB and SMB strategies.

In chapter 4 the concept of the Simulated Moving Bed Reactor (SMBR), based on the analogy with the True Moving Bed Reactor (TMBR) is introduced. The SMBR/TMBR systems combine two processes, reaction and separation, in one single unit. The constraints that must be fulfilled to achieve complete separation/reaction were the same as for the SMB/TMB case. The best operating conditions are found by simulations of the TMBR. Comparison between the transient and steady-state TMBR and TMB models are presented.

In chapter 5 new developments in the SMBR/TMBR model are presented. More steps are considered: mass transfer from the bulk fluid to the liquid film surrounding the adsorbent particle, and then the penetration through the pores of the adsorbent particle seeking sites for adsorption/reaction. The numerical simulation becomes much more complex and then improved numerical techniques must be used. LDF approximations were used considering reaction, adsorption and unsteady-state diffusion on porous particles, in a first approach and then a new detailed model taking into account the intraparticle radial profiles was presented. The results obtained for both models were compared.

In chapter 6 the perfusion chromatography concepts are used in the simulated moving bed technology. Simulated results for the BSA and Myoglobin proteins separation are presented and discussed. The optimization algorithm used to design a simulated moving bed applied to

the separation of proteins is presented. The operating conditions and optimal construction parameters are determined by considering the maximization of the performance parameters as objective function. Simulated results are shown and conclusions are drawn on the influence of column size, safety margin applied on the regeneration zones and minimum required product purities.

Finally, the general conclusions drawn from this work and the suggestions for the future are presented in chapter 7.

1.4 References

Azevedo D. C. S., A. E. Rodrigues, (1999) *Design of a Simulated Moving Bed in the Presence of Mass-Transfer Resistances*, AIChE J. **45**, 956-966.

Azevedo D. C. S., L. S. Pais, A. E. Rodrigues, (1999) *Enantiomers separation by simulation moving bed chromatography. Non-instantaneous equilibrium at the solid-fluid interface*, J. Chromatogr. A **865**, 187-200.

Azevedo, D. C. S., (2001) *Separation/Reaction in Simulated Moving Bed – Application to the Production of Industrial Sugars*, PhD dissertation, LSRE, University of Porto, Porto.

Broughton, D. B., and C. G. Gerhold, (1961) *Continuous Sorption Process employing Fixed Bed of sorbent and Moving Inlets and Outlets*, U.S. Patent N°. 2985589.

Broughton, D. B., (1968) *Molex: Case History of a Process*, Chem. Eng. Prog. **64**, 60-65.

Broughton, D. B., (1984) *Production-scale adsorptive separations of liquid mixtures by simulated moving-bed technology*, Sep. Sci. Technol. **19**, 723-736.

Gattuso M. J., B. McCulloch, J. W. Priegnitz, (1994) *UOP Sorbex Simulated Moving Bed technology – A cost effective route to chiral products*, in: Proceedings of the Chiral Europe '94 Symposium, Nice, France, 19-20.

Fortran 77/90 computer programs for all the numerical solutions of the models discussed in this thesis were developed. The use of the codes is demonstrated where they are first introduced in the thesis. Some of the subroutines used are public domain and can be obtained on the Internet

Gembicki S. A., A. R. Oraskar, J. A. Johnson, (1997) *Adsorption, liquid chromatography*, in: D. M. Ruthven (Ed.), Encyclopedia of Separation Technology, Wiley, New York, 172-199.

Haag J., A. V. Wouwer, S. Lehoucq, P. Saucez, (2001) *Modeling and simulation of a SMB chromatographic process designed for enantioseparation*, Control Engineering Practice **9**, 921-928.

Heikkilä, H., (1983) *Separating Sugars and Amino Acids with Chromatography*, Chem. Engng. **24**, 50-52.

Kaspereit M., P. Jandera, M. Škavrada, A. Seidel-Morgenstern, (2002) *Impact of adsorption isotherm parameters on the performance of enantioseparation using simulated moving bed chromatography*, J. Chromatogr. A **944**, 249-262.

Küsters E., C. Heuer, D. Wieckhusen, (2000) *Purification of an ascomycin derivative with simulated moving bed chromatography. A case study*, J. Chromatogr. A **874**, 155-165.

Mazzotti M., G. Storti, M. Morbidelli, (1997) *Optimal Operation of Simulated Moving Bed Units for Nonlinear Chromatographic Separations*, J. Chromatogr. A **769**, 3-24.

Nicoud R.-M., (1992) *The Simulated Moving Bed: A Powerful Chromatographic Process*, LC-GC Intl. **5**, 43-47.

Pais, L. S., J. M. Loureiro, and A. E. Rodrigues, (1997) *Modeling, Simulation and Operation of a Simulated Moving Bed Operation for Chromatographic Separation of 1,1'-bi-naphthol enantiomers*, J. Chromatogr. A **769**, 25-35.

Pais, L. M. S., (1999) *Chiral Separation by Simulated Moving Bed Chromatography*, PhD dissertation, LSRE, University of Porto, Porto.

Otani, S., (1973) *Adsorption Separates Xylenes*, Chem. Engng., September 17, 106-107.

Otani, S., T. Iwamura, K. Sando, M. Kanaoka, K. Matsumura, S. Akita, T. Yamamoto, I. Takeushi, T. Tsuchiya, Y. Noguchi, T. Mori, (1973) *Separation Process of Components of Feed Mixture Utilizing Solid Sorbent*, U.S. Patent No. 3761533.

Rearick, D., M. Kearney, D. Costesso, (1997) *Simulated moving-bed technology in the sweetener industry*, Chemtech. **27** 9, 36-40.

de Rosset A. J., R. W. Neuzil, D. B. Broughton (1981) *Industrial Applications of Preparative Chromatography*, in: A. E. Rodrigues and D. Tondeur (Eds.), Percolation Process: Theory and Applications, Sihjthoft & Noordhoff, 249-281.

Wu D.-J., Z. Ma, N.-H. L. Wang, (1999) *Optimization of throughput and desorbent consumption in simulated moving-bed chromatography for paclitaxel purification*, J. Chromatogr. A **855**, 71-89.

2. Simulated Moving Bed: Fundamentals and Numerical Strategies to Solve Transient and Steady-State Models.

In this section a description of the fundamental concepts of the Simulated Moving Bed (SMB) technology is made. The theoretical aspects that characterize the operation and design of the SMB for a binary system are presented. Transient and steady-state models for the SMB, based on the analogy with the True Moving Bed (TMB), are introduced. Models can be formulated in terms of systems of Partial Differential Equations (PDEs) and Ordinary Differential Equations (ODEs) or Partial Differential-Algebraic Equations (PDAEs) and Differential-Algebraic Equations (DAEs) for transient and steady-state situations, respectively when the algebraic equation for the adsorption equilibrium isotherm is substituted in the other model equations or kept as an independent equation. The objective of this chapter is to solve these four models by using available software: PDECOL and COLNEW for PDEs and ODEs, respectively and DASSL and COLDAE for PDAEs and DAEs, respectively. The test example of Glucose/Fructose separation will be used through out the chapter.

2.1 Simulated Moving Bed Technology

The Simulated Moving Bed (SMB) technology was introduced in the chemical industry in the beginning of the 60's by Universal Oil Products (UOP) (Broughton and Gerhold, 1961). Since then, the SMB technology has been largely used in chemical industry, especially for the separation of normal paraffins (Molex process, Broughton, 1968), recovery of p-xylene (Parex process, Broughton *et al.*, 1970), and the separation of glucose/fructose (Sarex process, de Rosset *et al.*, 1981; Hashimoto *et al.*, 1983). More recently, new applications use the SMB principles in the fine chemistry and pharmaceuticals (chiral separations). Several works have already been done showing its large potential with remarkable results (Gattuso *et al.*, 1996; Guest, 1997; Nicoud, 1997; Pais *et al.*, 1997a, 1997b, 2000).

To overcome some of the drawbacks in chromatographic separation, the simulated moving bed adsorbers have been developed (Hashimoto *et al.*, 1993). The SMB technology simulates the countercurrent movement between the solid and the liquid phases. The positions of the feed and withdraw points are changed along the columns, in the direction of the liquid flow. Due to the different affinities of the feed components, one moves in the solid phase direction (more retained feed component), while the other moves in the liquid phase direction (less retained feed component). The concept of the moving bed system can be illustrated by the difference of velocity of a running tortoise and a running rabbit (Hashimoto *et al.*, 1993). This concept is illustrated through Figure 2.1. The four sets of belt conveyers, shown in the figure and their moving rates indicate the movement of the adsorbent and its moving rate, respectively. The rate of each belt conveyer is identical. A less adsorptive component A (represented by the rabbit) and a more adsorptive component B (represented by a tortoise) are introduced into the middle of the belt conveyers. Rabbits can run faster than the movement of the belt conveyers, running in opposite direction. Tortoises cannot move faster than the belt conveyers so they move with the belt conveyers. In other words, a mixture of components A and B are fed continuously. The strongly adsorbed component B is adsorbed, and the less adsorptive component A, is eluted from the raffinate stream.

The modelling and understanding of the SMB technology has, in the last few years, achieved considerable advances (Ruthven and Ching, 1989; Storti *et al.*, 1993; Zhong and Guiochon, 1996; Mazzotti *et al.*, 1997; Yun *et al.*, 1997; Azevedo and Rodrigues, 1998).

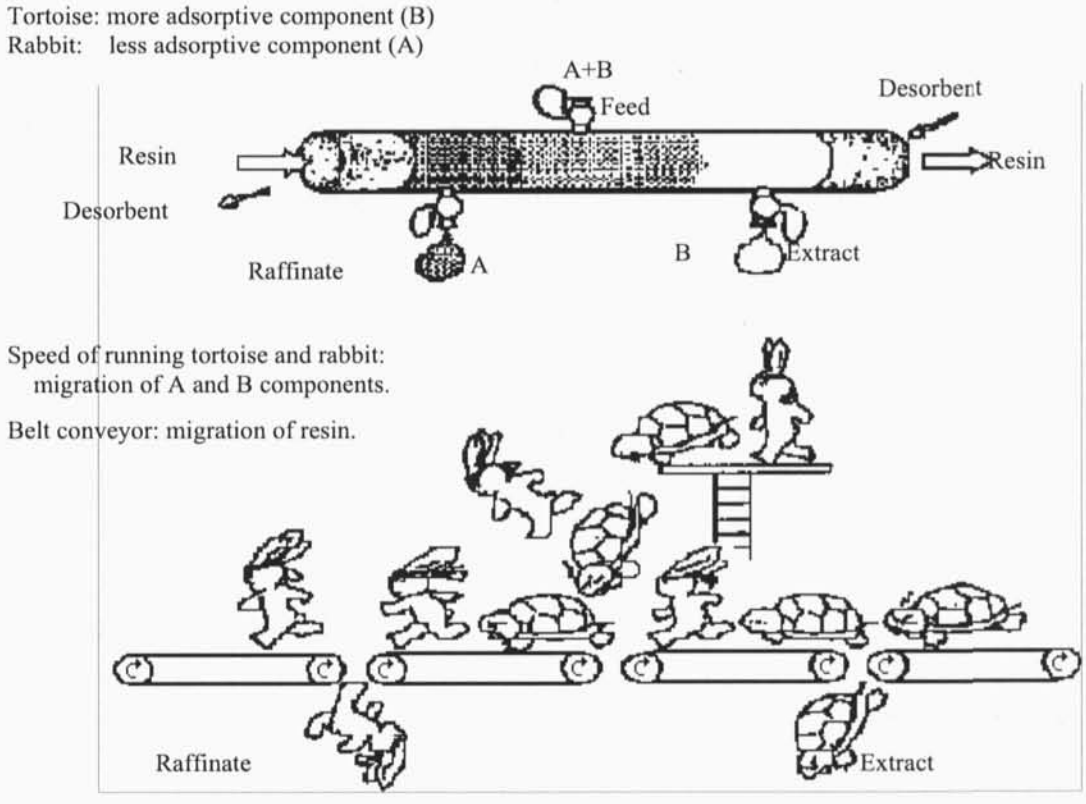

Figure 2.1 *Moving Bed Chromatographic Separation. From Hashimoto* et al. *(1993).*

A well known and widely system used to illustrate the application of the SMB technology for the separation of a binary system is the glucose/fructose system (Ching *et al.*, 1985, 1987; Hidajat *et al.*, 1986; Nicoud, 1995). A generic description of some of the theoretical aspects for the operating and design of the SMB for a binary system will be presented.

The Simulated Moving Bed adsorber is normally divided into three or four zones (Ruthven and Ching, 1989; Hashimoto *et al.*, 1993). In our case, a four-zone simulated moving bed would be described. A schematic diagram of a four-zone moving bed adsorber is shown in Figure 2.2.

The continuous SMB principle is described using the equivalent true moving bed (TMB) configuration. The adsorbent continuously moves down through the bed. Each of the four zones has a specific function. The feed solution, F, with components A and B, enters continuously at the feed point situated between the two central zones, III and II, where the separation takes place. Component A moves up to zone IV with the liquid flow because of

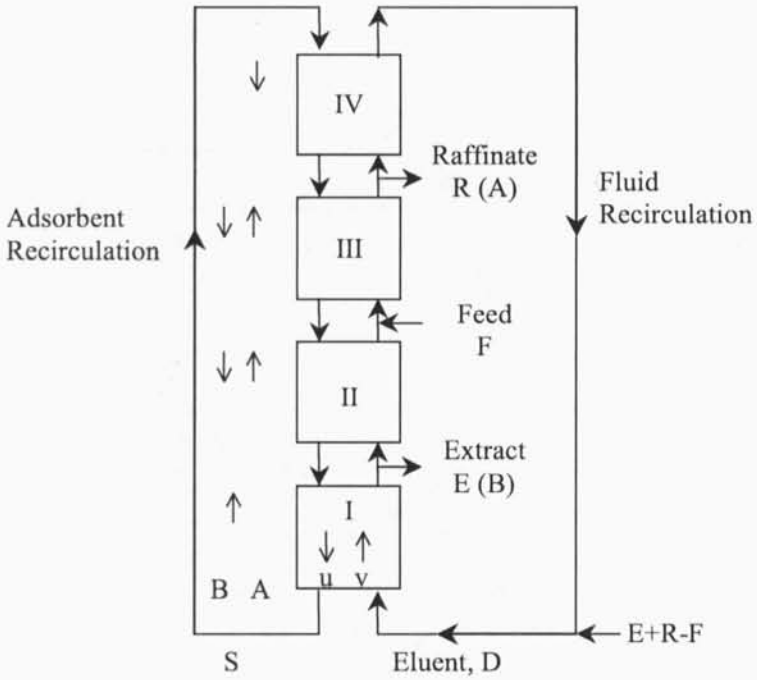

Figure 2.2 *Scheme of a four-section True Moving Bed separation unit. It also shows the flow rates direction of the two components in each section; fructose, represented by letter B, and glucose, represented by letter A, in each section.*

less adsorption onto the resin. Zone IV functions for adsorption of component A as well as for regeneration of the solvent. Component A is recovered at the top of zone III in the raffinate point, R. Component B, the strongly adsorbent component, is adsorbed on the solid and moves with the solid to zone I. Component B is recovered in the extract point, E, situated between zone I and II. The eluent used is assumed to be nonadsorbable.

To avoid the difficulties associated with the movement of the particles in the solid phase in a TMB unit, the SMB technology simulates the solid motion by switching periodically the feed and products withdrawal points, resulting a counter current flow of the liquid and the solid. Each section of the unit is divided into a finite number of connected fixed columns. The scheme of an equivalent SMB unit is shown in Figure 2.3. The draws in and off points are switched one column forward in the same direction of the liquid flow after each switch time period. The particular case shown in Figure 2.3, involves a 3-3-3-3 configuration, with a total of 12 columns.

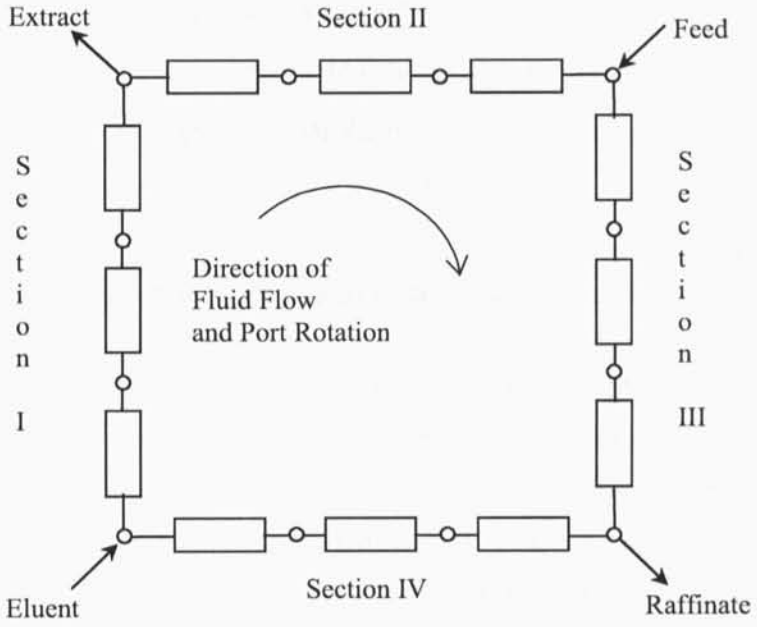

Figure 2.3 *Scheme of an equivalent SMB unit with 3-3-3-3 configuration.*

The two configurations SMB and TMB are equivalent under steady-state operation, *i.e.* both units achieve the same separation performance, when the relationships between the flow rates and velocities in both units are fulfilled. Table 2.1 shows the equivalence between the two systems (Leão *et al.*, 1997), where t^* is the switch time interval in the SMB system, L_c is the length of one column with cross-section area A, V is the corresponding volume which is assumed to be the same for all the columns, u_s is the interstitial solid velocity, ν_j^* and ν_j are

Table 2.1 *The equivalence between the SMB and TMB systems.*

	SMB	**TMB**
Solid phase		
velocity	*0*	$u_s = \dfrac{L_c}{t^*}$
flowrate	*0*	$Q_s = u_s(1-\varepsilon)A$
Liquid phase		
velocity	ν_j^*	$\nu_j = \nu_j^* - u_s$
flowrate	Q_j^*	$Q_j = Q_j^* - \varepsilon\dfrac{V_c}{t^*}$

the interstitial liquid velocities in the SMB system and in the equivalent TMB system, respectively, Q_S is the solid flow rate in the TMB system, Q_j^* and Q_j are the liquid flow rates in the SMB system and in the equivalent TMB system, respectively.

2.1.1 Theoretical Aspects: Separation Region and Process Parameters

Various operating parameters should be determined in order to fix the operating conditions or to design a simulated moving bed, in order to obtain a complete separation. The operating parameters that affect the separation performance are the internal flow rates in each section, Q_j. The other operating parameters to be selected are the switch time interval, t^* (equivalent to the solid flow rate Q_S in the equivalent TMB unit) and the feed concentration. The method used to estimate the operating conditions was the one developed by Ruthven and Ching (1989), considering the equilibrium theory and linear isotherms. The influence of the number of columns and/or their length and diameter, and the number of the intraparticle mass transfer unit, can also be studied.

Separation Region

The dimensionless key parameter that governs the steady-state concentration profile, γ_{ij}^*, is defined as the ratio between the liquid phase flux and the adsorbent phase flux of species i in section j of the system,

$$\gamma_{ij}^* = \frac{\textit{flux of i in the liquid phase}}{\textit{flux of i in the adsorbent}} = \frac{\varepsilon}{1-\varepsilon}\frac{v_j}{u_s}\frac{c_{ij}}{q_{ij}} \tag{2.1}$$

This relation is simplified for the case of a linear adsorption isotherm, $q_{ij} = K_i c_{ij}$,

$$\gamma_{ij}^* = \frac{\varepsilon}{1-\varepsilon}\frac{v_j}{u_s}\frac{1}{K_i} = \frac{\varepsilon}{1-\varepsilon}\gamma_j\frac{1}{K_i} \tag{2.2}$$

where $\gamma_j \left(= v_j/u_s\right)$ is the ratio between fluid and solid velocities in zone j, and $\varepsilon/(1-\varepsilon)$ is the ratio between fluid and solid volumes, c_{ij} and q_{ij} are the liquid phase and the adsorbed concentration of component i in zone j, respectively.

The value that the key parameter, γ_{ij}^{*}, takes can be used to know in which direction the flux of each product moves in each section of the bed. So, in order to achieve separation of the feed components A and B, it is necessary to fulfil the flux conditions for each section and product as described in Table 2.2.

Table 2.2 *Constraints for good separation.*

	Section			
	I	***II***	***III***	***IV***
γ_{Aj}^{*}		>1	>1	<1
γ_{Bj}^{*}	>1	<1	<1	

These inequalities are equivalent to the direction of the small arrows shown in Figure 2.2. It is in section III that the adsorption of the strongly component B takes place. The amount of component B adsorbed and transported by the adsorbent, should be more than that transferred with the liquid flow. Therefore, the parameter γ_{BIII}^{*} is less than 1 since the flux of component B transported by the fluid phase is lower than the flux of component B transported by the solid phase, using the definition presented in (2.2), $\frac{Q_{III}}{Q_S K_B} < 1$. On the other hand, the less adsorbed component A should be recovered from the raffinate stream and transported by the liquid flow. Thus γ_{AIII}^{*} is higher than 1, i.e., $\frac{Q_{II}}{Q_S K_A} > 1$. For section I and IV, the obtained inequalities are, $\frac{Q_I}{Q_S K_B} > 1$ and $\frac{Q_{IV}}{Q_S K_A} < 1$, respectively.

As in Ruthven and Ching (1989), or more recently, as in Zhong and Guiochon (1996), the flow rates in the different sections of a TMB system, are estimated using the following equations,

$$\frac{Q_I}{Q_S} = K_B\beta + \frac{\varepsilon}{1-\varepsilon} \tag{2.3}$$

$$\frac{(Q_I - Q_E)}{Q_S} = \frac{Q_{II}}{Q_S} = K_A\beta + \frac{\varepsilon}{1-\varepsilon} \tag{2.4}$$

$$\frac{(Q_I - Q_E + Q_F)}{Q_S} = \frac{Q_{III}}{Q_S} = \frac{K_B}{\beta} + \frac{\varepsilon}{1-\varepsilon} \tag{2.5}$$

$$\frac{(Q_I - Q_E + Q_F - Q_R)}{Q_S} = \frac{Q_{IV}}{Q_S} = \frac{K_A}{\beta} + \frac{\varepsilon}{1-\varepsilon} \tag{2.6}$$

where Q_I, Q_{II}, Q_{III}, Q_{IV} are the volumetric liquid flow rates in the various zones of the TMB, Q_S is the solid flow rate defined in Table 2.1, β is the safety coefficient in all four sections and is chosen to be slightly larger than 1 $\left(1 < \beta < \sqrt{K_B/K_A} = \sqrt{\alpha}\right)$, K_A, and K_B are the known adsorption equilibrium constants (in our case, K_A and K_B correspond to the equilibrium constants of glucose and fructose, respectively), and Q_D, Q_E, Q_F, and Q_R are the eluent, extract, feed, and raffinate volumetric flow rates, respectively. These algebraic equations (equations (2.3)-(2.6)) can be easily solved by eliminating Q_I:

$$Q_S = \frac{Q_F}{K_B/\beta - K_A\beta} \tag{2.7}$$

$$Q_E = Q_S\left(K_B - K_A\right)\beta = \frac{Q_F\left(K_B - K_A\right)\beta}{K_B/\beta - K_A\beta} \tag{2.8}$$

$$Q_R = Q_S\left(K_B - K_A\right)/\beta = \frac{Q_F\left(K_B - K_A\right)/\beta}{K_B/\beta - K_A\beta} \tag{2.9}$$

The value of Q_D, is then calculated using the global balance, that is, using the total inlet or outlet volumetric flow rates, $Q_F + Q_D = Q_E + Q_R$. In first approximation, we can say that we will have separation if at the end we get the following relationships for each section flow rates (Ruthven and Ching, 1989), $Q_I > Q_{III} > Q_{II} > Q_{IV}$. The limits proposed for the safety coefficient β, were $1 < \beta < \sqrt{\alpha}$. As close as β is to the lower limit, more the extract and the raffinate products concentrations are close to the feed. For β =1, and from equations (2.7)-(2.9), we obtain $Q_D = Q_E = Q_F = Q_S\left(K_B - K_A\right)$. Increasing β, Q_F decreases up to zero. Since the feed flow rate must be higher than zero, equation (2.7) gives the upper limit, $\beta < \sqrt{\alpha}$. In all the simulations made, the value of β used was approximately the two limits average, β=1.2.

The value of the switching time, t^*, can also be estimated by knowing that the solid-phase flow rate, Q_S i.e.,

$$t^* = \frac{L_c}{u_s} = \frac{(1-\varepsilon)L_c A}{Q_S} \tag{2.10}$$

Through the definition (2.2) and the previous conditions in γ_{ij}^* in Table 2.2, the region of complete separation in the $\gamma_{II} - \gamma_{III}$ and in the $\gamma_{IV} - \gamma_I$ planes, can be defined. An example of a region of complete separation is shown in Figure 2.4 considering linear isotherms with $K_A = 0.50$ and $K_B = 0.88$.

The definition of a complete separation region will be defined in the following chapters.

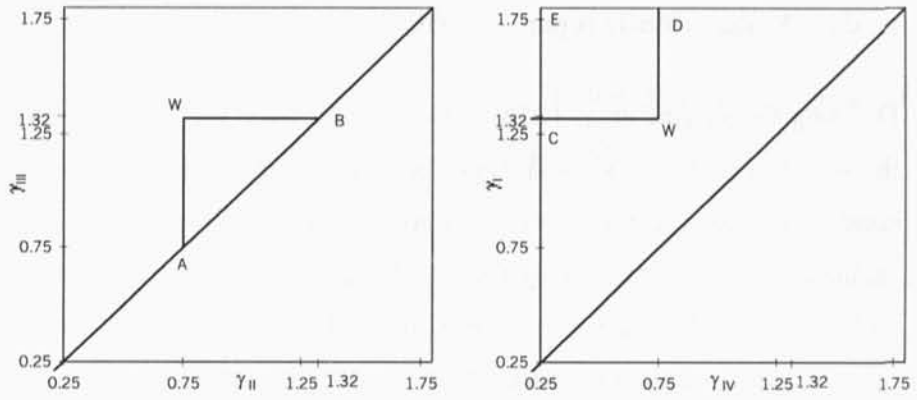

Figure 2.4 *Region of complete separation on the planes $\gamma_{II} - \gamma_{III}$ and $\gamma_{IV} - \gamma_I$ in terms of purity of the outlet streams, in the case of a system described by a linear isotherm with K_A=0.50 and K_B=0.88. The region of complete separation is defined by the triangle AWB on the $\gamma_{II} - \gamma_{III}$ plane, and by the square CWDE on the $\gamma_{IV} - \gamma_I$ plane. See next section for the definition of γ_{II} and γ_{III}.*

The typical concentration profile that appears in the SMB, when two components are separated successfully, is shown in Figure 2.12. Under these conditions, the concentration of component B is close to zero at the raffinate point and at the inlet point of the liquid in section *I* (desorbent point). The concentration of the less adsorptive component A is almost zero at the outlet of the liquid in zone *IV* and at the extract point.

Process Parameters

The most common used parameters to characterise the separation are: purity, recovery, solvent consumption, and productivity (Storti *et al.*, 1995).

1. **Purity (%)**; assuming that the more retained product B is recovered in the extract, $P_E = 100\frac{C_E^B}{C_E^A + C_E^B}$, is the purity of the extract. To maximize the purity of the extract is equivalent to minimize the concentration of product A in the extract. Similarly, if product A is to be recovered in the raffinate, $P_R = 100\frac{C_R^A}{C_R^A + C_R^B}$, is the purity of the raffinate, and must be maximised. The extract is pure, P_E=100%, if it does not contain product A, and raffinate is pure, P_R=100%, if it does not contain the product B.

   Defining the parameter γ_j (2.2), as the ratio between the liquid and solid velocities in the section j (= *I*, …, *IV*), and using the equilibrium theory to determine the operating conditions, we can reach the conditions of a complete separation. From the four sections in the system, namely the two middle sections have to be analysed, section *II* and section *III*. This is due to the proximity of these two sections to the feed point. So, the two sections contain products from the feed stream. The component B is adsorbed by the solid and moves down to zone *II* to be recovered in the extract point, the product A goes up with the liquid flow to zone *III* and is recovered in the raffinate point. Note that the fluid leaving section *IV* and solid leaving section *I*, are both regenerated and $\gamma_I > \frac{1-\varepsilon}{\varepsilon} K_B$ and $\gamma_{IV} < \frac{1-\varepsilon}{\varepsilon} K_A$ must be fulfilled. So, from Figure 2.5 we can analyse the effect of γ_{II} and γ_{III} on the system performance. We can also identify a specific region in the (γ_{II}, γ_{III}) plane where the separation is possible. This region is constrained by the following conditions:

$$\gamma_{II} < \frac{1-\varepsilon}{\varepsilon} K_B, \text{ and } \gamma_{III} > \frac{1-\varepsilon}{\varepsilon} K_A, \qquad (2.11)$$

   with the condition

$$\gamma_{III} > \gamma_{II} \qquad (2.12)$$

These three conditions are obtained by using the definition of γ_{ij}^{*}, (2.2), and the inequalities in Table 2.2.

The last condition, (2. 12), is a physical constraint since we cannot have negative feed flow rate. In the limit, when $Q_F = 0$ *ml/min*, we obtain $\gamma_{III} = \gamma_{II}$. For example, point C in Figure 2.5, corresponds to $\gamma_{III} = \gamma_{II} = 1$. Note that, this point C also corresponds to $\beta = \sqrt{\alpha} = 1.33$, and point W corresponds to $\beta = 1$.

For the case that we have for the upper limit, region defined by $\gamma_{II} > 1.32$, the state that prevails in sections *I* and *II* is the pure desorbent. In the case that the lower limit, region defined by $\gamma_{II} < 0.75$, the state in sections *III* and *IV* is again pure desorbent. In both cases no separation takes place.

The region of possible separation can be further divided. We obtain four regions, depending on the purity values of the outlet streams;

(1) *Complete separation region.* When the extract and raffinate streams are pure. This is the region where we get 100% of extract and raffinate purities, provided that the constraints on γ_I and γ_{IV}, mentioned above, are also fulfilled. For the case studied, where linear equilibrium isotherms were considered, the shape of the complete separation region, in $(\gamma_{II}, \gamma_{III})$ plane, is a single triangle defined by the points AWB (see Figure 2.5).

(2) *Pure extract region.* Region bounded by the vertical lines, $\gamma_{II} = \frac{1-\varepsilon}{\varepsilon} K_B$, on the right hand side, and $\gamma_{II} = \frac{1-\varepsilon}{\varepsilon} K_A$, on the left-hand side. Pure extract is obtained for all the operating conditions corresponding to points inside this region.

(3) *Pure raffinate region.* Region bounded by the horizontal lines $\gamma_{III} = \frac{1-\varepsilon}{\varepsilon} K_A$ from below, and $\gamma_{III} = \frac{1-\varepsilon}{\varepsilon} K_B$ from above. All the operating points inside this region lead to pure raffinate.

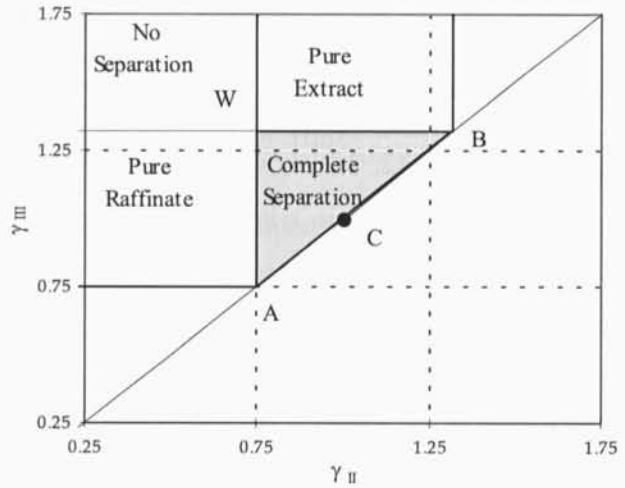

Figure 2.5 *Regions of the (γ_{II}, γ_{III}) plane with different separation regimes in terms of purity of the outlet streams. The constraints on γ_I and γ_{IV} must be fulfilled in order to obtain complete separation. System with linear isotherms with $K_A = 0.50$ and $K_B = 0.88$. Point W and point C correspond, respectively, to the lower and upper limits on the safety coefficient β,* $1 < \beta < \sqrt{\alpha}$.

(4) *No separation region*. The region remaining, rectangular region defined by $\gamma_{III} > \frac{1-\varepsilon}{\varepsilon} K_B$ and $\gamma_{II} < \frac{1-\varepsilon}{\varepsilon} K_A$, neither the extract nor the raffinate streams are pure. We get extract and raffinate purities less than 100%.

2. **Recovery (%)**; it is defined as the total desired product recovered in each flow. For the extract, $R_E = 100 \frac{C_E^B \, Q_E}{C_F^B \, Q_F}$, ratio between the mass flow of more retained product in the extract and the mass flow of the same species in the feed. Similarly, for the raffinate, $R_R = 100 \frac{C_R^A \, Q_R}{C_F^A \, Q_F}$.

3. **Solvent consumption (l/g)**, it is defined as, for the extract, the total quantity of solvent necessary to produce one gram of the more retained product, $S_E = \frac{Q_E + Q_F}{C_E^B Q_E}$.

Similarly for the raffinate, $S_R = \frac{Q_E + Q_F}{C_R^A Q_R}$.

4. **Productivity (g/hr l)**; an optimal design procedure must account for the maximisation of a productivity parameter, defined as, for the extract, the ratio between the mass flowrate of the more retained product in the extract and the stationary-phase volume, $\mathrm{Pr}_E = \frac{C_E^B Q_E}{V_S}$. Similarly, for the raffinate, $\mathrm{Pr}_R = \frac{C_R^A Q_R}{V_S}$.

We characterise the SMB unit or, alternatively the equivalent TMB unit operating conditions, mainly in terms of two performance parameters: purity and recovery. These two performance parameters allow, in first approximation, a selection of the range of operating conditions feasible for any given separation requirement. Once this range has been determined, the choice of the specific optimal operating conditions can be performed on the basis of economic considerations.

2.1.2 Model Description

The model used to predict the performance and concentration profiles in a SMB unit was developed based on the equivalence with the TMB concept, assuming:

- axial dispersion flow for the liquid phase;
- simple linear driving force (LDF) approximation to describe the intraparticle mass transfer;
- plug flow for the solid phase;

The LDF approximation for an isolated particle is:

$$\frac{\partial \langle q_{ij} \rangle}{\partial t} = k_i \left(q_{ij}^* - \langle q_{ij} \rangle \right) \tag{2.13}$$

This is the model used by Pais *et al.* (1997). At the solid/liquid interface, the solid phase concentration is related to the mobile phase concentration by the equilibrium isotherm equation $q_{ij}^* = f_{ij}(c_{1j}, c_{2j})$, where the subscripts i and j, respectively, relates to the system components, glucose, i=1, and fructose, i=2, and to the section number j=*I, ..., IV*, $\langle q_{ij} \rangle$ and c_{ij} are the average adsorbed concentration in the particle and liquid phase concentration of component i in section j, respectively, and k_i the intraparticle mass transfer coefficient of

component i. In this work we took into account two different combinations of the adsorption equilibrium for the components. First, we considered linear adsorption equilibrium for both components, as follows,

$$q_{ij}^{*} = K_i c_{ij} \tag{2.14}$$

K_i are the equilibrium constant of component i. For the second case, different adsorption equilibrium isotherms for each component were considered. For the component B, fructose, which is assumed to be the more strongly adsorbent component, a linear isotherm was considered, (2.14), and an isotherm equation similar to the multicomponent Langmuir, (2.15), was considered for the less retained component A, glucose.

$$q_{Aj}^{*} = \frac{K_A c_{Aj}}{1 + 0.001 c_{Bj} + 0.01030 c_{Bj}^{0.8}} \tag{2.15}$$

The equation (2.15) is similar to the one used in the Strube and Schmidt-Traub (1996).

The basic mass balance equations in the fluid phase of a TMB section volume element and in the adsorbent particles, depending of the user interest, can be written as:

1. *Transient True-Moving-Bed* (T-TMB), for the transient regime and,
2. *Steady-state True-Moving-Bed* (S-TMB), for the stationary regime of the TMB processes.

The second model (S-TMB), where the term concerning the time is not considered, constitutes a system of ordinary differential equations while a system of partial differential equations describes the transient model (T-TMB). For these two models the equilibrium isotherms (2.14) may be inserted into the differential equations code system or written as separate algebraic equations, especially if they are non-linear (2.15). In the case that the isotherm equilibrium equation is written separately as an algebraic equation the system is transformed into a differential-algebraic system. The mass balance equations over a volume element in the section j and in the adsorbent particles, as well as the initial and boundary conditions for the different models considered are shown in Table 2.3; in those equations ε is the column porosity, z the axial coordinate, t is the time variable, u_s and v_j are the interstitial solid and fluid velocities, and D_{L_j} is the axial dispersion coefficient in section j.

Equations (2.16-2.19) concern the T-TMB and equations (2.21-2.24) concern the S-TMB. The boundary conditions chosen for the two models, (2.20) for the T-TMB and (2.25) for the S-TMB, are the Danckwerts boundaries conditions. Notice that for the right boundary, $x = 1$, the conditions are different for the two models considered. For the S-TMB model is presented one more boundary condition for the average adsorbed concentration in the particle, $\langle q_{ij} \rangle$, due to the type of problem to be solved, a second order Boundary Value Problem. The equations can be expressed in a dimensionless form, after introducing spatial and time dimensionless variables, $x = z/L_j$ and $\theta = t\, u_s / L_j$, where L_j is the section length. They are represented in Table 2.4, equations (2.26-2.30) for the T-TMB and equations (2.31-2.35) for the S-TMB. The resulting model parameters are defined in Table 2.5. The adsorption equilibrium parameters have to be added to the previous parameters.

Considering the adsorption equilibrium equation, (2.18) or (2.23), in Table 2.3, written separately as an algebraic equation, a PDAE system for the TTMB model and a DAE system for the STMB is defined. Replacing relation (2.28) or (2.33) in (2.27) or (2.32), depending on the model considered, the PDAE or DAE system will be transformed into a PDE or ODE system.

The liquid flow rate Q_j, in the boundary conditions defined in Table 2.3 and Table 2.4, is related to the interstitial liquid phase velocity, v_j, by $Q_j = \varepsilon\, A\, v_j$. The internal flow rates are related, and so for each node we have, $Q_{IV} = Q_{Rec}$, $Q_I = Q_{Rec} + Q_D$, $Q_{II} = Q_I - Q_E$, $Q_{III} = Q_{II} + Q_F$, where Q_D is the eluent flow rate, Q_E the extract flow rate, Q_F the feed flow rate, Q_R the raffinate flow rate and Q_{Rec} is the recycling flow rate.

The model in Table 2.4, was the one used to compare four strategies to be presented. The set of equations (2.26-2.30), defines a problem of second order partial differential algebraic equations, PDAE's, due the presence of the algebraic equation (2.28) for each component in each of the four sections. The second order derivative term, representing the axial dispersion term, in (2.26), renders the model of parabolic nature, while the second equation (2.27), is hyperbolic. This set of equations can be transformed into a system of partial differential equations, PDE's, by incorporating the algebraic equations (2.28) into the mass balance equations, (2.26) and (2.27). If we consider the terms with respect to the time derivative equal to zero, i.e. $\frac{\partial c_{ij}}{\partial \theta} = \frac{\partial \langle q_{ij} \rangle}{\partial \theta} = 0$, the system of PDE's becomes a system of ordinary differential

Table 2.3 *Model equations for the Transient and Steady-State TMB.*

	Transient TMB	**Steady-State TMB**
Mass balance in a volume element of the bed	$D_{L_j}\frac{\partial^2 c_{ij}}{\partial z^2}-v_j\frac{\partial c_{ij}}{\partial z}+\frac{(1-\varepsilon)}{\varepsilon}u_s\frac{\partial\langle q_{ij}\rangle}{\partial z}=\frac{\partial c_{ij}}{\partial t}+\frac{(1-\varepsilon)}{\varepsilon}\frac{\partial\langle q_{ij}\rangle}{\partial t}$ 2.16	$D_{L_j}\frac{d^2 c_{ij}}{dz^2}-v_j\frac{dc_{ij}}{dz}+\frac{(1-\varepsilon)}{\varepsilon}u_s\frac{d\langle q_{ij}\rangle}{dz}=0$ 2.21
Mass balance in the particle	$u_s\frac{\partial\langle q_{ij}\rangle}{\partial z}+k_i\left[q_{ij}^*-\langle q_{ij}\rangle\right]=\frac{\partial\langle q_{ij}\rangle}{\partial t}$ 2.17	$u_s\frac{d\langle q_{ij}\rangle}{dz}+k_i\left[q_{ij}^*-\langle q_{ij}\rangle\right]=0$ 2.22
Linear adsorption equilibrium	$q_{ij}^*=K_i c_{ij}$ 2.18	$q_{ij}^*=K_i c_{ij}$ 2.23
Initial conditions	$c_{ij}(z,t=0)=\langle q_{ij}\rangle(z,t=0)=0$ 2.19	$c_{ij}(z)=\langle q_{ij}\rangle(z)=0$ 2.24
Boundary conditions	$z=0,\quad c_{ij,0}=c_{ij}-\frac{D_{L_j}}{v_j}\frac{\partial c_{ij}}{\partial z}$ $z=L_j,\quad \frac{\partial c_{ij}}{\partial z}=0,$ 2.20 $j=I\quad c_{iIV,L_{IV}}=\frac{Q_I}{Q_{IV}}c_{iI,0}$ $j=II,IV\quad c_{i(j-1),L_{j-1}}=c_{ij,0}$ $j=III\quad c_{iII,L_{II}}=\frac{Q_{III}}{Q_{II}}c_{iIII,0}-\frac{Q_F}{Q_{II}}c_i^F$ and $\langle q_{iIV}\rangle=\langle q_{iI,0}\rangle,\langle q_{iI}\rangle=\langle q_{iII,0}\rangle,\langle q_{iII}\rangle=\langle q_{iIII,0}\rangle,\langle q_{iIII}\rangle=\langle q_{iIV,0}\rangle$	$z=0,\quad c_{ij,0}=c_{ij}-\frac{D_{L_j}}{v_j}\frac{dc_{ij}}{dz}$ $z=L_j,\quad \frac{dc_{ij}}{dz}=0,$ 2.25 $j=I\quad c_{iIV,L_{IV}}=\frac{Q_I}{Q_{IV}}c_{iI,0}$ $j=II,IV\quad c_{i(j-1),L_{j-1}}=c_{ij,0}$ $j=III\quad c_{iII,L_{II}}=\frac{Q_{III}}{Q_{II}}c_{iIII,0}-\frac{Q_F}{Q_{II}}c_i^F$ and $\langle q_{iIV}\rangle=\langle q_{iI,0}\rangle,\langle q_{iI}\rangle=\langle q_{iII,0}\rangle,\langle q_{iII}\rangle=\langle q_{iIII,0}\rangle,\langle q_{iIII}\rangle=\langle q_{iIV,0}\rangle$

Table 2.4 *Dimensionless model equations for the transient TMB and for the Steady-State TMB described in the Table 2.3.*

	Transient TMB	**Steady-State TMB**
Mass balance in a volume element of the bed	$\frac{\partial c_{ij}}{\partial \theta} = \gamma_j \left[\frac{1}{Pe_j} \frac{\partial^2 c_{ij}}{\partial x^2} - \frac{\partial c_{ij}}{\partial x} \right] - \frac{(1-\varepsilon)}{\varepsilon} \alpha_j \left(q_{ij}^* - \langle q_{ij} \rangle \right)$ 2.26	$\frac{d^2 c_{ij}}{dx^2} = Pe_j \frac{dc_{ij}}{dx} + \frac{(1-\varepsilon)}{\varepsilon} \frac{Pe_j}{\gamma_j} \alpha_j \left[q_{ij}^* - \langle q_{ij} \rangle \right]$ 2.31
Mass balance in the particle	$\frac{\partial \langle q_{ij} \rangle}{\partial \theta} = \frac{\partial \langle q_{ij} \rangle}{\partial x} + \alpha_{ij} \left[q_{ij}^* - \langle q_{ij} \rangle \right]$ 2.27	$\frac{d \langle q_{ij} \rangle}{dx} = -\alpha_{ij} \left[q_{ij}^* - \langle q_{ij} \rangle \right]$ 2.32
Linear adsorption equilibrium	$q_{ij}^* = K_i c_{ij}$ 2.28	$q_{ij}^* = K_i c_{ij}$ 2.33
Initial conditions	$c_{ij}(x) = \langle q_{ij} \rangle (x) = 0$ 2.29	$c_{ij}(x) = \langle q_{ij} \rangle (x) = 0$ 2.34
Boundary conditions	$x = 0, \quad c_{ij,0} = c_{ij} - \frac{1}{Pe_j} \frac{\partial c_{ij}}{\partial x}$ $x = 1, \quad \frac{\partial c_{ij}}{\partial x} = 0,$ 2.30 $j = I \quad c_{iIV,L_{IV}} = \frac{Q_I}{Q_{IV}} c_{iI,0}$ $j = II, IV \quad c_{i(j-1),L_{j-1}} = c_{ij,0}$ $j = III \quad c_{iIII,L_{III}} = \frac{Q_{III}}{Q_{II}} c_{iIII,0} - \frac{Q_F}{Q_{II}} c_i^F$ and $\langle q_{iIV} \rangle = \langle q_{iI,0} \rangle$, $\langle q_{iI} \rangle = \langle q_{iII,0} \rangle$, $\langle q_{iII} \rangle = \langle q_{iIII,0} \rangle$, $\langle q_{iIII} \rangle = \langle q_{iIV,0} \rangle$	$x = 0, \quad c_{ij,0} = c_{ij} - \frac{1}{Pe_j} \frac{dc_{ij}}{dx}$ $x = 1, \quad \frac{dc_{ij}}{dx} = 0,$ 2.35 $j = I \quad c_{iIV,L_{IV}} = \frac{Q_I}{Q_{IV}} c_{iI,0}$ $j = II, IV \quad c_{i(j-1),L_{j-1}} = c_{ij,0}$ $j = III \quad c_{iIII,L_{III}} = \frac{Q_{III}}{Q_{II}} c_{iIII,0} - \frac{Q_F}{Q_{II}} c_i^F$ and $\langle q_{iIV} \rangle = \langle q_{iI,0} \rangle$, $\langle q_{iI} \rangle = \langle q_{iII,0} \rangle$, $\langle q_{iII} \rangle = \langle q_{iIII,0} \rangle$, $\langle q_{iIII} \rangle = \langle q_{iIV,0} \rangle$

equations, ODE's, of second order (2.31-2.35). This system can be transformed into a system of differential-algebraic equations, DAE's, if the equilibrium isotherms (2.33) are written as separate algebraic equations.

Table 2.5 *Dimensionless parameters for the TMB system.*

Number of mass transfer units	$\alpha_j = \frac{kL_j}{u_s}$
Peclet Number	$Pe_j = \frac{\nu_j L_j}{D_{L_j}}$
Ratio between fluid and solid interstitial velocities	$\gamma_j = \frac{\nu_j}{u_s}$
Ratio between solid and fluid volumes	$\frac{1-\varepsilon}{\varepsilon}$

2.2 Numerical Methods and Differential Equations Solvers

In this sub-section we discuss the numerical techniques that were used to solve the four models presented in Table 2.4, transient PDAE and PDE, and steady-state DAE and ODE, models. The techniques used for the discretization of the spatial variable, x, for both PDE and ODE models presented, were the orthogonal collocation on finite element methods. In the first case, the resulting ODE's leads to an initial value problem which is solved by using a time integrator. In the second case, after the discretization, we obtain a linear/non-linear system of algebraic equations that were solved by direct methods. A brief description of these techniques is made ending with the application for a case study. Different public domain solvers that were used to integrate numerically the differential equations systems obtained are presented. For the transient TMB model, the PDECOL code (Madsen and Sincovec, 1979) was used to solve the system of PDE's and the DASSL code (Petzold, 1982) used to solve the system obtained when the isotherm equation was written separately as an algebraic equation. For the steady-state TMB model, the codes COLNEW (Bader and Ascher, 1987) and COLDAE (Ascher and Petzold, 1991) were used, respectively.

2.2.1 Orthogonal collocation on finite elements

The collocation methods are based on the concept of interpolation of unequally spaced points, that is, choosing a polynomial that approximates the solution of a differential equation in the range of integration, $a \leq x \leq b$, and determining the coefficients of that function from a set of base points.

If we consider a second-order boundary value problem (BVP) in the form,

$$y'' = f(x, y(x), y'(x)), \qquad 0 < x < 1 \tag{2.36}$$

with the boundary conditions

$$y(0) = y(1) = 0 \tag{2.37}$$

the finite element method finds a piecewise polynomial approximation, $u(x)$, represented by

$$u(x) = \sum_{j=1}^{m} a_j \phi_j(x) \tag{2.38}$$

$u(x)$ is the polynomial to estimate the solution of (2.36), where $\phi_j(x)$ are the specified functions that are piecewise continuously differentiable, and a_j are the unknown constants. The functions $\phi_j(x)$ called basis functions, satisfy the boundary conditions (2.37) and the unknown constants, a_j, are determined by satisfying the BVP exactly at m points, x_i the collocation points, in the interval.

The orthogonal collocation method derives from the collocation method considering orthogonal polynomials as basic functions and considering the residuals estimated at the zeros of these polynomials, that is, at the collocation points.

Several series of orthogonal polynomials can be used for the numerical solution of differential equations. The Jacobi polynomials, Hermite cubic polynomials and B-splines are examples of orthogonal polynomials.

In some cases, the orthogonal collocation methods present some difficulties. To overcome these problems, the interval of integration is divided into subintervals and then, within each subinterval, the orthogonal collocation is applied. This method was proposed by Carey and Finlayson (1975), and consists in the division of the interval of integration into k subintervals, denominated finite elements, not necessarily with the same amplitude, and then applying the

orthogonal collocation in N_i interior points in each subinterval. The continuity of the function and of the first derivative at the interior breakpoints must be defined. In all the work done, polynomials of order three were used since it is an appropriate order (they have continuity of derivatives at the interior breakpoints) and gives good results. The Hermite cubic polynomials have this property, do not requiring extra conditions to make the solution and its first derivative continuous between elements.

Considering these polynomials as basic function, then two collocation points are necessary in each of the k subintervals. The optimal position of the collocation points is the two Gaussian points given by de Boor and Swartz (1973):

$$\xi_{kt} = x_k + \frac{h_k}{2} + \left(\frac{h_k}{2}\right) u_t, \quad k = 1, \ldots, NE, \quad t = 1, 2 \tag{2.39}$$

where u_t are the Gaussian points in $[-1, 1]$.

The two Gaussian points in $[-1, 1]$ are the zeros of the Legendre polynomial of degree two, $-\frac{1}{2} + \frac{3}{2}x^2$, or $u_1 = -\frac{1}{\sqrt{3}}$ and $u_2 = \frac{1}{\sqrt{3}}$. Considering the Legendre polynomial defined in the interval $[0, 1]$, the zeros are the points $u_1 = 0.2113248654$ and $u_2 = 0.7886751346$.

Thus, the two collocation points in each subinterval $[x_k, x_{k+1}]$ are given by,

$$\begin{aligned} \xi_{k1} &= x_k + \frac{h_k}{2} - \frac{h_k}{2}\left(\frac{1}{\sqrt{3}}\right) = x_k + h_k(0.2113248654) \\ \xi_{k2} &= x_k + \frac{h_k}{2} + \frac{h_k}{2}\left(\frac{1}{\sqrt{3}}\right) = x_k + h_k(0.7886751346) \end{aligned} \tag{2.40}$$

The $2k$ equations specified at the collocation points in addition to the two boundary conditions (2.37), define the system of non-linear algebraic equations of dimension $2k+2$, that determines the collocation solution a_j ($j = 1, \ldots, 2k+2$), and then the solution of the initial problem (2.36).

2.2.2 Method of Lines

Consider the second order partial differential equation,

$$\frac{\partial y}{\partial t} = f\left(t, x, y, \frac{\partial y}{\partial x}, \frac{\partial^2 y}{\partial x^2}\right), \qquad 0 < x < 1, \quad 0 < t \tag{2.41}$$

the method of lines, developed by Liskovets (1965), denominated MOL, solves time dependent partial differential equations (2.46). This technique first discretizes the spatial derivative by using finite difference or finite element methods such as collocation and Galerkin methods, and then integrate in time the resulting system of ordinary differential equations by using a time integrator code.

The PDE (2.41) formulation to be complete requires boundary conditions at $x = 0$ and/or $x = 1$ and an initial condition at $t = 0$,

$$y = y_0(x) \quad \text{at} \quad t = 0 \tag{2.42a}$$

$$\begin{aligned} b_1(y, y') &= \gamma_1(t) \quad \text{at} \quad x = 0 \\ b_2(y, y') &= \gamma_2(t) \quad \text{at} \quad x = 1 \end{aligned} \tag{2.42b}$$

The boundary conditions are incorporated into the discretization in the x-direction while the initial condition is used to start the resulting ODE initial value problem.

Discretization by finite differences in space leads to a large number of equations as shown by Davis (1984), since to retain accuracy, the spatial step size must be small. The method used in the present study, was the discretization by using the collocation method.

Applying this concept into the PDE (2.41) and considering the piecewise polynomial approximation of the form,

$$u(x,t) = \sum_{j=1}^{m} a_j(t)\phi_j(x) \tag{2.43}$$

The collocation step requires that the PDE (2.41) be satisfied by the approximate solution at the collocation points, per subinterval considered,

$$\sum_{j=1}^{m} a_j'(t)\phi_j(x_i) = f\left(t, x_i, \sum_{j=1}^{m} a_j(t)\phi_j(x_i), \sum_{j=1}^{m} a_j(t)\phi'_j(x_i), \sum_{j=1}^{m} a_j(t)\phi''_j(x_i)\right) \tag{2.44}$$
$$i = 1, \ldots, m-2$$

where $m = 2k+2$.

The resulting system has (m–2) equations in m unknowns coefficients a_j (t). The two necessary equations are obtained by applying the same procedure in the two boundary conditions (2.42b). The resulting ($2k$+2) equations obtained define a non-linear ordinary differential system initial value problem in t that can be solved by any available integration package.

2.2.3 Boundary-Value Problems for Differential-Algebraic Equations

Systems that are described by models that consider only relationships between variables and their derivatives take a form of an ODE. However, depending on the variable of interest, sometimes it is necessary to consider not only the relationship between variables and some of their derivatives but also relationships between variables. In these cases the system takes the form of a DAE (Differential-Algebraic Equation) represented by,

$$\begin{aligned} F(t, y, y') &= 0 \\ G(t, y) &= 0 \end{aligned} \tag{2.45}$$

where the algebraic constraints are expressed explicitly by $G(t,y)$=0.

In order to use standard ODE integrators to solve the DAE equations it is necessary to do same changes. It is necessary to convert the algebraic equations in the DAE to the form of an ordinary differential equation, which implies eliminating the variables whose derivatives do not appear in the equations (called the "algebraic variables"), leaving relations between the others (called the "differential variables").

An important property of DAE's is the index. The index of the DAE, can be defined as the minimum number of times that all or part of (2.45) must be differentiated with respect to t in order to determine y' as a continuous function of y and t (Brenan *et al.*, 1989). This property is important in the classification and in the behaviour of the DAE's. According to this definition, an implicit ODE has index zero and DAE involves a mixture of differentiations and integrations. Applying analytical differentiations, repeatedly if necessary, will lead to an explicit ODE system for all the unknowns, except for singular problems.

Considering the special case of a semi-explicit DAE,

$$y' = f(t, y, z) \tag{2.46a}$$

$$0 = g(t, y, z) \tag{2.46b}$$

where $y(t)$ are the differential variables and $z(t)$ are the algebraic variables. By differentiating the constraint equation in (2.46b) with respect to t, we obtain,

$$y' = f(t, y, z) \tag{2.47a}$$

$$g_y(t, y, z)\, y' + g_z(t, y, z)\, z' = -g_t(t, y, z) \tag{2.47b}$$

Assuming that g_z is nonsingular for all t, the system (2.47) is an implicit ODE and (2.46) has index one. Semi-explicit index-1 DAEs are very closely related to implicit ODEs. By solving (2.47b) in order to z and then substituting z into (2.47a) we yield an ODE in y. This procedure is not always recommended because the relationship between variables is modified and also the numerical solution (Brenan *et al.*, 1989). If g_z is singular the DAE has a higher index, i.e., index 2 or higher, a projection method is used as described in Ascher and Petzold (1991).

Some numerical methods used for solving parabolic PDE's can lead to DAE's. The method of lines (MOL) discretize the spatial derivatives, in our case, by orthogonal collocation approximation, and converted the PDE system into an ODE initial value problem. In some cases the resulting system not only had differential equations but also some algebraic constraints on the variables defining a DAE system.

2.2.3.1 Orthogonal collocation on finite elements

The method used to approximate the solution u of the DAE system is the collocation at Gaussian points, as previously explained. The constraints are treated like differential equations of order 0 and correspondingly the approximation to y is found in a piecewise discontinuous polynomial space. For an index-2 DAE system a projection collocation method on the constraint is used. This method will not be described here since the DAE system in study has index one, as shown later.

2.2.4 Parabolic Partial-Algebraic Differential Equations

2.2.4.1 Method of Lines

The mixed system of ODEs, PDEs and DAEs, are called PDAEs (Partial Differential-Algebraic Equations). There are several methodologies to solve PDAE's. Using the MOL method, which by a finite approximation in the spatial variable, x, by the use of either finite differences or finite elements, PDAE's are transfromed into a system of DAEs in time variable, t. The MOL approach used to discretize the spatial derivatives is computationally more efficient. The existing ODE solvers allow the choice of the time step in a way that maintains the accuracy and stability in the evolving solution. In the present study, orthogonal collocation method was used for the spatial discretization. Depending of the model used T-TMB and S-TMB, two different types of DAE systems are obtained. The DAE system resulting from the discretization of the PDAEs is an initial value DAE problem in the time variable t, while the DAE system, resulting from the steady-state model is a second-order boundary DAE problem in the spatial variable, x.

2.2.5 Mathematical software applied to the case study

All the programs used to obtain the solution of the differential problems were written in Fortran language. The problem to be solved is properly defined by constructing a main program and subprograms. The main program defines the initial conditions of the system and calls the package, depending on the type of problem, and performs the desired output for the numerical problem, as illustrated in Figure 2.6. COLNEW and COLDAE for the ODE and DAE boundary problem, and PDECOL and DASSL for the PDE and DAE initial value problem, respectively. All these four packages can be obtained from the electronic library netlib (http://www.netlib.org).

Figure 2.6 *Flow diagram of computer program to numerically solve the models presented in Table 2.4. The subroutine PACKAGE refers to the package used depending on the type of problem to be solved.*

2.2.5.1 Boundary-Value Problems for Differential-Algebraic Equations

COLDAE package (Ascher and Petzold, 1991) is a modification of the package COLNEW (Bader and Ascher, 1987). It works practically the same way as COLNEW and optionally, solves semi-explicit differential-algebraic equations with index at most 2, with constraints given by

$$\begin{aligned} y_i^{(m_i)}(x) &= f_i\left(x; s\left(y(x)\right), z(x)\right) && i = 1, \ldots, ncomp \\ 0 &= f_i\left(x; s\left(y(x)\right), z(x)\right) && i = ncomp+1, \ldots, ny \\ & && a < x < b \\ g_j\left(\zeta_j; s\left(y\left(\zeta_j\right)\right)\right) &= 0 && j = 1, \ldots, mstar \\ & && mstar = m_1 + m_2 + \ldots + m_{ncomp} \end{aligned} \tag{2.48}$$

where m_i is the order of the i differential equation; $y(x) = \left(y_1(x), y_2(x), \ldots, y_{ncomp}(x)\right)^T$ is an isolated differential solution components and $z = \left(z_1, z_2, \ldots, z_{ny}\right)^T$ are the algebraic solution components, $s\left(y(x)\right) = \left(y_1(x), y_1'(x), \ldots, y_1^{(m_1-1)}(x), y_2(x) \ldots, y_d(x), \ldots, y_d^{(m_d-1)}(x)\right)^T$ is the vector of unknowns that would result from converting (2.48) to a first-order system, $y_i^{(m_i)}$ is the $m_i = m(i)^{th}$ derivative of y_i ; $f_i\left(x; s(y), z\right)$ is a nonlinear function of

$s(y) = s\left(y(x)\right)$ and $z = z(x)$; $g_j\left(\zeta_j; s\left(y\right)\right)$ is a nonlinear function used to represent a boundary condition.

The boundary points satisfy $a \le \zeta_1 \le ... \le \zeta_{mstar} \le b$ and the orders m_i of the differential equations satisfy $1 \le m_i \le 4$.

The method used to approximate the solution u is collocation at Gaussian points, requiring m_i–1 continuous derivatives in the i^{th} component, $i = 1, \ldots, ncomp$. Here, k is the number of collocation points (stages) per subinterval and is chosen such that $k \ge \max\ m_i$.

A Runge-Kutta-monomial solution representation is used. For general semi-explicit index-2 DAEs, a selective projected collocation method is used, see Ascher and Spiteri (1994).

The COLDAE was used to solve the system defined by (2.31)-(2.33) with initial and boundary conditions (2.34), (2.35), where the algebraic equation (2.33) represents the equilibrium isotherm equation. This system defines a DAE system, with two differential variables $\left(\partial c_{ij}/\partial t, \partial \left\langle q_{ij} \right\rangle / \partial t\right)$ and three algebraic variables $\left(q_{ij}^{*}, \left\langle q_{ij} \right\rangle, c_{ij}\right)$. In this case that corresponds to first solve (2.33) and then compute $\partial c_{ij}/\partial t$ and $\partial \left\langle q_{ij} \right\rangle / \partial t$ from (2.31) and (2.32). The two algebraic variables c_{ij} and $\left\langle q_{ij} \right\rangle$ appears only in the equations defining the derivatives. Applying analytical differentiation, we will get an explicit ODE system for all the unknowns. The number of differentiations needed for this transformation is called the index of the DAE, as mentioned before. Differentiating the equilibrium isotherm equation (2.33) yields,

$$\frac{\partial q_{ij}^{*}}{\partial t} = K_i \frac{\partial c_{ij}}{\partial t} \tag{2.49}$$

Doing this, we obtain a differential equation for all the unknowns. The index of this system is one, since we only needed to differentiate once. Note that if we carry out the substitution for q_{ij}^{*} then the resulting system is an ODE as previously solved. The main program and the user written subroutines required to solve the specified DAE system is presented in Appendix A. The final size of the DAE system to be solved is of dimension 672 (⟨2 differential equations + 1 algebraic equation⟩ × 2 components × 4 sections × 14 finite elements × 2 interior collocation points) as illustrated in Table 2.6, as the tolerance on the solution and derivative values considered. An example of the steady-state internal concentration profiles obtained under

operating conditions properly chosen is very similar to the one obtained by using the COLNEW, Figure 2.12c and 2.12d, with the final results for the performance parameters obtained described in Table 2.9.

2.2.5.2 Parabolic Partial Differential-Algebraic Equations

For the PDAEs problems the package DASSL (Petzold, 1982a) was used. The DASSL package solves a system of initial value DAE's, and so to use it, we first need to transform the PDAE in t and x variables, into a system of DAE in t. To do that, the method of lines, MOL, was used. The spatial discretization was done by using the orthogonal collocation in Gaussian points with Hermite cubic polynomials as basis function. This subroutine, provided by the user, will be explained later. The initial value DAE system arising from the MOL method is then solved using the time integrator DASSL. DASSL solves a system of ordinary differential-algebraic equations (ODAEs) in t by using the backward differentiation formulas, BDF, of orders one through five.

To use DASSL we first need to transform the system of partial differential-algebraic equations, (2.26)-(2.30), in t and x, into an initial value ordinary differential-algebraic problem, in t, since both mass balance equations, (2.26) and (2.27), have time and spatial derivatives. After the discretization, the algebraic equations, the equations related to the adsorption equilibrium, are the same as before the discretization, (2.28). The algebraic relationship (2.28) is simple and linear and there is virtually no reason to work with it separately. However, when this relationship becomes non-linear, it is better to keep the algebraic form, not only because of the complexity of the problem but because it allows easy changes of the algebraic model equation. The sequence of operations taken for the spatial discretization, HERMCOL subroutine, is illustrated as a flow diagram in Figure 2.7.

The way to identify the difficulty of solving numerically a system of DAE's is the index, as previously mentioned. Nevertheless, we can define it in a simple way as the number of t-differentiation required to convert the algebraic equations into a differential form. In the present case the system of DAE's equations are of index 1, as demonstrated in the section 2.2.3.

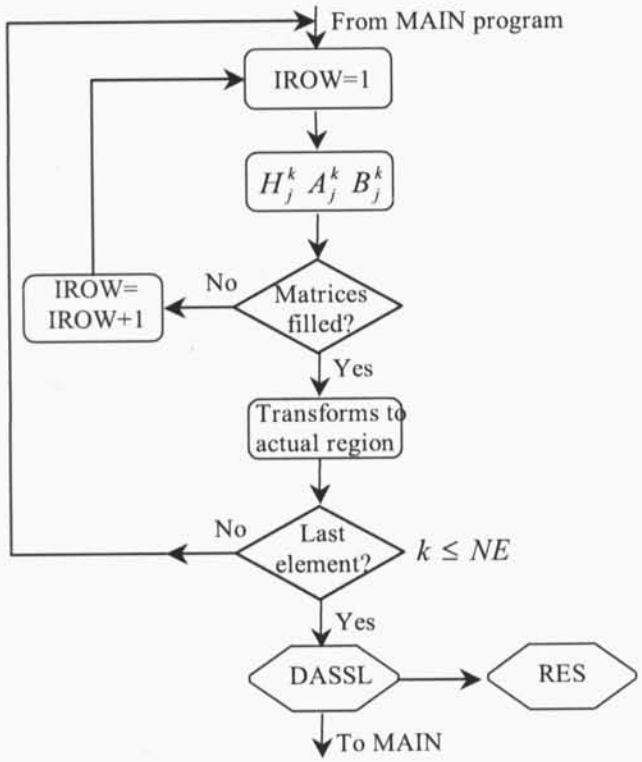

Figure 2.7 *Flow diagram of subroutine HERMCOL (one of the PACKAGE subroutine) that develops the discretization elements for the first and second derivatives carried out sequentially for each finite element, initial conditions are set and the problem takes the ODE form, defined in RES, to be integrated using the DASSL.*

A brief description of the orthogonal collocation method in finite elements using the Hermite cubic polynomials will be discussed.

2.2.5.2.1 Spatial discretization of the equations that describe the concentration

The collocation at the Gaussian points using Hermite cubic polynomials as basis functions, applied to the equations regarding to the liquid and average solid phase concentrations, (2.26-2.30), will be explained. Considering the solution in the following form,

$$c_{ij}(x,\theta) = \tilde{c}_{ij}(u_t,\theta) = \sum_{l=1}^{4} H_{tl}\left(u_t, h(k)\right) a_{ij,l+2k-2}(\theta)$$
$$\left\langle q_{ij} \right\rangle (x,\theta) = \tilde{q}_{ij}(u_t,\theta) = \sum_{l=1}^{4} H_{tl}\left(u_t, h(k)\right) b_{ij,l+2k-2}(\theta) \qquad (2.50)$$

for the liquid phase concentration and adsorbed concentration in the particle, respectively. In this section, we only describe the spatial discretization applied to the liquid phase concentration equations. For the average solid phase concentration equations, the procedure is equivalent. Let $X = \{x_k\}_{k=1}^{NE+1}$ define the spatial mesh of the interval $[0,1]$, as defined in Figure 2.8, with $h_k = x_{k+1} - x_k$, defining the mesh step size sequence $H = \{h_k\}_{k=1}^{NE}$. For any given collocation points (u_1, u_2), we define the new collocation point sequence $\Xi = \{\xi_{kj}\}_{k,j=1}^{NE,2}$ where,

$$\begin{aligned} \xi_{k1} &= x_k + u_1 h_k, \qquad i = 1,\ldots,NE \\ \xi_{k2} &= x_k + u_2 h_k, \qquad i = 1,\ldots,NE \end{aligned}, \tag{2.51}$$

The number of collocation points is $NT = 2.NE + 2$. The two ends points, x_1 and x_{NE+1}, are included into Ξ, to complete the sequence and to be used with the boundary conditions.

The matrix of the Hermite cubic polynomials H_{tl} in the two interior collocation points, (u_1, u_2), can be defined as,

$$\mathbf{H} = H_{tl}(u_t, h(k)) = \begin{bmatrix} H_{11}(u_1, h(k)) & H_{12}(u_1, h(k)) & H_{13}(u_1, h(k)) & H_{14}(u_1, h(k)) \\ H_{21}(u_2, h(k)) & H_{22}(u_2, h(k)) & H_{23}(u_2, h(k)) & H_{24}(u_2, h(k)) \end{bmatrix} \tag{2.52a}$$

with, as in Finlayson, (1980),

$$\begin{aligned} H_{t1}(u_t, h(k)) &= (1-u_t)^2 (1+2u_t) \\ H_{t2}(u_t, h(k)) &= u_t (1-u_t)^2 h(k) \\ H_{t3}(u_t, h(k)) &= u_t^2 (3-2u_t) \\ H_{t4}(u_t, h(k)) &= u_t^2 (u_t - 1) h(k) \end{aligned} \tag{2.52b}$$

The first and second derivatives for each element k, respectively, are obtained by differentiating (2.50) with respect to u_t, and gives:

$$\frac{\partial c_{ij}(x,\theta)}{\partial x} = \frac{1}{h(k)} \frac{\partial \tilde{c}_{ij}(u_t,\theta)}{\partial u_t} = \frac{1}{h(k)} \sum_{l=1}^{4} A_{tl}(u_t, h(k)) a_{ij,l+2k-2}(\theta) \tag{2.53a}$$

$$\frac{\partial^2 c_{ij}(x,\theta)}{\partial x^2} = \frac{1}{h(k)^2} \frac{\partial^2 \tilde{c}_{ij}(u_t,\theta)}{\partial u_t^2} = \frac{1}{h(k)^2} \sum_{l=1}^{4} B_{tl}(u_t, h(k)) a_{ij,l+2k-2}(\theta) \tag{2.53b}$$

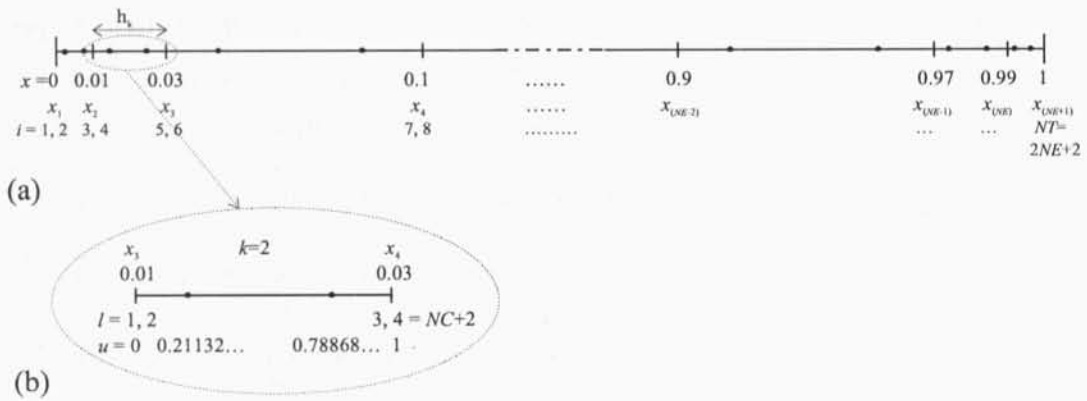

Figure 2.8 (a) *Subdivision of the solution domain into 14 finite elements. Two collocation points, NC=2, were chosen in each finite element considered.* | *, end points;* ı *, continuity between interior finite elements;* •*, interior collocation points within each finite element. Global numbering i.* ***(b)*** *Representation of the finite element 2 (k = 1, ..., NE) normalised between 0 and 1, with the two collocation points, u_1 and u_2, considered. Local numbering system I.*

the subscripts i and j are related to the components, glucose and fructose, and section, I, II, III, IV; k finite elements ($=1, \ldots, NE$); t interior collocation points ($=1, 2$); $l = 1, \ldots, 4$ parameters needed to define the Hermite cubic polynomial $H_{tl}(u_j)$, in each finite element, since the basis polynomial used are of degree three. Figure 2.8(b) shows the location of these points in element $k = 2$.

The matrices of the derivatives A_{tl} and B_{tl} representing the first and second derivatives of the polynomial H_{tl} in the t^{th} interior collocation point, are expressed, respectively, by

$$
\begin{aligned}
A_{t1}\left(u_t, h(k)\right) &= \left.\frac{\partial H_{t1}\left(u_t, h(k)\right)}{\partial u_t}\right|_{u_t, h(k)} = -6u_t(1-u_t) \\
A_{t2}\left(u_t, h(k)\right) &= \left.\frac{\partial H_{t2}\left(u_t, h(k)\right)}{\partial u_t}\right|_{u_t, h(k)} = (1-3u_t)(1-u_t)h(k) \\
A_{t3}\left(u_t, h(k)\right) &= \left.\frac{\partial H_{t3}\left(u_t, h(k)\right)}{\partial u_t}\right|_{u_t, h(k)} = 6u_t(1-u_t) \\
A_{t4}\left(u_t, h(k)\right) &= \left.\frac{\partial H_{t4}\left(u_t, h(k)\right)}{\partial u_t}\right|_{u_t, h(k)} = u_t(3u_t-2)h(k)
\end{aligned}
\qquad (2.54)
$$

and

$$B_{t1}(u_t, h(k)) = \left.\frac{\partial^2 H_{t1}(u_t, h(k))}{\partial u_t^2}\right|_{u_t, h(k)} = -6(1-2u_t)$$

$$B_{t2}(u_t, h(k)) = \left.\frac{\partial^2 H_{t2}(u_t, h(k))}{\partial u_t^2}\right|_{u_t, h(k)} = (6u_t - 4)h(k) \qquad (2.55)$$

$$B_{t3}(u_t, h(k)) = \left.\frac{\partial^2 H_{t3}(u_t, h(k))}{\partial u_t^2}\right|_{u_t, h(k)} = 6(1-2u_t)$$

$$B_{t4}(u_t, h(k)) = \left.\frac{\partial^2 H_{t4}(u_t, h(k))}{\partial u_t^2}\right|_{u_t, h(k)} = (6u_t - 2)h(k)$$

These matrices, and **H**, only depend of the new dimensionless axial coordinate u_t.

The four parameters a_{l+2k-2} in each element are estimated using four collocation points; the two boundary points (u = 0 and u = 1) and the two interior collocation points (u_1 and u_2). These two interior points are the zeros of the orthogonal quadratic polynomial of Legendre $P_2(u_j)$, u_1 = 0.2113248654 and u_2 = 0.7886751346, as previously mentioned. The concentration profiles near the two end nodes, 0 and 1, referring to the connection points between two neighbouring sections, varied abruptly as response to the step concentration input or output, becoming, the problem, numerically difficult to deal with. Trying to overcome this problem, the interval of integration is divided into subintervals, or finite elements, with different length depending on the distance to these two boundary points. The subintervals near the boundary points are the ones with small length, Figure 2.8. In the present study, the domain was divided into 14 interior subintervals *NE*, with 2 interior collocation points *NC*, in each subinterval.

Applying the usual procedures of orthogonal collocation into the differential equations that describes the system through the column, (2.26)-(2.28), may be expressed in collocation form represented by (2.56) for each t^{th} interior collocation point on the k^{th} element. These equations are formed by substitution of (2.50) and (2.53), which gives,

$$\sum_{l=1}^{4} H_{tl} \frac{\partial a_{ij,l+2k-2}}{\partial \theta} = \gamma_j \left[\frac{1}{Pe_j} \frac{1}{h(k)^2} \sum_{l=1}^{4} B_{tl} a_{ij,l+2k-2}(\theta) - \frac{1}{h(k)} \sum_{l=1}^{4} A_{tl} a_{ij,l+2k-2}(\theta) \right] - \\ - \frac{1-\varepsilon}{\varepsilon} \alpha_j \left[K_i \sum_{l=1}^{4} H_{tl} a_{ij,l+2k-2}(\theta) - \sum_{l=1}^{4} H_{tl} b_{ij,l+2k-2}(\theta) \right] \tag{2.56a}$$

$$\sum_{l=1}^{4} H_{tl} \frac{\partial b_{ij,l+2k-2}}{\partial \theta} = \frac{1}{h(k)} \sum_{l=1}^{4} A_{tl} b_{ij,l+2k-2}(\theta) + \\ + \alpha_j \left[K_i \sum_{l=1}^{4} H_{tl} a_{ij,l+2k-2}(\theta) - \sum_{l=1}^{4} H_{tl} b_{ij,l+2k-2}(\theta) \right] \tag{2.56b}$$

with $l = 1, \ldots, 4$; $j = 1, 2$; $k = 1, \ldots, NE$.

The matrices A_{tl} and B_{tl} approximate the first and second derivatives of the polynomial H_{tl} defined in (2.54)-(2.55), respectively. The components of the vector $\left[a_{ij}\ b_{ij}\right]$ are the unknown solution values at the interior collocation points. The collocation method determines these unknown coefficients, by satisfying the system of ODEs at the $(2 \times NE)$ points.

The equations (2.56) can be rearranged and simplified since the matrices **A**, **B** and **H**, for a time θ, are constants.

$$\sum_{l=1}^{4} H_{tl} \frac{\partial a_{ij,l+2k-2}}{\partial \theta} = \sum_{l=1}^{4} C_{tl} a_{ij,l+2k-2}(\theta) - \\ - \frac{1-\varepsilon}{\varepsilon} \alpha_j \left[\sum_{l=1}^{4} H_{tl} \left(K_i a_{ij,l+2k-2}(\theta) - b_{ij,l+2k-2}(\theta) \right) \right] \tag{2.57a}$$

$$\sum_{l=1}^{4} H_{tl} \frac{\partial b_{ij,l+2k-2}}{\partial \theta} = \sum_{l=1}^{4} A_{tl} b_{ij,l+2k-2}(\theta) + \\ + \alpha_j \left[\sum_{l=1}^{4} H_{tl} \left(K_i a_{ij,l+2k-2}(\theta) - b_{ij,l+2k-2}(\theta) \right) \right] \tag{2.57b}$$

where, $C_{tl} = \frac{1}{Pe_j} B_{tl} - A_{tl}$, $B_{tl} = \frac{1}{h(k)^2} B_{tl}$ and $A_{tl} = \frac{1}{h(k)} A_{tl}$ (2.58)

These equations form a system of $2.\left[n_i.n_j.(NC.NE)\right]$ equations with $2.\left[n_i.n_j.(NT)\right]$ unknowns coefficients, where 2 is the number of differential equations resulting from the

mass balance in a volume of the bed, and from the mass balance in the particle, n_i and n_j are the number of species and the number of sections in the system, respectively, NC is the number of internal collocation points, NE is the number of finite elements, and NT is the total number of collocation points. The boundary conditions equations, for $k=1$ $(u=0)$ and $k=NE$ $(u=1)$ and respectively, are used to estimate $n_i.n_j.(NC)$ coefficients of the solution vector, $\left[a_{ij}\ b_{ij}\right]$. Considering the boundary conditions and the mass balances equations (2.30) at each node, after the discretization we have,

$k=1,\ u=0$:

$$\begin{aligned}
&\frac{Q_{IV}}{Q_I}\sum_{l=1}^{4}H_{1l}a_{iIV,l+2NE-2}=\sum_{l=1}^{4}H_{0l}a_{iI,l}-\frac{1}{Pe_j}\sum_{l=1}^{4}A_{0l}a_{iI,l}\\
&\sum_{l=1}^{4}H_{1l}a_{iI,l+2NE-2}=\sum_{l=1}^{4}H_{0l}a_{iII,l}-\frac{1}{Pe_j}\sum_{l=1}^{4}A_{0l}a_{iII,l}\\
&\frac{Q_{II}}{Q_{III}}\sum_{l=1}^{4}H_{1l}a_{iII,l+2NE-2}+\frac{Q_F}{Q_{III}}c_i^F=\sum_{l=1}^{4}H_{0l}a_{iIII,l}-\frac{1}{Pe_j}\sum_{l=1}^{4}A_{0l}a_{iIII,l}\\
&\sum_{l=1}^{4}H_{1l}a_{iIII,l+2NE-2}=\sum_{l=1}^{4}H_{0l}a_{iIV,l}-\frac{1}{Pe_j}\sum_{l=1}^{4}A_{0l}a_{iIV,l}
\end{aligned}\qquad (2.59a)$$

$k=NE,\ u=1$:

$$\sum_{l=1}^{4}H_{1l}b_{ij,l+2NE-2}=\sum_{l=1}^{4}H_{0l}b_{ij+1,l}\qquad (2.59b)$$

Using these equations, (2.59), for each component i in section j, some unknowns can be directly estimated,

$$\begin{aligned}
a_{iI,1}&=\frac{1}{Pe}a_{iI,2}+\frac{Q_{IV}}{Q_I}a_{iIV,2NE+1}\\
a_{iII,1}&=\frac{1}{Pe}a_{iII,2}+a_{iI,2NE+1}\\
a_{iIII,1}&=\frac{1}{Pe}a_{iIII,2}+\left(\frac{Q_{II}}{Q_{III}}a_{iII,2NE+1}+\frac{Q_F}{Q_{III}}c_i^F\right)\\
a_{iIV,1}&=\frac{1}{Pe}a_{iIV,2}+a_{iIII,2NE+1}
\end{aligned}\qquad (2.60a)$$

and

$$\begin{aligned}
b_{iI,2NE+1}&=b_{iII,1}\\
b_{iII,2NE+1}&=b_{iIII,1}\\
b_{iIII,2NE+1}&=b_{iIV,1}\\
b_{iIV,2NE+1}&=b_{iI,1}
\end{aligned}\qquad (2.60b)$$

knowing that $H_{01}=1$, $H_{02}=H_{03}=H_{04}=0$; $A_{01}=A_{03}=A_{04}=0$, $A_{02}=h(1)$; and $H_{11}=H_{12}=H_{14}=0$, $H_{13}=1$; $A_{11}=A_{12}=A_{13}=0$, $A_{14}=h(NE)$.

The problem of no specified boundary conditions at $x=0$ for the average adsorbed concentration in the particle, $\langle q_{ij} \rangle$, and at $x=1$ for the liquid phase concentration, c_{ij}, was overcome by introducing additional equations resulting from the satisfaction of the mass balances in the particle, (2.27), and the mass balance in a volume element of the bed, (2.26) at the corresponding boundary. After the discretization we obtain,

for $k=1$, u=0:

$$\sum_{l=1}^{4} H_{0l} \frac{\partial b_{ij,l+2k-2}}{\partial \theta} = \sum_{l=1}^{4} A_{0l} b_{ij,l+2k-2} + \\ + \left[K_i \sum_{l=1}^{4} H_{0l} a_{ij,l+2k-2} - \sum_{l=1}^{4} H_{0l} b_{ij,l+2k-2} \right] \tag{2.61}$$

Simplifying,

$$\frac{\partial b_{ij,1}}{\partial \theta} = b_{ij,2} + \alpha_j \left[K_i a_{ij,1} - b_{ij,1} \right] \tag{2.62}$$

and for k=NE, u=1:

$$\sum_{l=1}^{4} H_{1l} \frac{\partial a_{ij,l+2NE-2}}{\partial \theta} = \gamma_j \left[\frac{1}{Pe_j} \sum_{l=1}^{4} B_{1l} a_{ij,l+2NE-2} - \sum_{l=1}^{4} A_{1l} a_{ij,l+2NE-2} \right] - \\ - \frac{1-\varepsilon}{\varepsilon} \alpha_j \left[K_i \sum_{l=1}^{4} H_{1l} a_{ij,l+2NE-2} - \sum_{l=1}^{4} H_{1l} b_{ij,l+2NE-2} \right] \tag{2.63}$$

The values of the coefficients $a_{ij,1}$ in (2.62), were estimated by using the expressions in (2.60a). Therefore, some coefficients can be removed by substitution of their values obtained for the two end points $u=0$ and $u=1$. The number of unknowns to be estimated is then reduced, and the same as the dimension of the differential equations system to be solved, that is, $n_i.n_j.(NC.NE+1)+n_i.n_j.(NC.NE+1)$ (first term with respect to the number of a_{ij} unknowns coefficients and the second term to the b_{ij} unknowns coefficients to be estimated). After the substitution and elimination of these coefficients, (2.60), the remaining ones were re-enumerated. After the elimination of the coefficients $a_{ij,1}$, the coefficients $a_{ij,2}$ will be designated by $a_{ij,1}$, and for $(l+2k-2)>2$ by $(l+2k-3)$. After the elimination of the

coefficients $b_{ij,2NE+1}$ the coefficient $b_{ij,2NE+2}$ will be designated by $b_{ij,2NE+1}$. Collecting (2.57), (2.60), (2.62) and (2.63), determines the system of equations which can be written in the following form:

if $k=1$

$$\begin{aligned}
&\left(\frac{H_{t1}}{Pe_j}+H_{t2}\right)\frac{\partial a_{ij,1}}{\partial\theta}+\sum_{l=3}^{4}H_{tl}\frac{\partial a_{ij,l-1}}{\partial\theta}+H_{t1}\frac{\partial}{\partial\theta}aa_{ij}= \\
&=\gamma_j\left[\frac{1}{Pe_j}\left(\left(\frac{B_{t1}}{Pe_j}+B_{t2}\right)a_{ij,1}+\sum_{l=3}^{4}B_{tl}a_{ij,l-1}+B_{t1}aa_{ij}\right)-\right. \\
&\left.-\left(\left(\frac{A_{t1}}{Pe_j}+A_{t2}\right)a_{ij,1}+\sum_{l=3}^{4}A_{tl}a_{ij,l-1}+A_{t1}aa_{ij}\right)\right]- \\
&-\frac{1-\varepsilon}{\varepsilon}\alpha_j\left[K_i\left(\left(\frac{H_{t1}}{Pe_j}+H_{t2}\right)a_{ij,1}+\sum_{l=3}^{4}H_{tl}a_{ij,l-1}+H_{t1}aa_{ij}\right)-\left(H_{t1}b_{ij,1}+\sum_{l=2}^{4}H_{tl}b_{ij,l}\right)\right]
\end{aligned} \tag{2.64a}$$

with $aa_{il}=\frac{Q_{IV}}{Q_I}a_{iIV,2NE}$, $aa_{iII}=a_{il,2NE}$, $aa_{iIII}=\frac{Q_{II}}{Q_{III}}a_{iII,2NE}+\frac{Q_F}{Q_{III}}c_i^F$, $aa_{iIV}=a_{iIII,2NE}$

if $2\le k\le NE-1$

$$\begin{aligned}
&\sum_{l=1}^{4}H_{tl}\frac{\partial a_{ij,l+2k-3}}{\partial\theta}=\gamma_j\left[\frac{1}{Pe_j}\left(\sum_{l=1}^{4}B_{tl}a_{ij,l+2k-3}\right)-\right. \\
&\left.-\left(\sum_{l=1}^{4}A_{tl}a_{ij,l+2k-3}\right)\right]-\frac{1-\varepsilon}{\varepsilon}\alpha_j\left[K_i\left(\sum_{l=1}^{4}H_{tl}a_{ij,l+2k-3}\right)-\left(\sum_{l=1}^{4}H_{tl}b_{ij,l+2k-2}\right)\right]
\end{aligned} \tag{2.64b}$$

if $k=NE$

$$\begin{aligned}
&\sum_{\substack{l=1\\l\neq3}}^{4}H_{tl}\frac{\partial a_{ij,l+2NE-3}}{\partial\theta}+H_{t3}\frac{\partial a_{ij,2NE}}{\partial\theta}=\gamma_j\left[\frac{1}{Pe_j}\left(\sum_{\substack{l=1\\l\neq3}}^{4}B_{tl}a_{ij,l+2NE-3}+B_{t3}a_{ij,2NE}\right)-\right. \\
&\left.-\left(\sum_{\substack{l=1\\l\neq3}}^{4}A_{tl}a_{ij,l+2NE-3}+A_{t1}a_{ij,2NE}\right)\right]-\frac{1-\varepsilon}{\varepsilon}\alpha_j \\
&\left[K_i\left(\sum_{\substack{l=1\\l\neq3}}^{4}H_{tl}a_{ij,l+2NE-3}+H_{t3}a_{ij,2NE}\right)-\left(\sum_{l=2}^{2}H_{tl}b_{ij,l+2NE-2}+H_{t4}b_{ij,2NE+1}+H_{t3}b_{ij+1,1}\right)\right]
\end{aligned} \tag{2.64c}$$

$$\frac{\partial a_{ij,2NE}}{\partial \theta} = \gamma_j \left[\frac{1}{Pe} \frac{2}{h(NE)} \left(3a_{ij,2NE-2} + a_{ij,2NE-1} - 3a_{ij,2NE} + 2a_{ij,2NE-1} \right) - a_{ij,2NE+1} \right] - \\ - \frac{1-\varepsilon}{\varepsilon} \left[K_i a_{ij,2NE} - b_{ij+1,1} \right] \quad , \quad (2.64d)$$

for the mass balance in a volume element of the bed. The equations for the mass balance in the particle are as follows; c_{ij} takes the values of $a_{ij,1}$ defined in (2.60a),

if $k = 1$

$$\frac{\partial b_{ij,1}}{\partial \theta} = b_{ij,2} + \alpha_j \left[K_i \left(c_{ij} \right) - b_{ij,1} \right] \quad (2.65a)$$

$$H_{t1} \frac{\partial b_{ij,1}}{\partial \theta} + \sum_{l=2}^{4} H_{tl} \frac{\partial b_{ij,l}}{\partial \theta} = \left[A_{t1} b_{ij,1} + \sum_{l=2}^{4} A_{tl} b_{ij,l} \right] + \\ + \alpha_j \left[K_i \left(\left(\frac{H_{t1}}{Pe_j} + H_{t2} \right) a_{ij,1} + \sum_{l=3}^{4} H_{tl} a_{ij,l-1} + H_{t1} aa_{ij} \right) - \left(H_{t1} b_{ij,1} + \sum_{l=2}^{4} H_{tl} b_{ij,l} \right) \right] \quad (2.65b)$$

if $2 \le k \le NE - 1$

$$\sum_{l=1}^{4} H_{tl} \frac{\partial b_{ij,l+2k-2}}{\partial \theta} = \sum_{l=1}^{4} A_{tl} b_{ij,l+2k-2} + \\ + \alpha_j \left[K_i \left(\sum_{l=1}^{4} H_{tl} a_{ij,l+2k-3} \right) - \left(\sum_{l=1}^{4} H_{tl} b_{ij,l+2k-2} \right) \right] \quad (2.65c)$$

if $k = NE$

$$\sum_{l=1}^{2} H_{tl} \frac{\partial b_{ij,l+2NE-2}}{\partial \theta} + H_{t4} \frac{\partial b_{ij,l+2NE+1}}{\partial \theta} + H_{t3} \frac{\partial b_{ij+1,1}}{\partial \theta} = \\ = \left[\sum_{l=1}^{2} A_{tl} b_{ij,l+2NE-2} + A_{t4} b_{ij,l+2NE+1} + A_{t3} b_{ij+1,1} \right] + \\ + \alpha_j \left[K_i \left(\sum_{\substack{l=1 \\ l \neq 3}}^{4} H_{tl} a_{ij,l+2NE-3} + H_{t4} a_{ij,2NE} \right) - \right. \\ \left. - \left(\sum_{l=1}^{2} H_{tl} b_{ij,l+2NE-2} + H_{t4} b_{ij,2NE+1} + H_{t3} b_{ij+1,1} \right) \right] \quad (2.65d)$$

The set of equations (2.64-2.65) defines a system of initial value problem in θ, which is to be integrated by DASSL. This set of equations can be expressed in a matrix form as the following:

$$[\mathrm{HaMAT}]\left[\frac{\partial a}{\partial \theta}\right] = \gamma_j \left\{\frac{1}{Pe_j}[\mathrm{BaMAT}] - [\mathrm{AaMAT}]\right\}[a] - \\ -\frac{1-\varepsilon}{\varepsilon}\alpha_j \left\{K_i[\mathrm{HaMAT}][a] - [\mathrm{HbMAT}][b]\right\} \tag{2.66a}$$

$$[\mathrm{HbMAT}]\left[\frac{\partial b}{\partial \theta}\right] = [\mathrm{AbMAT}][b] + \alpha_j \left\{K_i[\mathrm{HaMAT}][a] - [\mathrm{HbMAT}][b]\right\} \tag{2.66b}$$

with the initial conditions,

$$\mathbf{HaMAT}\begin{bmatrix} a_{1I,2}(0) \\ \vdots \\ a_{1I,2NE-1}(0) \\ a_{1I,2NE+1}(0) \\ a_{2I,1}(0) \\ \vdots \\ a_{2IV,1}(0) \\ \vdots \\ a_{2IV,2NE+1}(0) \end{bmatrix} = \begin{bmatrix} 0 \\ \vdots \\ 0 \\ 0 \\ 0 \\ \vdots \\ 0 \\ \vdots \\ 0 \end{bmatrix}, \quad \mathbf{HbMAT}\begin{bmatrix} b_{1I,2}(0) \\ b_{1I,3}(0) \\ \vdots \\ b_{1I,2NE+1}(0) \\ b_{2I,2}(0) \\ \vdots \\ b_{2IV,2}(0) \\ \vdots \\ b_{2IV,2NE+1}(0) \end{bmatrix} = \begin{bmatrix} 0 \\ 0 \\ \vdots \\ 0 \\ 0 \\ \vdots \\ 0 \\ \vdots \\ 0 \end{bmatrix}, \begin{bmatrix} a_{1I,2NE}(0) \\ a_{2I,2NE}(0) \\ \vdots \\ a_{2IV,2NE}(0) \\ b_{1I,2NE}(0) \\ b_{2I,2NE}(0) \\ \vdots \\ b_{1IV,2NE}(0) \\ b_{2IV,2NE}(0) \end{bmatrix} = \begin{bmatrix} 0 \\ 0 \\ \vdots \\ 0 \\ 0 \\ 0 \\ \vdots \\ 0 \\ 0 \end{bmatrix} \tag{2.67}$$

The matrices, **HaMAT** and **HbMAT**, have a well known sparse structure. Considering $NE = 3$, the matrix **HaMAT** can be defined as in Figure 2.9. The others matrices have similar shape.

The concentration values, c_{ij} and $\langle q_{ij} \rangle$, for each component in each section j, can then be evaluated by using the equation (2.50) at the collocation points in each subinterval as a function of θ. So, for the u_t point in the first finite element ($k = 1$),

$$\begin{aligned} c_{ij}(u_t) &= H_{t2}a_{ij,1} + H_{t3}a_{ij,2} + H_{t4}a_{ij,3} + H_{t1}aa_{ij} \\ \langle q_{ij} \rangle(u_t) &= H_{t1}b_{ij,1} + H_{t2}b_{ij,2} + H_{t3}b_{ij,3} + H_{t4}b_{ij,4} \end{aligned} \tag{2.68a}$$

for the u_t point, in the finite elements $k = 2$ to $k = NE - 1$,

$$\begin{aligned} c_{ij}(u_t) &= H_{t1}a_{ij,2k-2} + H_{t2}a_{ij,2k-1} + H_{t3}a_{ij,2k} + H_{t4}a_{ij,2k-1} \\ \langle q_{ij} \rangle(u_t) &= H_{t1}b_{ij,2k-1} + H_{t2}b_{ij,2k} + H_{t3}b_{ij,2k+1} + H_{t4}b_{ij,2k+2} \end{aligned} \tag{2.68b}$$

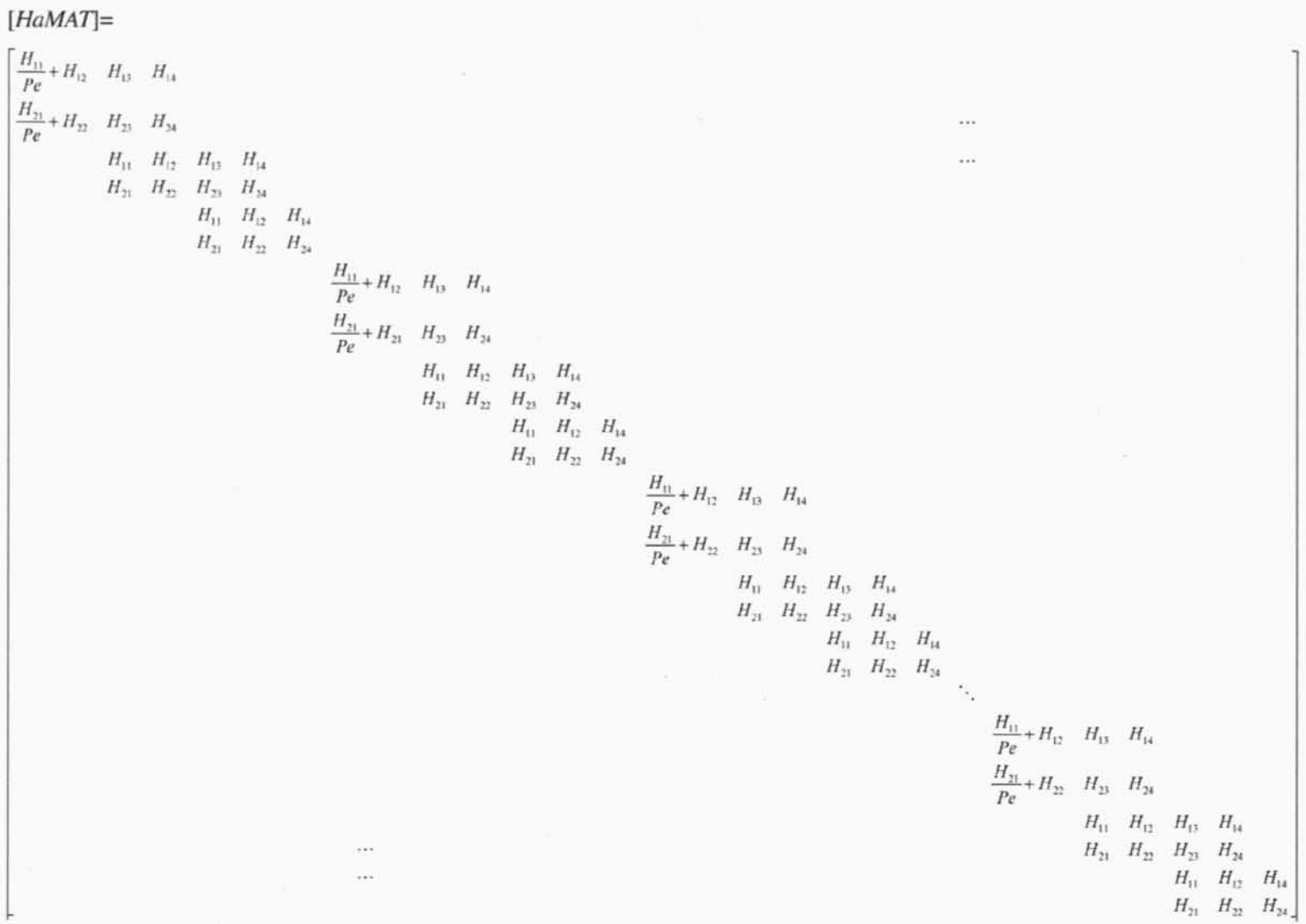

Figure 2.9 HaMAT *matrix representation considering three finite elements, NE=3, with two collocation points in each finite element.*

for the u_t point in the last finite element $(k=NE)$,

$$c_{ij}(u_t) = H_{t1}a_{ij,2NE-2} + H_{t2}a_{ij,2NE-1} + H_{t3}a_{ij,2NE} + H_{t4}a_{ij,2NE}$$
$$\langle q_{ij} \rangle (u_t) = H_{t1}b_{ij,2NE-1} + H_{t2}b_{ij,2NE} + H_{t3}b_{ij,2NE+1} + H_{t4}b_{ij+1,1} \qquad (2.68c)$$

The main program and the user written subroutines required for solving the specified PDAE system are presented in Appendix B.

2.2.5.3 Boundary-Value Problems for Ordinary Differential Equations

The software used for the solution of ODEs systems based on collocation was the COLNEW, described in Bader and Ascher, (1987). COLNEW is a modification of the package COLSYS (COLlocation for SYStems) described in Ascher *et al.* (1981). The FORTRAN-written code COLNEW has proved to be competitive with the other robust software for solving BVP's and to be particularly effective for difficult problems. It uses piecewise polynomial collocation at Gaussian points to determine the solution of the mixed-order system of equations multipoint boundary-value problems (BVP's).

Consider a mixed-order of *ncomp* nonlinear differential equations of orders $1 \le m_1 \le m_2 \le \ldots \le m_{ncomp} \le 4$,

$$y_i^{(m_i)}(x) = f_i\left(x; s(y)\right) \qquad a \le x \le b, \quad i = 1, \ldots, ncomp \qquad (2.69)$$

where m_i is the order of the i differential equation; $y(x) = \left(y_1(x), \ldots, y_{ncomp}(x)\right)^T$ is an isolated solution vector; and $s(y) = \left(y_1, y_1', \ldots, y_1^{(m_1-1)}, y_2, \ldots, y_{ncomp}, \ldots, y_{ncomp}^{(m_{ncomp}-1)}\right)^T$ is the vector of unknowns that would result from converting (2.69) to a first-order system. The result is subject to $m^* = \sum_{i-1}^{ncomp} m_i$ nonlinear multipoint separated boundary conditions

$$g_j\left(\zeta_j; s(y)\right) = 0 \qquad j = 1, \ldots, m^* \qquad (2.70)$$

where ζ_j is the location of the j^{th} boundary condition, $a \le \zeta_1 \le \zeta_2 \le \ldots \le \zeta_{m^*} \le b$.

To solve equations (2.69)-(2.70) numerically, we apply collocation at Gaussian points, using piecewise polynomial functions. If π is a partition of $[a, b]$

$$\begin{cases} \pi: a = x_1 < x_2 < \ldots < x_{NE} < x_{NE+1} = b \\ H_k = (x_k, x_{k+1}),\ h_k = x_{k+1} - x_k,\ k = 1, \ldots, NE \\ h = \max\limits_{1 \le k \le NE} h_k \end{cases} \tag{2.71}$$

and $P_{d,\pi} = \{u | u$ is a polynomial of order d (degree $< d$) on $H_k,\ k = 1, \ldots, NE\}$, then we seek an approximate solution $u = (u_1, \ldots, u_{ncomp})$ such that $u_i \in P_{d+m_i,\pi} \cap C^{(m_i-1)}[a, b]$, $i = 1, \ldots,$ *ncomp* or $u \in P_{d+m,\pi} \cap C^{(m-1)}[a, b]$. We require $d \geq m_i$, where d is the number of collocation points per subinterval.

The matrix problem is solved using an efficient implementation of Gaussian elimination with partial pivoting, developed by deBoor and Weiss (1980), and nonlinear problems are handled by use of a modified Newton method. Algorithms are included for estimating the error, and for mesh refinement. A redistribution of mesh points is automatically performed to roughly equidistribute the error.

The COLNEW was used to solve the system defined by (2.31), (2.32) with initial and boundary conditions (2.34), (2.35). This system defines an ODE since (2.33), the adsorption equilibrium isotherm, was inserted into the mass balance equations (2.31) and (2.32). The main program and the user written subroutines required for solving the specified ODE system are presented in Appendix C. The final size of the ODE system to be solved is of dimension 448 (2 differential equations × 2 components × 4 sections × 14 finite elements × 2 interior collocation points) as illustrated in Table 2.6.

The Table 2.6 also indicates the tolerance on the solution and derivative values considered. An example of the steady-state internal concentration profiles obtained under operating conditions properly chosen can be see in Figure 2.12b and in Table 2.9 the final results for the performance parameters obtained.

Table 2.6 *Relevant parameters for the four packages used.*

Code Name	Spatial Discretization	Time Integrator	Tolerance	System Dimension[c]
PDECOL	Collocation; B-splines basis	Gear's method	10^{-7}	448
DASSL	Collocation; Hermite cubic basis[a]	backward differentiation	10^{-7}	464/688[b]
COLNEW	modified B-splines basis	--	10^{-8}	448
COLDAE	collocation at Gaussian points; Runge-Kutta-monomial basis	--	10^{-8}	672

[a] provided by the user.
[b] isotherm equation included into the differential equation/work separately.
[c] These values depend on the number of finite elements considered.

2.2.5.4 Parabolic Partial Differential Equations

PDECOL, developed by N. K. Madsen of Lawrence Livermore Laboratory and R. F. Sincovec of Kansas State University (Madsen and Sincovec, 1979), is a package to solve numerically systems of nonlinear partial differential equations (NPDEs) in one space and one time dimension. It is based on the method of lines and implements finite element collocation methods, with B-splines as basis functions (de Boor, 1978), for the spatial discretization. The collocation procedure reduces the PDE system into an initial-value ODE system, which is solved with a time integrator derived from GEARIB (Hindmarsh, 1976) include in the PDECOL code. The time integration process is then accomplished by use of slightly modified standard techniques for the time dependent partial differential equations.

PDECOL solves general system of NPDEs of at most second order, on the interval $\left[x_L, x_R\right]$ for $t \geq t_0$ which is of the form,

$$\frac{\partial y}{\partial t} = f\left(t, x, y, y_x, y_{xx}\right) \tag{2.72}$$

$$y = \left(y_1, y_2, \ldots, y_{NPDE}\right)$$

where $$y_x = \left(\frac{\partial y_1}{\partial x}, \frac{\partial y_2}{\partial x}, \ldots, \frac{\partial y_{NDPE}}{\partial x}\right) \tag{2.73}$$

$$y_{xx} = \left(\frac{\partial^2 y_1}{\partial x^2}, \frac{\partial^2 y_2}{\partial x^2}, \ldots, \frac{\partial^2 y_{NPDE}}{\partial x^2}\right)$$

Each y_i is a function of the scalar quantities t and x ($i = 1, 2, \ldots, NPDE$), f represents an arbitrary vector valued function whose $NPDE$ components define the respective partial differential equations of the PDE system.

Depending on the particular type of equation, 0, 1 or 2 boundary conditions may be required for each equation in the system, imposed at x_L and/or x_R, of the form,

$$b(y, y_x) = \gamma(t) \tag{2.74}$$

where b and γ are arbitrary vector valued functions with $NPDE$ components and y, y_x and t are as above.

Each solution component y_k is assumed to be a known function of x at the initial time $t = t_0$ That is,

$$y_k(t_0, x) = \phi_k(x) \qquad k = 1, 2, \ldots, NPDE \tag{2.75}$$

where each $\phi_k(x)$ is a known function of x. The initial condition functions must be consistent with the boundary conditions (*i.e.*, the initial condition functions must satisfy the boundary condition for $t = t_0$).

The PDECOL was used to solve the system defined by (2.26), (2.27) with initial and boundary conditions (2.29), (2.30). This system defines a PDE since (2.29), the adsorption equilibrium isotherm, was inserted into (2.26) and (2.27), the corresponding mass balance equations. The main program and the user written subroutines required to solve the specified PDE system, is presented in Appendix D. The dimension of the initial-value ODE system, result of the spatial discretization by orthogonal collocation on finite elements, to be solved is 448 (16 differential equations × 14 finite elements × 2 interior collocation points) as is specified in Table 2.6, as the tolerance on the solution and derivative values considered. An example of the steady-state internal concentration profiles obtained under operating conditions properly chosen is very similar to the one obtained by using the COLNEW, Figure 2.12a and Table 2.9 the final results for the performance parameters obtained.

Notice that for this case, the finite elements considered have different length depending of the proximity to the end points. The finite elements near the end points are the ones with small length due the proximity to the connection points between different sections. In Figure 2.8 we can see the distribution of the collocation points in each different finite element.

2.3 Simulation Results and Discussion

Computer simulations were carried out to allow the estimation of the transient and steady-state concentration profiles of the glucose/fructose separation system, and to verify the effect of the strategy chosen to solve the model, in the final results. The model, as described in Table 2.4, was solved using the four packages previously mentioned, PDECOL, DASSL, COLNEW and COLDAE.

In all the simulations, the polynomials used were of order 3 and the tolerance, on the time integrator, set as described in Table 2.6. For the discretization of the spatial variable, the mesh used, except for DASSL, is illustrated in Figure 2.8. In this case a simple discretization mesh was used, that is, for the spatial discretization the number of finite elements was $NE = 4$ or 8, for the same number of interior collocation points. Decreasing the number of finite element corresponds to the decrease of the number of final ODEs to be solved by the integrator DASSL. The run time also decreases for the same maximum error criteria defined by the user, and considered equal to 0.01 for all the four packages. The error criteria is defined as the global error *er* (Pais, 1999):

$$er = er_E + er_R + er_A + er_B \tag{2.76a}$$

where er_E and er_R are the relative errors of the average concentration of the two components in the extract and in the raffinate, respectively, for two successive iterations; er_A and er_B are the relative errors between the amount of the less and the more retained component, respectively, that enters in the feed and leaves the system in the extract and raffinate streams:

$$er_E = \frac{\left|\overline{c}^A_{E_i} - \overline{c}^A_{E_{i-1}}\right|}{\overline{c}^A_{E_i}} + \frac{\left|\overline{c}^B_{E_i} - \overline{c}^B_{E_{i-1}}\right|}{\overline{c}^B_{E_i}}, \tag{2.76b}$$

$$er_R = \frac{\left|\overline{c}^A_{R_i} - \overline{c}^A_{R_{i-1}}\right|}{\overline{c}^A_{R_i}} + \frac{\left|\overline{c}^B_{R_i} - \overline{c}^B_{R_{i-1}}\right|}{\overline{c}^B_{R_i}}, \tag{2.76c}$$

$$er_A = \frac{\left|Q_F c^A_F - \left(Q_X \overline{c}^A_X + Q_R \overline{c}^A_R\right)\right|}{Q_F c^A_F}, \tag{2.76d}$$

$$er_B = \frac{\left|Q_F c^B_F - \left(Q_X \overline{c}^B_X - Q_R \overline{c}^B_R\right)\right|}{Q_F c^B_F}. \tag{2.76e}$$

The operating conditions and model parameters used in the simulation of the TMB are listed in Table 2.7. The operating conditions were estimated by the method developed by Ruthven and Ching (1989), considering the equilibrium theory, linear isotherms, and a safety parameter $\beta = 1.2$. All simulations were run in a Pentium II 300 MHz.

Table 2.7 *Operating conditions and models parameters used in the simulations of the TMB/SMB system, for the two models.*

Model Parameters	**Operating conditions**	**Columns**
SMB:	SMB:	SMB:
Pe = 2000	Feed conc. =30 g/l each	D_c =2.6 cm
$(1-\varepsilon)/\varepsilon = 1.5$	$t^* = 105$ s	$L_c = 11.5$ cm
α_{ij}= 3.15 (or $k_i = 0.01$ s^{-1})	$Q_{Rec} = 19.43$ ml/min[a]	Configuration: 3-3-3-3
K_{Gl}=0.314[b] K_{Fr}=0.625[b]	$Q_D = 10.22$ ml/min[a]	$L_j = 34.5$ cm
TMB:	$Q_E = 7.81$ ml/min[a]	
$\gamma_1 = 1.1246$ $\gamma_2 = 0.5649$	$Q_F = 3.02$ ml/min[a]	
$\gamma_3 = 0.7813$ $\gamma_4 = 0.3922$	$Q_R = 5.43$ ml/min[a]	

[a] values estimated by the method developed by Ruthven and Ching (1989).
[b] values measured at our laboratory.

Figure 2.10 shows the transient internal concentration profiles solutions for the two components for the T-TMB, under the conditions as described in Table 2.7, obtained by using the package PDECOL, (a), and obtained by using the package DASSL, (b), for cycle 1, 2 and 10, respectively. Different internal concentration profiles are obtained for the cycle 1, by using PDECOL and DASSL. After this cycle, the differences vanish. In cycle 2 and cycle 10, the solutions are very similar for both packages.

Figure 2.11 shows the steady-state internal concentration profiles solutions for the T-TMB, for the case study under the conditions in Table 2.7, obtained by using the four packages, PDECOL, (a), DASSL, (b), COLNEW, (c), and COLDAE, (d). Regardless the numerical package used, similar profile is obtained when the system reaches the steady-state, as expected. Although PDECOL and DASSL solve the TMB transient model, the steady-state solution, that obtained as $t \rightarrow \infty$, should be the same as that given by the ODE/DAE solvers, under the same conditions.

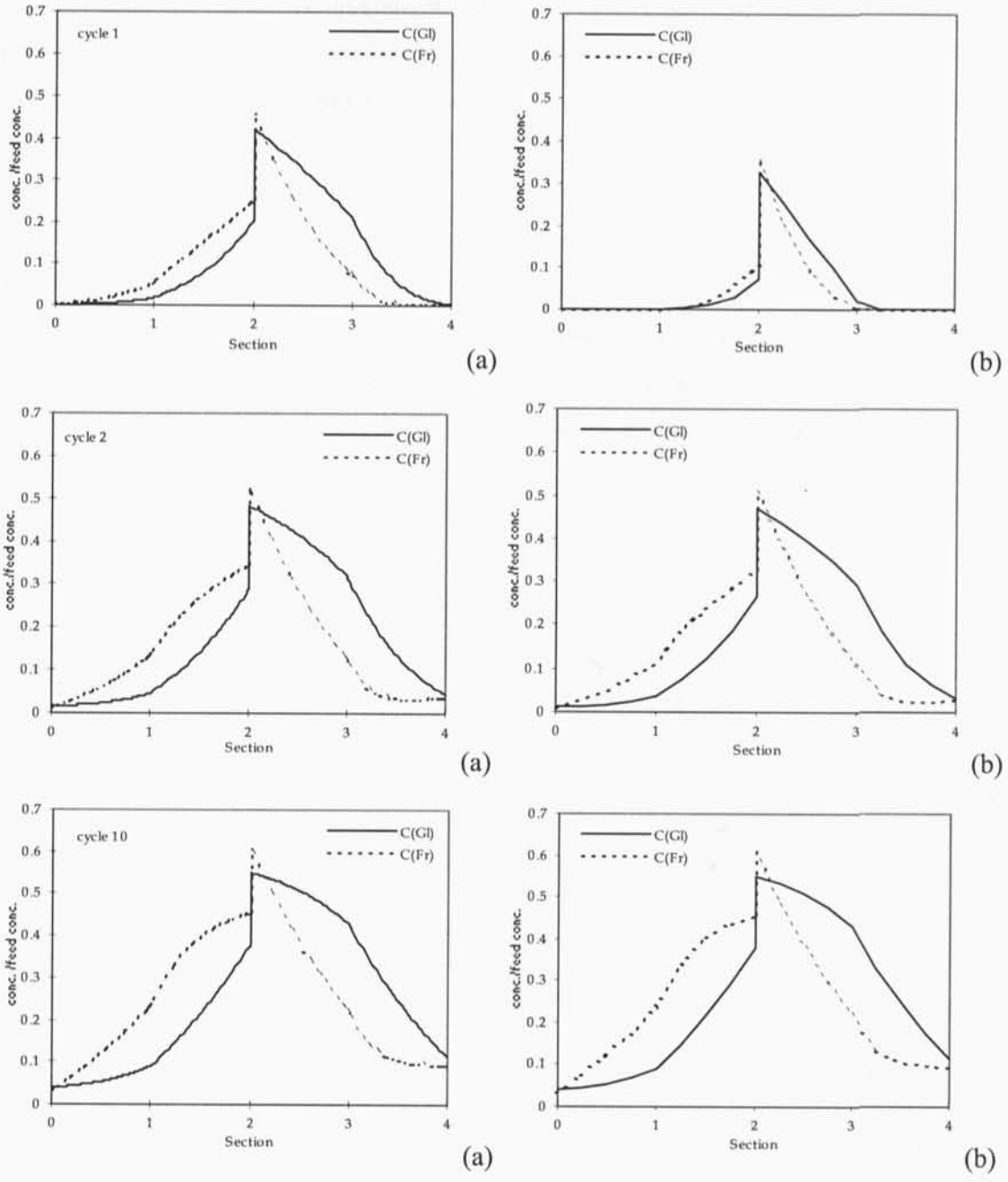

Figure 2.10 *Transient T-TMB internal concentration profiles for the TMB, under conditions described in Table 2.7, obtained by using the PDECOL, (a), and by using the DASSL, (b), for cycles 1, 2 and 10.*

Table 2.9 summarizes the final results for the performance parameters obtained by using the four different packages in the resolution of the mathematical model, as the corresponding run time consumed.

The performance parameters values obtained by using the PDECOL and DASSL, for the T2.7 case, in the resolution of mathematical model, are similar. Also, no significant differences are obtained, in the performance parameters values obtained by using the two ODE solvers, COLDAE and COLNEW. Figure 2.13(a) compares the internal concentration profile solutions obtained by the two PDE solvers. It can be seen that no significant differences in the internal concentration profiles were obtained for the two solvers. In the solution obtained by using the DASSL package, the mass balance is verified with an error of 0.7% for both components; for PDECOL the mass balance is verified with an error ≈0.05% for both components. These errors took into account the concentrations values in each of the four nodes, as shown in Table 2.10, under the conditions described in Table 2.7.

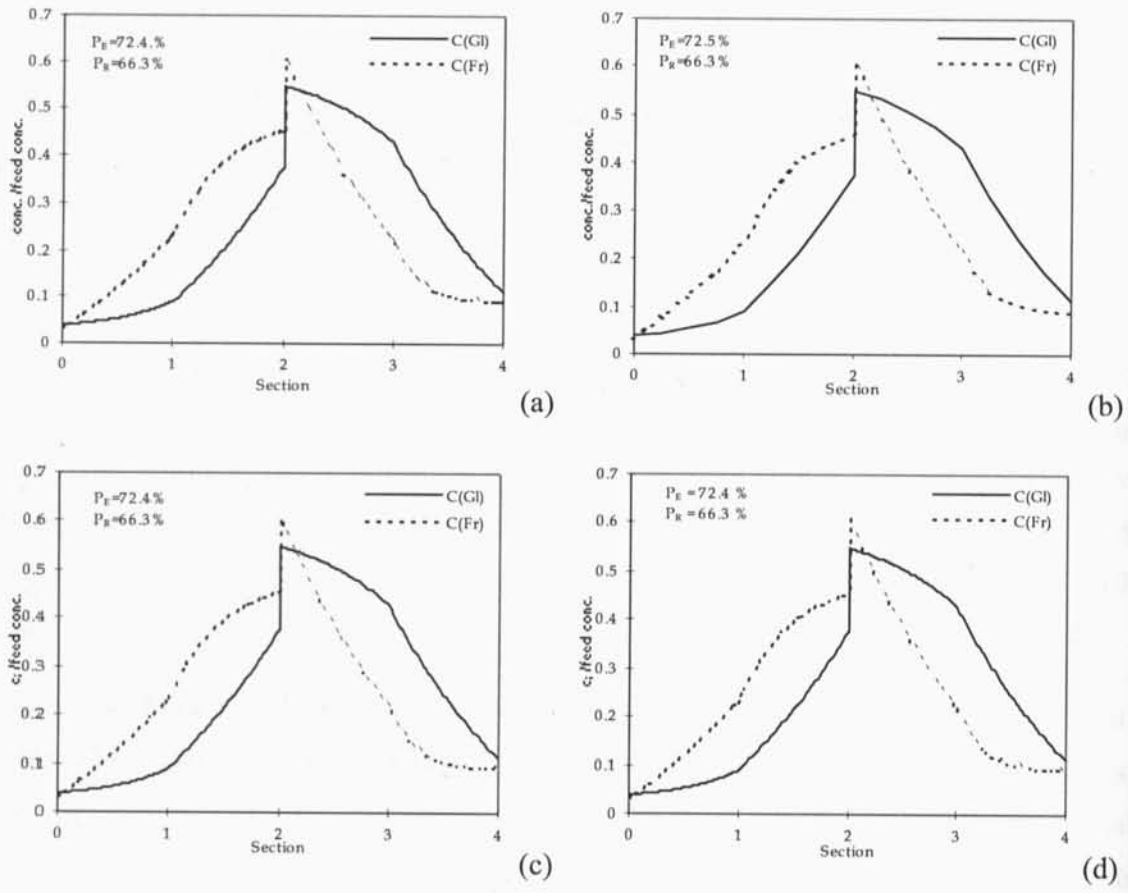

Figure 2.11 *Steady-state T-TMB internal concentration profiles solutions, under conditions described in Table 2.7, obtained by using the PDECOL, (a), DASSL, (b), COLNEW, (c), and COLDAE, (d).*

It can be seen that it is possible to obtain higher purity and recovery performances by increasing the length of each column, that is, by increasing the size of each section. Doing this, two model parameters, the mass transfer unit, α_{ij}, and the switching time, t^*, are also increased, as described in Table 2.8.

Table 2.8 *New operating conditions and models parameters used in the simulations of the TMB/SMB system, for the two models, to obtain higher purity and recovery performances.*

Model Parameters	**Operating conditions**	**Columns**
SMB:	SMB:	SMB:
$\alpha_{ij} = 8.21$ (or $k_i = 0.01\ s^{-1}$)	$T^* = 273.6$ s	$D_C = 2.6$ cm
TMB:		$L_C = 30.0$ cm
$\gamma_1 = 1.1221$ $\gamma_2 = 0.5631$		Configuration: 3-3-3-3
$\gamma_3 = 0.7793$ $\gamma_4 = 0.3970$		$L_j = 90.0$ cm

Steady-state solutions obtained are similar, regardless the numerical package used, as expected, Figure 2.12. The performance parameters values obtained by using the two ODE solvers, COLDAE and COLNEW, are similar as shown in Table 2.9 case T.2.8. The purity and recovery performance parameters obtained by using DASSL, in the resolution of mathematical model, are also similar to the ones obtained by the use of the others three packages. Figure 2.13(b) compares the internal concentration profile solutions obtained by the two PDE solvers, PDECOL and DASSL. The solution obtained by using the DASSL package, despite verifying the error criteria, the concentration balance it is not entirely verified; 0.7% obtained for glucose and 0.8% obtained for fructose, for PDECOL 0.04% and 0.1% for glucose and fructose, respectively. These errors took into account the concentration values in each of the four nodes, as shown in Table 2.10, under the conditions described in Table 2.8.

Table 2.9, summarizes the final results for the performances parameters obtained by using the four different packages in the resolution of the mathematical model, as the run time consumed with the new operating conditions. The value of tolerance and the number of finite elements considered in the four packages were similar to the values described in Table 2.6.

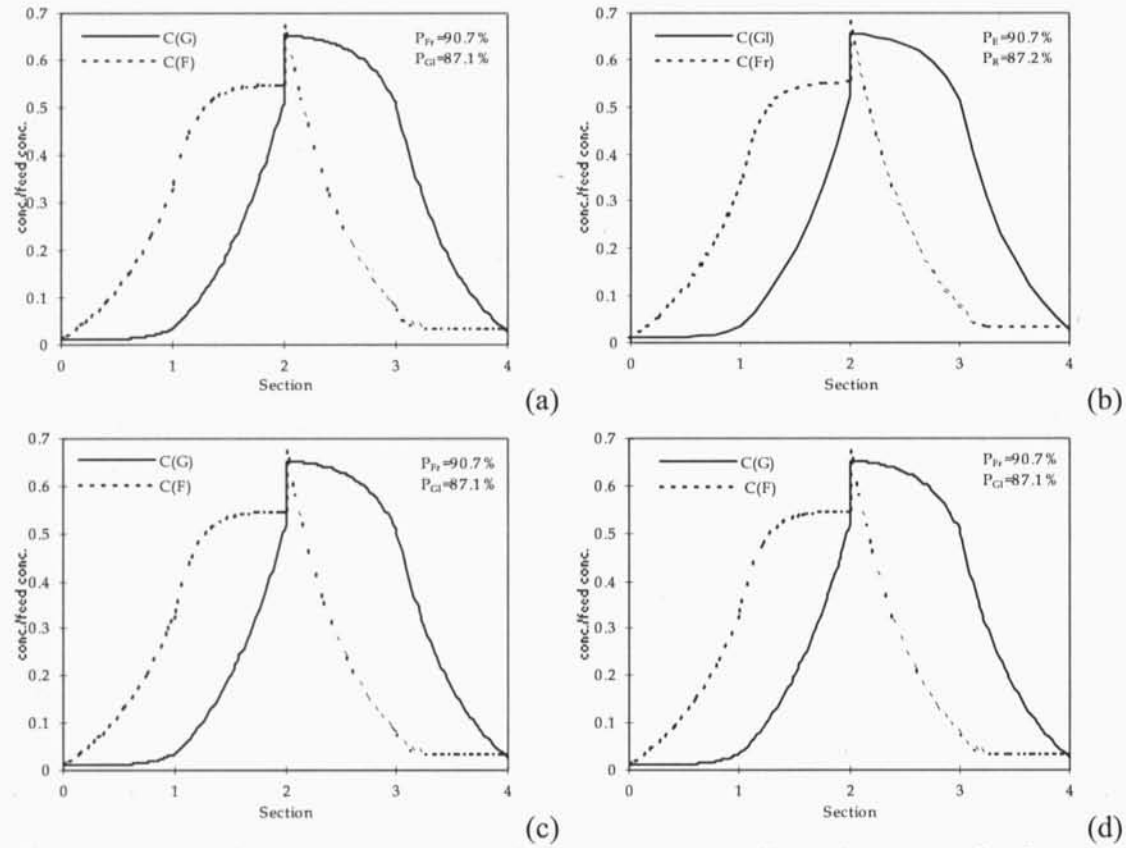

Figure 2.12 *Steady-state T-TMB internal concentration profiles solutions, under the new conditions described in Table 2.8, obtained by using the PDECOL, (a), DASSL, (b), COLNEW, (c), and COLDAE, (d).*

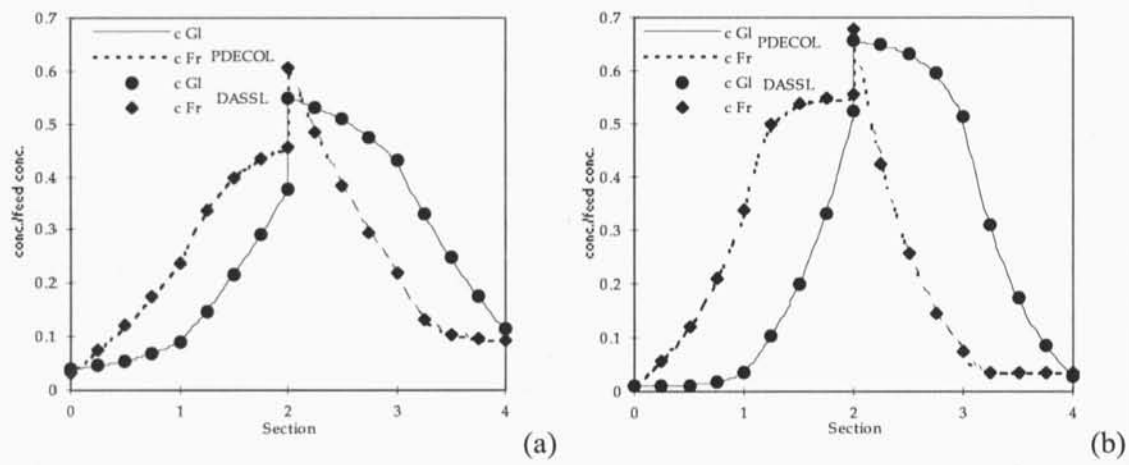

Figure 2.13 *Steady-state internal concentration profiles for the TMB, (a) under conditions described in Table 2.7, (b)) under the new conditions described in Table 2.8, obtained by using the PDECOL (straight and dash lines) and DASSL (• and ♦ points).*

Table 2.9 *Final results for the performance parameters obtained by using the four different packages in the resolution of the mathematical model, as the run time needed. T. 2.7 and T. 2.8 conditions described in Table 2.7 and Table 2.8, respectively. The values in brackets correspond to the values obtained by considering lower number of finite elements, for the case of using the DASSL.*

	PDECOL		DDASSL		COLNEW		COLDAE	
Operating conditions	**T 2.7**	**T 2.8**	**T 2.7**	**T 2.8**	**T 2.7**	**T 2.8**	**T 2.7**	**T 2.8**
P Fr (%)	72.4	90.7	72.5	90.7	72.4	90.7	72.4	90.7
P Gl (%)	66.3	87.1	66.3	87.2	66.3	87.1	66.3	87.1
R Fl (%)	61.0	86.6	61.4	87.7	60.9	86.5	60.9	86.5
R Gl (%)	76.9	91.1	77.3	91.9	76.8	91.1	76.8	91.1
S Fr (l/g)	0.240	0.169	0.238	0.166	0.240	0.169	0.240	0.169
S Gl (l/g)	0.190	0.160	0.189	0.159	0.190	0.160	0.190	0.160
Pr Fl (g/hr lS)	7.39	4.110	7.59	4.150	7.530	4.10	7.529	4.10
Pr Gl (g/hr lS)	9.504	4.132	9.564	4.350	9.501	4.320	9.501	4.320
Run Time (min)	108	56	>120 (3)	>120 (5)	0.26	0.47	0.20	0.12
NE	14		14 (6)		14		14	
Tolerance, *tol*	10^{-7}		10^{-7}		10^{-8}		10^{-8}	
Global error, *er*	0.01		0.01		0.01		0.01	

Table 2.10 *Comparison between the relative concentrations values obtained for the two components, fructose and glucose, in the four nodes extract, feed, raffinate and eluent, obtained for the TMB, under conditions described in Table 2.7 and in Table 2.8, by using the PDECOL and DASSL . With these values the concentration balance can be verified.*

	T. 2.7				T. 2.8			
	PDECOL		DASSL		PDECOL		DASSL	
points	**Gl**	**Fr**	**Gl**	**Fr**	**Gl**	**Fr**	**Gl**	**Fr**
extract	0.090	0.236	0.090	0.237	0.034	0.335	0.034	0.339
feed	0.549	0.605	0.550	0.607	0.522	0.549	0.524	0.554
raffinate	0.427	0.217	0.430	0.218	0.507	0.075	0.511	0.074
eluent	0.112	0.092	0.113	0.093	0.029	0.034	0.029	0.034

2.4 Conclusions

The models used to predict the transient and steady-state performance of the SMB were described based on the analogy with the TMB. A well known test system was considered for SMB operation: the glucose/fructose separation. The algebraic equation corresponding to the adsorption equilibrium isotherm is usually substituted in the others model equations, defining a system of partial differential equations (PDEs) and ordinary differential equations (ODESs) for the transient and the steady-state situation, respectively. However, this algebraic equation can be kept as independent defining a system of partial differential-algebraic equations (PDAEs) and differential-algebraic equations (DAEs) for transient and steady-state situations, respectively. Four available software packages were used to solve the four models presented: PDECOL and COLNEW for PDEs and ODEs, respectively, and DASSL and COLDAE for PDAEs and DAEs, respectively. Independently of the model type and the related numerical package, the TMB separation system was efficiently simulated, under properly selected conditions. The steady-state models can be used for a preliminary estimation of the concentration profiles and the performance parameters with less computational time. With the transient model, the user can have an exact representation of the evolution of internal concentration profiles through the time period and estimate how long the operation of an actual plant would take to reach the steady-state. Working with the adsorption equilibrium isotherm separately allows easy changes on the algebraic relationship and subsequent study.

The run time, for the system of DAEs, is slightly lower than that taken by the ODEs systems. However, the opposite situation occurs for the partial differential equations. The system of PDAEs needs more run time to be solved than the PDE system, for the same conditions for both types of systems. If we considered, for the system of PDAEs, a different domain subdivision into a small number of finite elements, we obtain similar results in less run time, with the same tolerances; however, we must be careful to confirm if the final results verify the mass balance.

2.5 References

Ascher U., J. Christiansen, R. D. Russell, (1981) *Collocation Software for Boundary-Value ODEs*, ACM Trans. Math Software **7**, 209-222.

Ascher U., and L. Petzold, (1991) *Projected Implicit Runge-Kutta Methods for Differential-Algebraic Equations*, SIAM J. Num. Anal. **28**, 1097-1120.

Ascher U. M., and R. J. Spiteri, (1994) *Collocation Software for Boundary Value Differential-Algebraic Equations*, SIAM J. Sci. Comput. **15**, 938-952.

Azevedo D. C. S., and A. E. Rodrigues, (1998) *Bi-Linear Driving Force Approach in the Simulation of Adsorptive Separation Processes: Application to Fixed and Simulated Moving Bed*, Proc. of CHEMPOR'98, Vol. II 849-856.

Bader G. and U. Ascher, (1987) *A New Basis Implementation for a mixed Order Boundary Value ODE Solver*, SIAM J. Scient. Stat. Comput. **8**, 483-500.

de Boor, C., and B. Swartz, (1973) *Collocation at Gaussian Points*, SIAM J. Numer. Anal. **10**, 582-606.

Brenan K., S. Campbell, L. Petzold, (1989) *Numerical Solution of Initial-Value Problems in Differential-Algebraic Equations*, Elsevier, New York.

Broughton, D. B., and C. G. Gerhold, (1961) *Continuous Sorption Process employing Fixed Bed of sorbent and Moving Inlets and Outlets*, U.S. Patent Nº. 2985589.

Broughton, D. B., (1968) *Molex: Case History of a Process*, Chem. Eng. Prog. **64**, 60-65.

Broughton, D. B., R. W. Neuzil, J. M. Pharis, C. S. Brearley, (1970) *The Parex Process For Recovering Paraxylene*, Chem. Eng. Prog. **66**, 70-75.

Carey, G. F., and B. A. Finlayson, (1975) *Orthogonal collocation on finite elements*, Chem. Engng. Sci. **30**, 587-596.

Ching C. B., D. M. Ruthven, K. Hidajat, (1985) *Experimental Study of a Simulated Counter-Current Adsorption System - III. Sorbex Operation*, Chem. Engng. Sci. **40**, 1411-1417.

Ching C. B., C. Ho, K. Hidajat, D. M. Ruthven, (1987) *Experimental Study of a Simulated Counter-Current Adsorption System - V. Comparation of Resin and Zeolite Adsorbents for Fructose-Glucose Separation at High Concentration*, Chem. Engng. Sci. **42**, 2547-2555.

Davis, E. M., (1984) *Numerical Methods and Modeling for Chemical Engineers*, John Wiley & Sons, Inc., New York.

Finlayson, B. A., (1980) *Nonlinear Analysis in Chemical Engineering*, McGraw-Hill Int. Book Company, New York.

Gattuso M. J., McCulloch B., House D. W., Baumann W. M., Gottschall K., (1996) *Simulated Moving Bed Technology - The Preparation of Single Enantiomer Drugs,* Pharmaceutical Technology Europe **8**, 20-25.

Guest, W. B., (1997) *Evaluation of Simulated Moving Bed Chromatographic for Pharmaceutical Process Development*, J. Chromatogr. A **760**, 159-162.

Hashimoto, K., S. Adachi, H. Noujima, A. Maruyana, (1983) *Models for the Separation of Glucose/Fructose Mixture using a Simulated Moving-Bed Adsorber*, J. Chem. Eng. Japan. **16**, 400-406.

Hashimoto, K., S. Adachi, Y. Shirai, M. Morishita, (1993) *Operation and Design of Simulated Moving-Bed Adsorbers*, in Preparative and Production Scale Chromatography, Edts. Ganetsos and Barker **61**, 273-299.

Hidajat, K., C. B Ching., D. M. Ruthven, (1986) *Numerical Solution of a Semi-Continuous Counter-Current Adsorbent Unit for Fructose-Glucose Separation*, Chem. Eng. J. **33**, B55-B61.

Hindmarsh A., (1976) *Preliminary Documentation of GEARIB - Solution of Implicit Systems of Ordinary Differential Equations with Banded Jacobian*, Report UCID-30130, Lawrence Livermore Laboratory.

Leão C. P., L. S. Pais, M. Santos, A. E. Rodrigues, (1997) *Simulated Moving Bed Adsorptive Reactor*, 2nd International Conference on Process Intensification in Practice, Edited by J. Semel, 143-155.

Liskovets, O. A., (1965) *The Method of Lines*, J. Diff. Eqs. **1**, 1308-1321.

Madsen N. K., R. F. Sincovec, (1979) *PDECOL: General Collocation Software for Partial Differential Equations*, ACM Trans. Math. Software **5**, 326-351.

Mazzotti M., G. Storti, M. Morbidelli, (1997) *Optimal Operation of Simulated Moving Bed Units for Non Linear Chromatography Separations*, J. Chromatogr. A **769**, 3-24.

Nicoud R. M., (1995) *The Simulated Moving Bed: A Powerful Chromatography Process*, LC-GC INTL **5**, 43-47.

Nicoud, R. M., (1997) *Recent Advances in Industrial Chromatographic Process*, In Recent Advances in Industrial Chromatographic Process, 15 May, Nancy, France.

Pais, L. S., J. M. Loureiro, A. E. Rodrigues, (1997a) *Separation of 1,1'-bi-naphthol enantiomers by Continuous Chromatography in Simulated Moving Bed*, Chem. Engng. Sci. **52**, 245-257.

Pais, L. S., J. M. Loureiro, A. E. Rodrigues, (1997b) *Modeling, Simulation and Operation of a Simulated Moving Bed Operation for Chromatographic Separation of 1,1'-bi-naphthol enantiomers*, J. Chromatogr. A **769**, 25-35.

Pais, L. M. S., (1999) *Chiral Separation by Simulated Moving Bed Chromatography*, PhD dissertation, LSRE, University of Porto, Porto.

Pais, L. S., J. M. Loureiro, A. E. Rodrigues, (2000) *Chiral Separation by SMB Chromatography*, Separation and Purification Technology **20**, 67-77.

Petzold L., (1982a) *A Description of DASSL: A Differential/Algebraic System Solver*, Rep. Sand. 82-8637, Sandia National Laboratory, Livermore.

Petzold L., (1982b) *Differential/algebraic equations are not ODEs*, SIAM J. Sci. Stat. Comput. **3**, 367-373.

Ruthven D. M. and C. B. Ching, (1989) *Counter-Current and Simulated Moving Bed Adsorption Separation Process*, Chem. Engng. Sci. **44**, 1011-1038.

de Rosset A. J., R. W. Neuzil, D. B. Broughton, (1981) *Industrial Applications of Preparative Chromatography*, in A. E. Rodrigues and D. Tondeur (Eds.), Percolation Process: Theory and Applications, Sihjthoft & Noordhoff, 249-281.

Storti, G., M. Mazzotti, M. Morbidelli, S. Carra, (1993) *Robust Design of Binary Countercurrent Adsorption Separation Process*, AIChE J. **39**, 471-492.

Storti G., R. Baciocchi, M. Mazzotti, M. Morbidelli, (1995) *Design of Optimal Operating Conditions of Simulated Moving Bed Adsorptive Separation Units*, Ind. Eng. Chem. Res. **34**, 288-301.

Strube, J., and H. Schmidt-Traub, (1996) *Parameter Estimation for the Simulation of Fluid Chromatography*, Computers Chem. Engng. **20**, 5641-5646.

Zhong, G., and G. Guiochon, (1996) *Analytical Solution for the Linear Ideal Model of Simulated Moving Bed Chromatography*, Chem. Engng. Sci. **51**, 4307-4319.

Yun, T., G. Zhong, G. Guiochon, (1997) *Simulated Moving Bed under Linear Condition: Experimental vs. Calculated Results*, AIChE J. **43**, 935-945.

3. Modelling and Simulation of SMB Chromatography

In the first part of this chapter, the glucose/fructose separation is presented as the case study. Some simulation results, for different operating conditions, are presented by solving the four different mathematical models previously used, T-TMB (transient TMB) and S-TMB (steady-state TMB), with the corresponding software packages. The effect of operating parameters on the separation region is discussed. In a first approximation, linear adsorption isotherms for both components, glucose and fructose were considered. A combination of nonlinear (glucose) and linear isotherms (fructose) is considered in a second approach. The influence of the type of isotherms and mass transfer coefficient on the complete separation region is performed. In these two cases, the intraparticle mass transfer is described by a homogeneous LDF (linear driving force).

Using the TMB strategy, a new model for the mass transfer on porous particle (LDF porous) is introduced and compared with the LDF model for homogeneous particles. A SMB formulation with the LDF for porous particle is also presented. This last model allows the observation of product histories and the periodic character of the cyclic steady state. The test system used was the separation of bi-naphthol enantiomers.

3.1 The case of Gl/Fr Separation

3.1.1. Steady-State Simulation Results from T-TMB and S-TMB Models using LDF approximation for homogeneous particles

The case study, based on the values shown in Table 3.1 and numerical parameters in Table 3.2, was addressed by simulation using the two models, T-TMB and S-TMB. The flow rates were estimated using the equilibrium model for the TMB, described in the previous section, developed by Ruthven and Ching (1989), considering linear isotherms and using a safety parameter of $\beta = 1.2$.

The numerical parameters that were used and that must be specified to implement the four packages, are described in Table 3.2. In the four packages, no initial guess to the solution was provided. During the numerical resolution the packages COLNEW (Bader and Ascher, 1987) and COLDAE (Ascher and Petzold, 1991), control the number of subintervals, whereas in the PDECOL (Madsen and Sincovec, 1979) and DASSL (Petzold, 1982) this value was constant and equal to *NE*, initially specified by the user. The steady state is considered to be achieved when the global error, *er* (3.1), is less than a maximum error defined by the user.

The global error *er*, as previously defined by equation (2.76) in Chapter 2, is defined as

$$er = er_E + er_R + er_A + er_B \tag{3.1 a}$$

where, er_E is the relative error of the average concentrations of the two components in the extract for two successive iterations:

$$er_E = \frac{\left|\overline{c}^{A}_{E_i} - \overline{c}^{A}_{E_{i-1}}\right|}{\overline{c}^{A}_{E_i}} + \frac{\left|\overline{c}^{B}_{E_i} - \overline{c}^{B}_{E_{i-1}}\right|}{\overline{c}^{B}_{E_i}} \tag{3.1 b}$$

er_R is the relative error of the average concentrations of the two components in the raffinate for two successive iterations:

$$er_R = \frac{\left|\overline{c}^{A}_{R_i} - \overline{c}^{A}_{R_{i-1}}\right|}{\overline{c}^{A}_{R_i}} + \frac{\left|\overline{c}^{B}_{R_i} - \overline{c}^{B}_{R_{i-1}}\right|}{\overline{c}^{B}_{R_i}} \tag{3.1 c}$$

er_A is the relative error between the amount of the less retained component that enters (in the feed stream) and leaves (in the extract and raffinate streams) the system:

$$er_A = \frac{\left|Q_F c_F^A - \left(Q_X \bar{c}_X^A + Q_R \bar{c}_R^A\right)\right|}{Q_F c_F^A} \qquad (3.1\ d)$$

er_B is the relative error between the amount of the more retained component that enters (in the feed stream) and leaves (in the extract and raffinate streams) the system:

$$er_B = \frac{\left|Q_F c_F^B - \left(Q_X \bar{c}_X^B + Q_R \bar{c}_R^B\right)\right|}{Q_F c_F^B} \qquad (3.1\ e)$$

Table 3.1a *Operating conditions and model parameters for the base case study. The flow rates were estimated using the equilibrium model for the SMB, as in Zhong and Guiochon (1996).*

SMB operating conditions:	**TMB Model parameters:**	**Columns:**
Feed conc. = 50.0 g/l each	Solid/Fluid volumes, $(1-\varepsilon)/\varepsilon = 1.5$	$D_c = 2.6$ cm
$t^* = 120$ sec	Number of mass transfer units, $\alpha_{ij} = 36.0$ ($k_i = 0.1\ s^{-1}$)	$L_c = 10.5$cm
$Q_{Rec} = 18.12$ ml/min	Peclet Number, Pe_j=2000	Configuration:
$Q_D = 10.69$ ml/min	Ratio between fluid and solid velocities:	3, 3, 3, 3
$Q_E = 7.62$ ml/min	$\gamma_I = 1.5840$, $\gamma_{II} = 0.8996$,	$L_j = 31.5$ cm
$Q_F = 2.23$ ml/min	$\gamma_{III} = 1.0996$, $\gamma_{IV} = 0.6252$	
$Q_R = 5.30$ ml/min	Linear equilibrium isotherm[a]: $K_{GI} = 0.50$, $K_{Fr} = 0.88$	

[a]values at ambient temperature, 30° C, with Duolite cation exchange resin in its Ca^{2+} exchanged form as adsorbent, Ching *et al.*, 1985.

Table 3.1b *Equivalence between TMB and SMB flow-rates.*

Section	TMB		SMB	
	Q_j (ml/min)	γ_j	Q_j^* (ml/min)	γ_j^*
I	17.66	1.58	28.81	2.58
II	10.04	0.90	21.19	1.90
III	12.27	1.10	23.42	2.10
IV	6.97	0.62	18.12	1.62
t^* (min)	---		2.0	

Table 3.2 *Numerical parameters used in the four packages.*

	COLNEW	COLDAE	PDECOL	DASSL
Number of collocation points per interval	4	4	2	2
Number of subintervals in the initial mesh, NE	10	10	14	10
Error tolerance, TOL	10^{-8}	10^{-8}	10^{-7}	10^{-7}
Global error, *er*	0.01	0.01	0.01	0.01

The steady-state internal profiles obtained by using the PDECOL are shown in Figure 3.1a (full squares for fructose (Fr) and full circles for glucose (Gl)) and the steady-state internal profiles obtained by using the COLNEW package (white squares for fructose (Fr) and white circles for glucose (Gl)), for the case study. Solving the PDAE system by using DASSL and the DAE system by using COLDAE, the resulting steady-state internal profile solutions are shown in Figure 3.1b.

The results obtained in both cases, considering the adsorption equilibrium isotherm as an independent equation or not, are very similar. The initial aim of the simulation study is to compare the two models, T-TMB and S-TMB, which describe the TMB system. With the results obtained by the use of the four software tools, PDECOL and COLNEW, DASSL and COLDAE, it is possible to know which one to use depending on our interest. Since the exact solution is not known, the choice will be made by comparing the final steady-state solutions obtained for each of the four models.

No significant differences can be found between the obtained solutions, Figure 3.1. However, DASSL solutions obtained in sections II and III, are slightly higher than those obtained with the others packages, Figure 3.1b. The glucose concentration values obtained by using PDECOL, in the Extract and Raffinate points were 0.00028 and 0.42, respectively, and 0.292 and 0.00042, for fructose concentration values. The glucose concentration values obtained by using the COLNEW, in the Extract and Raffinate points were 0.00026 and 0.42, respectively, and 0.292 and 0.00042, for fructose concentration values. We can see that the global balance is verified with an error around 0.1%. In Table 3.3, these and the others obtained values, in the four nodes, can be found. The global balance is also verified when using COLDAE. By

using DASSL, the error on the global balance is around 2%. The fructose concentration obtained in the raffinate, was lower than the one obtained by using the others three packages.

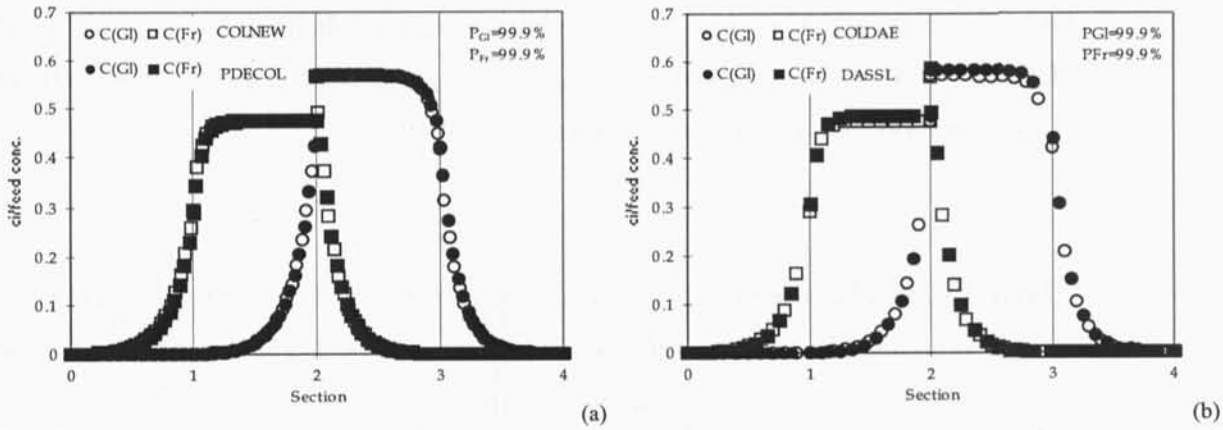

Figure 3.1 *Steady-state internal profiles for the case study under conditions described in Table 3.1 and 3.2, obtained by (a) using the PDECOL package and the COLNEW package, for the PDE/ODE system; and obtained by (b) using the DASSL package and the COLDAE package, for the PDAE/DAE system. Full squares and circles for fructose (Fr) and glucose (Gl), respectively, obtained with PDECOL/DASSL, and white squares and circles for fructose (Fr) and for glucose (Gl), respectively, obtained with COLNEW/COLDAE.*

Comparing the results of the performance parameters obtained in the steady-state solution and in the transient steady-state solutions, Table 3.3, we can see that no significant differences exist. Only the value of productivity obtained with DASSL is slightly higher than the values obtained by the others three packages. The computing time is lower when using the two ordinary differential solvers, COLNEW and COLDAE. DASSL needs more time to reach the steady-state solution, almost two hours. This behaviour was due to the fact that, to obtain the same precision in the solutions, it was necessary to increase the numbers of finite elements for the spatial discretization and therefore, increasing the dimension of the system to be solved in time.

Defining the relative and absolute error between the solutions obtained by the ordinary/algebraic equation solvers, O/As, and the partial algebraic/ordinary algebraic equation solvers, PA/OAs, solvers as,

$$\rho(\%) = \frac{\text{solution by O/As} - \text{solution by PA/OAs}}{\text{solution by O/As}} * 100 = \\ = \frac{\text{absolute error}}{\text{solution by O/As}} * 100 \qquad (3.2)$$

for each point, and applying to the previously results obtained by using COLNEW and PDECOL solvers, we obtained the graphs in Figures 3.2a and 3.2b. For COLDAE and DASSL we obtained the graphs in Figures 3.2c and 3.2d.

Table 3.3 *Relative concentration values obtained for the two components, Gl and Fr, in the four nodes: extract, feed, raffinate and eluent, and the T-TMB system performance parameters and run time obtained by using the four packages, for the case study.*

Relative Concentration [a]	COLNEW		PDECOL		DASSL		COLDAE	
	Gl	Fr	Gl	Fr	Gl	Fr	Gl	Fr
extract	0.00026	0.2920	0.00028	0.2920	0.00027	0.3000	0.00027	0.2900
feed	0.5700	0.5700	0.5700	0.5700	0.5800	0.5800	0.5700	0.5700
raffinate	0.4200	0.00042	0.4200	0.00042	0.4300	0.00031	0.4200	0.00042
eluent	0.00010	0.00026	0.00010	0.00026	0.00011	0.00027	0.00010	0.00026
Purity (%)	99.9	99.9	99.9	99.9	99.9	99.9	99.9	99.9
Recovery (%)	99.9	99.9	100.0	100.0	100.0	100.0	99.9	99.9
Solvent. Cons. (l/g)	0.116	0.116	0.115	0.115	0.112	0.113	0.116	0.116
Productivity (g/hr l)	16.65	16.65	16.69	16.77	17.20	17.03	16.65	16.65
Run Time (min)	0.30		30		124		0.13	

[a] Relative concentration defined as $c_i / c_{i,feed}$ with $c_{i,feed} = 50$ g/l.

Figure 3.2a shows that, the highest relative error is around 3%, close to the nodes. COLNEW, for this case study, gives a lower estimation of relative concentration comparing with the values obtained with PDECOL (Figure 3.2b), specially, in the estimation of Gl concentration, in section 3. The obtained relative error between COLDAE and DASSL solutions has a behaviour similar to the one obtained between COLNEW and PDECOL, Figure 3.2c. On the other hand, Figure 3.2d shows that, between COLDAE and DASSL, in certain points, the relative error reaches 30%. The Fr concentration near the raffinate node, takes very low

values, Figure 3.1, and small differences in the obtained solutions between both POAs solvers, can result in high relative error. COLDAE, for this case study, gives a lower estimation of relative concentration comparing with the values obtained by using DASSL, Figure 3.2d, in particular, in the Fr concentration values in section 2 and Gl concentration values in section 3.

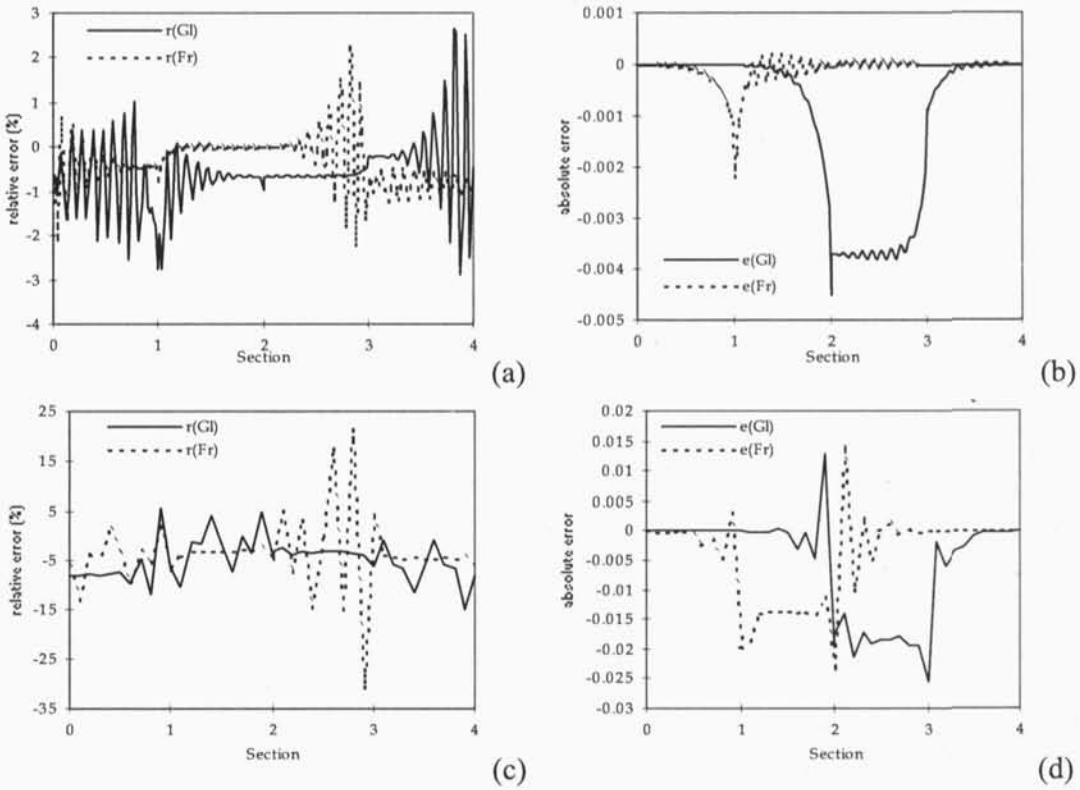

Figure 3.2 *Relative error,* ***(a)*** *and* ***(c)****, and absolute error,* ***(b)*** *and* ***(d)****, for the case study, comparing the obtained results using COLNEW / PDECOL, and COLDAE / DASSL, respectively.*

To study the effects of the operating variables on the SMB performance, only the steady-state results are important. Since no significant differences were obtained on the estimation of the final steady-state concentrations, by using the four packages, the choice took into account the run time needed.

3.1.2 Evolution of the internal profiles for transient operation of the TMB

With the PDECOL and DASSL packages, we solve the transient operating of the TMB. So, it is possible to evaluate the evolution of the transient internal profiles for the case study, under conditions described in Table 3.1 and 3.2. The internal profiles obtained, for cycles 1, 2, 3 and 10, are illustrated in Figure 3.3; (a) by using PDECOL and (b) by using DASSL.

One complete cycle corresponds to $\theta = 4$ ($\theta = t / (n_j \Delta t)$), where n_j is the number of columns in the section j, Δt is the time period, and t is the time of a complete cycle). Notice that for the study case, the number of columns per section is constant ($n_j = 3$).

We can observe that a small number of cycles is enough to reach the final steady state (cycle 10). As in the case study used in the previous section (section 2.3), the profiles obtained for cycle 1, by using PDECOL and DASSL, are different. However, that difference vanishes with the time, converging to identical solution.

In Figure 3.4 the evolution from cycle 1 up to cycle 10, of the transient internal profile for the TMB is shown for the reference case. The fronts of the less adsorbed component, glucose (full dots), moved until they reach the high value of purity, in zone III (zone defined by columns 6-9). The same occurs with the more retained component, fructose (white dots), which moves until they reach the high value of purity, in zone II (zone defined by columns 3-6). The two arrows in the figure show the way of evolution, one for each outlet stream.

All the results presented in the following sections are obtained with the COLNEW package since we are only concerned with the steady-state internal profiles.

3.1.3 Effect of operating variables

The effect of operating variables (rotation period, extract and feed flow rates, section length and number of intraparticle mass transfer) on the SMB/TMB performance is analysed. The SMB performance is characterised by purity, recovery, solvent consumption and adsorbent productivity, as described in the previous section. The effect of the operating variables on the system performance is analysed one at a time. The ranges considered, for each of the operating variables, are summarised in Table 3.4. For each case, the remaining operating conditions and model parameters were kept constants as previously described in Table 3.1.

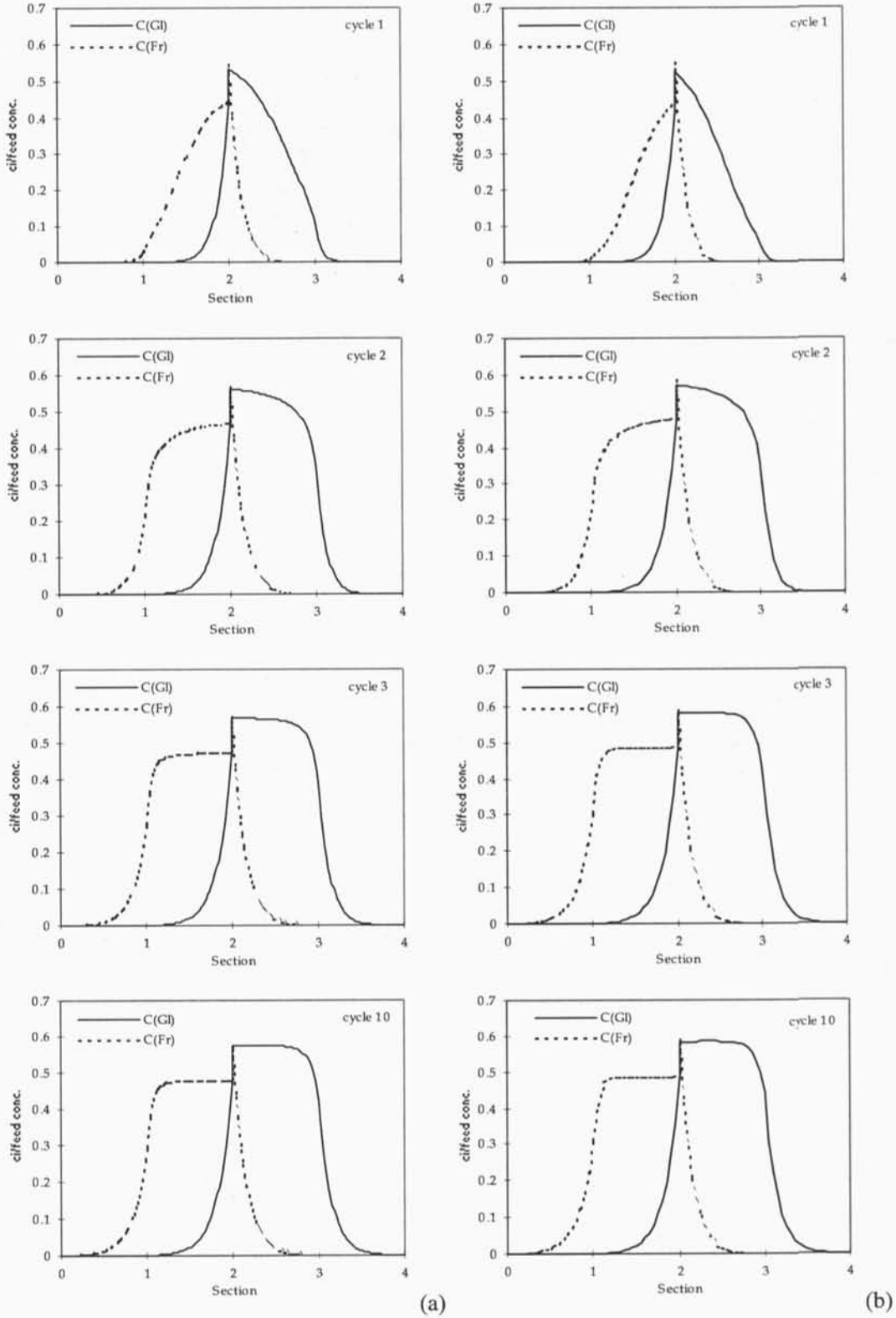

***Figure 3.3**. Transient TMB internal profiles for the case study under conditions described in Table 3.1 and 3.2, obtained by using PDECOL (a) and DASSL (b), for cycles 1, 2, 3 and 10.*

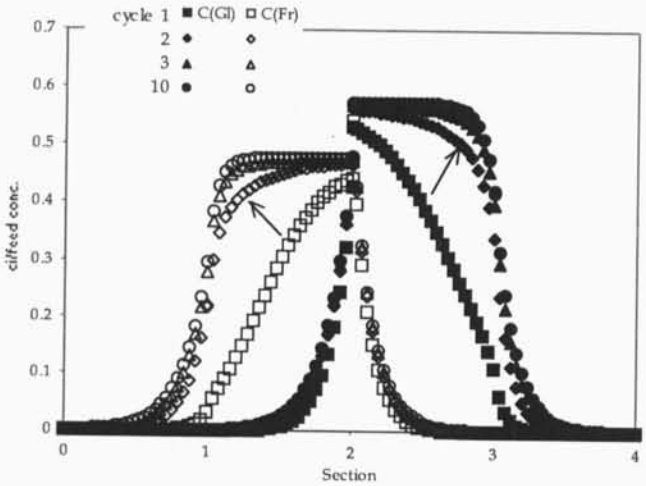

Figure 3.4. *Evolution of the transient internal profiles for the case study under conditions described in Table 3.1 and 3.2. Squares represent the internal profiles in cycle 1 and the circles the internal profiles in cycle 10, the diamonds and triangles represent the internal profiles for cycle 2 and 3, respectively (full, glucose and white, fructose). The two arrows show the way of the evolution, one for each outlet stream.*

Table 3.4 *Range of the operating variables for the study of the effect on the TMB performance. The others parameters are described in Table 3.1.*

Rotation period, t^*	106 - 136 *sec*
Extract flowrate, Q_E	3.62 - 11.62 *ml/min*
Feed flowrate, Q_F	0.23 - 8.23 *ml/min*
Total Balance[a] (total flow in=total flow out)	12.92 *ml/min*
Section lenght, L_j	10.5 *cm* -52.5 *cm*
intraparticle mass transfer rate, k	0.02 - 0.1 s^{-1}

[a] this value was kept constant in all the simulations.

3.1.3.1 Effect of the rotation period

The range of the rotation period used for the study of its effect on the system performance was $t^* \in [106,136] sec$. The other operating conditions were kept constants, Table 3.1. The results of the influence of the rotation period, t^*, on the system performance is shown in Figure 3.5. It can be seen that, for all the performance parameters, an optimum value of rotation period exists, $t^* \approx 120 sec$, where they hold the highest values (≈100%). For lower or higher rotation

period values, both extract and raffinate purity and recovery decrease. The rotation period is inversely proportional to the solid flow rate or directly proportional to the liquid recycling flow rate. So, changing the value of the liquid recycling flow rate instead of the rotation period we could obtain similar behaviour.

Another analysis could be made relating recovery with purity obtained for different values of rotation period. In Figure 3.6 that relationship can be seen. It is clear that it is possible to obtain simultaneously high purity and recovery in a TMB, although the region of high purity and recovery is narrow and must be very well chosen.

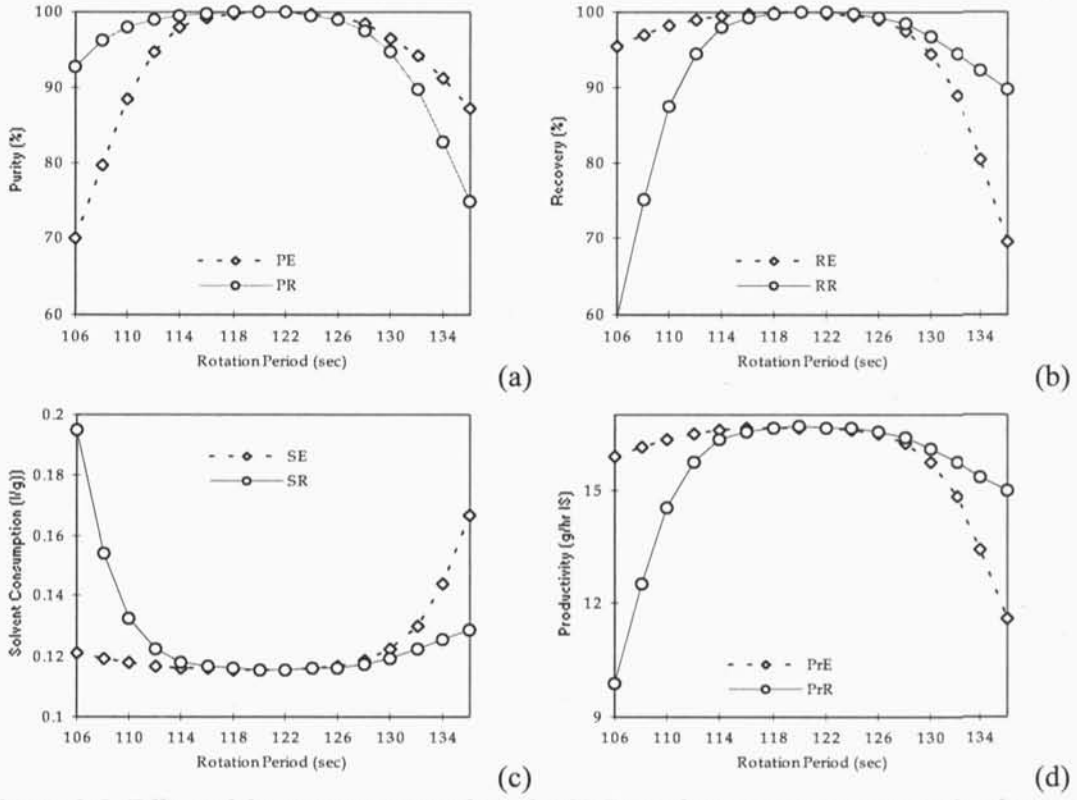

Figure 3.5 *Effect of the rotation period on the SMB performance parameters for the case study. The rotation period varied between 106 and 136 sec. The others operating conditions and model parameters were kept constant and the same as described in Table 3.1.* ***(a)*** *Rotation Period versus Purity,* ***(b)*** *Rotation Period versus Recovery,* ***(c)*** *Rotation Period versus Solvent Consumption,* ***(d)*** *Rotation Period versus Productivity.*

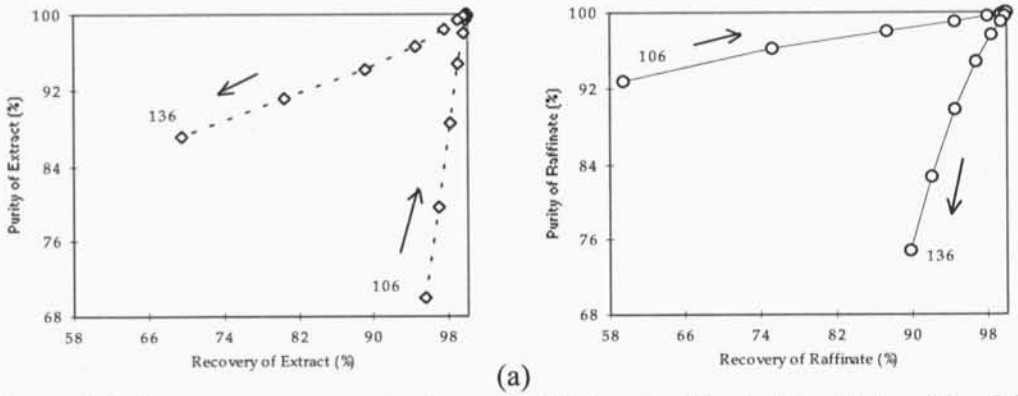

Figure 3.6 *Recovery versus purity for extract (a) and raffinate (b), obtained for different values of rotation period (106-136 sec) for the base case study. The others operating conditions and model parameters were kept constant and the same as described in Table 3.4. The two limits considered for the rotation period, 106 sec and 136 sec are referred with the equivalent values for the purity and recovery. The arrows show the evolution of the performance with the increase of the rotation period.*

3.1.3.2 Effect of the extract flow rate

The extract flow rate varied between 3.62 to 11.62 *ml/min*. Figure 3.7 shows the effect of the extract flow rate, Q_E, on the SMB performance.

The purity for both extract and raffinate is very sensitive to the change of extract flowrate. So, high values of purity can only be obtained in a narrow window of values of the extract flow rate. It can be seen that, depending on which direction Q_E is changed, the optimum value of the extract flow drastically affects the performance of one or the other product. Increasing the extract flow rate the liquid flow rate in section II, $Q_{II} = Q_I - Q_E$, will be lower. It is possible that the constraint in zone II is not verified; therefore, glucose will have a net flux in opposite direction and will contaminate the extract with decrease of purity of that stream. If the extract flow rate is decreased the raffinate flow rate will be increased, which will increase the liquid flow rate in section III. For this case, it is possible that the constraint in zone III is not verified; therefore, fructose will have a net flux in opposite direction and will contaminate the raffinate with decrease of purity of that stream.

High recovery for the extract and raffinate is also obtained only for a narrow window of values of extract flow rate. The only difference is that, for the case of the raffinate, the

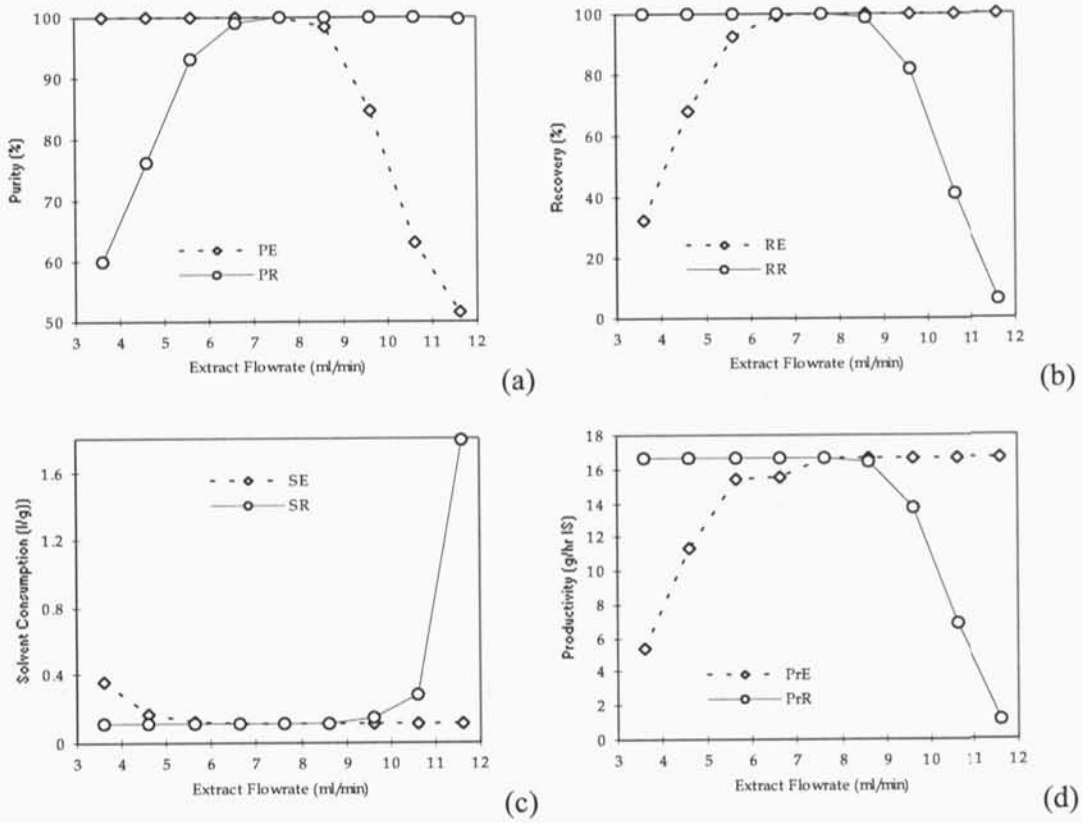

Figure 3.7 *Effect of the extract flowrate on the SMB performance parameters for the case study. The extract flowrate changed between 3.62 and 11.62 ml/min. The others operating conditions and model parameters were kept constant as described in Table 3.1, except the raffinate flowrate that changed with the extract flowrate in order to keep constant the total balance.* ***(a)*** *Extract Flowrate vs. Purity,* ***(b)*** *Extract Flowrate vs. Recovery,* ***(c)*** *Extract Flowrate vs. Solvent Consumption,* ***(d)*** *Extract Flowrate vs. Productiviiy.*

recovery decreases with the increase of the extract flowrate and increases for the extract. This behaviour was expected, according to the definition of extract and raffinate recovery.

As in the previous case, for the study of the effect of rotation period, the study of the behaviour of the purity versus recovery was done. Figure 3.8 shows that behaviour for the extract and raffinate for different extract flows rates. It shows that, it is possible to have simultaneously high purity and recovery for both extract and raffinate, but only for a very narrow region of values of extract flowrates. A small change in the extract flow rate leads to a situation of high purity and low recovery or the opposite, low purity and high recovery. This behaviour occurs for both outlet streams.

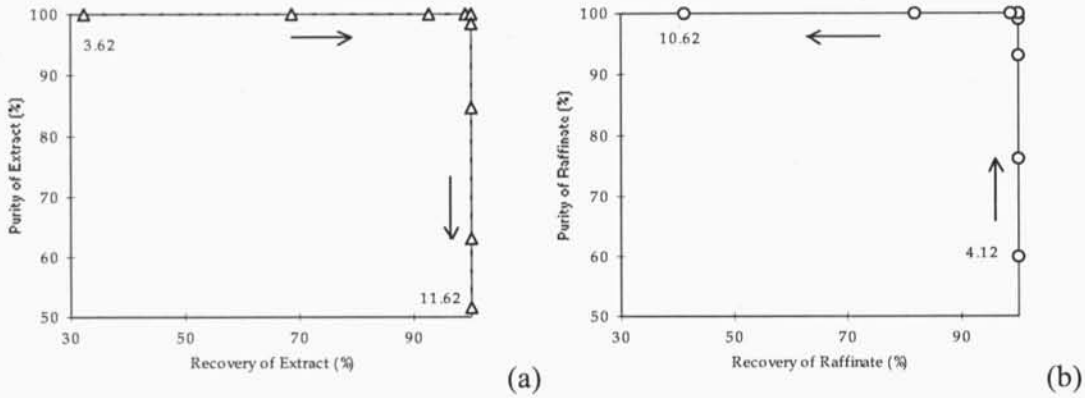

Figure 3.8 *Recovery versus purity for extract* ***(a)*** *and raffinate* ***(b)*** *obtained for different values of the extract flow rate (4.12-12.12 ml/min), for the case study. The others operating conditions and model parameters were kept constant and the same as described in Table 3.4, except the raffinate flowrate that changed with the extract flowrate in order to keep constant the total balance ($Q_R+Q_E=Q_D+Q_F$). The two limits considered for the extract flowrate, 4.12 ml/min and 12.12 ml/min are referred with the equivalent values for the purity and recovery. The arrows show the evolution of the performance with the increase of the extract flowrate.*

3.1.3.3 Effect of the feed flow rate

The feed flow rate varied between 0.23 to 8.23 *ml/min*. Figure 3.9 shows the effect of the feed flowrate on the SMB performance.

An increase of the feed flowrate improves the productivity and the solvent consumption, for both extract and raffinate. That is, higher values for the productivity and lower values for the solvent consumption are obtained. However, purity and recovery decrease with the increase of the feed flowrate. With the feed flowrate modification, the values of the liquid flowrates Q_{III} and Q_{IV} will be also, affected. They increase proportionally to the feed flow rate. Thus, the more retained product, Fr, will contaminate the raffinate stream and the product less retained, Gl, contaminates the extract.

Figure 3.10 shows the effect of the feed flow rate on the recovery versus purity. The behaviour is similar for both outlet streams, extract and raffinate. With the decrease of the feed flow rate, the purity and recovery, increases.

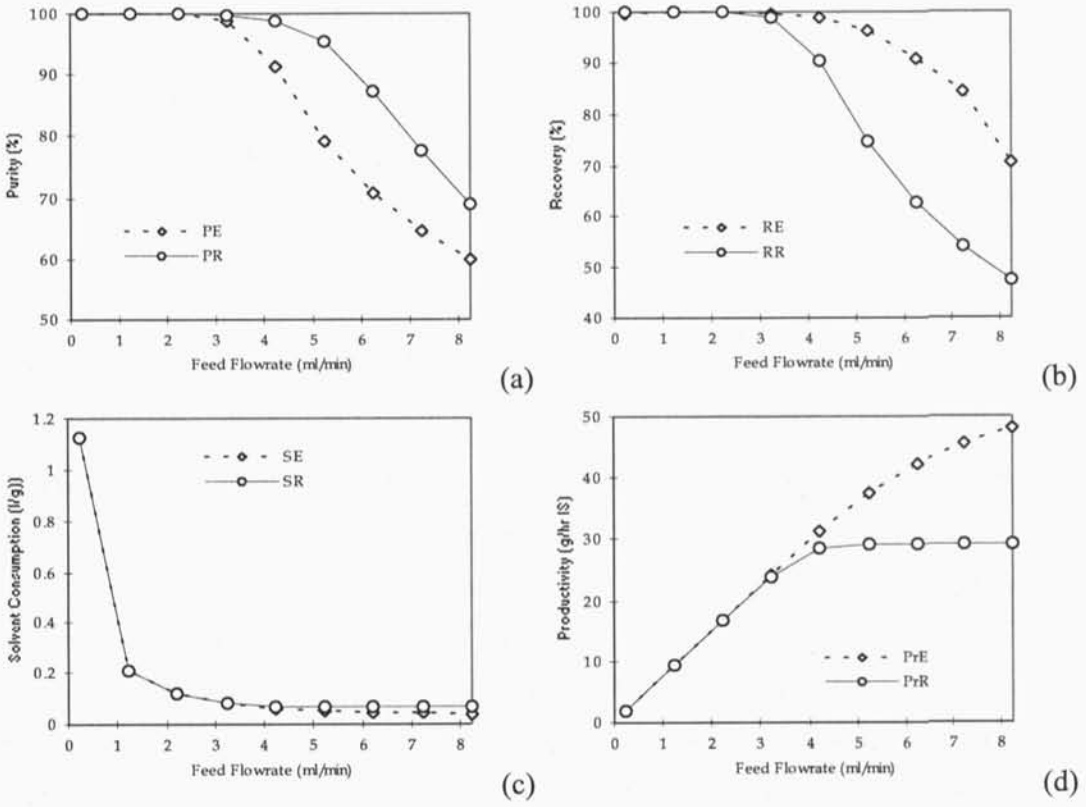

Figure 3.9 *Effect of the feed flow rate on the SMB performance parameters for the case study. The feed flowrate varied between 0.23 and 8.23 ml/min. The others operating conditions and model parameters were kept constant and the same as described in Table 3.4, except the eluent flowrate that changed with the feed flowrate in order to keep constant the total balance ($Q_R+Q_E=Q_D+Q_F$).* ***(a)*** *Feed Flowrate vs. Purity,* ***(b)*** *Feed Flowrate vs. Recovery,* ***(c)*** *Feed Flowrate vs. Solvent Consumption,* ***(d)*** *Feed Flowrate vs. Productivity.*

3.1.3.4 Effect of feed concentration

The feed concentration varied between 5*g/l* to 100*g/l* for each feed component. The operating conditions and model parameters are the same as described in Table 3.1.

The effect of the feed concentration on the Solvent Consumption and on the Productivity on the SMB for the case study, is shown in Figure 3.11. These results show that we can obtain, practically, the same results for solvent consumption for both feed components, extract and raffinate, also for the productivity. The solvent consumption decreases with the increase of the feed concentration. The productivity, with the increase of the feed concentration, increases.

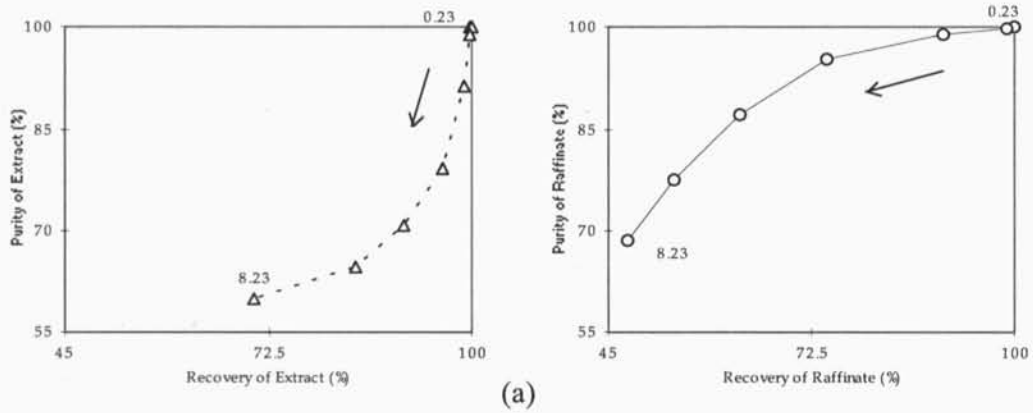

Figure 3.10 *Recovery versus purity for extract* ***(a)*** *and raffinate* ***(b)*** *obtained for different values of the feed flow rate (0.23-8.23 ml/min), for the case study. The others operating conditions and model parameters were kept constant and the same as described in Table 3.4, except the eluent flowrate that changed with the feed flowrate in order to keep constant the total balance ($Q_R+Q_E=Q_D+Q_F$). The two limits considered for the feed flowrate, 0.23 ml/min and 8.23 ml/min are referred with the equivalent values for the purity and recovery. The arrows show the evolution of the performance with the increase of the feed flowrate.*

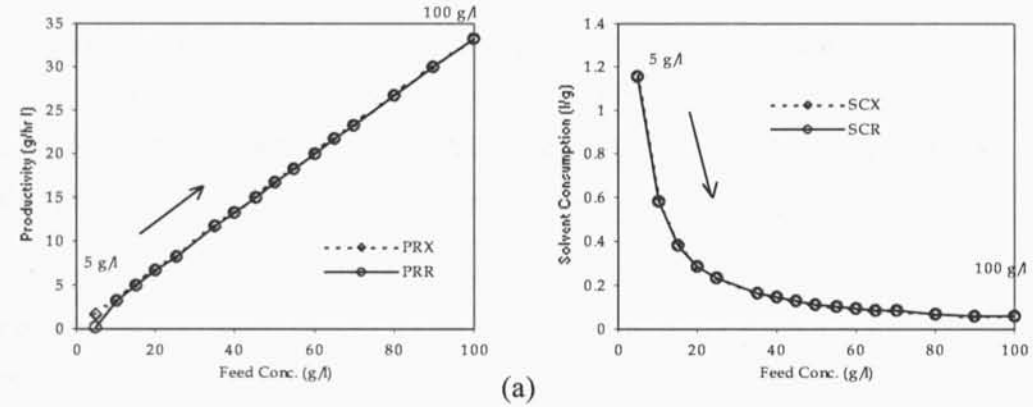

Figure 3.11 *Effect of the feed concentration on the Solvent Consumption and on the Productivity on the SMB for the case study. The feed concentration varied between 5 and 100 g/l. The others operating conditions and model parameters were kept constant and the same as described in Table 3.4.* ***(a)*** *Productivity versus Feed Concentration,* ***(b)*** *Solvent Consumption versus Feed Concentration.*

3.1.3.5 Effect of the section length and configuration

The operating conditions and model parameters are the same as in Table 3.1. The effect of the section length is described in Table 3.5 and shown in Figure 3.12. These results show that we can obtain, practically, complete separation using 12 columns configuration in the SMB pilot plant with 10.5 *cm* long columns. Different results were obtained considering different configurations for each section. Considering three columns per section the results obtained were slightly better than the ones obtained with 2-4-4-2 configuration, 99.9% for both Extract and Raffinate Purity and 99.8 for Extract Purity and 99.6 for Raffinate Purity, respectively.

Table 3.5 *Effect of the section length in the performance parameters. The others operating conditions and model parameters were kept constant and the same as described in Table 3.1.*

Configuration	L_j *(cm)*	P_E *(%)*	P_R *(%)*	R_E *(%)*	R_R *(%)*
1-1-1-1	10.5	94.3	92.7	92.6	94.4
2-2-2-2	21.0	99.3	99.2	99.2	99.3
3-3-3-3	31.5	99.9	99.9	99.9	99.9
4-4-4-4	42.0	100.0	100.0	100.0	100.0
5-5-5-5	52.5	100.0	100.0	100.0	100.0
2-4-4-2	L_1=L_4=21.0 L_2=L_3=42.0	99.8	99.6	99.5	99.8

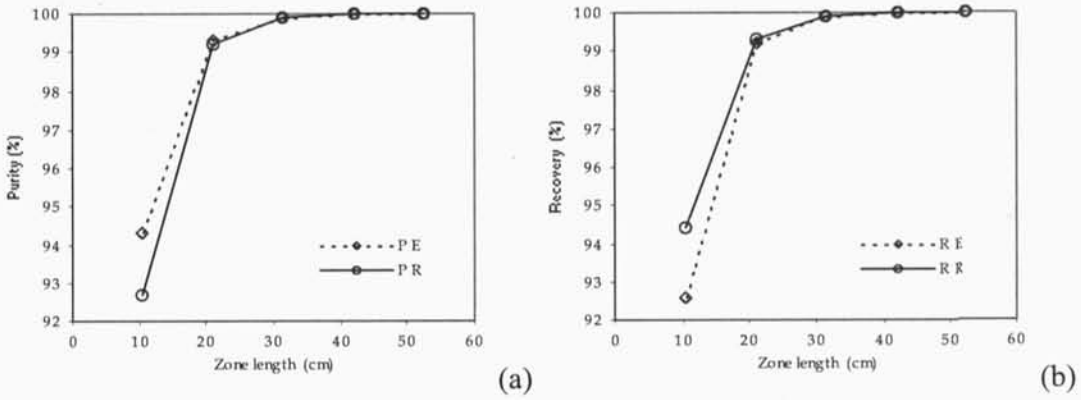

Figure 3.12 *Effect of the zone length in the performance parameters: (a) purity, (b) recovery. The others operating conditions and model parameters were kept constant and the same as described in Table 3.1.*

3.1.3.6 Effect of the number of intraparticle mass transfer units

a) on internal concentration profiles

The effect of the intraparticle mass transfer units, k, or the corresponding dimensionless number α, on the internal profiles of the SMB is shown in Figure 3.13. Simulations for three different values of α were made (α = 3.60, 7.20, 10.8 and 18.0 or $k = 0.01 s^{-1}$, $0.02\ s^{-1}$, $0.03\ s^{-1}$ and $0.05\ s^{-1}$). The results for α = 36.0, or $k = 0.1\ s^{-1}$, are illustrated in Figure 3.1. The mass transfer coefficient depends only on the intraparticle diffusivity of species and particle size. Therefore, increasing α, or k, by decreasing the particle size, improves the performance of the SMB.

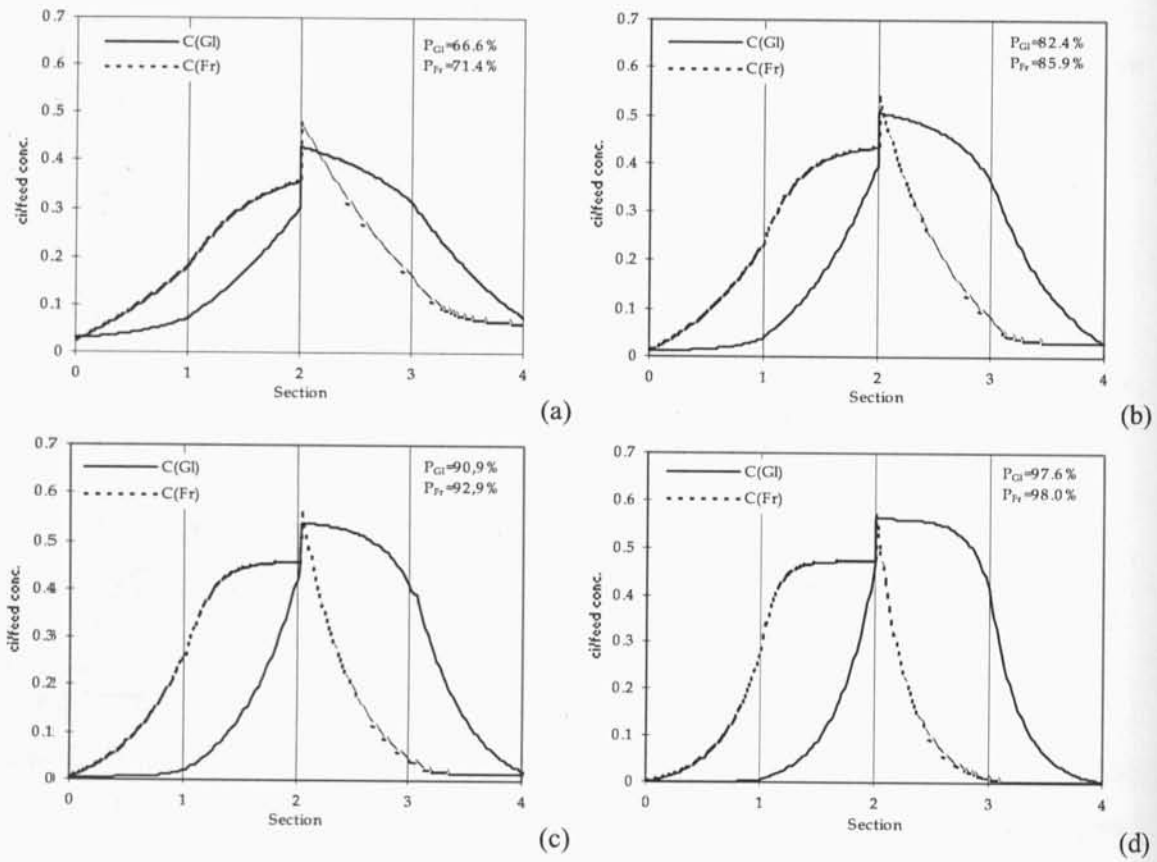

Figure 3.13 *Effect of the intraparticle mass transfer rate on the SMB steady-state internal profile.* ***(a)*** *α =3.60 or k =0.01 s^{-1};* ***(b)*** *α =7.20 or k =0.02 s^{-1};* ***(c)*** *α =10.8 or k =0.03 s^{-1};* ***(d)*** *α =18.0 or k =0.05 s^{-1}. The others operating conditions and model parameters were kept constant and the same as described in Table 3.1.*

With different values of k, a simultaneous study can be also made considering the effect of rotation period, feed and extract flow rates.

b) on Purity versus Recovery plots at various rotation period

Figure 3.14 shows the recovery versus purity in the extract and raffinate for different rotation periods and different values of k considered (number of intraparticle mass transfer units).

Through these figures we can see the effect of the value of k in the performance parameters purity and recovery for different values if rotation period. The obtained results confirm the conclusions obtained through the observation of the SMB internal profiles (Figure 3.13). That is, increasing the value of k (or α) the performance of the TMB will improve.

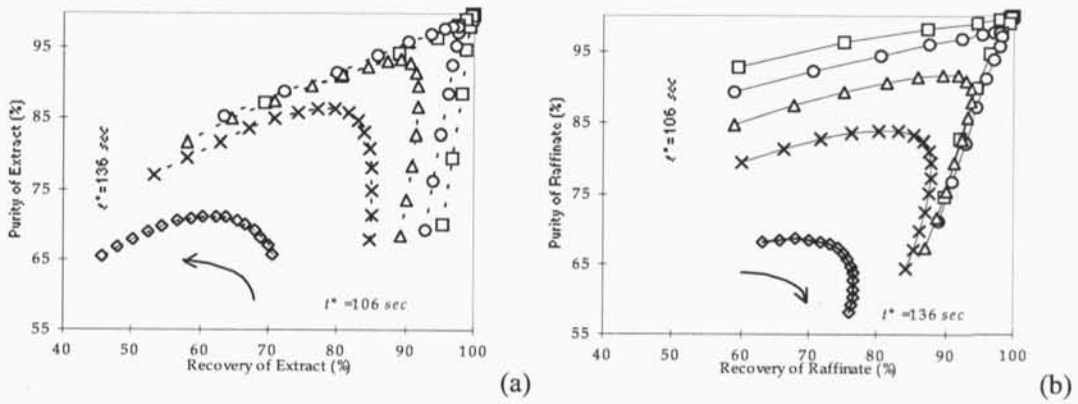

Figure 3.14 *Recovery vs. purity of extract* ***(a)*** *and Recovery vs. purity of raffinate* ***(b)*** *for different values of the intraparticle mass transfer rate (—□—$k = 0.1\ s^{-1}$, —o— $k = 0.05\ s^{-1}$, —Δ— $k = 0.03\ s^{-1}$, —x— $k = 0.02\ s^{-1}$, and —◊— $k = 0.01\ s^{-1}$) each for different values of rotation period, $t^* \in [106,136] sec$. The others operating conditions and model parameters were kept constant and as described in Table 3.1. The arrow shows the evolution of the performance parameters with the increase of the rotation period.*

For different values of k, the behaviour of the recovery versus purity is similar. And, the values of purity and recovery follows the decreases of k. For higher values of k is possible to obtained high purities and recoveries, although only in a narrow window of switch time interval values. To illustrate, look to the shape of the curve for $k = 0.01$ and for $k = 0.1\ s^{-1}$.

c) on Purity versus Recovery plots at various extract flow rate

Figure 3.15 shows the recovery versus purity in the extract and raffinate for different extract flowrate and for the different values of k considered (number of intraparticle mass transfer units). The behaviour of purity versus recovery is similar independently the value of k. The difference is in the region were we can obtain high performance. Only for higher values of k we obtain this region, thought for a restrict region of extract flowrate values.

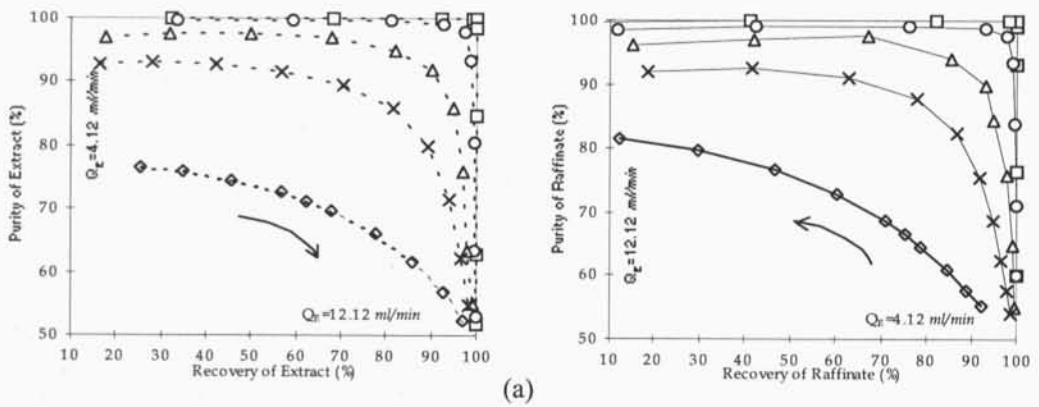

Figure 3.15 *Recovery vs. purity of extract* ***(a)*** *and Recovery vs. purity of raffinate* ***(b)*** *for different values of the intraparticle mass transfer rate (—□—$k = 0.1\ s^{-1}$, —o— $k=0.05\ s^{-1}$, —Δ— $k=0.03\ s^{-1}$, —×— $k=0.02\ s^{-1}$, and —◊— $k=0.01\ s^{-1}$) each for different values of extract flow $Q_E \in [4.12,12.12] ml/min$. The others operating conditions and model parameters were kept constant and as described in Table 3.1. The arrow shows the evolution of the performance parameters with the increase of the extract flowrate.*

d) on Purity versus Recovery plots at various feed flow rate

Figure 3.16 shows the recovery versus purity in the extract and recovery versus purity in the raffinate, for different values of feed flow rate, $Q_F \in [0.23,8.23] ml/min$, and for the different values of k considered (number of intraparticle mass transfer units). The behaviour of purity versus recovery is similar independently the value of k. High performance values are obtained for low values of feed flow rates.

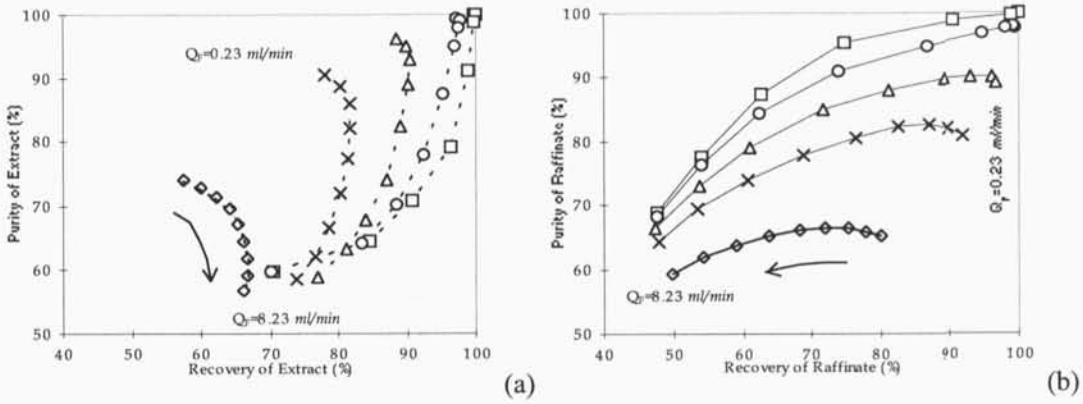

Figure 3.16 *Recovery vs. purity of extract* ***(a)*** *and Recovery vs. purity of raffinate* ***(b)*** *for different values of the intraparticle mass transfer rate (—□—$k = 0.1\ s^{-1}$, —o— $k=0.05\ s^{-1}$, —Δ— $k=0.03\ s^{-1}$, —×— $k=0.02\ s^{-1}$, and —◊— $k=0.01\ s^{-1}$) each for different values of feed flow, $Q_F \in [0.23, 8.23] ml/min$. The others operating conditions and model parameters were kept constant and as described in Table 3.4. The arrow shows the evolution of the performance parameters with the increase of the feed flowrate.*

3.1.3.7 $\gamma_{II} - \gamma_{III}$ plane analysis

The conditions for complete separation are defined in terms of the model parameter γ_{ij} $\left(= v_j / u_s\right)$, see (2.2) in the previous chapter, when linear adsorption isotherm are considered. This parameter, when related to zone II and III, plays a crucial role on the separation performance of the SMB/TMB system, see Table 2.2. Taking into account this consideration, a $\gamma_{II} - \gamma_{III}$ plane analysis was performed. Following the same methodology used previously to study the effect of the operating conditions and model parameters on the SMB performance, the $\gamma_{II} - \gamma_{III}$ plane was built by keeping constant the recycling flowrate (Q_{Rec} = 18.12 *ml/min*) and the solid flowrates, and so the γ_{IV} (=0.6252). The rotation period considered was of 2 *min*. The total balance was also kept constant in all the performed simulations and equal to 12.92 *ml/min*. The value for the mass transfer coefficient used was $k = 0.1\ s^{-1}$. Other operating conditions and model parameters are described in Table 3.1.

The obtained results were compiled and illustrated in Figure 3.17. The straight lines are related to the theoretical values (Storti *et al.*, 1993). The zone where separation can take place is defined by the two lines:

- $\gamma_{II} < \gamma_{III}$,
- $\gamma_{III} > 0.75$.

The first condition, represented by the diagonal line, $\gamma_{II} = \gamma_{III}$, defines the region where Q_F is equal to zero. This line represents a physical limitation. The second condition, $\gamma_{III} = 0.75$, is related to the conditions for the parameter γ_{III} to obtain separation, $\gamma_{III} > \frac{1-\varepsilon}{\varepsilon} K_A$. The closed squares are the numerical results based on the equivalence between the TMB and SMB, connected by a thin line. The $\gamma_{II} - \gamma_{III}$ plane obtained for the reference case shows four different regions: one region of complete separation, extract and raffinate purity ≥ 99.5%, one region of pure extract, extract purity ≥ 99.5%, one region of pure raffinate, raffinate purity ≥ 99.5%, and one region of no separation, extract and raffinate purity < 99.5%.

The effects of the extract (or raffinate) and feed (or eluent) flowrates on the TMB performance were also represented. For the reference case, the effect of the extract flowrate the feed and eluent flowrates were kept constant and equal to 2.23 and 10.69 *ml/min*, respectively. The others model parameters were kept constant and the same as in Table 3.1. The × points, in Figure 3.17, represent the numerical simulation results obtained, for the extract flowrate values between 3.62 and 11.62 *ml/min*. These results confirm the obtained in section 3.1.3.2, under the same conditions. For the reference case the effect of the feed flowrate, the extract and raffinate flowrates were kept constant and equal to 7.62 and 5.30 *ml/min*, respectively. The + points, in Figure 3.17, represent the numerical simulation results obtained, for the feed flowrate concentration values between 0.23 and 8.23 *ml/min*. These results confirm the obtained in section 3.1.3.3, under the same conditions.

In Table 3.6, the TMB performance parameters for the points A, B, C, D represented in Figure 3.17, are described, and also the obtained γ_j parameters.

The point A is in the separation region therefore, the purity values obtained, for both components, are approximately 100%. The point B and D lay respectively, in the pure extract and pure raffinate region. In B, the extract purity is 100% and the raffinate purity obtained is less than 95%. The opposite situation was obtained in point D, raffinate purity of 100% and extract purity less than 95%. Point C, due to the oblique line that separate the region of complete separation and of pure raffinate, lays in the no separation region where, for both components, the purity obtained are ≤ 95%. Theoretically, both points C and D, should lie on

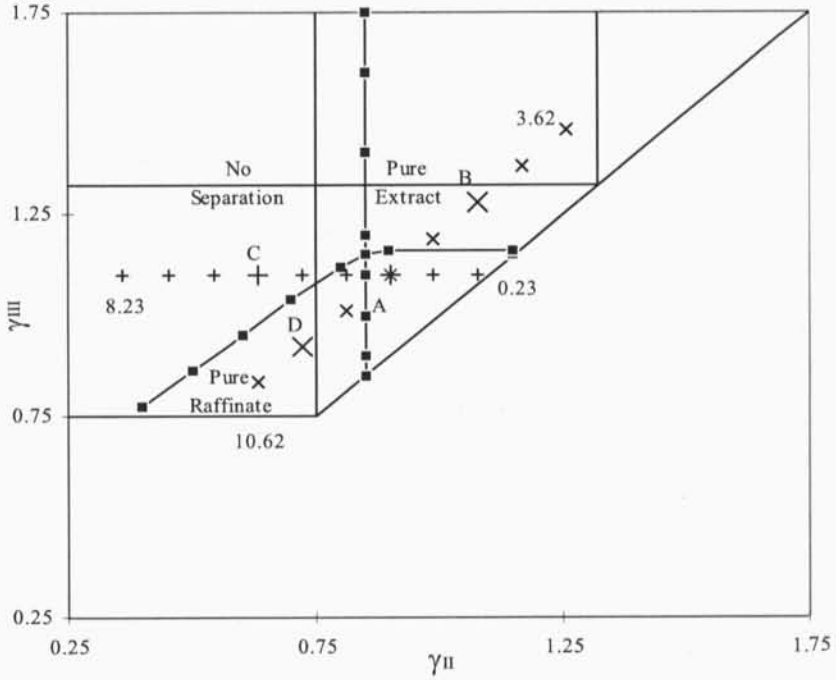

Figure 3.17 *Regions of operation of the TMB in a plot of the ratio of fluid/solid velocities in zone III versus Ratio of fluid/solid velocities in zone II considering linear isotherms for both components under conditions described in Table 3.4 and 3.1; the full squares (▪) represent numerical simulation results corresponding to purity values ≥ 99.5%for one or both outlet streams; the —line represents the theoretical limits; × and + represents the effect of extract and feed flowrates changes on the separation region of operating of the TMB, respectively. The performance parameters obtained for A, B, C and D points are described in Table 3.6.*

the pure raffinate zone, since $\gamma_{III} < 0.75$, see Table 3.6. However, for point C, $\gamma_I = 1.32$ (which should be higher than 1.32). This can explain the reduced area of pure raffinate region. In all the numerical simulations, the total inlet or outlet flowrates (the total balance) were kept constant so by increasing the feed flowrate, the eluent flowrate decreases, decreasing the flowrate in section I and consequently γ_I. The oblique line corresponds to a $Q_F \approx 5.23$ *ml/min.* The constraint in the γ_{IV} value is verified in all points ($\gamma_{IV} < 0.75$).

In section 3.1.3.6, the study of the effect of the intraparticle mass transfer units, k, on the TMB internal concentration profiles and on the performance parameters were made. The conclusion is that by increasing the value of k, the TMB performance will increase. All the simulation results obtained for different values of k, 0.1, 0.5 and 2.0 s^{-1}, were collected and

Table 3.6 *TMB performance parameters obtained for A, B, C, and D points illustrated in Figure 3.17.*

	A		B		C		D	
	Gl	**Fr**	**Gl**	**Fr**	**Gl**	**Fr**	**Gl**	**Fr**
Purity (%)	99.9	99.9	93.1	100	95.2	79.2	100	84.8
Recovery (%)	99.9	99.9	100	92.5	74.7	96.2	82.1	100
Solvent Cons. (*l/g*)	0.116	0.116	0.116	0.125	0.066	0.051	0.141	0.116
Productivity (*g/hrl*)	16.65	16.65	16.66	15.42	29.20	37.62	13.68	16.66
Region	**Separation**		**Pure Ext.**		**No Sep.**		**Pure Raf.**	
Operating conditions								
Q_D (ml/min)	10.69		10.69		7.69		10.69	
Q_E (ml/min)	7.62		5.62		7.62		9.62	
Q_F (ml/min)	2.23		2.23		5.23		2.23	
Q_R (ml/min)	5.30		7.30		5.30		3.30	
Model Parameters								
γ_I	1.58		1.58		1.32		1.58	
γ_{II}	0.90		1.08		0.63		0.72	
γ_{III}	1.10		1.28		1.10		0.92	
γ_{IV}	0.63		0.63		0.63		0.63	

represented into the $\gamma_I - \gamma_{III}$ plane, Figure 3.18. The influence of the k parameters on the separation region area was performed.

With higher k value, that is, lower mass transfer resistance, more defined triangular complete separation region is obtained and converges to the theoretical limits. However, the line of separation between no separation and pure raffinate regions remains oblique, not vanishing with the increase of the mass transfer coefficient.

Trying to understand such behaviour, several numerical simulations were performed for different values of total balance, 17.92 ml/min and 22.62 ml/min (higher than 12.92 ml/min, the value previously used). Figure 3.19 shows the different regions definitions obtained when the mass transfer resistance is not so important, $k = 2.0\ s^{-1}$. Increasing the total balance, for constant recycling flowrate (constant γ_{IV}), the oblique line converge to the theoretical limit line. That is, for a total balance of 22.62 ml/min, the constraint on γ_I is fulfilled, that is, $\gamma_I >$ 1.32.

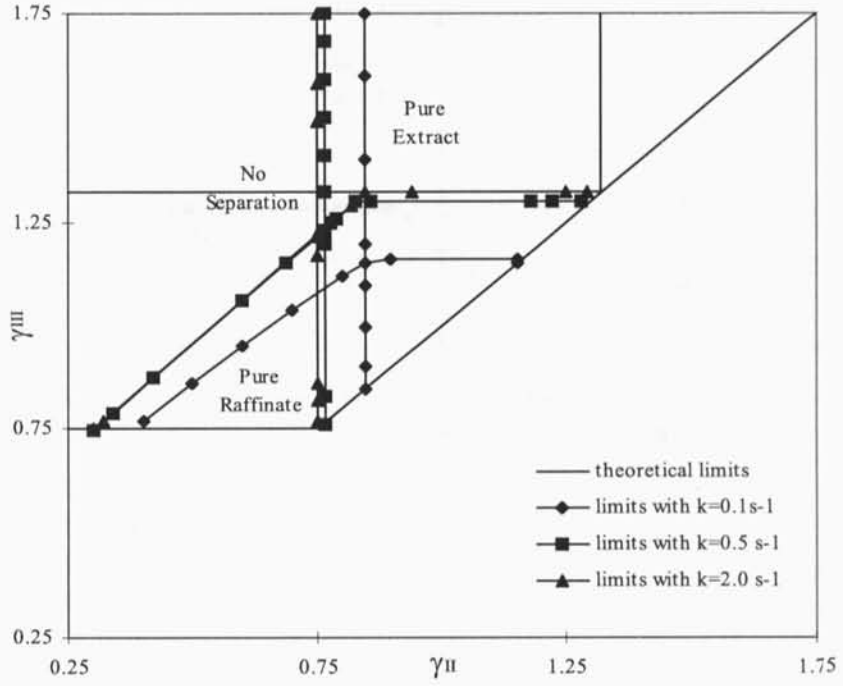

Figure 3.18 *Regions of operation of the TMB in a plot of the ratio of fluid/solid velocities in zone III versus Ratio of fluid/solid velocities in zone II considering linear isotherms for both components under conditions described in Table 3.4 and 3.1, for different values of the mass transfer resistance; the full diamonds (♦), the full squares (▪), and the full triangles (▲) represent the numerical simulation results corresponding to purity values ≥ 99.5% for one or both outlet streams, for k = 0.1 s^{-1}, k = 0.5 s^{-1}, and k = 2.0 s^{-1}, respectively; the —line represents the theoretical limits (Vertex: ♦ $\gamma_I = 1.47$, ▪ $\gamma_I = 1.34$, ▲ $\gamma_I = 1.32$).*

3.1.4 Influence of the Type of Isotherms on the Behaviour of the SMB

The target of this study is to verify the effect of other published equilibrium isotherms, for the glucose/fructose separation, on the behaviour of the SMB separation process. In all the simulations, the model used was the S-TMB model, (2.31-2.35) described in the foregoing chapter, based on the values shown in Table 3.7. The equation (2.33), equilibrium isotherm, was substituted by (3.2), for the linear case for both components and by (3.3) for linear/non linear for glucose and fructose, respectively.

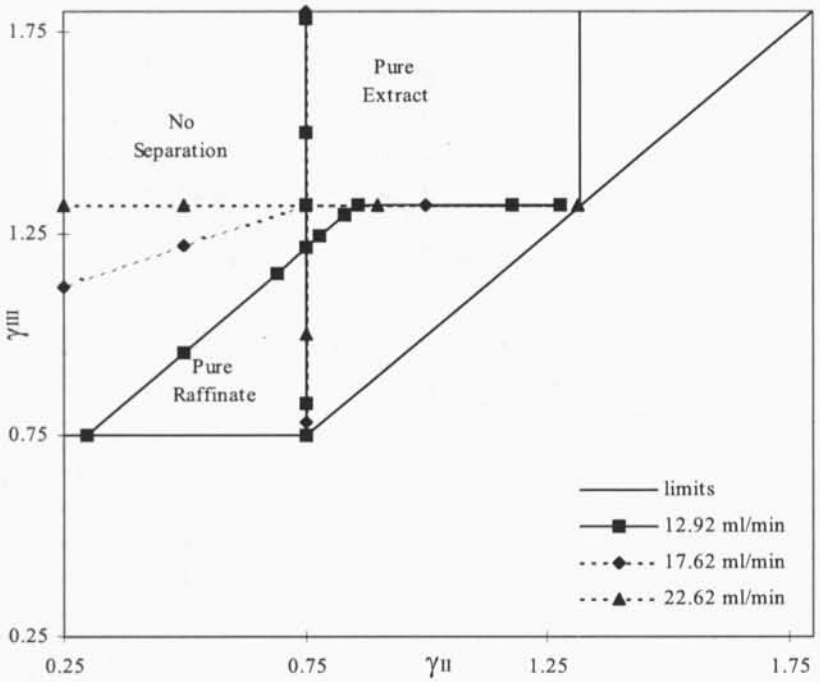

Figure 3.19 *Regions of operation of the TMB in a plot of the ratio of fluid/solid velocities in zone III versus Ratio of fluid/solid velocities in zone II considering linear isotherms for both components under conditions described in Table 3.1, with k = 2.0 s^{-1}, for different values of total balances; full squares (▪), full diamonds (♦) and full triangles (▲) represent the numerical simulation results corresponding to purity values ≥ 99.5% for one or both outlet streams, for 12.92, 17.62, and 22.62 ml/min, respectively; the —line represents the theoretical limits (Vertex: ▪ $\gamma_I = 1.32$, ♦ $\gamma_I = 1.64$, ▲ $\gamma_I = 2.08$).*

Linear/linear isotherms for both components

For both components, glucose and fructose, linear isotherms were considered,

$$q_{Gl} = K_{Gl}\, c_{Gl}\,, \text{ and} \tag{3.2a}$$

$$q_{Fr} = K_{Fr}\, c_{Fr} \tag{3.2b}$$

where q_i is the solid phase concentration of the component i expressed in *g/l*, and c_i is the concentration of the component i in the liquid phase expressed in *g/l*.

The values of the equilibrium coefficients, K_i, in the two above equations, (3.2), were, 0.3401 for glucose and 0.5634 for fructose and the selectivity factor (= K_{Fr}/K_{Gl}) is equal to 1.6566.

These values were taken from experiments performed at our laboratory. The numerical parameters used were the same as the ones described in Table 3.2.

Table 3.7a *Operating conditions and model parameters for the study case. The flowrates were estimated using the equilibrium model for the SMB/TMB as in Zhong and Guiochon (1996)*

Model parameters	**Operating conditions**	**Columns:**
SMB:	SMB:	SMB:
Peclet Number, Pe_j=2000	Feed conc.= 30 g/l each	D_c= 2.6 cm
Solid/Fluid ratio, $(1-\varepsilon)/\varepsilon$=1.5	t^* = 105 sec[a]	L_c= 11.5cm
Number mass transfer units, α_{ij} = 31.5		Configuration: 3, 3, 3, 3
(k_i = 0.1 s^{-1})	Q_{Rec} = 19.89 ml/min[b]	L_j= 34.5 cm
TMB:	Q_D= 8.23 ml/min[b]	
Ratio between fluid and solid velocities:	Q_E= 5.62 ml/min[b]	
γ_I=1.0142, γ_{II}=0.6122,	Q_F= 1.28 ml/min[b]	
γ_{III}=0.7039, γ_{IV}=0.4252	Q_R= 3.89 ml/min[b]	

[1] switching time, $t^* = L_c/u_s = (1-\varepsilon)\, L_c\, A / Q_s$
[2] values obtained through the operating conditions as in Zhong and Guiochon (1996).

Table 3.7b *Equivalence between TMB and SMB flow-rates.*

Section	TMB		SMB	
	Q_j (ml/min)	γ_j	Q_j^* (ml/min)	γ_j^*
I	14.15	1.01	28.11	2.01
II	8.54	0.61	22.50	1.61
III	9.82	0.70	23.78	1.70
IV	5.93	0.43	19.89	1.43
t^* (min)	---		1.75	

The steady-state internal profiles obtained by using the COLNEW and PDECOL solvers are shown in Figure 3.20(a), for the case study under conditions described in Table 3.7. The relative error obtained by using (3.1) is also shown, Figure 3.20(b). The steady-state concentration profiles obtained, by using the two solvers, are similar. The highest relative error obtained is less than 2%, obtained when the relative concentration, for both components,

takes values around zero, sections I and IV. Simulations were also made, now using COLDAE and DASSL solvers, for the ordinary algebraic and partial differential algebraic case, respectively. All the obtained results were compiled and described in Table 3.8. As in the previous case study, under conditions described in Table 3.1, the computing time is lower when using the ordinary differential solvers, COLNEW and COLDAE. The DASSL solver takes more time depending on the number of finite elements chosen.

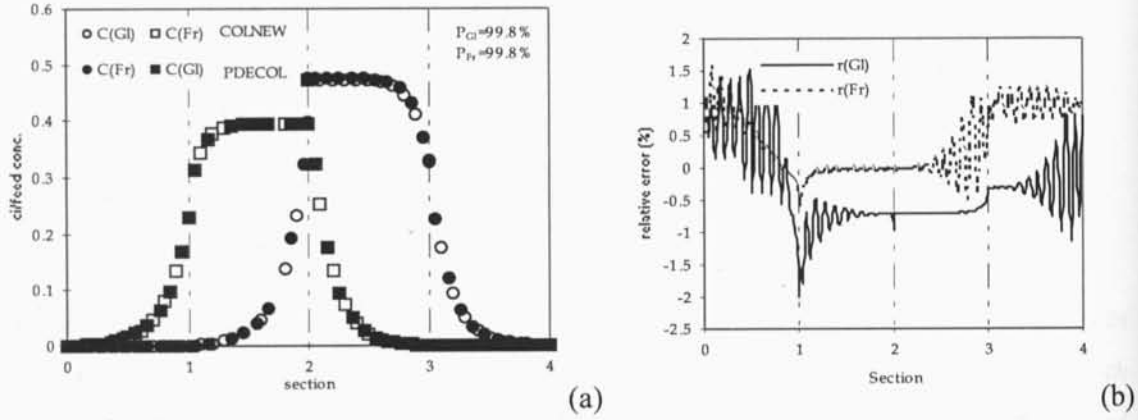

Figure 3.20 *(a) Steady-state internal profiles for the study case obtained using linear isotherms (3.2) for both components, with K_{Gl} = 0.3401 and K_{Fr} = 0.5634, and the operating conditions and model parameters as described in Table 3.7 and 3.2, and (b) corresponding relative error.*

Table 3.8 *T-TMB system performance parameters and run time, for the case study, under conditions described in Table 3.7 and 3.2, obtained by using the four solvers.*

	COLNEW		PDECOL		DASSL		COLDAE	
	Gl	Fr	Gl	Fr	Gl	Fr	Gl	Fr
Purity (%)	99.8	99.8	99.8	99.8	99.8	99.8	99.8	99.8
Recovery (%)	99.7	99.7	100.0	100.0	100.0	100.0	99.8	99.8
Solvent Cons. (l/g)	0.248	0.248	0.248	0.246	0.238	0.236	0.248	0.248
Productivity (g/hr l)	5.225	5.227	5.244	5.267	5.488	5.455	5.229	5.229
Run Time (min)	0.17		25		>120		0.15	

Linear/non-linear isotherms for the two components

To verify the effect of the equilibrium isotherms on the behaviour of the SMB, the results obtained in Strube and Schmidt-Traub (1996) were used. Fructose, the more strongly adsorbed component, was not influenced by the presence of glucose, so was described with a linear isotherm, (3.2b) as in the previous simulation. Glucose, on the contrary, was shown to be influenced by the presence of fructose, decreasing is adsorption. For glucose an isotherm equation adapted from Strube and Schmidt-Traub (1996), was used, (3.3),

$$q_{Gl} = \frac{K_{Gl} c_{Gl}}{1 + 0.01030 c_{Fr}^{0.8} + 0.001 c_{Fr}} \tag{3.3a}$$

$$q_{Fr} = K_{Fr}\, c_{Fr} \tag{3.3b}$$

where q_i is the solid phase concentration of the component i (g/l), c_i is the of the component i in the liquid phase (g/l).

Figure 3.21 shows the reprint of the experimental results with the isotherms equation (3.3a) for the glucose in the presence of fructose, using the values obtained by Strube and Schmidt-Traub (1996).

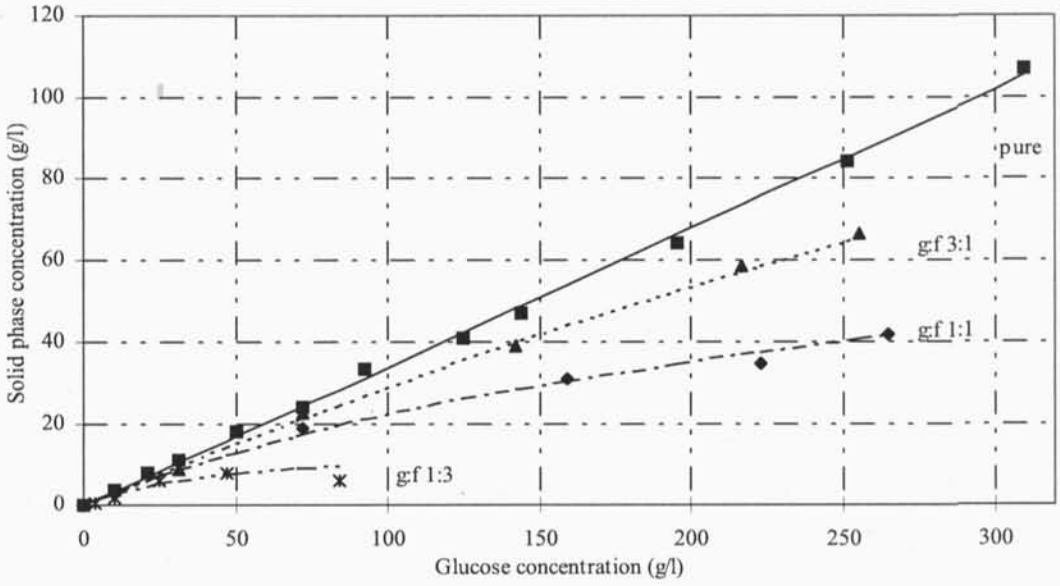

Figure 3.21 *Isotherms of glucose in the presence of fructose using equation (3.3a). Results taken from Strube and Schmidt-Traub (1996). The dots represent the experimental results and the lines the values obtained using the model similar to the multicomponent Langmuir.*

Due to numerical problems the above experimental isotherm was fitted by the equation,

$$q_{Gl} = \frac{0.3401 c_{Gl}}{1 + 0.004447 c_{Fr}} \tag{3.4}$$

Figure 3.22 shows the reprint of the experimental results for the isotherms for the glucose in the presence of fructose, now considering the isotherm equation (3.4).

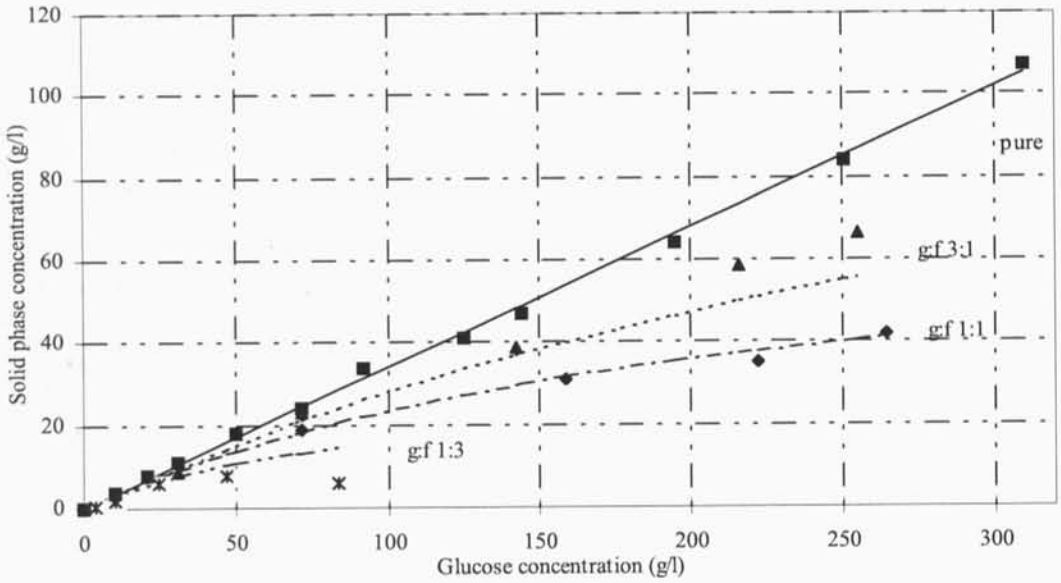

Figure 3.22 *Isotherms of glucose in the presence of fructose using equation (3.4), Langmuir equation modelled by using the experimental values obtained Strube and Schmidt-Traub (1996). The dots represent the experimental results and the lines the values obtained by using the isotherm equation (3.4).*

Figure 3.23 shows a 3-dimensional representation of the two models. Figure 3.23a represents the variation of the q_{Gl} for different values of c_{Gl} and c_{Fr} using the isotherm equation from Strube and Schmidt-Traub (3.3a) and Figure 3.23b using the fitted equation (3.4).

The results obtained with the equation (3.4), are similar to the model presented by Strube and Schmidt-Traub (1996) equation (3.3a). For low values of glucose concentration, up to 20 g/l, no significant differences were found between the values obtained by both isotherms. The differences increase proportionally with the glucose concentration. In Figure 3.24, we can see

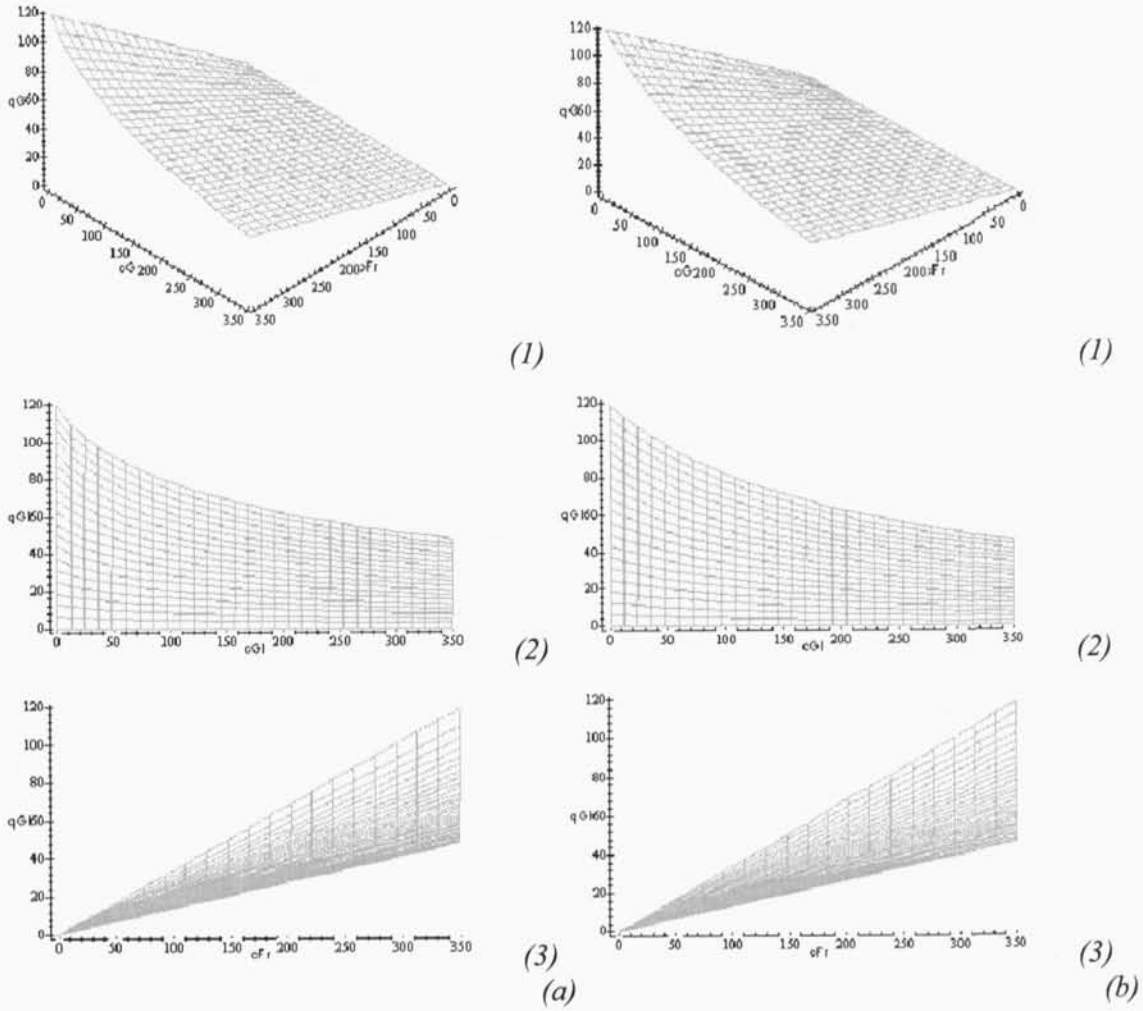

Figure 3.23 (a) *3-dimensional representation of the Langmuir equation model (3.3a) obtained by Strube and Schmidt-Traub (1996); and* ***(b)*** *3-dimensional representation of the Langmuir equation model used in the present work using the experimental values of Strube and Schmidt-Traub (1996) (3.4). (1) variation of q_{GI} for different values of c_{GI} and c_{Fr}; (2) 2-D plane showing the variation of q_{GI} for different values of c_{GI}; (3) 2-D plane showing the variation of q_{GI} for different values of c_{Fr}.*

the difference between the results obtained by using the two models. The relative error was estimated by

$$relative\ error(\%) = \frac{q_{Gl}\ by\ (3.4) - q_{Gl}\ by\ (3.3a)}{q_{Gl}\ by\ (3.4)} * 100 \qquad (3.5)$$

Since for the TMB steady-state simulations, the feed concentration used is 30 g/l, the Langmuir equation, (3.4), can be used. So, we used (3.2a), the isotherm for fructose, and (3.4), the isotherm for glucose.

Figure 3.25 shows steady-state concentration profiles obtained for the reference case.

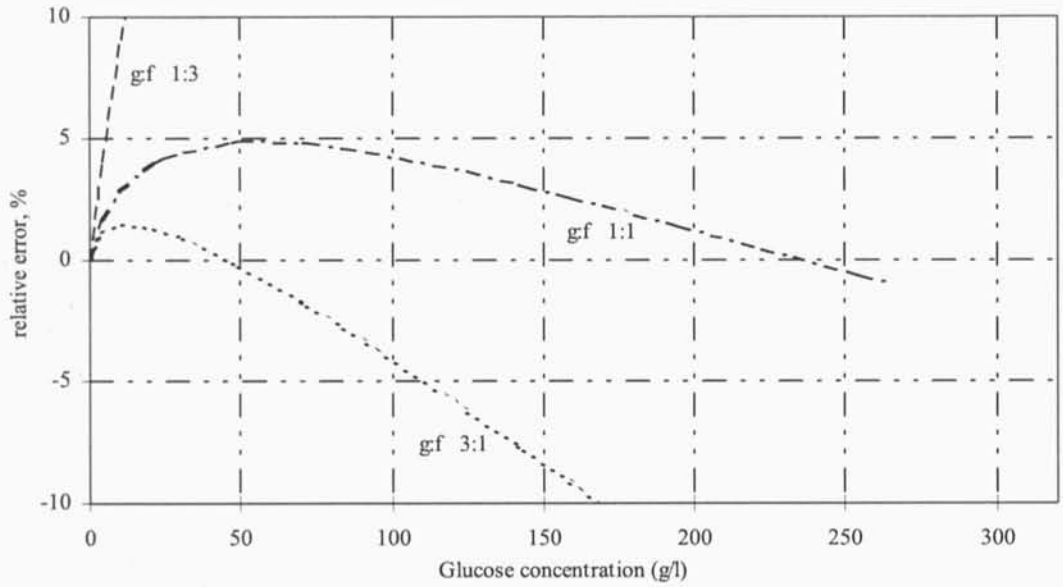

Figure 3.24 *Relative error, equation (3.5), versus glucose concentration for the obtained values by using the Langmuir equation (3.4) and by using the multicomponent Langmuir equation (3.3a).*

The performance parameters, P_{Fr} and P_{Gl}, obtained by using the two types of isotherm equations, are identical. Compare the performance parameters described in Table 3.8 and 3.9, for linear/linear and for linear/non-linear isotherms, respectively. The only tiny difference is in the glucose internal profile. This result was expected since the isotherm used takes into consideration the influence of the presence of fructose. Both simulations were performed with low feed concentration (30g/l). For low concentrations, both isotherms have, basically, a linear and similar behaviour. The SMB model with linear/non-linear equilibrium isotherm, consumes more computing time.

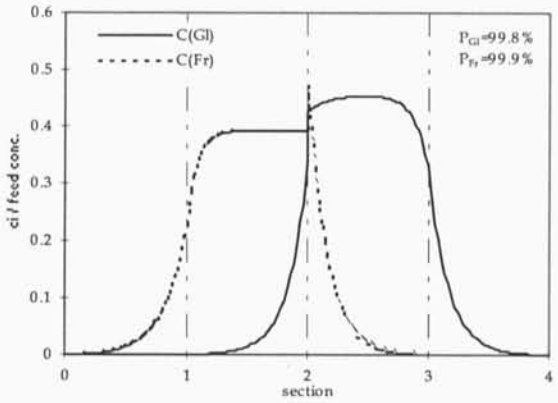

Figure 3.25 *Steady-state internal profiles for each TMB component obtained using the new Langmuir isotherm (3.4) for glucose and the linear isotherm for fructose equation (3.2a). The model parameters and operating conditions are as described in Table 3.7.*

Table 3.9 *T-TMB system performance parameters and run time, for the case study, under conditions as described in Table 3.7, obtained by using the four packages, considering, for glucose, the new Langmuir isotherm (3.4) and a linear isotherm (3.2a) for fructose.*

	COLNEW		PDECOL		DASSL		COLDAE	
	Gl	Fr	Gl	Fr	Gl	Fr	Gl	Fr
Purity (%)	99.8	99.9	99.9	99.8	100.0	99.9	99.8	99.9
Recovery (%)	99.9	99.8	100.0	100.0	100.0	100.0	99.9	99.8
Solvent Cons. (l/g)	0.248	0.248	0.246	0.247	0.240	0.239	0.248	0.248
Productivity (g/hr l)	5.235	5.228	5.267	5.254	5.400	5.438	5.236	5.229
Run Time (min)	25		88		57		15	

The simulations were repeated, now considering a high feed concentration value. The value was chosen to fall where the linearity of the isotherms was not verified. The operating conditions and model parameters were kept as in the previous simulation, Table 3.7. The feed concentration value, C, was considered equal to 225 g/l. Figure 3.26 shows the final results.

Looking at Figure 3.20a and Figure 3.26, no differences were found in the steady-state internal profiles by increasing the feed concentration, using linear isotherms in both components. The results confirm the linearity of the model, in other words, the feed concentration does not modify the internal profiles on relative concentration. The difference obtained is in the performance parameters, lower solvent consumption and higher productivity

with the increase of the feed concentration. Table 3.11 summarizes all the results obtained for all the simulations performed.

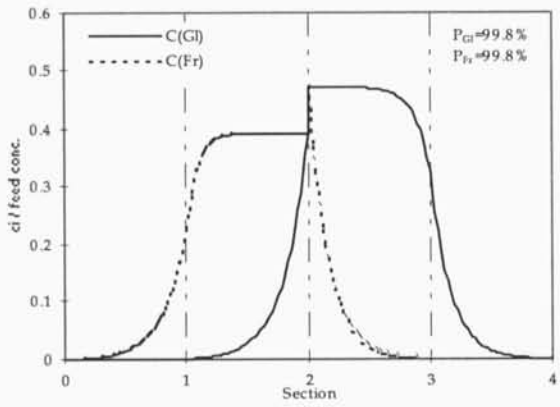

Figure 3.26 *Steady-state internal profiles for the TMB obtained using linear isotherms for glucose and fructose, equation (3.3), for a feed concentration, C=225 g/l. The model parameters and operating conditions are as described in Table 3.7.*

Figure 3.27 shows the results obtained using the non-linear isotherm equation (3.4), for glucose and 225 g/l for feed concentration. Table 3.10 shows the performance parameters and the computer time obtained, for each of the four software packages.

Table 3.10 *T-TMB system performance parameters and run time, for the case study, under conditions as described in Table 3.7, for a feed concentration C=225 g/l, obtained by using the four packages, considering, for glucose, the new Langmuir isotherm (3.4) and a linear isotherm(3.2a) for fructose.*

	COLNEW		PDECOL		DASSL		COLDAE	
	Gl	Fr	Gl	Fr	Gl	Fr	Gl	Fr
Purity (%)	99.8	100.0	99.8	100.0	100.0	100.0	99.8	100.0
Recovery (%)	100.0	99.8	100.0	100.0	100.0	100.0	100.0	99.8
Solvent Cons. (l/g)	0.033	0.033	0.033	0.033	0.032	0.032	0.033	0.033
Productivity (g/hr l)	39.296	39.217	39.431	39.498	40.790	40.380	39.296	39.217
Run Time (min)	36		87		72		27	

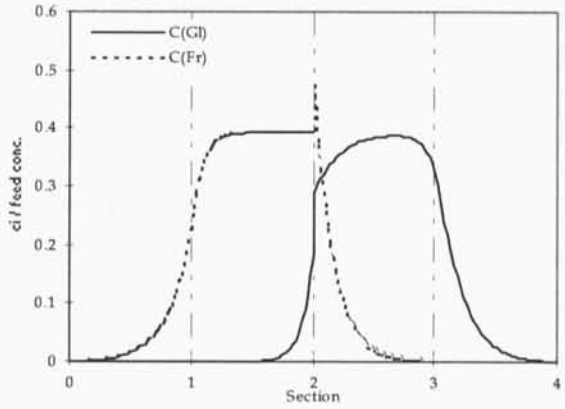

Figure 3.27 *Steady-state internal profiles for the TMB obtained using non linear Langmuir isotherm, equation (3.4), for glucose and linear isotherm, equation (3.2a), for fructose, for a concentration feed, C=225 g/l. The model parameters and operating conditions are as described in Table 3.7.*

Looking at the results obtained by using the non linear isotherm for glucose for low and higher feed concentration, some differences can be found. The component which was affected by increasing the feed concentration, was the glucose. However, the performance parameters obtained are similar. Table 3.11 shows the performance parameters, productivity, *P*, recovery, *R*, solvent consumption, *S*, and productivity, *Pr*, for both extract, fructose, and raffinate, glucose, obtained in all the simulations performed.

Table 3.11 *Performance parameters obtained, by using COLNEW, for a feed concentration 30 and 225 g/l, under conditions as described in Table 3.7.*

Feed Concentration. (g/l)	**30**				**225**			
Isotherms	*Linear, Linear*		*Langmuir, Linear*		*Linear, Linear*		*Langmuir, Linear*	
	Gl	**Fr**	**Gl**	**Fr**	**Gl**	**Fr**	**Gl**	**Fr**
Purity (%)	99.8	99.8	99.9	99.9	99.8	99.8	99.8	100.0
Recovery (%)	99.7	99.7	99.9	99.8	99.8	100.0	100.0	98.8
Solvent Cons. (l/g)	0.248	0.248	0.248	0.248	0.0331	0.033	0.033	0.033
Productivity (g/hr l)	5.225	5.227	5.235	5.228	39.214	39.316	39.296	39.217

3.1.5 Effect of the operating conditions on the TMB performance

The effect of the operating conditions for the glucose/fructose system by Simulated Moving Bed was studied. The performance parameters are characterised by purity, recovery, solvent consumption and adsorbent productivity. The model used was the model (2.32)-(2.36), described in preceding chapter, and based on the values shown in Table 3.7 and 3.2. The values that were kept constant are described in Table 3.12.

Table 3.12 *Operating conditions and model parameters that were kept constant to study the influence in the process performance.*

SMB operating conditions:	**TMB Model parameters:**
Feed conc. = 30 g/l each	Solid/fluid volumes, $(1-\varepsilon)/\varepsilon = 1.5$
$t^* = 105$ sec	
$Q_{Rec} = 19.89$ ml/min	Peclet number, $Pe_j = 2000$
Total Balance = $Q_D + Q_F = Q_E + Q_R = 9.51$ ml/min	
$D_c = 2.6$ cm	Ratio between fluid and solid velocities
$L_j = 31.5$ cm	in section IV, $\gamma_{IV} = 0.4252$

The conditions for complete separation are defined in terms of the model parameters γ_j ($= v_j / u_s$, fluid and solid velocities rate in the four sections of the TMB system). Those related with zone II and III, γ_{II} and γ_{III}, play a crucial role on the separation performance of the TMB, due to their proximity to the feed point situated between sections II and III.

As in the previous studied, in first approach we will consider linear isotherms, as equations (3.2), for both components, glucose and fructose. For the second study we consider different isotherms for the two components, linear for fructose, equation (3.3b), and Langmuir for glucose, equation (3.4).

A $\gamma_{II} - \gamma_{III}$ plane analysis was performed. The $\gamma_{II} - \gamma_{III}$ plane was built keeping constant the recycling flowrate ($Q_{Rec} = 19.89$ *ml/min*) and the rotation period ($t^* = 105$ *sec*). Therefore, the value of the ratio between the liquid flow rate and the adsorbent phase flow rate in section IV, γ_{IV}, is kept constant and equal to 0.425 (< 0.510, from the equilibrium theory). The total

flowrate balance was also kept constant in all the simulations performed and equal to 9.51 *ml/min*. Table3.12 summarizes the operating conditions and model parameters.

Figure 3.28 defines the different regions, using the values for the purity performance parameter, in the $\gamma_{II} - \gamma_{III}$ plane, where separation can take place. The straight lines are related to the theoretical values (Storti *et al.*, 1993). Top horizontal line, $\gamma_{III} = 0.845$, and left vertical line $\gamma_{II} = 0.510$. The closed squares are the numerical results based on the equivalence between the TMB and SMB, connected by a thin line, defining the complete separation region, for different values of mass transfer resistance, k, where purity higher than 99.5%, for both outlet components, is reached.

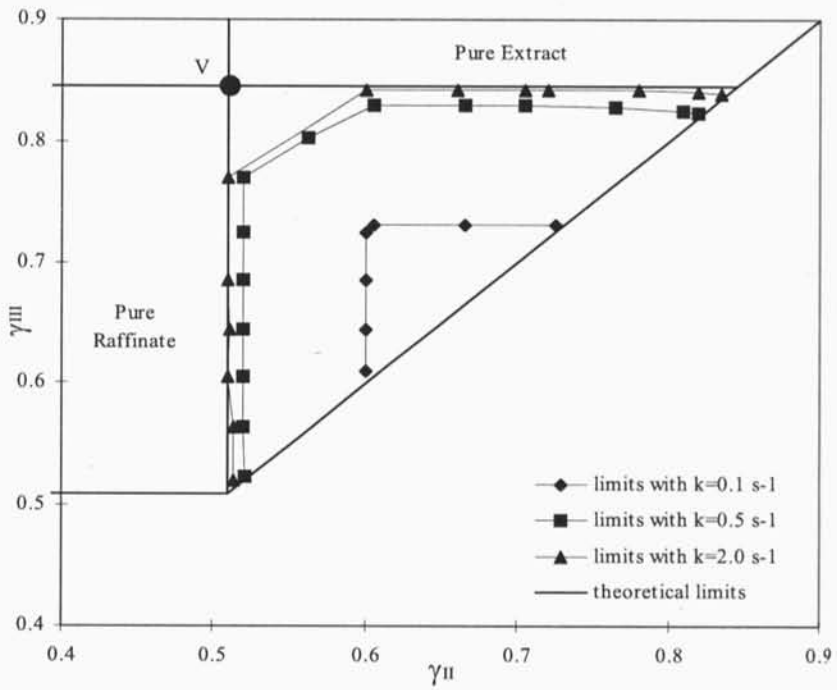

Figure 3.28 *Regions of operation of the TMB in a γ_{III} - γ_{II} plot considering linear isotherms for both components under conditions described in Table 3.12; the full diamonds (♦) represent numerical simulation results obtained for mass transfer resistance $k = 0.1\ s^{-1}$, the full squares (▪) represent numerical simulation results obtained for $k = 0.5\ s^{-1}$, the full triangles (▲) represent the numerical simulation results obtained for negligible mass transfer resistance $k = 2.0\ s^{-1}$, the — line represents the theoretical limits (Vertex: ♦ $\gamma_I = 1.56$, ▪ $\gamma_I = 1.46$, ▲ $\gamma_I = 1.45$).*

The area of separation increases with k, *i.e.*, lower mass transfer resistance, higher separation region we obtain improving the performance of the SMB, see Pais *et al.* (1997). The lines that define the triangle shaped region of complete separation converge to the theoretical limits, however, as in the previous study (section 3.1.3.7), the triangle is not complete. Notice that for small k ($k = 0.1\ s^{-1}$) the complete separation region is basically triangle shaped. With increase of the k, in other words, considering negligible the mass transfer, the γ_I values affect the SMB performance, as pointed out in Azevedo and Rodrigues (1999). In Azevedo and Rodrigues (1999), a different strategy was used to find the region of separation taking mass-transfer effects into consideration, for a linear equilibrium system, and intraparticle mass transfer described by a bi-LDF approximation. The value of γ_I is constant along a straight line parallel to the diagonal $\gamma_{II} = \gamma_{III}$, decreasing as gets away from the diagonal, as concluded before. Since the total balance is kept constant, the value of γ_I decreases when the feed flowrate increases. For $Q_F > 3.60\ ml/min$, γ_I becomes lower than the critical value, $\gamma_I > 0.8451$. The constraint concerning section IV is fulfilled, in all the simulations, since γ_{IV} is constant and equal to 0.4252 (< 0.5102).

Considering a higher total balance, $Q_D + Q_F = Q_E + Q_R = 12.89\ ml/min$, and lower mass transfer resistance, $k = 2.0\ s^{-1}$, we can obtained the expected triangle shaped complete separation region with limits equivalent to the limits estimated by the theoretical limits. The vertex point V, of a complete separation region corresponds to the better operating conditions (Pais, 1999). That can be shown comparing the values of γ_j for the vertex point V obtained for the two values of total balances considered, see Table 3.13. For both values of Q_{BAL}, γ_{II} and γ_{III} obtained are identical to the theoretical limits. However, γ_I, for lower Q_{BAL} is lower than the theoretical limit not satisfying the constraint in section I, placing point V in the pure extract region.

Now we will try to study the effect of the operating conditions on the TMB performance using the different isotherms equations for each component. Linear for fructose, equation (3.3b), and Langmuir for glucose, equation (3.4).

In Figure 3.29 we have the results of the simulations made for the reference case. The regions of separation for different values of k are defined. The region of complete separation is defined as explained in the previous case and following the operating conditions and model parameters presented in Table 3.12. The several points, connected by thin lines, are the numerical results defining the separation regions. The line that separates the complete

Table 3.13 *Operating conditions and γ_j parameters obtained for two values of total balance, Q_{BAL}, 9.51 and 12.89 ml/min, with Q_{Rec} = 19.89 ml/min, t^* = 1.75 mim and k = 2.0 s^{-1}.*

Total Balance, Q_{BAL} (ml/min)	**9.51**		**12.89**	
Q_D (ml/min)	4.81		8.22	
Q_E (ml/min)	3.61		7.03	
Q_F (ml/min)	4.70		4.67	
Q_R (ml/min)	5.90		5.86	
γ_I	0.770		1.014	
γ_{II}	0.511		0.511	
γ_{III}	0.848		0.845	
γ_{IV}	0.425		0.425	
	Gl	**Fr**	**Gl**	**Fr**
Purity (%)	81.1	99.8	99.5	99.7
Recovery (%)	99.8	76.7	99.7	99.5
Solvent Cons. (l/g)	0.0676	0.0880	0.0923	0.0925
Productivity (g/hr l)	19.209	14.756	19.070	19.021

separation region and the pure extract region is a straight line similar to the line obtained for the case of linear isotherms for both components. Notice that the fructose component, recovered in the extract, is described by a linear isotherm as in the previous example, explaining the similar behaviour. The line that separates the complete separation region and the pure raffinate region is different from the one obtained in the previous study since the isotherm for glucose was changed. Consequently, for a specific value of k, the complete separation region obtained is larger than the one obtained for linear isotherms for both components. As previously, the area of the complete separation region depends directly on the mass transfer resistance value. As previously with the Q_{BAL} initially used, for some values of Q_F the constraint in section I is not verified. The complete separation region does not have vertex, independently of value k, closed dots in Figure 3.29.

With Q_{BAL} = 12.89 *ml/min*, the shape of the complete separation region is as expected, open dots in Figure 3.29. The vertexes, V_1 and V_2 obtained for k = 0.1 and 2.0 s^{-1}, respectively, verifies the constraints in section I, that is, γ_1 = 1.1688 in V_1 and γ_1 = 0.9538 in V_2 (>0.8451).

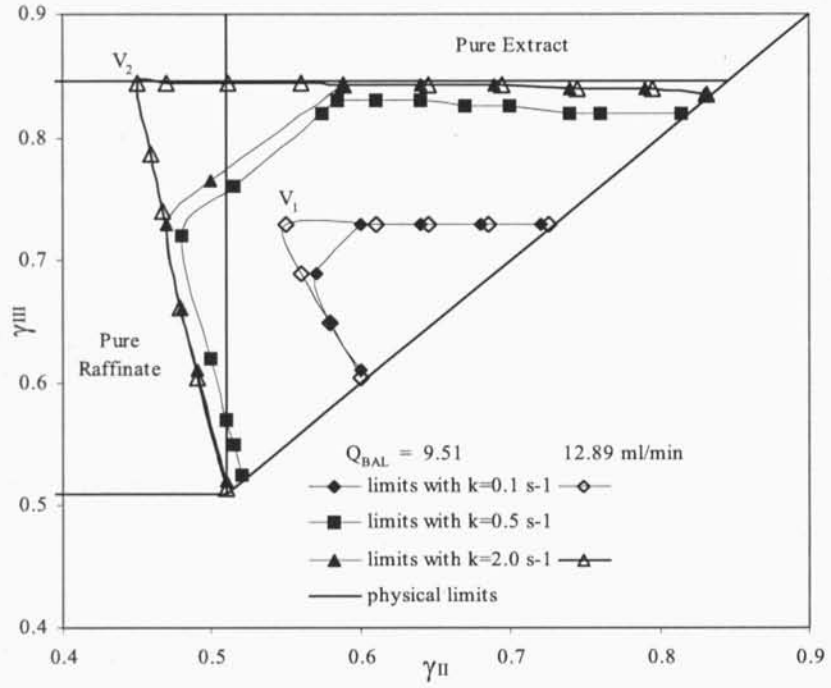

Figure 3.29 *Regions of operation of the TMB in a γ_{III} - γ_{II} plot considering linear isotherm for fructose and Langmuir for glucose under conditions described in Table 3.12; the full diamonds (♦) represent numerical simulation results obtained for mass transfer resistance $k = 0.1\ s^{-1}$, the full squares (▪) represent numerical simulation results obtained for $k = 0.5\ s^{-1}$, the full triangles (▲) represent the numerical simulation results obtained for negligible mass transfer resistance $k = 2.0\ s^{-1}$, the —represent the theoretical limits; the open diamonds (◊) and triangles (Δ) represents the numerical simulation results obtained for $k = 0.1$ and $2\ s^{-1}$, respectively for $Q_{BAL} = 12.89$ ml/min (Vertex: ♦ $\gamma_I = 0.97$, ◊ $\gamma_I = 1.17$, ▲ $\gamma_I = 0.85$, Δ $\gamma_I = 0.95$).*

3.2 TMB and SMB Models using LDF Approximation Model for Porous Particles

The chromatographic separation of 1,1'-bi-naphtol enantiomers with 3,5-dinitrobenzoyl phenylglycine bonded to silica gel stationary phases is used as an example (Pais 1999). Continuous chromatography in simulated moving bed (SMB) is analysed by modelling and simulation of the SMB.

A new model is developed for the prediction of the cyclic steady-state performance of the SMB. The new model assumes axial dispersion flow for the liquid phase, diffusion of the

species *i* inside particles described by a LDF approximation for porous particles, Figure 3.30, and takes into account multicomponent adsorption equilibrium.

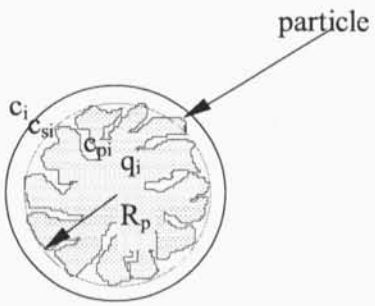

Figure 3.30 *Schematic stagnant particle representation.*

The SMB package allows the simulation of the pilot unit.

The work involves the following steps:

(i) development of a model for the SMB and numerical solution of model equations,

(ii) understanding SMB process by using the simulation package to predict the effect of operating variables on the SMB performance,

(iii) comparison with the operation of the SMB pilot unit for the bi-napthol system obtained in Pais *et al.* (1997) and the simulated results.

The model equations are described in Table 3.14 and dimensionless model equations are shown in Table 3.15, where *i* (*i*=*A*, *B*) refers to the species in the mixture, *j* (*j*=1, 2, 3, 4) is the section number, c_{ij} the concentration of component *i* in the adsorption section *j*, $\langle c_{p_{ij}} \rangle$ the mean pore concentration of component *i* in section *j* averaged over the particle, and $\langle q_{ij} \rangle$ the average adsorbed-phase concentration of species *i* in the section *j* of the TMB, q_{ij}^* adsorbed concentration in equilibrium with the fluid phase concentration c_{ij} (Pais *et al.*, (1997) model), or in equilibrium with the pore concentration $c_{p_{ij}}$ (model developed in chapter five), *z* the

Table 3.14 *Transient TMB model equations.*

	Pais *et al.* (1997) model – LDF for homogeneous particles	**This work - LDF model for porous particle**
Mass balance in volume element of the bed	$\varepsilon D_{L_j}\frac{\partial^2 c_{ij}}{\partial z^2}-\varepsilon v_j\frac{\partial c_{ij}}{\partial z}+(1-\varepsilon)u_s\frac{\partial\langle q_{ij}\rangle}{\partial z}=$ $=\varepsilon\frac{\partial c_{ij}}{\partial t}+(1-\varepsilon)\frac{\partial\langle q_{ij}\rangle}{\partial t}$ (3.6)	$\varepsilon D_{L_j}\frac{\partial^2 c_{ij}}{\partial z^2}-\varepsilon v_j\frac{\partial c_{ij}}{\partial z}+(1-\varepsilon)u_s\left[\frac{\partial\langle q_{ij}\rangle}{\partial z}+\varepsilon_p\frac{\partial\langle c_{p_{ij}}\rangle}{\partial z}\right]=$ $=\varepsilon\frac{\partial c_{ij}}{\partial t}+(1-\varepsilon)\left[\frac{\partial\langle q_{ij}\rangle}{\partial t}+\varepsilon_p\frac{\partial\langle c_{p_{ij}}\rangle}{\partial t}\right]$ (3.11)
Mass balance in the adsorbent particles	$u_s\frac{\partial\langle q_{ij}\rangle}{\partial z}+k\left(q_{ij}^*-\langle q_{ij}\rangle\right)=\frac{\partial\langle q_{ij}\rangle}{\partial t}$ (3.7)	$u_s\left[\frac{\partial\langle q_{ij}\rangle}{\partial z}+\varepsilon_p\frac{\partial\langle c_{p_{ij}}\rangle}{\partial z}\right]+k_p\left(c_{ij}-\langle c_{p_{ij}}\rangle\right)=\left[\frac{\partial\langle q_{ij}\rangle}{\partial t}+\varepsilon_p\frac{\partial\langle c_{p_{ij}}\rangle}{\partial t}\right]$ (3.12)
Boundary conditions	$z=0,\quad c_{ij}-\frac{D_{L_j}}{v_j}\frac{\partial c_{ij}}{\partial z}=c_{ij,0}$ $z=L_j,\quad \frac{\partial c_{ij}}{\partial z}=0\quad\text{and}\quad\langle q_{ij}\rangle=\langle q_{ij+1,0}\rangle$ (3.8)	$z=0,\quad c_{ij}-\frac{D_{L_j}}{v_j}\frac{\partial c_{ij}}{\partial z}=c_{ij,0}$ $z=L_j,\quad \frac{\partial c_{ij}}{\partial z}=0\quad\text{and}\quad\langle c_{p_{ij}}\rangle=\langle c_{p_{ij+1,0}}\rangle$ (3.13)
Multicomponent Adsorption equilibrium isotherm	$q_{Aj}^*=\frac{2.69c_{Aj}}{1+0.0336c_{Aj}+0.0466c_{Bj}}+\frac{0.10c_{Aj}}{1+c_{Aj}+3c_{Bj}}$ $q_{Bj}^*=\frac{3.73c_{Bj}}{1+0.0336c_{Aj}+0.0466c_{Bj}}+\frac{0.30c_{pBj}}{1+c_{Aj}+3c_{Bj}}$ (3.9)	$q_{Aj}^*=\frac{2.69c_{pAj}}{1+0.0336c_{pAj}+0.0466c_{pBj}}+\frac{0.10c_{pAj}}{1+c_{pAj}+3c_{pBj}}-\varepsilon_p c_{pAj}$ $q_{Bj}^*=\frac{3.73c_{pBj}}{1+0.0336c_{pAj}+0.0466c_{pBj}}+\frac{0.30c_{pBj}}{1+c_{pAj}+3c_{pBj}}-\varepsilon_p c_{pBj}$ (3.14)
Mass balances at the nodes of the inlet and outlet lines of the TMB	eluent node: $c_{i1,0}=\frac{v_4}{v_1}c_{i4,L_j}$, extract node: $c_{i2,0}=c_{i1,L_j}$ feed node: $c_{i3,0}=\frac{v_2}{v_3}c_{i2,L_j}+\frac{v_F}{v_3}c_i^F$, raffinate node: $c_{i4,0}=c_{i3,L_j}$ (3.10)	eluent node: $c_{i1,0}=\frac{v_4}{v_1}c_{i4,L_j}$, extract node: $c_{i2,0}=c_{i1,L_j}$ feed node: $c_{i3,0}=\frac{v_2}{v_3}c_{i2,L_j}+\frac{v_F}{v_3}c_i^F$, raffinate node: $c_{i4,0}=c_{i3,L_j}$ (3.15)

Table 3.15 Transient TMB dimensionless model equations.

	Pais *et al.* (1997) model – LDF for homogeneous particles	This work - LDF model for porous particle
Mass balance in volume element of the bed	$\frac{1}{Pe_j}\frac{\partial^2 c_{ij}}{\partial x^2}-\frac{\partial c_{ij}}{\partial x}+\frac{(1-\varepsilon)}{\varepsilon}\frac{1}{\gamma_j}\frac{\partial\langle q_{ij}\rangle}{\partial x}= =\frac{1}{\gamma_j}\frac{\partial c_{ij}}{\partial\theta}+\frac{(1-\varepsilon)}{\varepsilon}\frac{1}{\gamma_j}\frac{\partial\langle q_{ij}\rangle}{\partial\theta}$ (3.16)	$\frac{1}{Pe_j}\frac{\partial^2 c_{ij}}{\partial x^2}-\frac{\partial c_{ij}}{\partial x}+\frac{(1-\varepsilon)}{\varepsilon}\frac{1}{\gamma_j}\left[\frac{\partial\langle q_{ij}\rangle}{\partial x}+\varepsilon_p\frac{\partial\langle c_{Pij}\rangle}{\partial x}\right]= =\frac{1}{\gamma_j}\frac{\partial c_{ij}}{\partial\theta}+\frac{(1-\varepsilon)}{\varepsilon}\frac{1}{\gamma_j}\left[\frac{\partial\langle q_{ij}\rangle}{\partial\theta}+\varepsilon_p\frac{\partial\langle c_{Pij}\rangle}{\partial\theta}\right]$ (3.19)
Mass balance in the adsorbent particles	$\frac{\partial\langle q_{ij}\rangle}{\partial x}+\alpha_j\left(q_{ij}^{*}-\langle q_{ij}\rangle\right)=\frac{\partial\langle q_{ij}\rangle}{\partial\theta}$ (3.17)	$\left[\frac{\partial\langle q_{ij}\rangle}{\partial x}+\varepsilon_p\frac{\partial\langle c_{Pij}\rangle}{\partial x}\right]+\alpha_p\left(c_{ij}-\langle c_{Pij}\rangle\right)=\left[\frac{\partial\langle q_{ij}\rangle}{\partial\theta}+\varepsilon_p\frac{\partial\langle c_{Pij}\rangle}{\partial\theta}\right]$ (3.20)
Boundary conditions	$x=0,\quad c_{ij}-\frac{1}{Pe_j}\frac{\partial c_{ij}}{\partial x}=c_{ij,0}$ $x=1,\quad \frac{\partial c_{ij}}{\partial x}=0$ and $\langle q_{ij}\rangle=\langle q_{ij+1,0}\rangle$ (3.18)	$x=0,\quad c_{ij}-\frac{1}{Pe_j}\frac{\partial c_{ij}}{\partial x}=c_{ij,0}$ $x=1,\quad \frac{\partial c_{ij}}{\partial x}=0$ and $\langle c_{Pij}\rangle=\langle c_{Pij+1,0}\rangle$ (3.21)

Multicomponent adsorption equilibrium isotherm and the mass balances at the nodes of the inlet and outlet lines of the TMB are the same as in Table 3.14, (3.9-3.10) and (3.14-3.15), for the Pais *et al.* (1997) model and for this work model, respectively.

axial coordinate, t is the time variable, ε is the bed porosity (= 0.4), ε_p is the particle porosity (= 0.45), and D_{L_j} is the axial dispersion coefficient in section j.

Introducing the dimensionless variables $x = z/L_j$ and $\theta = t/\tau_s$ with $\tau_s = L_j/u_s = N_s \Delta T$ (where N_s is the number of columns per section) the model equations become as described in Table 3.15. The model parameters are:

$\frac{(1-\varepsilon)}{\varepsilon}$ ratio between solid and fluid volumes;

$\gamma_j = \frac{v_j}{u_s}$ ratio between fluid and solid velocities;

$Pe_j = \frac{v_j L_j}{D_{L_j}}$ Peclet number;

$\alpha_j = \frac{kL_j}{u_s} = k\tau_s$ number of intraparticle mass transfer units, for the Pais *et al.* (1997) model and,

$\alpha_{pj} = \frac{k_p L_j}{u_s} = k_p \tau_s$ number of intraparticle mass transfer units, for model developed in the present work.

The partial differential equations model was simplified by considering the terms in order to time, t, equal to zero, that is, $\frac{\partial c_{ij}}{\partial t} = \frac{\partial \langle q_{ij} \rangle}{\partial t} = \frac{\partial \langle c_{p_{ij}} \rangle}{\partial t} = 0$. The resulting dimensionless model is presented in Table 3.16, and then solved by using the COLNEW package (improved version of COLSYS (Ascher *et al.*, 1981) based on collocation at the Gaussian points as the method of approximation).

In the above equations, (Table 3.14-3.15), the liquid-phase concentrations of species A and B, c_A and c_B, respectively, are in g/l of solution, the adsorbent-phase concentrations are expressed in g/l of adsorbent, and the mean pore concentration, averaged over the particle, $\langle c_{p_A} \rangle$ and $\langle c_{p_B} \rangle$, are in g adsorbed/l of fluid in pores.

The mass transfer coefficient can be estimated by using the following relationship (Pais, 1999),

Table 3.16 *Steady-state TMB dimensionless model equations.*

	Pais *et al.* (1997) model – LDF for homogeneous particles	**This work - LDF model for porous particle**
Mass balance in volume element of the bed	$\frac{d^2c_{ij}}{dx^2} = Pe_j\left[\frac{dc_{ij}}{dx} - \frac{(1-\varepsilon)}{\varepsilon}\frac{1}{\gamma_j}\frac{d\langle q_{ij}\rangle}{dx}\right]$ (3.22)	$\frac{d^2c_{ij}}{dx^2} = Pe_j\frac{dc_{ij}}{dx} - \frac{(1-\varepsilon)}{\varepsilon}\frac{Pe_j}{\gamma_j}\left[\frac{d\langle q_{ij}\rangle}{dx} + \varepsilon_p\frac{d\langle c_{Pij}\rangle}{dx}\right]$ (3.25)
Mass balance in the adsorbent particles	$\frac{d\langle q_{ij}\rangle}{dx} = -\alpha_j\left(q_{ij}^{*} - \langle q_{ij}\rangle\right)$ (3.23)	$\left[\frac{d\langle q_{ij}\rangle}{dx} + \varepsilon_p\frac{d\langle c_{Pij}\rangle}{dx}\right] = -\alpha_p\left(c_{ij} - \langle c_{Pij}\rangle\right)$ (3.26)
Boundary conditions	$x=0, \quad c_{ij} - \frac{1}{Pe_j}\frac{dc_{ij}}{dx} = c_{ij,0}$ $x=1, \quad \frac{dc_{ij}}{dx} = 0 \quad \text{and} \quad \langle q_{ij}\rangle = \langle q_{ij+1,0}\rangle$ (3.24)	$x=0, \quad c_{ij} - \frac{1}{Pe_j}\frac{dc_{ij}}{dx} = c_{ij,0}$ $x=1, \quad \frac{dc_{ij}}{dx} = 0 \quad \text{and} \quad \langle c_{Pij}\rangle = \langle c_{Pij+1,0}\rangle$ (3.27)

Multicomponent adsorption equilibrium isotherm and the mass balances at the nodes of the inlet and outlet lines of the TMB are the same as in Table 3.14, (3.9-3.10) and (3.14-3.15), for the Pais *et al.* (1997) model and for this work model, respectively.

$$k_h = \frac{k_p}{\varepsilon_p + K} = \frac{k_p}{K_h} \tag{3.28}$$

obtained by using the equivalence between the linear driving force (LDF) model for homogeneous particles and the LDF model considering porous particles (model used in this work); k_h is the mass transfer coefficient used in the LDF model for homogeneous particles, k_p is the mass transfer coefficient used in the LDF model for porous particles evaluated by $k_p = \frac{15 D_{pe}}{R_p^2}$, $D_{pe} = \frac{\varepsilon_p D_m}{\tau}$ the effective pore diffusivity and R_p the particle radius (= 1.625×10^{-3} cm), D_m the molecular diffusivity (= 8.1×10^{-6} cm^2s^{-1}) by using the Wilke-Chang correlation (Reid *et al.*, 1987), $D_m = \frac{7.4\times10^{-8}(\phi M)^{1/2} T}{\eta V^{0.6}}$, M is the molecular weight of the solvent (g mol^{-1}), T is the temperature (K), η is the solvent viscosity (cP), V is the molar volume of the solute at its normal boiling temperature (cm^3mol^{-1}), ϕ is an association factor of the solvent (dimensionless, 2.6 if the solvent is water, 1.9 if it is methanol, 1.5 if it is ethanol, and 1.0 if it is unassociated), and τ the tortuosity (value between 2 and 8, in this work it was considered equal to 5), ε_p is the particle porosity (= 0.45), K_h $(= \varepsilon_p + K)$ is the initial slope of the isotherm considering the adsorbent as homogenous particle (K_{h_A} = 2.79, K_{h_B} = 4.03, the one used in Pais *et al.* (1997) work), and K is the initial slope of the isotherm considering only the adsorbed amount (excluding the amount in pores), $K_A \approx 2.79 - \varepsilon_p = 2.34$, $K_B \approx 4.03 - \varepsilon_p = 3.58$, the one used in this work. Using the equation (3.28) and the value of the mass transfer coefficient used in the LDF model for homogeneous particles, $k_p = 0.10$ s^{-1} (Pais *et al.*, 1997a; and Pais, 1999), it is possible to estimate the mass transfer coefficient for the LDF model for porous particles, $k_{pA} = k_p K_{hA} = 0.279$ s^{-1} and $k_{pB} = k_p K_{hB} = 0.403$ s^{-1}.

The Figure 3.31 presents the adsorption isotherms for the bi-naphtol enantiomers for the Pais *et al.* (1997) model, equation (3.9) (— line), and for the new model, equation (3.14) (▬ line).

The operating conditions used for the SMB simulation for the separation of the bi-naphthol enantiomers were those of Pais *et al.* (1997a), and presented in Table 3.17. The steady-state TMB model presented in Table 3.16 was used to simulate the SMB operation by predicting its performance and its internal concentration profiles.

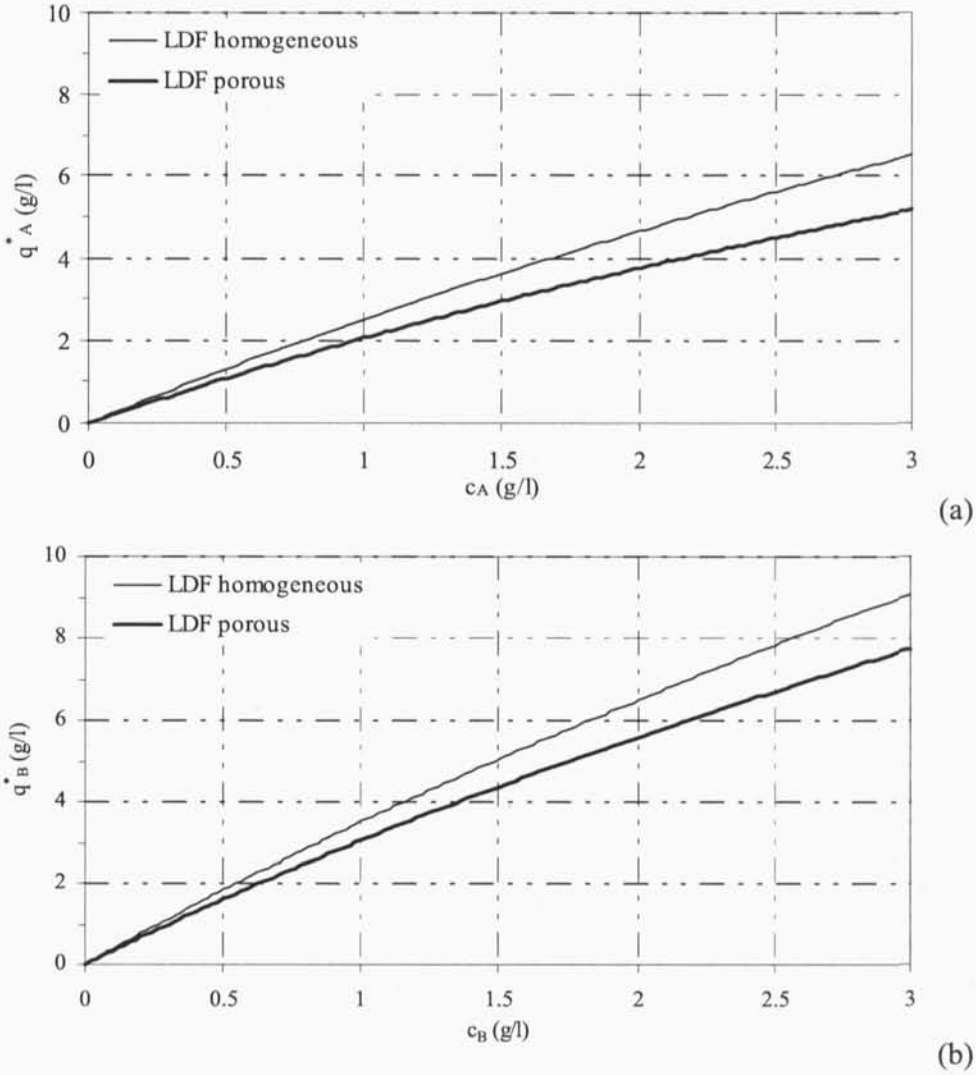

Figure 3.31 *Adsorption isotherms for the bi-naphthol enantiomers: (a) for the lees retained component; (b) for the more retained component. Thin line for the LDF model for homogeneous particles, equation (3.9), and thick line for LDF model considering porous particles, equation (3.14).*

The values of velocities ratios in each section were estimated according to the equilibrium theory:

$$\gamma_I > \frac{1-\varepsilon}{\varepsilon}\left(\varepsilon_p + K_B\right),\ \frac{1-\varepsilon}{\varepsilon}\left(\varepsilon_p + K_A\right) < \gamma_{II} < \gamma_{III} < \frac{1-\varepsilon}{\varepsilon}\left(\varepsilon_p + K_B\right),\ \gamma_{IV} < \frac{1-\varepsilon}{\varepsilon}\left(\varepsilon_p + K_A\right) \quad (3.29)$$

where K_A , and K_B are the equilibrium constant for the adsorbed amount (excluding the amount in pores) for the less and the more retained component, respectively. With $Q_{IV} = Q_{Rec}$

= 35.38 ml/min and fixed γ_{IV} = 3.76 (< 4.185). The value of γ_I was fixed as 6.65 (> 6.045). The velocities ratios γ_{II} and γ_{III}, determine the separation region, which depends on the feed. The values fixed were: γ_{II} = 4.23 (> 4.185) and γ_{III} = 4.72 (< 6.045). Taking into account these values, the remaining flowrates were calculated and presented in Table 3.17.

Table 3.17 *SMB and equivalent TMB operating conditions and model parameters used in the steady-state TMB model, with a feed concentration of* $C_A = C_B = 2.9$ *g/l.*

SMB operation conditions	**Equivalent TMB operating conditions**	**Model parameters:**
Columns: Diameter: 2.6 cm Length: 10.5 cm Number of columns: 8 Configuration: 2-2-2-2	Sections: Diameter: 2.6 cm Length: 21 cm Number of sections: 4	Solid/fluid volumes: 1.5 Peclet number: 2000 Mass transfer unit: $\alpha_{pA} = 100.4$ ($k_{pA} = 0.279$ s^{-1}) $\alpha_{pB} = 145.1$ ($k_{pB} = 0.403$ s^{-1})
Flow-rates (ml/min): Eluent: 21.45 Extract: 17.98 Feed: 3.64 Raffinate: 7.11 Recycling flow-rate: 35.38	Flow-rates (ml/min): Eluent: 21.45 Extract: 17.98 Feed: 3.64 Raffinate: 7.11	Ratio between fluid and solid Velocities: γ_I=6.65 γ_{II}=4.23 γ_{III}=4.72 γ_{IV}=3.76
Switch time interval: 3 min	Solid flow-rate: 11.15ml/min	$\varepsilon_p = 0.45$ $K_A = 2.34$ $K_B = 3.58$

Model equations (3.25-3.27, 3.14-3.15) were numerically solved by using the COLNEW package (Bader and Asher, 1987). The steady-state model is defined by a set of 16 non-linear ODE's, two ordinary differential equations, for each component in each of the four section of the TMB. No initial guess to the solution is provided and the solver COLNEW generates the initial mesh and controls it during the numerical solution, with 3 collocation points in each element. The error tolerance was set at 10^{-8}. When the global error, *er* (equation (3.1)), is less than 0.05%, maximum error defined by the user, the TMB steady-state final solution is achieved.

For the case studied and using the parameters presented in Table 3.17, the steady-state TMB solution took approximately 30 min (Pentium III 500 MHz). The effects of the rotation

period, extract and feed flow rates, section length and number of intraparticle mass transfer units on the SMB performance were studied by simulation. The reference flow rates were the same as the one used in Pais *et al.* (1997a). The internal profiles for the reference case are shown in Figure 3.32.

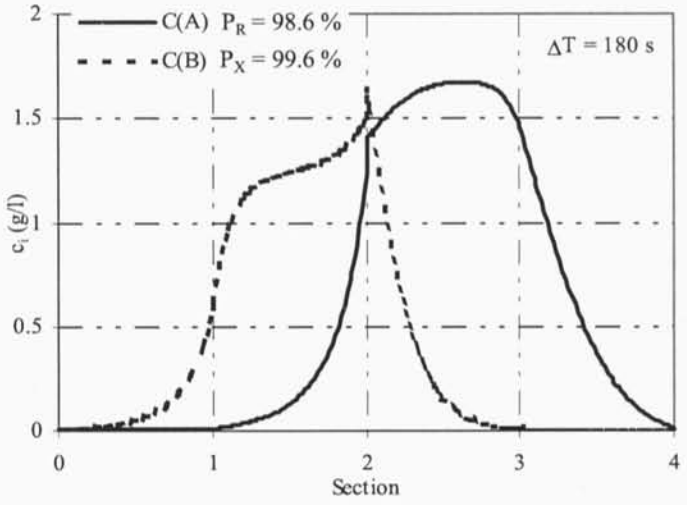

Figure 3.32 *Internal profiles for the reference case. Solid line for the less retained component dashed line for the more retained component under operating conditions as in Table 3.17.*

3.2.1 Effect of operating variables

3.2.1.1 Effect of the rotation period

The effect of the rotation period, t^*, on the SMB performance is shown in Figure 3.33. The other operating conditions and model parameters were kept constants, Table 3.17. It can be seen that, for the performance parameters, an optimum value of rotation period exists, $t^* \approx$ 180 sec. The black points in each graph of Figure 3.33 correspond to the optimum value obtained for the reference case. For lower or higher rotation period values, both extract and raffinate purity and recovery decrease. The region of high purity and recovery can be defined by relating recovery with purity obtained for different values of rotation period, Figure 3.16e and Figure 3.16f.

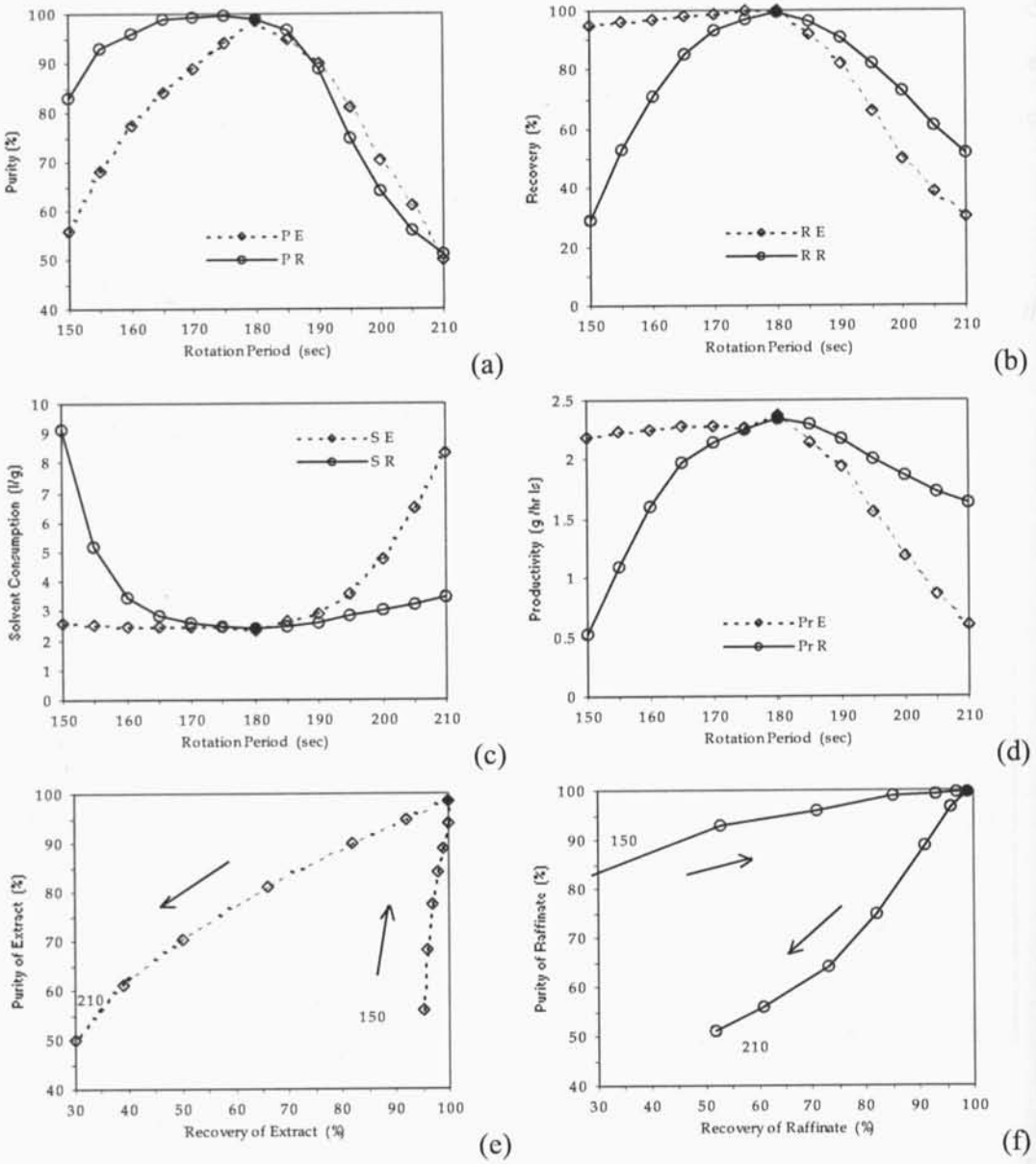

Figure 3.33 *Effect of the rotation period on the SMB performance parameters, $t^* \in$ [105, 210] sec. The others operating conditions and model parameters were kept constant as described in Table 3.17. (a) Rotation Period vs. Purity (b) Rotation Period vs. Recovery (c) Rotation Period vs. Solvent Consumption (d) Rotation Period vs. Productivity (e) Recovery vs. purity for extract (f) Recovery vs. recovery for raffinate (the arrows show the way of the rotation period increase).*

3.2.1.2 Effect of the extract flow rate

The effect of the extract flow rate Q_E on the SMB performance is shown in Figure 3.34. The purity for both extract and raffinate, is very sensitive to the change of extract flowrate. It can be seen that, depending on which direction Q_E is changed, the optimum value of the extract flowrate drastically affects the performance of one or the other product. The black points shown in the Figure 3.34, correspond to the optimum value obtained for the reference case. The reasons of such behaviour are the same as the ones described in the previous section.

Higher values of extract flowrate will decrease the liquid flowrate in section II modifying the flux of the extract in the opposite direction decreasing the purity in the extract. Lower values of extract flowrate implies higher values in the raffinate flowrate affecting the liquid flowrate in section III modifying the extract flux in opposite direction decreasing the raffinate purity.

Figure 3.34e and Figure 3.34f show the behaviour of the effect of the extract flowrate on the purity and recovery. It shows that, only for a narrow region of values of extract flowrates, it is possible to obtain simultaneously high purity and recovery for both extract and raffinate.

3.2.1.3 Effect of the feed flow rate

The effect of the feed flow rate Q_F on the SMB performance is shown in Figure 3.35. The concentration varied between 0.14 and 9.14 ml/min. An increase of the feed flowrate improves the productivity and the solvent consumption for the extract and raffinate. Opposite behaviour is obtained for the purity and recovery parameters. The results obtained are similar to the ones obtained in the studied of the influence of the operating variables with the previous TMB model. However different effect of the feed flowrate on the recovery versus purity is obtained for the extract and raffinate, Figure 3.35e and Figure 3.35f. With the decrease of the feed flowrate, the purity and recovery of the extract increase. The region of high purity and recovery for the raffinate is narrower, even so, sufficient to obtain simultaneously, high purity and recovery for both extract and raffinate.

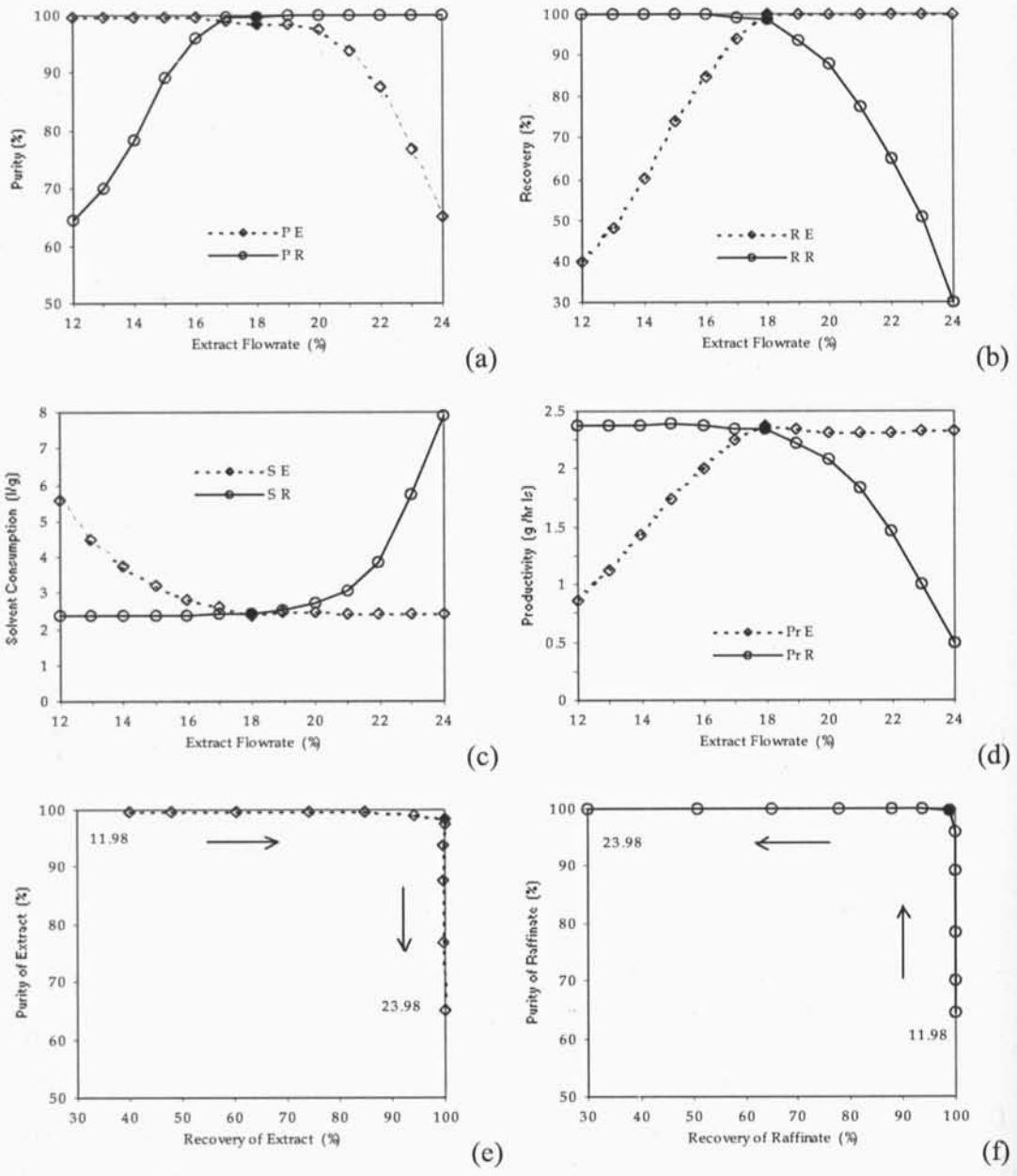

Figure 3.34 *Effect of the extract flowrate on the SMB performance parameters, $Q_E \in$ [11.98, 23.98] ml/min. The others operating conditions and model parameters were kept constant as described in Table 3.17. (a) Extract Flowrate vs. Purity (b) Extract Flowrate vs. Recovery (c) Extract Flowrate vs. Solvent Consumption (d) Extract Flowrate vs. Productivity (e) Recovery vs. purity for extract (f) Recovery vs. recovery for raffinate (the arrows show the way of the extract flowrate increase).*

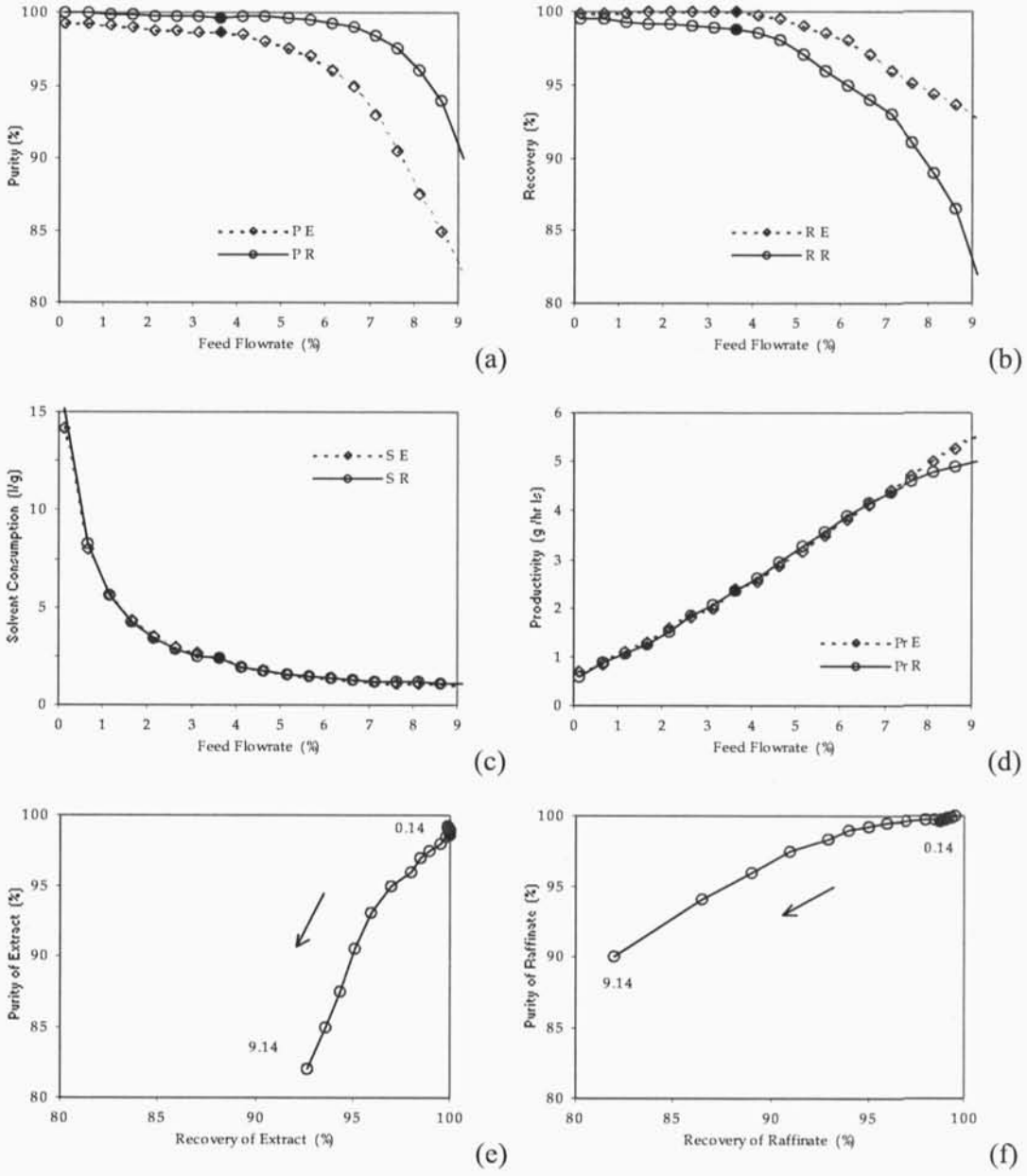

Figure 3.35 *Effect of the feed flow rate on the SMB performance parameters for the case study.* $Q_F \in [0.14; 9.14]$*ml/min. The others operating conditions and model parameters were kept constant and the same as described in Table 3.17, except the eluent flowrate that changed with the feed flowrate in order to keep constant the total balance* ($Q_R+Q_E=Q_D+Q_F$). ***(a)*** *Feed Flowrate vs. Purity,* ***(b)*** *Feed Flowrate vs. Recovery,* ***(c)*** *Feed Flowrate vs. Solvent Consumption,* ***(d)*** *Feed Flowrate vs. Productivity,* ***(e)*** *Recovery vs. Purity for Extract* ***(f)*** *Recovery vs. Purity for Raffinate. The arrows show the increase of the feed flowrate.*

3.2.1.4 Effect of the section length

The effect of the section length is displayed in Figure 3.36 for values between 10.5 *cm* (1 column/section) to 52.5 *cm* (5 columns/section). With the mass transfer coefficients, in the LDF model for porous particle, for the two components, $k_{pA} = 0.279\ s^{-1}$, $k_{pB} = 0.403\ s^{-1}$, no significant improvement in the system performance is observed for section length greater than 31.5 *cm* corresponding to 3 columns per section in the SMB configuration.

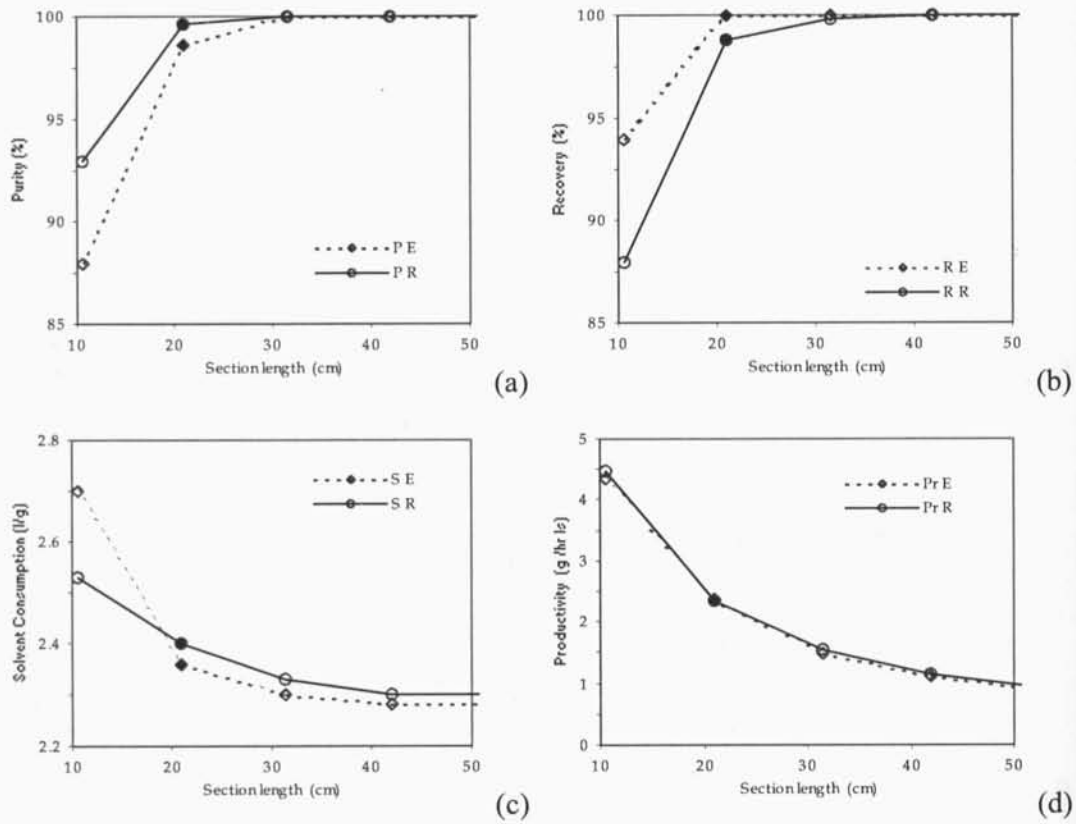

Figure 3.36 *Effect of the section length on the performance parameters: (a) purity, (b) recovery, (c) solvent consumption, (d) productivity. The others operating conditions and model parameters were kept constant and the same as described in Table 3.17.*

3.2.1.5 Effect of the number of intraparticle mass transfer units

The effect of the mass transport coefficient in the pores, k_p, or the corresponding dimensionless number, α_p, on the cyclic steady-state internal profiles of the SMB is shown in Figure 3.37 for $\alpha_{pA} = 50.22$ and $\alpha_{pB} = 72.54$ (or $k_{pA} = 0.1395\ s^{-1}$ and $k_{pB} = 0.2015\ s^{-1}$) and α_{pA}

= 502.2 and α_{pB} = 725.4 (or k_{pA} = 1.395 s^{-1} and k_{pB} = 2.015 s^{-1}). For α_{pA} = 100.44 and α_{pB} = 145.08 (or k_{pA} = 0.279 s^{-1} and k_{pB} = 0.403 s^{-1}), the reference case, is shown in Figure 3.32.

The mass transfer coefficients for the LDF model for porous particle were obtained having as source the values of the mass transfer coefficient used in the LDF for homogeneous particles (Pais *et al.*, 1997a), k_h = 0.05, 0.5 and 0.1 s^{-1}, respectively, and using the relationship (3.28). The performance parameters obtained for these three simulations are presented in Table 3.18. These coefficients depend on the effective diffusivity and particle size. By decreasing the particle size, the value of α_{pi} or k_{pi}, increases, improving the performance of the SMB.

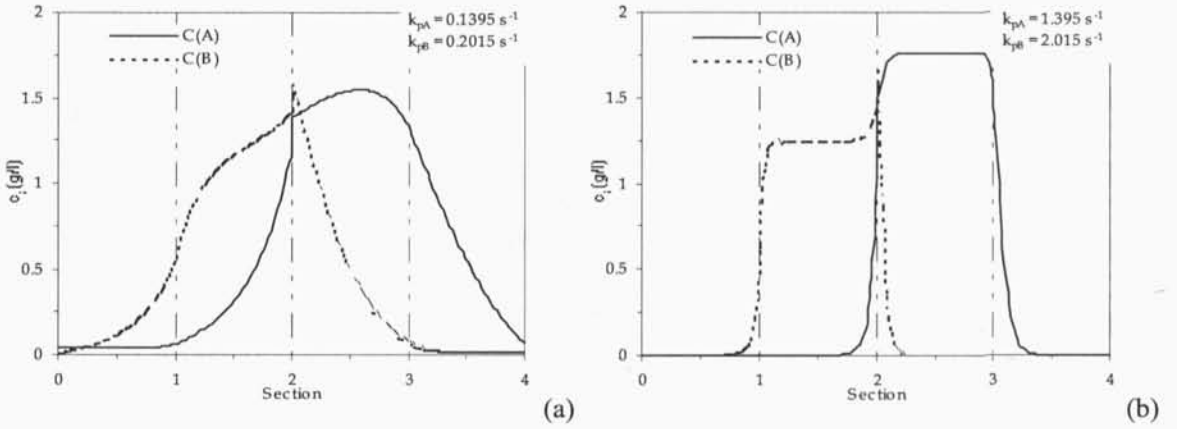

Figure 3.37 *Effect of the mass transport coefficient in the pores on the cyclic SMB steady-state internal profiles. (a) k_{pA} = 0.1395 s^{-1} and k_{pB} = 2.015 s^{-1} (or α_{pA} = 50.22 and α_{pB} = 72.54), (b) k_{pA} = 1.395 s^{-1} and k_{pB} = 2.015 s^{-1} (or α_{pA} = 502.2 and α_{pB} = 725.4). The others operating conditions and model parameters were kept constant and the same as described in Table 3.17.*

Table 3.18 *Effect of the mass transport coefficient in the pores on the performance parameters.*

k_h (s^{-1}) [a]	α_p		Purity (%)		Recovery (%)		Solvent Cons. (l/gr)		Productivity (g/hr l)	
	A	B	A (R)	B (E)	A (R)	B (E)	A (R)	B (E)	A (R)	B (E)
0.05	50.22	72.54	90.1	94.7	95.6	89.8	2.49	2.65	2.26	2.13
0.1	100.44	145.08	98.6	99.6	100	98.8	2.36	2.40	2.38	2.34
0.5	502.2	725.4	100	100	100	100	2.25	2.28	2.50	2.46

[a] coefficients as in Pais *et al.* (1997a).

3.2.2 Evolution of the internal profiles for the transient operation of the TMB

The evolution of the transient internal profiles for the TMB operation was also evaluated in the reference case by using the model equations described in Table 3.15, LDF model for porous particle, equations (3.19-3.21), and it is shown in Figure 3.38 for cycles 1, 2, 3 and 10 (cycle steady-state). The front of the less adsorbed species A is progressing in zone III leading to a A-rich raffinate stream. A number of cycles, 10, is sufficient to reach the final cyclic steady-state.

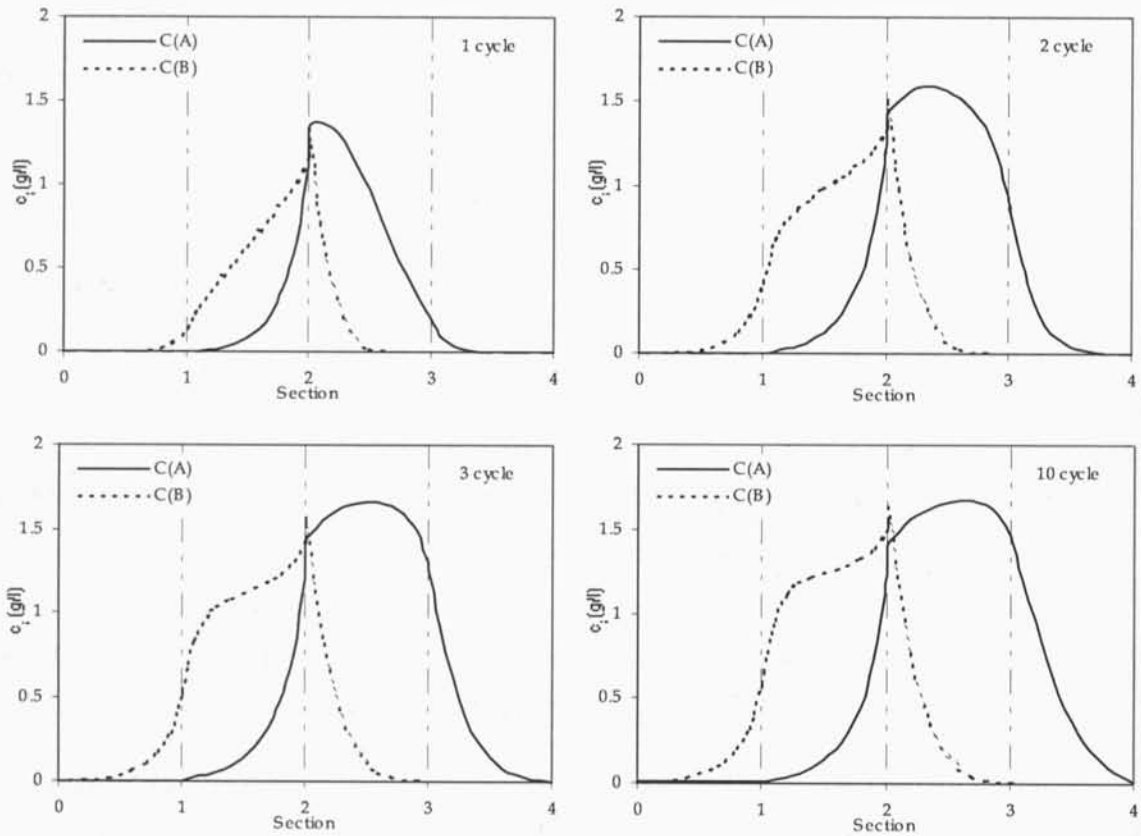

Figure 3.38 *Transient TMB internal profiles for the reference case obtained for cycles 1, 2, 3 and 10.*

3.2.3 Influence of the LDF type model approximation

The influence of the type of the LDF model considered can be analysed through Figure 3.39. As expected, no significant differences in the extract and raffinate profile concentrations

between the LDF model for homogenous particle and the LDF model for porous particle were found. The equivalence between the T-TMB models using LDF-homogeneous and LDF-porous approximation has been verified.

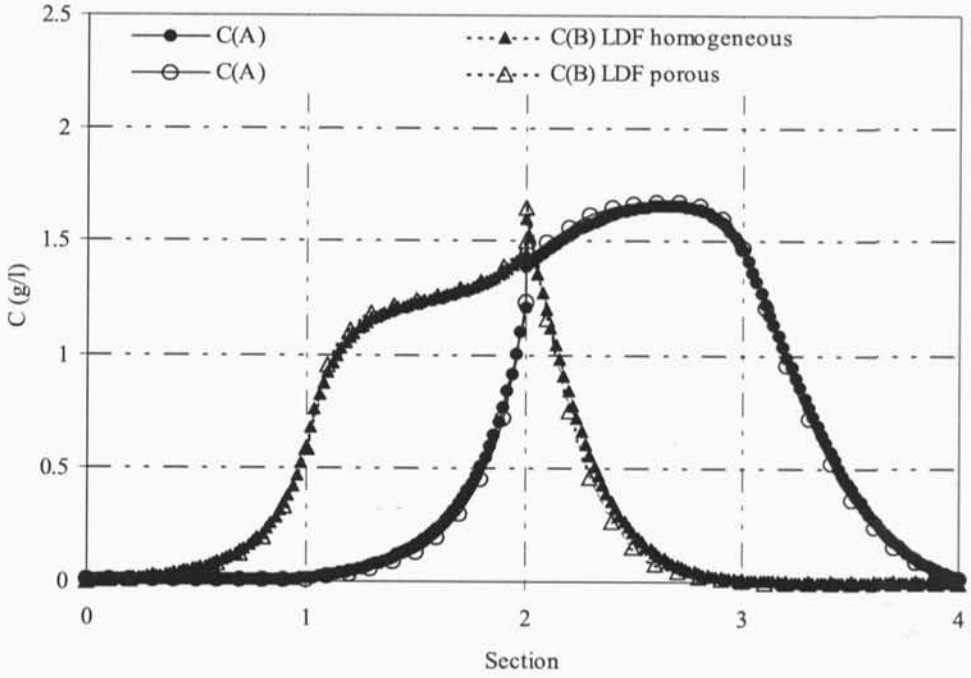

Figure 3.39 *Internal profiles for the case of LDF model for homogeneous particles (full circles for raffinate (A) and full triangles for extract (B)), and LDF model for porous particles (white circles for raffinate (A) and white triangles for extract (B)).*

With the LDF model for porous particle, the cyclic steady-state behaviour, characteristic of a SMB operation, can be simulated, Figure 3.40 and 3.41. The SMB operating conditions and model parameters used are described in Table 3.17. The number of mass transfer units per section for porous particles, k_{pi}, is the same for TMB and SMB (Table 3.17).

The model equations using a SMB strategy by using the LDF-porous approximation are presented in Table 3.19., see equations (3.34–3.37).

The model equations described in Table 3.19 represents the dimensionless model equations, where i (i=A, B) refers to the species in the mixture, k (k=1, 2, ...) is the column number, c_{ik} and $\langle q_{ik} \rangle$ fluid phase and average adsorbed phase concentration of species i in column k of

Table 3.19 *Transient SMB dimensionless model equations.*

	Pais *et al.* (1997) model – LDF for homogeneous particles	**This work - LDF model for porous particle**
Mass balance in volume element of the bed k	$\frac{\partial c_{ik}}{\partial \theta} = \gamma_k^* \left[\frac{1}{Pe_k} \frac{\partial^2 c_{ik}}{\partial x^2} - \frac{\partial c_{ik}}{\partial x} \right] - \frac{(1-\varepsilon)}{\varepsilon} \alpha_k \left(q_{ik}^* - \langle q_{ij} \rangle \right)$ (3.30)	$\frac{\partial c_{ik}}{\partial \theta} = \gamma_k^* \left[\frac{1}{Pe_j} \frac{\partial^2 c_{ik}}{\partial x^2} - \frac{\partial c_{ik}}{\partial x} \right] - \frac{(1-\varepsilon)}{\varepsilon} \left[\frac{\partial \langle q_{ik} \rangle}{\partial \theta} + \varepsilon_p \frac{\partial \langle c_{pik} \rangle}{\partial \theta} \right]$ (3.34)
Mass balance in the adsorbent particles	$\frac{\partial \langle q_{ik} \rangle}{\partial \theta} = \alpha_k \left(q_{ik}^* - \langle q_{ik} \rangle \right)$ (3.31)	$\left[\frac{\partial \langle q_{ik} \rangle}{\partial \theta} + \varepsilon_p \frac{\partial \langle c_{pik} \rangle}{\partial \theta} \right] = \alpha_{pk} \left(c_{ik} - \langle c_{pik} \rangle \right)$ (3.35)
Multicomponent Adsorption equilibrium isotherm	$q_{Ak}^* = \frac{2.69 c_{Ak}}{1 + 0.0336 c_{Ak} + 0.0466 c_{Bk}} + \frac{0.10 c_{Ak}}{1 + c_{Ak} + 3 c_{Bk}}$ $q_{Bk}^* = \frac{3.73 c_{Bk}}{1 + 0.0336 c_{Ak} + 0.0466 c_{Bk}} + \frac{0.30 c_{Bk}}{1 + c_{Ak} + 3 c_{Bk}}$ (3.32)	$q_{Ak}^* = \frac{2.69 c_{pAk}}{1 + 0.0336 c_{pAk} + 0.0466 c_{pBk}} + \frac{0.10 c_{pAk}}{1 + c_{pAk} + 3 c_{pBk}} - \varepsilon_p c_{pAk}$ $q_{Bk}^* = \frac{3.73 c_{pBk}}{1 + 0.0336 c_{pAk} + 0.0466 c_{pBk}} + \frac{0.30 c_{pBk}}{1 + c_{pAk} + 3 c_{pBk}} - \varepsilon_p c_{pBk}$ (3.36)
Boundary conditions	$x = 0, \quad c_{ik} - \frac{1}{Pe_k} \frac{\partial c_{ik}}{\partial x} = c_{ik,0}$ $x = 1, \quad c_{ik} = c_{ik+1,0}$ extract and raffinate nodes $c_{ik} = \frac{\nu_I^*}{\nu_{IV}^*} c_{ik+1,0}$ eluent node $c_k = \frac{\nu_{III}^*}{\nu_{II}^*} c_{ik+1,0} - \frac{\nu_F}{\nu_{II}^*} c_i^F$ feed node (3.33)	$x = 0, \quad c_{ik} - \frac{1}{Pe_k} \frac{\partial c_{ik}}{\partial x} = c_{ik,0}$ $x = 1, \quad c_{ik} = c_{ik+1,0}$ extract and raffinate nodes $c_{ik} = \frac{\nu_I^*}{\nu_{IV}^*} c_{ik+1,0}$ eluent node $c_k = \frac{\nu_{III}^*}{\nu_{II}^*} c_{ik+1,0} - \frac{\nu_F}{\nu_{II}^*} c_i^F$ feed node (3.37)

the SMB unit, respectively, $\langle c_{pik} \rangle$ the mean pore concentration of species i in column k averaged over the particle, and q_{ik}^{*} adsorbed concentration in equilibrium with the fluid phase concentration c_{ij} (Pais *et al.*, (1997) model). The variables x and θ are the dimensionless variables defined as $x = z/L_k$ and $\theta = t/t^{*}$, where z is the axial coordinate, t is the time variable, t^{*} is the switch time interval and L_k the length of the SMB column. The resulting model parameters are:

$\frac{1-\varepsilon}{\varepsilon}$ ratio between solid and fluid volumes;

$\gamma_k^{*} = \frac{v_k^{*}}{u_s} = \frac{v_k^{*}}{L_k/t^{*}}$ ratio between fluid and solid velocities;

$Pe_k = \frac{v_k^{*} Lk}{D_{L_k}}$ Peclet number;

$\alpha_k = \frac{kL_k}{u_s} = kt^{*}$ number of intraparticle mass transfer units, for the Pais *et al.* (1997) model and,

$\alpha_{pk} = \frac{k_p L_k}{u_s} = kt^{*}$ number of intraparticle mass transfer units, for model developed in the present work, where ε is the bed porosity, ε_p is the particle porosity, D_{L_k} is the axial dispersion coefficient, k the mass transfer coefficient used in the LDF model for homogeneous particles, and k_p is the mass transfer coefficient used in the LDF model for porous particles.

Figure 3.40 presents the concentration of the two components (a) in extract and (b) in raffinate, after cyclic steady-state is reached (after 10 full cycles the extract and raffinate concentration exhibit the same behaviour and values fraction after fraction). Figure 3.41 shows the evolution of the internal concentration profiles after cyclic steady-state is reached, during a switch time interval. Since the steady-state is achieved, the concentration profiles at the end of a switch time interval are the same at the beginning of this interval, but they are advanced one column.

The behaviour of the SMB model, using LDF-porous approximation, can be predicted in

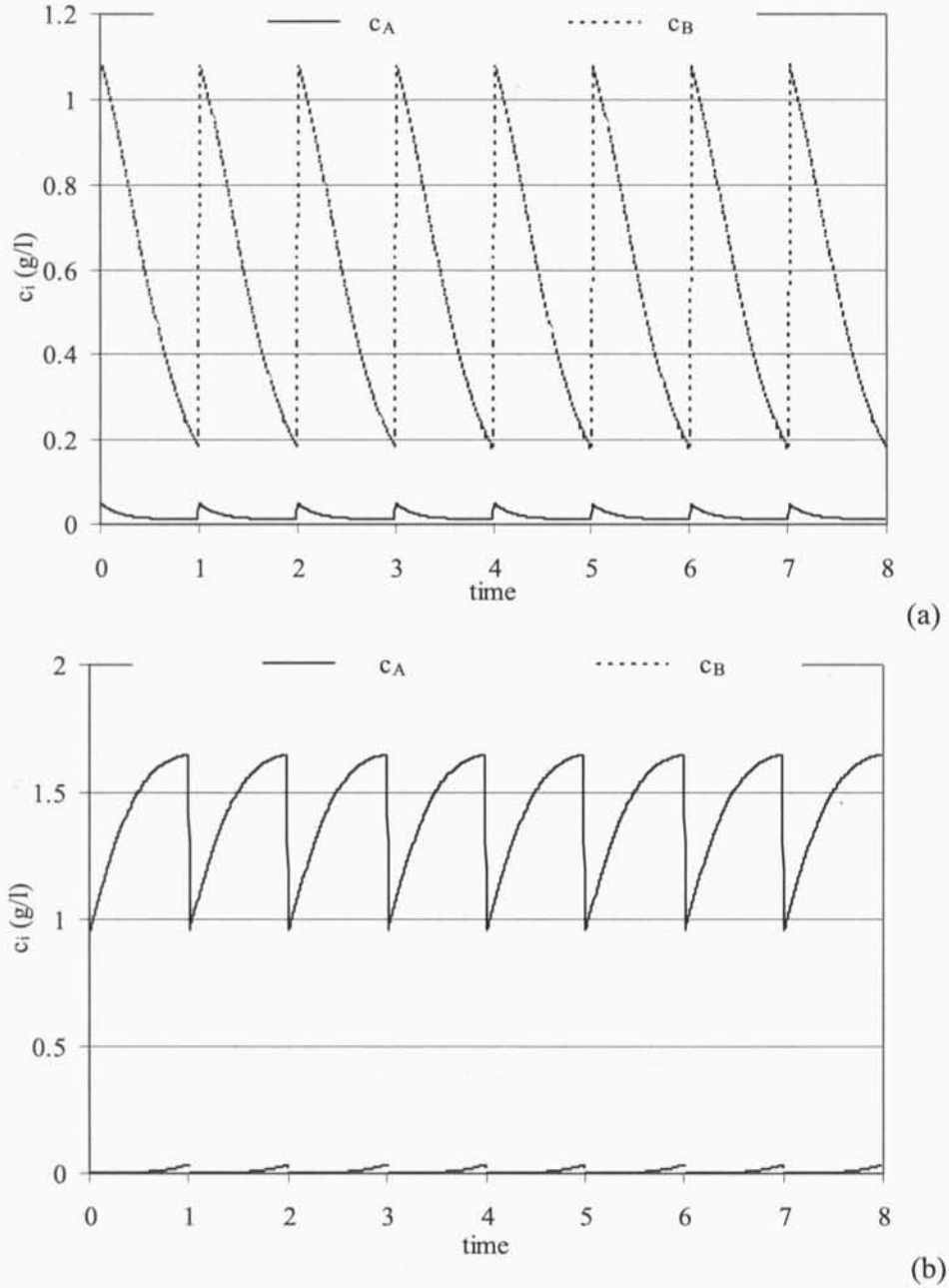

Figure 3.40 *Concentration profiles in (a) the extract and (b) raffinate for the SMB at cyclic-state and during a full cycle obtained by using the LDF model for porous particle. Dotted lines are for the more retained component; full line is for the less retained component.*

different ways: the exact transient evolution of concentration profiles, the average concentration evaluated at each switch time interval, and the instantaneous concentration evaluated at half time between two successive switching. Figure 3.42 shows the transient

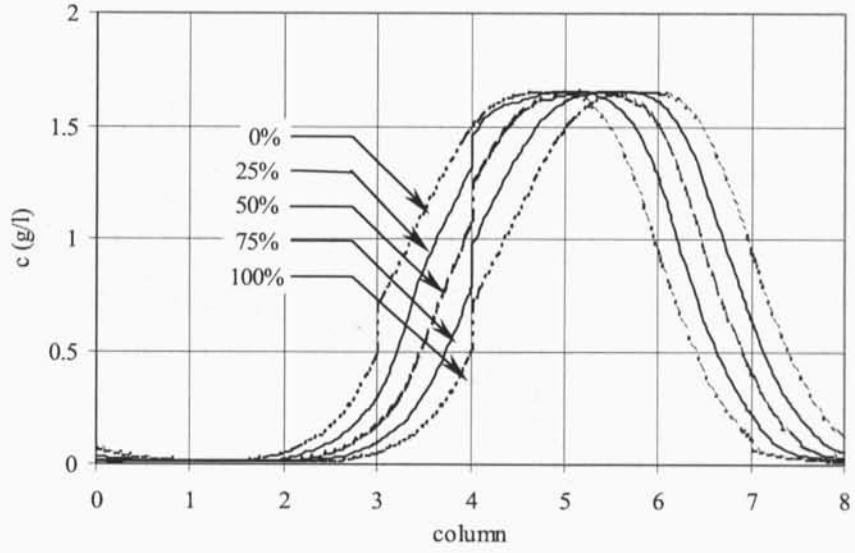

(a)

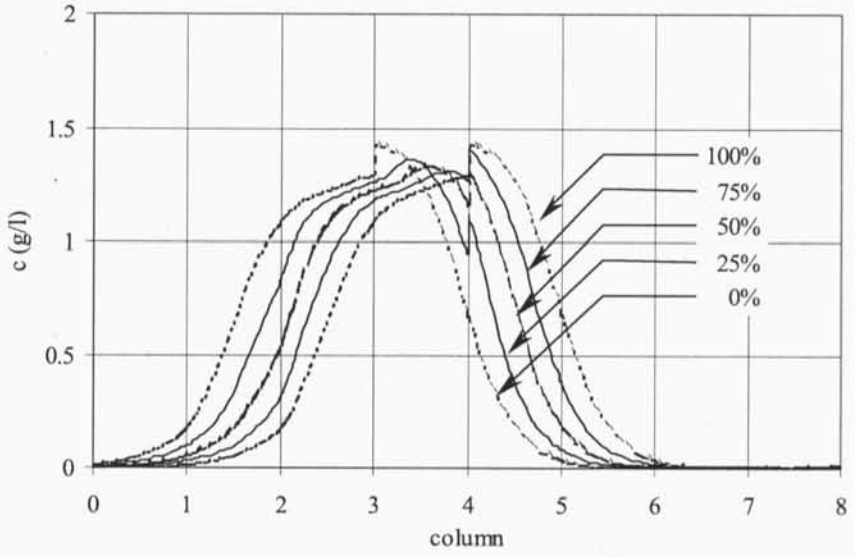

(b)

Figure 3.41 *Cyclic steady-state internal concentration profiles during a switch time interval (fraction) for the SMB obtained by using the LDF model for porous particle. Profiles for the less retained component (a) and for the more retained component (b) at the beginning, 25%, 50%, 75%, and at the end of a switch time interval (eluent at the beginning of column 1; extract between columns 2 and 3; feed between columns 4 and 5; raffinate between columns 6 and 7).*

evolution during the first five cycles (operating conditions are in Table 3.17). Although the switch time interval depends on the degree of subdivision of the bed, the duration of a full

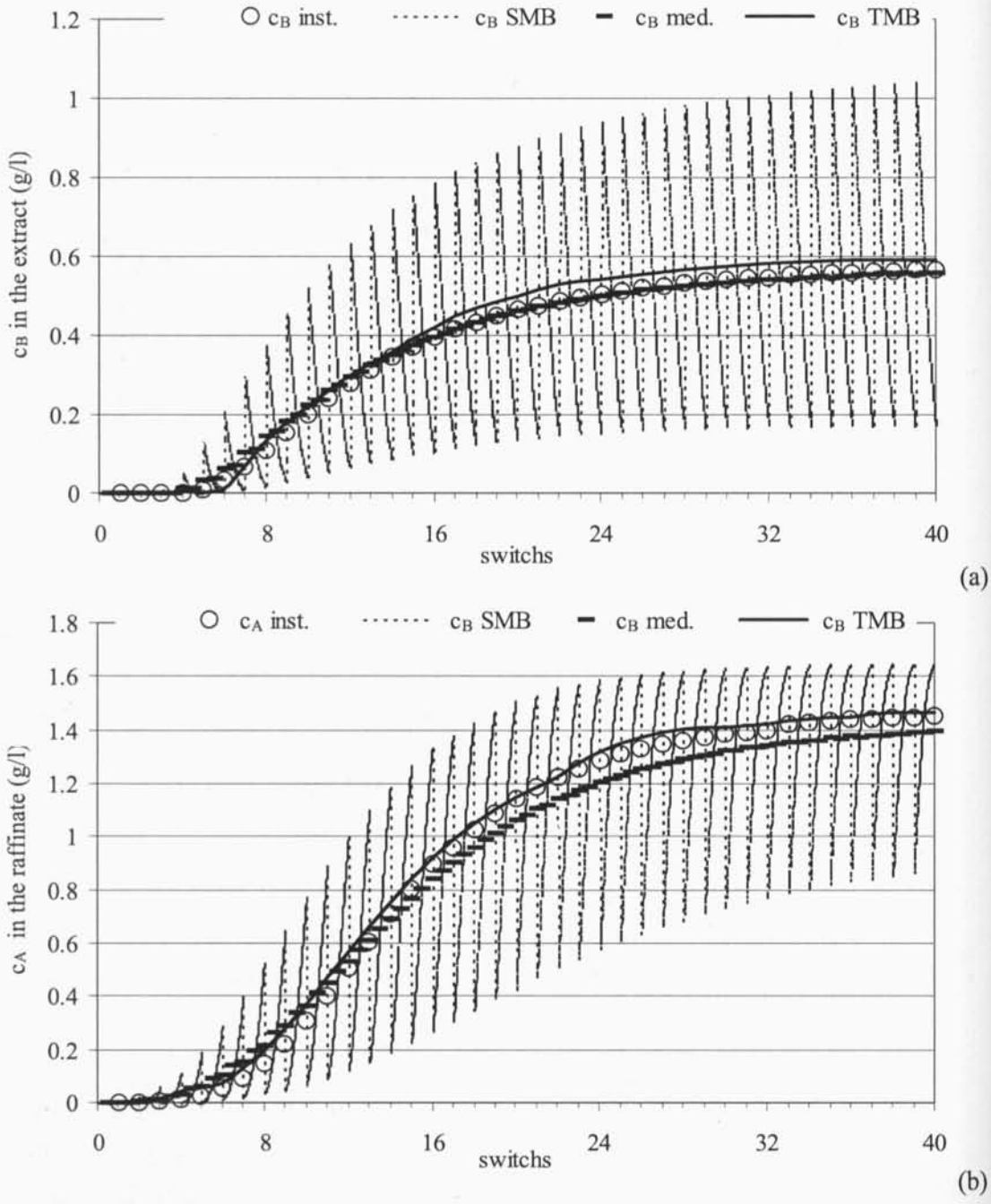

Figure 3.42 *Transient evolution (first five cycles) of the concentration (a) of the more retained component in the extract (b) of the less retained component in the raffinate obtained by using the LDF model for porous particle. The full line represents the values obtained in the TMB approach, the dotted line in the SMB approach, the step dotted line is the SMB approach with the average concentration over a switch time interval, the o o o line is the SMB instantaneous concentration evaluated half-period between switching.*

cycle is 24 minutes for all SMB cases, or after 8 switches.

There are some differences in the extract and raffinate concentrations between the TMB and the SMB models.

Figure 3.43 compares the steady-state internal concentration profiles, evaluated at half time between switching, for the TMB and SMB case. Same deviations occur between the behaviour of the two modelling approaches. The major difference occurs near the feed inlet point. This is due to the fact that the internal flow-rates in the TMB are smaller than in the SMB, (see Table 3.20), leading to a small dilution of the feed stream and mass balances for the feed node. As a consequence, near the feed inlet, TMB concentrations will be higher than in the corresponding SMB model. The opposite will occur near the eluent point, although the differences will be insignificant if concentrations are near zero, as it usually arises when flow-rates are well estimated.

Table 3.20 *Equivalence between TMB and SMB flow-rates.*

	TMB		**SMB**	
Section	Q_j	γ_j	Q_j^*	γ_j^*
I	49.40	6.65	56.83	7.65
II	31.42	4.23	38.85	5.23
III	35.06	4.72	42.49	5.72
IV	27.95	3.76	35.38	4.76
Pe	2000		1000	
u_s (cm /min)	3.5		3.5	
t^* (s)	---		180	
L_j (cm)	21		21	

Table 3.21 shows the values obtained for extract and raffinate purities and recoveries after the steady-state is reached, for the TMB and SMB approach. No significant differences between the purity performance parameter for the two approaches were found. The TMB approach gives slightly higher recovery for both extract and raffinate.

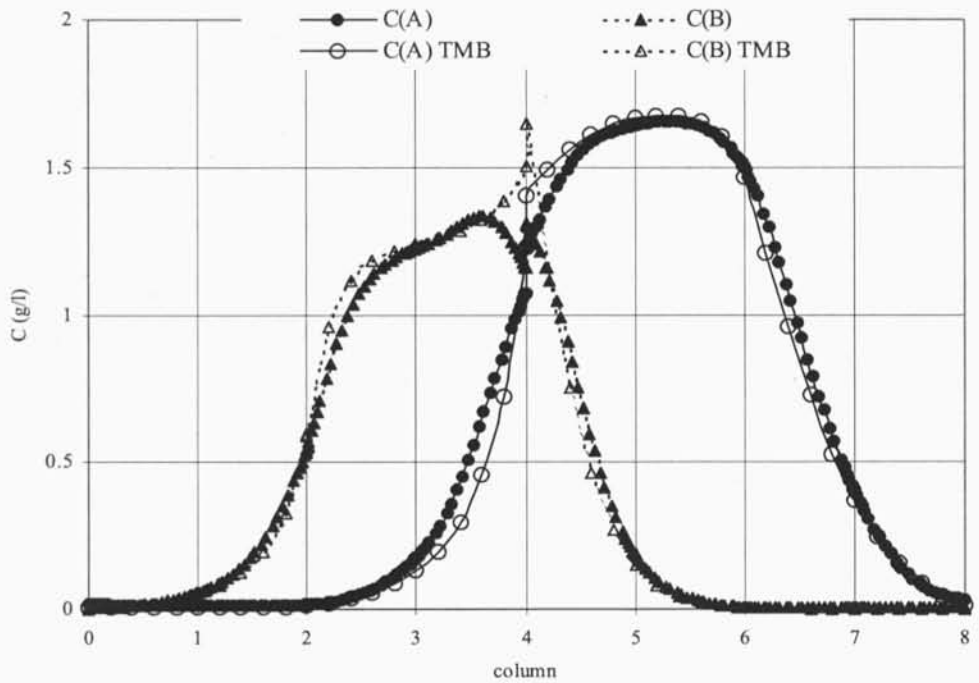

Figure 3.43 *Steady-state internal concentration profiles in the TMB approach and SMB case at half-time between switching obtained by using the LDF model for porous particle: less retained component A, more retained component B. The full circles and triangles are for the SMB approach; the white circles and triangles are for the TMB case (extract outlet column 2, feed inlet column 4, raffinate outlet column 6).*

Table 3.21*. Comparison between extract and raffinate purities and recoveries in the TMB and SMB approach obtained by using the LDF model for porous particle.*

	Extract		Raffinate	
Case	Purity (%)	Recovery (%)	Purity (%)	Recovery(%)
SMB	97.7	99.2	98.9	96.6
TMB	98.6	100	99.6	98.8

3.3 Conclusions

The True Moving Bed transient and steady-state models were used to predict internal concentrations profiles and performance of the Simulated Moving Bed using LDF approximation for homogeneous particles. The glucose/fructose separation system was used

to carry out the study with different operating conditions and model parameters used in the previous section. Under these conditions, the four mathematical model, PDEs/ODEs and PDAEs/DAEs model, were numerically solved with the related numerical package, PDECOL/COLNEW and DASSL/COLDAE, respectively. The steady-state model, owing to its lower computational time, was used to study the influence of the operating conditions on the SMB performance, namely the influence of the switch time interval, extract and feed flowrates, feed concentration, section length, and intraparticle mass transfer units. These results were presented in a $\gamma_{III} - \gamma_{II}$ plane for different values of γ_I. For linear isotherms for both components, the complete separation region presents a triangle shape, converging to the theoretical limits as the mass transfer resistance becomes less important. The same procedure was applied to the case of difference isotherms, linear for fructose and Langmuir type for glucose. The influence of the isotherm type was presented on the $\gamma_{III} - \gamma_{II}$ plane for different values of γ_I. The complete separation region shows a different shape due to the non-linearity of one of the isotherms. As the mass transfer resistance becomes less important, the area of the complete separation region increases. The $\gamma_{III} - \gamma_{II}$ plot provides, in both cases, an important tool for the choice of the SMB operating conditions. In all the $\gamma_{III} - \gamma_{II}$ plots, the limits were obtained for a minimum of 99.5% of purity of both products.

A new model for predicting the cyclic steady-state behaviour of the simulated moving bed (SMB) is developed. The model considers not only the axial dispersion flow for the bulk phase, and multicomponent adsorption equilibrium, but also the linear driving force (LDF) model for porous particles. Based on the TMB approach, the prediction of the performance of a SMB operation was performed, and also used to study the effects of the operating conditions on the SMB performance. If we are interested in the steady-state operation, the original transient TMB model can be replaced by a steady-state TMB model, which is not only simpler to implement, but also requires less computing time to be solved. The T-TMB models using LDF-homogeneous and LDF-porous approximation predicts similar results if appropriate equivalence relations are considered.

A SMB formulation with the LDF for porous particle is also presented. This last model allows the observation of product histories and the periodic character of the cyclic steady state.

3.4 References

Ascher U., J. Christiansen, R. D. Russell, (1981) *Collocation Software for Boundary-Value ODEs*, ACM Trans. Math. Software **7**, 209-222.

Azevedo D. C. S. and A. E. Rodrigues, (1999) *Design of a Simulated Moving Bed in the Presence of Mass-Transfer Resistances*, AIChE J. **45**, 956-966.

Bader G. and U. Ascher, (1987) *A New Basis Implementation for a mixed Order Boundary Value ODE Solver*, SIAM J. Scient. Stat. Comput. **8**, 483-500.

Ching C. B., D. M. Ruthven, K. Hidajat, (1985) *Experimental Study of a Simulated Counter-Current Adsorption System – III. Sorbex Operation*, Chem. Engng. Sci. 40, 1411-1417.

Madsen N. K., and R. F. Sincovec, (1979) *PDECOL: General Collocation Software for Partial Differential Equations*, ACM Trans. Math. Software **5**, 326-351.

Pais L. S., J. M. Loureiro, A. E. Rodrigues, (1997a) *Separation of 1,1'-bi-naphthol enantiomers by continuous chromatography in simulated moving bed*, Chem. Engng. Sci. **52**, 245-257.

Pais L. S., J. M. Loureiro, A. E. Rodrigues, (1997b) *Modeling, simulation and operation of a simulated moving bed eparation for continuous chromatographic separation of 1,1'-bi-naphthol enantiomers*, J. of Chromatogr. A **769**, 25-35.

Pais, L. M. S., (1999) *Chiral Separation by Simulated Moving Bed Chromatography*, PhD dissertation, LSRE, University of Porto, Porto.

Petzold L., (1982) *A Description of DASSL: A Differential/Algebraic System Solver*, Rep. Sand. 82-8637, Sandia National Laboratory.

Ruthven D. M., and C. B. Ching, (1989) *Counter-Current and Simulated Moving Bed Adsorption Separation Process*, Chem. Engng. Sci. **44**, 1011-1038.

Storti G., M. Mazzotti, M. Morbidelli, S. Carra, (1993) *Robust Design of Binary Countercurrent Adsorption Separation Process*, AIChE J. **39**, 471-492.

Strube, J., and H. Schmidt-Traub, (1996) *Dynamic Simulation of Simulation of Simulated-Moving-Bed Chromatographic Processes*, Computers Chem. Engng. **20**, S641-S643.

Zhong G., and G. Guiochon, (1996) *Analytical Solution for the Linear Ideal Model of Simulated Moving Bed Chromatography*, Chem. Engng. Sci. **51**, 4307-4319.

4. Simulated Moving Bed Adsorptive Reactor: Modelling and Simulation

In this chapter, modelling and simulation of the Simulated Moving Bed Reactor (SMBR) based on the analogy with the True Moving Bed Reactor (TMBR) (Leão and Rodrigues, 1997; Leão *et al.*, 1997; Azevedo, 2001) are addressed. An irreversible reaction was used as a test example in this work: the sucrose inversion and Glucose/Fructose separation. Models were formulated in terms of systems of partial differential equations and ordinary differential equations for transient and steady-state situations. Linear equilibrium isotherm for the reaction products, Michaelis-Menten model to describe the reaction rate and LDF for homogeneous particles approximation are considered. Due to the lower computational time, the steady-state TMBR model was used to find the best operating conditions. The effect of the operating parameters is addressed, namely the rotation period, extract flowrate, feed flowrate, feed concentration, section length and configuration, and number of intraparticle mass resistance.

4.1 Basic Idea of the SMBR

A Simulated Moving Bed Reactor (SMBR) is a continuous operation that combines chemical reaction and adsorptive separation within one single unit, based on the principle of SMB (Mazzotti *et al.* (1996)). The application of chromatographic reactors was initiated by Barker

research group in the 80s, in the biochemical field, and published by Ganetsos *et al.* (1993) and Hashimoto *et al.* (1993). Several studies have been made using the concept of the SMBR, namely the conversion of glucose to fructose for the production of high-fructose corn syrup (Hashimoto *et al.*, 1983; Ching *et al.*, 1986), the esterification of acetic acid catalyzed with ethanol on a highly cross linked sulphonic ion-exchange resin (Mazzotti *et al.*, 1996). Most recently the production of Bisphenol-A in a SMBR unit has been reported (Kawase *et al.*, 1999). The inversion of sucrose and separation of fructose from glucose, was carried out by Sarmidi and Barker (1993) using a continuous rotating annular chromatography. Since then, it became an example in study of SMBR (Meurer *et al.*, 1996; Ching and Lu, 1997; Leão *et al.*, 1997; Azevedo, 2001). The use of a SMBR for reversible reactions has also been studied (Meurer *et al.*,1997; Fricke *et al.*,1999; Lode *et al.*, 2001). The SMBR have been applied not only to liquid-phase reactions but also to gas-phase reactions; the hydrogenation of mesitylene (Fish *et al.*, 1986; Ray and Carr, 1995). The design of a SMBR process defines the process layout (size and number of columns used, length of the column) and the operating parameters that should leads to an optimised products separation and high reagent conversion.

The continuous SMBR principle is described using the equivalent true moving bed reactor (TMBR) configuration. As in the SMB case, the in and outlets points are used to define four distinct sections that can have different lengths, Figure 4.1. Each section plays an important role in the reaction/separation process. The feed stream, in our case containing sucrose, is introduced between sections II and III. It is then, converted to glucose and fructose. Due to different adsorption of the two products, they are recovered in different points. Glucose, the less adsorbed product, moves with the fluid phase and is recovered between sections III and IV. Fructose, is recovered between sections I and II, since it is the more adsorbed product and moves with the solid phase. Therefore, section III, is where the reaction and the separation of the two reaction products will take place, and due to that requires to be larger than the others three sections.

The movement of the solid phase is simulated by switching periodically, the feed point and the outlets points in the same direction as the fluid flow, through the bed.

For the SBMR and as an initial approach, we took into consideration all the assumptions made in the SMB case, to achieve complete separation of a binary mixture based on the constraints of the operating parameter $\gamma_{ij}^{*} = \frac{\varepsilon}{1-\varepsilon}\frac{v_j}{u_s}\frac{c_{ij}}{q_{ij}}$, the ratio between the fluxes of i transported by the liquid and solid phases, as described in Ruthven and Ching (1989). For the

case of a linear adsorption isotherm, $q_{ij} = K_i c_{ij}$, we have $\gamma_{ij}^{*} = \frac{\varepsilon}{1-\varepsilon}\frac{v_j}{u_s}\frac{1}{K_i}$ as described in section 2.1.

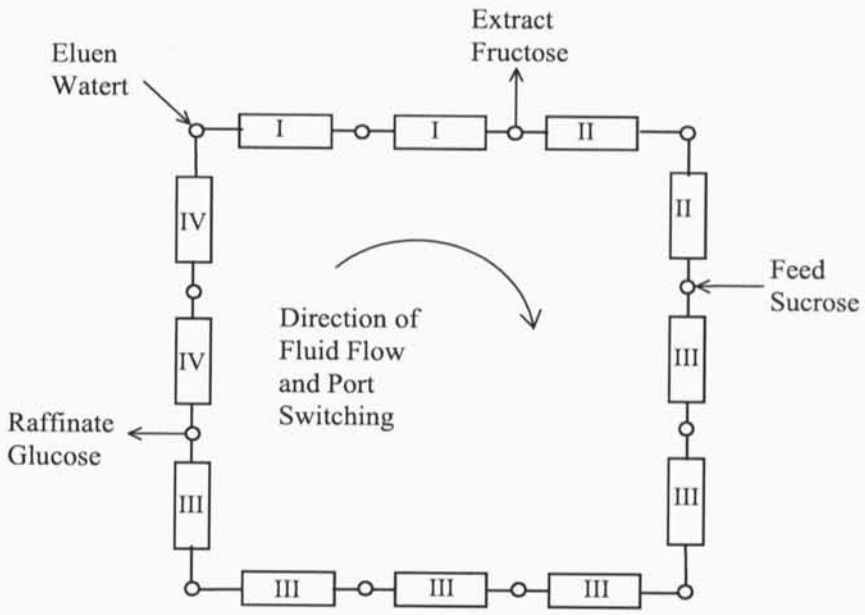

***Figure 4.1**. SMBR system configuration, with four sections, different number of columns per section, 2 2 6 2, respectively.*

4.1.1 Model Description

The SMBR models are similar to the models that have been proposed to simulate the SMB including the reaction terms. Simpler models, include differential mass balance in a bed volume element and take into account mass transfer between fluid and solid phase described by a LDF model (Hashimoto et al., 1983; Hashimoto et al., 1993; Kawase *et al.*, 2001) and more rigorous models consider axial dispersion (Meurer *et al.*, 1997). The adsorption isotherms are approximately linear and the reaction kinetics is described by a Michaelis-Menten equation.

The model used to predict the performance and concentration profiles in a SMBR unit, presented in this chapter, was developed based on the equivalence with the TMBR concept, assuming:

- axial dispersion flow for the liquid phase;

- simple linear driving force (LDF) approximation for homogeneous particles to describe the intraparticle mass transfer;
- plug flow for the solid phase;
- reaction, $\mathcal{R}$, on the liquid phase; and
- linear adsorption equilibrium; considering K_1=0, in other words, the sucrose is not adsorbed.

The first three assumptions were the same as for the TMB model described in chapter 2, (section 2.1.2), the last two conditions were added to account for the reaction.

The mass balance equations over a volume element in the section j (j = I, II, III, IV) and in the adsorbent particles are written:

- liquid phase:
  - i=1 (sucrose)

$$\varepsilon D_{L_j} \frac{\partial^2 c_{1j}}{\partial z^2} - \varepsilon v_j \frac{\partial c_{1j}}{\partial z} = - \upsilon_1 \varepsilon \mathcal{R} + \varepsilon \frac{\partial c_{1j}}{\partial t} \qquad (4.1)$$

  - i= 2, 3 (glucose and fructose)

$$\varepsilon D_{L_j} \frac{\partial^2 c_{ij}}{\partial z^2} - \varepsilon v_j \frac{\partial c_{ij}}{\partial z} + (1-\varepsilon)\, u_s \frac{\partial \langle q_{ij} \rangle}{\partial z} = -\upsilon_i \varepsilon \mathcal{R} + \varepsilon \frac{\partial c_{ij}}{\partial t} + (1-\varepsilon) \frac{\partial \langle q_{ij} \rangle}{\partial t} \qquad (4.2)$$

- solid phase:
  - i=2, 3 (glucose and fructose):

$$u_s \frac{\partial \langle q_{ij} \rangle}{\partial z} + k \left[q_{ij}^* - \langle q_{ij} \rangle \right] = \frac{\partial \langle q_{ij} \rangle}{\partial t} \qquad (4.3)$$

where $\langle q_{ij} \rangle$ and c_{ij} are the average adsorbed concentration in the particle and liquid phase concentration of product i in section j, (g/l), respectively, v_j and u_s are the interstitial liquid and solid phase velocities (m/min), ε is the column porosity, and υ_i is the stoichiometric coefficient of reaction. The coefficient υ_i is negative for the reagent, sucrose (i = 1), and positive for the reaction products, glucose and fructose (i = 2 and 3), that is, $\upsilon_1 = -1$, and $\upsilon_2 = \upsilon_3 = +1$. The first term in the model, (4.1), is the axial dispersion term. In the solid phase, (4.3), the equation for the sucrose component is not considered since the sucrose is not

adsorbed.

A linear equilibrium relation was taken into consideration,

$$q_{ij}^{*} = f(c_{ij}) = K_i\, c_{ij}, \text{ for } i = 2, 3 \tag{4.4}$$

and the reaction rate, $\mathcal{R}$, used was the Michaelis-Menten model,

$$\mathcal{R} = \frac{V_m . c_1 / Mw_1}{K_m + c_1 / Mw_1} . Mw_i \tag{4.5}$$

where $\mathcal{R}$, is the reaction rate velocity in *g/l-min*, c_1, is the sucrose concentration in *g/l* (Mw_i is the molecular weight of the component *i*), K_m, is the Michaelis constant in *moles/l*, and V_m,is the maximum reaction velocity in *moles/l-min*. In this work we considered K_m equal to 0.160*moles/l* and V_m variable (Bowski *et al.*, 1971).

The corresponding boundary and initial conditions for the problem are,

$$c_{ij}(z,0) = \langle q_{ij} \rangle (z,0) = 0 \tag{4.6a}$$

$$\begin{aligned} z = 0 \qquad & c_{ij} = c_{ij,0} - \frac{D_{L_j}}{v_j} \frac{\partial c_{ij}}{\partial z} \\ z = L_j \qquad & \frac{\partial c_{ij}}{\partial z} = 0 \quad \text{and} \quad \langle q_{ij} \rangle = \langle q_{ij+1,0} \rangle \end{aligned} \tag{4.6b}$$

The additional equations necessary for the resolution of the problem, for the boundary conditions, for each value of *j*, were the following:

$$c_{i1,0} = \frac{Q_{IV}}{Q_I} c_{i4,L_4} \qquad j = 1 \text{ (eluent node)} \tag{4.7a}$$

$$c_{i2,0} = c_{i1,L_1} \qquad j = 2 \text{ (extract node)} \tag{4.7b}$$

$$c_{i3,0} = \frac{Q_{II}}{Q_{III}} c_{i2,L_2} + \frac{Q_F}{Q_{III}} c_i^F \qquad j = 3 \text{ (feed node)} \quad (*) \tag{4.7c}$$

$$c_{i4,0} = c_{i3,L_3} \qquad j = 4 \text{ (raffinate node)} \tag{4.7d}$$

(*) for $i = 2$ e 3, i.e. for glucose and fructose, c_i^F is equal to zero, the feed is only formed with sucrose.

The equations (4.1-4.3), can be expressed in a dimensionless form. The dimensionless variables introduced were, $x = z / L_j$, axial distance z normalised by the length of each

section, $L_j = n_j L_c$, and $\theta = t/\tau_s$ with $\tau_s = L_c/u_s$, where n_j is the number of columns per section and L_c is the length of each column. The resulting model parameters are defined in Table 4.1, similar to the TMB system.

Table 4.1. *Dimensionless parameters for the TMBR system.*

Number of mass transfer units	$\alpha_c = \frac{kL_c}{u_s}, \quad \alpha_j = \frac{kL_j}{u_s}$
Peclet Number	$Pe_j = \frac{\nu_j L_j}{D_{L_j}}$
Ratio between fluid and solid interstitial velocities	$\gamma_j = \frac{\nu_j}{u_s}$
Ratio between solid and fluid volumes	$\frac{(1-\varepsilon)}{\varepsilon}$

The dimensionless model equations are,

- liquid phase:
  - $i = 1$ (sucrose)

$$\frac{\partial c_{1j}}{\partial \theta} = \frac{\gamma_j}{n_j}\left[\frac{1}{Pe_j}\frac{\partial c_{1j}^2}{\partial x^2} - \frac{\partial c_{1j}}{\partial x}\right] - \frac{L_c}{u_s}\mathcal{R} \tag{4.8}$$

  - $i = 2, 3$ (glucose and fructose)

$$\frac{\partial c_{ij}}{\partial \theta} = \frac{\gamma_j}{n_j}\left[\frac{1}{Pe_j}\frac{\partial c_{ij}^2}{\partial x^2} - \frac{\partial c_{ij}}{\partial x}\right] + \frac{L_c}{u_s}\mathcal{R} - \frac{(1-\varepsilon)}{\varepsilon}\alpha_c\left(q_{ij}^* - \langle q_{ij}\rangle\right) \tag{4.9}$$

- solid phase:
  - $i = 2, 3$ (glucose and fructose)):

$$\frac{\partial \langle q_{ij}\rangle}{\partial \theta} = \frac{1}{n_j}\frac{\partial \langle q_{ij}\rangle}{\partial x} + \alpha_c\left(q_{ij}^* - \langle q_{ij}\rangle\right) \tag{4.10}$$

Equations (4.8-4.10), the mass balance equations in each node (4.7), and the initial and boundaries conditions (4.6), define the TMBR model to be studied.

4.1.2 Performance Criteria

As for in the SMB, in the SMBR unit the outlet components must satisfy a strict purity specification. The operating conditions can be characterised in terms of three performance parameters: purity and recovery of the extract and raffinate, and conversion of sucrose.

1. **Purity**, of the extract is defined as follows, $P_E = 100\dfrac{C_E^{Fr}}{C_E^{Gl} + C_E^{Fr} + C_E^{Suc}}$. Similarly, for the raffinate, $P_R = 100\dfrac{C_R^{Gl}}{C_R^{Gl} + C_R^{Fr} + C_R^{Suc}}$. The extract is pure when P_E =100%, if it does not contain glucose and sucrose, whereas raffinate is pure for P_R =100%, if it does not contain fructose and sucrose.

2. **Recovery,** of the fructose in the extract is defined as $R_E^{Fr} = 100\dfrac{Q_E c_E^{Fr}}{Q_F c_F^{Suc}\left(\dfrac{M_w^{Fr}}{M_w^{Suc}}\right)}$ (M_w^i is the molecular weight of component *i*); a similar definition applies to the recovery of glucose in the raffinate.

3. **Conversion**, of sucrose is defined as follows, $X = 1 - \dfrac{Q_E C_E^{Suc} + Q_R C_R^{Suc}}{Q_F C_F^{Suc}}$. For $X = 1$, both draw-off products, raffinate and extract, do not contain sucrose. This means that all sucrose has been converted into glucose and fructose.

The definitions of solvent consumption and productivity are those already presented in chapter 2.

4.2 Numerical Methods

To solve the TMBR model numerically, the software package PDECOL (Madsen and Sincovec, 1979), based on the orthogonal collocation methods in finite elements, has been used to solve the dimensionless partial differential equations (4.8-4.10). A steady-state TMBR model can also be defined when the terms with respect to time derivative in equations (4.8-4.10) are equal to zero, i.e. $\dfrac{\partial c_{ij}}{\partial \theta} = \dfrac{\partial \langle q_{ij} \rangle}{\partial \theta} = 0$. To numerically solve the resulting set of ordinary differential equations, the software package COLNEW (Bader and Ascher, 1987)

was used. The numerical parameters considered for the two solvers are described in Table 4.3. Both processes went on until the sum of the following absolute errors, the global error *er*, was less than 1%:

- sum of relative differences between average extract and raffinate concentrations of two consecutives cycles (PDECOL) or iterations (COLNEW),
- Global molar balance error between sucrose and invert sugar (for each mole of sucrose that enters the TMBR, one mole of glucose and one mole of fructose must leave).

4.3 Simulation Results and Discussion

Several simulations were carried out to estimate the transient and steady state concentration solutions of the sucrose inversion and glucose/fructose separation system.

The operating conditions and models parameters used in the simulation of the TMBR are listed in Table 4.2. As initial approximation, the operating conditions were estimated by the method developed by Ruthven and Ching (1989), considering the equilibrium theory for nnon-reactive sysems, linear isotherms, and a safety parameter $\beta = 1.2$. The value of the mass transfer coefficient used in all the simulations was the same for fructose and glucose and equal to $k = 0.1\ s^{-1}$, and zero for sucrose since in the model, sucrose was considered as no adsorbed. The numerical parameters that were used and must be specified to implement the packages are described in Table 4.3. All the simulations were run in a Pentium II 300 MHz.

Figure 4.2 represents the steady-state concentration internal profiles for the transient model, equations (4.8-4.10) with boundary and initial conditions (4.6-4.7), obtained under the operating conditions described in Table 4.2 and 4.3, by using the PDECOL solver.

With the configuration 2-2-6-2, the sucrose was almost totally converted, in the section III, and high product purities were achieved. Considering, the same number of columns in all sections, 3-3-3-3, different product purities were achieved, Figure 4.3. The significant difference was on the raffinate purity, 98.4% with 2-2-6-2 and 86.3% with 3-3-3-3 configurations. The main difference between the two situations is in the length of section III, 63 and 31.5 cm, for the 2-2-6-2 and 3-3-3-3 configurations, respectively. Is in section III that the reaction takes place and the more retained product, fructose, is adsorbed. In the case of

section III with lower length, the more retained product is not completely adsorbed and contaminates the raffinate. Therefore the section III, should be longer than the other sections.

Table 4.2a *Operating parameters conditions and models parameters used in the simulations of the transient and steady-state TMBR models.*

SMBR Operating conditions	**TMBR Model Parameters**	**Columns**
Feed conc. = 5 *g/l* (Suc)	Pe = 2000	D_C =2.6 *cm*
t^* = 122 *s*[c]	$(1-\varepsilon)/\varepsilon = 1.5$	L_C = 10.5 *cm*
	$k_{Gl} = k_{Fr} = 0.1\ s^{-1}$, $k_{Suc} = 0.0$	
Q_{Rec} = 17.79 *ml/min*[a]	K_{Gl}=0.50[b] K_{Fr}=0.88[b] K_{Suc}=0.0[b]	Configuration:
Q_D = 11.90 *ml/min*[a]	K_m=0.160 *mol/l*[d]	2-2-6-2
Q_E = 8.00 *ml/min*[a]	V_m=0.0656 *mol/l-min*[d]	
Q_F = 1.15 *ml/min*[a]		
Q_R = 5.05 *ml/min*[a]	$\gamma_I = 1.7073$ $\gamma_{II} = 0.9778$	
	$\gamma_{III} = 1.0827$ $\gamma_{IV} = 0.6222$	

[a] values obtained through the operation conditions as in Ruthven and Ching (1989).
[b] values for a atmosphere temperature (=30°C, Ching *et al.* (1986)).
[c] switching time, $t^* = l/u_s = (1-\varepsilon)l\ A\ /\ Q_s$.
[d] values as in the work of Bowski *et al.* (1971).

Table 4.2b *Equivalence between TMBR and SMBR flow-rates.*

Section	TMB		SMB	
	Q_j (ml/min)	γ_j	Q_j^* (ml/min)	γ_j^*
I	18.72	1.71	26.69	2.71
II	10.72	0.98	21.69	1.98
III	11.87	1.08	22.84	2.08
IV	6.80	0.62	17.79	1.62
t^* (min)	---		2.03	

Table 4.3 *Numerical parameters used in the two software packages.*

	COLNEW	PDECOL
Number of collocation points per interval	4	2
Number of subintervals in the initial mesh, NE	10	14
Error tolerance, TOL	10^{-7}	10^{-7}
Global error, *er*	0.01	0.01

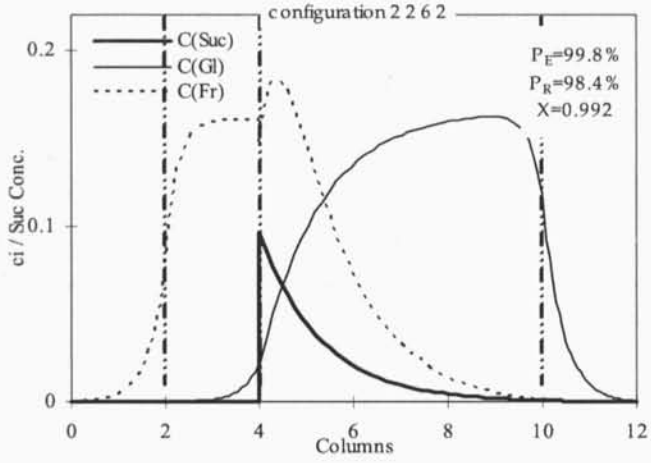

Figure 4.2 *Results obtained for the inversion of sucrose and glucose/fructose separation under conditions in Table 4.2 and numerical parameters described in Table 4.3, by using PDECOL solver.*

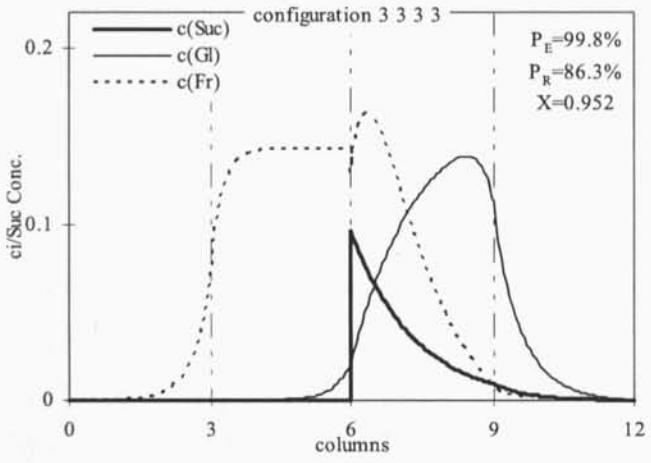

Figure 4.3 *Results obtained for the inversion of sucrose and glucose/fructose separation under conditions in Table 4.2 and numerical parameters described in Table 4.3, by using PDECOL solver, for the 3-3-3-3 configuration.*

4.3.1 Evolution of the internal profiles for the transient of the TMBR

When we solve the transient TMBR, for a 2-2-6-2 configuration, with the PDECOL package, it is possible to evaluate the evolution of the transient internal profiles for the reference case.

Figure 4.4 shows the internal profiles obtained for cycles 1, 2, 3 and 10, under conditions as described in Table 4.2. The numerical parameters used are in Table 4.3.

We can observe that with a limited number of cycles it is possible to reach the final cyclic steady-state (cycle 10).

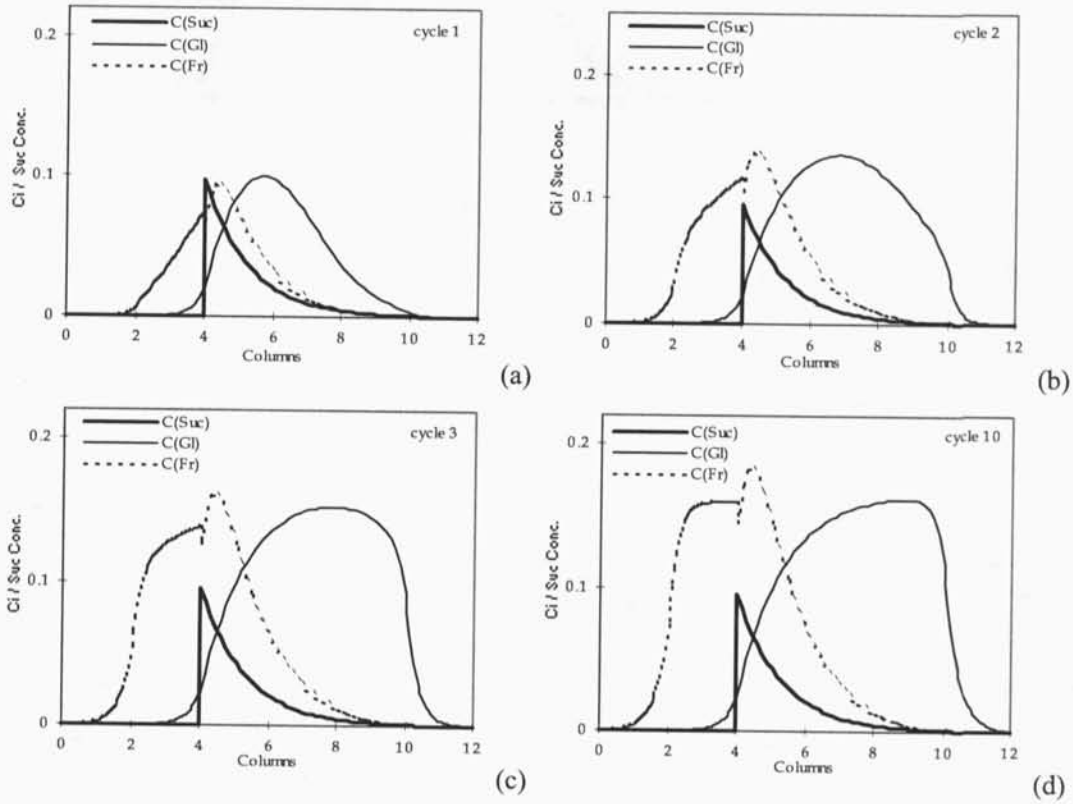

Figure 4.4 *Transient TMBR internal profiles for the case study under conditions described in Table 4.2 obtained by using PDECOL solver for cycles 1, 2, 3 and 10, respectively, with numerical parameters described in Table 4.3.*

In Figure 4.5 we can see the evolution, cycle 1 through cycle 10, of the transient internal profile for the TMBR study case. The fronts of the less adsorbed component, glucose (full squares), moved until they reach the high value of purity, in section III. The same occurs with the more retained product, fructose (full circles), which moves until it reaches the high value of purity, in section II. The two arrows in the figure show the way of evolution, one for each outlet products. The sucrose front is the same independently of the cycle (continuous line).

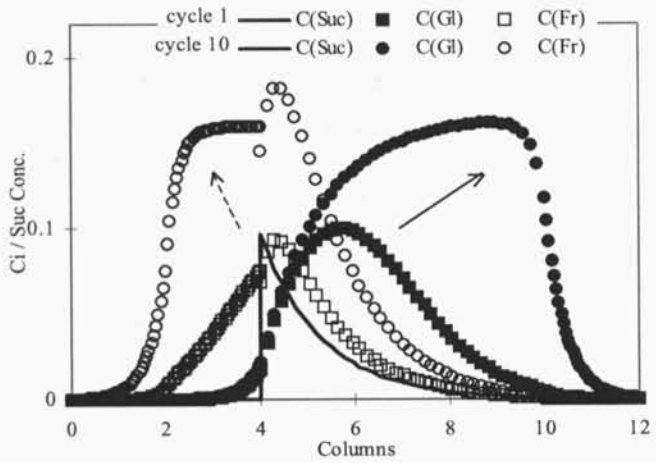

Figure 4.5 *Evolution of the transient internal profiles for the reference case under conditions described in Table 4.2 and 4.3. Squares represent the internal profiles in cycle 1 and circles represent the internal profiles in cycle 10 (full, glucose, and white, fructose), the continuous lines correspond to sucrose. The two arrows show the way of the evolution, one for each outlet stream.*

4.3.2 Comparison between the transient TMBR model and the steady-state TMBR

The model that describes the steady state TMBR is similar to the transient TMBR model with the following assumptions: $\frac{\partial c_{ij}}{\partial t} = \frac{\partial \langle q_{ij} \rangle}{\partial t} = 0$. So, the partial differential equations (4.8-4.10) became,

- liquid phase:
  - i=1 (sucrose)

$$\varepsilon D_{L_j} \frac{dc_{1j}^2}{dz^2} - \varepsilon v_j \frac{dc_{1j}}{dz} = -\upsilon_1 \varepsilon \mathcal{R} \tag{4.11}$$

  - i=2, 3 (glucose and fructose)

$$\varepsilon D_{L_j} \frac{dc_{ij}^2}{dz^2} - \varepsilon v_j \frac{dc_{ij}}{dz} + (1-\varepsilon) u_s \frac{d\langle q_{ij} \rangle}{dz} = -\upsilon_i \varepsilon \mathcal{R} \tag{4.12}$$

- solid phase:
  - i=2, 3 (glucose and fructose):

$$u_s \frac{d\langle q_{ij} \rangle}{dz} + k\left[q_{ij}^* - \langle q_{ij} \rangle \right] = 0 \tag{4.13}$$

The dimensionless model equations are:

- liquid phase:
  - $i = 1$ (sucrose)

$$\frac{dc_{1j}^2}{dx^2} = Pe_j \frac{dc_{1j}}{dx} + Pe_j \frac{L_j}{\gamma_j u_s} \mathcal{R} \tag{4.14}$$

  - $i = 2, 3$ (glucose and fructose)

$$\frac{dc_{ij}^2}{dx^2} = Pe_j \frac{dc_{ij}}{dx} - Pe_j \frac{L_j}{\gamma_j u_s} \mathcal{R} + Pe_j \frac{(1-\varepsilon)}{\varepsilon} \frac{\alpha_j}{\gamma_j} \left(q_{ij}^* - \langle q_{ij} \rangle \right) \tag{4.15}$$

- solid phase:
  - i=2, 3 (glucose and fructose):

$$\frac{d\langle q_{ij} \rangle}{dx} = -\alpha_j \left(q_{ij}^* - \langle q_{ij} \rangle \right) \tag{4.16}$$

The initial and boundary conditions are the same as in the previous model, (4.6-4.7). The resulting system, (4.14-4.16) and (4.6-4.7), was solved by using the COLNEW software package. The numerical parameters used are in Table 4.3.

The simulations obtained by using PDECOL and COLNEW solvers were compared in their capability to describe the SBMR processes.

The internal profiles obtained for the steady-state model under the same conditions as the previous model described in Table 4.2, by using the COLNEW solver is illustrated in Figure 4.6. The obtained results were very similar to those obtained by using the PDECOL solver, for the transient model, Figure 4.2.

Defining the relative and absolute error between the solutions obtained by the ordinary equation solver, OES, and the partial equation solver, PES, as,

$$\rho(\%) = \frac{\text{solution by OES} - \text{solution by PES}}{\text{solution by OES}} * 100 = \\ = \frac{\text{absolute error}}{\text{solution by OES}} * 100 \tag{4.17}$$

for each point, and applying to the previously results obtained by using COLNEW and PDECOL solvers, we obtained the graphs in Figures 4.7(a) and 4.7(b). The higher relative error obtained between the two steady-state solutions, was less than 3%, for the two products fo the reaction. However, for the sucrose, the relative error obtained in some points of section II, are around 30%, where the absolute error takes the smallest values (< 0.00001).

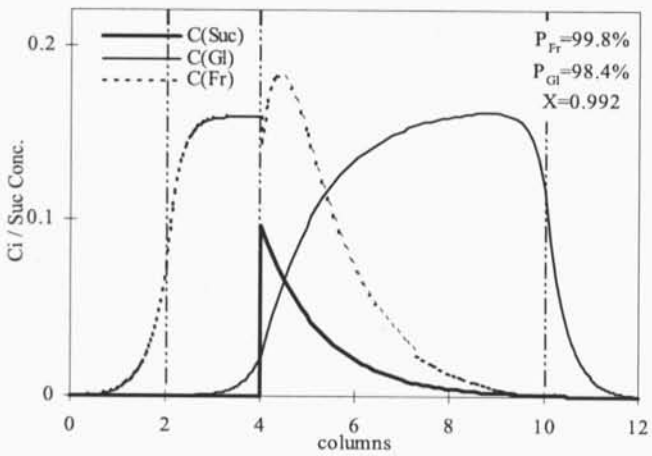

Figure 4.6 *Results obtained for the inversion of sucrose and glucose/fructose separation under conditions in Table 4.2 and 4.3 by using COLNEW solver.*

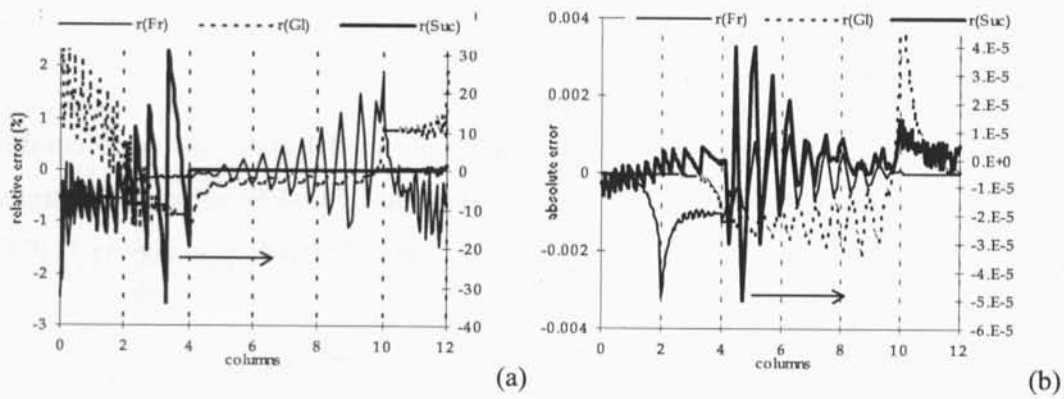

Figure 4.7 *Relative error (a) and absolute error (b), obtained for case study, comparing the obtained results by using PDECOL (transient model) and COLNEW (steady-state model) solvers.*

Table 4.4 summarizes the final results obtained by using the PDECOL and COLNEW codes in the estimation of the performance parameters and the steady-state liquid phase concentrations for the two components in the inlet and outlet nodes. Comparing the performance parameters obtained in the steady state and in the transient steady state, no significant differences can be found. The global balance is verified with error approximately or less than 1%. The computing time needed to solve the two models was very similar when using the PDECOL or the COLNEW solver, considering the numerical parameters described in Table 4.3. Notice that, the term concerning the reaction rate is non-linear.

Table 4.4. *TMBR system performance parameters, Gl and Fr components concentrations values obtained in the in and outlet points, and the run time needed by using the PDECOL, for the transient model, and COLNEW, for the steady-state model, solvers, under conditions described in Table 4.2, and the numerical parameters in Table 4.3.*

Performance	**PDECOL**		**COLNEW**	
	Gl	**Fr**	**Gl**	**Fr**
Purity (%)	98.4	99.8	98.4	99.8
Recovery (%)	99.4	99.7	99.4	98.7
Solvent Cons. (*l/g*)	4.384	4.323	4.339	4.367
Productivity (*g/hr l*)	0.445	0.451	0.447	0.450
Concentration (*g/l*):				
Extract	0.00068	0.376	0.00069	0.374
Feed	0.104	0.729	0.102	0.724
Raffinate	0.589	0.00192	0.594	0.0049
Eluent	0.00051	0.00028	0.0142	0.00764
Run Time (*min*)	42		37	

The choice depends on the user interest, in the transient or in the stationary regime of the TMBR processes. The model based on the steady state can be used for a preliminary estimation of the profiles and of the performance parameters of the TMBR processes. With the transient model, is possible to have, for each component, the exact profiles through the time period.

Since no significant differences were obtained on the estimation of the final steady-state concentrations, all the results presented in the following subsections were obtained by using the COLNEW solver.

4.4 Effect of operating variables

The effect of the operating variables (rotation period, extract and feed flowrates, section length, and number of intraparticle mass transfer) on the SMBR/TMBR performance is analysed. The TMBR performance is characterised by purity, recovery, solvent consumption and adsorbent productivity for the reaction products, and conversion of sucrose, as described in previous sections. The effect of the operating variables on the system performance was analysed one at a time. The ranges considered, for each of the operating variables, were summarised in Table 4.5. For each case, the remaining operating conditions and model parameters were kept constants as previously described in Table 4.2. The numerical parameters used are in Table 4.3.

Table 4.5 *Range of the operating variables for the study of the effect on the TMBR performance. The others parameters are described in Table 4.2.*

Rotation period, t^*	110 - 130 *sec*
Extract flowrate, Q_E	4.00 - 11.00 *ml/min*
Feed flowrate, Q_F	0.15 - 11.15 *ml/min*
Total Balance[a] (total flow in=total flow out)	13.05 *ml/min*
intraparticle mass transfer rate, k	0.02 - 1.0 s^{-1}

[a] this value was kept constant in all the simulations.

4.4.1 Effect of the rotation period

The range of the rotation period used for the study of its effect on the system performance was $t^* \in [110\text{-}130]$ *sec.* The other operating conditions were kept constant, Table 4.2. The results of the influence of the rotation period, t^*, on the system performance as in the conversion parameter, is shown in Figure 4.8.

It can be seen that an optimum value of rotation period exists, $t^* \approx 120$ *sec*, leading to higher performance parameters. The conversion parameter, X, decreases when the rotation period increases.

Another analysis could be made relating recovery with purity obtained for different values of rotation period. In Figure 4.9 that relationship can be seen. The region for high purity and recovery for both products, can be obtained, however it must be very well chosen since it is narrow.

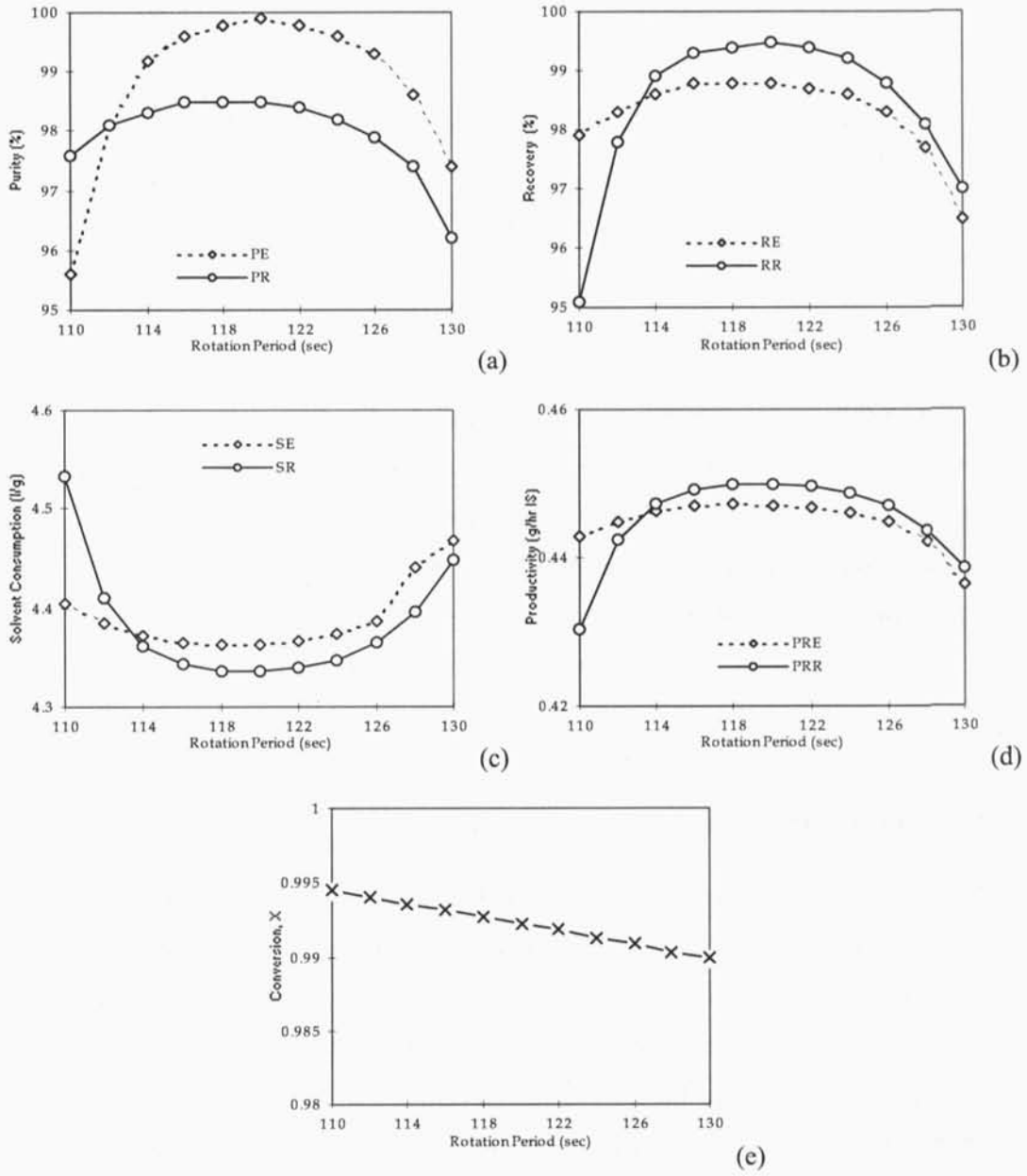

Figure 4.8 *Effect of the rotation period on the TMBR performance parameters for the case study. The rotation period varied between 110 and 130 sec. The others operating conditions and model parameters were kept constant and the same as described in Table 4.2 and numerical parameters in Table 4.3.* ***(a)*** *Rotation Period versus Purity,* ***(b)*** *Rotation Period versus Recovery,* ***(c)*** *Rotation Period versus Solvent Consumption,* ***(d)*** *Rotation Period versus Productivity,* ***(e)*** *Rotation Period versus Conversion.*

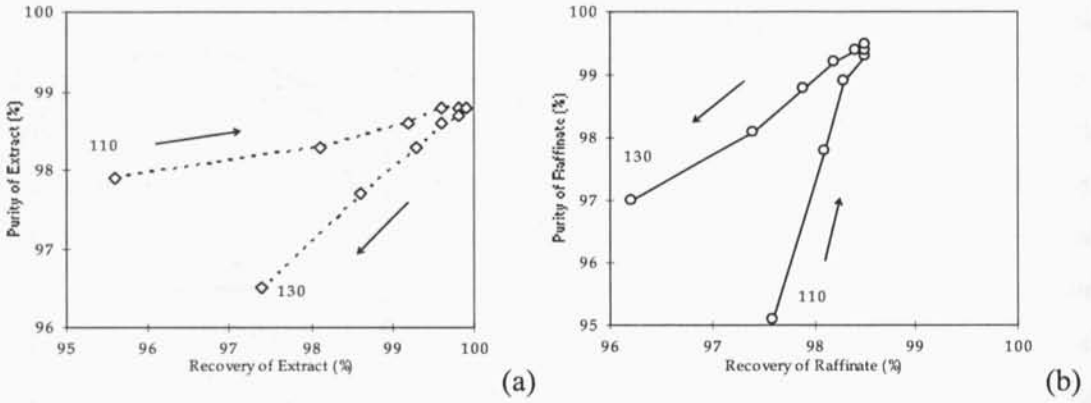

Figure 4.9 *Recovery vs purity for extract (a) and raffinate (b), obtained for different values of rotation period (110-130 sec) for the base case study. The others operating conditions and model parameters were kept constant and the same as described in Table 4.2. The two limits considered for the rotation period, 106 sec and 136 sec are referred with the equivalent values for the purity and recovery. The arrows show the evolution of the performance with the increase of the rotation period.*

4.4.2 Effect of the extract flow rate

The extract concentration varied between 4.00 to 11.00 *ml/min*. Figure 4.10 shows the effect of the extract flow rate, Q_E, on the TMBR performance and on the conversion parameter. The purity for both products, extract and raffinate, are very sensitive to the change of the extract flowrate. So, high values of purity can only be obtained in a narrow window of values of the extract flowrate. It can be seen that, depending on which direction Q_E is changed, the optimum value of the extract flow drastically affects the performance of one or the other product. This behaviour is similar to the one obtained on the TMB study, section 3.3.2. The conversion increases with the extract flowrate.

As in the previous case, the study of the behaviour of the purity versus recovery was done, Figure 4.11. It shows that, it is possible to have simultaneously high purity and recovery for both extract and raffinate, but only for a very narrow region of extract flowrate values.

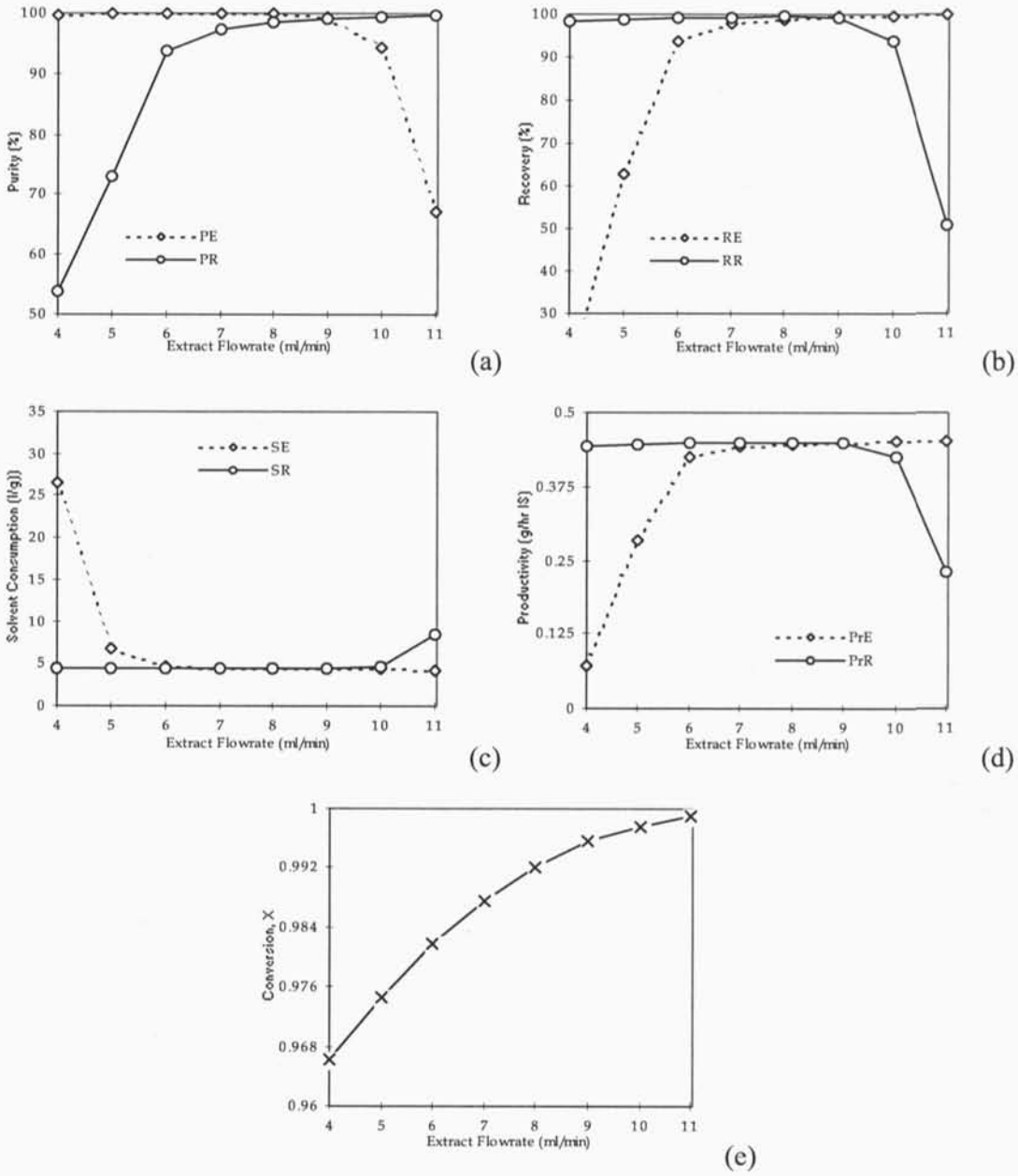

Figure 4.10 *Effect of the extract flowrate on the SMB performance parameters for the case study. The extract flowrate changed between 4.0 and 11.0 ml/min. The others operating conditions and model parameters were kept constant as described in Table 4.2, except the raffinate flowrate that changed with the extract flowrate in order to keep constant the total balance ($Q_R+Q_E=Q_D+Q_F$) and numerical parameters in Table 4.3.* ***(a)*** *Extract Flowrate versus Purity,* ***(b)*** *Extract Flowrate versus Recovery,* ***(c)*** *Extract Flowrate versus Solvent Consumption,* ***(d)*** *Extract Flowrate versus Productivity,* ***(e)*** *Extract Flowrate versus Conversion.*

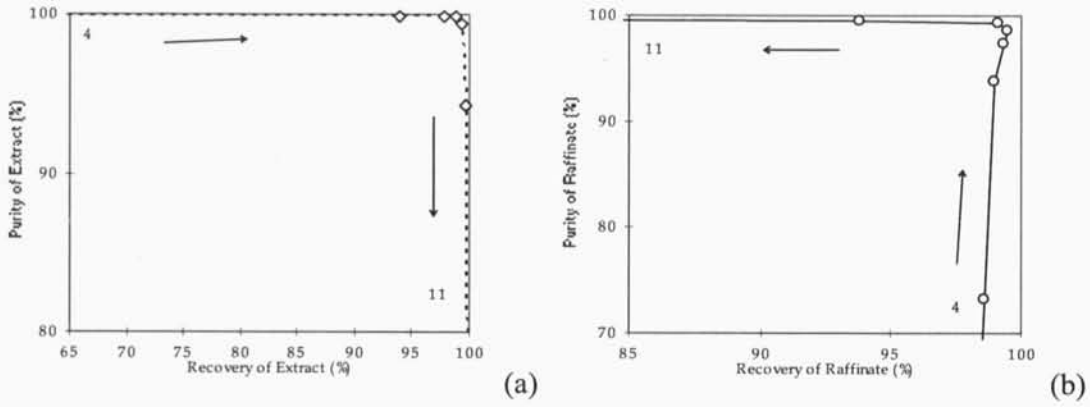

Figure 4.11 *Recovery versus purity for extract* ***(a)*** *and raffinate* ***(b)*** *obtained for different values of the extract flow rate (4.0-11.0 ml/min), for the case study. The others operating conditions and model parameters were kept constant and the same as described in Table 4.2, except the raffinate flowrate that changed with the extract flowrate in order to keep constant the total balance ($Q_R+Q_E=Q_D+Q_F$). The two limits considered for the extract flowrate, 4.0 ml/min and 11.0 ml/min are referred with the equivalent values for the purity and recovery. The arrows show the evolution of the performance with the increase of the extract flowrate.*

4.4.3 Effect of the feed flow rate

The feed flowrate concentration varied between 0.15 to 11.15 *ml/min*. Figure 4.12 shows the effect of the feed flowrate on the TMBR performance and on the conversion. An increase of the feed flowrate improves the productivity and the solvent consumption, for both extract and raffinate. The increase of the feed flowrate almost does not influence the conversion parameter.

Figure 4.13 shows the effect of the feed flowrate on the recovery versus purity. The behaviour is similar for both products. With the decrease of the feed flowrate, the purity and recovery, increase.

4.4.4 Effect of feed concentration

The feed concentration is also an important variable on the SMB performance, as we can verify from the solvent consumption and productivity definitions.

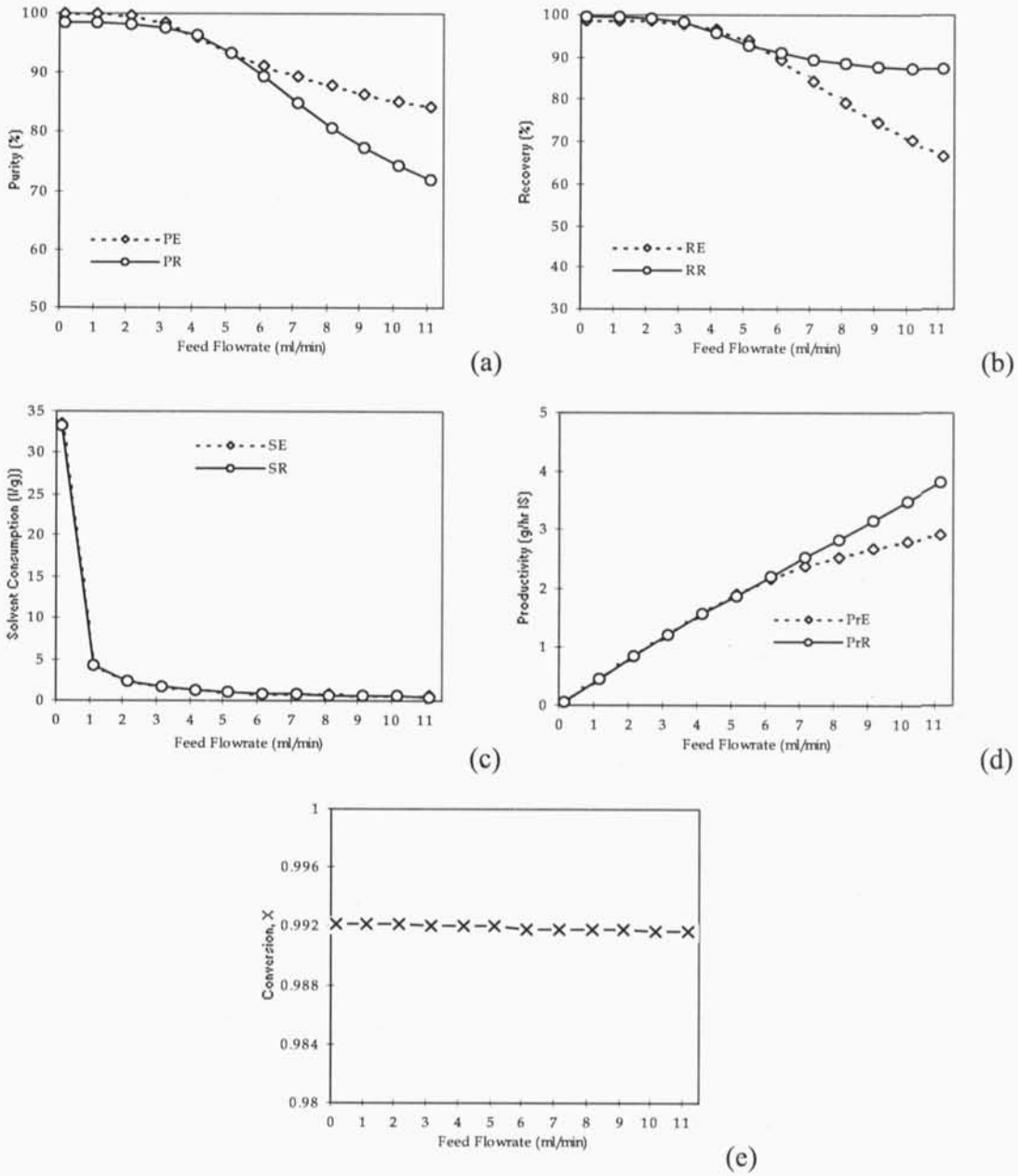

Figure 4.12 *Effect of the feed flow rate on the SMB performance parameters for the case study. The feed flowrate varied between 0.15 and 11.15 ml/min. The others operating conditions and model parameters were kept constant and the same as described in Table 4.2, except the eluent flowrate that changed with the feed flowrate in order to keep constant the total balance ($Q_R+Q_E=Q_D+Q_F$).* ***(a)*** *Feed Flowrate versus Purity,* ***(b)*** *Feed Flowrate versus Recovery,* ***(c)*** *Feed Flowrate versus Solvent Consumption,* ***(d)*** *Feed Flowrate versus Productivity,* ***(e)*** *Feed Flowrate versus Conversion.*

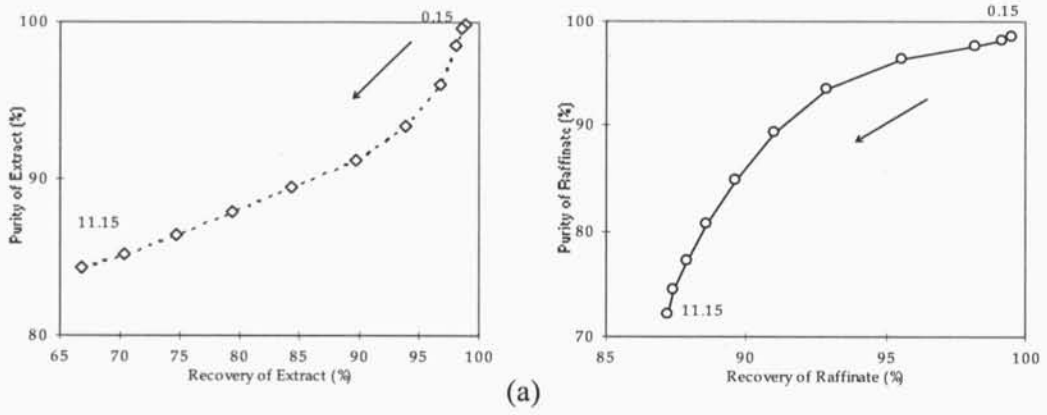

Figure 4.13 *Recovery versus purity for extract* ***(a)*** *and raffinate* ***(b)*** *obtained for different values of the feed flow rate (0.15-11.15 ml/min), for the case study. The others operating conditions and model parameters were kept constant and the same as described in Table 4.2, except the eluent flowrate that changed with the feed flowrate in order to keep constant the total balance ($Q_R+Q_E=Q_D+Q_F$). The two limits considered for the feed flowrate, 0.15 ml/min and 11.15 ml/min are referred with the equivalent values for the purity and recovery. The arrows show the evolution of the performance with the increase of the feed flowrate.*

For a system with linear adsorption isotherms, $q^* = K\,c$, the TMB flow-rates do not depend on the feed concentration values.

The feed concentration varied between 2.5*g/l* to 250*g/l* for the sucrose. The operating conditions and model parameters are the same as described in Table 4.2 and 4.3.

The effect of the feed concentration on the Solvent Consumption and on the Productivity on the TMBR for the case study is shown in Figure 4.14. These results show that we can obtain practically, the same results for extract and raffinate solvent consumption, and also for extract and raffinate productivity. The solvent consumption decreases as the feed concentration increases and the productivity increases as the feed concentration increases.

4.4.5 Effect of the section length and configuration

The operating conditions and model parameters were the same as in Table 4.2, except the number of columns per section. The effect of the section length is shown in Table 4.6.

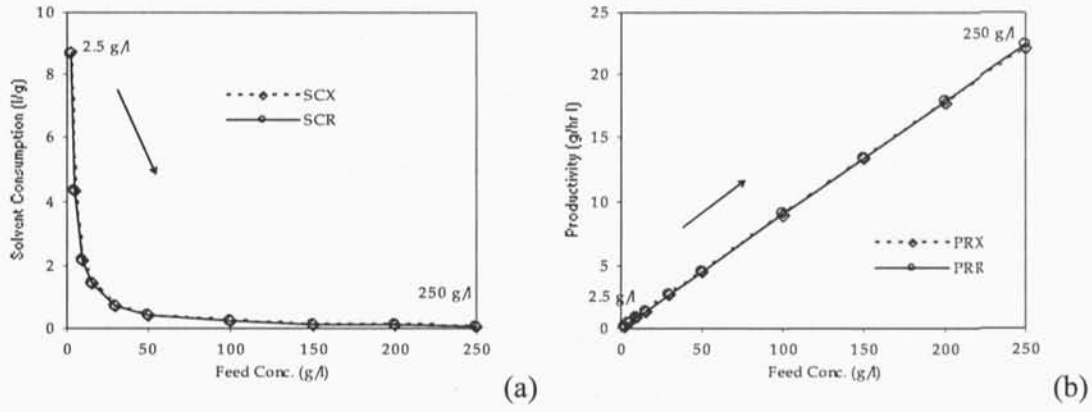

Figure 4.14. *Effect of the feed concentration on the Solvent Consumption and on the Productivity on the SMBR for the study case. The feed concentration varied between 2.5 and 250 gr/l. The others operating conditions and model parameters were kept constant and the same as described in Table 4.2 and 4.3.* ***(a)*** *Solvent Consumption versus Feed concentration,* ***(b)*** *Productivity versus Feed concentration.*

Table 4.6 *Effect of the section length in the performance parameters. The other operating conditions and model parameters were kept constant and the same as described in Table 4.2. The numerical parameters are in Table 4.3.*

Configuration	P_E (%)	P_R (%)	R_E (%)	R_R (%)	X
1 1 5 1	97.8	95.1	95.8	97.0	0.9808
2 2 6 2	99.8	98.4	98.7	99.4	0.9918
3 3 3 3	99.8	86.3	88.7	95.6	0.9187
2 4 4 2	99.6	93.2	94.7	97.7	0.9618
2 2 7 1	98.6	99.2	99.4	98.4	0.9960
2 2 5 3	99.9	96.7	97.4	99.0	0.9825
3 1 6 2	99.4	98.5	98.9	99.0	0.9918
3 3 7 3	100.0	99.3	99.5	99.8	0.9962
4 4 8 4	100.0	99.7	99.7	99.9	0.9983

These results show that we can obtain, practically, complete separation using 12 columns in the SMBR pilot plant, with 10.5*cm* long columns. Different results were obtained considering different configurations for each section. Higher purity and recovery values were obtained in the cases where section III was considered with more columns. The concentration profiles obtained for 3-3-3-3 and for a 2-2-6-2 configuration can be seen in Figure 4.2 and Figure 4.3. The raffinate purity increases, from 86.3% for 3-3-3-3 configuration to 98.4% for 2-2-6-2

configuration. The extract purity is the same. These two cases explain the reason why the section III must have a different length. Figure 4.15 compiles the two cases. The extract, feed and raffinate nodes are different for the two cases; 2, 4 and 10 for the 2-2-6-2 configuration and 3, 6, and 9 for the 3-3-3-3 configuration.

For a 12 columns configuration, with 2-2-6-2 and 2-2-7-1, satisfactory performance parameter were obtained. The effects of section I and II size on the TMBR steady-state concentration profiles, 2-2-6-2 and 3-1-6-2, can be seen in Figure 4.16. Grey lines for 3-1-6-2 configuration and black lines for the 2-2-6-2 configuration. The only difference was on the fructose concentration profile, due to the decrease of the column number of section I, from 2 to 3, and section II decrease from 2 to 1. The change on the fructose section I and II concentration profile, didn't affected the extract performance values, and very similar performance values and conversion parameter were obtained, for these two configuration.

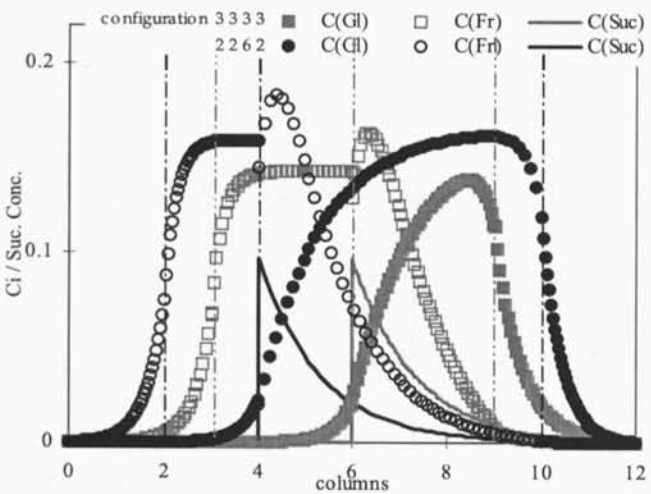

Figure 4.15 *Effect of the section configuration on the TMBR steady-state internal profile. 2 2 6 2 black circles (full glucose, white fructose) and black line sucrose; and 3 3 3 3 grey squares (full glucose, white fructose) and grey line sucrose. The operating conditions and model parameters were as described in Table 4.2. Extract: 2, feed: 4 and raffinate: 10, for 2-2-6-2 configuration; extract: 3, feed: 6 and raffinate: 9, for 3-3-3-3 configuration.*

4.4.6 Effect of the number of intraparticle mass transfer units

(a) on the internal concentration profiles

The effect of the intraparticle mass transfer units, k, (LDF for homogeneous particles) or the corresponding dimensionless number α, on the internal profiles of the TMBR is shown in Figure 4.17. Simulations for more three different values of k were made ($k=0.02\ s^{-1}$, $k=0.5\ s^{-1}$, $k=1.0\ s^{-1}$). For $k=0.1\ s^{-1}$ corresponds to the case study. The mass transfer coefficient depends only on the intraparticle diffusivity of species and on the particle size. Therefore, increasing α, or k, by decreasing the particle size, improves the TMBR performance.

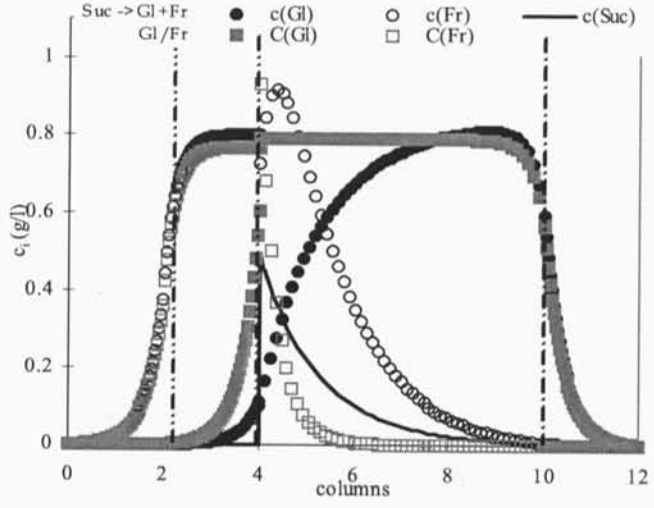

Figure 4.16 *Effect of the length of section I and II on the TMBR steady-state internal profile. 2 2 6 2 black circles (full glucose, white fructose) and black line sucrose; and 3 3 3 3 grey squares (full glucose, white fructose) and grey line sucrose. The operating conditions and model parameters used are described in Table 4.2. Extract: 2, feed: 4 and raffinate: 10, for 2-2-6-2 configuration; extract: 3, feed: 4 and raffinate: 10, for 3-1-6-2 configuration..*

4.5 Comparison between the transient TMBR and TMB models

The TMB steady-state model, equations (2.32 - 2.36), under the operating conditions and model parameters described in Table 4.7, was solved by using the COLNEW solver. The operating conditions and the models parameters used are similar to the ones used to solve the TMBR steady-state model, equations (4.14- 4.16), described in Table 4.2, and with numerical parameters described in Table 4.3. The only difference is on the feed composition: 5 g/l of sucrose for the TMBR case, and 2.5 g/l of glucose plus 2.5 g/l of fructose for the TMB case.

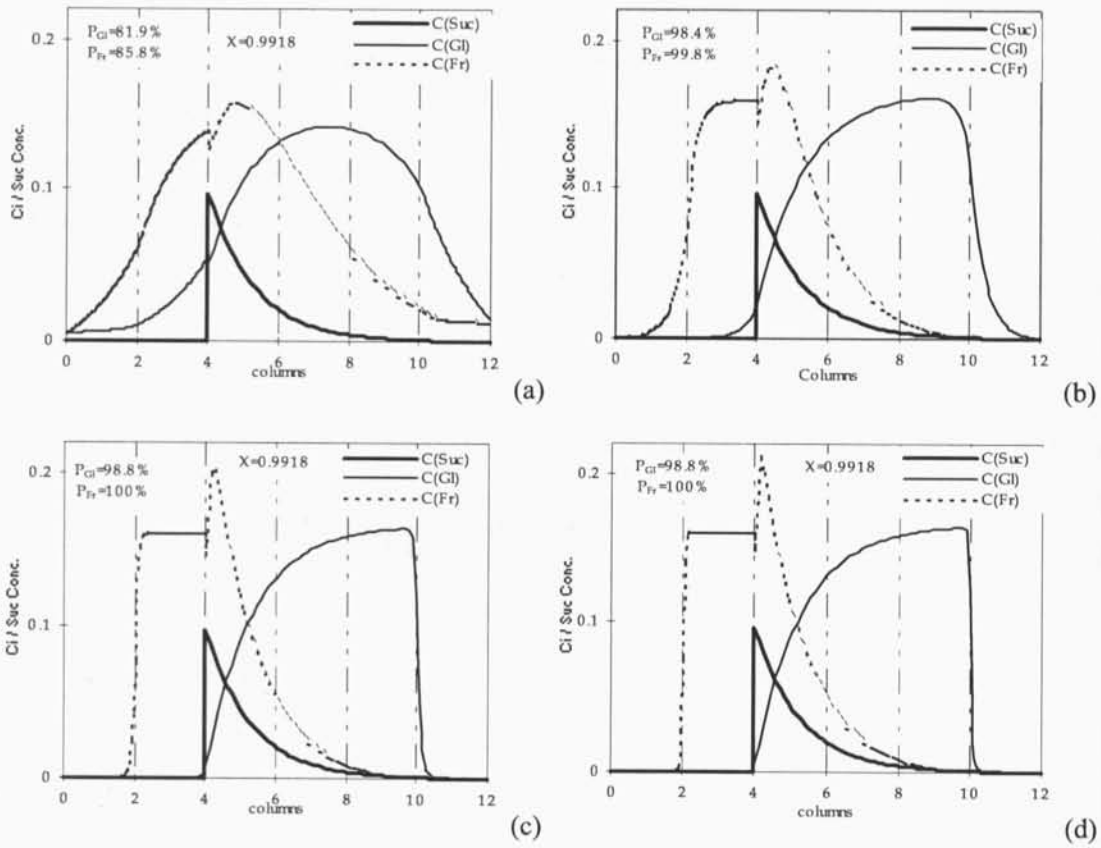

Figure 4.17 *Effect of the intraparticle mass transfer rate on the SMB steady-state internal profile.* ***(a)*** *k=0.02 s^{-1};* ***(b)*** *k=0.1 s^{-1};* ***(c)*** *k=0.5 s^{-1},* ***(d)*** *k=1.0 s^{-1}. The others operating conditions and model parameters were kept constant and the same as described in Table 4.2.*

Table 4.7 *Operating parameters conditions and models parameters used in the simulation of the steady-state TMB model. The equivalence between the TMB and SMB flowrates are the same as described in Table 4.2b.*

SMB Operating conditions	**TMB Model Parameters**	**Columns**
Feed conc. = 2.5 g/l (Gl) + 2.5 g/l (Fr)	Pe = 2000	D_C =2.6 cm
t^* = 122[c] s	$(1-\varepsilon)/\varepsilon$ = 1.5	L_C = 10.5 cm
Q_{Rec} = 17.79[a] ml/min	$k_{Gl} = k_{Fr}$ = 0.1 s^{-1}	Configuration:
Q_D = 11.90[a] ml/min	K_{GL}=0.50[b] K_{Fr}=0.88[b]	2-2-6-2
Q_E = 8.00[a] ml/min		
Q_F = 1.15[a] ml/min	γ_I = 1.7073 γ_{II}= 0.9778	
Q_R = 5.05[a] ml/min	γ_{III} = 1.0827 γ_{IV} = 0.6222	

[a] values obtained through the operation conditions as in Ruthven and Ching (1989).
[b] values for a atmosphere temperature (=30°C, Ching *et al.*, 1986).
[c] switching time, $t^* = l/u_s = (1-\varepsilon)l\,A\,/\,Q_s$.

The obtained results for the two cases considered are shown in Figure 4.18 and the performance parameters described in Table 4.8.

For the glucose/fructose separation system the glucose purity obtained was almost 100%, and 98.4% for the sucrose inversion and glucose/fructose separation, while no different obtained in the values for the extract purity, ≈ 99.9% for both cases. For the sucrose inversion and

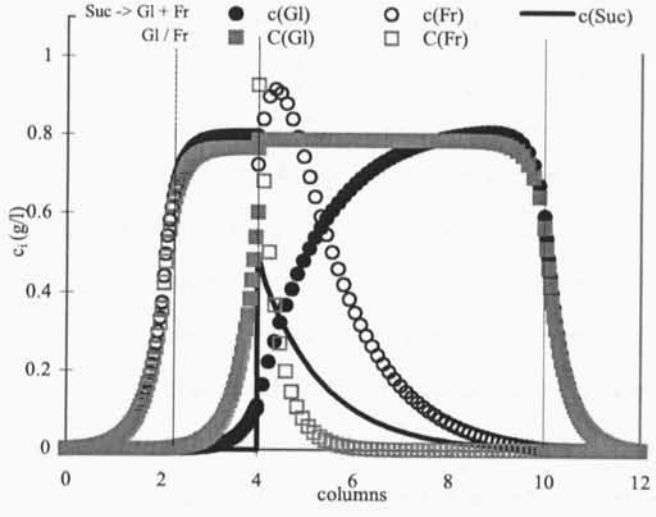

Figure 4.18 *Results obtained for the inversion of sucrose and glucose/fructose separation, black circles (full glucose, white fructose) and black line for sucrose concentration profiles; and for the glucose/fructose separation, grey squares (full glucose, white fructose), under conditions described in Table 4.2 and in Table 4.7, respectively, by using the COLNEW solver.*

Table 4.8 *Performance parameters obtained for the TMBR and TMB models under conditions as described in Table 4.2 and Table 4.7, respectively.*

Model	***TMBR***		***TMB***	
	Gl	***Fr***	***Gl***	***Fr***
Purity (%)	98.4	99.8	99.9	99.7
Recovery (%)	99.4	98.7	99.7	99.9
Solvent Consumption (l/g)	4.339	4.367	4.551	4.545
Productivity (g/hr l)	0.450	0.447	0.429	0.429
Run Time (min)	37		1	
Conversion, X	0.9918		----	

glucose/fructose system, the run time needed was higher, 37 min, comparing to the run time needed for the glucose/fructose separation system. This behaviour was, in one way, expected, since, for the first system, the size of the differential system has higher dimension, due to one more component and also due to the non-linear reaction term.

4.6 Conclusions

Transient and steady state models were presented, by using the TMBR concept, to model a simulated moving bed reactor, applied to the inversion of sucrose and fructose and glucose separation. The mathematical model presented is similar to the TMB model used to simulate the SMB process, adding the reaction term. A Michaelis-Menten model is used to describe the reaction rate, on the liquid phase. A linear equilibrium isotherm for the separation products and a LDF for homogeneous particles approximation are also considered. The obtained system can be presented as partial differential equations, for the transient situation, and as ordinary differential system equations, for the steady-state situation. It was shown that it is possible to obtain the internal steady-state concentration profile by using the PDEDOL and COLNEW solvers, for transient and steady-state situations, respectively.

The influence of the operating conditions on the SMBR/TMBR performance, namely the influence of the switching time interval, extract and feed flow-rates, section length and system configuration was addressed. It is possible to obtain high purity and recovery performances for both products simultaneously in a narrow window of operating conditions and model parameters. The section III, where reaction and adsorption of the more retained reaction product take place, should be longer than the other sections.

The comparison, under equivalent operating conditions of the TMB and TMBR showed that similar purity and recovery performance for the two products, glucose and fructose are obtained.

4.7 References

Azevedo, D. C. S., (2001) *Separation/Reaction in Simulated Moving Bed: Application to the Production of Industrial Sugars*, PhD dissertation, LSRE, University of Porto, Porto.

Bader G., and U. Ascher, (1987) *A New Basis Implementation for a Mixed Order Boundary Value ODE Solver*, SIAM J. Scient. Stat. Comput. **8**, 483-500.

Bowski, R. Saini, D. Y. Ryu, W. R. Vieth, (1971) *Kinetic Modeling of the Hydrolysis of sucrose by Invertase*, Biotechnology and Bioengineering **13**, 641-646.

Ching, B. C., Ho, D. M. Ruthven, (1986) *An Improved Adsorption Process for the Production of High-Fructose Syrup*, AIChE J. **32**, 1876-1880.

Ching, B. C., and Z. P. Lu, (1997) *Simulated Moving-Bed Reactor: Appliaction in Bioreaction and Separation*, Ind. Eng. Chem. Res. **36**, 152-159.

Fish, B., C. W. Carr, A. Rutherford, (1986) *The Continuous Countercurrent Moving Bed Chromatographic Reactor*, Chem. Engng. Sci. **41**, 661-668.

Fricke, J., M. Meurer, J. Dreisörner, H. Schmidt-Traub, (1999) *Effect of process parameters on the performance of a Simulation of a Simulate Moving Bed Chromatographic Reactor*, Chem. Engng. Sci. **54**, 1487-1492.

Ganetsos, G., P. E. Barker, J. N. Ajongwen, (1993) *Batch and Continuous Chromatographic Systems as Combined Bioreactor-Separators*, in Preparative and Production Scale Chromatography, Ganetsos, G., Barker, P. E., Eds.; Marcel Dekker Inc.; New York, 375-394.

Hashimoto, K., S. Adachi, H. Noujima, Y. Ueda, (1983) *A New Process Combined Adsorption and Enzyme Reaction for Producing Higher-Fructose Syrup*, Biotechnol. Bioeng. **25**, 2371-2393.

Hashimoto, K., S. Adachi, Y. Shirai, (1993) *Development of New Bioreactors of a Simulated Moving-Bed Type*, in Preparative and Production Scale Chromatography, Ganetsos, G., Barker, P. E., Eds.; Marcel Dekker Inc.; New York, 395-419.

Kawase, M., Y. Inoue, T. Araki, K. Hashimoto, (1999) *The Simulated-Moving-Bed Reactor for Production of Bisphenol A*, Catalysis Today **48**, 199-209.

Kawase, M., A. Pilgrim, T. Araki, K. Hashimoto, (2001) *Lactosucrose Production using a Simulated Moving Bed Reactor*, Chem. Engng. Sci. **56**, 453-458.

Leão C. P., and A. E. Rodrigues, (1997) *Modelling and Simulation of a SMBR pilot plant*, 15th IMACS World Congress on Scientific Computation, Modelling and Applied Mathematics, Achim Sydow Ed., 633-638.

Leão C. P., L.S Pais, M. Santos, A. E. Rodrigues, (1997) *Simulated Moving Bed Adsorptive Reactor*, 2nd International Conference on Process Intensification in Practice, J. Semel Eds., 143-155.

Madsen, N. K., and R. F. Sincovec, (1979) *PDECOL: General Collocation Software for Partial Differential Equations*, ACM Trans. Math. Soft. **5**, 326-351.

Lode, N., M. Houmard, C. Migliorini, M. Mazzotti, M. Morbidelli, (2001) *Continuous Reactive Chromatography*, Chem. Engng. Sci. **56**, 269-291.

Mazotti, A. Kruglov, B. Neri, D. Gelosa, M. Morbidelli, (1996) *A Continuous Chromatographic Reactor: SMBR*, Chem. Engng. Sci. **51**, 1827-1836.

Meurer, M., U. Altenhöner, J. Stube, A. Untiedt, H. Schmidt-Traub, (1996) *Dynamic Simulation of a Simulate-Moving-Bed Chromatographic Reactor for the Inversion of Sucrose*, Starch **48**, 452-457.

Meurer, M., U. Altenhöner, J. Stube, H. Schmidt-Traub, (1997) *Dynamic Simulation of a Simulate-Moving-Bed Chromatographic Reactors*, J. Chromatogr. A **769**, 71-79.

Ray, A. K., and R. W. Carr, (1995) *Numerical Simulation of a Simulated Countercurrent Moving Bed Chromatographic Reactor*, Chem. Engng. Sci. **50**, 3033-3041.

Ruthven, D. M., and C. B. Ching, (1989) *Counter-Current and Simulated Moving Bed Adsorption Separation Process*, Chem. Engng. Sci. **44**, 1011-1038.

Sarmidi, M. R., and P. E. Barker, (1993) *Simultaneous Biochemical Reaction and Separation in a Rotating Annular Chromatograph*, Chem. Engng. Sci. **48**, 2615-2623.

5. Modelling of TMBR Adsorber: New Developments

In this chapter a model is developed accounting not only for the reaction in the outer fluid phase but also inside the adsorbent particle. The resulting set of mass balance equations representing the fluid phase and the particle phase in a volume of element of the column and spherical particle shell element, respectively, are not easy solved. The standard LDF approximation for the diffusion/adsorption inside particles does not consider the reaction in the porous particle.

In a first approach, a polynomial approximation was used defining a new LDF model by using the coefficients in the Kim's (1989) LDF formulas. The resulting model is described by a system of PDEs defined by the mass balances for the outer liquid phase and for the averaged pore-intraparticle fluid phase, for each species. A steady-state TMBR model can be used, by considering the terms with respect to time derivative equal to zero. The effects of the particle radius have been studied on the performance parameters and on the TMBR concentration profiles. A γ_{II} - γ_{III} plane analysis based on the equilibrium theory for a non-reactive SMB system, has been performed.

A detailed new SMBR model, based on the TMBR analogy, is developed taking into account the intraparticle radial profiles. The numerical transient and steady-state solutions are obtained by using a combination of orthogonal collocation on finite element method and available PDE and ODE solvers, respectively. Numerical solutions are presented for linear

and non-linear reaction rate, and compared to those obtained with the new LDF approximation.

5.1 Model formulation and development

The TMBR model equations result from the mass balances over a volume element of the bed and at a particle level as shown in Figure 5.1. The steps considered were the transport of component *i* from the bulk solution to the particle surface through the liquid film; intraparticle diffusion of the component *i* into the particle, adsorption and reaction.

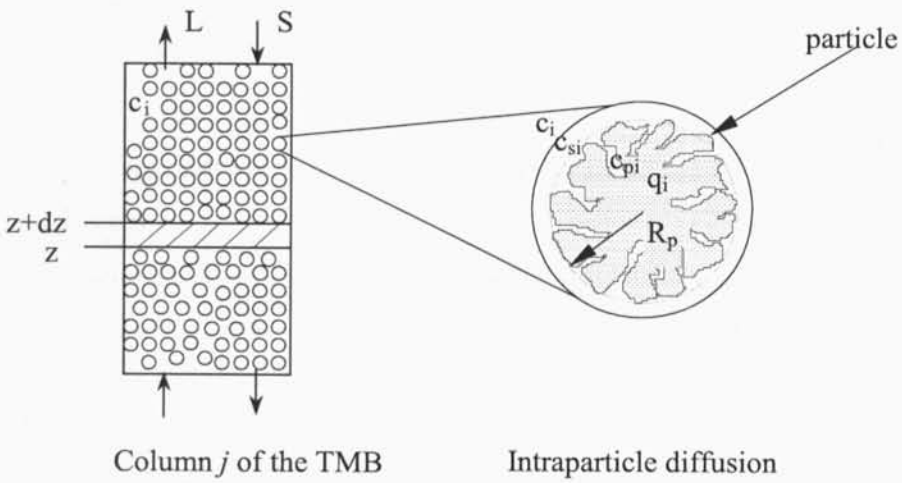

Figure 5.1. *Column and film and intraparticle diffusion of component i.*

The first step involves the mass transfer of the species *i* from the bulk fluid to the surface of the adsorbent particle. The diffusivity of species *i* is included. The second step involves the penetration of the species *i* through the pores of the adsorbent particle seeking sites for adsorption/reaction, where the reaction $\mathcal{R}$ takes place.

The mass balance of species *i* in outer liquid phase:

(*in* = *out* + *accumulation* +*reaction* + *transfer*)

$$\varepsilon D_{L_j} \frac{\partial^2 c_{ij}}{\partial z^2} = \varepsilon v_j \frac{\partial c_{ij}}{\partial z} + \varepsilon \frac{\partial c_{ij}}{\partial t} - \upsilon_i \varepsilon \mathcal{R} + \frac{3k_{fij}}{R_p}(1-\varepsilon)\left(c_{ij} - c_{sij}\right) \qquad (5.1)$$

In the above partial differential equation, D_{L_j} is the axial diffusion coefficient, v_j is the interstitial fluid velocity in the section j, υ_i is the stoichiometric coefficient of the reaction (negative for the reactant, sucrose ($i = 1$), and positive for the reaction products, glucose and fructose ($i = 2$ and 3), that is, $\upsilon_1 = -1$, and $\upsilon_2 = \upsilon_3 = +1$), c_{ij} is the concentration of species i in the adsorbent section j, c_{sij} represents the liquid phase concentration of species i at the solid-liquid interface, k_{fij} film-transfer coefficient for species i through liquid film, R_p is the particle radius, ε is the bed porosity, $\mathcal{R}$ is the reaction rate. For the sucrose inversion the reaction rate, $\mathcal{R}$, takes the form of Michaelis-Menten equation,

$$\mathcal{R} = \frac{k_r E_0 c_{Sucj}}{K_m + c_{Sucj}} \tag{5.2}$$

where k_r is the reaction rate constant, E_0 is the enzyme concentration and K_m the Michaelis constant.

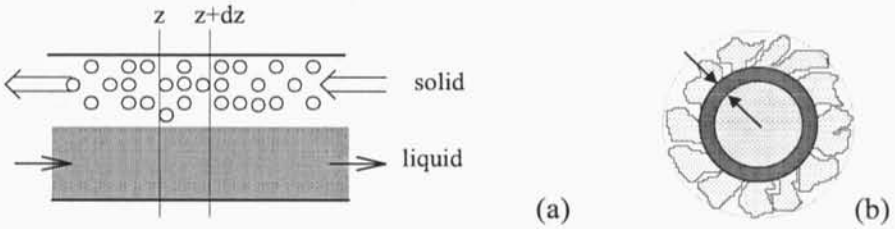

Figure 5.2. *Volume element of the column (a) and spherical particle shell element (b).*

The partial differential equation representing the mass balance of the pore-intraparticle fluid phase equation on a volume element of the section j and of species i, Figure 5.2(a), for the adsorption of species i is based on the following relationships:

$$u_s \frac{\partial \langle q_{ij} \rangle}{\partial z} + u_s \varepsilon_p \frac{\partial \langle c_{p_{ij}} \rangle}{\partial z} + \frac{3}{R_p} k_f \left(c_{ij} - c_{sij} \right) = \\ = \varepsilon_p \frac{\partial \langle c_{p_{ij}} \rangle}{\partial t} + \frac{\partial \langle q_{ij} \rangle}{\partial t} - \upsilon_i \left(\varepsilon_p + K_{enz} \right) \mathcal{R}\left(\langle c_{p_{ij}} \rangle \right) \tag{5.3}$$

Each term in the above equation is expressed in moles/m^3 particle.s. $\langle q_{ij} \rangle$ is the average adsorbed-phase concentration, mole adsorbed/m^3 particle, $\langle c_{p_{ij}} \rangle$ is the average pore concentration of species i, mole /m^3 fluid in pores, K_i the equilibrium constant of species i, ε_p is the particle porosity, u_s is the solid interstitial velocity defined as $= \frac{Q_s}{(1-\varepsilon)A} = \frac{L_c}{t^*}$, $\langle \mathcal{R}(c_{pij}) \rangle$ is the average reaction rate defined, by approximation, as $\frac{kE_0 \langle c_{p3j} \rangle}{K_m + \langle c_{p3j} \rangle}$, (for more details see following section), K_{enz} the equilibrium constant of the enzyme with adsorption isotherm equation $E_{ads} = K_{enz} E$.

If we considered the adsorption equilibrium described by the linear model

$$\langle q_{ij} \rangle = K_i \langle c_{p_{ij}} \rangle \tag{5.4}$$

then the differential equation (5.3) can be written as

$$u_s (K_i + \varepsilon_p) \frac{\partial \langle c_{p_{ij}} \rangle}{\partial z} + \frac{3k_f}{R_p} (c_{ij} - c_{sij}) = (K_i + \varepsilon_p) \frac{\partial \langle c_{p_{ij}} \rangle}{\partial t} - \upsilon_i (\varepsilon_p + K_{enz}) \langle \mathcal{R}(c_{pij}) \rangle \tag{5.5}$$

The corresponding initial condition is based on the assumption that at time $t = 0$ there is no species i in the liquid. Therefore the initial and boundary conditions can be represented as follows

$$c_{ij}(z,0) = 0, \quad c_{sij}(z,0) = 0, \quad \langle c_{p_{ij}} \rangle (z,0) = 0 \tag{5.6}$$

$$z = 0 \qquad c_{ij} = c_{ij,0} - \frac{D_{L_j}}{\nu_j} \frac{\partial c_{ij}}{\partial z} \tag{5.7a}$$

$$z = L_j \qquad \frac{\partial c_{ij}}{\partial z} = 0, \quad \langle q_{ij} \rangle = \langle q_{ij+1,0} \rangle \quad \langle c_{p_{ij}} \rangle = \langle c_{p_{ij+1,0}} \rangle \quad c_{sij} = c_{sij+1,0} \tag{5.7b}$$

$$j = I \qquad c_{iIV,L_{IV}} = \frac{v_I}{v_{IV}} c_{iI,0}$$

and $$j = II, IV \qquad c_{i(j-1),L_{j-1}} = c_{ij,0} \tag{5.7c}$$

$$j = III \qquad c_{iII,L_{II}} = \frac{v_{III}}{v_{II}} c_{iIII,0} - \frac{v_F}{v_{II}} c_i^F$$

Looking at the two differential equations that define the system to be solved, (5.1) and (5.5), we have three unknowns, c_{ij}, c_{sij}, and $\left\langle c_{pij} \right\rangle$. The third equation, that must be added to the system, is the one that links the two unknowns, c_{ij}, c_{sij}, which are the concentrations of the liquid-phase of species i in the adsorbent section j and of species i at the liquid-particle interface, respectively.

Considering a stagnant spherical particle shell element, the partial differential equation representing the pore diffusion, adsorption and reaction can be written as follows,

$$\varepsilon_p \frac{\partial c_{pij}}{\partial t} + \frac{\partial q_{ij}}{\partial t} = \frac{1}{r^2} \frac{\partial}{\partial r} \left(r^2 D_{pe} \frac{\partial c_{pij}}{\partial r} \right) + \upsilon_i \mathcal{R}\left(c_{pij}\right) \tag{5.8}$$

where D_{pe} is the effective pore diffusion coefficient (m^2/min), r the particle radial coordinate, R_p is the particle radius.

If the diffusivity is constant and if the equilibrium isotherm is linear, $q_{ij} = K_i c_{pij}$, then we get

$$\left(K_i + \varepsilon_p\right) \frac{\partial c_{pij}}{\partial t} = D_{pe} \frac{1}{r^2} \frac{\partial}{\partial r} \left(r^2 \frac{\partial c_{pij}}{\partial r} \right) + \upsilon_i \mathcal{R}\left(c_{pij}\right) \tag{5.9}$$

with the boundary conditions,

$$r = 0, \qquad \frac{\partial c_{pij}}{\partial r} = 0 \tag{5.10a}$$

$$r = R_p, \qquad \left. \frac{\partial c_{pij}}{\partial r} \right|_{r=R_p} = \frac{k_f}{D_{pe}} \left(c_{ij} - c_{sij} \right) \tag{5.10b}$$

where k_f is the film mass-transfer coefficient, D_{pe} is the effective pore diffusion coefficient.

Some analytical solutions to the equation (5.9) without chemical reaction are available in several works (Alopaeus, 2000; Li and Yang, 1999; Başağaoğlu *et al.*, 2000) each one with proper simplifications. The LDF approximation has been widely used in various problems that involve intraparticle diffusion, however with no chemical reaction. Averaging equation (5.9) without chemical reaction term, over the particle volume and using the LDF approximation we obtain,

$$\frac{\partial \langle c_{pij} \rangle}{\partial t} = \frac{15 D_{pe}}{R_p^2} \frac{1}{(K_i + \varepsilon_p)} \left(c_{psij} - \langle c_{pij} \rangle \right) \tag{5.11}$$

The unknown term c_{psij} is the liquid surface concentration, that is, at $r = R_p$, and can be considered time dependent or independent. Averaging equation (5.9) over the particle volume is not so straightforward due to the presence of the term concerning the chemical reaction $\mathcal{R}(c_{pij})$. Kim (1989) developed LDF approximations, which take into account a first order reaction, adsorption with linear isotherm, and unsteady-state diffusion in porous particles. Following the methodology illustrated in Kim (1989), it is possible to obtain the exact solution of equation (5.9), assuming that the surface concentration vary in time given by $f(\xi)$,

$$c_p(\rho,\theta) = \frac{2}{\rho} \sum_{n=1}^{\infty} (-1)^{n+1} n\pi \sin n\pi\rho \; e^{-\lambda_n \theta} \int_0^{\theta} e^{\lambda_n \xi} f(\xi) d\xi \tag{5.12}$$

where $\lambda_n = \phi^2 + n^2\pi^2$ with $\phi = R_p \sqrt{\frac{k'}{D_{pe}}}$ the Thiele modulus, $\theta = \frac{D_{pe}}{R_p^2 (K_i + \varepsilon_p)} t$ and $\rho = \frac{r}{R_p}$ the dimensionless parameters. This solution was obtained by using the method of separation of variables and solved the eigenvalue problem (Ramkrishna and Amundson, 1985). After averaged over a particle volume, the solution can be written as:

$$\langle c_p \rangle(\theta) = 3 \int_0^1 c(\rho,\theta) \rho^2 d\rho = 6 \sum_{n=1}^{\infty} e^{-\lambda_n \theta} \int_0^{\theta} e^{\lambda_n \xi} f(\xi) d\xi \tag{5.13}$$

Equation (5.13) can be written in a different way, after several mathematical manipulations (expanding the integral after integrated by parts successively and substituted in equation (5.13),

$$\langle c_p \rangle(\theta) = f(\theta) \sum_{n=1}^{\infty} \frac{6}{\lambda_n} - \frac{df}{d\theta} \sum_{n=1}^{\infty} \frac{6}{\lambda_n^2} + \frac{d^2 f}{d\theta^2} \sum_{n=1}^{\infty} \frac{6}{\lambda_n^3} - + \ldots + \sum_{n=1}^{\infty} \frac{e^{-\lambda_n \theta}}{\lambda_n} \cdot \left(-f(0) + \frac{1}{\lambda_n} \frac{df}{d\theta}\bigg|_{\theta=0} - \frac{1}{\lambda_n^2} \frac{d^2 f}{d\theta^2}\bigg|_{\theta=0} + - \ldots \right) \tag{5.14}$$

The terms with $e^{-\lambda_n \theta}$ vanishes with the time θ thus equation (5.14) can be simplified,

$$\langle c_p \rangle(\theta) = s_1 f(\theta) - s_2 \frac{df}{d\theta} + s_3 \frac{d^2 f}{d\theta^2} - s_4 \frac{d^3 f}{d\theta^3} + - \ldots \tag{5.15}$$

where the s_i coefficients, for various values of the Thiele modulus ϕ, were defined as,

$$s_i = \sum_{n=1}^{\infty} \frac{6}{\lambda_n^i} \tag{5.16}$$

These coefficients (see Table 5.1) decreases rapidly as the index i increase, turning the derivatives of f less important as the order of derivative increases. Differentiated (5.15) and truncated the terms with derivatives of orders higher then three, the new expression for the averaged concentration can be obtained,

$$\frac{d\langle c_p \rangle}{dt} = \frac{D_{pe}}{R_p^2 (K_i + \varepsilon_p)} \frac{s_1}{s_2} \left(c_{ps} - \langle c_p \rangle \right) \tag{5.17}$$

The coefficients in the LDF formula are listed the terms coefficients up to the first order in Table 5.1 and Figure 5.3. Notice that in the case of no reaction, $\phi = 0$, equation (5.17) become,

$$\frac{d\langle c_p \rangle}{dt} = \frac{15 D_{pe}}{R_p^2 (K_i + \varepsilon_p)} \left(c_{ps} - \langle c_p \rangle \right) \tag{5.18}$$

Equation (5.18) is equivalent to the LDF model approximation with no reaction case, equation (5.11).

The next step is to fit these values into an equation to enable to predict, for any value of ϕ, the value of the coefficient s_1/s_2.

The method used to fit the several values was the least-squares method. Looking at Figure 5.3, the relationship between s_1/s_2 and ϕ is nonlinear. The non-linear relationship that would better fit the data was described by a parabola, i.e., a second order polynomial, defined as $15 + a\phi + b\phi^2$. The reason to force the independent coefficient to be 15, is due to the value of the coefficient s_1/s_2 for the case of no reaction, $\phi = 0$, see Table 5.1. Defining the sum of the squares of the residuals, S_r, as

$$S_r = \sum_{i=1}^{n} \left((s_1/s_2)_i - \left(15 + a\phi_i + b\phi_i^2 \right) \right)^2 \tag{5.19}$$

The values of the a, b coefficients are determined to minimize equation (5.19). The least-squares fit, by using MAPLE V (Char *et al.*, 1992), was,

$$\overline{s_1/s_2} = 15 + 1.4932\phi + 2.0039\phi^2 \tag{5.20}$$

The fit of the second order model, equation (5.20), is represented in Figure 5.4. Polynomials with higher order can be also obtained however the coefficients of higher order terms are

practically irrelevant, for instance, the polynomial of degree three obtained is [15 + 0.8491 ϕ + 2.0275 ϕ^2 - 0.0001729 ϕ^3]. The standard error of the estimation based on the regression polynomial is $s = \sqrt{\frac{S_r}{n-(m+1)}}$, where m is the order of polynomial and n the number of points. In our case, with $m = 2$ and n = 8, $s = \sqrt{\frac{S_r}{8-(2+1)}} = 4.5780$, with a correlation coefficient $r = \sqrt{\frac{S_t - S_r}{S_t}} = 0.9972$. These results indicate that 99.72% of the original uncertainty has been explained by the model. This result supports the conclusion that the quadratic equation represents an excellent fit, as is also evident from Figure 5.4.

Table 5.1. *Coefficient in LDF formulas.*

Source: Kim (1989)

ϕ	s_1	s_2	s_1/s_2
0	1	1/15	15
1	0.9391	0.05565	16.88
2	0.8060	0.03550	22.70
5	0.4801	0.007212	66.56
10	0.2700	0.001200	225.0
20	0.1425	0.0001688	844.4
50	0.0588	1.152×10^{-5}	5104
100	0.0297	1.470×10^{-6}	20202

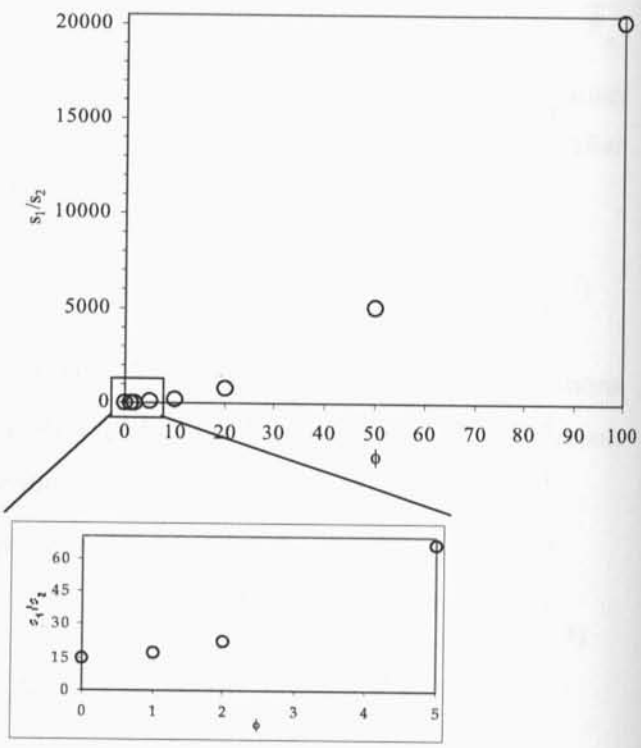

Figure 5.3. ϕ *versus* s_1/s_2.

In Table 5.2, the values of the s_1/s_2 coefficients are listed for various ϕ values for the LDF formulas obtained by Kim (1989) and for the new second order model. The coefficients

rapidly increase with the increasing of ϕ. The squares deviations for different values of ϕ were also estimated and shown in Table 5.2. The approximation accuracy shows no path.

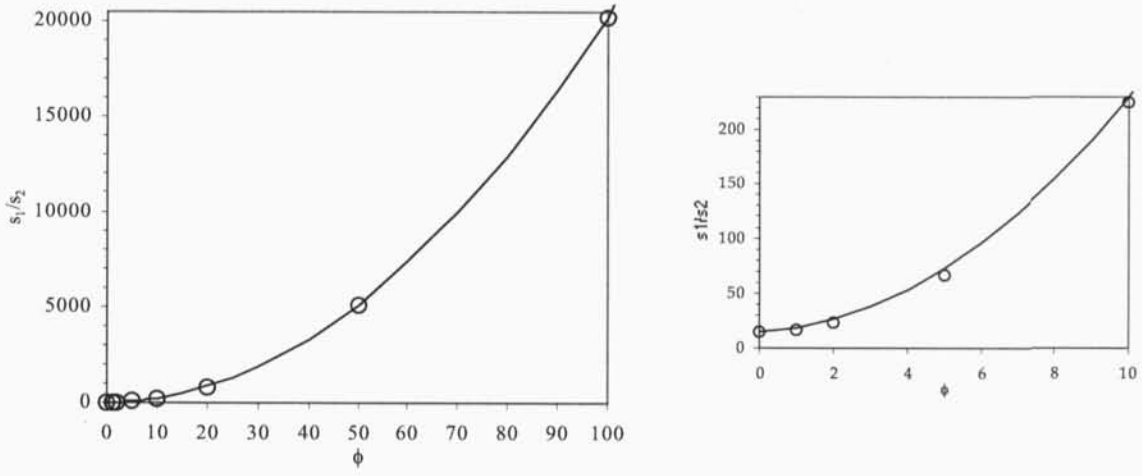

Figure 5.4 *Fit of a second order polynomial* $\overline{s_1/s_2} = 15 + 1.4932\phi + 2.0039\phi^2$. *The dots correspond to the values of* s_1/s_2 *for various* ϕ *values.*

Table 5.2. *Coefficient in LDF formulas,* s_1/s_2, *obtained by Kim (1989), by the second order polynomial,* $\overline{s_1/s_2}$, *and the squares deviations, for different values of* ϕ.

ϕ	s_1/s_2	$\overline{s_1/s_2}$	$\left(s_1/s_2 - \overline{s_1/s_2}\right)^2$
0	15	15	0
1	16.88	18.50	2.62
2	22.70	26.00	10.90
5	66.56	72.56	36.04
10	225.0	230.32	28.32
20	844.4	846.41	4.10
50	5104	5099.33	21.07
100	20202	20203.02	1.74

The new model that would be used to predict, for various ϕ values, the s_1/s_2 coefficients in the LDF formula, is as follows

$$\overline{s_1/s_2} = 15.f(\phi) = 15.\left(1 + 0.09955\phi + 0.1336\phi^2\right), \text{ with} \qquad (5.21a)$$

$$f(\phi) = 1 + 0.09955\phi + 0.1336\phi^2 \tag{5.21b}$$

Notice that, for the case of no reaction, $\phi = 0$, the value for s_1/s_2 is 15.

Back to the SMBR/TMBR system, to the point that was presented the partial differential equation concerning pore diffusion, adsorption and reaction model, equation (5.9) with the boundary conditions described in (5.10). Now we can consider that the chemical reaction occurs, i.e, that the term $\mathcal{R}(c_{pij})$ will be considered.

The boundary condition at the right hand side, considering chemical reaction, equation (5.10b), and using the new LDF model, equation (5.21), then we have

$$\frac{3k_f}{R_p}\left(c_{ij} - c_{sij}\right) = \frac{D_{pe}}{R_p^2}\left(c_{pij}\Big|_{r=R_p} - \left\langle c_{pij}\right\rangle\right).\left\{15.\left(1 + 0.09955\phi + 0.1336\phi^2\right)\right\} \tag{5.22}$$

For $\phi = 0$, equation (5.22) is equivalent to the case when the LDF approximation is applied to the boundary equation at the right hand side without considering chemical.

Applying this relationship, (5.22), into the partial differential equation (5.5), we obtain

$$\frac{\partial\left\langle c_{pij}\right\rangle}{\partial t} = u_s\frac{\partial\left\langle c_{pij}\right\rangle}{\partial z} + \frac{15.D_{pe}}{R_p^2\left(\varepsilon_p + K_i\right)}f(\phi)\left(c_{sij} - \left\langle c_{pij}\right\rangle\right) + \upsilon_i\frac{\left(\varepsilon_p + K_{enz}\right)}{\left(\varepsilon_p + K_i\right)}\left\langle\mathcal{R}(c_{pij})\right\rangle \tag{5.23}$$

In this case ϕ, the Thiele modulus, is defined as

$$\phi = R_p\sqrt{\frac{k'}{D_{pe}}} \tag{5.24}$$

The constant k', in equation (5.24), was obtained by using a simplified reaction model $\mathcal{R}(c_{pij})$. We assumed that the reaction follows the Michaelis-Menten model equation (5.2). If we considered a first order reaction and $K_m >> c_{pSuc}$ then,

$$\mathcal{R}(c_{pij}) = k'c_{pSuc} \text{ with } k' = \frac{k_r E_0}{K_m} \tag{5.25}$$

Considering this new reaction model, (5.25), and after averaging, we can say that

$$\left\langle\mathcal{R}(c_{pij})\right\rangle = \left\langle k'c_{pSuc}\right\rangle = k'\left\langle c_{pSuc}\right\rangle \tag{5.26}$$

From (5.22), we can obtain the third equation that is needed to obtain the value of c_{sij}, the liquid phase concentration of species i at the particle surface (mol.m^{-3}). Solving (5.22) for c_{sij}, and considering the mass Biot number Bi_m, as previously defined, we obtain

$$c_{sij} = \frac{1}{\frac{Bi_m}{5} + \left(1 + 0.09955\phi + 0.1336\phi^2\right)} \left(\frac{Bi_m}{5} c_{ij} + \left(1 + 0.09955\phi + 0.1336\phi^2\right) \left\langle c_{p_{ij}} \right\rangle \right) \tag{5.27}$$

The new LDF approximation with chemical reaction, linear equilibrium isotherm, film diffusion, axial dispersion for fluid flow, gives the following system of PDEs:

$$\frac{\partial c_{ij}}{\partial t} = D_{L_j} \frac{\partial^2 c_{ij}}{\partial z^2} - v_j \frac{\partial c_{ij}}{\partial z} + \upsilon_i \left(k' c_{Sucj}\right) - \frac{(1-\varepsilon)}{\varepsilon} \frac{15.D_{pe}}{R_p^2} f(\phi) \left(c_{sij} - \left\langle c_{p_{ij}} \right\rangle \right) \tag{5.28a}$$

$$\frac{\partial \left\langle c_{p_{ij}} \right\rangle}{\partial t} = u_s \frac{\partial \left\langle c_{p_{ij}} \right\rangle}{\partial z} + \upsilon_i \frac{\left(\varepsilon_p + K_{enz}\right)}{\left(\varepsilon_p + K_i\right)} \left(k' \left\langle c_{p\,Sucj} \right\rangle \right) + \\ + \frac{1}{\left(\varepsilon_p + K_i\right)} \frac{15.D_{pe}}{R_p^2} f(\phi) \left(c_{sij} - \left\langle c_{p_{ij}} \right\rangle \right) \tag{5.28b}$$

$$c_{sij} = \frac{1}{\frac{Bi_m}{5f(\phi)} + 1} \left(\frac{Bi_m}{5f(\phi)} c_{ij} + \left\langle c_{p_{ij}} \right\rangle \right) \tag{5.28c}$$

where ϕ is defined by (5.24) and $f(\phi)$ by (5.21b). The corresponding initial and boundary conditions are

$$c_{ij}(z,0) = 0, \quad \left\langle c_{p_{ij}} \right\rangle (z,0) = 0, \quad c_{sij}(z,0) = 0 \tag{5.29a}$$

$$z = 0 \qquad c_{ij,0} = c_{ij} - \frac{D_{L_j}}{v_j} \frac{\partial c_{ij}}{\partial z} \tag{5.29b}$$

$$z = L_j \qquad \frac{\partial c_{ij}}{\partial z} = 0, \qquad \left\langle c_{p_{ij}} \right\rangle = \left\langle c_{p_{ij+1,0}} \right\rangle$$

with the following node balance equations to solve the presented model, containing the information of the fluid-phase concentration in the left-hand side boundary, $z = 0$,

$$j = I \qquad c_{iIV,L_{IV}} = \frac{v_I}{v_{IV}} c_{iI,0}$$

$$j = II, IV \qquad c_{i(j-1),L_{j-1}} = c_{ij,0} \tag{5.29c}$$

$$j = III \qquad c_{iII,L_{II}} = \frac{v_{III}}{v_{II}} c_{iIII,0} - \frac{v_F}{v_{II}} c_i^F$$

The model defined by equations (5.28-5.29) can be represented in a dimensionless form after introducing the dimensionless variables for space and time, $x = z/L_j$ and $\theta = t/\tau_s$ with $\tau_s = L_c/u_s$ the switching time interval, where $L_j = n_j L_c$ the section j length, L_c the length of each column, and n_j the number of columns in section j.

$$\frac{\partial c_{ij}}{\partial \theta} = \frac{\gamma_j}{n_j}\left(\frac{1}{Pe_j}\frac{\partial^2 c_{ij}}{\partial x^2} - \frac{\partial c_{ij}}{\partial x} + \upsilon_i Da_j c_{Sucj} - \frac{(1-\varepsilon)}{\varepsilon} k_p \tau_j f(\phi)\left(c_{sij} - \left\langle c_{pij}\right\rangle\right)\right) \tag{5.30a}$$

$$\frac{\partial \left\langle c_{pij}\right\rangle}{\partial\theta} = \frac{1}{n_j}\left(\frac{\partial \left\langle c_{pij}\right\rangle}{\partial x} + \upsilon_i \gamma_j Da_j \frac{\left(\varepsilon_p + K_{enz}\right)}{\left(\varepsilon_p + K_i\right)}\left\langle c_{pSucj}\right\rangle + \right.$$
$$\left. + \gamma_j \frac{k_p \tau_j}{\left(\varepsilon_p + K_i\right)} f(\phi)\left(c_{sij} - \left\langle c_{pij}\right\rangle\right)\right) \tag{5.30b}$$

$$c_{sij} = \frac{1}{\frac{Bi_m}{5f(\phi)} + 1}\left(\frac{Bi_m}{5f(\phi)} c_{ij} + \left\langle c_{pij}\right\rangle\right) \tag{5.30c}$$

With the initial and boundary conditions,

$$c_{ij}(x,0) = 0, \quad \left\langle c_{pij}\right\rangle(x,0) = 0, \quad c_{sij}(x,0) = 0 \tag{5.31a}$$

$$x = 0 \qquad c_{ij,0} = c_{ij} - \frac{1}{Pe_j}\frac{\partial c_{ij}}{\partial x}$$

$$x = 1 \qquad \frac{\partial c_{ij}}{\partial x} = 0, \qquad \left\langle c_{pij}\right\rangle = \left\langle c_{pij+1,0}\right\rangle \tag{5.31b}$$

with the node balance equations (5.29).

The resulting model parameters are defined in Table 5.3. Equations (5.30-5.31-5.29c), define the transient SMBR/TMBR model to be studied.

A steady-state SMBR/TMBR model can be used, by considering the terms with respect to time derivative equal to zero, i.e. $\frac{\partial c_{ij}}{\partial\theta} = \frac{\partial \left\langle c_{pij}\right\rangle}{\partial\theta} = 0$;

$$\frac{\partial^2 c_{ij}}{\partial x^2} = Pe_j\left(\frac{\partial c_{ij}}{\partial x} - \upsilon_i Da_j c_{Sucj} + \frac{(1-\varepsilon)}{\varepsilon} k_p \tau_j f(\phi)\left(c_{sij} - \left\langle c_{pij}\right\rangle\right)\right) \tag{5.32a}$$

$$\frac{\partial\left\langle c_{p_{ij}}\right\rangle}{\partial x}=-\upsilon_i\gamma_j Da_j\frac{\left(\varepsilon_p+K_{enz}\right)}{\left(\varepsilon_p+K_i\right)}\left\langle c_{p\,Sucj}\right\rangle-\gamma_j\frac{k_p\tau_j}{\left(\varepsilon_p+K_i\right)}f(\phi)\left(c_{sij}-\left\langle c_{p_{ij}}\right\rangle\right) \qquad (5.32b)$$

$$c_{sij}=\frac{1}{\frac{Bi_m}{5f(\phi)}+1}\left(\frac{Bi_m}{5f(\phi)}c_{ij}+\left\langle c_{p_{ij}}\right\rangle\right) \qquad (5.32c)$$

With the initial and boundary conditions defined in (5.31) and the node balance equations (5.29).

Table 5.3. *Dimensionless parameters for the SMBR/TMBR system defined.*

Peclet Number	$Pe_j=\frac{\nu_j L_j}{D_{L_j}}$
Ratio between solid and fluid volumes	$\frac{1-\varepsilon}{\varepsilon}$
Ratio between fluid and solid velocities	$\gamma_j=\frac{\nu_j}{u_s}$
Damköhler Number	$Da_j=k'\tau_j$
Biot Number	$Bi_m=\frac{k_f R_p}{D_{pe}}$
Thiele Modulus	$\phi=R_p\sqrt{\frac{k'}{D_{pe}}}$
Number of pore diffusion units	$Nd_j=k_p\tau_j$
Mass transport coefficient in the pores, (min^{-1})	$k_p=\frac{15D_{pe}}{R_p^2}$
Liquid space time (min)	$\tau_j=\frac{L_j}{\nu_j}$
Reaction rate constant (min^{-1})	$k'=\frac{k_r E_0}{K_m}$

5.2 Operating conditions and model parameters estimation

5.2.1 Operating conditions

In chapter 4, the concept of Simulated Moving Bed Reactor was explained by analogy with the True Moving Bed Reactor. The equilibrium theory applied to the separation of the reaction products in a non-reactive SMB was used to define the adequate operating conditions for the SMBR/TMBR case (Fricke *et al.*, 1999), due to the similarities between them, namely the definition of four sections. These conditions are sufficient for the discussion of a reactive process for fast reaction kinetics as compared to the resident time, since reaction products are then formed in the feed port neighbourhood and most of the unit is utilized for their separation, opposite reaction kinetics must be taken into account (Lode *et al.*, 2001).

Adsorption equilibrium data, mass transfer and reaction parameters for sucrose inversion and glucose-fructose separation, and column axial dispersion were measured in our laboratory, see Azevedo and Rodrigues (2001), and shown in Table 5.4.

Table 5.4. *Model parameters and operating conditions for the SMBR/TMBR system defined.*

Model parameters		**SMBR operating conditions**	**TMBR operating conditions**
$Pe = 1500$		$T = 50°C$	$\gamma_I = 0.95$
$Bi_m = 100$		$C_F = 80g$ sucrose$/l$	$\gamma_{II} = 0.45$
$k_r = 50.32\,\text{min}^{-1}$	$K_m = 23\,\text{g/l}$	$E_0 = 0.250g/l$	$\gamma_{III} = 0.65$
$K_{enz} = 5$	$\varepsilon_p = 0.1$	$t^* = 3.4min$	$\gamma_{IV} = 0.33$
$k_{pFr} = k_{pGl} = 2.14\ \text{min}^{-1}$		$Q_{Rec} = 24ml/min$	**Columns**
$k_{pSuc} = 1.45\ \text{min}^{-1}$		$Q_D = 11.38ml/min$	$d_c = 2.6cm$
$K_{Fr} = 0.43$	$K_{Gl} = 0.17$	$Q_E = 9.11ml/min$	$L_c = 29cm$
$K_{Suc} = 0.00$		$Q_F = 3.62ml/min$	Configuration:
$R_p = 0.016$ cm		$Q_R = 5.89ml/min$	3 –2 –5 –2

The operating conditions (flow rates and switching time) used in the simulations were estimated by using the corresponding relationships.

$$\gamma_j = \frac{Q_j\, t^*}{\varepsilon V_c} - 1 \tag{5.33}$$

The relationships used for the SMB/TMB linear equilibrium system, Ruthven and Ching (1989), can be used to estimate the initial values of the SMBR/TMBR velocity ratios, γ_j,

$$\gamma_I > \frac{1-\varepsilon}{\varepsilon}\left(K_{Fr} + \varepsilon_p\right) \tag{5.34a}$$

$$\frac{1-\varepsilon}{\varepsilon}\left(K_{Gl} + \varepsilon_p\right) < \gamma_{II} < \gamma_{III} < \frac{1-\varepsilon}{\varepsilon}\left(K_{Fr} + \varepsilon_p\right) \tag{5.34b}$$

$$\gamma_{IV} < \frac{1-\varepsilon}{\varepsilon}\left(K_{Gl} + \varepsilon_p\right) \tag{5.34c}$$

Notice the presence of the term ε_p in the inequalities. The reaction only takes place in section III, and sections I and IV are regenerating sections. Consequently, the two conditions (5.34a) and (5.34c), guarantee the regeneration of the eluent, having no effect on the SMBR/TMBR performance in terms of conversion and purity. For section IV, a flowrate of 24ml/min is considered due to the SMB unit flowrate range (20 – 120 ml/min). With $Q_{IV} = 24ml/min$ and fixed $\gamma_{IV} = 0.325$ (<0.405), the switching time, t^*, was estimated by (5.33), and equal to 3.4min. The γ_I value fixed is 0.95 (>0.795). The velocity ratios γ_{II} and γ_{III}, determine the separation region, which depends on the feed. The simulation performed, the values of the velocity ratios in section II and III, γ_{II} and γ_{III}, where fixed and calculated for a specific value of the feed flowrate. Fixed $\gamma_{II} = 0.45$ (>0.405) and $\gamma_{III} = 0.65$ (<0.795) and by using the relationship (5.33) the flow rates in the remaining sections were estimated.

In the SMB, the feed flowrate was calculated by the difference of the flow rates in section III and II: $Q_F = Q_{III} - Q_{II}$. The eluent flowrate was calculated by the difference of the flow rates in section I and IV: $Q_E = Q_I - Q_{IV}$. The extract flowrate was calculated by the difference of the flow rates in section I and II: $Q_X = Q_I - Q_{II}$. The raffinate flowrate was calculated by using the value of the sum of the inlet/outlet streams: $\left(Q_{Bal} = Q_F + Q_E = Q_X + Q_R\right)$.

The recycle flowrate, Q_{Rec}, is the flowrate in section IV, $Q_{Rec} = Q_{IV} = 24ml/min$. The sucrose feed concentration, C_F, and the quantity of the enzyme invertase, which catalyses the inversion of sucrose, C_{enz}, were the same as in Azevedo and Rodrigues (2000) work as the equilibrium constants for fructose and glucose, K_{Fr} and K_{Gl}.

Table 5.4 summarizes the operating conditions used in the simulations and also the model parameters.

5.2.2 Model parameters

The Wilke-Chang equation, Reid et al. (1987), was used to predict the molecular diffusion coefficient of solute M in solvent S:

$$D_m = 7.4\times10^{-8}\frac{(\phi M_S)^{1/2}T}{\eta_S V_M^{0.6}} \tag{5.35}$$

where D_m the molecular diffusion coefficient (cm^2/s), ϕ the association factor of solvent S (ϕ = 2.6 since the solvent is water), M_S the molecular weight of the solvent (water ≈18), T the temperature (= 323K), η_S the solvent viscosity ≈0.6 cP, V_M the molar volume of solute M at normal boiling temperature. As no experimental data to obtain this value exist, the method based on the Le Bas additive volume table, Reid *et al.* (1987) was used, ≈ 340.4 cm^3/mol for sucrose, and ≈ 177.6 cm^3/mol for glucose and fructose. Then we get, $D_{m_{Suc}} \approx 8.25\times10^{-6} cm^2/s$ and $D_{m_{Fr}} \approx D_{m_{Gl}} \approx 1.22\times10^{-5} cm^2/s$.

The effective diffusivity, D_{pe} (cm2/s), is then estimated by, $D_{pe} = D_m\frac{\varepsilon_p}{\tau}$, where ε_p the particle porosity (= 0.1, value obtained experimentally), and τ the tortuosity factor (= 2). We then get $D_{pe\,Suc} \approx 4.12\times10^{-7} cm^2/s$ and $D_{pe\,Fr} \approx D_{pe\,Gl} \approx 6.09\times10^{-7} cm^2/s$.

The film mass transfer coefficients, k_f, for sucrose and fructose/glucose, was estimated by using the correlation of Wilson and Geankoplis, $Sh = \frac{1.09}{\varepsilon}Sc^{0.33}Re^{0.33}$, where $Sh = 2k_f R_p/D_m$ is the Sherwood number, k_f the film mass transfer coefficient, cm/s, R_p the particle radius, cm, $Sc = \frac{\mu_f}{\rho_f D_m}$ the Schmidt number, and $Re = \frac{u_0\rho_f d_p}{\mu_f}$ the Reynolds number, with μ_f the fluid viscosity ≈ 0.60×10^{-2} g/cm-s, ρ_f the fluid density ≈ 1g/cm^3, u_0 the mean velocity ≈ 0.0924 cm/s and d_p the particle diameter ≈ 0.0320 cm. We obtained the Sherwood numbers, for sucrose and fructose and glucose, Sh_{Suc} = 19 and $Sh_{Fr} = Sh_{Gl}$ = 16.7, and $k_{f\,Suc}$ = 0.29 cm/min and $k_{f\,Fr} = k_{f\,Gl}$ = 0.38 cm/min for the film mass transfer coefficients.

According to these values, it is possible to estimate the Biot number for mass transfer,

$$Bi_m = \frac{k_f R_p}{D_{pe}} \approx \begin{cases} 190, & \text{for Sucrose} \\ 170, & \text{for Glucose and Fructose} \end{cases}.$$

The Peclet number considered was constant and equal to 1500.

With the values of the effective diffusivity and the particle radius it is possible to estimate the mass transport coefficient in the pores, k_p, according to the following equation,

$$k_p = \frac{15D_{pe}}{R_p^2} = \begin{cases} k_{p_{Suc}} = 1.45 \\ k_{p_{Fr}} = k_{p_{Gl}} = 2.14 \end{cases} min^{-1}.$$

Table 5.4 summarizes the model parameters used in the simulations.

5.3 Performance Criteria

The SMBR/TMBR outlet/inlet flow rates calculated and described in Table 5.4, must satisfy a strict purity and reaction conversion specifications. The definitions of extract purity (P_E, %), raffinate purity (P_R, %), recovery of the fructose in the extract (R_E^{Fr}, %), recovery of glucose in the raffinate (R_R^{Gl}, %) and conversion of sucrose (X) are similar to those already presented in section 4.1.2. and are as follows:

$P_E = 100\dfrac{C_E^{Fr}}{C_E^{Fr} + C_E^{Gl} + C_E^{Suc}}$, a similar definition to the purity of the raffinate;

$R_E^{Fr} = 100\dfrac{Q_E c_E^{Fr}}{Q_F c_F^{Suc}\left(\dfrac{M_w^{Fr}}{M_w^{Suc}}\right)}$, a similar definition to the recovery of glucose in the raffinate;

and $X = 1 - \dfrac{Q_E C_E^{Suc} + Q_R C_R^{Suc}}{Q_F C_F^{Suc}}$.

The area that defines the complete separation region was stable by considering 99% or more for the reaction conversion and 95% or more for the extract purity and raffinate purity, see Figure 5.7.

The safety margin parameter β, considered was 1.2, approximately the center of the β range located at $1 < \beta < \sqrt{\alpha} = \sqrt{\dfrac{K_{Fr}}{K_{Gl}}} = 1.59$. At low values of β, the SMBR/TMBR operating conditions are very near to the zone of no separation, as previously verified (section 2.1). At

high values of β, the eluent flowrate increases and consequently the products becomes more diluted.

5.4 Simulation Results and Discussion

Performance parameters and steady-state concentration profiles for the sucrose inversion and glucose/fructose separation are presented. The system defined by the set of equations (5.27-5.26-5.24), was solved numerically by using the solver COLNEW software package (Bader and Ascher, 1987). Since the TMBR unit is composed by four sections and in each section three components, the steady-state model is defined by a set of 24 ODE's, after the substitution of equation (5.27c) in the corresponding two remaining equations. No initial guess to the solution is provided and the solver COLNEW generates the initial mesh and controls it during the numerical resolution, with 3 collocation points in each element. The error tolerance was set at 10^{-8}. When the global error is less than 0.5%, maximum error defined by the user, the SMBR/TMBR steady-state final solution is achieved. The global error *er*, is defined as the sum of the relative error, of the average concentrations of the two components in the extract and raffinate, respectively, for two consecutive iterations (see equations (3.1b) and (3.1c) in section 3.1.1) and, the relative error between the amount of the component that enters in the feed stream and leaves, in the extract and raffinate streams, the system (for each mole of sucrose, one mole of glucose and one mole of fructose are formed).

For the case studied and using the parameters presented in Table 5.4, the solution of the steady-state TMBR model took approximately 10 min (Pentium II 300 MHz). Table 5.5 shows the performance parameters obtained for this reference case with the corresponding steady-state internal concentration profiles obtained with the simulation solver, in Figure 5.5.

Table 5.5. *Performance parameters obtained for the reference case, under operating conditions and model parameters in Table 5.4.*

Performance parameters	Extract	Raffinate
Purity (%)	100	100
Recovery (%)	99.9	99.9

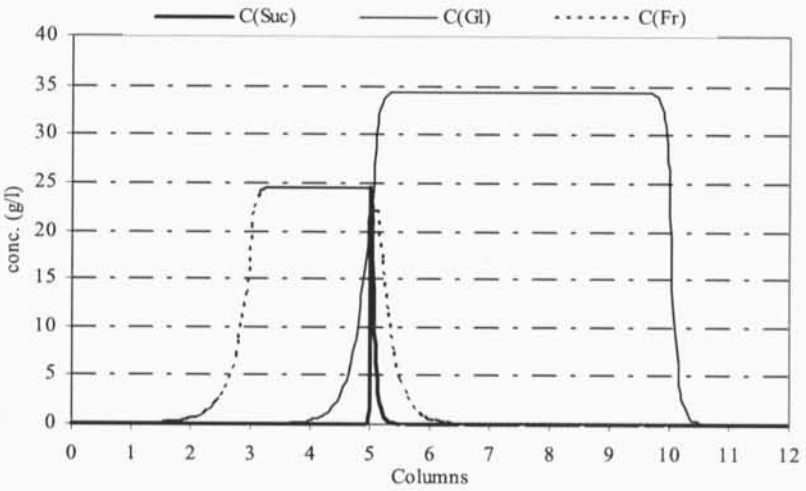

***Figure 5.5**. Steady-state internal concentration profiles for the reference case, under operating conditions and model parameters in Table 5.4.*

5.4.1 Effect of particle radius

In order to analyze the effect of the particle radius on the performance parameters and on the SMBR/TMBR concentration profiles the model presented, described by equations (5.32-5.31-5.29), was solved for several values of R_p as described in Table 5.6. The model parameters used in simulations are similar to the conditions described previously in Table 5.4 with the exceptions for the parameters described in Table 5.6, the particle radius R_p, the mass transport coefficient k_p, the film mass transfer coefficient k_f, and consequently the Biot number for mass transfer Bi_m, and the Thiele Modulus ϕ. Also the performance parameters, obtained in the simulations are summarized. The operating conditions were kept constants and the same as described in Table 5.4.

The effects of the increase of the particle radius on the purity and recovery of the two products are shown in Figure 5.6. Higher particle radius (R_p = 0.256 cm) leads to lower purity and recovery products. For the three situations simulated, the sucrose concentration, Figure 5.6a, decreases to zero, in zone III, very rapidly. No significant differences exist and the reaction is almost complete. The glucose and fructose concentrations level, Figure 5.6b and 5.6c, respectively, increases and, almost no existing for higher particle radius, consequently increasing the products concentration on the extract and raffinate points increasing the purity and recovery.

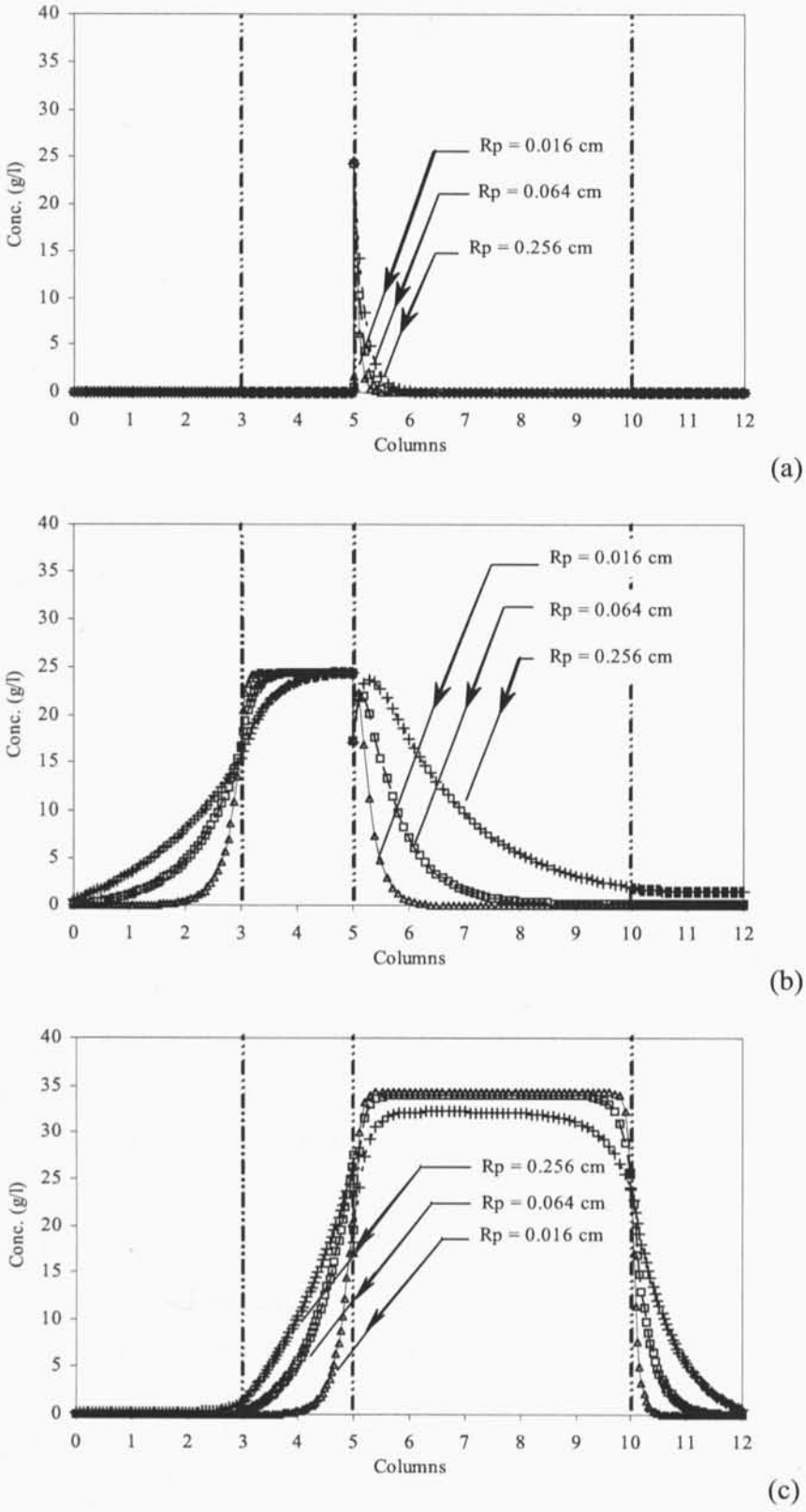

Figure 5.6. *SMBR/TMBR steady-state internal profiles obtained for three different values of R_p, 0.016, 0.064, and 0.256 cm, for (a) sucrose, (b) glucose, and (c) fructose, Table 5.6, the others model parameters and operating conditions in Table 5.4.*

Table 5.6. *Model parameters used for the study of the radius particle effects in the SMBR/TMBR performance parameters.*

Model parameters		R_p (cm)		
		0.016	0.064	0.256
k_p (min^{-1})	Gl/Fr	2.14	0.13	0.008
	Suc	1.45	0.09	0.006
k_f ($cm.min^{-1}$)	Gl/Fr	0.38	0.15	0.06
	Suc	0.29	0.12	0.05
Bi_m	Gl/Fr	167.0	264.0	417.0
	Suc	190.0	300.0	474.0
ϕ	Suc	2.38	9.52	38.1
Performance parameters (%)	P_E	100	99.1	92.6
	P_R	100	99.4	92.4
	R_E	99.9	99.3	92.2
	R_R	99.9	99.0	92.6

5.4.2 Complete separation region

The region where both extract and raffinate purities are approximately 100% (≥ 99.0%) is determined and represented in Figure 5.7. This prediction was based on the SMB/TMB separation assumptions. The conversion/separation region was determined by considering:

. the velocity ratios, γ_I and γ_{IV}, and the switch time, t^*, after properly selected, as indicated above, were kept constants in all the simulations $\gamma_I = 0.95$, $\gamma_{IV} = 0.33$ and $t^* = 3.4$ min;

. the complete separation region is represented in the (γ_{II}, γ_{III}) plane, with location determined by performing simulations along lines parallel to the diagonal of the (γ_{II}, γ_{III}) plane, with purity performance ≥ 99.0%.

The results are illustrated in Figure 5.7(a), for the model parameters described in Table 5.4 and using the steady-state TMBR model (5.33-5.32-5.30c). Four different situations are presented depending on the purity performances obtained in each simulation: (•) complete conversion of sucrose and purity of both products ≥ 99.0%, (o) no separation occurs, i.e, purity performance < 99.0% for both products, (◊) only extract purity is ≥ 99.0%, (□) only raffinate purity is ≥ 99.0%. The triangle defined by the dashed lines, given by (5.34b), is the region of complete separation for the case of SMB/TMB separation. The region of complete separation/conversion region has a triangular shape as in the case of SMB/TMB. The region on the right-hand side of the triangle, corresponds to the region where $P_E \geq 99.0\%$ whereas

$P_R < 99\%$, since the constraint (5.34b) is not fulfilled. The same for the region on the left-hand side of the triangle which corresponds to $P_R \geq 99.0\%$ and $P_E < 99\%$.

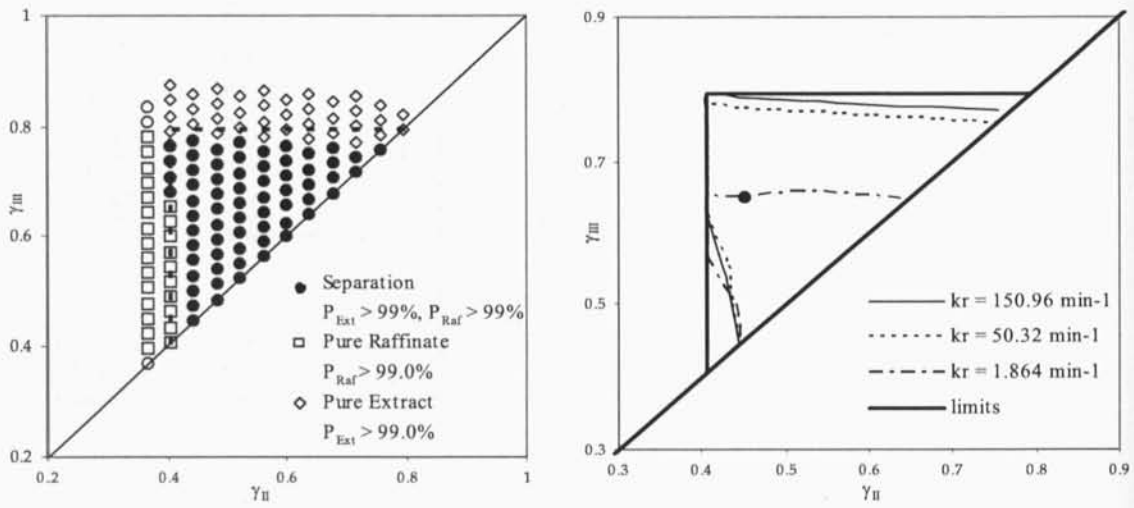

(a) (b)

Figure 5.7 *SMBR/TMBR performance for the sucrose inversion and glucose/fructose separation in the (γ_{II}, γ_{III}) plane. Different regions are defined in terms of purity of the two outlet products, as legend in the figure. (a) The presented points define parallel lines to the diagonal at different feed flow rate, Q_F, (b) effects of the reaction rate coefficient k_r, on the reaction/separation region; the dot point (•) corresponds to the reference case under conditions described in Table 5.4.*

The effect of the reaction rate coefficient k_r, on the reaction/separation region is shown in Figure 5.7(b). The triangle shaped separation/reaction region becomes smaller as the reaction rate coefficient decreases. Three regions are defined for three different values of k_r, 1.864, 50.32 and 150.96 min^{-1}, with purity performance $\geq 99.0\%$.

Figure 5.8 illustrates the separation/reaction region obtained for lower purity performance specifications, $\geq 90\%$. For lower purity specification the separation/reaction region is greater compared with the area defined for higher purity specification under the same operating conditions. The vertex of the triangle in the γ_{II} -γ_{III} plane, lies outside the region defined by the equilibrium theory limits.

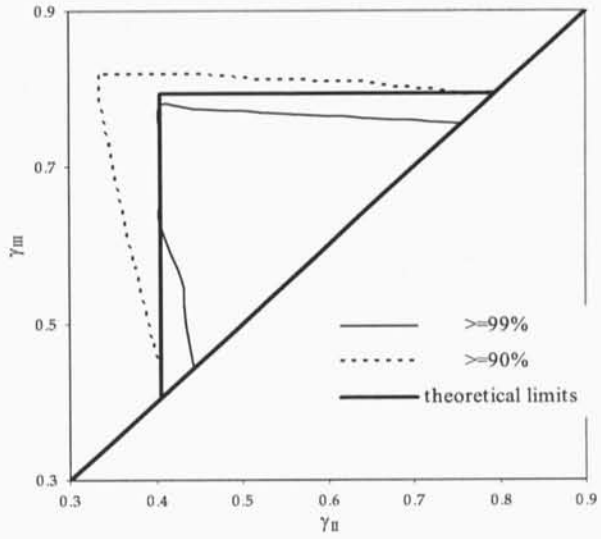

Figure 5.8 *Effect of the purity specification on the separation/reaction region for the SMBR/TMBR for the sucrose inversion and glucose/fructose separation in the (γ_{II}, γ_{III}) plane.*

5.5 New developments on the TMBR system

A new SMBR model, based on the TMBR analogy, was developed in the present work. Two sets of mass balances equations were considered, one for the outer fluid and other for the particle phases for each component, defining a PDE system in time with two spatial variables, column length, z, and radial position in the particle, r. All simulations were performed by using a combination of the method of orthogonal collocation on finite element (OCFE) and available PDE and ODE solvers. A steady-state model was also considered by setting the terms with respect to time derivatives equal to zero.

The equations for the mass balance of species i in outer fluid phase are

$$\varepsilon D_{L_j} \frac{\partial^2 c_{ij}}{\partial z^2} = \varepsilon \nu_j \frac{\partial c_{ij}}{\partial z} + \varepsilon \frac{\partial c_{ij}}{\partial t} - \upsilon_i \varepsilon \mathcal{R} + \frac{3}{R_p} k_f (1-\varepsilon)\left(c_{ij} - c_{sij}\right) \tag{5.36}$$

with the initial and boundary conditions,

$$c_{ij}(z,0) = 0, \quad c_{sij}(z,0) = 0 \tag{5.37a}$$

$$z = 0 \qquad c_{ij,0} = c_{ij} - \frac{D_{L_j}}{\nu_j} \frac{\partial c_{ij}}{\partial z} \tag{5.37b}$$

$$z = L_j \qquad \frac{\partial c_{ij}}{\partial z} = 0, \qquad c_{sij} = c_{sij+1,0} \tag{5.37c}$$

$$\text{and} \quad \begin{cases} j = I & c_{iIV,L_{IV}} = \dfrac{\nu_I}{\nu_{IV}} c_{iI,0} \\ j = II, IV & c_{i(j-1),L_{j-1}} = c_{ij,0} \\ j = III & c_{iII,L_{II}} = \dfrac{\nu_{III}}{\nu_{II}} c_{iIII,0} - \dfrac{\nu_F}{\nu_{II}} c_i^F \end{cases} \tag{5.37d}$$

where c_{ij} and c_{sij} represent the solid concentration of component i in the adsorbent section j and the liquid phase concentration at the solid-liquid interface, respectively.

Considering a spherical particle shell element, the partial differential equation representing the mass balance inside the particle in a volume of the section j and of species i for the adsorption of species i, pore diffusion, and reaction can be written as follows,

$$\frac{\partial q_{ij}}{\partial t} + \varepsilon_p \frac{\partial c_{pij}}{\partial t} - \upsilon_i \left(\varepsilon_p + K_{enz}\right) \mathcal{R}\left(c_{pij}\right) = \frac{1}{r^2} \frac{\partial}{\partial r}\left(r^2 D_{pe} \frac{\partial c_{pij}}{\partial r} \right) + u_s \frac{\partial q_{ij}}{\partial z} + \varepsilon_p u_s \frac{\partial c_{pij}}{\partial z} \tag{5.38}$$

with $q_{ij}(r,z,t) = f\left(c_{pij}(r,z,t)\right)$.

If the diffusivity is constant and if the equilibrium isotherm is linear, $q_{ij} = K_i c_{pij}$, then we get

$$\left(\varepsilon_p + K_i\right) \frac{\partial c_{pij}}{\partial t} = \frac{1}{r^2} \frac{\partial}{\partial r}\left(r^2 D_{pe} \frac{\partial c_{pij}}{\partial r} \right) + \upsilon_i \left(K_{enz} + \varepsilon_p\right) \mathcal{R}\left(c_{p3j}\right) + u_s \left(\varepsilon_p + K_i\right) \frac{\partial c_{pij}}{\partial z} \tag{5.39}$$

with the boundary conditions,

$$r = 0, \qquad \frac{\partial c_{pij}}{\partial r} = 0 \tag{5.40a}$$

$$r = R_p, \qquad \left.\frac{\partial c_{pij}}{\partial r}\right|_{r=R_p} = \frac{k_f}{D_{pe}} \left(c_{ij} - c_{sij}\right) \tag{5.40b}$$

In the above equation the term $c_{sij} = c_{pij}\big|_{r=R_p}$ is the liquid concentration of species i at $r = R_p$.

As a validation of the previous particle equation, the averaged operation can be considered,

$$\left(K_i + \varepsilon_p\right) \frac{\partial \left\langle c_{pij} \right\rangle}{\partial t} + \frac{3k_f}{R_p} \left(c_{ij} - c_{sij}\right) = u_s \left(K_i + \varepsilon_p\right) \frac{\partial \left\langle c_{pij} \right\rangle}{\partial z} - \upsilon_i \left(\varepsilon_p + K_{enz}\right) \left\langle \mathcal{R}\left(c_{p3j}\right) \right\rangle \tag{5.41}$$

by considering a linear adsorption equilibrium model $\langle q_{ij} \rangle = K_i \langle c_{p_{ij}} \rangle$. All the initial considerations are presented: the accumulation in the pores, the accumulation in the stationary phase, intraparticle diffusion, adsorption and the reaction term. The initial and boundary conditions are similar to (5.40).

The new model with chemical reaction, linear equilibrium isotherm, film diffusion, axial dispersion for fluid flow, gives the following differential system equations

$$\frac{\partial c_{ij}}{\partial t} = D_{L_j} \frac{\partial^2 c_{ij}}{\partial z^2} - \nu_j \frac{\partial c_{ij}}{\partial z} + \upsilon_i \mathcal{R}(c_{3j}) - \frac{(1-\varepsilon)}{\varepsilon} \frac{3.k_f}{R_p} (c_{ij} - c_{sij}) \tag{5.42}$$

$$\frac{\partial c_{pij}}{\partial t} = \frac{1}{(\varepsilon_p + K_i)} \frac{1}{r^2} \frac{\partial}{\partial r} \left(r^2 D_{pe} \frac{\partial c_{pij}}{\partial r} \right) + \upsilon_i \frac{(K_{enz} + \varepsilon_p)}{(\varepsilon_p + K_i)} \mathcal{R}(c_{p3j}) + u_s \frac{\partial c_{pij}}{\partial z} \tag{5.43}$$

with the initial conditions and boundary conditions,

$$c_{ij}(z,0) = 0, \quad c_{pij}(r,z,0) = 0\ ,\ c_{sij}(z,0) = 0 \tag{5.44a}$$

$$z = 0 \qquad c_{ij,0} = c_{ij} - \frac{D_{L_j}}{\nu_j} \frac{\partial c_{ij}}{\partial z} \tag{5.44b}$$

$$z = L_j \qquad \frac{\partial c_{ij}}{\partial z} = 0, \quad c_{sij} = c_{sij+1,0} \tag{5.44c}$$

and

$$r = 0, \qquad \frac{\partial c_{pij}}{\partial r} = 0 \tag{5.45a}$$

$$r = R_p, \qquad \left. \frac{\partial c_{pij}}{\partial r} \right|_{r=R_p} = \frac{k_f}{D_{pe}} \left(c_{ij} - c_{pij}\big|_{r=R_p} \right) \tag{5.45b}$$

Knowing that,

$$\langle c_{p_{ij}} \rangle = \frac{\int_0^{R_p} c_{pij} r^2 dr}{\int_0^{R_p} r^2 dr} = \frac{3}{R_p^3} \int_0^{R_p} c_{pij} r^2 dr \tag{5.46}$$

which corresponds to the mean pore concentration of component *i* in section *j* averaged over the particle.

Assuming that the reaction $\mathcal{R}(c_{ij})$, follows the Michaelis-Menten equation (5.2), and moreover $K_m >> c_{jSuc}$, the reaction rate is,

$$\mathcal{R}(c_{ij}) = k' c_{3j} \text{ with } k' = \frac{k_r E_0}{K_m} \tag{5.47}$$

or, for a non-linear reaction,

$$\mathcal{R}(c_{ij}) = k' \frac{c_{3j}}{1 + \frac{1}{K_m} c_{3j}} = k' \frac{c_{3j}}{1 + \delta\, c_{3j}} \tag{5.48}$$

The model defined by equations (5.42-5.45) can be represented in a dimensionless form after introducing the dimensionless variables for space, radial space and time, $x = z/L_j$, $\rho = r/R_p$ and $\theta = t/\tau_s$ with $\tau_s = L_c/u_s$ the switch time interval, where $L_j = n_j L_c$ the section j length, L_c the length of each column, and n_j the number of columns in section j, C_{03j} is the feed concentration. All partial derivatives and integrals can then be expressed in terms of these new independent variables:

$$\frac{\partial}{\partial z} = \frac{1}{L_j}\frac{\partial}{\partial x}; \quad \frac{\partial^2}{\partial z^2} = \frac{1}{L_j^2}\frac{\partial^2}{\partial x^2}; \quad \frac{\partial}{\partial t} = \frac{1}{\tau_s}\frac{\partial}{\partial \theta}; \quad \frac{\partial}{\partial r} = \frac{1}{R_p}\frac{\partial}{\partial \rho}; \quad \frac{\partial^2}{\partial r^2} = \frac{1}{R_p^2}\frac{\partial^2}{\partial \rho^2}$$

$$\int_0^{R_p} f(r)dr = R_p \int_0^1 f(\rho)d\rho .$$

Following this normalization, the model equations (5.43-5.45) become:

$$\frac{\partial c_{ij}}{\partial \theta} = \frac{\gamma_j}{n_j}\left(\frac{1}{Pe_j}\frac{\partial^2 c_{ij}}{\partial x^2} - \frac{\partial c_{ij}}{\partial x} + \upsilon_i \tau_j k' c_{3j} - \frac{(1-\varepsilon)}{\varepsilon}\frac{3k_f}{R_p}\tau_j \left(c_{ij} - c_{pij}\big|_{\rho=1}\right)\right) \tag{5.49}$$

$$\frac{\partial c_{pij}}{\partial \theta} = \frac{\gamma_j}{n_j\left(K_i + \varepsilon_p\right)}\left[\upsilon_i\left(K_{enz} + \varepsilon_p\right) Da_j c_{p3j} + \tau_j \frac{D_{pe}}{R_p^2}\left(\frac{\partial^2 c_{pij}}{\partial \rho^2} + \frac{2}{\rho}\frac{\partial c_{pij}}{\partial \rho}\right)\right] + \frac{1}{n_j}\frac{\partial c_{pij}}{\partial x} \tag{5.50}$$

and

$$\left\langle c_p \right\rangle_{ij} = \frac{\int_0^1 c_{pij}\rho^2 d\rho}{\int_0^1 \rho^2 d\rho} = 3\int_0^1 c_{pij}\rho^2 d\rho \tag{5.51}$$

With the initial and boundary conditions,

$$c_{ij}(x,0) = 0, \quad c_{pij}(\rho, x, 0) = 0 \tag{5.52a}$$

$$x=0 \qquad c_{ij,0}=c_{ij}-\frac{1}{Pe_j}\frac{\partial c_{ij}}{\partial x}$$

$$x=1 \qquad \frac{\partial c_{ij}}{\partial x}=0, \qquad c_{p_{ij}}=c_{p_{ij+1,0}} \tag{5.52b}$$

and the node balance equations:

$$\begin{cases} j=I & c_{iI,0}=c_{iIV,L_{IV}}\dfrac{\nu_{IV}}{\nu_I} \\ j=II,IV & c_{ij,0}=c_{i(j-1),L_{j-1}} \\ j=III & c_{iIII,0}=c_{iII,L_{II}}\dfrac{\nu_{II}}{\nu_{III}}+\dfrac{\nu_F}{\nu_{III}}c_i^F \end{cases} \tag{5.52c}$$

$$\rho=0 \qquad \frac{\partial c_{pij}}{\partial \rho}=0$$

$$\rho=1 \qquad \frac{\partial c_{pij}}{\partial \rho}=Bi_m\left(c_{ij}-c_{pij}\big|_{\rho=1}\right) \tag{5.52d}$$

The model equations (5.49-5.52) was defined by a PDE system with two sets of mass balance equations, one for the outer fluid and one for the particle phases for each component, respectively. For the particle phase, (5.50), with their associated initial (5.32a) and boundary conditions at $\rho = 0$ and $\rho = 1$, (5.52d), an OCFE for the discretization of the radial coordinate ρ, was applied. The cubic Hermite polynomials were used as basis function. The interval $0 \le \rho \le 0$ was divided into NE subintervals, with two collocation points within each subinterval. The solution c_{pij} in the kth subinterval of ρ was approximated by:

$$c_{pij}(\rho_t,x,\theta)=\sum_{l=1}^{4}a_{l+2k-2}^{ij}(x,\theta)H_{il} \tag{5.53}$$

where ρ_t are the collocation points within each subinterval of ρ, with $t=1,2$. The cubic Hermite polynomials $H_{il}(\rho_t)$, with $l=1,...,4$, were defined over $[\rho_k,\rho_{k+1}]$, as in Finlayson, (1980). The first and second derivatives for each element k, are obtained by differentiating (33.a) with respect to ρ_t. The a_{l+2k-2}^{ij}, with $k=1,...,\mathrm{NE}$ are the basis function coefficients to be determined. After the discretization process, we obtained a system of $(3*4)(2*NE)$ PDE in the new basis function coefficients a^{ij}'s dependent on the in one-space dimension, the bed axial coordinate x $\left(c_{pij}(\rho,x,\theta)\rightarrow a_k^{ij}(x,\theta)\right)$. The system resulting from the above discretization step, in conjunction with the mass balance equation in the liquid phase (5.49),

$(3*4\ (1+2*NE))$ equations, were numerically integrated with the PDECOL package (Madsen and Sincovec, 1979). For each component *i* and each section *j*:

- equation (5.49);
- $(2*NE)$ equations resulting from the discretization of particle equation (5.50):

k=1 and *t*=1, 2, *i*=1,2,3 and *j*=1, 2, 3, 4

$$\left(H_{t1}+\sum_{l=3}^{4}H_{tl}\right)\frac{\partial a_1^{ij}}{\partial\theta}=$$

$$=\frac{1}{n_j}\left\{D_{ap}\left[\left(\frac{1}{h_1^2}B_{t1}+\frac{2}{\omega_t h_1^2}A_{t1}\right)a_1^{ij}+\sum_{l=3}^{4}\left(\frac{1}{h_1^2}B_{tl}+\frac{2}{\omega_t h_1^2}A_{tl}\right)a_l^{ij}\right]\right. \tag{5.54a}$$

$$\left.+\upsilon_i k^*\left[\left(H_{t1}a_1^{3j}+\sum_{l=3}^{4}H_{tl}a_l^{3j}\right)\right]+\left[H_{t1}\frac{\partial a_1^{ij}}{\partial x}+\sum_{l=3}^{4}H_{tl}\frac{\partial a_1^{ij}}{\partial x}\right]\right\}$$

k=2, …, *NE*-1 and *t*=1, 2, *i*=1,2,3 and *j*=1, 2, 3, 4

$$\sum_{l=1}^{4}H_{tl}\frac{\partial a_{l+2k-3}^{ij}}{\partial\theta}=\frac{1}{n_j}\left\{D_{ap}\left[\sum_{l=1}^{4}\left(\frac{1}{h_k^2}B_{tl}+\frac{2}{(\varpi_t h_k+\rho_k)}\frac{1}{h_k}A_{tl}\right)a_{l+2k-3}^{ij}\right]\right.$$

$$\left.+\upsilon_i k^*\left[\sum_{l=1}^{4}H_{tl}a_{l+2k-3}^{3j}\right]+\left[\sum_{l=1}^{4}H_{tl}\frac{\partial a_{l+2k-3}^{ij}}{\partial x}\right]\right\} \tag{5.54b}$$

k=*NE* and *t*=1, 2, *i*=1,2,3 and *j*=1, 2, 3, 4

$$\sum_{l=1}^{2}H_{tl}\frac{\partial a_{l+2NE-3}^{ij}}{\partial\theta}+\left(H_{t3}-Bi_m H_{t4}\right)\frac{\partial a_{2NE}^{ij}}{\partial\theta}=$$

$$=\frac{1}{n_j}\left\{D_{ap}\left[\sum_{l=1}^{2}\left(\frac{1}{h_{NE}^2}B_{tl}+\frac{2}{(\omega_{NE}h_{NE}+\rho_{NE})}\frac{1}{h_{NE}}A_{tl}\right)a_{l+2NE-3}^{ij}+\right.\right.$$

$$+\left(\frac{1}{h_{NE}^2}\left(B_{t3}-Bi_m B_{t4}\right)+\frac{2}{(\omega_{NE}h_{NE}+\rho_{NE})}\frac{1}{h_{NE}}\left(A_{t3}-Bi_m A_{t4}\right)\right)a_{2NE}^{ij}+$$

$$\left.+Bi_m\left(\frac{1}{h_{NE}^2}B_{t4}+\frac{2}{(\omega_{NE}h_{NE}+\rho_{NE})}\frac{1}{h_{NE}}A_{t4}\right)C_{ij}(x,\theta)\right]-$$

$$+\upsilon_i k^*\left[\sum_{l=1}^{2}H_{tl}a_{l+2NE-3}^{3j}+\left(H_{t3}-Bi_m H_{t4}\right)a_{2NE}^{3j}+Bi_m H_{t4}C_{3j}(x,\theta)\right]+$$

$$\left.+\left[\sum_{l=1}^{2}H_{tl}\frac{\partial a_{l+2NE-3}^{ij}}{\partial x}+\left(H_{t3}-Bi_m H_{t4}\right)\frac{\partial a_{2NE}^{ij}}{\partial x}+Bi_m H_{t4}\frac{\partial C_{ij}(x,\theta)}{\partial x}\right]\right\}- \tag{5.54c}$$

$$-Bi_m H_{t4}\frac{\partial C_{ij}(x,\theta)}{\partial\theta}$$

with $D_{ap} = \dfrac{D_{pe}\tau_s}{R_p^2\left(K_i + \varepsilon_p\right)}$ and $k^* = k'\tau_s \dfrac{\left(K_{enz} + \varepsilon_p\right)}{\left(K_i + \varepsilon_p\right)}$. This set of equations can be expressed in a matrix form, as following:

$$[HMAT]\left[\frac{\partial a^{ij}}{\partial \theta}\right] = \frac{1}{n_j}\left\{D_{ap}\left([CMAT]\left[a^{ij}\right] + [CVEC]c_{ij}\right) + \right.$$
$$+ \upsilon_i k^*\left([HMAT]\left[a^{3j}\right] + [CVEC]c_{3j}\right) + \left.\left([HMAT]\left[\frac{\partial a^{ij}}{\partial x}\right] + [CVEC]\frac{\partial c_{ij}}{\partial x}\right)\right\} - \qquad (5.55)$$
$$-[HVEC]\frac{\partial c_{ij}}{\partial \theta}$$

with the initial conditions:

$$\begin{aligned}\left[a^{ij}(x,0)\right] &= -[HMAT]^{-1}[CVEC]c_{ij}(x,0)\\ c_{ij}(x,0) &= 0\end{aligned} \qquad (5.56)$$

and the boundary conditions (5.52a-5.52c).

The matrices, **HMAT** and **CMAT**, and the vectors, **HVEC** and **CVEC**, have a sparse structure. Considering *NE* (= *Ner*) = 4 and $i = 1$, the structure of **HMAT** and **HVEC**, can be defined as in Figure 5.9. The elements not shown are zero. The other matrix and vector have similar structure.

Figure 5.10 shows the strategy used to obtain the numerical solutions of the PDE system in the model by using the package PDECOL.

$$[HMAT] = \begin{bmatrix}
H_{11} & H_{13} & H_{14} & & & & & \\
H_{21} & H_{23} & H_{24} & & & & & \\
 & H_{11} & H_{12} & H_{13} & H_{14} & & & \\
 & H_{21} & H_{22} & H_{23} & H_{24} & & & \\
 & & & H_{11} & H_{12} & H_{13} & H_{14} & \\
 & & & H_{21} & H_{22} & H_{23} & H_{24} & \\
 & & & & & H_{11} & H_{12} & H_{13} - Bi_m H_{14} \\
 & & & & & H_{21} & H_{22} & H_{23} - Bi_m H_{24}
\end{bmatrix} \qquad [HVEC] = \begin{bmatrix} \\ \\ \\ \\ \\ \\ Bi_m H_{14} \\ Bi_m H_{24} \end{bmatrix}$$

***Figure 5.9 HMAT** and **HVEC** matrix representation, considering four finite elements, NE(=Ner)=4, with two collocation points in each.*

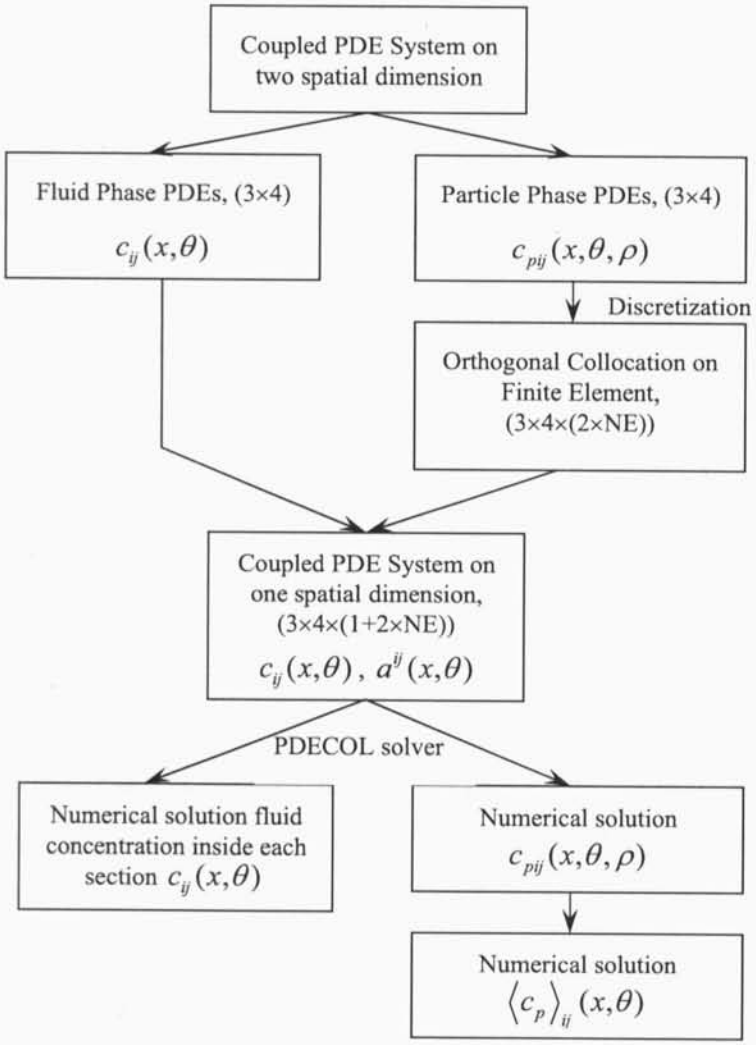

Figure 5.10 *Solution strategy, considering NE finite elements for the radial coordinate.*

A steady-state SMBR/TMBR model can be used, by considering the terms with respect to time derivative, in equations (5.49-5.50), equal to zero, i.e. $\frac{\partial c_{ij}}{\partial \theta} = \frac{\partial c_{pij}}{\partial \theta} = 0$;

$$\frac{\partial^2 c_{ij}}{\partial x^2} = Pe_j \left(\frac{\partial c_{ij}}{\partial x} - \upsilon_i Da_j c_{3j} + \frac{(1-\varepsilon)}{\varepsilon} \frac{3k_f}{R_p} \tau_j \left(c_{ij} - c_{pij}\big|_{\rho=1} \right) \right) \tag{5.57}$$

$$\frac{\partial c_{pij}}{\partial x} = -\frac{\gamma_j}{\left(\varepsilon_p + K_i\right)} \left(\frac{D_{pe}}{R_p^2} \tau_j \left(\frac{\partial^2 c_{pij}}{\partial \rho^2} + \frac{2}{\rho} \frac{\partial c_{pij}}{\partial \rho} \right) + \upsilon_i \left(\varepsilon_p + K_{enz} \right) Da_j c_{p3j} \right) \tag{5.58}$$

and

$$\left\langle c_{p_{ij}} \right\rangle = 3 \int_0^1 c_{pij} \rho^2 d\rho \tag{5.59}$$

With the initial and boundary conditions defined in (5.52).

The ODE model, (5.57) and (5.58), was numerically solved by using the COLNEW solver which incorporates a new basis representation replacing B-splines, and improvements for the linear and nonlinear algebraic equation solvers, after the discretization of the radial coordinate. The ODE system, in the axial coordinate, to be solved was,

$$\frac{\partial^2 c_{ij}}{\partial x^2} = Pe_j \left(\frac{\partial c_{ij}}{\partial x} - \upsilon_i Da_j c_{3j} + \frac{(1-\varepsilon)}{\varepsilon} \frac{3k_f}{R_p} \tau_j \left(c_{ij} - a^{ij}_{2NE} \right) \right) \tag{5.60}$$

$$\begin{aligned} [HMAT]\left[\frac{\partial a^{ij}}{\partial x}\right] = -\Big\{ D_{ap} \left([CMAT]\left[a^{ij}\right] + [CVEC] c_{ij} \right) + \\ + \upsilon_i k^* \left([HMAT]\left[a^{3j}\right] + [CVEC] c_{3j} \right) \Big\} - [HVEC] \frac{\partial c_{ij}}{\partial x} \end{aligned} \tag{5.61}$$

Due to the solver constraints, it was only possible to consider two finite element, in each section, for the discretization of the variable ρ, giving a total of $3\times(2\times Nex)+3 = 15$ ordinary-differential equations in one-space dimension. However, it was possible to use it with a higher number of finite elements by section after some modifications on the original COLNEW solver in way to accept a higher number of differential equations.

5.6 Simulation results

The values of velocity ratios in each section were estimated according to the equilibrium model theory based on the equations (5.34), as described previously in section 5.2. The values of the equilibrium constant for the more and the less retained component, K_{Fr}, and K_{Gl}, used were equal 0.43 and 0.17, respectively, and considering sucrose not adsorbed, $K_{Suc} = 0$, as previously presented. The switching time, t^*, was estimated from the following expression,

$$t^* = \left(\gamma_j + 1\right) . \frac{\varepsilon . V_c}{Q_j} \tag{5.62}$$

Assuming a flowrate of 24 ml/min for section IV, $Q_{IV} = Q_{Rec}$, and a fixed value of γ_{IV} equal to 0.33 (< 0.405). The value of γ_I was fixed an equal to 0.95 (> 0.795). The velocities ratios γ_{II} and γ_{III}, determine the separation region, which depends on the feed. The values fixed were: $\gamma_{II} = 0.45$ (> 0.405) and $\gamma_{III} = 0.65$ (< 0.795), and with a feed flowrate of 3.62 ml/min. With these values, the remaining flow-rates were calculated and presented in Table 5.7, as all the

operating conditions and model parameters used in the simulations (similar to the one used in the new LDF approximation).

Table 5.7 *Model parameters and operating conditions for the SMBR/TMBR system defined (similar to the operating conditions used for the previous model, Table 5.4).*

Model parameters	**SMBR operating conditions**	**TMBR operating conditions**
Pe = 100 (1500) $Bi_{m\,Suc}$ = 190 $Bi_{m\,Fr}$ = $Bi_{m\,Gl}$ = 167 k_r = 50.32 min^{-1} K_m = 23 g/l k' = 0.547 min^{-1} K_{enz} = 5 ε_p = 0.1 ε = 0.4 R_p = 0.016 cm β = 1.2 $k_{f\,Fr}$ = $k_{f\,Gl}$ = 0.38 cm/min $k_{f\,Suc}$ = 0.29 cm/min $k_{p\,Fr}$ = $k_{p\,Gl}$ = 2.16 min^{-1} $k_{p\,Suc}$ = 1.44 min^{-1} K_{Fr} = 0.43 K_{Gl} = 0.17 K_{Suc} = 0.0 Da_I = 5.85 Da_{II} = 8.27 Da_{III} = 14.31 Da_{IV} = 11.45 D_{peFr} = D_{peGl} = 0.36×10^{-4} cm^2/min D_{peSuc} = 0.24×10^{-4} cm^2/min	T= 50°C C_F = 80 g Suc/l E_0 = 0.250 g/l t^* = 3.4 min Q_{Rec} = 24 ml/min Q_D = 11.38 ml/min Q_E = 9.11 ml/min Q_F = 3.62 ml/min Q_R = 5.89 ml/min Q_{IV}/Q_I = 0.34 $Q_F/Q_{III}*C_F$ = 24.62 Q_{II}/Q_{III} = 0.69	γ_I = 0.95 γ_{II} = 0.45 γ_{III} = 0.65 γ_{IV} = 0.33 u_s = 8.53 cm/min Solid flow-rate: 27.17 ml/min Columns d_c = 2.6 cm L_c = 29 cm A_c = 5.309 cm^2 V_c= 153.97 cm^3 Configuration 3-2-5-2

5.6.1 Transient solutions

In Table 5.8, the equivalence between the TMBR and SMBR flowrates is shown.

Table 5.8 *Equivalence between TMBR and SMBR flow-rates.*

Section	TMBR		SMBR	
	Q_j (ml/min)	γ_j	Q_j^* (ml/min)	γ_j^*
I	17.28	0.95	35.40	1.95
II	8.15	0.45	26.27	1.45
III	11.77	0.65	29.89	1.65
IV	5.89	0.33	24.00	1.33
t^* (min)	---		3.4	

In all the simulation performed, the global error, *er* used was equal or less than 0.0095. However, in several situations, see Table 5.9, this value was not reached and then, the end criterion was the maximum number of iterations ($200 \geq k_{max}$). When this occurs, the global balance (balance between the feed and each of the separation products) is not verified.

The numerical parameters that were used and that must be specified by the user to implement the solvers, are described in Table 5.9. For the steady-state solutions, obtained by using the COLNEW solver, the influence of the number of collocation points per interval in the final solutions, was made.

Table 5.9 *Numerical parameters used in the solvers.*

	COLNEW	**PDECOL**
Number of collocation points per interval, *Nc*	2, 3, 4	2
Number of subintervals in the initial mesh, *Nint*	20	20
Error tolerance, *tol*	10^{-8}	10^{-8}
Global Error, *er*	0.0095	0.0095

Figure 5.11, shows the internal pore concentration of the three components, Suc, Gl and Fr, in a specific position of the TMBR, after the feed point (beginning of section III), for six different time, θ = 1, 2, 3, 4, 8, and 88. The computer run time consumed to solve the system was very high, more than 50h, to reach the cyclic transient steady-state solutions. However, from Figure 5.11f, for θ = 88, after the system reaches the cyclic transient steady-state, we can see that the particle concentration of the two components, Gl and Fr, are not similar, as expected.

Figure 5.12, shows the internal pore concentration of the three components, in the four most important positions on the TMBR: extract, feed, raffinate and eluent positions, in other words, beginning of section II, III, IV, and I, for two different time, θ =1, and 40. When the TMBR system reaches the transient steady-state, after θ =40, the particles in zone II transport fructose, and in zone III glucose.

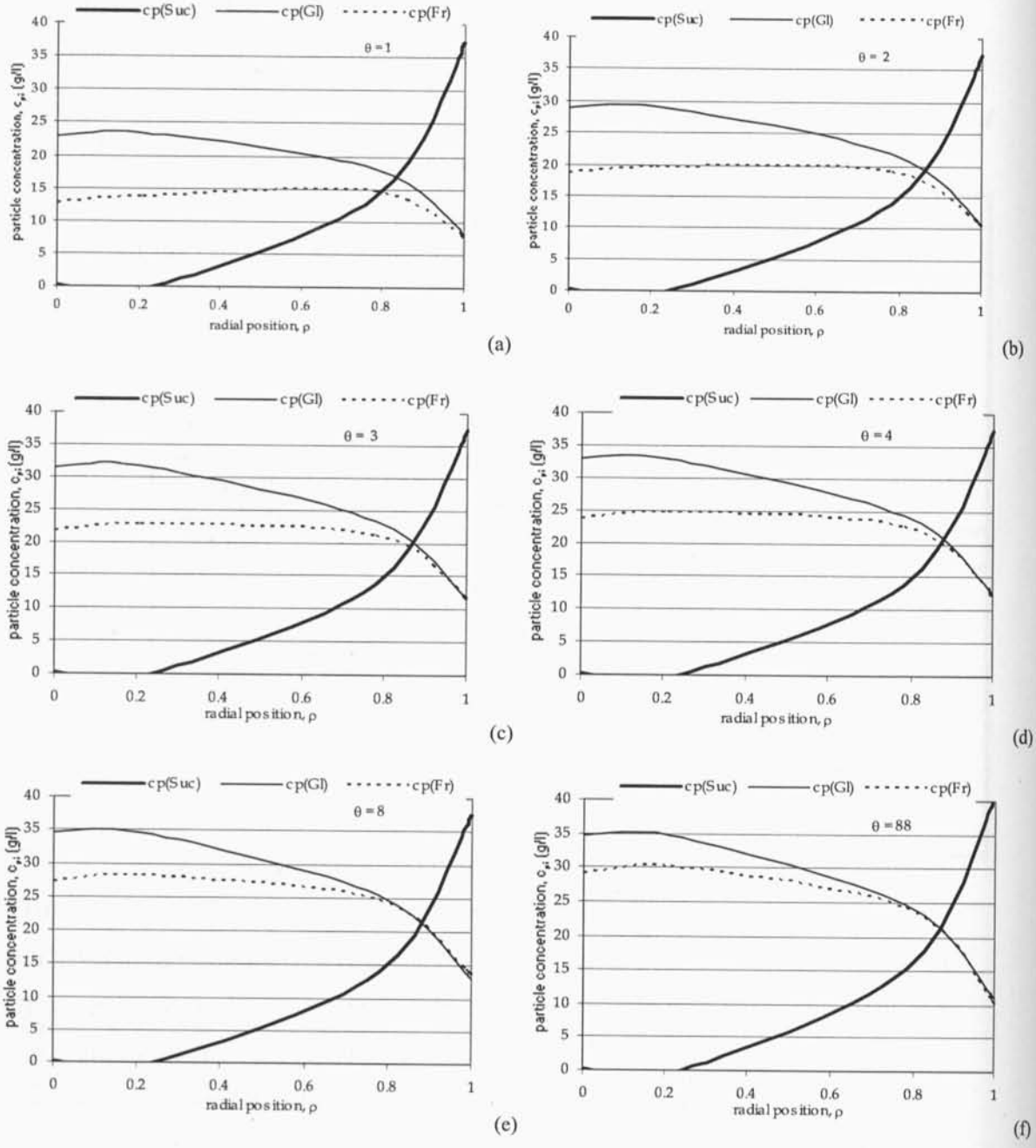

Figure 5.11 *Internal pore concentration of the three components, Suc, Gl and Fr, in a specific position of the TMBR, after the feed point (beginning of section III), for 6 different time, θ.*

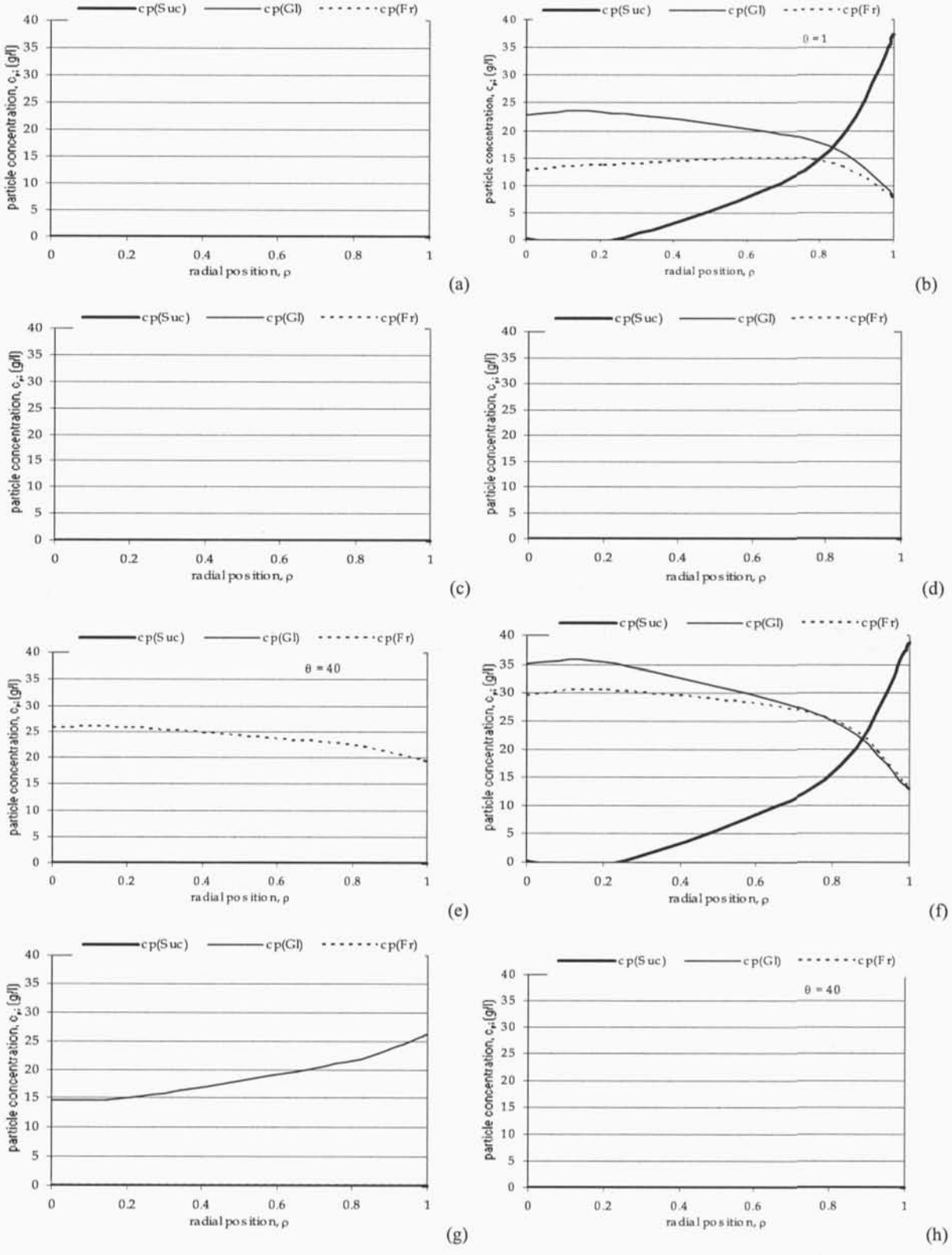

Figure 5.12 *Internal pore concentration of the three components, in the four most important positions on the TMBR: beginning of section II, III, IV, and I, for different time: $\theta = 1$ (a-d), and $\theta = 40$ (e-h).*

Figure 5.13, shows the transient TMBR internal profiles for liquid concentration, c_{ij}, and the mean pore concentration of component i in section j averaged over the particle, $\langle c_p \rangle_{ij}$, obtained by using (22), for three different time, θ =4, 8, and 40.

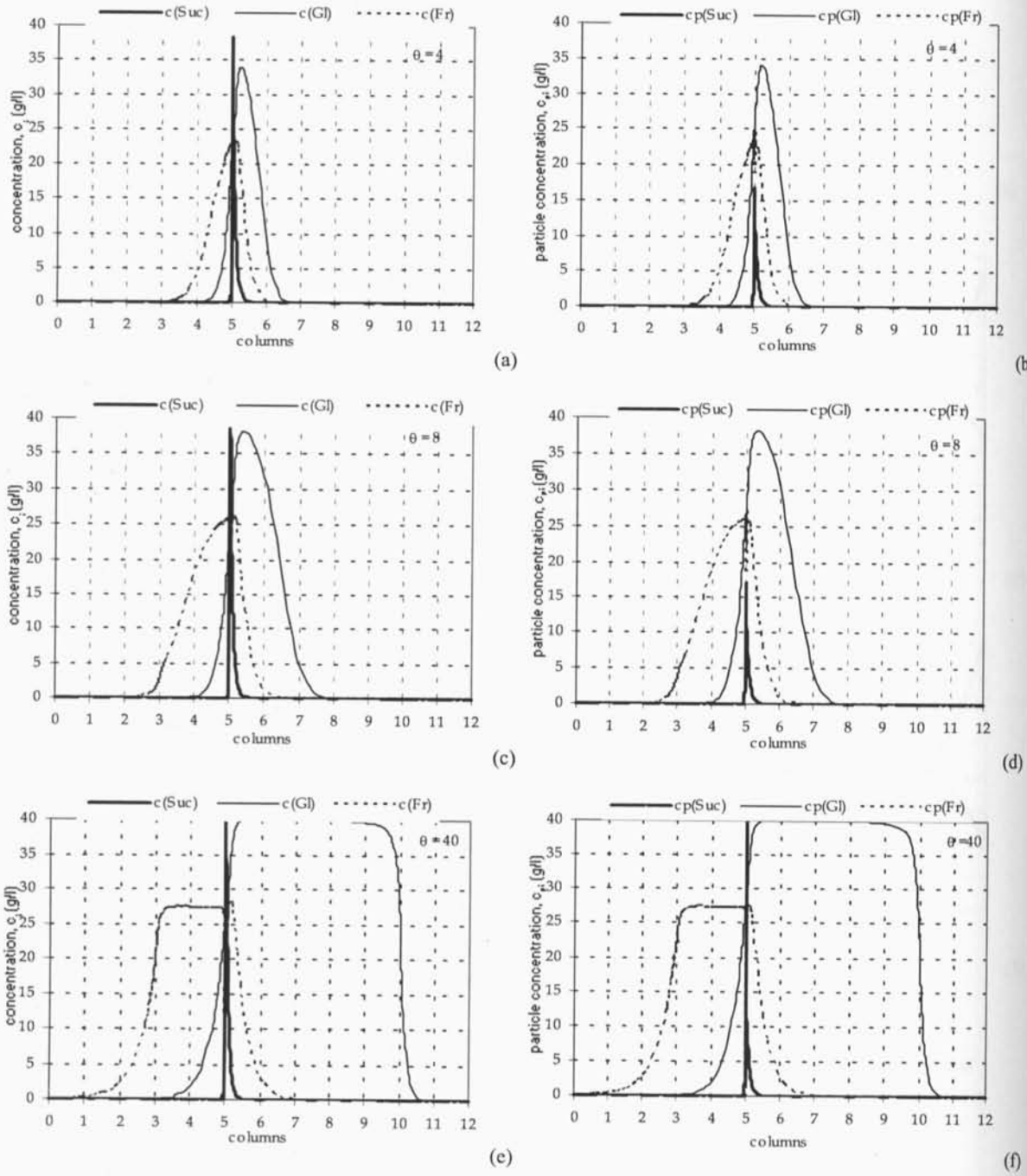

Figure 5.13 *Transient TMBR internal profiles (a-c-e) for liquid concentration, and (b-d-f) mean pore concentration of component i in section j averaged over the particle, obtained by using (5.41), for different time θ.*

Figure 5.14, shows the evolution of the transient internal concentration profiles for the two reaction products, glucose and fructose.

Figure 5.15, shows the steady-state internal concentration profiles for the sucrose reaction and glucose-fructose separation. The purities obtained were, for the two components, Gl and Fr, 99.9 and 100%, respectively.

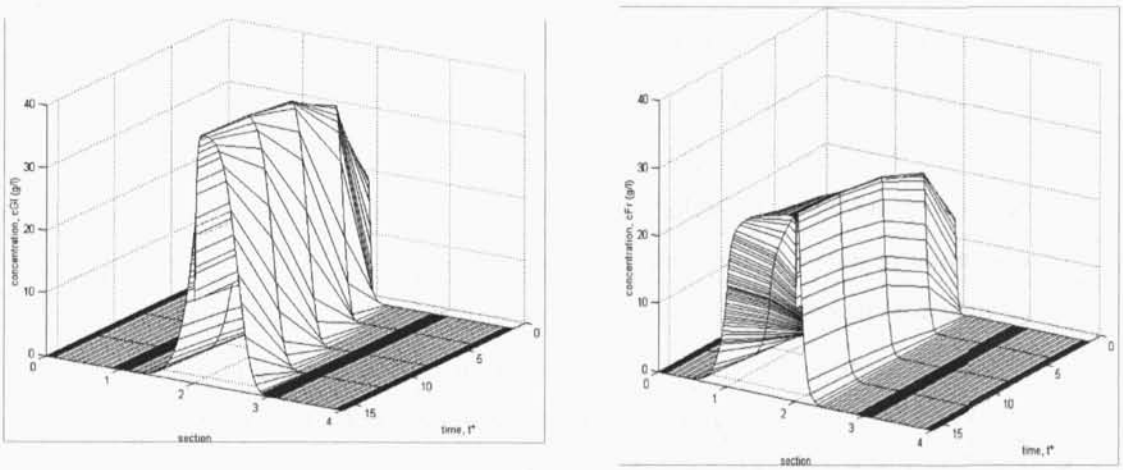

Figure 5.14 *Transient internal concentration profiles evolution, for the two reaction products, glucose and fructose.*

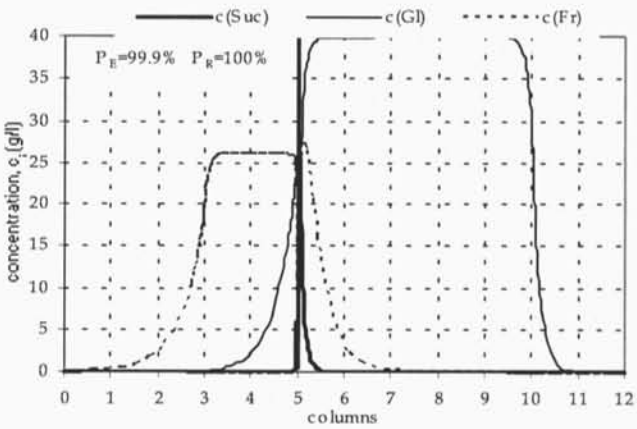

Figure 5.15 *Transient steady-state internal concentration profiles for the sucrose reaction and glucose-fructose separation under operating conditions described in Table 5.7.*

5.6.2 Steady-state solutions

The study of the influence of the number, *Ner*, and positions, $r(l)$, of the finite elements to be used in the discretization of the radial position ρ, was studied by using the steady-state model (5.60-5.61).

The model parameters and operating conditions used in all the simulation are described in Table 5.7. The other parameters, described in Table 5.9, were kept constant. Several situations were considered to reach to the TMBR steady-state solutions, as described in Table 5.10. The run time was obtained for 3, 4 and 5 collocation points per finite element in the radial position ρ, respectively. In most situations, the stop criteria error was not verified after the maximum number of iterations, k_{max}, specified. The symbol (-) was used to indicate these situations with the corresponding error value obtained. In some cases, the increase on the number of collocation points does not lead to better final results in terms of purities. The increase of the run time was not only due to the dimension of the ODE system to be solved but also due to the need of more iterations to reach the specified error, defined by the user. For example, for *Ner*=3 and with no isovolumetric discretization points (0; 0.79; 0.95; 1), with two collocation points the run time needed was higher than the one required for the case with four and five collocations points, since less iterations were needed to obtained the stop criteria error. With this table we can conclude that, for this particular case study, the isovolumetric discretization of the particle spatial radius is not a good solution. The points must be near the left boundary, x=1, see Figure 5.16. The best results were obtained by considering two or three finite intervals with three or four collocations points in each.

The isovolumetric discretization of the spatial domain in the particles was done considering grids with identical volumes. The formula, used for different value of number of points l, and for spherical geometries, was

$$x_l = \left(\frac{l - 0.5}{Ne} \right)^{1/3}, \quad l = 1,\ 2,\ ...,\ Ne \tag{5.63}$$

Figure 5.17 shows the steady-state concentration profiles obtained under the conditions described in Table 5.9, and with $Ner = 2$ ($r(l)$ = 0; 0.95; 1) with four collocation points. The profiles are very similar to the ones obtained by using the model with the new LDF approximation with chemical reaction described in previously section (Figure 5.5).

The internal concentration profile obtained for the two models, transient in Figure 5.15 and steady-state in Figure 5.17, are somewhat different. The maximum concentration values

obtained, for both components, for the transient model, are higher than the obtained values for the steady-state model. By using PDECOL, the maximum concentration value for fructose reaches the 25 g/l and 40g/l for the glucose. By using COLNEW, the maximum concentration values are below 25 g/l for fructose and below 35 g/l for glucose. Table 5.11 shows the concentration values for glucose and fructose in the extract and raffinate nodes obtained by using the two packages.

Table 5.10 *Parameters used in the radial position discretization for the steady-state model. The run time was obtained for 3, 4 and 5 collocation points per finite element in the radial position ρ, respectively; (-) indicates that the stop criteria error was not verified after the maximum number of iterations, k_{max}, was reached.*

Ner	*r(l)*	N. ODEs	R.T. (min)	P_E (%)	P_R (%)	er_{Fr}	er_{Gl}
2	0; 0.50; 1	15	-, -, -	100 [a]	99.9 [a]	0.1800	0.1300
2	0; 0.79; 1*	15	-, -, -	100 [a]	100 [a]	0.0870	0.0170
2	0; 0.90; 1	15	-, -, -	99.9 [b]	100 [b]	0.0310	0.0060
2	**0; 0.95; 1**	**15**	**3, 3, 3**	**99.9** [c]	**100** [c]	**0.0093**	**0.0018**
2	0; 0.99; 1	15	2, 12, 19	99.9 [c]	100 [c]	0.0003	0.0002
3	0; 0.63; 0.91; 1*	21	- , -, -	100 [b]	100 [b]	0.0290	0.0002
3	**0; 0.79; 0.95; 1**	**21**	**20, 13, 13**	**100** [c]	**100** [c]	**0.0086**	**0.0009**
4	0; 0.55; 0.79; 0.94; 1*	27	-, -, -	99.9 [b]	100 [b]	0.0230	0.0007
4	0; 0.63; 0.79; 0.95; 1	27	-, -, -	99.9 [b]	100 [b]	0.0230	0.0007
4	0; 0.79;0.87; 0.95; 1	27	- , -, -	99.9 [b]	100 [b]	0.0230	0.0007

* isovolumetric discretization

[a] $er > 0.0095$ (global balance not closed)
[b] $er \approx 0.0095$
[c] $er < 0.0005$

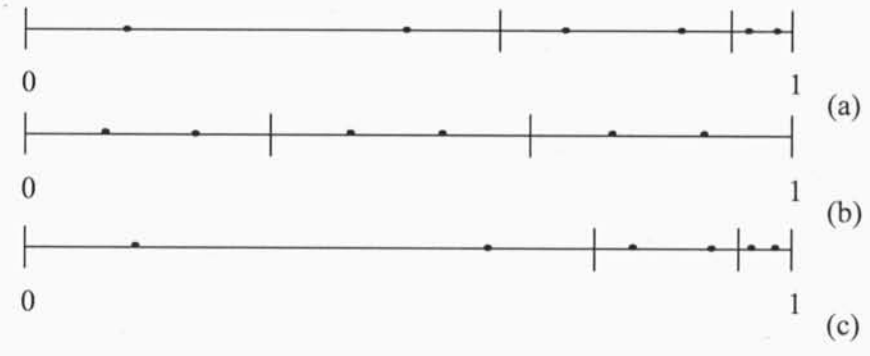

Figure 5.16 *(a) isovolumetric, (b) equidistant, and (c) user defined, discretization of the spatial particles domain, ρ, for Ner=3 with two collocation point in each subinterval.*

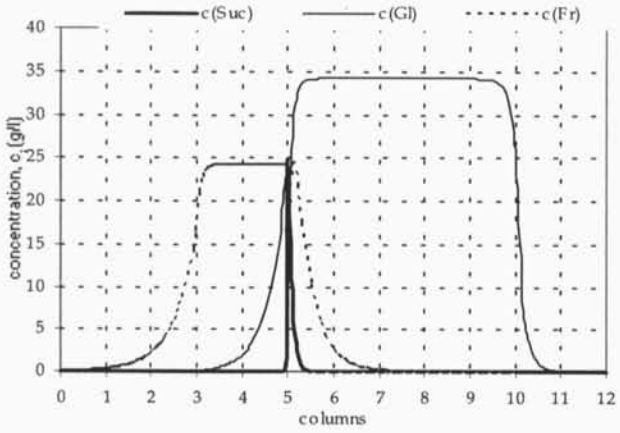

Figure 5.17 *Steady-state internal concentration profiles for the sucrose reaction and glucose-fructose separation, under operating conditions described in Table 5.7.*

Table 5.11 *Concentration values for the two components, Gl and Fr, in the extract and raffinate nodes obtained by using PDECOL (transient model) and COLNEW (steady-state model) for the case study.*

	PDECOL				COLNEW			
	Ne=2, *tol*=10^{-8}		*Ne*=3, *tol*=10^{-5}		*Ner*=3, *tol*=10^{-8}		*Ner*=2, *tol*=10^{-8}	
	Gl	**Fr**	**Gl**	**Fr**	**Gl**	**Fr**	**Gl**	**Fr**
Extract	0.0205	18.267	0.0511	15.429	0.00737	16.546	0.0156	16.532
Raffinate	28.309	0.0113	25.033	0.00548	25.842	0.00746	25.808	0.0116

Figure 5.18 shows the transient steady-state internal concentration profiles obtained after increasing the number of collocation points per interval and decreasing the tolerance error to 10^{-5}. The run time used to reach the steady-state was lower than the one obtained for the previous case, however still higher (> 240 min). The global balance was not verified. The fructose concentration obtained in the extract node was lower. The glucose concentration obtained in the raffinate node lower than the one obtained in the previous case and similar to the one obtained by using the steady-state model.

Figure 5.19 shows the internal pore concentration of the three components for three different times, $\theta = 2$, 4, 12 and 40. For $\theta = 12$, the fructose concentration values starts to be lower and not equal to the glucose concentration value. Explaining the behaviour of the decreasing of the fructose concentration values in the liquid phase as previously mentioned.

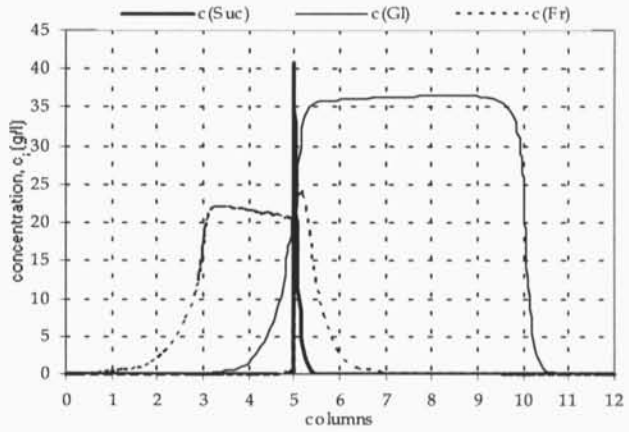

Figure 5.18 *Transient Steady-state internal concentration profiles for the sucrose reaction and glucose-fructose separation obtained with Ne=3, Nint=20 and, tol=10^{-5}.*

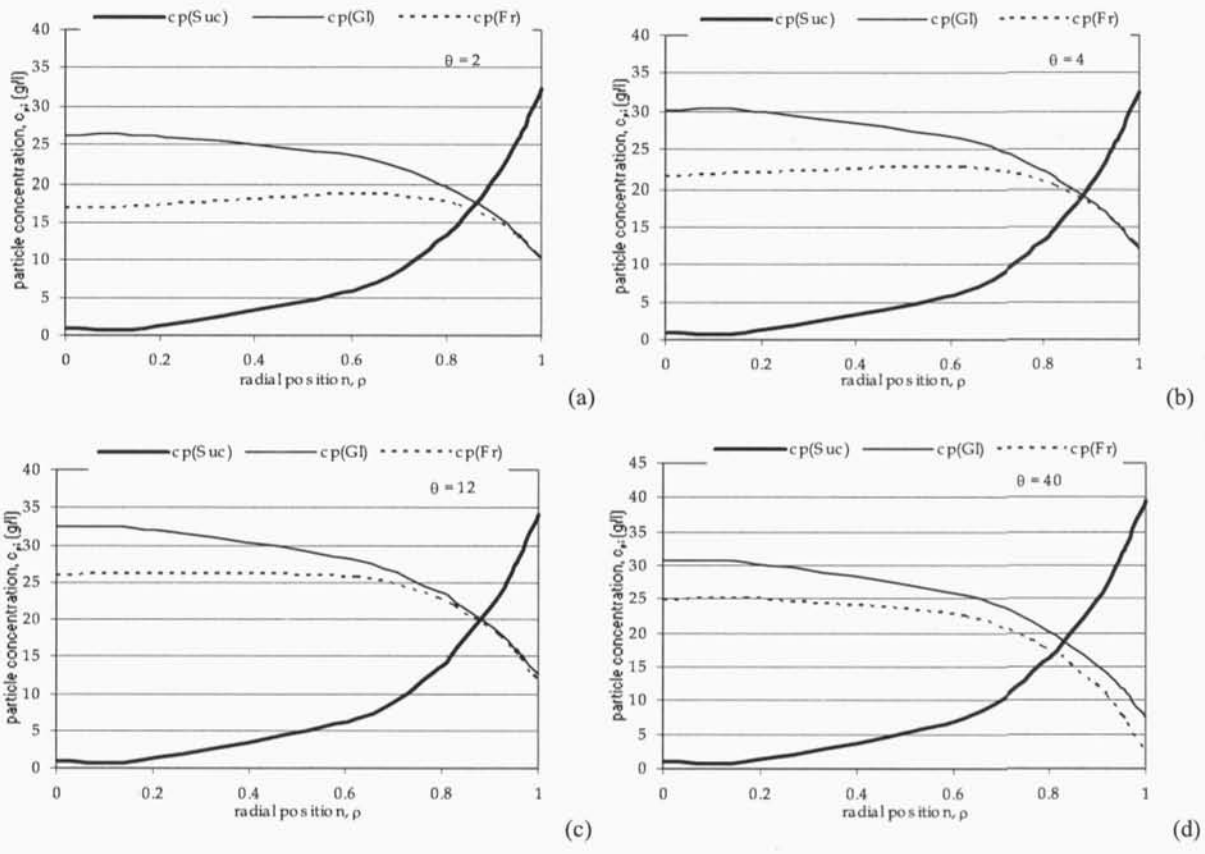

Figure 5.19 *Internal pore concentration of the three components, Suc, Gl and Fr, in a specific position of the TMBR, after the feed point (beginning of section III), for 4 different period of time, θ=2, 4, 12 and 40, with Ne=3, Nint=20 and, tol=10^{-5}.*

5.6.3 Model without reaction

The dimensionless mass balance equations to be solved in this case are, for the particle

$$\frac{\partial c_{pij}}{\partial \theta} = \frac{\gamma_j}{n_j\left(K_i+\varepsilon_p\right)}\left[\tau_j \frac{D_{pe}}{R_p^2}\left(\frac{\partial^2 c_{pij}}{\partial \rho^2}+\frac{2}{\rho}\frac{\partial c_{pij}}{\partial \rho}\right)\right]+\frac{1}{n_j}\frac{\partial c_{pij}}{\partial x} \tag{5.64a}$$

or, in matricial form,

$$\begin{aligned}[HMAT]\left[\frac{\partial a^{ij}}{\partial \theta}\right] = \frac{\gamma_j}{n_j\left(K_i+\varepsilon_p\right)}\left\{\tau_j \frac{D_{pe}}{R_p^2}\left([CMAT]\left[a^{ij}\right]+[CVEC]c_{ij}\right)\right\}+ \\ +\frac{1}{n_j}\left([HMAT]\left[\frac{\partial a^{ij}}{\partial x}\right]+[CVEC]\frac{\partial c_{ij}}{\partial x}\right)-[HVEC]\frac{\partial c_{ij}}{\partial \theta}\end{aligned} \tag{5.64b}$$

and,

$$\frac{\partial c_{ij}}{\partial \theta} = \frac{\gamma_j}{n_j}\left(\frac{1}{Pe_j}\frac{\partial^2 c_{ij}}{\partial x^2}-\frac{\partial c_{ij}}{\partial x}-\frac{(1-\varepsilon)}{\varepsilon}\frac{3k_f}{R_p}\tau_j\left(c_{ij}-c_{pij}\big|_{\rho=1}\right)\right) \tag{5.65a}$$

or,

$$\frac{\partial c_{ij}}{\partial \theta} = \frac{\gamma_j}{n_j}\left(\frac{1}{Pe_j}\frac{\partial^2 c_{ij}}{\partial x^2}-\frac{\partial c_{ij}}{\partial x}-\frac{(1-\varepsilon)}{\varepsilon}\frac{3k_f}{R_p}\tau_j\left(c_{ij}-a^{ij}_{2NE}\right)\right) \tag{5.65b}$$

for the outer liquid phase.

The steady-state model, (5.59) without the term concerning the reaction is

$$\frac{\partial c_{pij}}{\partial x} = -\frac{\gamma_j}{\left(\varepsilon_p+K_i\right)}\left(\frac{D_{pe}}{R_p^2}\tau_j\left(\frac{\partial^2 c_{pij}}{\partial \rho^2}+\frac{2}{\rho}\frac{\partial c_{pij}}{\partial \rho}\right)\right) \tag{5.66a}$$

or, in matricial form,

$$[HMAT]\left[\frac{\partial a^{ij}}{\partial x}\right] = -\frac{\gamma_j}{\left(\varepsilon_p+K_i\right)}\left\{\tau_j \frac{D_{pe}}{R_p^2}\left([CMAT]\left[a^{ij}\right]+[CVEC]c_{ij}\right)\right\}-[HVEC]\frac{\partial c_{ij}}{\partial x} \tag{5.66b}$$

and

$$\frac{\partial^2 c_{ij}}{\partial x^2} = Pe_j\left(\frac{\partial c_{ij}}{\partial x}+\frac{(1-\varepsilon)}{\varepsilon}\frac{3k_f}{R_p}\tau_j\left(c_{ij}-c_{pij}\big|_{\rho=1}\right)\right) \tag{5.67a}$$

or,

$$\frac{\partial^2 c_{ij}}{\partial x^2} = Pe_j\left(\frac{\partial c_{ij}}{\partial x}+\frac{(1-\varepsilon)}{\varepsilon}\frac{3k_f}{R_p}\tau_j\left(c_{ij}-a^{ij}_{2NE}\right)\right) \tag{5.67b}$$

The internal concentration profile obtained, Figure 5.20, was as expected. Figure 21, shows the pore concentration profile in a specific position of the TMB, after the feed point (beginning of section III). The particle, in that position, transports more glucose than fructose. It can be confirmed by looking to the feed point (column 5) in Figure 5.20.

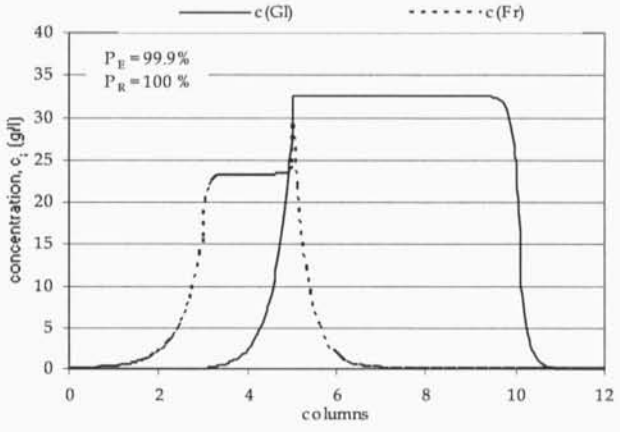

Figure 5.20 *Steady-state internal concentration profiles for the glucose-fructose separation obtained with Ner=3 and Nint=20.*

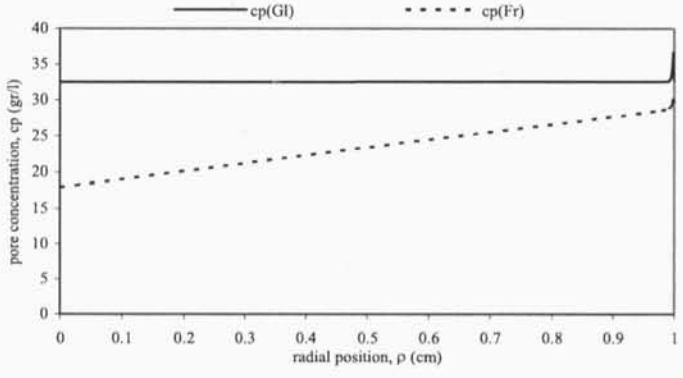

Figure 5.21 *Radial concentration profiles for the steady-state internal for the glucose-fructose separation obtained with Ner=3 and Nint=20, in a specific position of the TMB, after the feed point (beginning of section III).*

5.6.4 Model with non-linear reaction

The reaction rate, $\mathcal{R}$ (mol/l-min), considered takes the form of the Michaelis-Menten equation (5.48) previously described for a non-linear reaction,

$$\mathcal{R} = \frac{kE_0 c_{Suc}}{K_m + c_{Suc}} = k' \frac{c_{Suc}}{1 + \delta c_{Suc}} \quad \text{with} \quad k' = \frac{kE_0}{K_m} \quad \text{and} \quad \delta = \frac{1}{K_m}$$

where k is the reaction rate constant (min^{-1}), E_0 is the enzyme concentration ($mol.m^{-3}$) and K_m the Michaelis constant ($mol.l^{-1}$).

Since the concentration of sucrose, c_{Suc}, is in g/l, the reaction rate, $\mathcal{R}$ in g/l-min, takes the following form,

$$\mathcal{R} = k' \frac{c_{Suc}/M_{Suc}}{1+\delta\, c_{Suc}/M_{Suc}} . M_i \tag{5.68}$$

where M_i is the molecular weight of the component i, i=1, 2, 3 (Suc = 342, Gl = Fr = 180).

Transient model

The transient model equations with non linear reaction in dimensionless form is,

$$\frac{\partial c_{pij}}{\partial \theta} = \frac{\gamma_j}{n_j\left(K_i+\varepsilon_p\right)}\left[\upsilon_i\left(K_{enz}+\varepsilon_p\right)\tau_j k' \frac{c_{p3j}}{1+\delta c_{p3j}} + \tau_j \frac{D_{pe}}{R_p^2}\left(\frac{\partial^2 c_{pij}}{\partial \rho^2}+\frac{2}{\rho}\frac{\partial c_{pij}}{\partial \rho}\right)\right] + \frac{1}{n_j}\frac{\partial c_{pij}}{\partial x} \tag{5.69a}$$

or, in matricial form,

$$\begin{aligned}[HMAT]\left[\frac{\partial a^{ij}}{\partial \theta}\right] = \frac{\gamma_j}{n_j\left(K_i+\varepsilon_p\right)}\Bigg\{ & \upsilon_i\left(K_{enz}+\varepsilon_p\right)\tau_j k' \frac{\left([HMAT]\left[a^{3j}\right]+[HVEC]c_{3j}\right)}{1+\delta\left([HMAT]\left[a^{3j}\right]+[HVEC]c_{3j}\right)} + \\ & + \tau_j \frac{D_{pe}}{R_p^2}\left([CMAT]\left[a^{ij}\right]+[CVEC]c_{ij}\right)\Bigg\} + \\ & + \frac{1}{n_j}\left([HMAT]\left[\frac{\partial a^{ij}}{\partial x}\right]+[CVEC]\frac{\partial c_{ij}}{\partial x}\right) - [HVEC]\frac{\partial c_{ij}}{\partial \theta}\end{aligned} \tag{5.69b}$$

and,

$$\frac{\partial c_{ij}}{\partial \theta} = \frac{\gamma_j}{n_j}\left(\frac{1}{Pe_j}\frac{\partial^2 c_{ij}}{\partial x^2} - \frac{\partial c_{ij}}{\partial x} + \upsilon_i \tau_j k' \frac{c_{3j}}{1+\delta c_{3j}} - \frac{(1-\varepsilon)}{\varepsilon}\frac{3k_f}{R_p}\tau_j\left(c_{ij} - c_{pij}\big|_{\rho=1}\right)\right) \tag{5.70a}$$

or,

$$\frac{\partial c_{ij}}{\partial \theta} = \frac{\gamma_j}{n_j}\left(\frac{1}{Pe_j}\frac{\partial^2 c_{ij}}{\partial x^2} - \frac{\partial c_{ij}}{\partial x} + \upsilon_i \tau_j k' \frac{c_{3j}}{1+\delta c_{3j}} - \frac{(1-\varepsilon)}{\varepsilon}\frac{3k_f}{R_p}\tau_j\left(c_{ij} - a^{ij}_{2NE}\right)\right) \tag{5.70b}$$

The transient solutions obtained, by using the PDECOL package, are very similar to the one obtained for the model with linear reaction, *i.e.* no significant different were found by changing the type of reaction. The error tolerance was the same as the others numerical parameters. Much higher computational run time was needed to obtain the transient steady-state solutions. Figure 5.22 shows the relative error between the two solutions, linear and non

linear reaction, obtained. The higher relative error values, ≈20%, were obtained for very low concentrations.

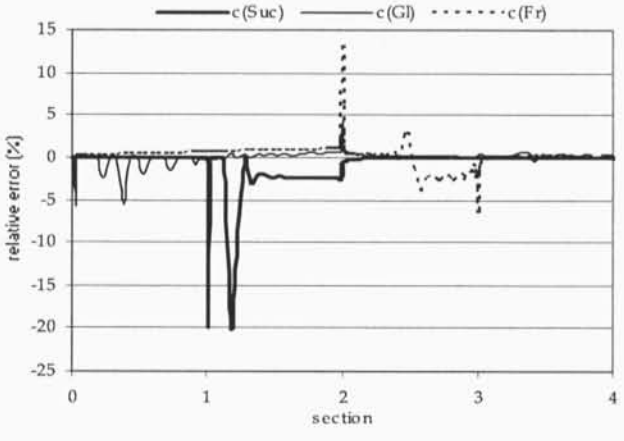

Figure 5.22 *Relative error obtained between the transient steady-state internal concentration profiles with linear and non linear reaction; Ner=3 and Nint=20.*

Steady-state model

The steady-state dimensionless mass balance equations

$$\frac{\partial c_{pij}}{\partial x} = -\frac{\gamma_j}{\left(\varepsilon_p + K_i\right)}\left(\frac{D_{pe}}{R_p^2}\tau_j\left(\frac{\partial^2 c_{pij}}{\partial \rho^2} + \frac{2}{\rho}\frac{\partial c_{pij}}{\partial \rho}\right) + \upsilon_i\left(K_{enz} + \varepsilon_p\right)\tau_j k' \frac{c_{p3j}}{1+\delta c_{p3j}}\right) \tag{5.71a}$$

or, in matricial form,

$$\begin{aligned}\left[HMAT\right]\left[\frac{\partial a^{ij}}{\partial x}\right] = -\frac{\gamma_j}{\left(\varepsilon_p + K_i\right)}\Bigg\{ & \tau_j \frac{D_{pe}}{R_p^2}\left(\left[CMAT\right]\left[a^{ij}\right] + \left[CVEC\right]c_{ij}\right) + \\ & + \upsilon_i\left(K_{enz} + \varepsilon_p\right)\tau_j k' \frac{\left(\left[HMAT\right]\left[a^{3j}\right] + \left[HVEC\right]c_{3j}\right)}{1+\delta\left(\left[HMAT\right]\left[a^{3j}\right] + \left[HVEC\right]c_{3j}\right)}\Bigg\} \\ & - \left[HVEC\right]\frac{\partial c_{ij}}{\partial x}\end{aligned} \tag{5.71b}$$

and

$$\frac{\partial^2 c_{ij}}{\partial x^2} = Pe_j\left(\frac{\partial c_{ij}}{\partial x} - \upsilon_i \tau_j k' \frac{c_{3j}}{1+\delta c_{3j}} + \frac{(1-\varepsilon)}{\varepsilon}\frac{3k_f}{R_p}\tau_j\left(c_{ij} - c_{pij}\big|_{\rho=1}\right)\right) \tag{5.72a}$$

or,

$$\frac{\partial^2 c_{ij}}{\partial x^2} = Pe_j \left(\frac{\partial c_{ij}}{\partial x} - \upsilon_i \tau_j k' \frac{c_{3j}}{1+\delta c_{3j}} + \frac{(1-\varepsilon)}{\varepsilon} \frac{3k_f}{R_p} \tau_j \left(c_{ij} - a^{ij}_{2NE} \right) \right) \qquad (5.72b)$$

The steady-state solutions obtained, by using the COLNEW package, are very similar to the one obtained for the model with linear reaction, *i.e.* no significant different were found by changing the type of reaction. The error tolerance was the same as the others numerical parameters.

5.7 Conclusions

A SMBR/TMBR model was developed accounting not only for the reaction in the outer fluid phase but also inside the adsorbent particle. The new model was analyzed through simulations for the sucrose inversion and glucose/fructose separation. Two different approaches were presented. By using the coefficients in the Kim's (1989) LDF formulas, a polynomial approximation was used defining a new LDF model, for chemical reaction in the porous particle. Linear equilibrium isotherms, film diffusion and axial dispersion for fluid flow were also considered. Some of the model parameters and the operating conditions used on the SMBR/TMBR system simulation were estimated under the same constraints as for the SMB/TMB system. It has been shown that the performances parameters, purity and recovery, decrease while particle radius increases. The sucrose inversion is slightly affected. The reaction/separation region has a triangular shape similar to those found for the SMB/TMB separation equilibrium theory. The effect of the reaction rate coefficient k_r, on the reaction/separation region was also studied. The triangle shaped separation/reaction region becomes smaller as the reaction rate coefficient decreases. For lower purity specification, ≥ 90.0%, the separation/reaction region becomes greater compared with the area defined for higher purity specification, ≥ 99.0%, under the same operating conditions and model parameters. The vertex of the triangle in the γ_{II} -γ_{III} plane, lies outside the region defined by the equilibrium theory limits.

The second approach uses a detailed new TMBR model, taking into account the intraparticle radial profiles. To solve the resulting system of PDE/ODE, a combination of orthogonal collocation on finite element method and available PDE solver (PDECOL) and ODE solver (COLNEW), respectively, were used. With the presented models, not only the transient

steady-state fluid-phase concentration profiles of the components can be obtained, but also the profiles of the concentration inside the porous particle in a specific place of the bed. Much higher computational run time was needed to obtain the steady-state solutions, being very sensitive to tolerances and numerical parameters adjust.

5.8 References

Alopaeus V. (2000) *Mass-Transfer Calculation Methods for Transient Diffusion within Particles*, AIChE J. **46**, 2369-2372.

Azevedo, D. C. S., A. E. Rodrigues (2001) *Design Methodology and Operation of a Simulated Moving Bed Reactor for the Inversion of Sucrose and Glucose-Fructose Separation*, Chem. Eng. J. **3**, 131-139.

Bader, G., U. Ascher (1987) *A New Basis Implementation for a Mixed Order Boundary Value ODE Solver*, SIAM J. Scient. Stat. Comput. **8**, 483-498.

Başağaoğlu H., T. R. Ginn, B. J. McCoy, M. A. Mariño (2000) *Linear Driving Force Approximation to a Radial Diffusive Model*, AIChE J. **46**, 2097-2105

Char, B., K. Geddes, G. Gonnet, B. Leong, M. Monagen, S. Watt, (1992) *First Leaves: A Tutorial Introduction to Maple V*, New York: Spinger-Verlag.

Fricke, J., M. Meurer, J. Dreisörner, H. Schmidt-Traub (1999) *Effect of Process Parameters on the Performance of a Simulated Moving Bed Chromatographic Reactor*, Chem. Engng. Sci. **54**, 1487-1492.

Kim, D. H., (1989) *Linear Driving Force Formulas for Diffusion and Reaction in Porous Catalysts*, AIChE J. **35,** 343-346.

Li, Z. and R. T. Yang, (1999) *Concentration Profile for Linear Driving Force Model for Diffusion in a Particle*, AIChE J. **45**, 196-200.

Lode, F., M. Houumard, C. Migliorini, M. Mazzotti, M. Morbidelli, (2001) *Continuous Reactive Chromatography*, Chem. Engng. Sci. **56**, 269-291.

Madsen, N. K., and R. F. Sincovec, (1979) *PDECOL: General Collocation Software for Partial Differential Equations*, ACM Trans. Math. Software **5**, 326-351.

Ramkrishna, D. and N. R. Amundson, (1985) *Linear operator methods in Chemical Engineering*, Prentice-Hall: Englewood Cliffs, NJ.

Reid, R. C., J. M. Prausnitz, B. E. P., (1987) *The properties of Gases & Liquids*, Fourth Edition, McGraw-Hill, Inc.

Ruthven, D. M., Ching, C. B. (1989) *Counter-Current and Simulated Moving Bed Adsorption Separation Process*, Chem. Engng. Sci. **44**, 1011-1038.

6. Model with intraparticle diffusion and convection development in proteins separation

The applications for purified proteins have grown considerably over recent years due to their biological and nutritional properties especially in the fields of biochemistry and medicine. Adsorptive separations by liquid chromatography are important processes in biotechnology for the purification of proteins, Leitão *et al.*, (2002).

The objective of this chapter is to assess the use of the Simulated Moving Bed (SMB) technology in the separation of proteins by considering perfusive particles.

The set of equations that describes the system are the mass balance equations for each component, in the outer fluid and in the particle phases. The mass transfer from the bulk phase to the fluid film surrounding the adsorbent particle is also considered. In the particle, the mass transfer through the pores includes convection and diffusion.

A mixture of two proteins: Bovine Serum Albumin (BSA) and Myoglobin (MYO), is considered as an example.

6.1 Introduction

Theoretical analysis of intraparticle convection effects in chromatography with permeable particles have been developed by several authors. For a porous slab with half-thickness, ℓ

(Rodrigues *et al.*, 1982), the augmented effective diffusivity owing to intraparticle convection, $\tilde{D}_{pe}$, is related to the intraparticle effective diffusivity, D_{pe}, by the following relationship:

$$\tilde{D}_{pe} = \frac{D_{pe}}{f(\lambda_p)} \tag{6.1}$$

where

$$f(\lambda_p) = \frac{3}{\lambda_p}\left(\frac{1}{\tanh \lambda_p} - \frac{1}{\lambda_p}\right). \tag{6.2}$$

The enhancement of diffusivity by convection, $\tilde{D}_{pe}$, is then $1/f(\lambda_p)$. The enhancement factor, $1/f(\lambda_p)$, of diffusivity by convection is shown in Figure 6.1.

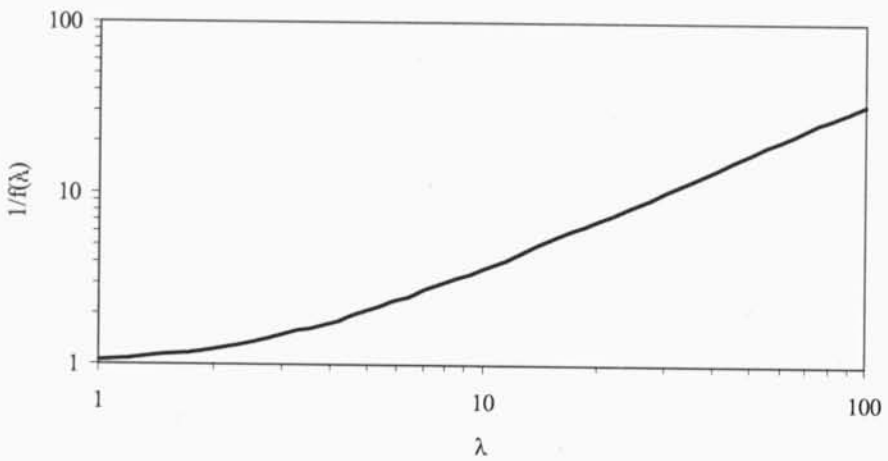

Figure 6.1. *The enhancement factor, $1/f(\lambda_p)$, of diffusivity by convection (Rodrigues, 1997).*

The relative importance of convective and diffusive fluxes can be expressed by the intraparticle Peclet number,

$$\lambda_p = v_0 \ell / D_{pe} \tag{6.3}$$

where v_0 is the intraparticle convective velocity inside large pores. The function $f(\lambda_p)$ approaches unity, when $\lambda_p << 1$ (particles with no throughpores, or with pores too small to allow a sufficient level of intraparticle convection) and to $3/\lambda_p = 3D_{pe}/v_0\ell$ when λ_p is large. In this case, the convection-augmented diffusivity, D_{pe} becomes proportional to v_0. Equations (6.1) and (6.2) are still valid for spherical pellets (Carta *et al.*, 1992), if the intraparticle Peclet

number is defined as $\lambda_p = v_0 R_p / (3D_{pe})$, where R_p is the particle radius. The ratio $\tilde{D}_{pe}/D_{pe}$, representing the enhancement of intraparticle transport caused by convection, was then found analytically as a series expansion of Legendre polynomials, dependent on λ_p.

For chromatographic process, the measure of the column performance is conveniently expressed in terms of the height equivalent to a theoretical plate (HETP). Intraparticle convection effects in this case are accounted, by addition of the convective enhancement factor, $1/f(\lambda_p)$; an modified form of the dimensionless Van Deemter equation as (Rodrigues, 1993)

$$HETP = A + \frac{B}{u_0} + C f(\lambda_p)\, u_0 \tag{6.4}$$

where u_0 is the bed superficial velocity for the spherical pellets of radius R_p. The A and B terms account, respectively, for hydrodynamic dispersion and molecular diffusion, as in the classical van Deemter equation, $A = a'\, d_p$, with a' depending on the quality of the column packing, and $B = 2\, D_m$, where D_m is the molecular diffusivity of the particle in solution. The C term is due to intraparticle mass transfer kinetics. For spherical particles and inert tracers this term is given by (Carta and Rodrigues, 1993)

$$C = \frac{1}{30} \frac{\varepsilon_p (1-\varepsilon_b) b^2}{\left[\varepsilon_b + \varepsilon_p (1-\varepsilon_b) b\right]^2} \varepsilon_p \frac{d_p^2}{D_{pe}} \tag{6.5}$$

where $b = 1 + \left[(1-\varepsilon_p)/\varepsilon_p\right] K$.

After replacing the A, B and C terms in the extended Van Deemter equation, we obtain

$$h = \frac{HETP}{d_p} = a' + \frac{2D_m}{u_0 d_p} + \frac{1}{30} \frac{\varepsilon_p (1-\varepsilon_b) b^2}{\left[\varepsilon_b + \varepsilon_p (1-\varepsilon_b) b\right]^2} \varepsilon_p \frac{d_p}{D_{pe}} f(\lambda_b) u_0 \tag{6.6}$$

where h is the reduced *HETP*.

The values of all the unknowns in (6.6), a', D_{pe}, B_p, ε_p, ε_b, B_b, R_p, D_m, were the same as the ones considered in Leitão *et al.*, (2002). Table 6.1 shows the values for these parameters.

Table 6.1. *Parameters values for Rodrigues equation (6.6) from Leitão et al., (2002).*

Protein	a'	D_{pe} (cm^2/s)	B_p (cm^2)	D_m (cm^2/s)	$\alpha \times 100$
MYO	12	2.14×10^{-7}	7.2×10^{-12}	16.1×10^{-7}	0.388
BSA	12	0.70×10^{-7}	6.0×10^{-12}	5.30×10^{-7}	0.323

Bed permeability, B_b, is obtained form the slope of the plot $\Delta P/L$ versus the bed superficial velocity, u_0. In laminar flow, the pressure drop ΔP across a bed of length L packed with particles of diameter d_p is given by Darcy's law, $\Delta P/L = \mu u_0/B_b$, where μ is the fluid viscosity,

$$B_b = \left(\varepsilon_b^3 d_p^2\right)/\left[150\left(1-\varepsilon_b\right)^2\right] \tag{6.7}$$

and ε_b is the bed porosity. For the POROS HQ/M column, $20\mu m$ particles, the bed permeability is $1.4\times10^{-9}\ cm^2$ and the bed porosity is 0.30.

The Darcy's law can be written as in Biressi *et al.*, (2000)

$$\frac{\Delta P}{L} = \mu u_0/B_b = \frac{\left(1-\varepsilon_b\right)^2}{\varepsilon_b^3}\frac{150\mu}{d_p^2}u_0 = \frac{\varphi}{d_p^2}u_0 = \Phi u_0 \tag{6.8}$$

The pellet porosity was estimated, ε_p = 0.5. In Table 6.1 $\alpha = \left(1-\varepsilon_b\right)B_p/B_b$ is the split ratio, i.e. the fraction of flow rate entering the column that goes through the macropores of the pellets by convection. The particle permeability, B_p, was obtained experimentally (Leitão *et al.*, 2002), however, it can be defined as

$$B_p = \frac{\varepsilon_p^3}{150\left(1-\varepsilon_p\right)^2}d_m^2 = \frac{a\varepsilon_p^3}{150\left(1-\varepsilon_p\right)^2}d_{pore}^2 \tag{6.9}$$

where d_m is the diameter of the microspheres inside the particle, d_{pore} is the pore diameter, $a = d_m^2/d_{pore}^2$ is a constant Rodrigues *et al.*, (1992).

The intraparticle convective velocity inside large pores, v_0, in laminar flow is related with the bed superficial velocity, u_0, by Rodrigues *et al.*, (1996)

$$v_0 = \frac{B_p}{B_b}u_0 \tag{6.10}$$

In Leitão *et al.*, (2002) work, BSA and MYO adsorption equilibrium isotherms follow a Langmuir isotherm almost rectangular in shape, of the type $q^* = Q_m K_L\, c^*/\left(1+K_L\, c^*\right)$, where Q_m is the maximum adsorbed concentration and K_L is the Langmuir equilibrium constant. The MYO adsorption isotherm can be reduced to the linear form $q^* = K_i\, c^*$, where K_i is the adsorption coefficient. Using the values obtained in Leitão *et al.*, (2002), the adsorption isotherms used are $q^* = 1.59\, c^*$ for the MYO protein and $q^* \approx 4.02\, c^*$ for the BSA protein. The last one corresponds to adsorption equilibrium isotherm with a higher value of salt concentration that the one considered.

Other model parameters must be considered as the Peclet number, *Pe*, and the intraparticle Peclet number, λ_p. The film mass transfer coefficient, k_f, was calculated from the correlation $Sh = k_f d_p / D_m = 47.5 Re^{1.22}$ as considered in Leitão *et al.*, (2002). The Reynolds number can be defined as $Re = u \rho_f d_p / (\mu_f)$ where u is the mean velocity, ρ_f the fluid density, d_p, particle diameter, μ_f the fluid viscosity.

Perfusion chromatography is a technique characterised by the combination of convective and diffusive solute transport within the internal pores of individual particles. From the theoretical models developed to explain the dynamic of retention of solutes in perfusion supports, it was derived that efficiency of a separation was independent of the flow-rate and only dependent slightly on the particle diameter (Rodrigues *et al.*, 1991; Rodrigues, 1997; Garcia *et al.*, 2000). In perfusion chromatography (flow-through particle chromatography), stationary particles used are designed to enable a better access of molecules to the inner of these through two classes of pores: *throughpores* (6000-8000 Å), which cross the stationary phase particle from side to side and allow the transport of molecules into the interior of the particle by convective flow and *diffusive pores* (800-1500 Å), interconnecting the *throughpore* network and enabling the transport by diffusion, Figure 6.2. In this way, molecules travel by convection through the column to the stationary phase particle, such as in convectional chromatography. Since there, molecules cross the stationary phase particles by means of a combination of convective and diffusive transport, thus, accelerating the transport of molecules through the particles. The benefits of perfusion chromatography are greater at high mobile-phase velocities (1000-5000 cm/h and beyond), where intraparticle convective transport greatly exceeds the rate of diffusion transport.

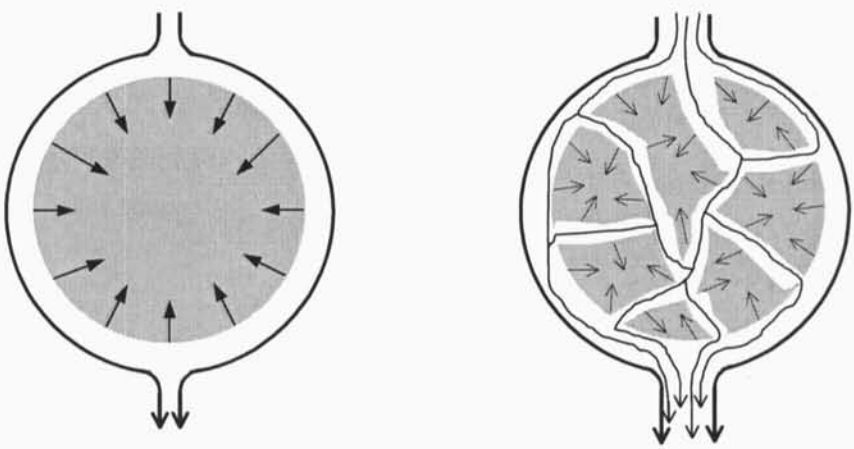

Figure 6.2. *Conventional and perfusion chromatography stationary phase particle (from Garcia et al., (2000)).*

6.2 TMB steady-state intraparticle diffusion/convection model equations

Mathematical models describing the intraparticle transport in permeable chromatography have been developed, becoming more realistic but more difficult to be solved. In Leitão work, Leitão and Rodrigues, (1999), and Leitão *et al.*, (2002), the technique implemented to obtain the solution of the intraparticle diffusion/convection model is presented also with the inherent difficulties: the equations for the throughpores are written in spherical coordinates, increasing the final number of PDEs equations (in time and in one spatial coordinates) to be solved. In this section we intend not only, to study the influence of the diffusion on the SMB/TMB performance but also the influence of the intraparticle convection. The steady-state model described takes into account the new LDF model approximation (described in section 5.1) without reaction, that is ϕ=0, see equation (6.13), linear equilibrium isotherm, film diffusion, axial dispersion for fluid flow and convection. The dimensionless TMB steady-state mass balance equations for the protein in the bed fluid, throughpores and microparticles considered are written as follows,

· *for the particles*

$$\frac{\partial \langle c_p \rangle_{ij}}{\partial x} = -\frac{\gamma_j}{(\varepsilon_p + K_i)} \tilde{k}_p \tau_j \left(c_{sij} - \langle c_p \rangle_{ij} \right) \tag{6.11}$$

· *for the fluid phase in the bed*

$$\frac{\partial^2 c_{ij}}{\partial x^2} = Pe_j \left(\frac{\partial c_{ij}}{\partial x} + \frac{(1-\varepsilon)}{\varepsilon} \tilde{k}_p \tau_j \left(c_{sij} - \langle c_p \rangle_{ij} \right) \right) \tag{6.12}$$

· *relationship between the liquid phase concentration and the particle surface concentration, c_{sij}*

$$c_{sij} = \frac{1}{\frac{\tilde{Bi}_m}{5} + 1} \left(\frac{\tilde{Bi}_m}{5} c_{ij} + \langle c_p \rangle_{ij} \right) \tag{6.13}$$

· *initial conditions*

$$c_{ij}(x,0) = \langle c_p \rangle_{ij}(x,0) = c_{sij}(x,0) = 0 \tag{6.14a}$$

· *boundary conditions*

$$x = 0 \qquad c_{ij,0} = c_{ij} - \frac{1}{Pe_j} \frac{\partial c_{ij}}{\partial x} \tag{6.14b}$$

$$x=1 \qquad \frac{\partial c_{ij}}{\partial x}=0, \qquad \left\langle c_p \right\rangle_{ij}=\left\langle c_p \right\rangle_{ij+1,0} \tag{6.14c}$$

Four equations, one for each four node, must be added (equations (5.24c) previously defined in section 5) to the system defined (6.11-6.14).

The model parameters defined in the model equations (6.11-6.14) are as follows:

· axial Peclet number

$$Pe_j=\frac{v_j L_j}{D_{L_j}} \tag{6.15a}$$

where v_j is the bed superficial velocity and D_{Lj} is the axial dispersion coefficient.

· intraparticle Peclet number

$$\lambda_p=v_0\frac{\ell}{D_{pe}}=v_0\frac{R_p}{3D_{pe}} \tag{6.15b}$$

as defined in equation (6.3).

· Ratio between solid and fluid volume fraction

$$\frac{1-\varepsilon}{\varepsilon} \tag{6.15c}$$

· Ratio between fluid and solid velocities

$$\gamma_j=\frac{v_j}{u_s} \tag{6.15d}$$

where v_j is the interstitial fluid velocity in section j and u_s the solid interstitial velocity.

· Biot number

$$\tilde{B}i_m=\frac{k_f R_p}{\tilde{D}_{pe}} \tag{6.15e}$$

where k_f if the film mass transfer coefficient, R_p is the particle radius and $\tilde{D}_{pe}$ is the augmented effective diffusivity by intraparticle convection.

· Liquid space time

$$\tau_j=\frac{L_j}{v_j} \tag{6.15f}$$

where L_j is the length of section j.

· Mass transport coefficient in the pores

$$\tilde{k}_p=\frac{15\tilde{D}_{pe}}{R_p^2} \tag{6.15g}$$

Before running the optimisation problem, a simulation of the two proteins separation was performed. The system defined, (6.11-6.15), was solved numerically by using the solver COLNEW (Bader and Ascher, 1987). No initial guess to the solution is provided and the solver COLNEW generates the initial mesh and controls it during the numerical resolution, with 3 collocation points in each element. The error tolerance was set at 10^{-8}. When the global error (defined as in the previous sections) is less than 0.05%, maximum error defined by the user, the steady-state solution is achieved. The model parameters and operating conditions used are described in Table 6.1 and Table 6.2(a). In Table 6.2(b), the equivalence between the TMB and SMB flowrates is shown. With the steady-state model (6.11-6.15), the influence of the intraparticle convection can be studied by changing the value of the intraparticle Peclet number, λ_p. Thus, the different values obtained for the enhancement of diffusivity by convection, $\tilde{D}_{pe}$, the values of Biot number, $\tilde{Bi}_m$, and the mass transport coefficients in the pores, $\tilde{k}_p$, are replaced by the model parameters D_{pe}, Bi_m and k_p respectively, as described in Table 6.2(c).

Figure 6.3, shows the simulation profiles for the two different situations to study the influence of the intraparticle convection in the SMB unit. Table 6.3 describes the different concentrations values obtained in the four nodes, extract, feed, raffinate and eluent, for the two components, and the final extract and raffinate purity obtained.

No significant differences between the two situations are obtained. The obtained profiles for the two components along the four sections are basically the same. The full squares and diamonds correspond to the case of no intraparticle convection, λ_p=0, for myoglobin and BSA, respectively, and white squares and diamonds for the case considering the intraparticle convection. Observing the different model parameters obtained for the two situations, with and without intraparticle convection, Table 6.2(a) and (c), they are of the same order. Only the value of $\tilde{D}_{pe}$ for the BSA component in the section I, is higher comparing to the others and, consequently, the corresponding values of $\tilde{k}_p$ and $\tilde{Bi}_m$. In fact, is on section I that is evident a difference between the two profiles. Nevertheless this behaviour in section I, the concentrations obtained, for the two components, on the extract are the same, considering or not the intraparticle convection (Table 6.3).

Table 6.2 *Model parameters and operating conditions for the SMB/TMB system defined* ***(a)*** *with intraparticle convection, $\lambda_p \neq 0$;* ***(b)*** *equivalence between TMB and SMB flow-rates;* ***(c)*** *model parameters for $\lambda_p = 0$.*

(a)

Model parameters								
Section	BSA				Myo			
	$\tilde{B}i_m$	$\tilde{k}_p$ (s^{-1})	$\tilde{D}_{pe}$ (cm^2/s)	λ_p	$\tilde{B}i_m$	$\tilde{k}_p$ (s^{-1})	$\tilde{D}_{pe}$ (cm^2/s)	λ_p
I	0.40	4.87	3.26×10^{-7}	12.88	0.33	5.87	3.92×10^{-7}	4.24
II	0.85	2.31	1.54×10^{-7}	5.39	0.51	3.79	2.53×10^{-7}	1.78
III	0.60	3.24	2.16×10^{-7}	8.14	0.44	4.46	2.97×10^{-7}	2.68
IV	0.99	1.98	1.32×10^{-7}	4.37	0.54	3.59	2.40×10^{-7}	1.44

$Pe = 2500$	$\varepsilon_p = 0.5$	$K_{Myo} = 1.59$	$k_{f\,Myo} = 0.0078\ cm/min$
$d_p = 20\mu m$	$\varepsilon = 0.3$	$K_{BSA} = 4.02$	$k_{f\,BSA} = 0.0078\ cm/min$

SMB operating conditions		TMB operating conditions	
$T = 25\ ^oC$	$t^* = 612\ s$	$\gamma_I = 12.56$	$\gamma_{II} = 5.3$
$C_F = 10\ g/l$ each		$\gamma_{III} = 8$	$\gamma_{IV} = 4.3$
$Q_{Rec} = 24\ ml/min$	$Q_E = 37.84\ ml/min$	Solid flow-rate = 4.53 ml/min	
	$Q_X = 33.31\ ml/min$	**Columns**	
	$Q_F = 12.23\ ml/min$	$d_c = 2.6\ cm$	$L_c = 29\ cm$
	$Q_R = 16.76\ ml/min$	Configuration: 2-2-2-2	

(b)

Section	TMB		SMB	
	Q_j (ml/min)	γ_j	Q^*_j (ml/min)	γ^*_j
I	57.31	12.66	61.84	13.66
II	24.00	5.30	28.53	6.30
III	36.23	8.00	40.76	9.00
IV	19.47	4.30	24.00	5.30
t^* (min)	---		10.2	

(c)

Model parameters
$Bi_{mBSA} = 1.86$
$Bi_{mMyo} = 0.614$
$k_{pBSA} = 1.046\ s^{-1}$
$k_{pMyo} = 3.209\ s^{-1}$
$D_{peBSA} = 0.70\times10^{-7}\ cm^2/s$
$D_{peMyo} = 2.12\times10^{-7}\ cm^2/s$

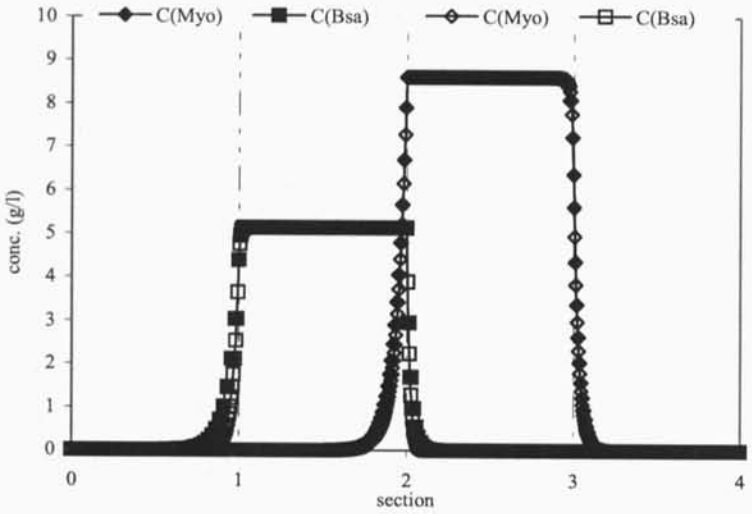

Figure 6.3 *Steady-state concentration profiles for a simulated moving bed separation under conditions summarised in Table 6.2, full dots for the case without intraparticle convection and white dots for the case with intraparticle convection.*

Table 6.3. *TMB concentrations values obtained for the two components in the four nodes without or with intraparticle convection, under the conditions described in Table 6.1 and Table 6.2.*

Conc. (g/l)	*With intraparticle convection*		*Without intraparticle convection*	
	Myo	*BSA*	*Myo*	*BSA*
Extract	6.67×10^{-7}	3.71	1.31×10^{-7}	3.71
Feed	8.64	6.70	8.64	6.72
Raffinate	7.22	7.57×10^{-11}	7.21	4.13×10^{-6}
Eluent	2.69×10^{-10}	2.80×10^{-11}	6.07×10^{-12}	1.47×10^{-6}
Performance Purity (%)	100.0	100.0	99.9	100
Productivity (g/hr l)	8.50	8.48	8.50	8.48

6.2.1 γ_{II} - γ_{III} plane analysis

Based on the linear equilibrium parameters, Table 6.2, and on equilibrium theory, described in section 2 the region of complete separation for the SMB unit can be defined in a γ_{II} - γ_{III} plane.

In the case of linear isotherms (Ruthven and Ching, 1989) and knowing that the component more retained is collected in the extract, BSA, while the less retained component, Myo, is collected in the raffinate,

$$\gamma_I > \frac{1-\varepsilon}{\varepsilon}\left(K_{BSA}+\varepsilon_p\right) \tag{6.16a}$$

$$\frac{1-\varepsilon}{\varepsilon}\left(K_{Myo}+\varepsilon_p\right) < \gamma_{II} < \gamma_{III} < \frac{1-\varepsilon}{\varepsilon}\left(K_{BSA}+\varepsilon_p\right) \tag{6.16b}$$

$$\gamma_{IV} < \frac{1-\varepsilon}{\varepsilon}\left(K_{Myo}+\varepsilon_p\right) \tag{6.16c}$$

Knowing that is on the two central sections that the separation is carried on, a two dimensional graphic can be performed defining the triangle region of complete separation.

For the system in study in this work, (6.16b) is given by

$$4.877 < \gamma_{II} < \gamma_{III} < 10.547 \tag{6.17}$$

The different values of γ_j obtained for the system in study are listed in Table 6.2, γ_I =12.56, γ_{II} =5.3, γ_{III} =8.0, γ_{IV} =4.3. Comparing these values with the previous constraints (6.16) it is possible to observe that they are all verified, γ_I >10.547 and γ_{IV} < 4.877.

The region of complete separation in the γ_{II} - γ_{III} plane for the BSA/Myo separation system and a feed concentration of C_F = 10 *g/l* for each component, is shown in Figure 6.4. The thick line represents the limits of the region of complete separation from the equilibrium theory, (6.16), while the thin lines represent regions for lower purities obtained from the model (6.11-6.14). As expected, the region of complete separation increases as the purities decrease and at 96% purity the limits almost coincides with the theoretical one. The circle represents the location of the system in study under conditions summarised in Tables 6.1 and 6.2. The vertex of each triangle-shaped region corresponds to the optimal operating point in terms of productivity and solvent consumption. So, the productivity can be increased, maintaining the purities, by working much closer to the vertex of the triangle (diamond point). This point was obtained under conditions summarised in Table 6.4, keeping constant the others conditions. Since the steady-state concentrations and the parameters performance obtained for the case with and without intraparticle convection are very similar, only the results for the case of $\lambda_p \neq 0$ are listed. The square point, represents the location of the operating conditions calculated using the detailed model and the optimisation routine (see description in the next section).

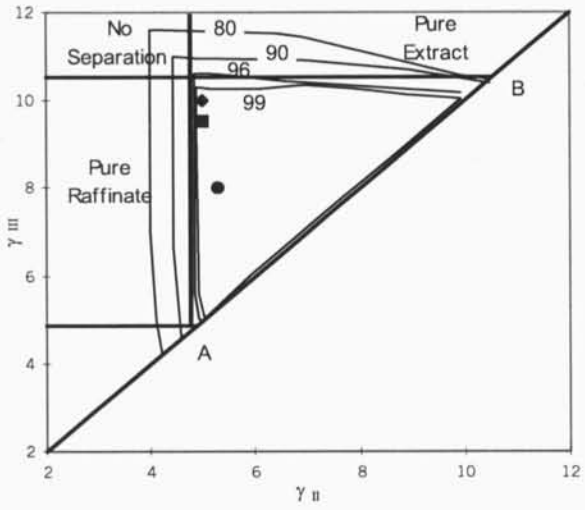

Figure 6.4 *TMB/SMB performance for the proteins separation in the γ_{II} - γ_{III} plane. Four regions are defined in terms of purity of the two components, no separation, pure extract, pure raffinate and complete separation triangle region. The circle, (●), represents the location of the system under conditions summarised in Tables 6.1 and 6.2, the diamond, (♦), represents the location of the system with higher productivity, and the square, (▪), represents the location of the optimal operating condition for η=0.8.*

Table 6.4. *Some operating conditions for the SMB and the concentrations values obtained for the two components in the four nodes for $\lambda_p \neq 0$, (♦) point on Figure 6.4.*

Conc. (g/l)	*Myo*	*BSA*		
Extract	3.15×10^{-3}	6.58	$\gamma_{II} = 5.0$	$\gamma_{III} = 10.0$
Feed	9.75	9.48	$Q_I^{SMB} = 61.84$ *ml/min*	$Q_{Rec} = 24.00$ *ml/min*
Raffinate	8.68	2.08×10^{-3}	$Q_{II}^{SMB} = 27.17$ *ml/ min*	$Q_E = 37.84$ *ml/min*
Eluent	5.41×10^{-10}	1.23×10^{-10}	$Q_{III}^{SMB} = 49.81$ *ml/ min*	$Q_X = 34.67$ *ml/min*
Performance Purity (%)	100.0	100.0	$Q_{IV}^{SMB} = 24.00$ *ml/ min*	$Q_F = 22.64$ *ml/min*
Productivity (g/hr l)	15.7	15.7		$Q_R = 25.81$ *ml/min*
	$\lambda_{pI} = 4.23$ $\lambda_{pII} = 1.68$ $\lambda_{pIII} = 3.35$ $\lambda_{pIV} = 1.44$	$\lambda_{pI} = 12.88$ $\lambda_{pII} = 5.09$ $\lambda_{pIII} = 10.17$ $\lambda_{pIV} = 4.37$		

6.2.2 The optimisation problem and procedure

With the specific considerations, to be described in this section, a combination of the Biressi *et al.*, (2000) and Azevedo and Rodrigues, (2001) works, the design and optimisation of a simulated moving bed unit applied to the proteins separation, was performed. It is necessary the knowledge of the equilibrium isotherms, the Van Deemter equation and a correlation for pressure drop. The results obtained in the optimisation have been compared with the predicted results by the equilibrium theory. The observed deviations have been put in evidence and discussed.

The SMB operating conditions to be fulfilled must follow some characteristics. The optimisation procedure uses the following information:

- adsorption equilibrium isotherms, that define the separation region and defines the adequate γ_j values, see section 2;
- Van Deemter equation for the height equivalent to a theoretical plate $HETP_j$; (6.4), where u_j is the superficial velocity in the j-th section, and the constants A, B, C and Φ depending on physical properties; and
- correlation for estimating pressure drop by using the Kozeny-Kárman equation, (6.8).

The last two equations are used in addition to the model equation, (6.11-6.14), that describes the steady-state SMB/TMB intraparticle diffusion/convection model.

The parameter η is defined as the dimensionless distance of a certain (γ_{II}, γ_{III}) pair to the optimum point given by the equilibrium theory $\left(\gamma_{II}^{eq},\ \gamma_{III}^{eq}\right)$. In other words

$$\eta = \frac{\gamma_{III} - \gamma_{II}}{\gamma_{III}^{eq} - \gamma_{II}^{eq}} = \frac{\gamma_{III} - \gamma_{II}}{\nu\left(K_{BSA} - K_{myo}\right)} \tag{6.18}$$

η=1, corresponds to the distance of the vertex of the complete region predicted by the equilibrium theory.

In order to begin the optimisation procedure some of the parameters must be fixed, the distribution of columns in each section, feed concentration, and the SMB fluid flowrate in section I. By assuming a value to the SMB fluid flowrate in section I, $Q_I^{SMB} = 10^3$ *ml/min*, all the other flowrates and column cross-section are calculated by using this value. Since the pressure drop is proportional to the throughput of the plant, the productivity will be the highest when pressure drop is the highest possible in the plant. Therefore, we set the pressure drop in section I, which is where the fluid velocity is maximum, equal to the allowable upper limit, hence fixing the value of the product $u_I L$. From the adsorption isotherms it is possible to predict the values of γ_I and γ_{IV}, assuming equilibrium, which guarantee the proper behaviour

of section I and IV, i.e., complete regeneration of the eluent and the adsorbent, respectively, in the most general case of non linear adsorption isotherms. Proper safety margins β, can be included.

The productivity, *Pr* in *gr/hr l*, is defined as the ratio between the mass flowrate of the product in the extract or raffinate, and the stationary-phase volume, as previously defined in section 2,

$$Pr_{Ext} = \frac{C_{Ext}^{BSA} Q_X}{V_s}, \qquad Pr_{Raf} = \frac{C_{Raf}^{Myo} Q_R}{V_s} \tag{6.19}$$

The algorithm, described in Figure 6.5, illustrates the optimisation strategy adopted, with the convergence loops considered. The main loop is on η. For each value of η, a low value in the begin of the simulation study is considered, a low initial value of the column length, L_c, is chosen. Inside the L_c loop, two loops are considered where the values of γ_{II} and γ_{III} are estimated. If both purities are not satisfied, the column length is increased until the condition is verified. In this loop, for each section, different values of the augmented effective diffusivity $\tilde{D}_{pe}$ (intraparticle convection) are also calculated. With this is possible to study the influence of the intraparticle convection on the process system performance.

6.2.3 Design results and discussion

Analysis of the influence of the optimal parameters on the system purity requirements was performed.

Several computations were performed for several values of η, with and without considering the intraparticle convection term, leading to the plot shown in Figure 6.6 and results summarized in Table 6.5. All the values were obtained for purities (extract and raffinate) equal to 99% for the BSA/Myo separation system under conditions described in Tables 6.1 and 6.2. Considering the intraparticle convection in the system in study, the obtained values of productivity are higher than the ones obtained without the intraparticle convection, for both outlets. However, for both situations, the optimal operating condition is readily obtained at the same value of η=0.8, where the maximum of productivity, for both outlets, is achieved. The column length is also represented in the same figure. L_c varies slowly for η values lower than the optimal one and rapidly increases for higher values. For the case of no intraparticle convection, higher values of column length and lower productivities are found, related to the case of intraparticle convection. When the maximum value of productivity is obtained, with purity requirement equal to 99%, two optimal design parameters are identified: L_c = 9.0 cm

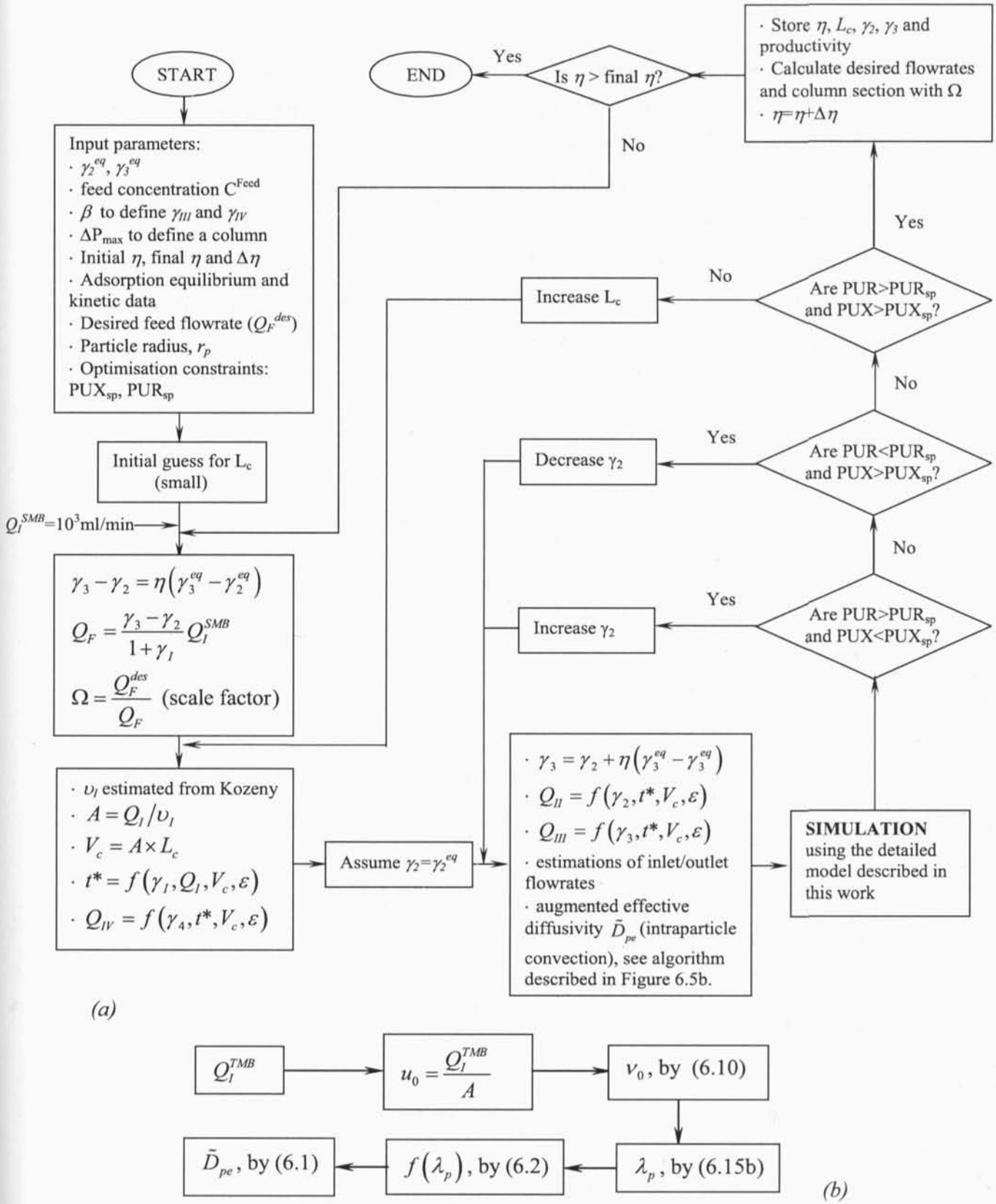

Figure 6.5. ***(a)*** *Diagram of the optimisation algorithm;* ***(b)*** *procedure to obtain the value of* $\tilde{D}_{pe}$*, when intraparticle convection is considered on the model.*

and η=0.8, model with intraparticle convection, and L_c= 10.5 cm and η=0.8, model without intraparticle convection, for both outlets. Increasing the column directly the volume increases, consequently lower productivities without intraparticle convection system. The differences obtained in SMB operating conditions in the two cases are only on the flowrates that directly or indirectly depend on the values of γ_{II} and γ_{III}. The switching time for λ_p=0 is higher since the L_c is lower than for the case of $\lambda_p \neq 0$ (Table 6.5). The optimal point in the γ_{II} - γ_{III} plane is illustrated in Figure 6.4 as the square point with coordinates (4.98; 9.51). The point obtained for λ_p=0 is not shown since the obtained values are very similar to the previous one (4.93; 9.46).

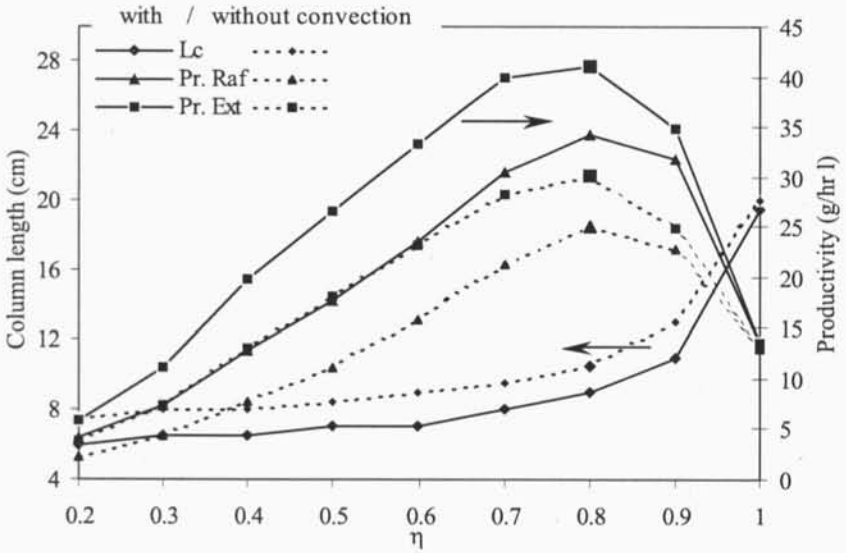

Figure 6.6 *Productivity and optimal column length as a function of η with purity equal to 99% for the system described in Tables 6.1 and 6.2. Straight and dash lines correspond to obtained simulation values with and without intraparticle convection, respectively. The maximum corresponds to the optimal point (▲ for raffinate and ▪ for extract).*

6.2.3.1 Effect of purity requirements

It is known that highest are the purity requirements more critical the separation performance becomes. Figure 6.7 shows the influence of the purities on the productivities and column length. As expected, productivities decrease as the required purity increases. The column length increases when the required purity increases. On the other hand the optimal value of η increases when purity decreases, as shown in Figure 6.8. This behaviour is expected since by

decreasing the purity requirement, the area of complete separation predicted by the equilibrium theory increases, increasing the η value.

Table 6.5. *TMB concentrations values obtained for the two components in the four nodes and the flowrates with or without intraparticle convection through the optimisation procedure for* $\eta=0.8$.

	With intraparticle convection		*Without intraparticle convection*	
Conc. (g/l)	*Myo*	*BSA*	*Myo*	*BSA*
Extract	0.048	4.72	0.046	4.67
Feed	7.67	7.22	7.83	7.18
Raffinate	6.51	0.049	6.61	0.059
Eluent	0.000087	0.00060	0.21×10^{-6}	0.0039
Purity (%)	99.2	99.0	99.1	99.1
	λ_{pI}=4.77 λ_{pII}=1.89 λ_{pIII}=3.60 λ_{pIV}=1.53	λ_{pI}=14.48 λ_{pII}=5.75 λ_{pIII}=10.94 λ_{pIV}=4.65		
	Q_{Rec} = 371 *ml/min* Q_E = 629 *ml/min* Q_X = 562 *ml/min* Q_F = 266 *ml/min* Q_R = 333 *ml/min* t^*=2.82 *min* γ_I = 12.66 γ_{II} = 4.98 γ_{III} = 9.51 γ_{IV} = 4.06 (square (▪) in Figure 6.4)		Q_{Rec} = 371 *ml/min* Q_E = 629 *ml/min* Q_X = 566 *ml/min* Q_F = 266 *ml/min* Q_R = 329 *ml/min* t^*=3.83 *min* γ_I = 12.66 γ_{II} = 4.93 γ_{III} = 9.46 γ_{IV} = 4.06	

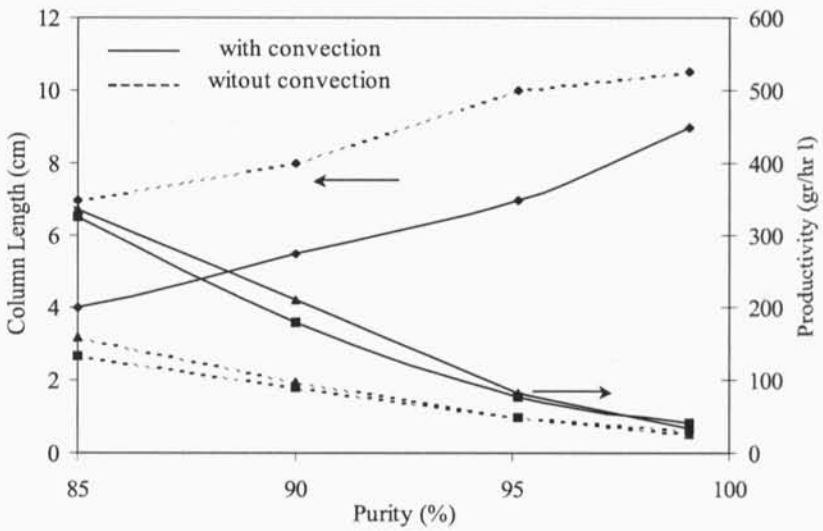

Figure 6.7 *Optimal productivity (▲ for raffinate and ▪ for extract) and column length (♦) for various purities specifications for the system described in Table 6.1 and 6.2.*

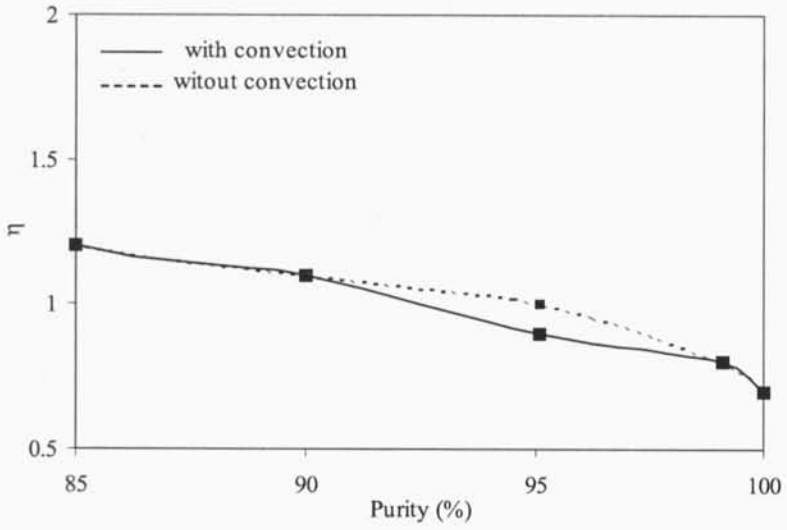

Figure 6.8 *Values of η leading to productivity for various purities specifications for the system described in Table 6.1 and 6.2.*

6.2.3.2 Effect of particle size

Several optimisation calculations were performed to study the influence of the particle size on the system in study. Four different particle diameter are considered: d_p= 20, 40, 80 and 160 μm. In all cases the corresponding optimal values γ_{II} and γ_{III} and η estimated for the same purity equal to 99%, are the same. Figures 6.9 and 6.10 show the column length and productivity, respectively, as a function of the particle radius for a purity of 99%. The effect of the intraparticle convection can also be analysed. The column length increases and the corresponding productivity decreases when the particle size increases, with or without considering intraparticle convection. However, the column length needed for a specific particle radius, by considering the intraparticle convection influence is slightly lower than when convection is absent. Opposite behaviour has the productivity for the same values of particle radius. The obtained values of the enhancement factor, $1/f(\lambda_p)$, of diffusivity by convection, under the conditions described in Table 6.1 and Table 6.2 for both proteins, is shown in Table 6.6. With these values we can observe how significant is the influence of the intraparticle convection on the SMB/TMB process. The influence becomes more significant as the enhancement factor increases (6.1).

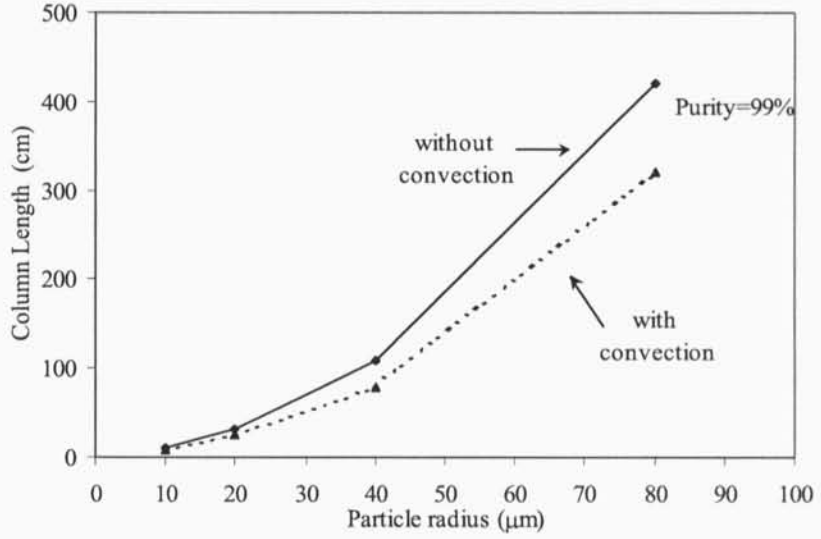

Figure 6.9 *Column length as a function of particle radius for a purity specification of 99%, for the system described in Table 6.1 and 6.2.*

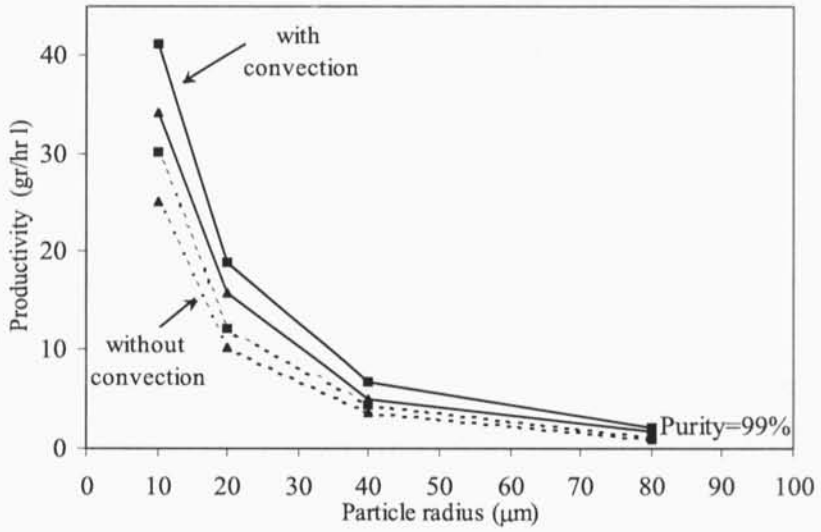

Figure 6.10 *Productivity as a function of particle radius for a purity specification of 99%, (▲ for raffinate and ▪ for extract), for the system described in Table 6.1 and 6.2.*

Table 6.6. *Enhancement factor, $1/f(\lambda_p)$, of diffusivity by convection, under the conditions described in Table 6.1 and Table 6.2.*

Protein	*Section I*	*Section II*	*Section III*	*Section IV*
MYO	2.01	1.22	1.66	1.15
BSA	5.18	2.32	4.01	1.97

The region of complete separation was also estimated for a particle radius of $20\mu m$ for purities specification of 99%, under the same operating conditions summarized in Table 6.1 and 6.2. The obtained results are shown in Figure 6.11. Increasing the particle radius, the triangle-shaped region of complete separation decreases. However, the vertex that corresponds to the optimum operating point in terms of productivity, is almost the same, as can be seen by the optimal points obtained for different values of η, for the three particle radius considered. For a particle radius of 40 μm and for purity specification of 99%, the obtained region of complete separation was very small not being represented. The arrow shows the direction of increasing of the η parameter.

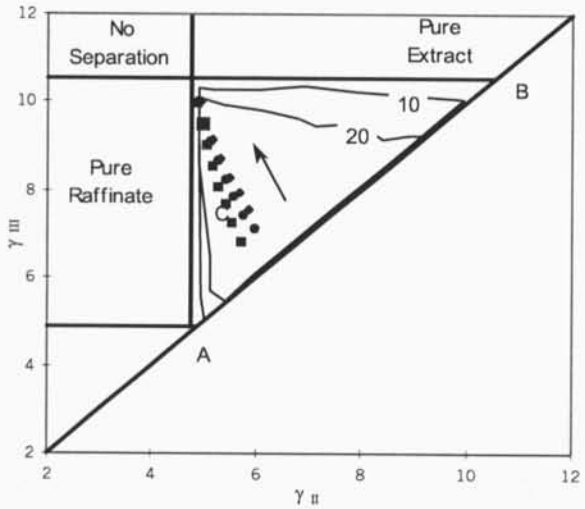

Figure 6.11 *Triangle- shaped complete separation region obtained for R_p=10 and 20μm, thin lines, for the system described in Table 6.1 and 6.2. The several points correspond to the simulation point for several values of η (♦ R_p=10μm, • R_p=20μm, ■ R_p=40μm). The arrow shows the way of η increasing.*

6.3 Equilibrium stage model

Using the model described previously, LDF model for porous particle, for the TMB system,

$$\varepsilon D_{L_j}\frac{\partial^2 c_{ij}}{\partial z^2}-\varepsilon v_j\frac{\partial c_{ij}}{\partial z}+(1-\varepsilon)u_s\left[\frac{\partial\langle q\rangle_{ij}}{\partial z}+\varepsilon_p\frac{\partial\langle c_p\rangle_{ij}}{\partial z}\right]= \\ =\varepsilon\frac{\partial c_{ij}}{\partial t}+(1-\varepsilon)\left[\frac{\partial\langle q\rangle_{ij}}{\partial t}+\varepsilon_p\frac{\partial\langle c_p\rangle_{ij}}{\partial t}\right] \tag{6.20}$$

The steady-state solutions of the TMB system can be estimated by solving a different model which requires lower computing time. By cancelling the accumulation terms and neglecting the axial term, considering the unit as a series of several stages connected by the fluid and solid countercurrent flows we obtain the following system,

$$Q_j^{TMB}\left(c_{ij,n-1}-c_{ij,n}\right)+Q_{ST}\left[\left(q_{ij,n+1}-q_{ij,n}\right)+\varepsilon_p\left(c_{ij,n+1}-c_{ij,n}\right)\right]=0 \qquad (6.21)$$

where $c_{ij,n}$ is the fluid concentration of the component i of section j in the stage n ($=L_c/HETP$), $q_{ij,n}$ is the solid concentration of the component i of section j in the stage n, ε_p particle porosity, Q_j^{SMB} and Q_j^{TMB} are the flowrates in section j of the SMB and TMB units, respectively, Q_{ST} is the solid flowrate in the TMB unit and ε is the porosity. The two unit performance, SMB and TMB, achieve the same steady-state separation performance when the following relationships are satisfied and taken into consideration:

$$\begin{aligned} Q_j^{TMB} &= Q_j^{SMB}-\frac{\varepsilon}{(1-\varepsilon)}Q_{ST} \\ Q_{ST} &= (1-\varepsilon)\frac{V}{t^*} \end{aligned} \qquad (6.22)$$

V is the volume of a column, and t^* is the switch time in the SMB unit.

The number of stages in each section corresponds to the number of theoretical plates in the section; the HETP previously defined (6.4), characterises its efficiency. c_{ij} and q_{ij} are related through the isotherm equations. In this work, the isotherm equations considered are linear so (6.21) defines coupled linear algebraic equations that were solved using Gauss elimination algorithm.

Figure 6.12 shows the concentration profiles obtained by using the two models defined, intraparticle diffusion/convection model (6.11-6.14), red lines, and the equilibrium stage model (6.21), black lines, under conditions described in Table 6.1 and 6.2.

The number of theoretical plates, *HETP*, and the number of stages, n, obtained in each of the four sections are summarized in Table 6.7. In all the simulations, only one value of n in each section was used and equal to the maximum of ($L_c/HETP_{\text{Myo}}$, $L_c/HETP_{\text{BSA}}$). With the same error criteria, the number of stages is higher when intraparticle convection is important.

The optimisation procedure, previously described, was also implemented now by using the equilibrium stage model. The same maximum value of productivity, with purity requirement equal to 99% for both outlets, was obtained for the same pair of optimal design parameters: L_c= 9.0 cm and η=0.8. However, this value was also achieved for the case where the intraparticle convection was not included. With the equilibrium stage model higher purities

were achieved. Figure 6.13 shows the concentrations profiles obtained by using the two models defined: (6.11-6.14), red lines, and (6.21), black lines, for the optimal operating condition previously identified.

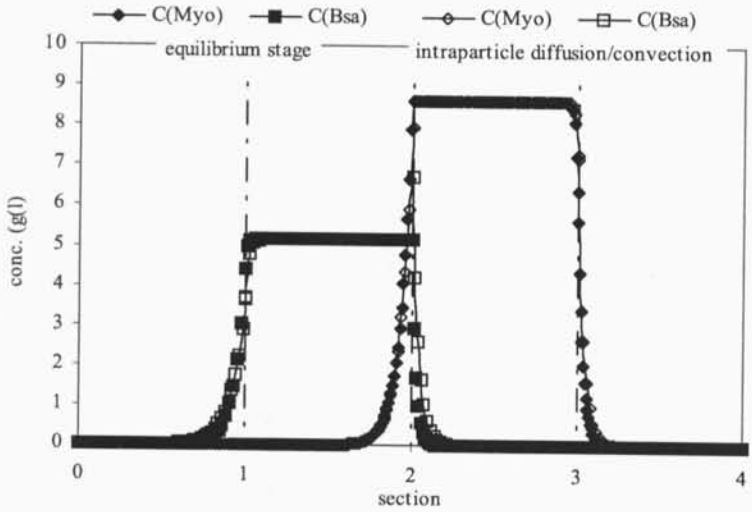

Figure 6.12 *Steady-state concentration profiles for the two models defined: intraparticle diffusion/convection model (6.11-6.14), white dots, and the equilibrium stage model (6.21), full dots, under conditions described in Table 6.1 and 6.2.*

Table 6.7. *Number of theoretical plates HETP, and the number of stages n, in each section, for the model (6.21).*

	Protein	Section I			Section II		
		HETP	λ_p	*n*	*HETP*	λ_p	*n*
With intra particle convection	Myo	0.189	4.24	153	0.131	1.78	221
	BSA	0.281	12.88		0.251	5.39	
Witout intra particle convection	Myo	0.328		88	0.151		191
	BSA	0.122			0.524		
	Protein	Section III			Section IV		
		HETP	λ_p	*n*	*HETP*	λ_p	*n*
With intra particle convection	Myo	0.161	2.70	180	0.115	1.44	251
	BSA	0.268	8.14		0.239	4.37	
Witout intra particle convection	Myo	0.216		133	0.127		227
	BSA	0.779			0.430		

Table 6.8 shows the outlet and inlet concentrations values for the two components obtained for the two models with intraparticle convection. For the case of no intraparticle convection the concentration values obtained in each outlet were very similar, as illustrated in Figure 6.14.

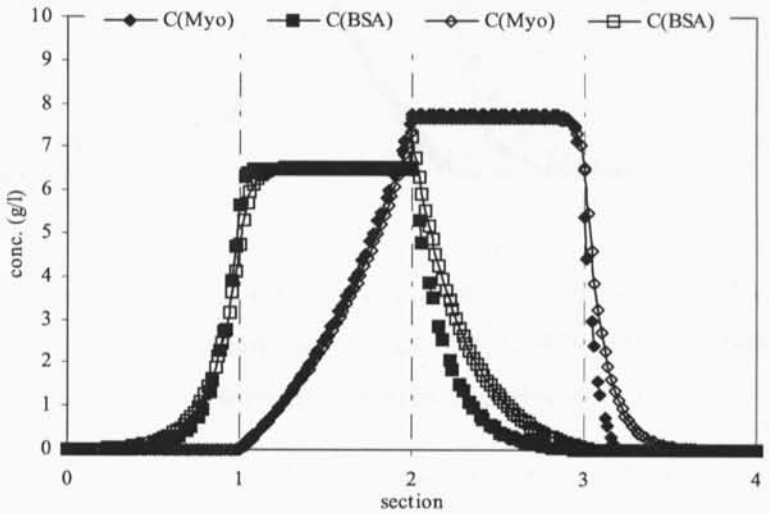

Figure 6.13 *Steady-state concentration profiles for the two models considered: intraparticle diffusion/convection model defined by (6.11-6.14), white dots, and the equilibrium stage model defined by (6.21), full dots, for the optimal conditions described in Table 6.5.*

Table 6.8. *TMB concentrations values obtained for the two components in the four nodes by using the two models, intraparticle diffusion/convection model defined by (6.11-6.14) and the equilibrium stage model defined by (6.21), under the conditions described in Table 6.1 and Table 6.2.*

Conc. (g/l)	*intraparticle diffusion/convection model*		*equilibrium stage model*	
	Myo	*BSA*	*Myo*	*BSA*
Extract	0.048	4.72	0.00	5.66
Feed	7.67	7.22	7.76	6.51
Raffinate	6.51	0.049	5.40	0.0028
Eluent	0.000087	0.00060	0.00	0.00031
Performance Purity (%)	99.2	99.0	99.0	99.0

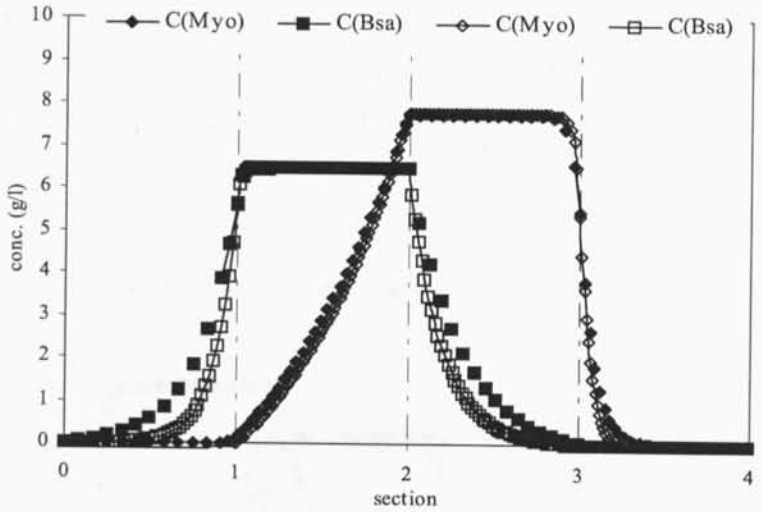

Figure 6.14 *Steady-state concentration profiles for the equilibrium stage model (6.20-6.21), with (white dots) and without (full dots) the intraparticle convection term, for the optimal operating conditions described in Table 6.5.*

6.4 Conclusions

This work illustrates the application of the simulated moving bed technology to the separation of proteins by considering perfusive particles, namely for the BSA/Myoglobin separation. The TMB steady-state model described takes into account the new LDF model approximation, linear equilibrium isotherm, film diffusion, axial dispersion for fluid flow and intraparticle diffusion/convection. Based on the equilibrium theory, the operating conditions and model parameters were estimated. An analysis of the separation region, on an γ_{II} - γ_{III} plane, was performed taken into account the influence of the intraparticle convection term. The highest productivity was obtained for a given separation constraints on purity and on pressure drop. An optimisation procedure was performed to study the effects on the separation performance of several parameters, such as the particle size and purity requirement. The choice on the optimal SMB operating conditions can be made by taking into account these results balanced with the economic cost that were not included as optimisation variables in this study.

In this example, it was evidenced that intraparticle convection affects the column length needed and the productivity for a specific particle radius of the process, without affecting the purity of the components. It was shown that the intraparticle convection model and the equilibrium stage model are equivalent.

6.5 References

Azevedo, C. S. D., and A. E. Rodrigues, (2001) *Design methodology and operation of a simulated moving bed reactor for the inversion of sucrose and glucose-fructose separation*, Chem. Eng. J. **82**, 95-107.

Bader, G., and U. Ascher, (1987) *A New Basis Implementation for a mixed Order Boundary Value ODE Solver*, SIAM J. Scient. Stat. Comput. **8**, 483.

Biressi, G., O. Ludemann-Hombourger, M. Mazzotti, R. M. Nicoud, M. Morbidelli, (2000) *Design and optimisation of a simulated moving bed unit: role of deviations from equilibrium theory*, J. Chromatogr. A **876**, 3-15.

Carta, G., M. Massaldi, M. Gregory, and D. J. Kirwan, (1992) *Chromatography with permeable supports: theory and comparison with experiments*, Sep. Technol. **4**, 62-72.

Carta, G., and A. E. Rodrigues, (1993) *Diffusion and convection in chromatographic processes using permeable supports with a bidisperse pore structure*, Chem. Eng. Science. **48**, 3927-3935.

Garcia, M. C., M. L. Marina, M. Torre, (2000) *Perfusion Chromatography: an emergent technique for the analysis of food proteins*, J. Chromatogr. A **880**, 169-187.

Leitão, A., and A. E. Rodrigues, (1999) *Modeling and simulation of protein adsorption in permeable chromatographic packings: a double linear driving force model*, Biochemical Engineering Journal **3**, 131-139.

Leitão, A., M. Li, A. E. Rodrigues, (2002) *The role of intraparticle convection in protein adsorption by liquid chromatography using POROS 20 HQ/M particles*, Biochemical Engineering Journal **11**, 33-48.

Rodrigues, A. E., B. J. Ahn, A. Zoulalian, (1982) *Intraparticle-forced convection effect in catalyst diffusivity measurements and reactor design*, AIChE J. **28**, 541.

Rodrigues, A. E., Z. P. Lu, J. M. Loureiro, (1991) *Residence time distribution of inert and linearly adsorbed species in separations engineering*, Chem. Eng. Sci. **46**, 2765.

Rodrigues, A. E., J. C. Lopes, Z. P. Lu, J. M. Loureiro, M. M. Dias, (1992) *Importance of intraparticle convection in the performance of chromatographic processes*, J. Chromatogr. A **590**, 93-100.

Rodrigues, E. A., (1993) *An Extended Van Deemter Equation (Rodrigues Equation) for Performing Chromatographic Processes Using Large-Pore, Permeable Packings*, LC-GC **6**, 20-29.

Rodrigues, E. A., C. Chenou, M. Rendueles de la Vega, (1996) *Protein separation by liquid chromatography using permeable POROS Q/M particles*, Chem. Eng. J. **61**, 191-201.

Rodrigues, E. A., (1997) *Permeable Packings and Perfusion Chromatography in Protein Separation*, J. Chromatogr. B **699**, 47-61.

Ruthven, D. M., and C. B. Ching, (1989) *Counter-Current and Simulated Moving Bed Adsorption Separation Process*, Chem. Engng. Sci. **44**, 1011-1038.

7. Conclusions and suggestions for future work

This work deals with new extensions in the modelling and simulation of Simulated Moving Bed (SMB) and Simulated Moving Bed Reactor (SMBR) processes applied to chiral, sugar and proteins systems.

The simplified LDF approximation for homogeneous particles was first used in the transient and steady-state models. Depending of the way of presentation of the equilibrium isotherm, as a part of the mass balance equations or as an independent algebraic equation, different methods and simulation techniques can be used: PDE solved by using PDECOL, PDAE solved by using OCFE+DASSL, ODE solved by COLNEW, and DAE solved by using COLDAE (software packages available on the internet). This partition becomes more significant for non-linear relationships. The γ_{II} - γ_{III} plane analysis allows the choice of the best operating conditions in order to obtain high productivities.

The LDF approximation for porous particles is then presented and used with the TMB approach and SMB formulation. Both LDF approximations with equivalence relationships predict similar results.

A similar procedure was applied to study a SMBR/TMBR system. In the TMB simpler model, a reaction term, described by a Michaelis-Menten equation, was added. This first model was applied to the sucrose inversion and glucose/fructose separation. An extension to this model was carried out considering not only the reaction in the outer fluid phase but also inside the adsorbent particle. The detailed new TMBR model, taking into account the intraparticle radial

profiles, was developed. Due to the characteristics of the model, a combination of orthogonal collocation on finite element method and the available PDE solver and ODE solver, for the transient and steady-state models, respectively, were used. It was possible to simulate the concentration evolution inside the porous particle, in a specific position of the bed. However, this model requests higher computing efforts being very sensitive to tolerances and numerical parameters modifications. Using the coefficients in the Kim's (1989) LDF formulas, a polynomial approximation is used defining a new LDF model for porous particle with chemical reaction. The use of this new approximation allows the study of the effects of the kinetic constant and the particle size on the SMB performance.

The mass transfer phenomena in SMB process was introduced and used to the SMB process applied to protein separation (BSA/Myoglobin). An optimization procedure was applied to the BSA/Myoglobin separation. Based on the TMB analogy, two equivalents models were presented: the intraparticle diffusion/convection model and the equilibrium stage model. The operating conditions and optimal construction parameters are estimated by considering the maximization of the performance parameters as objective function. It was evidenced that the intraparticle convection affects the column length needed and the productivity for a specific particle radius of the process, without affecting the purity of the components.

In the following paragraphs, some suggestions are made for future research.

- Concerning the modelling of SMB, new models for large-pore particles, with non-linear isotherms applied to the protein separation, such be addressed.
- With respect to the simulation of a SMBR, explore and apply more robust numerical techniques to the detailed new TMBR model developed in this work.
- The methodology of design and optimization may be extended to more complex systems, including reversible reactions, non-linear adsorption equilibrium and large-pore supports. As far as economic factors are concerned, we also suggest the inclusion of cost function as objective function of the presented design/optimization algorithm.
- A 'friendly' user SMB/SMBR package can be developed, predicting not only the final steady-state concentration profiles of the system components but also the optimization and parameter estimation.

A: Source code for the Steady-State TMB model using COLDAE

```
C       Program STMBdae.f
C       Steady-state TMB: dc/dt e dq/dt=0, GL
-> FR Separation
C       LDF - Linear Driving Force Model
C       SECTION BY SECTION
C       PROBLEM DEFINITON IN SUBROUTINE FSUB
C************ INITIALIZATION ***************
      IMPLICIT DOUBLE PRECISION (A-H,O-Z)
      DOUBLE PRECISION ZETA(6),
FSPACE(1449000), TOL(6), Z(6), Y(2)
      DOUBLE PRECISION LC, LJ,BETA
      INTEGER M(4), IPAR(12), ISPACE(39025),
LTOL(6)
      DIMENSION
Q(4),V(4),R(4),Q1(4),Q2(4),C1(4),C2(4),C10(4)
,C20(4)
C
      COMMON /FCAL1/EP,PE,ALF
      COMMON /FCAL2/RF1,RF31,RF32
      COMMON /FCAL3/RR,AKFR,AKGL
      COMMON /FCAL5/CONS1,CONS2,CONS3,CONS4
C
C       SUBROUTINES DEFINITION
      EXTERNAL FSUB,DFSUB,GSUB,DGSUB,GETTIM
C
      CHARACTER*9 FR
      CHARACTER TAB
      TAB=CHAR(9)
C
C       INPUT - MODEL PARAMETERS:
      OPEN
(UNIT=12,FILE='DATTMB',STATUS='OLD')
C                       SMB FLOWRATES (ML/MIN):
C       RECYCLING, ELUENT, EXTRACT, FEED,
RAFFINATE
      READ(12,*) QR,QEL,QEX,QFE,QRA
C                       S.TIME (s), FEED CONC.
(g/l), PARAMETER β:
      READ(12,*) RP,CAFE,BETA
C       PARAMETERS ( ε ; PE ; K ):
      READ(12,*) EP,PE,AK
C       EQUILIBRIUM CONSTANTS (KFR/FGL,
MORE/LESS RETAINED)
      READ(12,*) AKFR,AKGL
C       COLUNS ( DC (cm) ; LC(cm) ; NCS ):
      READ(12,*) DC,LC,NCS
      CLOSE (12)
C
C       DEFINITION OUTPUT FILE RESULTS NAME
C       NRP=100.D0*QEX
C       NRP=INT(RP)
C       NRP=NCS*1000.D0+NRP+BETA*1000000.D0

NRP=QEX*100.D0+QFE*100000.D0+AK*1000000.D0
      ILETRAS=1
      IDIGITOS=7
      FR(1:ILETRAS+1)='J'
C
      DO 500 I=1,IDIGITOS
        NCHAR=NRP/10**(IDIGITOS-I)
        NRP=NRP-NCHAR*10**(IDIGITOS-I)
        FR(ILETRAS+I:ILETRAS+I+1)=CHAR(48+NCHA
R)
  500 CONTINUE
C
C       OUTPUT:
      OPEN(UNIT=6,FILE=FR)
      CALL GETTIM (IHR,IMIN,ISEC,I100TH)
      WRITE(6,9002)IHR,IMIN,ISEC,I100TH
 9002
FORMAT(I2,':',I2.2,':'I2.2,':',I2.2,'',A,'m')
      WRITE(6,101)AKFR,AKGL,CAFE
  101 FORMAT(/2X,17HTMB FRU/GLU:
KFR=,F5.3,2X,6H  KGL=,F5.3,2X,
     *                4H  C=,F5.1,4H G/L/)
      WRITE(6,117)
  117 FORMAT(/2X,35HCASE OF LINEAR ADSORPTION
ISOTHERMS)
C
C       COLUNS, SMB:
      AC=DC*DC*3.141592654D0/4.D0
      VC=AC*LC
      LJ=FLOAT(NCS)*LC
      VSP=4.D0*FLOAT(NCS)*VC*(1.D0-EP)
      WRITE(6,102)
  102 FORMAT(2X,8HCOLUMNS:)
      WRITE(6,103) NCS,DC,LC,AC,LJ,VC,BETA
  103 FORMAT(2X,32HNUMBER OF COLUMNS PER
SECTION : ,I1/
```

```
     *       2X,5HDC = ,F6.4,4H CM ,6X,5HLC =
,F7.4,3H CM/
     *       2X,5HAC = ,F6.4,4H CM2,6X,5HLJ =
,F7.4,3H CM/
     *       2X,5HVC = ,F6.3,4H CM3,6X,5HBE =
,F6.4/)
C
C       SMB FLOWRATES (ml/min):
      Q(4)=QR
      Q(1)=QR+QEL
      Q(2)=QR+QEL-QEX
      Q(3)=QR+QEL-QEX+QFE
      WRITE(6,104)
  104 FORMAT(2X,4HSMB:)
      WRITE(6,105) QR,RP,QEL,Q(1),QEX,Q(2),
     *             QFE,Q(3),QRA,Q(4)
  105 FORMAT(2X,5HQR = ,F5.2,7H
ML/MIN,4X,5HRP = ,F6.2,2H S/
     *       2X,5HQEL =,F5.2,7H
ML/MIN,4X,5HQ1 = ,F6.3,7H ML/MIN/
     *       2X,5HQEX =,F5.2,7H
ML/MIN,4X,5HQ2 = ,F6.3,7H ML/MIN/
     *       2X,5HQFE =,F5.2,7H
ML/MIN,4X,5HQ3 = ,F6.3,7H ML/MIN/
     *       2X,5HQRA =,F5.2,7H
ML/MIN,4X,5HQ4 = ,F6.3,7H ML/MIN/)
C
C       FLOWRATES (ml/min), VELOCITIES (cm/s)
C       SOLID VELOCITY (cm/s)
C       RATIO FLUID/SOLID VELOC. TMB SECTION:
      QST=EP*VC/RP*60.D0
      AL=EP*AC*60.D0
      US=LC/RP
      DO 2 J=1,4
        Q(J)=Q(J)-QST
        V(J)=Q(J)/AL
        R(J)=V(J)/US
    2 CONTINUE
C
      WRITE(6,106)
  106 FORMAT(2X,4HTMB:)
      WRITE(6,107) QST,US
  107 FORMAT(2X,6HQST = ,F6.3,7H
ML/MIN,3X,5HUS = ,F6.4,5H CM/S)
      WRITE(6,108) (J,Q(J),J,V(J),J,R(J),
J=1,4)
  108 FORMAT(4(2X,1HQ,I1,3H = ,F6.3,7H
ML/MIN,3X,1HV,I1,3H = ,F6.4,
     *       5H CM/S,3X,1HR,I1,3H = ,F6.4/))
C
C       OTHERS MODEL PARAMETERS:
      ALF=AK*RP*FLOAT(NCS)
      RF1=Q(4)/Q(1)
      RF31=QFE/Q(3)*CAFE
      RF32=Q(2)/Q(3)
      WRITE(6,109)
  109 FORMAT(2X,17HMODEL PARAMETERS:)
      WRITE(6,110) EP,PE
  110 FORMAT(2X,6HEP  = ,F6.4,6X,5HPE =
,F5.0)
      WRITE(6,111) AK,ALF
  111 FORMAT(2X,5HK  = ,E10.4,4H 1/S,6X,6HALF
= ,E10.4)
      WRITE(6,112) RF1,RF31,RF32
  112 FORMAT(2X,6HRF1 = ,F6.4,6X,7HRF31 =
,F7.4,4X,7HRF32 = ,F6.4)
C
      FEED=QFE*CAFE
C
C       ***** COLDAE PARAMETERS *****
C       NUMBER OF O.D.E.s
      NCOMP=4
C       O.D.E.s ORDER
      M(1)=1
      M(2)=1
      M(3)=2
      M(4)=2
C       NO OF CONSTRAINTS (A.E.s)
      NY=2
C       IPAR()  VALUES; LINEAR PROBLEM
      IPAR(1) = 0
C       COLLOCATION POINTS PER SUBINTERVAL
      IPAR(2) = 4
C       INITIAL UNIFORM MESH OF 50SUBINTERVALS
      IPAR(3) = 50
      IPAR(8) = 0
C       DIMENSION OF REAL WORK ARRAY FSPACE IS
      IPAR(5) = 1449000
C    DIMENSION OF INTEGER WORK ARRAY ISPACE IS
      IPAR(6) = 39025
C  (THESE DIMENSIONS OF  FSPACE  AND  ISPACE
C  ENABLE  COLDAE  TO USE MESHES OF UP TO ...
C    INTERVALS.)
C       PRINT NOT FULL OUTPUT.
      IPAR(7) = 1
C       INITIAL APPROXIMATION IS NOT PROVIDED
      IPAR(9) = 0
C       NOT A REGULAR PROBLEM
      IPAR(10) = 2
C       NO OF FIXED POINTS IN THE MESH
      IPAR(11) = 0
C       INDEX OF THE DAE
      IPAR(12)=1
C       TOLERANCES ON  ALL COMPONENTS
      IPAR(4) = 6
      DO 10 I=1,6
        LTOL(I) = I
   10   TOL(I) = .1D-9
C
C       INITIAL VALUES
        C1=0.0D0
        C2=0.0D0
        DO 99 I=1,4
          C1(I)=0.0D0
          C2(I)=0.0D0
          Q1(I)=0.0D0
          Q2(I)=0.0D0
          C10(I)=0.0D0
          C20(I)=0.0D0
   99    CONTINUE
C
C       ITERATIONS
      DO 333 JJ=1,40
C
C       FOR EACH SECTION J
        DO 11 J=1,4
          ALEFT = 0.D0
          ARIGHT = 1.D0
C
C       LOCATIONS OF SIDE CONDITIONS
          ZETA(1) = 0.D0
          ZETA(2) = 0.D0
          ZETA(3) = 1.D0
          ZETA(4) = 1.D0
          ZETA(5) = 1.D0
          ZETA(6) = 1.D0
C
C       VARIABLES UPDATE
C       SECTION I
          IF (J.EQ.1) THEN
            CONS1= RF1*C1
            CONS2= RF1*C2
            CONS3=Q1(2)
            CONS4=Q2(2)
          ENDIF
C
C       SECTION II
          IF (J.EQ.2) THEN
            CONS1= C1
            CONS2= C2
            CONS3=Q1(3)
            CONS4=Q2(3)
          ENDIF
C
C       SECTION III
          IF (J.EQ.3) THEN
            CONS1=RF32*C1+RF31
            CONS2=RF32*C2+RF31
            CONS3=Q1(4)
            CONS4=Q2(4)
          ENDIF
C
C       SECTION IV
          IF (J.EQ.4) THEN
```

```
          CONS1=C1
          CONS2=C2
          CONS3=Q1(1)
          CONS4=Q2(1)
        ENDIF
C
        RR=R(J)
C
C       ****** CALL  COLDAE ******
        CALL COLDAE (NCOMP, NY, M, ALEFT,
ARIGHT, ZETA, IPAR, LTOL, TOL,
     *   DUMMY, ISPACE, FSPACE, IFLAG, FSUB,
DFSUB, GSUB, DGSUB, DUMMY)
C
C     CHECK FOR CONVERGENCE AND PROBLEMS
C       IF(IFLAG.NE.1) THEN
C         WRITE(6,401)IFLAG
C  401  FORMAT(//1X,'THERE IS A PROBLEM
IDENTIFIED BY COLDAE. IFLAG=',
C     *                  1X,I3)
C         STOP
C       ELSE
C
C     PRINT THE OBTAINED APPROXIMATE SOLUTION
AT POINTS X= 0,.05, ...,
        X = 0.D0
        WRITE(6,131)
  131   FORMAT(46H   X   C(G)    C(F)    PG
PF     GG     GF/)
 132    FORMAT (I2,7D15.5)
C
C       *** CALL SUBROUTINE APPSLN ***
        DO 555 III=1,51
          CALL APPSLN (X,Z,Y,FSPACE,ISPACE)
C
C       ** P, GG E DE GF  ESTIMATION **
          IF (Z(3).EQ.0) THEN
            P=0.D0
            ELSE
            P=100.D0*Z(3)/(Z(3)+Z(5))
          ENDIF
          IF (Z(1).EQ.0)THEN
            GG=0.D0
          ELSE
            GG=EP/(1-EP)*RR*Z(3)/Z(1)
          ENDIF
          IF (Z(2).EQ.0.D0)THEN
           GF=0.D0
          ELSE
           GF=EP/(1-EP)*RR*Z(5)/Z(2)
          ENDIF
        IF (JJ.EQ.40)THEN
         WRITE(6,132)
J,X,Z(3),Z(5),P,(100.D0-P),GG,GF
        ENDIF
C
C       CHANGING VARIABLES
          IF (III.EQ.51) THEN
            C1=Z(3)
            C2=Z(5)
          ENDIF
          IF (III.EQ.1) THEN
            Q1(J)=Z(1)
            Q2(J)=Z(2)
          ENDIF
          X = X + .020D0
  555   CONTINUE
        ER1=DABS(C1(1)*QEX+C1(3)*QRA-
FEED)/FEED
        ER2=DABS(C2(1)*QEX+C2(3)*QRA-
FEED)/FEED
        ER3=DABS(C1(1)-
C10(1))/DABS(C1(1))+DABS(C2(1)-
C20(1))/DABS(C2(1))
        ER4=DABS(C1(3)-
C10(3))/DABS(C1(3))+DABS(C2(3)-
C20(1))/DABS(C2(3))
        ER=ER1+ER2+ER3+ER4
C       ENDIF
C
C       PU, RE, CON. AND PROD. ESTIMATION
          IF
((JJ.EQ.40).OR.(ER.LE.0.001D0))THEN
            IF (J.EQ.1)THEN
              PUX=100.D0*C2(1)/(C1(1)+C2(1))
               RCX=100.D0*QEX*C2(1)/FEED
               SCX=(QEL+QFE)/QEX/C2(1)
               PRX=60.D0*QEX*C2(1)/VSP
             ENDIF
             IF (J.EQ.3)THEN

PUR=100.D0*C1(3)/(C1(3)+C2(3))
               RCR=100.D0*QRA*C1(3)/FEED
               SCR=(QEL+QFE)/QRA/C1(3)
               PRR=60.D0*QRA*C1(3)/VSP
             ENDIF
          ENDIF
   11    CONTINUE
C
C       VARIABLES UPDATE
                C10(1)=C1(1)
                C1(1)=0.0D0
                C20(1)=C2(1)
                C2(1)=0.0D0
                C10(3)=C1(3)
                C1(3)=0.0D0
                C20(3)=C2(3)
                C2(3)=0.0D0
C
       IF(ER.LE.0.001D0)GOTO 1000
  333 CONTINUE
C
       CALL GETTIM(IHR,IMIN,ISEC,I100TH)
       WRITE(6,9002)IHR,IMIN,ISEC,I100TH
C
C       END
 1000 CONTINUE
C
      WRITE(6,127) PUX,PUR
  127 FORMAT(2X,8HEXTRACT:,7X,10HRAFFINATE:/
     *       2X,5HPUX =,F5.1,5X,5HPUR
=,F5.1,3X,1H%)
      WRITE(6,128) RCX,RCR,SCX,SCR
  128 FORMAT(2X,5HRCX =,F5.1,5X,5HRCR
=,F5.1,3X,1H%/
     *       2X,5HSCX =,F9.4,3X,5HSCR
=,F9.4,4H L/G)
      WRITE(6,129) PRX,PRR
  129 FORMAT(2X,5HPRX =,F7.4,3X,5HPRR
=,F7.4,8H G/HR LS/)
      WRITE(6,130)ER
 130 FORMAT(5x,5herro=f8.4)
      CLOSE(6)
      STOP
      END
C
C       SUBROUTINE FSUB
      SUBROUTINE FSUB (X, Z, Y, F)
      IMPLICIT REAL*8 (A-H,O-Z)
C
      DIMENSION Z(6), F(6), Y(2)
C
      COMMON /FCAL1/EP,PE,ALF
      COMMON /FCAL3/RR,AKFR,AKGL
C
C   * DIFERENTIAL EQUATIONS AND VARIABLES*
C               F(1)=DQ1/DX, F(2)=DQ2/DX,
F(3)=D2C1/DX2, F(4)=D2C2/DX2
C               F(5)=0, F(6)=0
C               Z(1)=Q1, Z(2)=Q2, Z(3)=C1,
Z(4)=DC1/DX, Z(5)=C2, Z(6)=DC2/DX
C               Y(1)=Q*1, Y(2)=Q*2
        F(1)=-ALF*(Y(1)-Z(1))
        F(2)=-ALF*(Y(2)-Z(2))
        F(3)=PE*Z(4)+(1.D0-
EP)/EP*PE/RR*ALF*(Y(1)-Z(1))
        F(4)=PE*Z(6)+(1.D0-
EP)/EP*PE/RR*ALF*(Y(2)-Z(2))

        F(5)=-AKGL*Z(3)+Y(1)
        F(6)=-AKFR*Z(5)+Y(2)
C
      RETURN
```

```
      END
C
C       SUBROUTINE DFSUB
      SUBROUTINE DFSUB (X, Z, Y, DF)
      IMPLICIT REAL*8 (A-H,O-Z)
      DIMENSION Z(6), Y(2), DF(6,8)
C
      COMMON /FCAL1/EP,PE,ALF
      COMMON /FCAL3/RR,AKFR,AKGL
      COMMON /FCAL2/RF1,RF31,RF32
C
C *** INITIALIZATION OF F JACOBIAN MATRIX ***
      DO 3 I=1,6
        DO 5 J=1,8
          DF(I,J)=0.D0
  5     CONTINUE
  3   CONTINUE
C
      DF(1,1)=ALF
      DF(1,7)=-ALF
      DF(2,2)=ALF
      DF(2,8)=-ALF
      DF(3,4)=PE
      DF(3,1)=-(1.D0-EP)/EP*PE/RR*ALF
      DF(3,7)=(1.D0-EP)/EP*PE/RR*ALF
      DF(4,6)=PE
      DF(4,2)=-(1.D0-EP)/EP*PE/RR*ALF
      DF(4,8)=(1.D0-EP)/EP*PE/RR*ALF
      DF(5,3)=-AKGL
      DF(5,7)=+1.D0
      DF(6,5)=-AKFR
      DF(6,8)=+1.D0
      RETURN
      END
C
C       SUBROUTINE GSUB
      SUBROUTINE GSUB (I, Z, G)
      IMPLICIT REAL*8 (A-H,O-Z)
C
      DIMENSION Z(6)
      DOUBLE PRECISION G
C
      COMMON /FCAL1/EP,PE,ALF
      COMMON /FCAL2/RF1,RF31,RF32
      COMMON /FCAL5/CONS1,CONS2,CONS3,CONS4
C
C       *** BOUNDARY CONDITIONS
      GO TO (1,2,3,4,5,6), I
   1  G=Z(3)-1.D0/PE*Z(4)-CONS1
      RETURN
   2  G=Z(5)-1.D0/PE*Z(6)-CONS2
      RETURN
   3  G=Z(4)
      RETURN
   4  G=Z(6)
      RETURN
   5  G=Z(1)-CONS3
      RETURN
   6  G=Z(2)-CONS4
      RETURN
      END
C
C       SUBROUTINE DGSUB
      SUBROUTINE DGSUB (I, Z, DG)
      IMPLICIT REAL*8 (A-H,O-Z)
C
      DIMENSION Z(6), DG(6)
C
      COMMON /FCAL1/EP,PE,ALF
      COMMON /FCAL2/RF1,RF31,RF32
C
C*** INITIALIZATION OF G JACOBIAN MATRIZ
      DO 25 J=1,6
  25     DG(J) = 0. D0
      GO TO (1,2,3,4,5,6), I
    1 DG(3)=1.D0
      DG(4)=-1.D0/PE
      RETURN
    2 DG(5)=1.D0
      DG(6)=-1.D0/PE
      RETURN
    3 DG(4)=1.D0
      RETURN
    4 DG(6)=1.D0
      RETURN
    5 DG(1)=1.D0
      RETURN
    6 DG(2)=1.D0
      RETURN
      END
C
```

```
C input file model parameters and operating
conditions
C the others are estimated during the program
C
C 12.92d0,10.69d0,7.62d0,2.23d0,5.30d0
C 120.d0,50.d0,1.2d0
C 0.40d0,2000.D0,0.1d0
C 0.88d0,0.50d0
C 2.6d0,10.5d0,2
C
```

B: Source code for the Transient model using DASSL

```
C             PROGRAM FOR DDASSL.
C       THIS VERSION IS IN DOUBLE PRECISION.
C      PROGRAM USED FOR THE MODEL T-TMB
C             (4 SECTIONS).
C          (FRUTOSE/GLUCOSE SEPARATION)
C      SPATIAL DISCRETIZATION WITH
C        HERMITE POLYNOMIALS
C      ------------------------------------
C***ROUTINES CALLED  DDASSL,RES,JAC
C
       IMPLICIT DOUBLE PRECISION(A-H,O-Z)
       integer maxneq,maxord
       parameter (maxneq=850,maxord=5)
       integer lrw,liw
       parameter
(lrw=40+(maxord+4)*maxneq+maxneq**2,liw=20+ma
xneq)
c
       DOUBLE PRECISION LC,LJ,T
       EXTERNAL RES,JAC,hermite
       DOUBLE PRECISION
Y(maxneq),YY(maxneq),RWORK(lrw),YPRIME(maxneq
),
     *
erro(maxneq),DELTA(maxneq),ATOL(maxneq),hu(51
),xpon(51)
       INTEGER INFO(15),IWORK(liw)
       DIMENSION Q(4),V(4),root(4),pos(4)
       DIMENSION H(2,4),A(2,4),B(2,4)
       DIMENSION CONC(16,51)
       COMMON /FCAL1/EP,PE,ALF
       COMMON /FCAL2/RF1,RF31,RF32,akgl,akfr
       COMMON /FCAL3/R(4)
       common /fcal4/nc,ne,neq,neq1,hk(26)
       COMMON
/MATRIZ1/BMAT(maxneq/2,maxneq/2),AMAT(maxneq,
maxneq),
     *
HMAT(maxneq,maxneq),HDMAT(maxneq,maxneq)
       common
/matriz3/hd1(maxneq/2),a1(maxneq/2),h1(maxneq
/2),
     *
b1(maxneq/2),hb2(maxneq/2),ab2(maxneq/2)
     *
,ha2(maxneq/2),aa2(maxneq/2),ba2(maxneq/2)
       common /pontos/XBKPT(22)

       external gettim
       CHARACTER*9 FR
       CHARACTER TAB
       TAB=CHAR(9)
       TOUT=0.D0
       cont=1
       DETAT=.1d0
       T=0.d0
        cte110=0.d0
        cte120=0.d0
        cte210=0.d0
        cte220=0.d0
        cte130=0.d0
        cte230=0.d0
        cte140=0.d0
        cte240=0.d0
        qte110=0.d0
        qte120=0.d0
        qte210=0.d0
        qte220=0.d0
        qte130=0.d0
        qte230=0.d0
        qte140=0.d0
        qte240=0.d0
C
C      Input - model parameters:
C      ------------------------------------

OPEN(UNIT=12,FILE='dattmb2',STATUS='OLD')
c      elements number, Gl and Fr constants
       READ(12,*) NE,akgl,akfr
C      SMB flowrates(ml/min):
       READ(12,*) QR,QEL,QEX,QFE,QRA
C      rotation period (s), feed
concentration(g/l):
       READ(12,*) RP,CAFE
C      parameters ( e ; Pe ; k ):
       READ(12,*) EP,PE,AK
C      columns ( Dc (cm) ; Lc(cm) ; NCS ):
       READ(12,*) DC,LC,NCS
       close(12)
```

```
C     Output:
C     ----------------------------------
      NRP=10.d0*ne
c      NRP=INT(RP)
      NRP=NRP+ak*100000.d0
      iletras=2
      idigitos=7
      FR(1:iletras+1)='yy'
      DO 500 i=1,idigitos
        NCHAR=NRP/10**(idigitos-i)
        NRP=NRP-NCHAR*10**(idigitos-i)

FR(iletras+i:iletras+i+1)=CHAR(48+NCHAR)
  500 CONTINUE
c
      open(unit=15,file=FR)
      OPEN(UNIT=16,FILE='matrizes')
      WRITE(15,101)
  101 FORMAT(/2X,39Htmb fru/glu: Linear
Driving Force Model)
c
C     DDASSL parameters:
      KPRINT = 3
      IPASS = 1
      NERR = 0
      RTOL = 1.D-7
      ATOL(1) = 1.D-7
c
      NC=2
      NPDE=16
      NEQ1= NC*NE*NPDE
      neq=neq1+16
      nce=nc*ne
c
      root(2)=.2113248654051871d0
      root(3)=.7886751345948129d0
c
      NOUT=1200.d0/detat
      IF (KPRINT .GE. 2) THEN
        WRITE (15,110) NEQ,RTOL,ATOL(1)
      ENDIF
 110    FORMAT(/1X'NEQ='I3,'  RTOL='E10.1,'
ATOL=',E10.1)
C
      DO 115 I = 1,15
 115  INFO(I) = 0
      INFO(3)=1
      INFO(11)=1
c
      WRITE(15,106) akgl,akfr
  106   FORMAT(/2X'kgl='f6.3,'   kfr='f6.3)
      WRITE(15,107)
  107   FORMAT(/2X,35Hcase of linear
adsorption isotherms)
c
c     subintervals definition
      NPTS=NE+1
      XBKPT(1)=0.D0
      do i=2,npts
        xbkpt(i)=xbkpt(i-1)+1.d0/ne
       enddo
c      endif
c
c     x points to obtain solution
      NPP=51
      DPX=1.D0/(NPP-1)
      do K=1,npp
        XPON(K)=DBLE(K-1)*DPX
      enddo
c
      XLEFT=XBKPT(1)
      XRIGHT=XBKPT(NPTS)
      do k=1,ne
         hk(k)=xbkpt(k+1)-xbkpt(k)
      enddo
c
C     Columns:
C     ----------------------------------
      AC=DC*DC*3.141592654D0/4.D0
      VC=AC*LC
      LJ=FLOAT(NCS)*LC
      VSP=4.D0*FLOAT(NCS)*VC*(1.D0-EP)
      WRITE(15,102)
  102   FORMAT(2X,8HColumns:)
      WRITE(15,103) NCS,DC,LC,AC,LJ,VC
  103   FORMAT(2X,32HNumber of columns per
section : ,I1/
     *       2X,5HDc = ,F6.4,4H cm ,6X,5HLc =
,F7.4,3H cm/
     *       2X,5HAc = ,F6.4,4H cm2,6X,5HLj =
,F7.4,3H cm/
     *       2X,5HVc = ,F7.3,4H cm3/)
C     SMB flowrates in each section (ml/min):
C     ----------------------------------
      Q(4)=QR
      Q(1)=QR+QEL
      Q(2)=QR+QEL-QEX
      Q(3)=QR+QEL-QEX+QFE
      WRITE(15,104)
  104   FORMAT(2X,4HSMB:)
      WRITE(15,105) QR,RP,QEL,Q(1),QEX,Q(2),
     *              QFE,Q(3),QRA,Q(4)
  105   FORMAT(2X,5HQR = ,F5.2,7H
ml/min,4X,5HRP = ,F6.2,2H s/
     *          2X,5HQEL =,F5.2,7H
ml/min,4X,5HQ1 = ,F6.3,7H ml/min/
     *          2X,5HQEX =,F5.2,7H
ml/min,4X,5HQ2 = ,F6.3,7H ml/min/
     *          2X,5HQFE =,F5.2,7H
ml/min,4X,5HQ3 = ,F6.3,7H ml/min/
     *          2X,5HQRA =,F5.2,7H
ml/min,4X,5HQ4 = ,F6.3,7H ml/min/)
C     Flowrates (ml/min) and velocities
(cm/s)
C     solid velocity (cm/s)
C     liquid / solid velocity ratio in each
TMB section:
C     ----------------------------------
      QST=EP*VC/RP*60.D0
      AL=EP*AC*60.D0
      US=LC/RP
      do J=1,4
        Q(J)=Q(J)-QST
        V(J)=Q(J)/AL
        R(J)=V(J)/US
      enddo
      WRITE(15,96)
  96    FORMAT(2X,4HTMB:)
      WRITE(15,97) QST,US
  97    FORMAT(2X,6HQST = ,F6.3,7H
ml/min,3X,5HUS = ,F6.4,5H cm/s)
      WRITE(15,98) (J,Q(J),J,V(J),J,R(J),
J=1,4)
  98    FORMAT(4(2X,1HQ,I1,3H = ,F6.3,7H
ml/min,3X,1HV,I1,3H = ,F6.4,
     *       5H cm/s,3X,1HR,I1,3H = ,F6.4/))
C     others model parameters:
C     ----------------------------------
      ALF=AK*RP*FLOAT(NCS)
      RF1=Q(4)/Q(1)
      RF31=QFE/Q(3)*CAFE
      RF32=Q(2)/Q(3)
      WRITE(15,99)
  99    FORMAT(2X,17HModel parameters:)
      WRITE(15,80) EP,PE
  80    FORMAT(2X,6HEP  = ,F6.4,6X,5HPE =
,F5.0)
      WRITE(15,81) AK,ALF
  81    FORMAT(2X,5Hk  = ,E10.4,4H
1/s,6X,6HALF = ,E10.4)
      WRITE(15,82) RF1,RF31,RF32
  82    FORMAT(2X,6HRF1 = ,F6.4,6X,7HRF31 =
,F6.4,4X,7HRF32 = ,F6.4)
c
      TRE1=0.D0
      TRE2=1.D0
      EXTA1=0.D0
      EXTB1=0.D0
      RAFA1=0.D0
      RAFB1=0.D0
      EXTA2=0.D0
      EXTB2=0.D0
      RAFA2=0.D0
      RAFB2=0.D0
```

```
      FEED=QFE*CAFE
c
      WRITE(15,73)
   73    FORMAT(///2X,8HResults:,/)
      WRITE(15,131) TAB,TAB,TAB,TAB,TAB,TAB
  131
FORMAT(1HX,A1,4HC(G),A1,4HC(F),A1,4HP(G),A1,4
HP(F)
     *    ,A1,2HNQ,A1,1HH)
c
c     initial values
      do 999 i=1,neq
         y(i)=0.0d0
         yy(i)=100.d0
         yprime(i)=0.0d0
 999     delta(i)=0.0d0
c
      do i=1,neq1/2
        do j=1,neq1/2
           hmat(i,j)=0.d0
           hdmat(i,j)=0.d0
           amat(i,j)=0.d0
        enddo
      enddo
      do i=1,neq1/2
        do j=1,neq1/2
          bmat(i,j)=0.d0
        enddo
        hd1(i)=0.d0
        h1(i)=0.d0
        a1(i)=0.d0
        b1(i)=0.d0
        hb2(i)=0.d0
        ab2(i)=0.d0
        ha2(i)=0.d0
        aa2(i)=0.d0
      enddo
ccccccccccccccccccccccccccccccccccccccccccc
c     matrix estimation
c     subinterval 1
       CALL HERMITE(hk(1),h,a,b)
c     cycle, 1 - number of cij (2*4)
      do j=1,8
c     nc = number of interior collocation
points
        do jj=1,nc
          hmat(nce*(j-1)+jj,nce*(j-
1)+1)=h(jj,1)/PE+h(jj,2)
          hmat(nce*(j-1)+jj,nce*(j-
1)+2)=h(jj,3)
          hmat(nce*(j-1)+jj,nce*(j-
1)+3)=h(jj,4)
      hdmat(nce*(j-1)+jj,nce*(j-
1)+1)=hmat(nce*(j-1)+jj,nce*(j-1)+1)
      hdmat(nce*(j-1)+jj,nce*(j-
1)+2)=hmat(nce*(j-1)+jj,nce*(j-1)+2)
      hdmat(nce*(j-1)+jj,nce*(j-
1)+3)=hmat(nce*(j-1)+jj,nce*(j-1)+3)
c
       bmat(nce*(j-1)+jj,nce*(j-
1)+1)=(b(jj,1)/PE+b(jj,2))/hk(1)/hk(1)
       bmat(nce*(j-1)+jj,nce*(j-
1)+2)=b(jj,3)/hk(1)/hk(1)
       bmat(nce*(j-1)+jj,nce*(j-
1)+3)=b(jj,4)/hk(1)/hk(1)
c
          amat(nce*(j-1)+jj,nce*(j-
1)+1)=(a(jj,1)/PE+a(jj,2))/hk(1)
          amat(nce*(j-1)+jj,nce*(j-
1)+2)=a(jj,3)/hk(1)
          amat(nce*(j-1)+jj,nce*(j-
1)+3)=a(jj,4)/hk(1)
c
        do i=1,3
c     for the qij
c     neq1 = nc*ne*npde
          hmat(neq1/2+nce*(j-
1)+jj,neq1/2+nce*(j-1)+i)=h(jj,i+1)
          hdmat(neq1/2+nce*(j-
1)+jj,neq1/2+nce*(j-1)+i)=h(jj,i+1)
       amat(neq1/2+nce*(j-
1)+jj,neq1/2+nce*(j-1)+i)=a(jj,i+1)/hk(1)
        enddo
       enddo
      enddo
ccccccccccccccccccccccccccccccccccc
c     subinterval 2 to ne-1
        do k=2,ne-1
          CALL HERMITE(hk(k),h,a,b)
          do j=1,8
           do jj=1,nc
             do i=1,4
               hmat(nce*(j-1)+nc*k+jj-
nc,nce*(j-1)+i+nc*k-3)=h(jj,i)
               hdmat(nce*(j-1)+nc*k+jj-
nc,nce*(j-1)+i+nc*k-3)=
     *           hmat(nce*(j-1)+nc*k+jj-
nc,nce*(j-1)+i+nc*k-3)
               bmat(nce*(j-1)+nc*k+jj-
nc,nce*(j-1)+i+nc*k-3)=b(jj,i)/
     *          hk(k)/hk(k)
               amat(nce*(j-1)+nc*k+jj-
nc,nce*(j-1)+i+nc*k-3)=a(jj,i)/
     *          hk(k)
c
              hmat(nce*(j+7)+nc*k+jj-
nc,nce*(j+7)+i+nc*k-3)=h(jj,i)
              hdmat(nce*(j+7)+nc*k+jj-
nc,nce*(j+7)+i+nc*k-3)=
     *           hmat(nce*(j+7)+nc*k+jj-
nc,nce*(j+7)+i+nc*k-3)
             amat(nce*(j+7)+nc*k+jj-
nc,nce*(j+7)+i+nc*k-3)=a(jj,i)/
     *          hk(k)
           enddo
         enddo
        enddo
      enddo
ccccccccccccccccccccccccccccccccccccccccccc
c     subinterval ne
        CALL HERMITE(hk(ne),h,a,b)
        do j=1,8
         do jj=1,nc
          do i=1,2
            hmat(nce*(j-1)+jj+nce-nc,nce*(j-
1)+nce-3+i)=h(jj,i)
            hdmat(nce*(j-1)+jj+nce-
nc,nce*(j-1)+nce-3+i)=
     *           hmat(nce*(j-1)+jj+nce-
nc,nce*(j-1)+nce-3+i)
            bmat(nce*(j-1)+jj+nce-nc,nce*(j-
1)+nce-3+i)=b(jj,i)/
     *           hk(ne)/hk(ne)
            amat(nce*(j-1)+jj+nce-nc,nce*(j-
1)+nce-3+i)=a(jj,i)/
     *           hk(ne)
c
            hmat(nce*(j+7)+jj+nce-
nc,nce*(j+7)+nce-3+i)=h(jj,i)
           hdmat(nce*(j+7)+jj+nce-
nc,nce*(j+7)+nce-3+i)=
     *        hmat(nce*(j+7)+jj+nce-
nc,nce*(j+7)+nce-3+i)
            amat(nce*(j+7)+jj+nce-
nc,nce*(j+7)+nce-3+i)=a(jj,i)/
     *           hk(ne)
         enddo
c
            hmat(nce*(j-1)+jj+nce-nc,nce*(j-
1)+nce)=h(jj,4)
          hdmat(nce*(j-1)+jj+nce-nc,nce*(j-
1)+nce)=
     *        hmat(nce*(j-1)+jj+nce-
nc,nce*(j-1)+nce)
            bmat(nce*(j-1)+jj+nce-nc,nce*(j-
1)+nce)=b(jj,4)/
     *        hk(ne)/hk(ne)
           amat(nce*(j-1)+jj+nce-nc,nce*(j-
1)+nce)=a(jj,4)/
     *        hk(ne)
c
            hmat(nce*(j+7)+jj+nce-
nc,nce*(j+7)+nce)=h(jj,4)
```

```
            hdmat(nce*(j+7)+jj+nce-
nc,nce*(j+7)+nce)=
     *       hmat(nce*(j+7)+jj+nce-
nc,nce*(j+7)+nce)
            amat(nce*(j+7)+jj+nce-
nc,nce*(j+7)+nce)=a(jj,4)/
     *          hk(ne)
          enddo
         enddo
c      qij equations vectors
       do jj=1,2
c      equations for u=0
c       first subinterval k=1
         hb2(jj)=h(jj,1)
         ab2(jj)=a(jj,1)/hk(1)
         hb2(nce+jj)=h(jj,1)
         ab2(nce+jj)=a(jj,1)/hk(1)
         hb2(2*nce+jj)=h(jj,1)
         ab2(2*nce+jj)=a(jj,1)/hk(1)
         hb2(3*nce+jj)=h(jj,1)
         ab2(3*nce+jj)=a(jj,1)/hk(1)
         hb2(4*nce+jj)=h(jj,1)
         ab2(4*nce+jj)=a(jj,1)/hk(1)
         hb2(5*nce+jj)=h(jj,1)
         ab2(5*nce+jj)=a(jj,1)/hk(1)
         hb2(6*nce+jj)=h(jj,1)
         ab2(6*nce+jj)=a(jj,1)/hk(1)
         hb2(7*nce+jj)=h(jj,1)
         ab2(7*nce+jj)=a(jj,1)/hk(1)
c       last subinterval k=NE
         hb2(3*nce-(nc-jj))=h(jj,3)
         ab2(3*nce-(nc-jj))=a(jj,3)/hk(ne)
         hb2(4*nce-(nc-jj))=h(jj,3)
         ab2(4*nce-(nc-jj))=a(jj,3)/hk(ne)
         hb2(5*nce-(nc-jj))=h(jj,3)
         ab2(5*nce-(nc-jj))=a(jj,3)/hk(ne)
         hb2(6*nce-(nc-jj))=h(jj,3)
         ab2(6*nce-(nc-jj))=a(jj,3)/hk(ne)
         hb2(7*nce-(nc-jj))=h(jj,3)
         ab2(7*nce-(nc-jj))=a(jj,3)/hk(ne)
         hb2(8*nce-(nc-jj))=h(jj,3)
         ab2(8*nce-(nc-jj))=a(jj,3)/hk(ne)
         hb2(nce-(nc-jj))=h(jj,3)
         ab2(nce-(nc-jj))=a(jj,3)/hk(ne)
         hb2(2*nce-(nc-jj))=h(jj,3)
         ab2(2*nce-(nc-jj))=a(jj,3)/hk(ne)
        enddo
c      cij equations vectors
       do jj=1,2
c      equations for u=1
c       first subinterval k=1
         ha2(jj)=h(jj,1)*rf1
         aa2(jj)=a(jj,1)*rf1/hk(1)
         ba2(jj)=b(jj,1)*rf1/hk(1)/hk(1)
         ha2(nce+jj)=h(jj,1)*rf1
         aa2(nce+jj)=a(jj,1)*rf1/hk(1)
         ba2(nce+jj)=b(jj,1)*rf1/hk(1)/hk(1)
         ha2(2*nce+jj)=h(jj,1)
         aa2(2*nce+jj)=a(jj,1)/hk(1)
         ba2(2*nce+jj)=b(jj,1)/hk(1)/hk(1)
         ha2(3*nce+jj)=h(jj,1)
         aa2(3*nce+jj)=a(jj,1)/hk(1)
         ba2(3*nce+jj)=b(jj,1)/hk(1)/hk(1)
         ha2(4*nce+jj)=h(jj,1)*rf32
         aa2(4*nce+jj)=a(jj,1)*rf32/hk(1)

ba2(4*nce+jj)=b(jj,1)*rf32/hk(1)/hk(1)
         ha2(5*nce+jj)=h(jj,1)*rf32
         aa2(5*nce+jj)=a(jj,1)*rf32/hk(1)

ba2(5*nce+jj)=b(jj,1)*rf32/hk(1)/hk(1)
         ha2(6*nce+jj)=h(jj,1)
         aa2(6*nce+jj)=a(jj,1)/hk(1)
         ba2(6*nce+jj)=b(jj,1)/hk(1)/hk(1)
         ha2(7*nce+jj)=h(jj,1)
         aa2(7*nce+jj)=a(jj,1)/hk(1)
         ba2(7*nce+jj)=b(jj,1)/hk(1)/hk(1)
c       last subinterval k=NE
         ha2(nce-(nc-jj))=h(jj,3)
         aa2(nce-(nc-jj))=a(jj,3)/hk(ne)
         ba2(nce-(nc-
jj))=a(jj,3)/hk(ne)/hk(ne)
         ha2(2*nce-(nc-jj))=h(jj,3)
         aa2(2*nce-(nc-jj))=a(jj,3)/hk(ne)
         ba2(2*nce-(nc-
jj))=a(jj,3)/hk(ne)/hk(ne)
         ha2(3*nce-(nc-jj))=h(jj,3)
         aa2(3*nce-(nc-jj))=a(jj,3)/hk(ne)
         ba2(3*nce-(nc-
jj))=a(jj,3)/hk(ne)/hk(ne)
         ha2(4*nce-(nc-jj))=h(jj,3)
         aa2(4*nce-(nc-jj))=a(jj,3)/hk(ne)
         ba2(4*nce-(nc-
jj))=a(jj,3)/hk(ne)/hk(ne)
         ha2(5*nce-(nc-jj))=h(jj,3)
         aa2(5*nce-(nc-jj))=a(jj,3)/hk(ne)
         ba2(5*nce-(nc-
jj))=a(jj,3)/hk(ne)/hk(ne)
         ha2(6*nce-(nc-jj))=h(jj,3)
         aa2(6*nce-(nc-jj))=a(jj,3)/hk(ne)
         ba2(6*nce-(nc-
jj))=a(jj,3)/hk(ne)/hk(ne)
         ha2(7*nce-(nc-jj))=h(jj,3)
         aa2(7*nce-(nc-jj))=a(jj,3)/hk(ne)
         ba2(7*nce-(nc-
jj))=a(jj,3)/hk(ne)/hk(ne)
         ha2(8*nce-(nc-jj))=h(jj,3)
         aa2(8*nce-(nc-jj))=a(jj,3)/hk(ne)
         ba2(8*nce-(nc-
jj))=a(jj,3)/hk(ne)/hk(ne)
        enddo
ccccccccccccccccccccccccccccccccccccccccccc
      write(16,*)TOUT
       do i=1,neq+8
         do j=1,neq+8

if((hmat(i,j).ne.0.d0).or.(hdmat(i,j).ne.0.d0
))then

write(16,111)i,j,hmat(i,j),bmat(i,j),amat(i,j
),hb2(j),ab2(j)
           endif
         enddo
       enddo
      close(16)
c
  111      format('(',i3,',',i3,')=',e14.5,
e14.5, e14.5, e14.5, e14.5)
  113      format('(',i3,')=',e14.5)
ccccccccccccccccccccccccccccccccccccccccccc
      write(*,*) npp,ne
      write(15,*) npp,ne
      call GETTIM (ihr, imin, isec, i100th)
      write(15,9002)ihr, imin, isec, i100th
 9002 format(i2,':',i2.2,':',i2.2,':',i2.2,'
',A,'m')
ccccccccccccccccccccccccccccccccccccccccccc
c
      TRE1=0.D0
      TRE2=1.D0
c
      EXTA1=0.D0
      EXTB1=0.D0
      RAFA1=0.D0
      RAFB1=0.D0
      EXTA2=0.D0
      EXTB2=0.D0
      RAFA2=0.D0
      RAFB2=0.D0
c
   10 TOUT=TOUT+DETAT
      DO 170 IOUT = 1,NOUT
ccccc
c       balan1=qex*cte110+qra*cte130
c       balan2=qex*cte210+qra*cte230
c       perc1=dabs((balan1-feed))/feed*100.d0
c       perc2=dabs((balan2-feed))/feed*100.d0
c       if
((perc1.lt.1.d0).and.(perc2.lt.1.d0))then
c          goto 43434
c       endif
c
       do i=1,neq
         erro(i)=dabs(y(i)-yy(i))
```

```
        enddo
        small=1d20
        do i=1,neq
          erro1=dmax1(small,erro(i))
        enddo
        if (erro1.lt..1d-7) then
           INDEX=989
           goto 43434
        endif
cccc
        CALL HERMITE(hk(1),h,a,b)
        do j=1,nc
c
hd1(2*NE*(4)+j)=RF31*h(j,1)*100.d0*dexp(-
100.d0*T)
c
hd1(2*NE*(5)+j)=RF31*h(j,1)*100.d0*dexp(-
100.d0*T)
          h1(nce*4+j)=RF31*h(j,1)
          h1(nce*5+j)=RF31*h(j,1)
          a1(nce*4+j)=RF31*a(j,1)/hk(1)
          a1(nce*5+j)=RF31*a(j,1)/hk(1)
          b1(nce*4+j)=RF31*b(j,1)/hk(1)/hk(1)
          b1(nce*5+j)=RF31*b(j,1)/hk(1)/hk(1)
        enddo
cccc
c       write(15,*)tout
       write(*,*) tout
c
       do i=1,neq
         yy(i)=y(i)
       enddo
c
          CALL
DDASSL(RES,NEQ,T,Y,YPRIME,TOUT,INFO,RTOL,ATOL
,IDID,
     *
RWORK,LRW,IWORK,LIW,RPAR,IPAR,JAC)
           HU = RWORK(7)
           NQU = IWORK(8)
c
c      results apresentation for each cycle (1
cycle => tout=4)
c      subinterval 1  (conc(j) cG1, conc(j+2)
cF1)
          pos(1)=xbkpt(1)+hk(1)*root(2)
          pos(2)=xbkpt(1)+hk(1)*root(3)
          pos(3)=xbkpt(1)+hk(1)*root(4)
          do jj=1,4
            if(jj.eq.1)then

cte110=RF1*y(neq1+15)+1.d0/PE*y(1)

cte210=RF1*y(neq1+16)+1.d0/PE*y(nce+1)
             qte120=y(nce*15+nce+1)
             qte220=y(nce*15+nce+2)
             cte1=cte110
             cte2=cte210
             cte3=qte120
             cte4=qte220
            endif
            if(jj.eq.2)then

cte120=y(neq1+9)+1.d0/PE*y(2*nce+1)

cte220=y(neq1+10)+1.d0/PE*y(3*nce+1)
             qte130=y(nce*15+nce+3)
             qte230=y(nce*15+nce+4)
             cte1=cte120
             cte2=cte220
             cte3=qte130
             cte4=qte230
            endif
            if(jj.eq.3)then
             cte130=RF32*y(neq1+11)+RF31+
     *        1.d0/PE*y(4*nce+1)
             cte230=RF32*y(neq1+12)+RF31+
     *        1.d0/PE*y(5*nce+1)
             qte140=y(15*nce+nce+5)
             qte240=y(15*nce+nce+6)
             cte1=cte130
             cte2=cte230
             cte3=qte140
             cte4=qte240
            endif
            if(jj.eq.4)then

cte140=y(neq1+13)+1.d0/PE*y(6*nce+1)

cte240=y(neq1+14)+1.d0/PE*y(7*nce+1)
             qte110=y(15*nce+nce+7)
             qte210=y(15*nce+nce+8)
             cte1=cte140
             cte2=cte240
             cte3=qte110
             cte4=qte210
            endif
c
            do j=1,nc
             conc(2*jj-1,j)=0.d0
             conc(jj*2,j)=0.d0
             conc(2*jj+7,j)=0.d0
             conc(2*jj+8,j)=0.d0
             call hermite(hk(1),h,a,b)
             conc(2*jj-1,j)=h(j,1)*cte1+
     *                      h(j,2)*y(1+(jj-
1)*2*nce)
             conc(jj*2,j)=h(j,1)*cte2+
     *                     h(j,2)*y(nce+1+(jj-
1)*2*nce)
             conc(2*jj+7,j)=h(j,1)*cte3+
     *
h(j,2)*y(2*nce*(jj-1)+8*nce+1)
             conc(2*jj+8,j)=h(j,1)*cte4+
     *
h(j,2)*y(2*nce*(jj-1)+9*nce+1)
               do i=3,4
                conc(2*jj-1,j)=conc(2*jj-1,j)+
     *            h(j,i)*y(2*nce*(jj-1)+i-1)

conc(2*jj,j)=conc(2*jj,j)+h(j,i)*
     *            y(2*nce*(jj-1)+nce+i-1)
               conc(2*jj+7,j)=conc(2*jj+7,j)+
     *            h(j,i)*y(2*nce*(jj-
1)+8*nce+i-1)
               conc(2*jj+8,j)=conc(2*jj+8,j)+
     *            h(j,i)*y(2*nce*(jj-
1)+9*nce+i-1)
              enddo
            enddo
          enddo
          icont=icont+1
c      results presentation for each cycle (1
cycle=>tout=4)
          if
((int(tout*1000+0.5d0)/1000).eq.(4*cont))
then
            write(15,145)tout
            write(*,145)tout
            posi=0.00d0
  145       format(5H t = ,f5.1)

write(15,700)posi,cte110,cte210,cte120,cte220
,
     *
cte130,cte230,cte140,cte240

write(*,700)posi,cte110,cte210,cte120,cte220,
     *
cte130,cte230,cte140,cte240
           do j=1,nc

write(15,700)pos(j),conc(1,j),conc(2,j),conc(
3,j),conc(4,j),
     *
conc(5,j),conc(6,j),conc(7,j),conc(8,j)

write(*,700)pos(j),conc(1,j),conc(2,j),conc(3
,j),conc(4,j),
     *
conc(5,j),conc(6,j),conc(7,j),conc(8,j)
           enddo
         endif
c        endif
```

```
c     subinterval 2 to NE=NE-1
      do kk=2,ne-1
          pos(1)=xbkpt(kk)+hk(kk)*root(2)
          pos(2)=xbkpt(kk)+hk(kk)*root(3)
          pos(3)=xbkpt(kk)+hk(kk)*root(4)
          call hermite(hk(kk),h,a,b)
          do jj=1,4
            do j=1,nc
               conc(2*jj-1,nc*kk+j-nc)=0.d0
               conc(2*jj,nc*kk+j-nc)=0.d0
               conc(2*jj+7,nc*kk+j-nc)=0.d0
               conc(2*jj+8,nc*kk+j-nc)=0.d0
               do i=1,4
                conc(nc*jj-1,nc*kk+j-
nc)=conc(2*jj-1,nc*kk+j-nc)+
     *           h(j,i)*y(2*nce*(jj-
1)+2*kk+i-3)
                conc(nc*jj,nc*kk+j-
nc)=conc(2*jj,nc*kk+j-nc)+
     *           h(j,i)*y(2*nce*(jj-
1)+nce+2*kk+i-3)
                conc(nc*jj+7,nc*kk+j-
nc)=conc(2*jj+7,nc*kk+j-nc)+
     *           h(j,i)*y(2*nce*(jj-
1)+neq1/2+2*kk+i-3)
                conc(nc*jj+8,nc*kk+j-
nc)=conc(2*jj+8,nc*kk+j-nc)+
     *           h(j,i)*y(2*nce*(jj-
1)+18*ne+2*kk+i-3)
               enddo
            enddo
          enddo
          if
((int(tout*1000+0.5d0)/1000).eq.(4*cont))
then
            write(15,700)xbkpt(kk),y(2*kk-
2),y(nce+2*kk-2),
     *      y(2*nce+2*kk-2),y(3*nce+2*kk-
2),y(4*nce+2*kk-2),
     *      y(5*nce+2*kk-2),y(6*nce+2*kk-
2),y(7*nce+2*kk-2)
            write(*,700)xbkpt(kk),y(2*kk-
2),y(nce+2*kk-2),
     *      y(2*nce+2*kk-2),y(3*nce+2*kk-
2),y(4*nce+2*kk-2),
     *      y(5*nce+2*kk-2),y(6*nce+2*kk-
2),y(7*nce+2*kk-2)
            do j=1,nc

write(15,700)pos(j),conc(1,2*kk+j-
2),conc(2,2*kk+j-2),
     *       conc(3,2*kk+j-2),conc(4,2*kk+j-
2),conc(5,2*kk+j-2),
     *       conc(6,2*kk+j-2),conc(7,2*kk+j-
2),conc(8,2*kk+j-2)

write(*,700)pos(j),conc(1,2*kk+j-
2),conc(2,2*kk+j-2),
     *       conc(3,2*kk+j-2),conc(4,2*kk+j-
2),conc(5,2*kk+j-2),
     *       conc(6,2*kk+j-2),conc(7,2*kk+j-
2),conc(8,2*kk+j-2)
            enddo
          endif
        enddo
c     subinterval NE
        pos(1)=xbkpt(ne)+hk(ne)*root(2)
        pos(2)=xbkpt(ne)+hk(ne)*root(3)
        pos(3)=xbkpt(ne)+hk(ne)*root(4)
        do jj=1,4
           if(jj.eq.1)then
             cte110=y(neq1+9)
             cte210=y(neq1+10)
             qte144=y(neq1+3)
             qte244=y(neq1+4)
             cte1=cte110
             cte2=cte210
             cte3=qte144
             cte4=qte244
           endif
           if(jj.eq.2)then
             cte120=y(neq1+11)
             cte220=y(neq1+12)
             qte111=y(neq1+5)
             qte211=y(neq1+6)
             cte1=cte120
             cte2=cte220
             cte3=qte111
             cte4=qte211
           endif
           if(jj.eq.3)then
             cte130=y(neq1+13)
             cte230=y(neq1+14)
             qte122=y(neq1+7)
             qte222=y(neq1+8)
             cte1=cte130
             cte2=cte230
             cte3=qte122
             cte4=qte222
           endif
           if(jj.eq.4)then
             cte140=y(neq1+15)
             cte240=y(neq1+16)
             qte133=y(neq1+1)
             qte233=y(neq1+2)
             cte1=cte140
             cte2=cte240
             cte3=qte133
             cte4=qte233
           endif
           call hermite(hk(ne),h,a,b)
           do j=1,nc
            conc(nc*jj-1,nce+j-2)=cte1*h(j,3)
            conc(nc*jj,nce+j-2)=cte2*h(j,3)
            conc(nc*jj+7,nce+j-2)=cte3*h(j,3)
            conc(nc*jj+8,nce+j-2)=cte4*h(j,3)
            do i=1,2
             conc(nc*jj-1,nce+j-2)=conc(2*jj-
1,nce+j-2)+
     *        h(j,i)*
     *        y(2*nce*(jj-1)+i+nce-3)
             conc(nc*jj,nce+j-
2)=conc(2*jj,nce+j-2)+
     *        h(j,i)*
     *        y(2*nce*(jj-1)+i+2*nce-3)
             conc(nc*jj+7,nce+j-
2)=conc(2*jj+7,nce+j-2)+
     *         h(j,i)*
     *         y(2*nce*(jj-1)+neq1/2+nce+i-3)
             conc(nc*jj+8,nce+j-
2)=conc(2*jj+8,nce+j-2)+
     *         h(j,i)*
     *         y(2*nce*(jj-1)+18*ne+nce+i-3)
            enddo
             conc(nc*jj-1,nce+j-2)=conc(2*jj-
1,nce+j-2)+
     *         h(j,4)*
     *         y(2*nce*(jj-1)+nce)
             conc(nc*jj,nce+j-
2)=conc(2*jj,nce+j-2)+
     *         h(j,4)*
     *         y(2*nce*(jj-1)+2*nce)
             conc(nc*jj+7,nce+j-
2)=conc(2*jj+7,nce+j-2)+
     *         h(j,4)*
     *         y(2*nce*(jj-1)+neq1/2+nce)
             conc(nc*jj+8,nce+j-
2)=conc(2*jj+8,nce+j-2)+
     *         h(j,4)*
     *         y(2*nce*(jj-1)+18*ne+nce)
          enddo
        enddo
c
c     results apresentation for each cycle (1
cicle=>tout=4)

if((int(tout*1000+0.5d0)/1000).eq.(4*cont))
then
          cont=cont+1
          write(15,700)xbkpt(ne),y(2*(ne)-
2),y(nce+2*(ne)-2),
     *      y(2*nce+2*(ne)-2),y(3*nce+2*(ne)-
2),y(4*nce+2*(ne)-2),
```

```
     *       y(5*nce+2*(ne)-2),y(6*nce+2*(ne)-
2),y(7*nce+2*(ne)-2)
              write(*,700)xbkpt(ne),y(2*(ne)-
2),y(nce+2*(ne)-2),
     *       y(2*nce+2*(ne)-2),y(3*nce+2*(ne)-
2),y(4*nce+2*(ne)-2),
     *       y(5*nce+2*(ne)-2),y(6*nce+2*(ne)-
2),y(7*nce+2*(ne)-2)
            do j=1,nc
            write(15,700)pos(j),conc(1,2*ne+j-
2),conc(2,2*ne+j-2),
     *       conc(3,2*ne+j-2),conc(4,2*ne+j-
2),conc(5,2*ne+j-2),
     *       conc(6,2*ne+j-2),conc(7,2*ne+j-
2),conc(8,2*ne+j-2)
            write(*,700)pos(j),conc(1,2*ne+j-
2),conc(2,2*ne+j-2),
     *       conc(3,2*ne+j-2),conc(4,2*ne+j-
2),conc(5,2*ne+j-2),
     *       conc(6,2*ne+j-2),conc(7,2*ne+j-
2),conc(8,2*ne+j-2)
          enddo
          posf=1.d0

write(15,700)posf,cte110,cte210,cte120,cte220
,
     *
cte130,cte230,cte140,cte240

write(*,700)posf,cte110,cte210,cte120,cte220,
     *
cte130,cte230,cte140,cte240
          endif
cc
      IF ((TOUT.GE.TRE1).AND.(TOUT.LE.TRE2))
THEN
         EXTA1=EXTA1+cte110*DETAT
         EXTB1=EXTB1+cte210*DETAT
         RAFA1=RAFA1+cte130*DETAT
         RAFB1=RAFB1+cte230*DETAT
      END IF

      IF (TOUT.GE.TRE2) THEN
         TRE1=TRE1+1.D0
         TRE2=TRE2+1.D0

       ER1=DABS(EXTA1-
EXTA2)/dabs(EXTA1)+DABS(EXTB1-
EXTB2)/dabs(EXTB1)
       ER2=DABS(RAFA1-
RAFA2)/dabs(RAFA1)+DABS(RAFB1-
RAFB2)/dabs(RAFB1)
       ER3=DABS(EXTA1*QEX+RAFA1*QRA-
FEED)/FEED
       ER4=DABS(EXTB1*QEX+RAFB1*QRA-
FEED)/FEED
       ER=ER1+ER2+ER3+ER4
c
       IF (ER.LE.0.01D0) GOTO 43434

       IF
((TRE1.GT.500.D0).AND.((ER1+ER2).LT.0.5D-9))
THEN
        INDEX=99
        GO TO 43434
       END IF

       IF (TRE1.GT.600.D0) THEN
        INDEX=999
        GO TO 43434
       END IF

       EXTA2=EXTA1
       EXTA1=0.D0
       EXTB2=EXTB1
       EXTB1=0.D0
       RAFA2=RAFA1
       RAFA1=0.D0
       RAFB2=RAFB1
       RAFB1=0.D0

     ENDIF

 170   TOUT=TOUT+DETAT
ccccccccccccccccccccccccccccccccccccccccccc
700
format(t2,f5.3,f9.6,f9.6,f9.6,f9.6,f9.6,
     *       f9.6,f9.6,f9.6)
ccccccccccccccccccccccccccccccccccccccccccc
43434      write(15,145)tout
           write(*,145)tout
ccccccccccccccccccccccccccccccccccccccccccc

if((cte110.ne.0.d0).or.(cte210.ne.0.d0))then
           PUX=100.D0*cte210/(cte110+cte210)
           else
           PUX=0.d0
         endif
         if(cte210.ne.0.d0)then
           SCX=(QEL+QFE)/QEX/cte210
           else
           SCX=0.d0
           endif
           RCX=100.D0*QEX*cte210/FEED
           PRX=60.D0*QEX*cte210/VSP

if((cte130.ne.0.d0).or.(cte230.ne.0.d0))then
           PUR=100.D0*cte130/(cte130+cte230)
           else
           PUR=0.d0
         endif
         if(cte130.ne.0.d0)then
           SCR=(QEL+QFE)/QRA/cte130
           else
           SCR=0.d0
         endif
           RCR=100.D0*QRA*cte130/FEED
           PRR=60.D0*QRA*cte130/VSP
c
  300 CONTINUE
c
      call GETTIM (ihr, imin, isec, i100th)
      write(15,9002)ihr, imin, isec, i100th
c
      WRITE(15,127) PUX,PUR
  127
FORMAT(2X,8HExtract:,7X,10HRaffinate:/
     *       2X,5HPUX =,F5.1,5X,5HPUR
=,F5.1,3X,1H%)
      WRITE(15,128) RCX,RCR,SCX,SCR
  128   FORMAT(2X,5HRCX =,F5.1,5X,5HRCR
=,F5.1,3X,1H%/
     *       2X,5HSCX =,F8.4,3X,5HSCR
=,F7.4,4H 1/g)
      WRITE(15,129) PRX,PRR
  129   FORMAT(2X,5HPRX =,F7.4,3X,5HPRR
=,F7.4,8H g/hr 1S/)
      WRITE(15,130) ER,INDEX
  130
FORMAT(/,2X,'ER=',F6.4,4X,'INDEX=',I4/)
      CLOSE(15)
C
      STOP
 5555     END
c
c ***************************************
      SUBROUTINE HERMITE(hkk,h,a,b)
      IMPLICIT DOUBLE PRECISION(A-H,O-Z)
c     hkk - subinterval size
c     h - matrix of the coefficient
c     a- matrix of first derivatives
c     b- matrix of second derivatives
      DIMENSION
h(2,4),a(2,4),b(2,4),h9(4),b9(2),h19(4),b19(2
)
      double precision hkk
c
      common /fcal4/nc,ne,neq,neq1,hk(26)
c
       data
h9/.8849001794597505d0,.1314458557658021d0
     *
,.1150998205402495d0,.3522081090086452d-01/
       data a9/.2886751345948129d0/
```

```
      data
b9/.3464101615137755d+01,.2732050807568877d+0
1/
c
      h(1,1)=h9(1)
      h(1,2)=h9(2)*hkk
      h(1,3)=h9(3)
      h(1,4)=-h9(4)*hkk
      h(2,1)=h9(3)
      h(2,2)=h9(4)*hkk
      h(2,3)=h9(1)
      h(2,4)=-h9(2)*hkk
c
      a(1,1)=-1.d0
      a(1,2)=a9*hkk
      a(1,3)=1.d0
      a(1,4)=-a9*hkk
      a(2,1)=-1.d0
      a(2,2)=-a9*hkk
      a(2,3)=1.d0
      a(2,4)=a9*hkk
c
      b(1,1)=-b9(1)
      b(1,2)=-b9(2)*hkk
      b(1,3)=b9(1)
      b(1,4)=-(b9(2)-2.d0)*hkk
      b(2,1)=b9(1)
      b(2,2)=(b9(2)-2.d0)*hkk
      b(2,3)=-b9(1)
      b(2,4)=b9(2)*hkk
c
      RETURN
      END
c
c ****************************************
      SUBROUTINE
RES(T,Y,YPRIME,DELTA,IRES,RPAR,IPAR)
      IMPLICIT DOUBLE PRECISION(A-H,O-Z)
      integer maxneq
      parameter (maxneq=850)
      DIMENSION
Y(maxneq),YPRIME(maxneq),DELTA(maxneq),AKI(ma
xneq),
     *          RJ(maxneq)
c
      COMMON /FCAL1/EP,PE,ALF
      COMMON /FCAL3/R(4)
      common /fcal4/nc,ne,neq,neq1,hk(26)
      COMMON /FCAL2/RF1,RF31,RF32,akgl,akfr
      COMMON
/MATRIZ1/BMAT(maxneq/2,maxneq/2),AMAT(maxneq,
maxneq),
     *
HMAT(maxneq,maxneq),HDMAT(maxneq,maxneq)
      common
/matriz3/hd1(maxneq/2),a1(maxneq/2),h1(maxneq
/2),
     *
b1(maxneq/2),hb2(maxneq/2),ab2(maxneq/2)
     *
,ha2(maxneq/2),aa2(maxneq/2),ba2(maxneq/2)
c
      do j=1,2*ne
        aki(j)=akgl
        rj(j)=r(1)
      enddo
      do j=4*ne+1,6*ne
        aki(j)=akgl
        rj(j)=r(2)
      enddo
      do j=8*ne+1,10*ne
        aki(j)=akgl
        rj(j)=r(3)
      enddo
      do j=12*ne+1,14*ne
        aki(j)=akgl
        rj(j)=r(4)
      enddo
      do j=2*ne+1,4*ne
        aki(j)=akfr
        rj(j)=r(1)
      enddo
      do j=6*ne+1,8*ne
        aki(j)=akfr
        rj(j)=r(2)
      enddo
      do j=10*ne+1,12*ne
        aki(j)=akfr
        rj(j)=r(3)
      enddo
      do j=14*ne+1,16*ne
        aki(j)=akfr
        rj(j)=r(4)
      enddo
c
      do j=1,ne*16
         delta(j)=0.d0
         delta(j+16*ne)=0.d0
         do i=1,16*ne
            delta(j)=delta(j)+
     *
(rj(j)*(1.d0/PE*bmat(j,i)-amat(j,i))*y(i)-
     *               (1.d0-
ep)/ep*alf*(aki(j)*hmat(j,i)*y(i)-
     *
hmat(j+16*ne,i+16*ne)*y(i+16*ne)))
c
            delta(j+16*ne)=delta(j+16*ne)+
     *
(amat(j+16*ne,i+16*ne)*y(i+16*ne)+
     *
alf*(aki(j)*hmat(j,i)*y(i)-
     *
hmat(j+16*ne,i+16*ne)*y(i+16*ne)))
         enddo

delta(j)=delta(j)+(rj(j)*(1.d0/PE*b1(j)-
a1(j))-
     *               (1.d0-
ep)/ep*alf*(aki(j)*h1(j)))
           delta(j+16*ne)=delta(j+16*ne)+
     *                alf*(aki(j)*h1(j))
c     addition of the 8 a's and b's terms
c     first subinterval
           if((j.eq.1).or.(j.eq.2))then

delta(j)=delta(j)+(rj(j)*(1.d0/PE*ba2(j)-
aa2(j))*
     *         y(neq1+15)-(1.d0-ep)/ep*alf*
     *         (aki(j)*ha2(j)*y(neq1+15)-
hb2(j)*y(neq1+1)))

delta(j+16*ne)=delta(j+16*ne)+ab2(j)*y(neq1+1
)+
     *        alf*(aki(j)*ha2(j)*y(neq1+15)-
hb2(j)*y(neq1+1))
           endif

if((j.eq.(2*ne+1)).or.(j.eq.(2*ne+2)))then

delta(j)=delta(j)+(rj(j)*(1.d0/PE*ba2(j)-
aa2(j))*
     *         y(neq1+16)-(1.d0-ep)/ep*alf*
     *         (aki(j)*ha2(j)*y(neq1+16)-
hb2(j)*y(neq1+2)))

delta(j+16*ne)=delta(j+16*ne)+ab2(j)*y(neq1+2
)+
     *        alf*(aki(j)*ha2(j)*y(neq1+16)-
hb2(j)*y(neq1+2))
           endif

if((j.eq.(4*ne+1)).or.(j.eq.(4*ne+2)))then

delta(j)=delta(j)+(rj(j)*(1.d0/PE*ba2(j)-
aa2(j))*
     *         y(neq1+9)-(1.d0-ep)/ep*alf*
     *         (aki(j)*ha2(j)*y(neq1+9)-
hb2(j)*y(neq1+3)))

delta(j+16*ne)=delta(j+16*ne)+ab2(j)*y(neq1+3
)+
     *        alf*(aki(j)*ha2(j)*y(neq1+9)-
hb2(j)*y(neq1+3))
```

```
            endif

if((j.eq.(6*ne+1)).or.(j.eq.(6*ne+2)))then

delta(j)=delta(j)+(rj(j)*(1.d0/PE*ba2(j)-
aa2(j))*
     *          y(neq1+10)-(1.d0-ep)/ep*alf*
     *          (aki(j)*ha2(j)*y(neq1+10)-
hb2(j)*y(neq1+4)))

delta(j+16*ne)=delta(j+16*ne)+ab2(j)*y(neq1+4
)+
     *        alf*(aki(j)*ha2(j)*y(neq1+10)-
hb2(j)*y(neq1+4))
            endif

if((j.eq.(8*ne+1)).or.(j.eq.(8*ne+2)))then

delta(j)=delta(j)+(rj(j)*(1.d0/PE*ba2(j)-
aa2(j))*
     *          y(neq1+11)-(1.d0-ep)/ep*alf*
     *          (aki(j)*ha2(j)*y(neq1+11)-
hb2(j)*y(neq1+5)))

delta(j+16*ne)=delta(j+16*ne)+ab2(j)*y(neq1+5
)+
     *        alf*(aki(j)*ha2(j)*y(neq1+11)-
hb2(j)*y(neq1+5))
            endif

if((j.eq.(10*ne+1)).or.(j.eq.(10*ne+2)))then

delta(j)=delta(j)+(rj(j)*(1.d0/PE*ba2(j)-
aa2(j))*
     *          y(neq1+12)-(1.d0-ep)/ep*alf*
     *          (aki(j)*ha2(j)*y(neq1+12)-
hb2(j)*y(neq1+6)))

delta(j+16*ne)=delta(j+16*ne)+ab2(j)*y(neq1+6
)+
     *        alf*(aki(j)*ha2(j)*y(neq1+12)-
hb2(j)*y(neq1+6))
            endif

if((j.eq.(12*ne+1)).or.(j.eq.(12*ne+2)))then

delta(j)=delta(j)+(rj(j)*(1.d0/PE*ba2(j)-
aa2(j))*
     *          y(neq1+13)-(1.d0-ep)/ep*alf*
     *          (aki(j)*ha2(j)*y(neq1+13)-
hb2(j)*y(neq1+7)))

delta(j+16*ne)=delta(j+16*ne)+ab2(j)*y(neq1+7
)+
     *        alf*(aki(j)*ha2(j)*y(neq1+13)-
hb2(j)*y(neq1+7))
            endif

if((j.eq.(14*ne+1)).or.(j.eq.(14*ne+2)))then

delta(j)=delta(j)+(rj(j)*(1.d0/PE*ba2(j)-
aa2(j))*
     *          y(neq1+14)-(1.d0-ep)/ep*alf*
     *          (aki(j)*ha2(j)*y(neq1+14)-
hb2(j)*y(neq1+8)))

delta(j+16*ne)=delta(j+16*ne)+ab2(j)*y(neq1+8
)+
     *        alf*(aki(j)*ha2(j)*y(neq1+14)-
hb2(j)*y(neq1+8))
            endif
c     last subinterval
            if((j.eq.(2*ne-
1)).or.(j.eq.(2*ne)))then

delta(j)=delta(j)+(rj(j)*(1.d0/PE*ba2(j)-
aa2(j))*
     *      y(neq1+9)-(1.d0-ep)/ep*alf*
     *      (aki(j)*ha2(j)*y(neq1+9)-
hb2(j+4*ne)*y(neq1+3)))

delta(j+16*ne)=delta(j+16*ne)+ab2(j)*y(neq1+3
)+
     *      alf*(aki(j)*ha2(j)*y(neq1+9)-
hb2(j+4*ne)*y(neq1+3))
            endif
            if((j.eq.(4*ne-
1)).or.(j.eq.(4*ne)))then

delta(j)=delta(j)+(rj(j)*(1.d0/PE*ba2(j)-
aa2(j))*
     *      y(neq1+10)-(1.d0-ep)/ep*alf*
     *     (aki(j)*ha2(j)*y(neq1+10)-
hb2(j+4*ne)*y(neq1+4)))

delta(j+16*ne)=delta(j+16*ne)+ab2(j)*y(neq1+4
)+
     *     alf*(aki(j)*ha2(j)*y(neq1+10)-
hb2(j+4*ne)*y(neq1+4))
            endif
            if((j.eq.(6*ne-
1)).or.(j.eq.(6*ne)))then

delta(j)=delta(j)+(rj(j)*(1.d0/PE*ba2(j)-
aa2(j))*
     *      y(neq1+11)-(1.d0-ep)/ep*alf*
     *     (aki(j)*ha2(j)*y(neq1+11)-
hb2(j+4*ne)*y(neq1+5)))

delta(j+16*ne)=delta(j+16*ne)+ab2(j)*y(neq1+5
)+
     *     alf*(aki(j)*ha2(j)*y(neq1+11)-
hb2(j+4*ne)*y(neq1+5))
            endif
            if((j.eq.(8*ne-
1)).or.(j.eq.(8*ne)))then

delta(j)=delta(j)+(rj(j)*(1.d0/PE*ba2(j)-
aa2(j))*
     *          y(neq1+12)-(1.d0-ep)/ep*alf*
     *       (aki(j)*ha2(j)*y(neq1+12)-
hb2(j)*y(neq1+6)))

delta(j+16*ne)=delta(j+16*ne)+ab2(j)*y(neq1+6
)+
     *         alf*(aki(j)*ha2(j)*y(neq1+12)-
hb2(j)*y(neq1+6))
            endif
            if((j.eq.(10*ne-
1)).or.(j.eq.(10*ne)))then

delta(j)=delta(j)+(rj(j)*(1.d0/PE*ba2(j)-
aa2(j))*
     *          y(neq1+13)-(1.d0-ep)/ep*alf*
     *        (aki(j)*ha2(j)*y(neq1+13)-
hb2(j)*y(neq1+7)))

delta(j+16*ne)=delta(j+16*ne)+ab2(j)*y(neq1+7
)+
     *         alf*(aki(j)*ha2(j)*y(neq1+13)-
hb2(j)*y(neq1+7))
            endif
            if((j.eq.(12*ne-
1)).or.(j.eq.(12*ne)))then

delta(j)=delta(j)+(rj(j)*(1.d0/PE*ba2(j)-
aa2(j))*
     *          y(neq1+14)-(1.d0-ep)/ep*alf*
     *         (aki(j)*ha2(j)*y(neq1+14)-
hb2(j)*y(neq1+8)))

delta(j+16*ne)=delta(j+16*ne)+ab2(j)*y(neq1+8
)+
     *         alf*(aki(j)*ha2(j)*y(neq1+14)-
hb2(j)*y(neq1+8))
            endif
            if((j.eq.(14*ne-
1)).or.(j.eq.(14*ne)))then

delta(j)=delta(j)+(rj(j)*(1.d0/PE*ba2(j)-
aa2(j))*
     *          y(neq1+15)-(1.d0-ep)/ep*alf*
```

```
     *        (aki(j)*ha2(j)*y(neq1+15)-
hb2(j)*y(neq1+1)))

delta(j+16*ne)=delta(j+16*ne)+ab2(j)*y(neq1+1
)+
     *         alf*(aki(j)*ha2(j)*y(neq1+15)-
hb2(j)*y(neq1+1))
              endif
              if((j.eq.(16*ne-
1)).or.(j.eq.(16*ne)))then

delta(j)=delta(j)+(rj(j)*(1.d0/PE*ba2(j)-
aa2(j))*
     *          y(neq1+16)-(1.d0-ep)/ep*alf*
     *        (aki(j)*ha2(j)*y(neq1+16)-
hb2(j)*y(neq1+2)))

delta(j+16*ne)=delta(j+16*ne)+ab2(j)*y(neq1+2
)+
     *         alf*(aki(j)*ha2(j)*y(neq1+16)-
hb2(j)*y(neq1+2))
              endif
          enddo
cc
          do j=1,ne*16
             do i=1,16*ne
              delta(j)=delta(j)-
hdmat(j,i)*yprime(i)
              delta(j+16*ne)=delta(j+16*ne)-
     *
        hdmat(j+16*ne,i+16*ne)*yprime(i+16*ne)
             enddo
              delta(j)=delta(j)-hd1(j)
              if((j.eq.1).or.(j.eq.2))then
                delta(j)=delta(j)-
ha2(j)*yprime(neq1+15)
                delta(j+16*ne)=delta(j+16*ne)-
hb2(j)*yprime(neq1+1)
              endif

if((j.eq.(2*ne+1)).or.(j.eq.(2*ne+2)))then
                delta(j)=delta(j)-
ha2(j)*yprime(neq1+16)
                delta(j+16*ne)=delta(j+16*ne)-
hb2(j)*yprime(2+neq1)
              endif

if((j.eq.(4*ne+1)).or.(j.eq.(4*ne+2)))then
                delta(j)=delta(j)-
ha2(j)*yprime(neq1+9)
                delta(j+16*ne)=delta(j+16*ne)-
hb2(j)*yprime(3+neq1)
              endif

if((j.eq.(6*ne+1)).or.(j.eq.(6*ne+2)))then
                delta(j)=delta(j)-
ha2(j)*yprime(neq1+10)
                delta(j+16*ne)=delta(j+16*ne)-
hb2(j)*yprime(4+neq1)
              endif

if((j.eq.(8*ne+1)).or.(j.eq.(8*ne+2)))then
                delta(j)=delta(j)-
ha2(j)*yprime(neq1+11)
                delta(j+16*ne)=delta(j+16*ne)-
hb2(j)*yprime(5+neq1)
              endif

if((j.eq.(10*ne+1)).or.(j.eq.(10*ne+2)))then
                delta(j)=delta(j)-
ha2(j)*yprime(neq1+12)
                delta(j+16*ne)=delta(j+16*ne)-
hb2(j)*yprime(6+neq1)
              endif

if((j.eq.(12*ne+1)).or.(j.eq.(12*ne+2)))then
                delta(j)=delta(j)-
ha2(j)*yprime(neq1+13)
                delta(j+16*ne)=delta(j+16*ne)-
hb2(j)*yprime(7+neq1)
              endif

if((j.eq.(14*ne+1)).or.(j.eq.(14*ne+2)))then
                delta(j)=delta(j)-
ha2(j)*yprime(neq1+14)
                delta(j+16*ne)=delta(j+16*ne)-
hb2(j)*yprime(8+neq1)
              endif
c
              if((j.eq.(2*ne-
1)).or.(j.eq.(2*ne)))then
                delta(j)=delta(j)-
ha2(j)*yprime(neq1+9)
                delta(j+16*ne)=delta(j+16*ne)-
hb2(j)*yprime(neq1+3)
              endif
              if((j.eq.(4*ne-
1)).or.(j.eq.(4*ne)))then
                delta(j)=delta(j)-
ha2(j)*yprime(neq1+10)
                delta(j+16*ne)=delta(j+16*ne)-
hb2(j)*yprime(4+neq1)
              endif
              if((j.eq.(6*ne-
1)).or.(j.eq.(6*ne)))then
                delta(j)=delta(j)-
ha2(j)*yprime(neq1+11)
                delta(j+16*ne)=delta(j+16*ne)-
hb2(j)*yprime(5+neq1)
              endif
              if((j.eq.(8*ne-
1)).or.(j.eq.(8*ne)))then
                delta(j)=delta(j)-
ha2(j)*yprime(neq1+12)
                delta(j+16*ne)=delta(j+16*ne)-
hb2(j)*yprime(6+neq1)
              endif
              if((j.eq.(10*ne-
1)).or.(j.eq.(10*ne)))then
                delta(j)=delta(j)-
ha2(j)*yprime(neq1+13)
                delta(j+16*ne)=delta(j+16*ne)-
hb2(j)*yprime(7+neq1)
              endif
              if((j.eq.(12*ne-
1)).or.(j.eq.(12*ne)))then
                delta(j)=delta(j)-
ha2(j)*yprime(neq1+14)
                delta(j+16*ne)=delta(j+16*ne)-
hb2(j)*yprime(8+neq1)
              endif
              if((j.eq.(14*ne-
1)).or.(j.eq.(14*ne)))then
                delta(j)=delta(j)-
ha2(j)*yprime(neq1+15)
                delta(j+16*ne)=delta(j+16*ne)-
hb2(j)*yprime(1+neq1)
              endif
              if((j.eq.(16*ne-
1)).or.(j.eq.(16*ne)))then
                delta(j)=delta(j)-
ha2(j)*yprime(neq1+16)
                delta(j+16*ne)=delta(j+16*ne)-
hb2(j)*yprime(2+neq1)
              endif
          enddo
ccccc  equation for qij for u=0
           delta(neq1+1)=-
yprime(neq1+1)+(y(1+16*ne)
     *
+alf*(aki(1)*(RF1*y(neq1+15)+1.d0/PE*y(1))-
y(neq1+1)))
           delta(neq1+2)=-
yprime(neq1+2)+(y(2*ne+1+16*ne)
     *
+alf*(aki(6*ne+1)*(RF1*y(neq1+16)+1.d0/PE*y(2
*ne+1))-y(neq1+2)))
           delta(neq1+3)=-
yprime(neq1+3)+(y(4*ne+1+16*ne)
     *
+alf*(aki(1)*(y(neq1+9)+1.d0/PE*y(4*ne+1))-
y(neq1+3)))
```

```
        delta(neq1+4)=-
yprime(neq1+4)+(y(6*ne+1+16*ne)
     *
+alf*(aki(6*ne+1)*(y(neq1+10)+1.d0/PE*y(6*ne+
1))-y(neq1+4)))
        delta(neq1+5)=-
yprime(neq1+5)+(y(8*ne+1+16*ne)
     *
+alf*(aki(1)*(RF32*y(neq1+11)+RF31*100.d0*dex
p(-100.d0*T)+
     *   1.d0/PE*y(8*ne+1))-y(neq1+5)))
        delta(neq1+6)=-
yprime(neq1+6)+(y(10*ne+1+16*ne)
     *
+alf*(aki(6*ne+1)*(RF32*y(neq1+12)+RF31*100.d
0*dexp(-100.d0*T)+
     *   1.d0/PE*y(10*ne+1))-y(neq1+6)))
        delta(neq1+7)=-
yprime(neq1+7)+(y(12*ne+1+16*ne)
     *
+alf*(aki(1)*(y(neq1+13)+1.d0/PE*y(12*ne+1))-
y(neq1+7)))
        delta(neq1+8)=-
yprime(neq1+8)+(y(14*ne+1+16*ne)
     *
+alf*(aki(6*ne+1)*(y(neq1+14)+1.d0/PE*y(14*ne
+1))-y(neq1+8)))
ccccc equation for cij for u=1
c       delta(neq1+9)=yprime(neq1+9)-
(rj(1)*(1.d0/(PE*hk(ne)*hk(ne))
c     *    *(6.d0*y(2*ne-
2)+2.d0*hk(ne)*y(2*ne-1)-6.d0*y(neq1+9)+
c     *     4.d0*hk(ne)*y(2*ne))-y(2*ne))-
c     *     (1.d0-
ep)/ep*alf*(aki(1)*y(2*ne*16+9)-y(neq1+1)))
       delta(neq1+9)=-yprime(neq1+9)+(rj(1)*(-
y(2*ne)))-
     *     (1.d0-ep)/ep*alf*(aki(1)*y(neq1+9)-
y(neq1+3))
c       delta(neq1+10)=yprime(neq1+10)-
(rj(1)*(1.d0/(PE*hk(ne)*
c     *    hk(ne))*(6.d0*y(2*ne-
2+2*ne)+2.d0*hk(ne)*y(2*ne-1+2*ne)-
c     *      6.d0*y(neq1+10)+
c     *     4.d0*hk(ne)*y(2*ne+2*ne))-
y(2*ne+2*ne))-
c     *     (1.d0-
ep)/ep*alf*(aki(6*ne+1)*y(neq1+10)-
y(neq1+2)))
       delta(neq1+10)=-
yprime(neq1+10)+(rj(1)*(-y(2*ne+2*ne)))-
     *     (1.d0-
ep)/ep*alf*(aki(6*ne+1)*y(neq1+10)-y(neq1+4))
c       delta(neq1+11)=yprime(neq1+11)-
(rj(1)*(1.d0/(PE*hk(ne)*
c     *    hk(ne))*(6.d0*y(2*ne-
2+4*ne)+2.d0*hk(ne)*y(2*ne-1+4*ne)-
c     *      6.d0*y(neq1+11)+
c     *     4.d0*hk(ne)*y(2*ne+4*ne))-
y(2*ne+4*ne))-
c     *     (1.d0-
ep)/ep*alf*(aki(1)*y(2*ne*16+11)-y(neq1+3)))
       delta(neq1+11)=-
yprime(neq1+11)+(rj(1)*(-y(2*ne+4*ne)))-
     *     (1.d0-
ep)/ep*alf*(aki(1)*y(neq1+11)-y(neq1+5))
c       delta(neq1+12)=yprime(neq1+12)-
(rj(1)*(1.d0/(PE*hk(ne)*
c     *    hk(ne))*(6.d0*y(2*ne-
2+6*ne)+2.d0*hk(ne)*y(2*ne-1+6*ne)-
c     *      6.d0*y(neq1+12)+
c     *     4.d0*hk(ne)*y(2*ne+6*ne))-
y(2*ne+6*ne))-
c     *     (1.d0-
ep)/ep*alf*(aki(6*ne+1)*y(2*ne*16+12)-
y(neq1+4)))
       delta(neq1+12)=-
yprime(neq1+12)+(rj(1)*(-y(2*ne+6*ne)))-
     *     (1.d0-
ep)/ep*alf*(aki(6*ne+1)*y(neq1+12)-y(neq1+6))
c       delta(neq1+13)=yprime(neq1+13)-
(rj(1)*(1.d0/(PE*hk(ne)*
c     *    hk(ne))*(6.d0*y(2*ne-
2+8*ne)+2.d0*hk(ne)*y(2*ne-1+8*ne)-
c     *      6.d0*y(neq1+13)+
c     *     4.d0*hk(ne)*y(2*ne+8*ne))-
y(2*ne+8*ne))-
c     *     (1.d0-
ep)/ep*alf*(aki(1)*y(2*ne*16+13)-y(neq1+5)))
       delta(neq1+13)=-
yprime(neq1+13)+(rj(1)*(-y(2*ne+8*ne)))-
     *     (1.d0-
ep)/ep*alf*(aki(1)*y(neq1+13)-y(neq1+7))
c       delta(neq1+14)=yprime(neq1+14)-
(rj(1)*(1.d0/(PE*hk(ne)*
c     *    hk(ne))*(6.d0*y(2*ne-
2+10*ne)+2.d0*hk(ne)*y(2*ne-1+10*ne)-
c     *      6.d0*y(neq1+14)+
c     *     4.d0*hk(ne)*y(2*ne+10*ne))-
y(2*ne+10*ne))-
c     *     (1.d0-
ep)/ep*alf*(aki(6*ne+1)*y(2*ne*16+14)-
y(neq1+6)))
       delta(neq1+14)=-
yprime(neq1+14)+(rj(1)*(-y(2*ne+10*ne)))-
     *     (1.d0-
ep)/ep*alf*(aki(6*ne+1)*y(neq1+14)-y(neq1+8))
c       delta(neq1+15)=yprime(neq1+15)-
(rj(1)*(1.d0/(PE*hk(ne)*
c     *    hk(ne))*(6.d0*y(2*ne-
2+12*ne)+2.d0*hk(ne)*y(2*ne-1+12*ne)-
c     *      6.d0*y(neq1+15)+
c     *     4.d0*hk(ne)*y(2*ne+12*ne))-
y(2*ne+12*ne))-
c     *     (1.d0-
ep)/ep*alf*(aki(1)*y(2*ne*16+15)-y(neq1+7)))
       delta(neq1+15)=-
yprime(neq1+15)+(rj(1)*(-y(2*ne+12*ne)))-
     *     (1.d0-
ep)/ep*alf*(aki(1)*y(neq1+15)-y(neq1+1))
c       delta(neq1+16)=yprime(neq1+16)-
(rj(1)*(1.d0/(PE*hk(ne)*
c     *    hk(ne))*(6.d0*y(2*ne-
2+14*ne)+2.d0*hk(ne)*y(2*ne-1+14*ne)-
c     *      6.d0*y(neq1+16)+
c     *     4.d0*hk(ne)*y(2*ne+14*ne))-
y(2*ne+14*ne))-
c     *     (1.d0-
ep)/ep*alf*(aki(6*ne+1)*y(2*ne*16+16)-
y(neq1+8)))
       delta(neq1+16)=-
yprime(neq1+16)+(rj(1)*(-y(2*ne+14*ne)))-
     *     (1.d0-
ep)/ep*alf*(aki(6*ne+1)*y(neq1+16)-y(neq1+2))
c
      RETURN
      END
C -----------------------------------------
      SUBROUTINE
JAC(T,Y,YPRIME,PD,CJ,RPAR,IPAR)
      IMPLICIT DOUBLE PRECISION(A-H,O-Z)
      DIMENSION Y(1),YPRIME(1),PD(1,1)
      RETURN
      END
c  -----------------------------------------
```

```
C input file model parameters and operating
C conditions the others are estimated during
C the program
C
C 14, 0.88d0,0.50d0
C 12.92d0,10.69d0,7.62d0,2.23d0,5.30d0
C 120.d0,50.d0
C 0.40d0,2000.D0,0.1d0
C 2.6d0,10.5d0,2
C
```

C: Source code for the Steady-State TMB model using COLNEW

```
C       Program STMBode.f
C       Steady-state TMB: dc/dt and
C dq/dt=0, Gl -> Fr Separation
C   LDF - Linear Driving Force Model
C       Section by Section
C       Problem definition in
C       Subroutine FSUB
C               INITIALISATION
        IMPLICIT DOUBLE PRECISION (A-H,O-Z)
        DOUBLE PRECISION ZETA(6),
FSPACE(808700), TOL(6), Z(6)
      DOUBLE PRECISION LC, LJ
      INTEGER M(4), IPAR(11), ISPACE(26000),
LTOL(6)
      DIMENSION
Q(4),V(4),R(4),Q1(4),Q2(4),C1(4),C2(4),C10(4)
,C20(4)
C
      COMMON /FCAL1/EP,PE,ALF
      COMMON /FCAL2/RF1,RF31,RF32
      COMMON /FCAL3/RR,AKFR,AKGL
      COMMON /FCAL5/CONS1,CONS2,CONS3,CONS4
C
      EXTERNAL FSUB,DFSUB,GSUB,DGSUB,GETTIM
CC      INPUT - MODEL PARAMETERS:
OPEN (UNIT=12,FILE='dattmb',STATUS='OLD')
C       S.TIME(s), FEED CONC. (g/l), T.BAL.:
      READ(12,*) RP,CAFE,QBAL
C  PARAMETERS ( E ; PE ; K ), PARAMETER BETA:
      READ(12,*) EP,PE,AK,BETA
C          RATIO FLUID/SOLID VELOCITIES ZONE
           II AND III,
C         SMB RECYCLING FLOWRATE (ML/MIN):
      READ(12,*)R(2),R(3),QR
C       K VALUE (KFR, KGL MORE, LESS RETAINED)
      READ(12,*)AKFR,AKGL
C       COLUMNS ( DC (CM); LC(CM); NCS ):
      READ(12,*) DC,LC,NCS
      CLOSE (12)
 9999 CONTINUE
C
C       OUTPUT:
OPEN(UNIT=6,FILE='RSTMBODE')
       CALL GETTIM (IHR, IMIN, ISEC, I100TH)
      WRITE(6,9002)IHR, IMIN, ISEC, I100TH
 9002 FORMAT(I2,':',I2.2,':',I2.2,':',I2.2,'
',A,'m')
        WRITE(6,101)
  101 FORMAT(/2X,39Htmb fru/glu: Linear
Driving Force Model)
      WRITE(6,116)AKGL,AKFR,CAFE
  116 FORMAT(/2X,5Hkgl= ,F6.4,2X,7H  kfr=
,F6.4,2X,5H  C= ,F5.1,4H g/l/)
      WRITE(6,117)
  117 FORMAT(/2X,35HCASE OF LINEAR ADSORPTION
ISOTHERMS)
C
C       COLUMNS, SMB:
AC=DC*DC*3.141592654D0/4.D0
      VC=AC*LC
      LJ=FLOAT(NCS)*LC
      VSP=4.D0*FLOAT(NCS)*VC*(1.D0-EP)
      WRITE(6,102)
  102 FORMAT(2X,8HColumns:)
      WRITE(6,103) NCS,DC,LC,AC,LJ,VC
  103 FORMAT(2X,32HNumber of columns per
section : ,I1/
     *       2X,5HDc = ,F6.4,4H cm ,6X,5HLc =
,F7.4,3H cm/
     *       2X,5HAc = ,F6.4,4H cm2,6X,5HLj =
,F7.4,3H cm/
     *       2X,5HVc = ,F6.3,4H cm3/)
      US=LC/RP
C
C       SOLID VEL. (cm/s) RATIO FLUID/SOLID
TMB SECTION.
       QST=EP*VC/RP*60.D0
       AL=EP*AC*60.D0
       V(2)=R(2)*US
       V(3)=R(3)*US
       Q(2)=V(2)*AL
       Q(3)=V(3)*AL
       Q(2)=Q(2)+QST
       Q(3)=Q(3)+QST
       QS=(1-EP)*AC*US*60.d
C
C       SMB FLOWRATES (ml/min):
      Q(4)=QR
      QRA=Q(3)-Q(4)
      QEX=QBAL-QRA
```

```
      QFE=Q(3)-Q(2)
      QEL=QBAL-QFE
      Q(1)=QR+QEL
      WRITE(6,104)
  104 FORMAT(2X,4HSMB:)
      WRITE(6,105) QR,RP,QEL,Q(1),QEX,Q(2),
QFE,Q(3),QRA,Q(4)
  105 FORMAT(2X,5HQR = ,F5.2,7H
ml/min,4X,5HRP = ,F6.2,2H s/
     *       2X,5HQEL =,F5.2,7H
ml/min,4X,5HQ1 = ,F6.3,7H ml/min/
     *       2X,5HQEX =,F5.2,7H
ml/min,4X,5HQ2 = ,F6.3,7H ml/min/
     *       2X,5HQFE =,F5.2,7H
ml/min,4X,5HQ3 = ,F6.3,7H ml/min/
     *       2X,5HQRA =,F5.2,7H
ml/min,4X,5HQ4 = ,F6.3,7H ml/min/)
      DO 2 J=1,4
      Q(J)=Q(J)-QST
      V(J)=Q(J)/AL
      R(J)=V(J)/US
    2 CONTINUE
      WRITE(6,106)
  106 FORMAT(2X,4HTMB:)
      WRITE(6,107) QST,US
  107 FORMAT(2X,6HQST = ,F6.3,7H
ml/min,3X,5HUS = ,F6.4,5H cm/s)
      WRITE(6,108) (J,Q(J),J,V(J),J,R(J),
J=1,4)
  108 FORMAT(4(2X,1HQ,I1,3H = ,F6.3,7H
ml/min,3X,1HV,I1,3H = ,F6.4,
     *       5H cm/s,3X,1HR,I1,3H = ,F6.4/))
C
C       OTHERS MODEL PARAMETERS:
      ALF=AK*RP*FLOAT(NCS)
      RF1=Q(4)/Q(1)
      RF31=QFE/Q(3)*CAFE
      RF32=Q(2)/Q(3)
      WRITE(6,109)
  109 FORMAT(2X,17HModel parameters:)
      WRITE(6,110) EP,PE
  110 FORMAT(2X,6HEP  = ,F6.4,6X,5HPE =
,F5.0)
      WRITE(6,111) AK,ALF
  111 FORMAT(2X,5Hk  = ,E10.4,4H 1/s,6X,6HALF
= ,E10.4)
      WRITE(6,112) RF1,RF31,RF32
  112 FORMAT(2X,6HRF1 = ,F6.4,6X,7HRF31 =
,F7.4,4X,7HRF32 = ,F6.4)
C
       FEED=QFE*CAFE
C
C       **** COLNEW PARAMETERS******
C       NUMBER OF O.D.Es.
      NCOMP=4
C       O.D.E.s ORDER
      M(1)=1
      M(2)=1
      M(3)=2
      M(4)=2
C       LINEAR PROBLEM
      IPAR(1) = 0
C       4 COLLOCATION POINTS PER SUBINTERVAL
      IPAR(2) = 4
C       INITIAL UNIFORM MESH OF 50 SUBINT.
      IPAR(3) = 50
      IPAR(8) = 0
C   DIMENSION OF REAL WORK ARRAY FSPACE IS...
      IPAR(5) = 808700
C  DIMENSION OF INTEGER WORK ARRAY ISPACE IS
      IPAR(6) = 26000
C       PRINT NOT FULL OUTPUT.
      IPAR(7) = 1
C       NO INITIAL GUESS FOR SOL. IS PROVIDED
      IPAR(9) = 0
C       REGULAR PROBLEM
      IPAR(10) = 0
C       NO OF FIXED POINTS IN THE MESH
      IPAR(11) = 0
C       TOLERANCES ON ALL COMPONENTS
      IPAR(4) = 6
      DO 10 I=1,6
       LTOL(I) = I
   10  TOL(I) = .1D-8
C
C       INITIAL VALUES
       C1=0.0D0
       C2=0.0D0
       DO 99 I=1,4
         C1(I)=0.0D0
         C2(I)=0.0D0
         Q1(I)=0.0D0
         Q2(I)=0.0D0
         C10(I)=0.0D0
         C20(I)=0.0D0
  99   CONTINUE
C
C       ITERATIONS
      DO 333 JJ=1,50
C
C       FOR EACH SECTION J
       DO 11 J=1,4
         ALEFT = 0.D0
         ARIGHT = 1.D0
C
C       LOCATIONS OF SIDE CONDITIONS
         ZETA(1) = 0.D0
         ZETA(2) = 0.D0
         ZETA(3) = 1.D0
         ZETA(4) = 1.D0
         ZETA(5) = 1.D0
         ZETA(6) = 1.D0
C
C       VARIABLES UPDATE
C       SECTION I
         IF (J.EQ.1) THEN
           CONS1= RF1*C1(4)
           CONS2= RF1*C2(4)
           CONS3=Q1(2)
           CONS4=Q2(2)
         ENDIF
C
C       SECTION II
         IF (J.EQ.2) THEN
           CONS1= C1(1)
           CONS2= C2(1)
           CONS3=Q1(3)
           CONS4=Q2(3)
         ENDIF
C
C       SECTION III
         IF (J.EQ.3) THEN
           CONS1=RF32*C1(1)+RF31
           CONS2=RF32*C2(1)+RF31
           CONS3=Q1(4)
           CONS4=Q2(4)
         ENDIF
C
C       SECTION IV
         IF (J.EQ.4) THEN
           CONS1=C1(3)
           CONS2=C2(3)
           CONS3=Q1(1)
           CONS4=Q2(1)
         ENDIF
C
         RR=R(J)
C
C       ****** CALL  COLNEW ***********
C
         CALL COLNEW (NCOMP, M, ALEFT,
ARIGHT, ZETA, IPAR, LTOL, TOL,
     * DUMMY, ISPACE, FSPACE, IFLAG,
FSUB,DFSUB,GSUB,DGSUB,DUMMY)
C
C  PRINT OBTAINED APX. SOL. PTS X=0,.05,...,1
C
         X = 0.d0
         WRITE(6,131)
 131     FORMAT(1h1,46h   x   C(G)    C(F)
PG     PF      GG      GF/)
 132     FORMAT (i2,7d15.5)
C
C       *** CALL SUBROUTINE APPSLN ***
```

```
          DO 555 III=1,51
            CALL APPSLN (X,Z,FSPACE,ISPACE)
C
C       ** P, GG E DE GF  ESTIMATION **
              P=100.D0*Z(3)/(Z(3)+Z(5))
               GG=EP/(1-EP)*RR*Z(3)/Z(1)
               GF=EP/(1-EP)*RR*Z(5)/Z(2)
          IF (JJ.EQ.50) THEN
               WRITE(6,132)
J,X,Z(3),Z(5),P,(100.D0-P),GG,GF
            ENDIF
C
C       CHANGING VARIABLES
            IF (III.EQ.51) THEN
              C1(J)=Z(3)
              C2(J)=Z(5)
            ENDIF
            IF (III.EQ.1) THEN
              Q1(J)=Z(1)
              Q2(J)=Z(2)
            ENDIF
            X = X + .020D0
  555     CONTINUE
          ER1=DABS(C1(1)*QEX+C1(3)*QRA-
FEED)/FEED
          ER2=DABS(C2(1)*QEX+C2(3)*QRA-
FEED)/FEED
          ER3=DABS(C1(1)-
C10(1))/DABS(C1(1))+DABS(C2(1)-
C20(1))/DABS(C2(1))
          ER4=DABS(C1(3)-
C10(3))/DABS(C1(3))+DABS(C2(3)-
C20(3))/DABS(C2(3))
          ER=ER1+ER2+ER3+ER4
C
C       PU., RE., CONS. AND PROD. ESTIMATION
            IF
((JJ.EQ.50).OR.(ER.LE.0.001D0))THEN
              IF (J.EQ.1)THEN
                 PUX=100.D0*C2(1)/(C1(1)+C2(1))
                  RCX=100.D0*QEX*C2(1)/FEED
                  SCX=(QEL+QFE)/QEX/C2(1)
                  PRX=60.D0*QEX*C2(1)/VSP
                ENDIF
                IF (J.EQ.3)THEN

PUR=100.D0*C1(3)/(C1(3)+C2(3))
                  RCR=100.D0*QRA*C1(3)/FEED
                  SCR=(QEL+QFE)/QRA/C1(3)
                  PRR=60.D0*QRA*C1(3)/VSP
                ENDIF
            ENDIF
   11     CONTINUE
C
C       VARIABLES UPDATE
              C10(1)=C1(1)
              C1(1)=0.0D0
              C20(1)=C2(1)
              C2(1)=0.0D0
              C10(3)=C1(3)
              C1(3)=0.0D0
              C20(3)=C2(3)
              C2(3)=0.0D0
C
       IF(ER.LE.0.001D0)GOTO 1000
  333 CONTINUE
C
       CALL GETTIM (IHR, IMIN, ISEC, I100TH)
       WRITE(6,9002)IHR, IMIN, ISEC, I100TH
C
C       END
 1000 CONTINUE
C
       WRITE(6,127) PUX,PUR
  127 FORMAT(2X,8HExtract:,7X,10HRaffinate:/
     *       2X,5HPUX =,F5.1,5X,5HPUR
=,F5.1,3X,1H%)
      WRITE(6,128) RCX,RCR,SCX,SCR
  128 FORMAT(2X,5HRCX =,F5.1,5X,5HRCR
=,F5.1,3X,1H%/
     *       2X,5HSCX =,F8.4,3X,5HSCR
=,F7.4,4H 1/g)
       WRITE(6,129) PRX,PRR
  129 FORMAT(2X,5HPRX =,F7.4,3X,5HPRR
=,F7.4,8H g/hr lS/)
       WRITE(6,130)ER
  130 FORMAT(5x,5herro=,f8.4)
       CLOSE(6)
      STOP
      END
C
C       SUBROUTINE FSUB
SUBROUTINE FSUB (X, Z, F)
      IMPLICIT REAL*8 (A-H,O-Z)
      DIMENSION Z(6), F(4)
      COMMON /FCAL1/EP,PE,ALF
      COMMON /FCAL3/RR,AKFR,AKGL
C
C       DIFERENTIAL EQUATIONS AND VARIABLES
C     F(1)=DQ1/DX, F(2)=DQ2/DX,
F(3)=D2C1/DX2, F(4)=D2C2/DX2
C     Z(1)=Q1, Z(2)=Q2, Z(3)=C1, Z(4)=DC1/DX,
Z(5)=C2, Z(6)=DC2/DX
C
       F(1)=-ALF*(AKGL*Z(3)-Z(1))
       F(2)=-ALF*(AKFR*Z(5)-Z(2))
       F(3)=PE*Z(4)+(1.D0-
EP)/EP*PE/RR*ALF*(AKGL*Z(3)-Z(1))
       F(4)=PE*Z(6)+(1.D0-
EP)/EP*ALF*PE/RR*(AKFR*Z(5)-Z(2))
      RETURN
      END
C
C       SUBROUTINE DFSUB
SUBROUTINE DFSUB (X, Z, DF)
      IMPLICIT REAL*8 (A-H,O-Z)
      DIMENSION Z(6), DF(4,6)
      COMMON /FCAL1/EP,PE,ALF
      COMMON /FCAL3/RR,AKFR,AKGL
      COMMON /FCAL2/RF1,RF31,RF32
C
C        INITIALIZATION OF F JACOBIAN MATRIX
      DO 3 I=1,4
        DO 5 J=1,6
          DF(I,J)=0.D0
  5     CONTINUE
  3   CONTINUE
      DF(1,3)=-ALF*AKGL
      DF(1,1)=ALF
      DF(2,5)=-ALF*AKFR
      DF(2,2)=ALF
      DF(3,3)=(1.D0-EP)/EP*PE/RR*ALF*AKGL
      DF(3,4)=PE
      DF(3,1)=-(1.D0-EP)/EP*PE/RR*ALF
      DF(4,5)=(1.D0-EP)/EP*PE/RR*ALF*AKFR
      DF(4,6)=PE
      DF(4,2)=-(1.D0-EP)/EP*PE/RR*ALF
      RETURN
      END
C
C       SUBROUTINE GSUB
SUBROUTINE GSUB (I, Z, G)
      IMPLICIT REAL*8 (A-H,O-Z)
      DIMENSION Z(6)
      DOUBLE PRECISION G
      COMMON /FCAL1/EP,PE,ALF
      COMMON /FCAL2/RF1,RF31,RF32
      COMMON /FCAL5/CONS1,CONS2,CONS3,CONS4
C
C       BOUNDARY CONDITIONS
      GO TO (1,2,3,4,5,6), I
   1  G=Z(3)-1.D0/PE*Z(4)-CONS1
      RETURN
   2  G=Z(5)-1.D0/PE*Z(6)-CONS2
      RETURN
   3  G=Z(4)
      RETURN
   4  G=Z(6)
      RETURN
   5  G=Z(1)-CONS3
      RETURN
   6  G=Z(2)-CONS4
      RETURN
      END
```

```
C
C       SUBROUTINE DGSUB
SUBROUTINE DGSUB (I, Z, DG)
      IMPLICIT REAL*8 (A-H,O-Z)
      DIMENSION Z(6), DG(6)
      COMMON /FCAL1/EP,PE,ALF
      COMMON /FCAL2/RF1,RF31,RF32
C
C       INITIALIZATION OF G JACOBIAN MATRIZ
      DO 25 J=1,6
   25    DG(J) = 0. D0
      GO TO (1,2,3,4,5,6), I
    1 DG(3)=1.D0
      DG(4)=-1.D0/PE
      RETURN
    2 DG(5)=1.D0
      DG(6)=-1.D0/PE
      RETURN
    3 DG(4)=1.D0
      RETURN
    4 DG(6)=1.D0
      RETURN
    5 DG(1)=1.D0
      RETURN
    6 DG(2)=1.D0
      RETURN
      END
```

```
C input file model parameters and operating
C conditions the others are estimated during
C the program
C
C 120.d0,50.d0,12.92d0
C 0.40d0,2000.D0,0.1d0,1.2d0
C 0.8996d0,1.0996d0,18.12d0
C 0.88d0,0.50d0
C 2.6d0,10.5d0,2
C
```

D: Source code for the Transient model using PDECOL

```
C          PROGRAM: TMBFG.FOR
C          LINEAR DRIVING FORCE MODEL
C         PROGRAM USED FOR THE MODEL
C        T-TMB (4 SECTIONS).
C      (FRUCTOSE/GLUCOSE SEPARATION)
C
       IMPLICIT DOUBLE PRECISION (A-H,O-Z)
       DOUBLE PRECISION LC,LJ
       DIMENSION
XBKPT(15),SCTCH(200),WORK(150092),IWORK(1020)
       DIMENSION USOL(16,51),XPON(51)
       DIMENSION Q(4),V(4)
C
       COMMON /ENDPT/XLEFT,XRIGHT
       COMMON /GEAR0/DTUSED,NQ,NSTEPS,NF,NJ
       COMMON /FCAL1/EP,PE,ALF
       COMMON /FCAL2/RF1,RF31,RF32
       COMMON /FCAL3/R(4)
       COMMON /FCAL4/DCT(8),DQT(8)
C
       EXTERNAL GETTIM
       CHARACTER*9 FR
       CHARACTER TAB
       TAB=CHAR(9)
C
C      INPUT - MODELPARAMETERS:
       OPEN
(UNIT=12,FILE='DATTMB2',STATUS='OLD')
C  SMB FLOWRATES(ML/MIN):
       READ(12,*) QR,QEL,QEX,QFE,QRA
C            ROTATION   PERIOD   (S)   AND   FEED
CONCENTRATION (G/L):
       READ(12,*) RP,CAFE,CBFE
C      PARAMETERS ( E ; PE ; K ):
       READ(12,*) EP,PE,AK
C      COLUNMS ( DC (CM) ; LC(CM) ; NCS ):
       READ(12,*) DC,LC,NCS
       CLOSE(12)
C      OUTPUT:
C      ------------------------------------
       NRP=INT(1000.D0*AK)
       ILETRAS=1
       IDIGITOS=4
       FR(1:ILETRAS+1)='A'
       DO 500 I=1,IDIGITOS
            NCHAR=NRP/10**(IDIGITOS-I)
            NRP=NRP-NCHAR*10**(IDIGITOS-I)

FR(ILETRAS+I:ILETRAS+I+1)=CHAR(48+NCHAR)
  500 CONTINUE
C
       OPEN(UNIT=15,FILE=FR)
       CALL GETTIM (IHR, IMIN, ISEC, I100TH)
       WRITE(15,9002)IHR, IMIN, ISEC, I100TH
 9002   FORMAT(I2,':',I2.2,':',I2.2,':',I2.2,'
',A,'M')
C
       WRITE(15,101)
  101    FORMAT(/2X,41HTMB    FRU/GLU:    LINEAR
DRIVING FORCE MODEL//)
C      ---------------------------------
C    PDECOL PARAMETERS:
       NPDE=16
       NINT=14
       KORD=4
       NCC=2
       MF=22
       INDEX=1
       IWORK(1)=150092
       IWORK(2)=1020
       T0=0.D0
       DT=1.D-6
       EPS=1.D-7
       NPTS=NINT+1
       XBKPT(1)=0.D0
       XBKPT(2)=0.01D0
       XBKPT(3)=0.03D0
       XBKPT(4)=0.1D0
       XBKPT(13)=0.97D0
       XBKPT(14)=0.99D0
       XBKPT(15)=1.D0
       DO 1 K=5,12
            XBKPT(K)=0.1D0+0.1D0*DBLE(K-4)
    1 CONTINUE
       XLEFT=XBKPT(1)
       XRIGHT=XBKPT(NPTS)
       TOUT=0.D0
C
       CONT=1
C
```

```
      WRITE(15,116)
  116 FORMAT(/2X,22HKGL=0.314    KFR=0.625/)
      WRITE(15,117)
  117 FORMAT(/2X,36HCASE OF LINEAR ADSORPTION
ISOTHERMS//)
C
C     COLUNMS:
      AC=DC*DC*3.141592654D0/4.D0
      VC=AC*LC
      LJ=FLOAT(NCS)*LC
      VSP=4.D0*FLOAT(NCS)*VC*(1.D0-EP)
C
      WRITE(15,102)
  102 FORMAT(2X,8HCOLUMNS:)
      WRITE(15,103) NCS,DC,LC,AC,LJ,VC
  103  FORMAT(2X,32HNUMBER   OF   COLUMNS   PER
SECTION : ,I1/
     *       2X,5HDC = ,F6.4,4H CM ,6X,5HLC =
,F7.4,3H CM/
     *       2X,5HAC = ,F6.4,4H CM2,6X,5HLJ =
,F7.4,3H CM/
     *       2X,5HVC = ,F6.3,4H CM3/)
C
C     FLOWRATES IN SMB (ML/MIN):
      Q(4)=QR
      Q(1)=QR+QEL
      Q(2)=QR+QEL-QEX
      Q(3)=QR+QEL-QEX+QFE
      WRITE(15,104)
  104 FORMAT(2X,4HSMB:)
      WRITE(15,105) QR,RP,QEL,Q(1),QEX,Q(2),
     *              QFE,Q(3),QRA,Q(4)
  105      FORMAT(2X,5HQR      =      ,F5.2,7H
ML/MIN,4X,5HRP = ,F6.2,2H S/
     *                     2X,5HQEL   =,F5.2,7H
ML/MIN,4X,5HQ1 = ,F6.3,7H ML/MIN/
     *                     2X,5HQEX   =,F5.2,7H
ML/MIN,4X,5HQ2 = ,F6.3,7H ML/MIN/
     *                     2X,5HQFE   =,F5.2,7H
ML/MIN,4X,5HQ3 = ,F6.3,7H ML/MIN/
     *                     2X,5HQRA   =,F5.2,7H
ML/MIN,4X,5HQ4 = ,F6.3,7H ML/MIN/)
C
C     FLOWRATES (ML/MIN) E VELOCITIES (CM/S)
C     SOLID VELOCITY (CM/S)
C     RATIO LIQUID VELOCITY / SOLIDVELOCITY
C     IN TMB SECTIONS:
      QST=EP*VC/RP*60.D0
      AL=EP*AC*60.D0
      US=LC/RP
      DO 2 J=1,4
           Q(J)=Q(J)-QST
           V(J)=Q(J)/AL
           R(J)=V(J)/US
    2 CONTINUE
      WRITE(15,106)
  106 FORMAT(2X,4HTMB:)
      WRITE(15,107) QST,US
  107      FORMAT(2X,6HQST      =      ,F6.3,7H
ML/MIN,3X,5HUS = ,F6.4,5H CM/S)
      WRITE(15,108)      (J,Q(J),J,V(J),J,R(J),
J=1,4)
  108    FORMAT(4(2X,1HQ,I1,3H    =    ,F6.3,7H
ML/MIN,3X,1HV,I1,3H = ,F6.4,
     *       5H CM/S,3X,1HR,I1,3H = ,F6.4/))
C     ------------------------------------
C     OTHERS PARAMETERS OF THE MODL:
      ALF=AK*RP*FLOAT(NCS)
       RF1=Q(4)/Q(1)
      RF31=QFE/Q(3)*CAFE
      RF32=Q(2)/Q(3)
C
      WRITE(15,109)
  109 FORMAT(2X,17HMODEL PARAMETERS:)
      WRITE(15,110) EP,PE
  110   FORMAT(2X,6HEP     =   ,F6.4,6X,5HPE   =
,F5.0)
      WRITE(15,111) AK,ALF
  111 FORMAT(2X,5HK   = ,E10.4,4H 1/S,6X,6HALF
= ,E10.4)
      WRITE(15,112) RF1,RF31,RF32
  112   FORMAT(2X,6HRF1   =   ,F6.4,6X,7HRF31   =
,F6.4,4X,7HRF32 = ,F6.4)
C
C PDECOL PARAMETERS:
      DETAT=0.01D0
      TRE1=0.D0
      TRE2=1.D0
      EXTA1=0.D0
      EXTB1=0.D0
      RAFA1=0.D0
      RAFB1=0.D0
      EXTA2=0.D0
      EXTB2=0.D0
      RAFA2=0.D0
      RAFB2=0.D0
C
      DO 6 K=1,8
              DCT(K)=0.D0
              DQT(K)=0.D0
    6 CONTINUE
C
      FEED=QFE*CAFE
WRITE(15,113)
  113 FORMAT(///2X,8HRESULTS:,/)
C
      DPX=1.D0/50.D0
      DO 3 K=1,51
                XPON(K)=DBLE(K-1)*DPX
    3 CONTINUE
      NPP=51
C
   10 TOUT=TOUT+DETAT
      CALL PDECOL(T0,TOUT,DT,XBKPT,EPS,NINT,
     * KORD,NCC,NPDE, MF,INDEX,WORK,IWORK)
C
      IF (INDEX.NE.0) GOTO 100
C
      CALL
VALUES(XPON,USOL,SCTCH,NPDE,NPP,NPP,0,WORK)
C
      IF   ((TOUT.GE.TRE1).AND.(TOUT.LE.TRE2))
THEN

EXTA1=EXTA1+USOL(1,51)*DETAT

EXTB1=EXTB1+USOL(2,51)*DETAT

RAFA1=RAFA1+USOL(5,51)*DETAT

RAFB1=RAFB1+USOL(6,51)*DETAT
      END IF
C
      IF (TOUT.GE.TRE2) THEN
              TRE1=TRE1+1.D0
              TRE2=TRE2+1.D0
        ER1=DABS(EXTA1-
EXTA2)/DABS(EXTA1)+DABS(EXTB1-
EXTB2)/DABS(EXTB1)
          ER2=DABS(RAFA1-
RAFA2)/DABS(RAFA1)+DABS(RAFB1-
RAFB2)/DABS(RAFB1)
          ER3=DABS(EXTA1*QEX+RAFA1*QRA-
FEED)/FEED
          ER4=DABS(EXTB1*QEX+RAFB1*QRA-
FEED)/FEED
          ER=ER1+ER2+ER3+ER4
C
PUX=100.D0*USOL(2,51)/(USOL(1,51)+USOL(2,51))
           RCX=100.D0*QEX*USOL(2,51)/FEED
              SCX=(QEL+QFE)/QEX/USOL(2,51)
              PRX=60.D0*QEX*USOL(2,51)/VSP

PUR=100.D0*USOL(5,51)/(USOL(5,51)+USOL(6,51))

RCR=100.D0*QRA*USOL(5,51)/FEED
              SCR=(QEL+QFE)/QRA/USOL(5,51)
              PRR=60.D0*QRA*USOL(5,51)/VSP
C
            IF (ER.LE.0.01D0) GOTO 100
            IF
((TRE1.GT.200.D0).AND.((ER1+ER2).LT.0.005D0))
THEN
```

```
                INDEX=99
                GO TO 100
            END IF
C
            IF (TRE1.GT.500.D0) THEN
                INDEX=999
                GO TO 100
            END IF
C
             EXTA2=EXTA1
             EXTA1=0.D0
             EXTB2=EXTB1
             EXTB1=0.D0
             RAFA2=RAFA1
             RAFA1=0.D0
             RAFB2=RAFB1
             RAFB1=0.D0
C
C      APRESENTATION OF RESULTS FOR EACH CICLE
(1 CICLE=>TOUT=4)
        IF
((INT(TOUT*1000+0.5)/1000).EQ.(4*CONT)) THEN
          CONT=CONT+1
          WRITE(15,145)TOUT
  145     FORMAT(4HT = ,F5.1)
          WRITE(15,131)
TAB,TAB,TAB,TAB,TAB,TAB
          DO 8 J=1,4
              DO 9 K=1,51
            IF
(USOL(2*J,K).NE.0.D0.OR.USOL(2*J-
1,K).NE.0.D0) THEN
                P=100.D0*USOL(2*J-
1,K)/(USOL(2*J-1,K)+USOL(2*J,K))
                    ELSE
                        P=0.D0
                  ENDIF
              IF (USOL(2*J+7,K).NE.0.D0) THEN
                    GG=EP/(1-
EP)*R(J)*USOL(2*J-1,K)/USOL(2*J+7,K)
                    ELSE
                    GG=0.D0
                  ENDIF
              IF (USOL(2*J+8,K).NE.0.D0) THEN
                    GF=EP/(1-
EP)*R(J)*USOL(2*J,K)/USOL(2*J+8,K)
                    ELSE
                      GF=0.D0
               ENDIF
               WRITE(15,132)  XPON(K)+DBLE(J-
1),TAB,USOL(2*J-1,K),
     *
TAB,USOL(2*J,K),TAB,P,TAB,(100.D0-P),
     *              TAB,GG,TAB,GF
    9       CONTINUE
    8     CONTINUE
          WRITE(15,127) PUX,PUR
          WRITE(15,128) RCX,RCR,SCX,SCR
          WRITE(15,129) PRX,PRR
        ENDIF
        END IF
        GOTO 10
  100 CONTINUE
C
      CALL GETTIM (IHR, IMIN, ISEC, I100TH)
      WRITE(15,9002)IHR, IMIN, ISEC, I100TH
      WRITE(15,127) PUX,PUR
  127 FORMAT(2X,8HEXTRACT:,7X,10HRAFFINATE:/
     *               2X,5HPUX   =,F5.1,5X,5HPUR
=,F5.1,3X,1H%)
      WRITE(15,128) RCX,RCR,SCX,SCR
  128     FORMAT(2X,5HRCX      =,F5.1,5X,5HRCR
=,F5.1,3X,1H%/
     *               2X,5HSCX   =,F8.4,3X,5HSCR
=,F7.4,4H L/G)
      WRITE(15,129) PRX,PRR
  129     FORMAT(2X,5HPRX      =,F7.4,3X,5HPRR
=,F7.4,8H G/HR LS/)
      WRITE(15,130) INDEX
  130 FORMAT(/,2X,'INDEX=',I5/)
      WRITE(15,*)TOUT
      WRITE(15,131) TAB,TAB,TAB,TAB,TAB,TAB
  131
FORMAT(1HX,A1,4HC(G),A1,4HC(F),A1,5HPU(G),A1,
5HPU(F),A1,2HGG
     *         ,A1,2HGF)
      DO 94 J=1,4
          DO 95 K=1,51
            P=100.D0*USOL(2*J-
1,K)/(USOL(2*J-1,K)+USOL(2*J,K))
            GG=EP/(1-EP)*R(J)*USOL(2*J-
1,K)/USOL(2*J+7,K)
            GF=EP/(1-
EP)*R(J)*USOL(2*J,K)/USOL(2*J+8,K)
            WRITE(15,132)    XPON(K)+DBLE(J-
1),TAB,USOL(2*J-1,K),
     *
TAB,USOL(2*J,K),TAB,P,TAB,(100.D0-P),
     *                    TAB,GG,TAB,GF
  132     FORMAT (F7.4,6(A1,F9.5))
   95   CONTINUE
   94 CONTINUE
C
      CLOSE(15)
      STOP
      END
C+++++++++++++++++++++++++++++++++++++++++++
C           SUBROUTINE F
C         PDE'S AND ODE'S DEFINITION
C     ----------------------------------
      SUBROUTINE F(T,X,U,UX,UXX,FVAL,NPDE)
      IMPLICIT DOUBLE PRECISION (A-H,O-Z)
      DIMENSION U(16),UX(16),UXX(16),FVAL(16)
      COMMON /FCAL1/EP,PE,ALF
      COMMON /FCAL3/R(4)
      COMMON /FCAL4/DCT(8),DQT(8)
C
      DO 1 J=1,4

FVAL(2*J+7)=UX(2*J+7)+ALF*(0.314D0*U(2*J-1)-
U(2*J+7))

FVAL(2*J+8)=UX(2*J+8)+ALF*(0.625D0*U(2*J)-
U(2*J+8))
          FVAL(2*J-1)=R(J)*(UXX(2*J-1)/PE-
UX(2*J-1))-
     *                                    (1.D0-
EP)/EP*ALF*(0.314D0*U(2*J-1)-U(2*J+7))
          FVAL(2*J)=R(J)*(UXX(2*J)/PE-
UX(2*J))-
     *                                    (1.D0-
EP)/EP*ALF*(0.625D0*U(2*J)-U(2*J+8))
    1 CONTINUE
C
      IF (X.EQ.0.D0) THEN
            DO 2 K=1,8
              DQT(K)=FVAL(K+8)
    2   CONTINUE
      END IF
IF (X.EQ.1.D0) THEN
          DO 3 K=1,8
            DCT(K)=FVAL(K)
    3   CONTINUE
      END IF
      RETURN
      END
C+++++++++++++++++++++++++++++++++++++++++++
C             SUBROUTINE BNDRY
C          DEFINITON OF BOUNDARY CONDITIONS
C     ----------------------------------
      SUBROUTINE
BNDRY(T,X,U,UX,DBDU,DBDUX,DZDT,NPDE)
      IMPLICIT DOUBLE PRECISION (A-H,O-Z)
      DIMENSION U(16),UX(16),DZDT(16)
      DIMENSION DBDU(16,16),DBDUX(16,16)
      COMMON /FCAL1/EP,PE,ALF
      COMMON /FCAL2/RF1,RF31,RF32
      COMMON /FCAL4/DCT(8),DQT(8)
C
C     INICIALIZATION:
            DO 1 K=1,16
              DZDT(K)=0.D0
              DO 2 J=1,16
               DBDU(K,J)=0.D0
```

```
                        DBDUX(K,J)=0.D0
    2   CONTINUE
    1 CONTINUE
C
      IF (X.GT..5D0) GOTO 10
C     X=0:
           DO 3 K=1,8
              DBDU(K,K)=1.D0
              DBDUX(K,K)=-1.D0/PE
    3 CONTINUE
C
      DZDT(1)=RF1*DCT(7)
      DZDT(2)=RF1*DCT(8)
      DZDT(3)=DCT(1)
      DZDT(4)=DCT(2)
      DZDT(5)=RF31*100.D0*DEXP(-
100.D0*T)+RF32*DCT(3)
      DZDT(6)=RF31*100.D0*DEXP(-
100.D0*T)+RF32*DCT(4)
      DZDT(7)=DCT(5)
      DZDT(8)=DCT(6)
      RETURN
10 CONTINUE
C
C     X=1:
           DO 4 K=1,8
              DBDU(K+8,K+8)=1.D0
    4 CONTINUE
      DZDT(9)=DQT(3)
      DZDT(10)=DQT(4)
      DZDT(11)=DQT(5)
      DZDT(12)=DQT(6)
      DZDT(13)=DQT(7)
      DZDT(14)=DQT(8)
      DZDT(15)=DQT(1)
      DZDT(16)=DQT(2)
      RETURN
      END
C+++++++++++++++++++++++++++++++++++++++++++++
++++++++++++++++
C                     SUBROUTINE UINIT
C           DEFINITION OF INITIAL CONDITIONS
C     ------------------------------------
      SUBROUTINE UINIT(X,U,NPDE)
      IMPLICIT DOUBLE PRECISION (A-H,O-Z)
      DIMENSION U(16)
      COMMON /ENDPT/XLEFT,XRIGHT
C
      DO 1 K=1,16
            U(K)=0.D0
    1 CONTINUE
      RETURN
      END
C+++++++++++++++++++++++++++++++++++++++++

C input file model parameters and operating
C conditions the others are estimated during
C the program
C
C 12.92d0,10.69d0,7.62d0,2.23d0,5.30d0
C 120.d0,50.d0,50.d0
C 0.40d0,2000.D0,0.1d0
C 0.88d0,0.50d0
C 2.6d0,10.5d0,2
C
```

E: Modelling intraparticle diffusion, adsorption and reaction (with spatial discretization)

E.1 Numerical solutions

The partial differential equation to be solved is the following,

$$\upsilon_i \frac{\left(\varepsilon_p + K_{enz}\right)}{\left(\varepsilon_p + K_i\right)} \Re\left(c_{pi}\right) + \frac{D_{pe}}{\left(\varepsilon_p + K_i\right)} \left(\frac{\partial^2 c_{pi}}{\partial r^2} + \frac{2}{r} \frac{\partial c_{pi}}{\partial r} \right) = \frac{\partial c_{pi}}{\partial t} \tag{E.1}$$

with the boundary and initial conditions,

$$r = 0, \qquad \frac{\partial c_{pi}}{\partial r} = 0 \tag{E.2a}$$

$$r = R_p, \qquad \left.\frac{\partial c_{pi}}{\partial r}\right|_{r=R_p} = \frac{k_f}{D_{pe}} \left(c_i - c_{pi}\big|_{r=R_p} \right) \tag{E.2b}$$

$$t = 0, \qquad c_{pi} = 0, \; i = 1, 2, 3 \qquad c_S = 80, \; c_G = c_F = 0, \; \forall_r \tag{E.2c}$$

where c_{pi} the pore concentration of component i (g/l), k_f is the film mass-transfer coefficient (cm.min^{-1}), D_{pe} is the effective pore diffusion coefficient (cm^2.min-1), $\Re\left(c_{pi}\right)$ is reaction rate defined by the linear relation $k' c_{pS}$ (g/l.min^{-1}), ε_p the particle porosity, K_i the equilibrium constant of component i, K_{enz} the equilibrium constant of the enzyme with linear adsorption

isotherm relationship. The differential equation that represents the mass balance of the pore-intraparticle fluid phase, to be solved not only considers the transient but also a reaction term, constant diffusivity and linear equilibrium isotherm, $q_i = K_i c_{pi}$. The υ_i is the stoichiometric coefficient of reaction equal to $\begin{cases} -1, i = sucrose \\ +0.526, i = glu\cos e, fructose \end{cases}$.

After introducing the dimensionless variables for the space $\rho = x/R_p$, with R_p the particle radius (cm), the differential equation to be solved becomes,

$$\frac{\partial c_{pi}}{\partial t} = \upsilon_i \frac{K_{enz} + \varepsilon_p}{K_i + \varepsilon_p} k' c_{pS} + \frac{1}{K_i + \varepsilon_p} \frac{D_{pe}}{R_p^2} \left(\frac{\partial^2 c_{pi}}{\partial \rho^2} + \frac{2}{\rho} \frac{\partial c_{pi}}{\partial \rho} \right) \qquad \text{(F3)}$$

with the boundary and initial conditions,

$$\rho = 0, \qquad \left. \frac{\partial c_{pi}}{\partial \rho} \right|_{\rho=0} = 0 \qquad \text{(E.4a)}$$

$$\rho = 1, \qquad \left. \frac{\partial c_{pi}}{\partial \rho} \right|_{\rho=1} = Bi_m \left(c_i - c_{pi}\big|_{\rho=1} \right) \qquad \text{(E.4b)}$$

$$t = 0, \qquad \begin{aligned} & c_{pi} = 0, \ i = 1,2,3 \\ & c_S = 80, \ c_G = c_F = 0, \ \forall_\rho \end{aligned} \qquad \text{(E.4c)}$$

with Bi_m the Biot number defined as $= k_f R_p / D_{pe}$.

The system of partial differential equations, PDE, (E.3-E.4) would be solved by using two different solvers: PDECOL (Madsen and Sincovec, 1979) and DASSL (Petzold, 1982)..

To be solved by using the PDECOL, some modifications must be done, since the system of differential equations are not defined for $r = 0$, however for all the points $r \neq 0$ is a quantity well defined. To overcome this problem the Rule of L'Hospital (Piskounov, 1990) was applied:

be $f(x)$ and $g(x)$ two functions that satisfied the Cauchy conditions in a certain segment $[a,b]$ and nulls for $x = a$, that is, $f(x) = g(x) = 0$. If, the limit of the coefficient $\frac{f'(x)}{g'(x)}$ exists when $x \to a$, then, $\lim_{x \to a} \frac{f(x)}{g(x)}$ exists and $\lim_{x \to a} \frac{f(x)}{g(x)} = \lim_{x \to a} \frac{f'(x)}{g'(x)}$.

For $r = 0$, and after applying the Rule of L'Hospital, the differential equation to be solved becomes,

$$3\frac{\partial^2 c_{pi}}{\partial r^2}\bigg|_{r=0} - \frac{\rho_p k}{D_{pe}} c_{pi} = \frac{\partial c_{pi}}{\partial t}$$

The rule was only applied to the term not defined for $r = 0$,

$$\frac{1}{r^2}\frac{\partial}{\partial r}\left(r^2 \frac{\partial c_{pi}}{\partial r}\right)$$

$$\lim_{r\to 0} \frac{\dfrac{\partial}{\partial r}\left(r^2 \dfrac{\partial c_{pi}}{\partial r}\right)}{r^2} = \frac{0}{0} = \lim_{r\to 0} \frac{2r\dfrac{\partial c_{pi}}{\partial r} + r^2 \dfrac{\partial^2 c_{pi}}{\partial r^2}}{r^2} = \lim_{r\to 0} \frac{2\dfrac{\partial c_{pi}}{\partial r}}{r} + \lim_{r\to 0} \frac{\partial^2 c_{pi}}{\partial r^2} =$$

$$= \frac{0}{0} + \frac{\partial^2 c_{pi}}{\partial r^2}\bigg|_{r=0} = \lim_{r\to 0} \frac{2\dfrac{\partial^2 c_{pi}}{\partial r^2}}{1} + \frac{\partial^2 c_{pi}}{\partial r^2}\bigg|_{r=0} = 2\frac{\partial^2 c_{pi}}{\partial r^2}\bigg|_{r=0} + \frac{\partial^2 c_{pi}}{\partial r^2}\bigg|_{r=0} = 3\frac{\partial^2 c_{pi}}{\partial r^2}\bigg|_{r=0}$$

The differential equations to be solved are,

$$\rho = 0, \quad \frac{\partial c_{pi}}{\partial t} = \upsilon_i \frac{K_{enz} + \varepsilon_p}{K_i + \varepsilon_p} k' c_{pS} + \frac{1}{K_i + \varepsilon_p} \frac{D_{pe}}{R_p^2}\left(3\frac{\partial^2 c_{pi}}{\partial \rho^2}\right) \tag{E.5a}$$

$$0 < \rho \le 1, \quad \frac{\partial c_{pi}}{\partial t} = \upsilon_i \frac{K_{enz} + \varepsilon_p}{K_i + \varepsilon_p} k' c_{pS} + \frac{1}{K_i + \varepsilon_p} \frac{D_{pe}}{R_p^2}\left(\frac{\partial^2 c_{pi}}{\partial \rho^2} + \frac{2}{\rho}\frac{\partial c_{pi}}{\partial \rho}\right) \tag{E.5b}$$

with the boundary and initial conditions defined in (4).

To use DASSL, also some modifications must be done to the system to be solved. The PDE system, in time, *t*, and in the spatial variable, ρ, is transformed into a initial value problem.

The method of orthogonal collocation in finite elements with the Hermite polynomials as basis function. In each subinterval, *k*, the approximated solutions of the concentration in the particle as the derivatives, defined as:

$$c_{pi}(t,\rho) = \tilde{c}_{pi}(t,u_j) = \sum_{l=1}^{4} H_{il}[u_j, h_k] a_{l+2k-2}(t) \tag{E.6a}$$

$$\frac{\partial c_{pi}(t,\rho)}{\partial \rho} = \frac{1}{h_k}\frac{\partial \tilde{c}_{pi}(t,u_j)}{\partial u_j} = \frac{1}{h_k}\sum_{l=1}^{4} A_{il}[u_j, h_k] a_{l+2k-2}(t) \tag{E.6b}$$

$$\frac{\partial^2 c_{pi}(t,\rho)}{\partial \rho^2} = \frac{1}{h_k^2}\frac{\partial^2 \tilde{c}_{pi}(t,u_j)}{\partial u_j^2} = \frac{1}{h_k^2}\sum_{l=1}^{4} B_{il}[u_j, h_k] a_{l+2k-2}(t) \tag{E.6c}$$

The new coordinate u_j, is defined, in each of the k subinterval ($0 \le u \le 1$), as:

$$u = \frac{\rho - \rho_k}{h_k} \qquad h_k = \rho_{k+1} - \rho_k \tag{E.7}$$

The functions H_{tl}, A_{tl}, and B_{tl} are the basis polynomials as defined in Finlayson (1989).

To obtained the estimation of the four parameters a_{l+2k-2} in each of the subinterval, four collocations points are needed. Two of them are the boundary points, u=0 and u=1, and the others two, the interiors points, the zeros of the Legendre polynomial $P_2^{(0,0)}(u_j)$, u_1=0.2113248654 and u_2=0.7886751346.

By using the two boundary conditions of the model equation, (4.b), we obtain,

$$k=1;\ u=0 \qquad \frac{1}{h_1}\frac{d\tilde{c}_{pi}}{du}\bigg|_{u=0} = a_2 = 0 \tag{E.8a}$$

$$k=NE;\ u=1 \qquad \frac{1}{h_{NE}}\frac{d\tilde{c}_{pi}}{du}\bigg|_{u=1} = Bi\left(c_i - \tilde{c}_{pi}\big|_{u=1}\right) \tag{E.8b}$$

$$a_{2NE+2} = Bi\left(c_i - a_{2NE+1}\right)$$

Two of the (2 NE+2) parameters to be estimated can be eliminated, remaining (2 NE) unknowns and (2 NE) equations.

Therefore, and after elimination of the two previous estimated parameters, the pore concentration of component *i* can be write as,

k=1, first subinterval

$$\tilde{c}_{pi} = H_{t1}a_1^i + H_{t3}a_2^i + H_{t4}a_3^i$$

$2 \le k \le$ NE-1

$$\tilde{c}_{pi} = \sum_{l=1}^{4} H_{tl}a_{l+2k-3}^i$$

k=NE, last subinterval

$$\tilde{c}_{pi} = \sum_{l=1}^{2} H_{tl}a_{l+2NE-3}^i + \left(H_{t3} - Bi_m H_{t4}\right)a_{2NE}^i + Bi_m H_{t4}c_i$$

The final initial value problem to be solved, after the applying the orthogonal collocation in finite elements is,

k=1 and t=1, 2, i=1,2,3 and j=1, 2, 3, 4

$$H_{t1}\frac{\partial a_1^i}{\partial t}+\sum_{l=3}^{4}H_{tl}\frac{\partial a_l^i}{\partial t}=D_p\left[\left(\frac{1}{h_1^2}B_{t1}+\frac{2}{\omega_t h_1^2}A_{t1}\right)a_1^i+\sum_{l=3}^{4}\left(\frac{1}{h_1^2}B_{tl}+\frac{2}{\omega_t h_1^2}A_{tl}\right)a_l^i\right]$$
$$-\upsilon_i k^*\left[H_{t1}a_1^3+\sum_{l=3}^{4}H_{tl}a_l^3\right] \qquad \text{(E.9a)}$$

k=2, …, NE-1 and t=1, 2, i=1,2,3 and j=1, 2, 3, 4

$$\sum_{l=1}^{4}H_{tl}\frac{\partial a_{l+2k-3}^i}{\partial t}=D_p\left[\sum_{l=1}^{4}\left(\frac{1}{h_k^2}B_{tl}+\frac{2}{(\varpi_t h_k+\rho_k)}\frac{1}{h_k}A_{tl}\right)a_{l+2k-3}^i\right]$$
$$-\upsilon_i k^*\left[\sum_{l=1}^{4}H_{tl}a_{l+2k-3}^3\right] \qquad \text{(E.9b)}$$

k=NE and t=1, 2, i=1,2,3 and j=1, 2, 3, 4

$$\sum_{l=1}^{2}H_{tl}\frac{\partial a_{l+2NE-3}^i}{\partial t}+(H_{t3}-Bi_m H_{t4})\frac{\partial a_{2NE}^i}{\partial t}=$$
$$=D_p\left[\sum_{l=1}^{2}\left(\frac{1}{h_{NE}^2}B_{tl}+\frac{2}{(\omega_{NE}h_{NE}+\rho_{NE})}\frac{1}{h_{NE}}A_{tl}\right)a_{l+2NE-3}^i+\right.$$
$$+\left(\frac{1}{h_{NE}^2}(B_{t3}-Bi_m B_{t4})+\frac{2}{(\omega_{NE}h_{NE}+\rho_{NE})}\frac{1}{h_{NE}}(A_{t3}-Bi_m A_{t4})\right)a_{2NE}^i+$$
$$\left.+Bi_m\left(\frac{1}{h_{NE}^2}B_{t4}+\frac{2}{(\omega_{NE}h_{NE}+\rho_{NE})}\frac{1}{h_{NE}}A_{t4}\right)c_i\right]- \qquad \text{(E.9c)}$$
$$-\upsilon_i k^*\left[\sum_{l=1}^{2}H_{tl}a_{l+2NE-3}^3+(H_{t3}-Bi_m H_{t4})a_{2NE}^3+Bi_m H_{t4}c_3\right]$$

with $D_{pi}=\frac{1}{K_i+\varepsilon_p}\frac{D_{pe}}{R_p^2}$ and $k_i^*=\frac{1}{K_i+\varepsilon_p}(K_{enz}+\varepsilon_p)k'$;

Resulting a system with [3.(2.NE)] parameters to be estimated, (2.NE) parameters for each of the three components.

After rearranging and in the matricial form, the system to be solved becomes,

$$[HMAT]\left[\frac{\partial a^i}{\partial t}\right]=D_{pi}([CMAT][a^i]+[CVEC]c_i)-\upsilon_i k_i^*([HMAT][a^3]+[HVEC]c_3)$$

with initial conditions,

$$[HMAT][a^i]-[HVEC]c_i=0\text{, with } c_3=80.0 \text{ and } c_1=c_2=0.0 \qquad \text{(E.10)}$$

The parameter coefficients matrix, $[HMAT]$, of dimension [3.(2.NE)] which defines the number of parameters $[a^i]$, to be estimated. The used matrices, with NE=4,can be defined as,

$$[HMAT]^i = \begin{bmatrix} H_{11} & H_{13} & H_{14} & & & & & \\ H_{21} & H_{23} & H_{24} & & & & & \\ & H_{11} & H_{12} & H_{13} & H_{14} & & & \\ & H_{21} & H_{22} & H_{23} & H_{24} & & & \\ & & & H_{11} & H_{12} & H_{13} & H_{14} & \\ & & & H_{21} & H_{22} & H_{23} & H_{24} & \\ & & & & & H_{11} & H_{12} & H_{13} - Bi_{mi} H_{14} \\ & & & & & H_{21} & H_{22} & H_{23} - Bi_{mi} H_{24} \end{bmatrix}^i$$

$$[CMAT]^i = [BMAT]^i + \frac{2}{u_t h_k + \rho_k} [AMAT]^i$$

$$[HVEC]^i = \begin{bmatrix} 0 \\ 0 \\ 0 \\ 0 \\ 0 \\ 0 \\ Bi_{mi} H_{14} \\ Bi_{mi} H_{24} \end{bmatrix}^i, \quad [CVEC]^i = \begin{bmatrix} 0 \\ 0 \\ 0 \\ 0 \\ 0 \\ 0 \\ Bi_{mi}\left(B_{14} + \frac{2}{u_t h_{NE} + \rho_{NE}} A_{14} \right) \\ Bi_{mi}\left(B_{24} + \frac{2}{u_t h_{NE} + \rho_{NE}} A_{24} \right) \end{bmatrix}^i$$

, where the subscript i, defines each of the three components.

The results obtained by using the initial value problem, (E.8-E.9), and by using the PDE system (E.3-E.4), considering the operating conditions and parameters as defined in Table E.1, are illustrated in the following figures. The value of c_i, the fluid concentration, was considered constant and equal to 80 g/l for the sucrose and 0 g/l for both glucose and fructose components.

***Table E.1**. Model parameters used in the model.*

$R_p = 0.016$ cm	$A_p = 0.00322$ cm^2
	$V_p = 0.00001716$ cm^3
$\varepsilon_p = 0.1$	$K_{enz} = 5$
$D_{peS} = 0.412 \times 10^{-6}$ cm^2/s	$D_{peG} = D_{peF} = 0.609 \times 10^{-6}$ cm^2/s
$k_{fS} = 0.2935$ cm/min	$k_{fG} = k_{fF} = 0.3812$ cm/min
$K_F = 0.43$	$K_G = 0.17$
$K_S = 0.0$	$k' = 0.547$ min^{-1}
$Bi_{mS} = 189.9$	$Bi_{mG} = Bi_{mF} = 166.9$
$\upsilon_S = -1$	$\upsilon_G = \upsilon_F = +0.526$
$M_S = 342$	$M_G = M_F = 180$

The numeric parameters and the total number of equations to be solved used in the two solvers are described in Table E.2.

Table E.2. *Relevant parameters for the two solvers.*

	PDECOL	DASSL
Spatial Discretization	Collocation; B-spines basis	Collocation, Hermite cubic basis
Time integrator	Gear's method	Backward differentiation
Number of collocation points per interval, NCC	2	2
Number of subintervals in the initial mesh, NE	14	14
Total number of ODE to be solved	NCC.NE.3 = 84	NCC.NE.3 = 84
Error tolerance	10^{-7}	10^{-7}

Following the main program and the subroutines where the model equations (E.3-E.4) are defined using PDECOL. The model parameters and some of the operations conditions are defined in the MAIN program. Additional information are provided as comments. The PDE system is defined in SUBROUTINE F(T,X,U,UX,UXX,FVAL,NPDE) where FVAL(1), FVAL(2) and FVAL(3) are the three differential equations (E.3), for i = 1, 2 and 3, respectively. The specification of the boundary conditions defined by equations (E.4), are defined in SUBROUTINE BNDRY(T,X,U,UX,DBDU,DBDUX,DZDT,NPDE). The initial conditions are specified in SUBROUTINE UINIT(X,U,NPDE)

```
C   MAIN PROGRAMME: PARTICLE.FOR
C           TO SOLVE THE MODEL:
C            PORE-INTRAPARTICLE
DIFFUSION, REACTION EQUATION
C        (SUCROSE INVERSION +
C      FRUTOSE/GLUCOSE SEPARATION)
C      ---------------------------
C
       IMPLICIT  DOUBLE  PRECISION  (A-
H,O-Z)
       DOUBLE PRECISION LC
C
C      DIMENSION DEFINITION
       DIMENSION
XBKPT(15),SCTCH(200),WORK(4050904),I
WORK(3630)
       DIMENSION
USOL(3,51),XPON(51),YCONC(51),CONCM(
3)

       COMMON /ENDPT/XLEFT,XRIGHT
C
C      INPUT - MODEL PARAMETERS
C
       OPEN
(UNIT=12,FILE='DATTMB_C',STATUS='OLD
')
C
C       ROTATION PERIOD (S) AND
C     FEED CONCENTRATION (G/L):
       READ(12,*) RP,CSFE
C PARAMETERS (E; EP; RP; PE; BETA):
```

```
      READ(12,*) EP,EPP,RPP,PE,BETA
C       COLUNMS (DC (CM); LC(CM);
 C    NCSI; NCSII; NCSIII; NCSIV):
      READ(12,*)
DC,LC,NCS(1),NCS(2),NCS(3),NCS(4)
C     MICHAELIS-MENTEN CONSTANTS:
C       K (MIN-1); KM (G/L);
C     CONC. ENZ:  KENZ (G/L):
      READ(12,*) AKVM,AKM,AKENZ,CENZ
C     CONSTANTS KSUC, KGL, KFR:
      READ(12,*) AKSUC,AKGL,AKFR
C       RATIO FLUID/SOLID VELOCITIES
ZONE II, R(2) AND III, R(3);
C   RECYCLING FLOWRATE, QR (ML/MIN)
      READ(12,*) R(2),R(3),QR
      CLOSE(12)
C
C     OUTPUT DEFINITION:
C     PDECOL PARAMETERS:
C
C     NINT=NUMBER OF SUBINTERVALS
C   FOR X IN PDECOL,
C     NCC=NUMBER COLLOCATION POINTS
C     NPDE=NUMBER OF PDE'S
      NINT=14
      NCC=2
      NPDE=3
C
      KORD=4
      MF=22
      INDEX=1
      IWORK(1)=4050904
      IWORK(2)=3630
      T0=0.D0
C
C     EPS = TOLERANCE
            DT=1.D-9
            EPS=1.D-10
C
C       NPTS=NUMBER OF POINTS IN THE
INTERVALS FOR PDECOL
            NPTS=NINT+1
            XBKPT(1)=0.D0
            XBKPT(2)=0.1D0
            XBKPT(3)=0.2D0
            XBKPT(4)=0.3D0
            XBKPT(5)=0.4D0
            XBKPT(6)=0.5D0
            XBKPT(7)=0.6D0
            XBKPT(8)=0.7D0
            XBKPT(9)=0.8D0
            XBKPT(10)=0.9D0
            XBKPT(11)=0.95
            XBKPT(12)=0.99D0
            XBKPT(13)=0.995D0
            XBKPT(14)=0.999D0
            XBKPT(15)=1.D0
            XLEFT=XBKPT(1)
            XRIGHT=XBKPT(NPTS)
            TOUT=0.D0
C
C     FLOWRATES IN THE TMB SECTIONS
C (ML/MIN),
C     SOLID VELOCITY (CM/S)
C     RATIO LIQUID VELOCITY / SOLID
CVELOCITY
C
            DO 2 J=1,4
          Q(J)=Q(J)-QST
          V(J)=Q(J)/AL
          R(J)=V(J)/US
C        TAU(J) ; TAUS(J) (S)
          TAU(J)=ALJ(J)/V(J)
          TAUS(J)=ALJ(J)/US
    2       CONTINUE
C
OTHERS PARAMETERS OF THE MODEL:
C     REACTION CONSTANTS (MIN-1),
C     DAMKOHLER NUMBER
            AKL=AKVM*CENZ/AKM
            DO 12 J=1,4
         DA(J)=AKL*(TAU(J)/60.D0)
   12       CONTINUE
C
C  MOLECULAR DIFFUSIVITY, DM, CM2/S
      ASSOFAC=2.6D0
      MOLECU=18.D0
      TEMPE=273.D0+50.D0
      VISCO=0.6D0
      VOLSUC=340.4D0
      VOLFR=177.6
      DMSUC=7.4D-
8*((ASSOFAC*MOLECU)**(0.5D0)*TEMPE)/
      *
(VISCO*(VOLSUC)**(0.6D0))
      DMFR=7.4D-
8*((ASSOFAC*MOLECU)**(0.5D0)*TEMPE)/
      *
(VISCO*(VOLFR)**(0.6D0))
C EFFECTIVE DIFFUSIVITY, DPE, CM2/S
      TORTU=2.D0
      DPES=DMSUC*EPP/TORTU
      DPEF=DMFR*EPP/TORTU
C    SHERWOOD NUMBER, SH,
C  SHCMIDT, SC, REYNOLDS, RE G/CM-S
      UF=0.01D0*0.6D0
C     G/CM3
      DENSITY=1.D0
      SCSUC=UF/(DENSITY*DMSUC)
      SCFR=UF/(DENSITY*DMFR)
C     CM/S
      UMEAN=V(3)
      REY=(UMEAN*DENSITY*2.D0*RPP)/(
UF)
C           FILM  MASS  TRANSFER,  KF
(CM/MIN)
      AKFS=((1.09D0/EP*(SCSUC)**(0.3
3D0)*(REY)**(0.33D0))*DMSUC/
      *
(2.D0*RPP))*60.D0
      AKFF=((1.09D0/EP*(SCFR)**(0.33
D0)*(REY)**(0.33D0))*DMFR/
      *
(2.D0*RPP))*60.D0
C     BIOT NUMBER
      BIOS=(AKFS/60.D0)*RPP/DPES
```

```
      BIOF=(AKFF/60.D0)*RPP/DPEF
C     KP (S-1)- FOR SUC ; GL/FR
      AKPS=(15.D0*DPES/(RPP*RPP))
      AKPF=(15.D0*DPEF/(RPP*RPP))
C
C     THIELE MODULUS
      THIES=RPP*DSQRT((AKL)/(DPES/60
.D0))
      THIEF=RPP*DSQRT((AKL)/(DPEF/60
.D0))
C     F(PHI)
      FPHIS=1+0.09955D0*THIES+0.1336
D0*THIES*THIES
      FPHIF=1+0.09955D0*THIEF+0.1336
D0*THIEF*THIEF
C
C     WRITE ALL THE VALUES:
C
            DETAT=0.01D0
C
   10       TOUT=TOUT+DETAT
C
            CALL
PDECOL(T0,TOUT,DT,XBKPT,EPS,NINT,KOR
D,NCC,NPDE,
     *  MF,INDEX,WORK,IWORK)
C
      CALL    VALUES(XPON,USOL,SCTCH,
NPDE,NPP,NPP,0,WORK)
C
C     MEAN   PARTICLE   CONCENT.   FOR
EACH TIME
C     CALL D01GAF
C
      DO K=1,3
               DO I=1,51

YCONC(I)=USOL(K,I)*XPON(I)*XPON(I)
               ENDDO
               IFAIL=1
               CALL
D01GAF(XPON,YCONC,51,ESTIMATE,ERROR,
IFAIL)
               IF(IFAIL.EQ.0)THEN

CONCM(K)=3.D0*ESTIMATE
                  ERRORC=ERROR
               ENDIF
      ENDDO
C
C     WRITE VALUES CONCENTRATION
C
            GOTO 10
C
  100       CONTINUE
C
            STOP
            END

C   Subroutines used in the PDECOL
C
C       F SUBROUTINE
C      PDE'S AND ODE'S DEFINITION
      SUBROUTINE
F(T,X,U,UX,UXX,FVAL,NPDE)
      IMPLICIT DOUBLE PRECISION (A-
H,O-Z)
      DIMENSION
U(3),UX(3),UXX(3),FVAL(3)
C     3 EQUATIONS - ONE FOR EACH
C     COMPONENT - SUC, GL, FR -
     COMMON …
C
C     FOR X=0, THE RULE OF
C     L'HOSPITAL WAS APPLIED, PDE
C     NOT DEFINED IN X=0.
      IF(X==XLEFT)THEN
       FVAL(1)=1.D0/(AKSUC+EPP)*(
     * -(AKENZ+EPP)*AKL/60.D0*U(1)
     *
+DPES/(RPP*RPP)*(3.D0*UXX(1)))
       FVAL(2)=1.D0/(AKGL+EPP)*(
     * 0.526D0*(AKENZ+EPP)*AKL/
     *  60.D0*U(1)+DPEF/(RPP*
     *  RPP)*(3.D0*UXX(2)))
      FVAL(3)=1.D0/(AKFR+EPP)*(
     *   0.526D0*(AKENZ+EPP)*AKL
     *   /60.D0*U(1) +DPEF/(RPP*
     *  RPP)*(3.D0*UXX(3)))
      ELSE
       FVAL(1)=1.D0/(AKSUC+EPP)*(
     *-(AKENZ+EPP)*AKL/60.D0*U(1)
     * +DPES/(RPP*RPP)*(UXX(1)+
     * 2.D0/(X)*UX(1)))
       FVAL(2)=1.D0/(AKGL+EPP)*(
     *   0.526D0*(AKENZ+EPP)*AKL
     *   /60.D0*U(1)+DPEF/(RPP*
    * RPP)*(UXX(2)+2.D0/(X)*UX(2)))
       FVAL(3)=1.D0/(AKFR+EPP)*(
     *  0.526D0*(AKENZ+EPP)*AKL/
     *  60.D0*U(1)+DPEF/(RPP*RPP)*
     *  (UXX(3)+2.D0/(X)*UX(3)))
      ENDIF
C
            RETURN
            END

C       SUBROUTINE BNDRY
C   BOUNDARY CONDITIONS DEFINITIONS
C     ---------------------------
      SUBROUTINE
BNDRY(T,X,U,UX,DBDU,DBDUX,DZDT,NPDE)
      IMPLICIT DOUBLE PRECISION (A-
H,O-Z)
      DIMENSION U(3),UX(3),DZDT(3)
      DIMENSION DBDU(3,3),DBDUX(3,3)
C
      COMMON …
C
C     INITIALIZATION:
      DO 1 K=1,3
         DZDT(K)=0.D0
         DO 2 J=1,3
            DBDU(K,J)=0.D0
            DBDUX(K,J)=0.D0
    2     CONTINUE
```

```
    1 CONTINUE
C
      IF (X.GT..5D0) GOTO 10
C
C     X=0:
C     ------------------------
            DO 4 K=1,3
         DBDUX(K,K)=1.D0
    4       CONTINUE
C
            RETURN
   10       CONTINUE
C
C     X=1:
C     ------------------------
      DO 5 K=1,3
         DBDUX(K,K)=1.D0
    5 CONTINUE
      DBDU(1,1)=BIOS
      DBDU(2,2)=BIOF
      DBDU(3,3)=BIOF
      DZDT(1)=80.D0*BIOS*(10.D0*DEXP
     (-10.D0*T))
C      RETURN
            END
C
C        UINIT SUBROUTINE
C    INITIALS CONDITIONS DEFINITION
C     ---------------------------
      SUBROUTINE UINIT(X,U,NPDE)
      IMPLICIT DOUBLE PRECISION (A-
     H,O-Z)
      DIMENSION U(3)
C
            COMMON ...
C
      DO 1 K=1,3
         U(K)=0.D0
    1 CONTINUE
C
      RETURN
      END
C
```

Figure E.1 shows the concentration variation of the three components along the particle at (a) beginning, t =1, (b) t =15 and (c) transient steady-state. Notice that the concentrations of the glucose and fructose, along the time, tends to the same value. Figure E.2, shows the mean pore concentration averaged over the particle, for the three components, along the time. Both obtained by using the DASSL. By using the PDECOL, Figure E.3 shows the concentration variation of the three components along the particle at (a) beginning, t =1, (b) t =15 and (c) transient steady-state. Notice that the concentrations of the glucose and fructose, along the time, tends to the same value. Figure E.4, shows the mean pore concentration averaged over the particle, for the three components, along the time.

Validation of the model solved by using the DASSL solver:

Verification in the steady-state:

sucrose

- flux through the biofilm (*moles/min*) = $k_f A_p \left(c_S - c_{pS}\big|_{\rho=1} \right) =$

  $0.2935 \times 0.003217 \times (80\text{-}78.19861)/1000 =$

  1.7×10^{-6} *g/min* / 342 = 4.97×10^{-9} *moles/min*

- *moles/min* consumed by reaction = $\langle \Re(c_p) \rangle . V_p =$

$$= 3.\left(\left(K_{enz} + \varepsilon_p \right) k' . \int_0^1 c_{pS} . \rho^2 d\rho \right) . V_p = 3.\left(\left(K_{enz} + \varepsilon_p \right) k' . \frac{\left\langle c_p \right\rangle_S}{3} \right) . \frac{4}{3} \pi . R_p^3 =$$

$(5.1 \times 0.547 \times 35.53785) \times 0.00001716/1000 =$

1.7×10^{-6} *g/min* / 342 = 4.97×10^{-9} *moles/min*

glucose / fructose

- flux through the biofilm (*moles/min*) = $k_f A_p \left(c_{pG}\big|_{\rho=1} - c_G \right) =$

  $0.3812 \times 0.003217 \times (0.72937-0)/1000 =$

  0.894×10^{-6} *g/min* / 180 = 4.97×10^{-9} *moles/min*

- *moles/min* consumed by reaction $\left\langle \Re\left(c_p\right) \right\rangle . V_p =$

$$3.\left(\left(K_{enz} + \varepsilon_p \right) 0.526 . k' . \int_0^1 c_{pS} . \rho^2 d\rho \right) . V_p = 3.\left(\left(K_{enz} + \varepsilon_p \right) 0.526 . k' . \frac{\left\langle c_p \right\rangle_S}{3} \right) . \frac{4}{3} \pi . R_p^3 =$$

$(5.1 \times 0.526 \times 0.547 \times 35.53785) \times 0.00001716/1000 =$

8.95×10^{-7} *g/min* / 180 = 4.97×10^{-9} *moles/min*

Looking to the previous obtained results, all are the same and equal to 4.97×10^{-9} *moles/min.* At the steady-state, the concentration of sucrose consumed by reaction is equal to the concentration of glucose and fructose formed.

Doing the estimation by using the mean pore concentration averaged over the particle values obtained along the time, Figure E.2:

(80.0-35.53785) × 0.526 = 23.38709 g/l ≠ 15.90408 g/l of Gl/Fr

(only ≈ 68% of glucose/fructose produced!)

Validation of the model solved by using the PDECOL solver:

Verification in the steady-state:

sucrose

- flux through the biofilm (*moles/min*) = $k_f A_p \left(c_S - c_{pS}\big|_{\rho=1} \right)$

  $0.2935 \times 0.003217 \times (80-78.19866)/1000 =$

  1.7×10^{-6} *g/min* / 342 = 4.97×10^{-9} *moles/min*

- *moles/min* consumed by reaction = $\left\langle \Re\left(c_p\right) \right\rangle . V_p =$

$$3.\left(\left(K_{enz}+\varepsilon_p\right)k'.\int_0^1 c_{pS}.\rho^2 d\rho\right).V_p = 3.\left(\left(K_{enz}+\varepsilon_p\right)k'.\frac{\langle c_p\rangle_S}{3}\right).\frac{4}{3}\pi.R_p^3 =$$

$$= (5.1\times0.547\times35.53729)\times0.00001716/1000 =$$

$$1.7\times10^{-6}\ g/min\ /\ 342 = 4.97\times10^{-9}\ moles/min$$

glucose / fructose

- flux through the biofilm (*moles/min*) $= k_f A_p\left(c_{pG}\big|_{\rho=1} - c_G\right) =$

$$0.3812\times0.003217\times(0.72945-0)/1000 =$$

$$0.895\times10^{-6}\ g/min\ /\ 180 = 4.97\times10^{-9}\ moles/min$$

- *moles/min* consumed by reaction $\langle\Re(c_p)\rangle.V_p =$

$$3.\left(\left(K_{enz}+\varepsilon_p\right)k'.\int_0^1 c_{pS}.\rho^2 d\rho\right).V_p = 3.\left(\left(K_{enz}+\varepsilon_p\right)k'.\frac{\langle c_p\rangle_S}{3}\right).\frac{4}{3}\pi.R_p^3 =$$

$$(5.1\times0.526\times0.547\times35.53729)\times0.00001716/1000 =$$

$$0.895\times10^{-6}\ g/min\ /\ 180 = 4.97\times10^{-9}\ moles/min$$

Looking to the previous obtained results, no differences were obtained between the two solvers.

Undertaking the estimation by using the mean pore concentration averaged over the particle values obtained along the time, Figure E.3, only ≈ 68% of glucose/fructose was produced,

$$(80.0 - 35.53729) \times 0.526 = 23.38739\ g/l \neq 15.89718\ g/l \text{ of Gl/Fr}$$

All the results, obtained for the solutions by using DASSL and PDECOL, are summarized in Table E.3.

Table E.3. *Validation of the model solved by using the PDECOL and DASSL solvers, in the steady-state*

		DASSL		PDECOL	
		Suc	Gl / Fr	Suc	Gl / Fr
With film	flux through the biofilm (*moles/min*)	4.97×10^{-9}	4.97×10^{-9}	4.97×10^{-9}	4.97×10^{-9}
	moles/min consumed by reaction	4.97×10^{-9}	4.97×10^{-9}	4.97×10^{-9}	4.97×10^{-9}
Without film	*moles/min* consumed by reaction	5.09×10^{-9}	5.09×10^{-9}	5.09×10^{-9}	5.09×10^{-9}

In Table E.3 we can also see the verification of the system balance for the case without considering the film $(Bi_m \to \infty)$.

By considering $Bi_m \to \infty$, the right boundary condition, (E.4b), was adjust to the following,

$$\rho = 1, \qquad c_{pi}\big|_{\rho=1} = c_i \tag{E.11a}$$

To use DASSL, (E.11a) was transformed into

$$k = NE;\ u = 1 \qquad a_{2NE+1} = c_i \tag{E.b11}$$

replacing the equation (E.7b). Consequently, the equation (E.8c), replaced by,

k=NE and t=1, 2, i=1,2,3 and j=1, 2, 3, 4

$$\begin{aligned}
&\sum_{l=1}^{2} H_{tl}\frac{\partial a^i_{l+2NE-3}}{\partial t} + H_{t4}\frac{\partial a^i_{2NE}}{\partial t} = \\
&= D_{pi}\left[\sum_{l=1}^{2}\left(\frac{1}{h_{NE}^2}B_{tl} + \frac{2}{(\omega_{NE}h_{NE} + \rho_{NE})}\frac{1}{h_{NE}}A_{tl}\right)a^i_{l+2NE-3} + \right. \\
&+\left(\frac{1}{h_{NE}^2}B_{t4} + \frac{2}{(\omega_{NE}h_{NE} + \rho_{NE})}\frac{1}{h_{NE}}A_{t4}\right)a^i_{2NE} + \\
&\left.+\left(\frac{1}{h_{NE}^2}B_{t3} + \frac{2}{(\omega_{NE}h_{NE} + \rho_{NE})}\frac{1}{h_{NE}}A_{t3}\right)c_i\right] - \\
&-\upsilon_i k_i^*\left[\sum_{l=1}^{2} H_{tl}a^3_{l+2NE-3} + H_{t4}a^3_{2NE} + H_{t3}c_3\right]
\end{aligned} \tag{E.12}$$

The DASSL final results were illustrated in Figure E.5 and Figure E.6; the mean pore concentration along the time and the concentration variation for three different value of t, respectively, for the model without considering the Bi_m. The PDECOL final results were illustrated in Figure E.7 and Figure E.8; the mean pore concentration along the time and the concentration variation for three different value of t, respectively, for the model without considering the Bi_m.

By using both PDECOL and DASSL, the flux through the biofilm were equal to the moles/min consumed by reaction, however, using the mean pore concentration averaged over the particle values obtained along the time, only 68% of glucose and fructose were produced.

To confirm the obtained results, the steady-state problem was considered and solved. The term with respect to time equal was set to zero, i.e. $\frac{\partial c_{pi}}{\partial t} = 0$, in the system (E.3). The steady-

state ODE system resulted was then solved by using MAPLE V (Char *et al.*, 1992) with mathematical methods. The model parameters used were the same as for the one used in the previous models, described in Table E.1.

The resultant ODE system to be solved was,

$$\begin{aligned}
&\frac{\partial^2 c_{pS}}{\partial \rho^2} + \frac{2}{\rho}\frac{\partial c_{pS}}{\partial \rho} - k'.(K_{enz} + \varepsilon_p)\frac{R_p^2}{D_{peS}} c_{pS} = 0 \\
&\frac{\partial^2 c_{pG}}{\partial \rho^2} + \frac{2}{\rho}\frac{\partial c_{pG}}{\partial \rho} + 0.526.k'.(K_{enz} + \varepsilon_p)\frac{R_p^2}{D_{peS}} c_{pS} = 0 \\
&\frac{\partial^2 c_{pF}}{\partial \rho^2} + \frac{2}{\rho}\frac{\partial c_{pF}}{\partial \rho} + 0.526.k'.(K_{enz} + \varepsilon_p)\frac{R_p^2}{D_{peS}} c_{pS} = 0
\end{aligned} \qquad \text{(E.13)}$$

and using the boundary conditions as for the case without considering the film, (E.4a) and (E.10).

The obtained exact solution was of the form,

$$\begin{aligned}
c_{pS}(\rho) &= 0.742609\frac{\sinh(5.372782.\rho)}{\rho} \\
c_{pG}(\rho) &= -0.264405\frac{\sinh(5.372782.\rho)}{\rho} + 28.483967 \\
c_{pF}(\rho) &= -0.264405\frac{\sinh(5.372782.\rho)}{\rho} + 28.483967
\end{aligned} \qquad \text{(E.14)}$$

and illustrated in Figure E.9. The relative error between the MAPLE V steady-state and PDECOL transient steady-state pore concentration solutions of the three components along the particle, obtained was illustrated in Figure E.10. The values obtained for the relative error, were irrelevant, less than 0.023%. Figure E.11 illustrated the obtained relative error between the two PDE solvers, DASSL and PDECOL. Also, no significant differences were obtained, less than 0.020%. In Table E.4, for several values of ρ, the obtained solution by using the three solvers described, can be compared.

Table E.4. *Obtained results, for same values of* ρ, *by using the three solvers: DASSL, MAPLE V and PDECOL, for the solution of the problem in study.*

	c_{pS}			c_{pG}			c_{pF}		
ρ	DASSL	Maple V	PDECOL	DASSL	Maple V	PDECOL	DASSL	Maple V	PDECOL
0.0	3.989	3.990	3.989	27.060	27.063	27.060	27.056	27.063	27.060
0.1	4.184	4.185	4.184	26.991	26.994	26.991	26.986	26.994	26.991
0.2	4.803	4.803	4.802	26.771	26.774	26.771	26.766	26.774	26.771
0.3	5.956	5.956	5.955	26.360	26.363	26.360	26.356	26.363	26.360
0.4	7.853	7.854	7.853	25.685	25.688	25.685	25.681	25.688	25.685
0.5	10.849	10.850	10.849	24.618	24.621	24.618	24.615	24.621	24.618
0.6	15.520	15.521	15.50	22.955	22.958	22.955	22.953	22.958	22.955
0.7	22.789	22.791	22.790	20.367	20.369	20.367	20.366	20.369	20.367
0.8	34.138	34.139	34.139	16.327	16.329	16.327	16.326	16.329	16.327
0.9	51.938	51.939	51.939	9.990	9.991	9.990	9.990	9.991	9.990
1.0	80.000	80.000	80.000	0.000	0.000	0.000	0.000	0.000	0.000

Results obtained by using the DASSL (after discretization of the spatial terms)

- With Bi_m

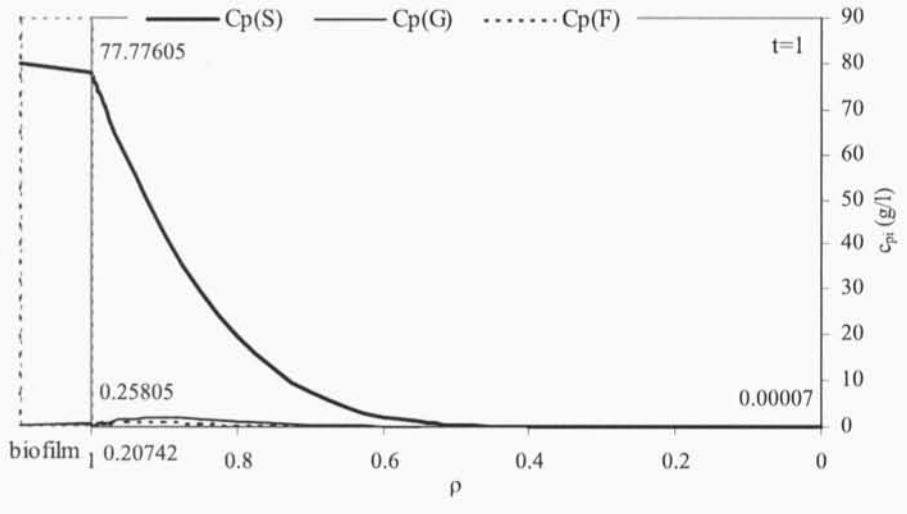

(a)

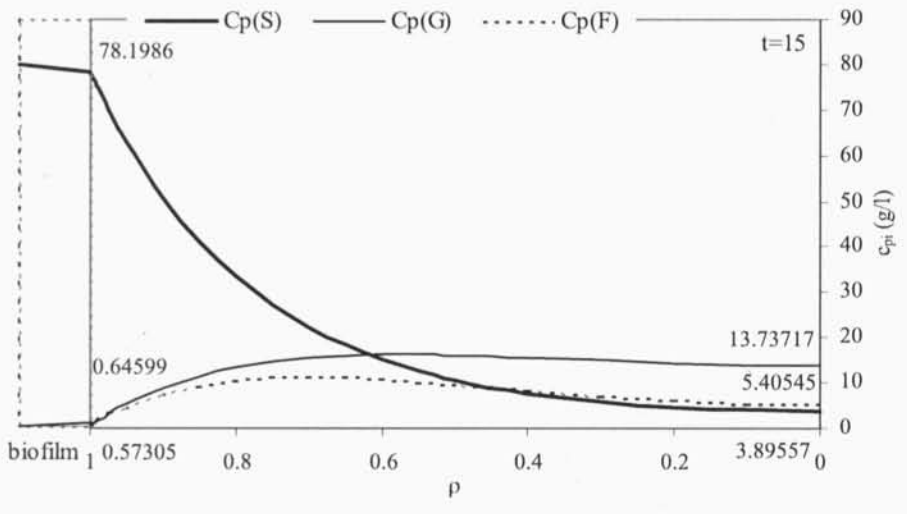

(b)

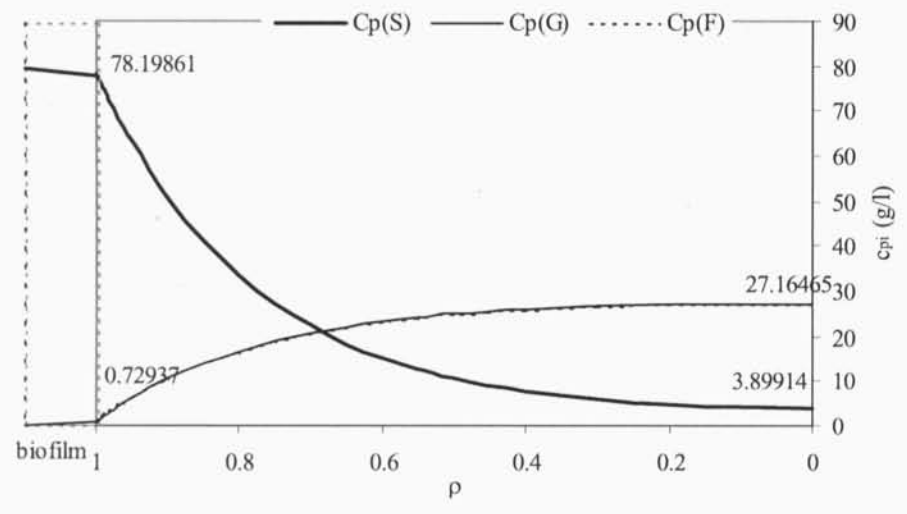

(c)

***Figure E.1**. Pore concentration variation of the three components along the particle for (a) initial of the study,* t *=1, (b)* t *=15, (c) final steady-state.*

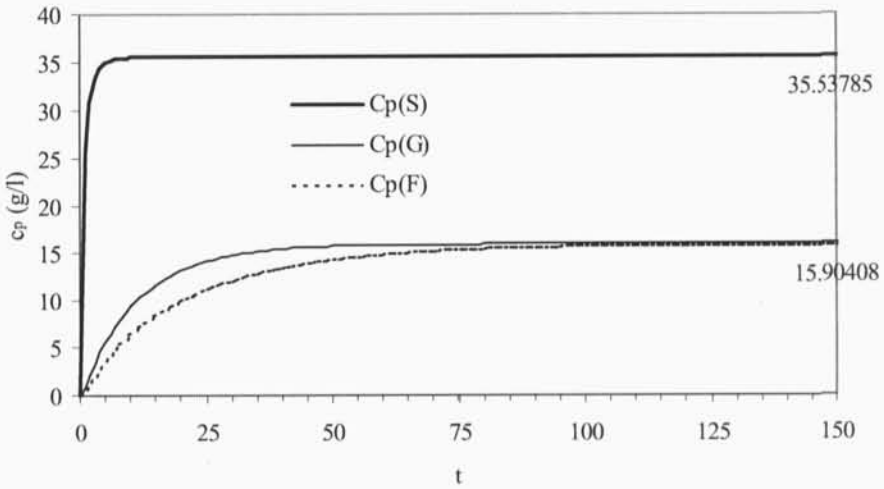

Figure E.2. *Mean pore concentration averaged over the particle, for the three components, along the time.*

Results obtained by using the PDECOL

- With Bi_m

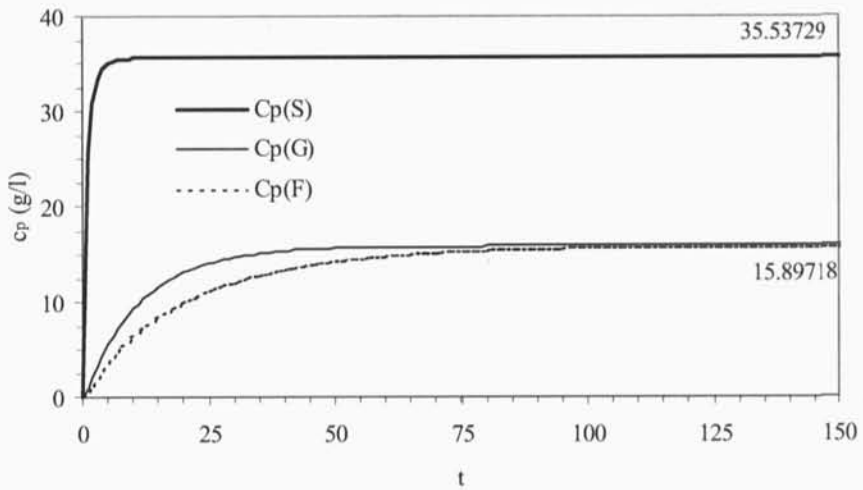

Figure E.3. *Mean pore concentration averaged over the particle, for the three components, along the time.*

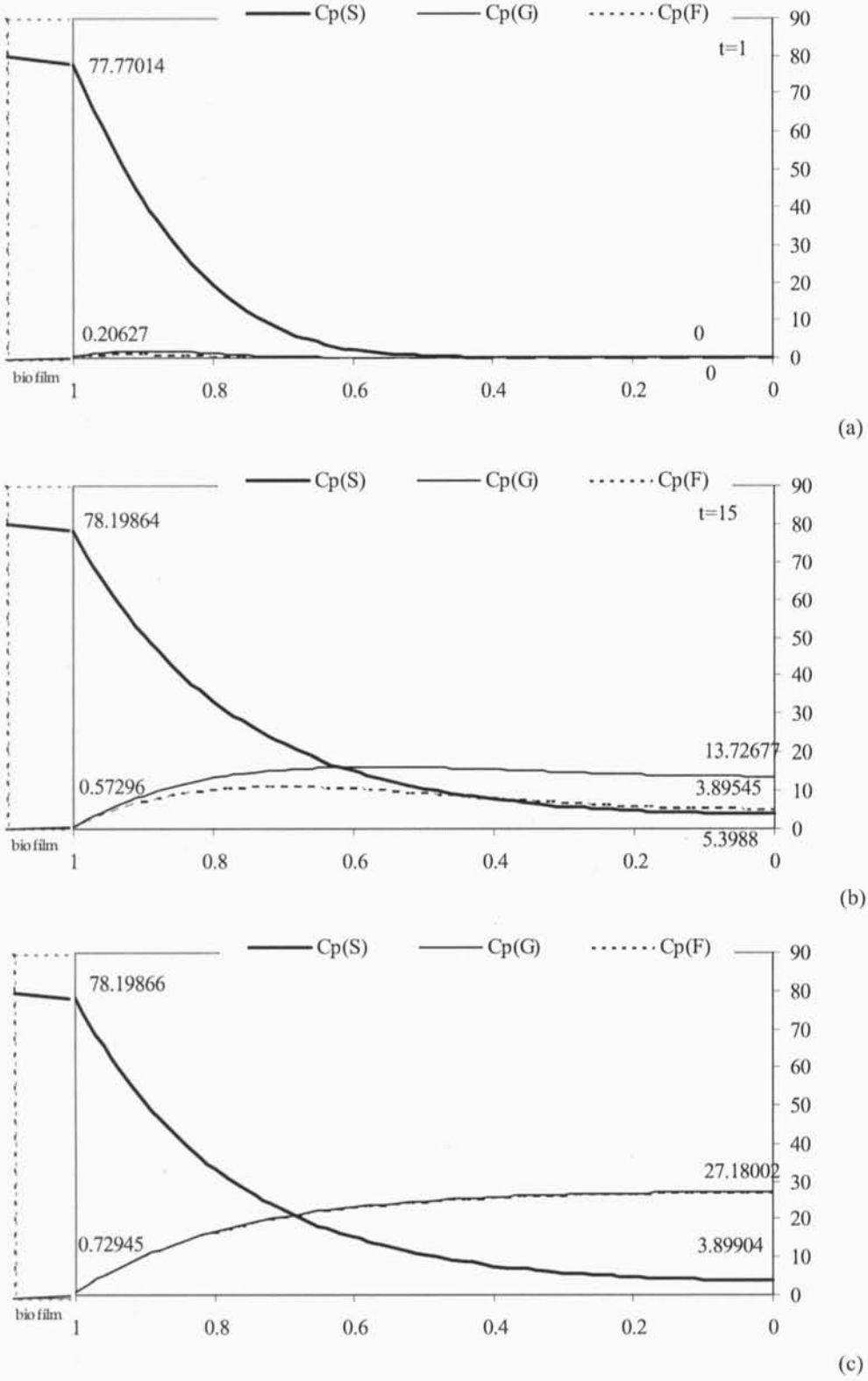

Figure E.4. *Pore concentration variation of the three components along the particle for (a) initial of the study, t =1, (b) t =15, (c) final steady-state.*

Results obtained by using the DASSL (after discretization of the spatial terms)

- Without Bi_m

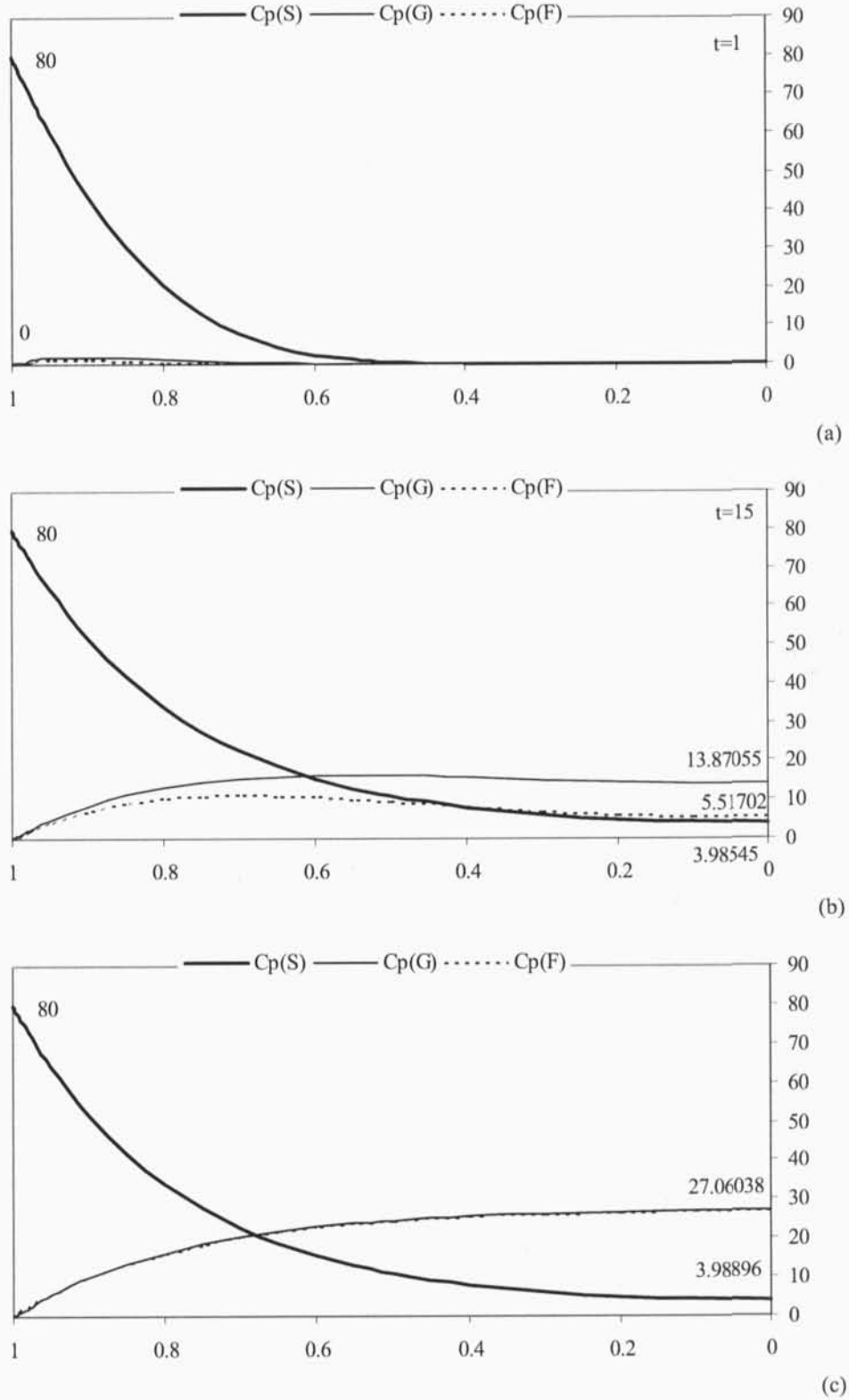

Figure E.5. *Pore concentration variation of the three components along the particle for (a) initial of the study, t =1, (b) t =15, (c) final steady-state.*

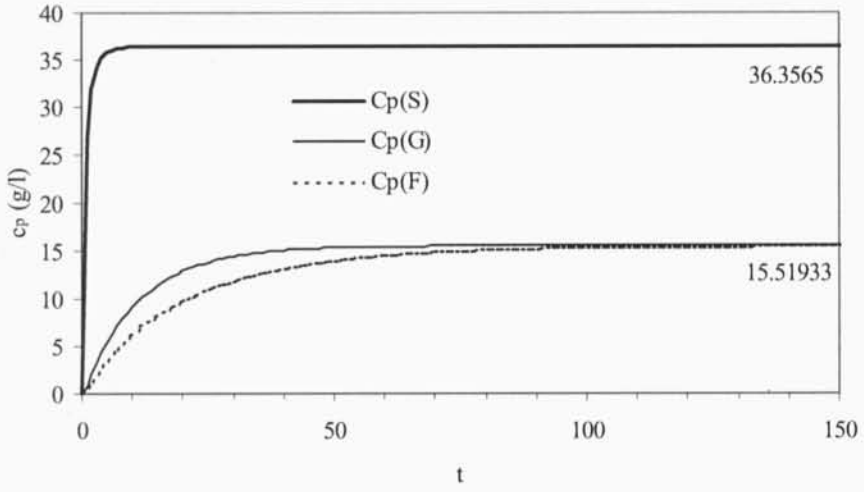

Figure E.6. *Mean pore concentration averaged over the particle, for the three components, along the time.*

Results obtained by using the PDECOL

- Without Bi_m

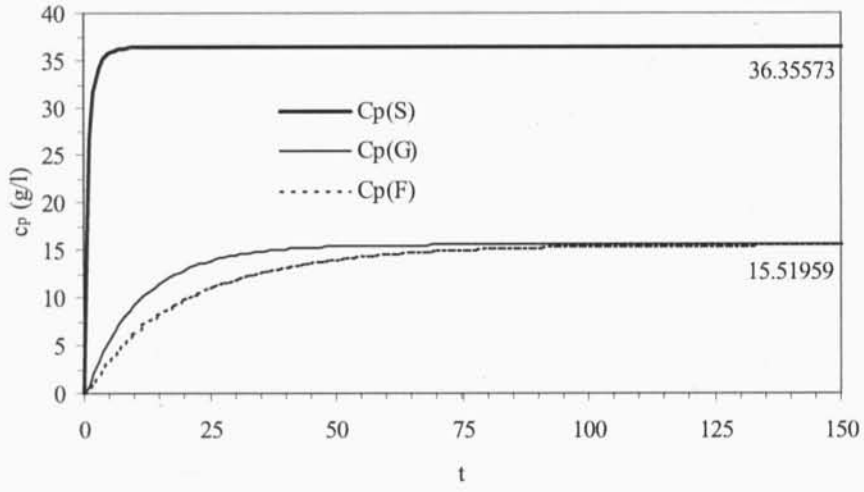

Figure E.7. *Mean pore concentration averaged over the particle, for the three components, along the time.*

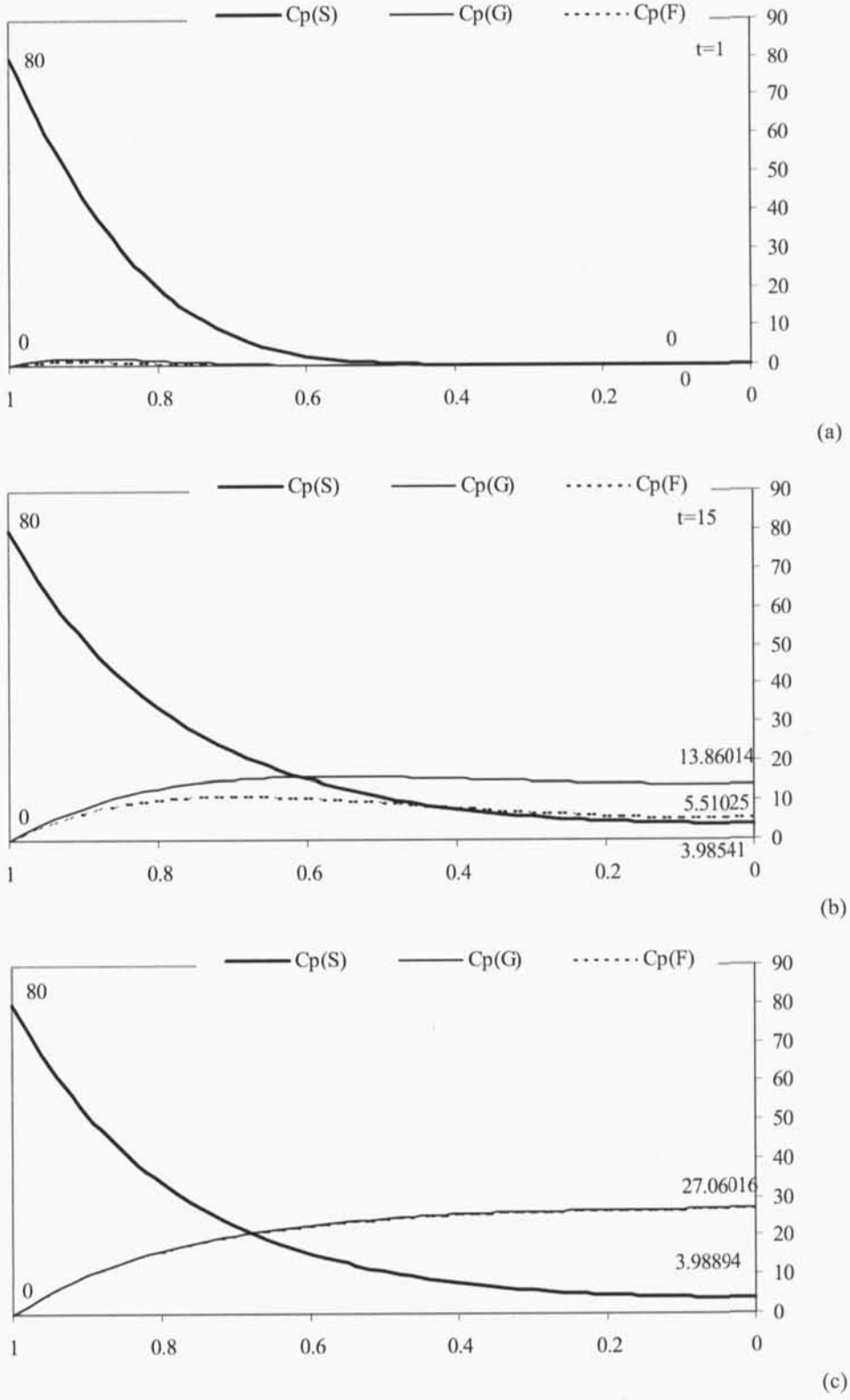

Figure E.8. *Pore concentration variation of the three components along the particle for (a) initial of the study, t =1, (b) t =15, (c) final steady-state.*

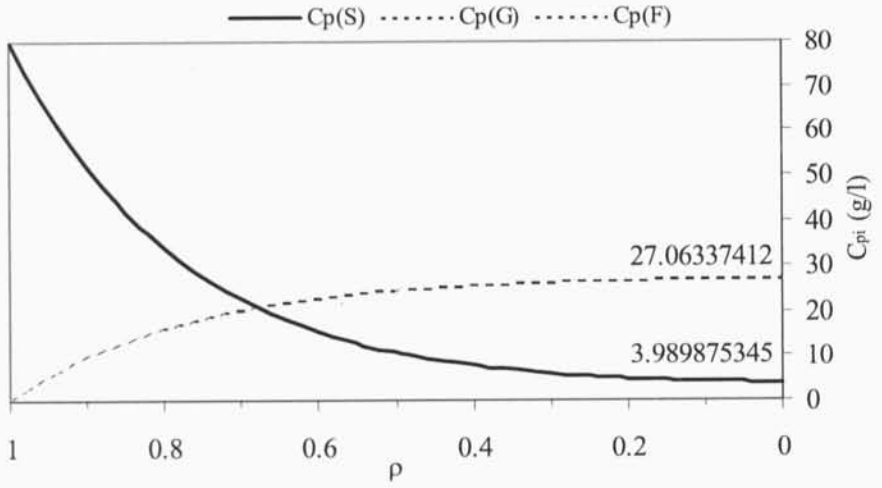

***Figure E.9**. Steady-state pore concentration variation of the three components along the particle, obtained by using MAPLE V (mathematical methods).*

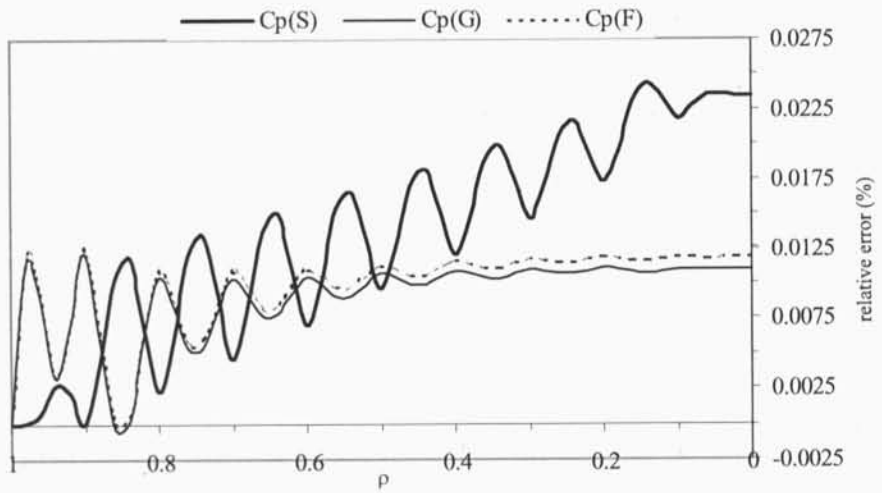

***Figure E.10**. Relative error between the MAPLE V steady-state and PDECOL transient steady-state pore concentration solutions of the three components along the particle, obtained, for the case without* Bi_m.

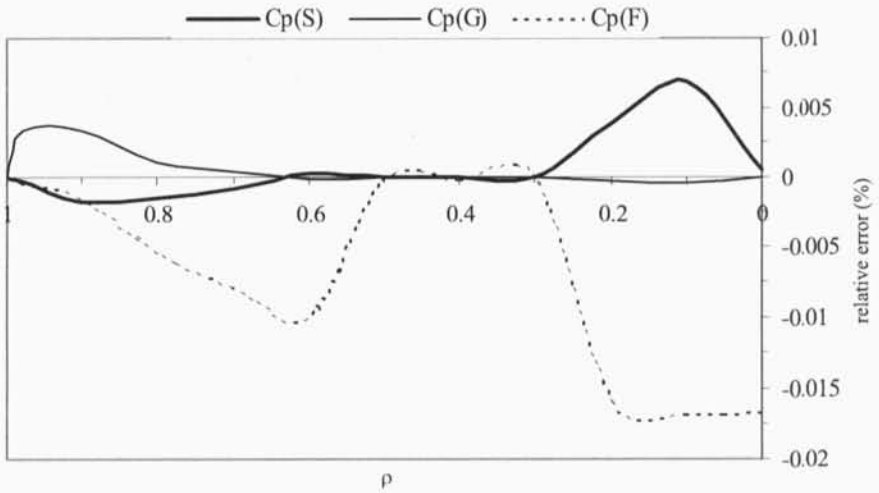

***Figure E.11**. Relative error between the DASSL and PDECOL transient steady-state pore concentration solutions of the three components along the particle obtained, for the case without Bi_m.*

E.2 References

Char, B., K. Geddes, G. Gonnet, B. Leong, M. Monagen, S. Watt, (1992) *First Leaves: A Tutorial Introduction to Maple V*, New York: Spinger-Verlag.

Madsen, N. K., and R. F. Sincovec, (1979) *PDECOL: General Collocation Software for Partial Differential Equations*, ACM Trans. Math. Software **5**, 326-351.

Petzold, L. R., (1982) *A description of DASSL: A Differential/Algebraic System Solver*, Rep. Sand. 82-8637, Sandia National Laboratory, Livermore.

Piskounov, N., (1990) *Cálculo Diferencial e Integral*, Vol. I, Lopes da Silva Eds., Porto.